An Experimental Study of Causes and Repair of Cracking of 1¼Cr-½Mo Steel Equipment

API PUBLICATION 938
MAY 1996

American Petroleum Institute
1220 L Street, Northwest
Washington, D.C. 20005

SPECIAL NOTES

(1) API publications necessarily address problems of a general nature. With respect to particular circumstances, local, state, and federal laws and regulations should be reviewed.

(2) API is not undertaking to meet the duties of employers, manufacturers, or suppliers to warn and properly train and equip their employees, and others exposed, concerning health and safety risks and precautions, nor undertaking their obligations under local, state, or federal laws.

(3) Information concerning safety and health risks and proper precautions with respect to particular materials and conditions should be obtained from the employer, the manufacturer or supplier of that material, or the material safety data sheet.

(4) Nothing contained in any API publication is to be construed as granting any right, by implication or otherwise, for the manufacture, sale, or use of any method, apparatus, or product covered by letters patent. Neither should anything contained in the publication be construed as insuring anyone against liability for infringement of letters patent.

(5) Generally, API standards are reviewed and revised, reaffirmed, or withdrawn at least every five years. Sometimes a one-time extension of up to two years will be added to this review cycle. This publication will no longer be in effect five years after its publication date as an operative API standard or, where an extension has been granted, upon republication. Status of the publication can be ascertained from the API Authoring Department [telephone (202) 682-8000]. A catalog of API publications and materials is published annually and updated quarterly by API, 1220 L Street, N.W., Washington, D.C. 20005.

FINAL REPORT TO
THE AMERICAN PETROLEUM INSTITUTE
OF RESEARCH UNDER THE GUIDANCE OF
THE TASK GROUP ON MATERIALS AND CORROSION RESEARCH
OF THE
COMMITTEE ON CORROSION AND MATERIALS

AN EXPERIMENTAL STUDY OF CAUSES AND REPAIR OF CRACKING OF 1¼Cr-½Mo STEEL EQUIPMENT

MAY 1996

Contractor:
The Materials Properties Council, Inc.
Investigator: M. Prager

Subcontractor:
Department of Materials Science
University of Tennessee
Investigators: C. D. Lundin, P. Liu,
C. Y. P. Qiao, G. Zhou and K. K. Khan

FOREWORD

The origin of this project was an in-depth study for API of numerous reported incidents of cracking of equipment of 1Cr-½Mo and 1¼Cr-½Mo-Si steels. The report to API is an explanation of the problem and the basis for further work to help prevent and repair such cracking. Metallurgical reports, fabrication records and service histories were reviewed. Worldwide research on the subject by steelmakers and studies of these alloys and similar materials in related applications were considered. In many cases, the cracking was major and cracks propagated in service. Emphasis in the report was placed on the causes of crack initiation during fabrication or of their appearance after only a short time in service.

It was concluded that major contributions to the cracking were from poor design, fabrication and operating practices which should be corrected using reasonable precautions and well known technology. Such action would prevent future vessels from entering service with preexisting cracks or initiating cracks in service. However, there was strong evidence that some of the plates and forgings used for vessel construction were more prone to cracking than others or have disturbingly low toughness. This study was intended to recommend ways to eliminate detrimental fabrication practices and materials.

Fabrication and repair operations must be upgraded because subsurface cracks which cannot be readily detected may occur and then emerge in service. Repairs have been troublesome.

Specifically, the study was developed to address the materials, fabrication and repair issues of greatest concern.

Under API and MPC Task Groups, Chaired by J. McLaughlin. The objectives of the Phase II Study were established as follows:

1) Develop an understanding of the fabrication/welding factors that affect cracking of Cr-Mo equipment, including the effects of PWHT and preheat temperature.
2) Develop an understanding of the inherent material properties that affect cracking of Cr-Mo equipment. This was to include the effects of impurities in the steel and initial condition of the steel (i.e., annealed vs. normalized and tempered).
3) Define a controlled deposition (temper bead) procedure for repair and initial fabrication that will produce a fine grain, more damage tolerant, microstructure in the weld heat affected zone (HAZ).
4) Determine the effect of using lower carbon, lower strength fillers for repair welds. Experience suggests that depending on conditions, the use of a low carbon filler can either improve or impair the performance of a repaired weld.

Appreciation is expressed to API for support. Portions of the work were cost shared by MPC, PVRC and WRC.

This work resulted in important new physical simulation, weldability and notched bar test methods. Fresh insight was gained into the heat affected zone metallurgy of this important class of materials.

Dr. M. Prager
Executive Director, Materials Properties Council, Inc.

CONTENTS

An Experimental Study of Causes and Repair of Cracking of 1¼Cr-½Mo Steel Equipment

C. D. Lundin, P. Liu, C. Y. P. Qiao, G. Zhou, K. K. Khan and M. Prager

Executive Summary

A multitask experimental study was conducted to provide the petroleum industry with solutions to recurring incidents of cracking in the application of welded 1¼Cr-½Mo steel for hydrogen processing equipment. The principal objective was to develop recommendations for the elimination of cracking that occurred during fabrication or early in operating life, was associated with repairs or was found after extended service exposure at elevated temperature.

Vessel and equipment experience has shown that the majority of weld cracking problems have occurred at temperatures in excess of 850°F. Further, little or no problems have been found for operation at temperatures below 800°F. Thus, a cutoff temperature of 825°F has been suggested for invoking the precautions, considerations and recommendations regarding the potential for coarse grained weld HAZ (CGHAZ) cracking in 1¼Cr-½Mo steels.

The research plan followed was proposed as a Phase II study at the conclusion of a survey and investigation (Phase I) conducted for API by MPC and reported in September, 1990.

The objectives of Phase II were to: determine what compositional and other material issues influence cracking; evaluate controlled deposition repair techniques; determine the suitability of low carbon filler materials; and understand the role of fabrication and welding practices on susceptibility to cracking.

The program succeeded in all objectives. It was found that fabrication, repair- and service-related cracking often have the same roots and are responsive to the same remedial action. Problems arise where there is low heat affected zone ductility. The following conclusions and recommendations are therefore provided.

For Applications of 1¼Cr-½Mo Steel at 825°F and Higher

(a) It is strongly recommended that Class 1 (60/35 ksi tensile, yield strength) materials be specified in preference to Class 2 (75/45 ksi tensile, yield strength), accelerated cooled materials.

(b) High PWHT temperatures were found to be necessary to improve heat affected zone ductility. PWHT requirements are related to welding variables and material composition. Fabrication guidelines are provided herein with specific PWHT recommendations depending on composition, desired strength and welding variables.

(c) High PWHT temperatures may be used without undesirably impairing creep strength and charpy impact values provided carbon content is not too high.

(d) Certain materials display a high sensitivity to cracking. Materials Composition Factors (MPC-5, MPC-7) have been identified and can be used to screen the materials. All of the elements included in the factors may not normally be included in the specification requirements and thus the range of elements controlled must be especially requested with the accuracy defined in Appendix B.

(e) Design, fabrication and materials specifications may now be prepared to assure freedom from cracking.

(f) Controlled deposition welding techniques and low carbon filler metals may be implemented in repair strategies when performance objectives and materials are identified.

(g) A number of screening tests have been demonstrated as suitable for determining material sensitivity to fabrication-related cracking. These include (Gleeble) simulated heat affected zone cracking, spiral notch rupture and large scale (PREVEW) weldability tests. These tests are not intended as requirements for material purchase. However, if the composition suggests that the material may be sensitive to reheat and in-service cracking, it may be wise to consider these tests to define the extent of anticipated problems.

(h) Studies of smooth and notch bar stress rupture behavior of simulated CGHAZ specimens provided insight into the effect of PWHT, heat input and microstructure on creep rate, ductility and cracking tendency.

(i) The results of this work have shown that the term "creep embrittlement" when applied to the low

---

Final report to API on *Prevention and Repair of Cracking in Chrome Moly Equipment*, MPC, September, 1990.

ductility in-service cracking in the low Cr-Mo materials is inappropriate. The low ductility behavior is essentially inherent from the initiation of service and is a combined result of the material factors in terms of chemistry, resistance to tempering and the degree of thermal treatment provided prior to service. No embrittlement was found to be caused by service in the creep range and, therefore, the use of the term creep embrittlement to describe service behavior of 1¼Cr-½Mo HAZ is not appropriate.

Report Overview and Conclusions

The attached report documents a comprehensive and complex study of cracking associated with an alloy for use at elevated temperatures. The Research Plan was developed and reported in an MPC document *Final Report to API—Prevention and Repair of Cracking in Chrome-Moly Equipment*. It was presented originally as a two year plan for Phase II to be conducted under the guidance of the API Task Group on Corrosion and Materials Research which prioritized the program tasks as follows:

1. *Effects of Fabrication and Welding*
   Develop an understanding of the fabrication/welding factors that affect cracking of Cr-Mo equipment. This will include the effects of PWHT and preheat temperature
2. *Materials Variables*
   Develop an understanding of the inherent material properties that affect cracking of Cr-Mo equipment. This will include the effects of impurities in the steel and initial condition of the steel (i.e., annealed vs. normalized and tempered).
3. *Controlled Deposition Repair Procedures*
   Define a Controlled deposition (temper bead) procedure for repair and initial fabrication that will produce a fine grain microstructure in the heat affected zone (HAZ).
4. *Filler Metals*
   Determine the effect of using lower carbon, lower strength fillers for repair welds. Experience suggests that depending on conditions, the use of a lower carbon filler can either improve or impair the performance of a repaired weld.

Additional work on hydrogen effects originally suggested by MPC received a low priority and was not pursued.

While the objectives of the tasks are defined separately, the work was performed in a testing plan that most efficiently explored the various interrelated issues. Appendix J indicates the relationships of the various tasks as originally described.

The various studies in Phase II that are documented and attached here are:

(a) Update of the Literature Survey (Appendix A)

(b) Compositional and Microstructural Studies, Heat Affected Zone Transformation and Metallurgical Characteristics (Appendixes B and C)

(c) Assessment of Reheat Cracking Susceptibility (Appendix D)

(d) Predicting Reheat Cracking Susceptibility Based on Chemical Composition (Appendix E)

(e) Toughness Study (Appendix F)

(f) Microstructural and Fractographic Evaluations (Appendix G)

(g) Notch Bar and Smooth Bar Stress-Rupture Studies (Appendix H)

(h) Repair Welding (Appendix I)

(i) Original Phase II Plan (Appendix J)

The overall logic of the program was as follows:

1. obtain a broad range of materials;
2. select small scale notch tests to screen material variables for susceptibility to elevated temperature cracking;
3. screen and rank materials on the basis of HAZ behavior;
4. validate ranking and test predictions by large scale tests;
5. systematically evaluate material variables using small scale tests;
6. examine repair procedures on sensitive heats with large scale tests;
7. use a notched bar rupture test for simulation of cracking in-service;
8. examine the effects of materials and fabrication variables on in-service cracking probability; and
9. rank materials and heat treatments for in-service cracking tendency.

A total of seventeen commercial heats were obtained and information on others was utilized. Based on analyses of the behavior of the more than twenty heats it has been concluded that the hardest areas in the weld heat affected zones of 1¼Cr-½Mo steel respond relatively slowly to PWHT and may display low ductility at elevated temperatures. Ductility depends on material composition, weld heat input and PWHT conditions. While these qualitative characteristics were not surprising, the quantitative details which emerged from the study were. For example:

(a) heat affected zone ductilities among the materials varied by a factor of ten;

(b) coarse *grained* heat affected zones of high carbon materials tended to display low ductility, perhaps only a fraction of 1% to failure, even after PWHT;

(c) for a given heat input and hardness, creep rates of coarse *grained* heat affected zones varied by as much as a factor of 10 depending on composition (transformation microstructure);

(d) the ductilities of some heats were improved significantly by heat treatment while others reached a plateau and remained relatively notch sensitive;

(e) smooth bar and notched bar stress-rupture lives of the materials were found to vary by as much as a factor of ten;

(f) there is no evidence that the materials become brittle in time (creep embrittlement). Instead, it is concluded that brittleness is a consequence of the as-tempered microstructure which must be softened significantly before ductility can be observed;

(g) creep rates and smooth bar rupture lives of simulated HAZs were only slightly affected by tempering temperatures from 1250°F–1350°F. However, the ratios of notch to smooth bar lives and ductilities tended to improve;

(h) the PWHT temperature necessary to reduce significantly notch sensitivity in the heat affected zones varied among the heats by as much as 100°F. Fabrication and repair procedures should take this into account;

(i) controlled deposition techniques and low carbon filler metals may be used to reduce the tendency for cracking during heat treatment and service;

(j) materials that were found to display PWHT cracking susceptibility tended to rate poorer expectations for service;

(k) as a result of this work the compositional factors identified as useful are shown below. All quantities are expressed in wt %. (See Appendix E for a more detailed description of these factors);

$$\text{MPC Factor-5} = [\text{Cfn}(\text{Tramp} + \text{Sin})\text{Alfn}] - 1$$

$$\text{Cfn} = (5\text{C} + 1000\text{Nb} + 100\text{V} + 50\text{Ti} - 0.5) + 1$$

$$\text{Tramp} = 2[4.3(\text{Sn} + \text{As}) + 150\text{Sb} + \text{Cu} + 50(\text{P} - 0.01)]$$

$$\text{Sfn} = 1 + 30(\text{S} - 0.02\ \text{Tramp});$$

$$\text{For Sfn} < 1, \quad \text{Sfn} = 1$$

$$\text{Alfn} = 1 + 15(\text{Al} - 0.015);$$

$$\text{For Alfn} < 1, \quad \text{Alfn} = 1$$

$$\begin{aligned}\text{MPC Factor-7} = {} & 2(\text{C} - 0.12) - 0.25(\text{Mn} - 0.6) \\ & + 150\text{Nb} + 15\text{V} + 15\text{Ti} - 100\text{B} \\ & + 40(\text{P} - 0.010) + 5(\text{S} - 0.015) \\ & + 10(\text{Al} - 0.010) \\ & + 20(\text{Cu}/100 + \text{Sn}/3 + \text{As}/3 + 3\text{Sb})\end{aligned}$$

MPC Factor-5 combines a carbon function (strength), a tramp element function (embrittlement), a sulfur function (embrittlement) and an aluminum function. The combination of these functions is shown in the factor as presented in Fig. 3. MPC Factor-7 (Fig. 4) utilizes the concept of a lower limit threshold as a basis for the effect of the elements in an additive fashion. It is believed that the sensitivity to reheat/PWHT cracking can be assessed by either of these factors and a reasonable correlation exists with fabrication behavior. Using MPC Factor-5 the limiting value for the onset of a potential for reheat/PWHT cracking is 2.0 and for MPC Factor-7 the limiting value is 0.5.

(l) it is recommended that carbon content should be in the range of 0.10–0.13% to achieve satisfactory material properties with minimum fabrication problems;

(m) it is also recommended that users specify materials and processes to obtain Class 1 (60-85 UTS) to reduce problems during fabrication, repair and service. There is no difference between allowable stresses for Class 1 and Class 2 in the creep range; and

(n) it is considered that a similar factor concept be applieded to 1Cr- ½Mo materials. The Cr ranges overlap. The Si content is the basic differential. Excluding this difference in Si, the basic considerations are applicable. However, a slightly different factor may have been derived if a number of 1Cr-½Mo heats had been included.

Recommendations for Vessel Fabrication and Repair

Introduction

The key results of this program on means of mitigating cracking either during PWHT or in-service are presented in the form of guidelines for fabrication and repair. The discussion of the research results that support these recommendations is presented in the next section and the experimental results are contained in the various Appendixes. The guideline flow charts were derived in consideration of the data and the experience of the investigators and those in the petroleum industry. The repair recommendations offered are firm at this time, but tests of the efficacy of the low carbon weld metal continue.

Fabrication Guidelines

The fabrication guidelines are presented in the form of a flow chart (Fig. 1) that will direct the user to the considerations necessary for successful fabrication of vessels and components of 1¼Cr-½Mo steel for use at elevated temperatures into the creep temperature regime (>825°F). The fabrication guidelines recommend that the users first establish the composition of the material of construction and consider the strength level (Class) to be employed.

Guidelines are offered for both the Class 1 (60–85 ksi) and Class 2 (75–100 ksi) strength levels. The initial material strength (hardness) during fabrication will be dictated by the final strength or Class desired in the vessel or component. The material must be purchased at a specific strength/hardness level so that the application of the required PWHT schedules does not reduce the base metal strength below that for the design Class desired. For example, a quenching and tempering (Q & T) operation may be required to maintain Class 2 strength after the desired PWHT exposure. It is evident from the testing accomplished here that the higher the initial strength of the material the more likely the occurrence of reheat/PWHT cracking in a sensitive material and if the material enters service with the HAZ only moderately tempered to preserve the high end of the strength level, in-service HAZ cracking is also more likely. The research also strongly suggests that the vessel or component should be PWHT high in the

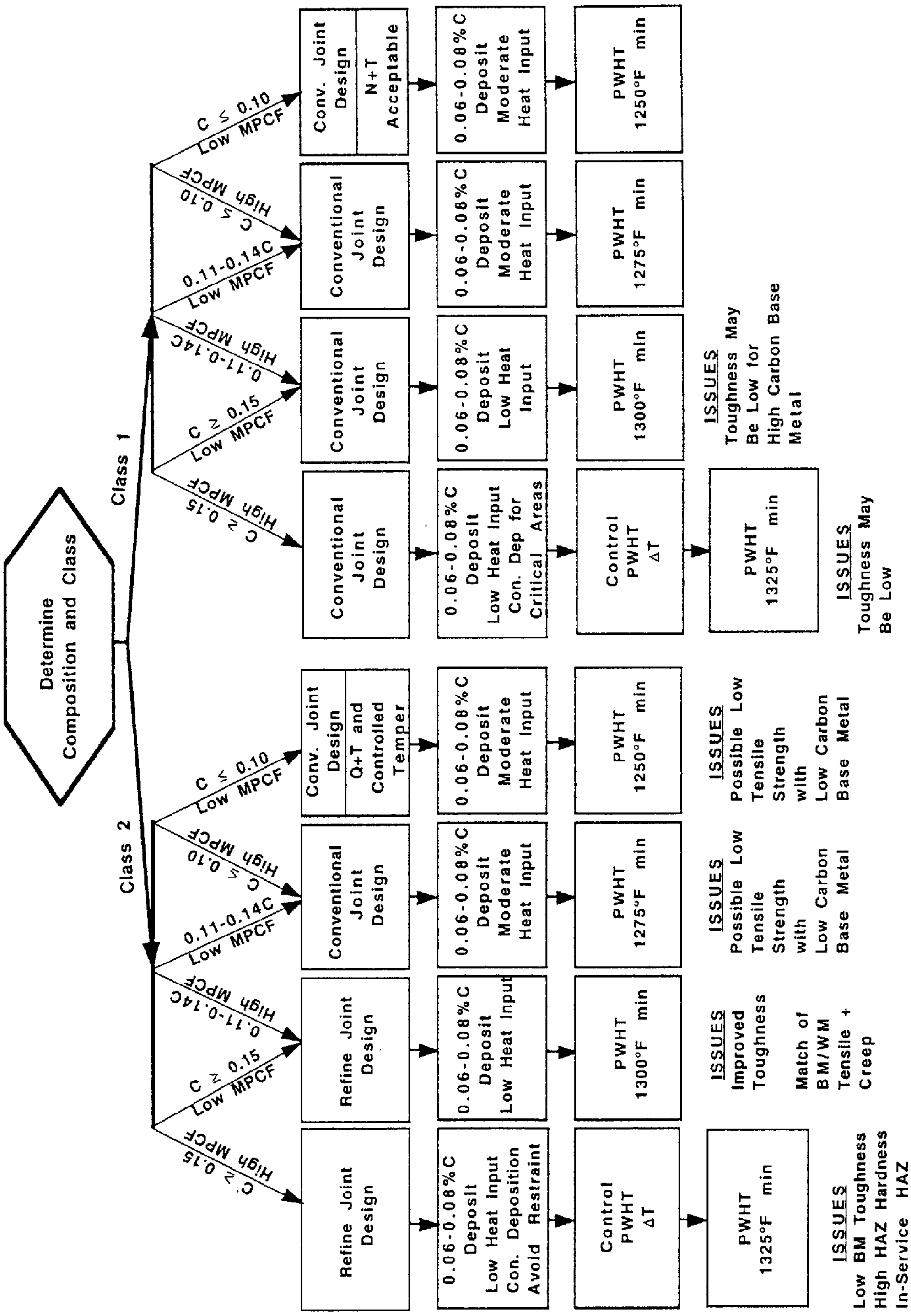

Fig. 1—Fabrication guidelines

PWHT range and certainly above 1250°F in any event in order to impart good HAZ ductility.

PWHT at high temperatures will more rapidly reduce strength levels and may cause loss in toughness, bringing further considerations to bear in terms of properties. This study of the coarse grained HAZ creep properties also showed that the strength of the HAZ for a given material was not significantly affected by the degree of PWHT, but notch sensitivity was greatly increased by relatively low PWHT. Further, in the considerations for design it must be recognized that when time-dependent properties govern, the ASME allowable stresses are substantially the same for both Classes of material (above 900°F). Thus, it would be prudent to select a Class 1 strength level for these applications.

The composition of the material should be considered from several standpoints. Today, most 1¼Cr-½Mo-Si steel is furnished to relatively low J and X-bar factors (J factors of <200 and X-bar levels less than 15) which are readily attainable with current steel making practice. However, to avoid crack susceptible heats, we propose a newly defined MPC Factor. Several were evaluated. Of these MPC Factors, 5 or 7 should be employed, and the satisfactory performance cutoff maximum values for the factors are: 2.0 for MPC Factor-5 and 0.5 for MPC Factor-7. These factors assess the sensitivity toward reheat/PWHT cracking and in-service sensitivity to low ductility HAZ cracking. It is also important to consider the carbon content of the material because of its major effect on hardenability (ability to attain a specific strength [hardness] level during the initial heat treatment; e.g., Q & T or N & T). The carbon content also plays a major role in the level of toughness that can be maintained after PWHT. The higher carbon content materials tend to experience a greater loss in toughness with a given PWHT.

When the strength class, carbon content and MPC Factor have been determined, the flow charts may be entered in the appropriate column to determine the basic considerations in fabrication that will aid in avoiding PWHT as well as in-service cracking and property degradation.

Guideline Details Class 2 Properties

Case 1. The Class 2 properties column, which is characterized by a carbon content $\geq 0.15\%$ and a high MPC Factor, represents the most critical material for fabrication. The initial direction calls for a "refined joint design" that should include all means for reducing the fabrication and operational stresses and should invoke the requirement that all joints be full penetration welded and utilize the least amount of filler metal. The weld crowns should be removed and ground flush with the plate surface for butt welds and the contour of the fillet welds should be ground such as to provide a smooth transition to the base material (blend ground). The grinding scratches should be transverse to the weld axis and the final grinding should be done with fine wheels. The sequencing of welds should be considered carefully so as to minimize long range residual stresses.

"Refined joint design" is a generic term that reflects the optimum placement and configuration of weld joints in order to avoid excessive long range residual stresses and stress raisers that can trigger the initiation of reheat cracking. The application of butt joints, which have the smallest amount of filler metal added (narrow groove technology), limits the generation of residual stresses that span significant distances and cause distortions that contribute to the stress redistribution which triggers reheat cracking. A secondary consideration is the employment of "refined joint details" such as the surface dressing of the overfill in butt joints, which reduces stress raisers and mitigates the occurrence of reheat cracks in the butt weld HAZ. It is known that properly made butt welds with no surface of internal discontinuities are relatively immune to any exacerbating factors that contribute to reheat cracking. Sit-on nozzles that employ fillet welds are to be avoided as well as fillet welds that are not properly contoured and fared into the base metal at the toes. Lack of fusion at the root of fillet welds is also to be avoided. In general, welds should not be placed in regions of natural stress elevation or where the stress state from both the fabrication and operation standpoints is high or unknown. ASME B & PV Code Section VIII provides some guidance in Part UG, UHA and UHT, in addition to the appendixes. The 1988 Hague Conference paper by Cane also describes "refined joint designs." Naturally the sensitivity of the material to reheat cracking plays a part in the potential for cracking and to this end the MPC factors that are given cutoff limits for sensitivity should be considered when the types of joints to be employed are selected.

The weld deposit carbon content should be aimed at the 0.06–0.08% range as this carbon content range provides sufficient elevated temperature strength without the potential for excessive hardness in the weld deposit. Extensive Pressure Vessel Research Council (PVRC) research has showed that little benefit is gained in terms of elevated temperature strength as the weld metal carbon content is raised much above the 0.06–0.08% level. Preheat should be 300°F minimum, in accordance with ASME recommendations. A postweld hold at the preheat temperature is advisable when the section size exceeds one-half inch. Low weld heat input should be utilized, employing small passes that induce low temperature transformation products to yield a better ductility response during PWHT and higher creep rates to redistribute the strains attendant with reduction in welding residual stresses. Small passes also provide for maximum overlap in the base metal HAZ and thus will limit the extent of the coarse grained region remaining after welding is complete (it is the coarse grained region that has the maximum potential for cracking). As an example, the number of passes to insure low heat input should exceed approximately 16 for a 1 in. thick plate. Controlled deposition procedures should be considered strongly dependent upon the MPC factor and carbon content. The employment of controlled deposition procedures similar to those defined in Appendix I can be used with success in refining the base metal HAZ microstructure thus minimizing the potential occurrence of reheat/PWHT cracking or cracking in the HAZ in-service.

PWHT should be performed at a minimum of 1325°F with controls placed on the heat-up rate and the ΔT within the vessel during the PWHT treatment to minimize stresses. The high PWHT will greatly desensitize the HAZ tendency toward low ductility cracking in-service.

Several issues must be addressed for the fabrication of the high carbon and high MPC Factor materials. Loss in base metal toughness, upon the high temperature PWHT, is a concern and efforts to combat this loss may involve limited heat treatment and tempering before fabrication in the attempt to maintain toughness after completion of fabrication. However, the higher the strength of the initial base material the higher the potential for cracking problems. High carbon content materials with high levels of carbide forming elements (which contribute to the MPC Factor) may cause the retention of high base metal HAZ hardness after fabrication and influence certain applications for which the hardness level is a consideration. The high hardness HAZs are also more sensitive to HAZ cracking in-service and will cause consideration for a significant level of in-service inspection of the welds, especially early on in operation.

The high carbon and high MPC Factor conditions are the most critical in the fabrication of a vessel and component and will involve the most carefully considered fabrication steps to be invoked.

Case 2. If the MPC Factor is low with a high carbon content or a high MPC Factor with the carbon content in the recommended range of 0.11–0.14%, certain relaxation in fabrication procedures can be invoked. These are basically that controlled deposition welding procedures are probably not necessary and the PWHT temperature can be reduced to 1300°F minimum. The reduction in PWHT temperature will no doubt improve toughness response upon PWHT and the base metal and weld metal tensile and creep strength will most likely have a better match. The degree of in-service inspection can probably be relaxed after the initial start-up, although the attention to joint design details and the contouring of the welds should be followed rigorously.

Case 3. With the optimum range of carbon content and a low MPC Factor or a low carbon ($\leq 0.10\%$) content and a high MPC Factor relaxation to conventional joint designs and normal treatment of weld contours and grinding can be accomplished. Moderate heat input welding can be employed and the PWHT temperature reduced to 1275°F minimum. Better retention of toughness will be affected. However, at the low carbon level the tensile strength may be reduced to values approaching the lower limit of the Class 2 properties if extended PWHT times are employed.

Case 4. For a carbon content ($\leq 0.10\%$) and a low MPC Factor the chance of reheat/PWHT or in-service HAZ cracking is minimal and the PWHT temperature can be reduced to 1250°F minimum. However, this condition of low carbon and low MPC Factor may require a Q & T heat treatment for the base metal prior to fabrication with a controlled tempering temperature to maintain Class 2 properties.

It should be noted that Class 2 offers no advantage as far as allowable stresses for service in the creep range. Thus specification of Class 1 facilitates fabrication with no lower allowable stress and improved ductility.

Class 1 Properties

The columns representing Class 1 properties in the Fabrication Guidelines are less restrictive in fabrication procedures than those for Class 2 properties because the lower strength (hardness) of the base material provides for a greater degree of stress relaxation during PWHT and for better redistribution of stress during transient conditions in-service. This tends to reduce the potential for coarse grained HAZ cracking during PWHT or as a function of time for in-service exposure.

Conventional joint designs and the 0.06–0.08% weld deposit carbon content range are recommended with alteration of welding and PWHT procedures depending on the carbon content and MPC Factor.

For the most restrictive case of the high carbon content ($> 0.15\%$) and high MPC Factor, low weld heat input is recommended with controlled deposition welding procedures employed in critical weld regions. Control of the PWHT process should be undertaken with careful control of thermal gradients (ΔT) and PWHT should be accomplished at 1325°F. As with the Class 2 considerations, the base metal toughness may be significantly reduced by the more severe PWHT schedule and this should be attended to by the overall heat treatment schedule for the base material.

If the MPC Factor is reduced at the high carbon level or the carbon content is reduced to the recommended range of 0.11–0.14% with a high MPC Factor, the PWHT temperature may be reduced and a relaxation in the employment of controlled deposition welding procedures may be effected. Again, a concern for a reduced toughness at the 1300°F PWHT temperature may be evident with the high carbon material.

As the carbon content is further reduced and in combination with the MPC Factor as shown in the guidelines, the PWHT may be reduced to 1275°F minimum.

With a low carbon content and low MPC Factor the chance for HAZ cracking either during PWHT or in-service is virtually eliminated and the PWHT temperature may be reduced to 1250°F. Normalization will most likely be adequate to retain the Class 1 properties even at the low carbon level.

Repair Guidelines

The considerations for repair are presented in the Repair Guidelines flow chart (Fig. 2) which is divided into two categories depending on the required life of the vessel subsequent to repair.

The long term repair scenario (greater than 2 years)

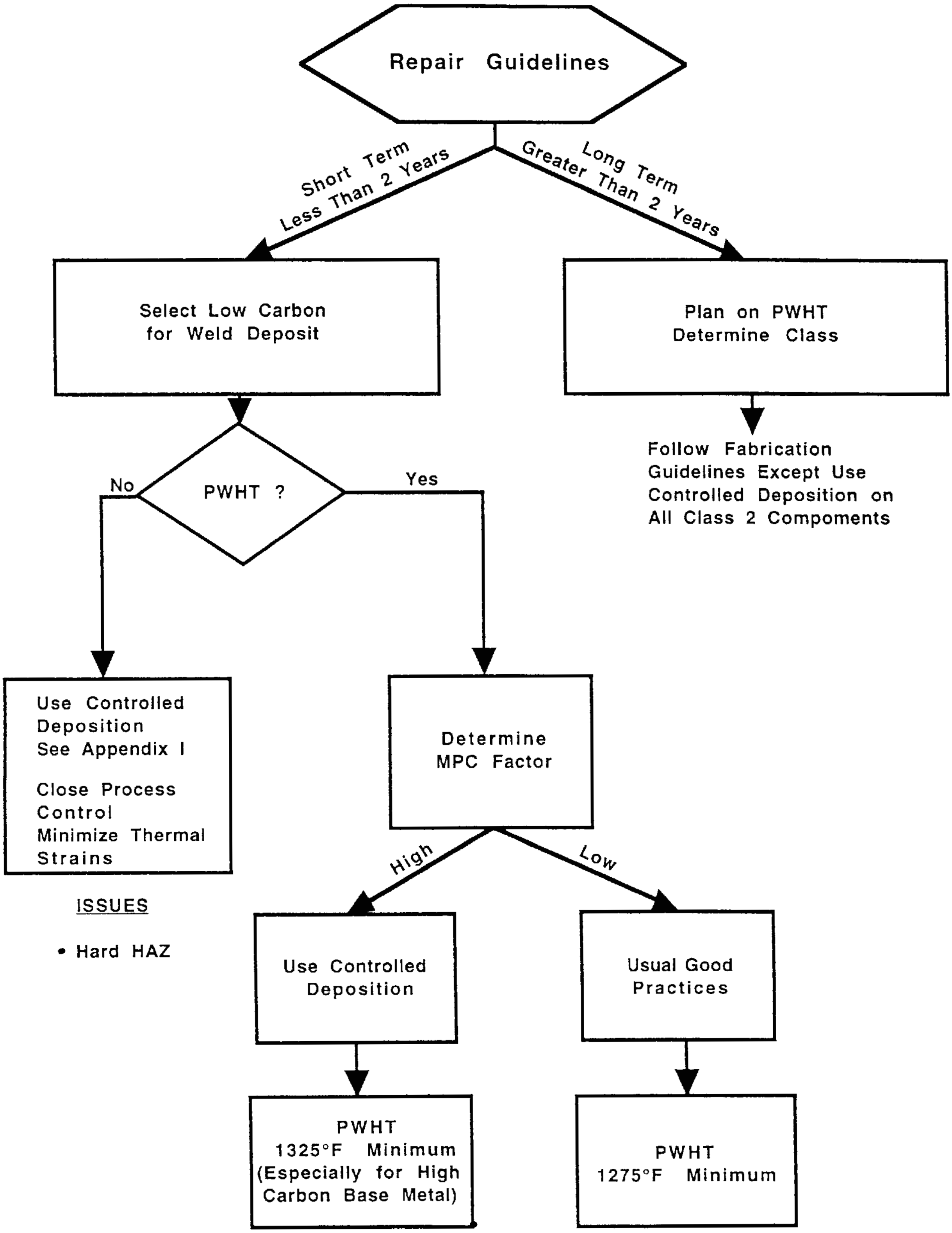

Fig. 2—Repair Guidelines

invokes considerations similar to the original fabrication and requires controlled deposition welding procedures on Class 2 components. The column in the Fabrication Guidelines appropriate to the carbon content and MPC Factor should be employed for long term repairs.

Short term repairs (less than 2 years) are governed by the considerations in the Repair Guidelines and it is recommended that a low carbon weld metal (0.025–0.035% carbon), E8018-B2L, be employed. (The AWS is currently changing the designation for the "L" Grade of the B2 class to reflect that the strength will not normally meet the 80,000 ksi level.) The use of this filler metal will aid in mitigating weld cracking problems (including cold cracking) and reduce the level of residual stresses that will occur as a result of localized repair. Furthermore, the creep properties of the low carbon weld metal will be adequate for short term service after repair.

If PWHT is to be employed, the MPC Factor should be determined and if the Factor is high, controlled deposition weld procedures should be used together with PWHT of 1325°F minimum. If the MPC Factor is low, normal welding practices can be employed and PWHT should be accomplished at 1275°F minimum. These precautions will mitigate the cracking potential and provide adequate creep behavior for the less than 2 year anticipated additional life.

The election to repair without PWHT involves many factors, but significant considerations should be given to this option if the component is to be used at elevated temperatures, especially in the creep regime, since PWHT related metallurgical changes will occur as a function of operational time thus softening the repair and relaxing the residual stresses. If the decision is to repair without the application of PWHT, the controlled deposition procedures defined in Appendix I should be used together with close process control to minimize thermal strains during welding and equipment start-up after repair. The elimination of the coarse grained HAZ by use of the controlled deposition procedures will result in the virtual elimination of the type of cracking responsible for most problems in the 1¼Cr-½Mo system. The issue of hard HAZs must be addressed in terms of the service environment for the component or vessel.

Repairs by their very nature are critical operations for which all precautions and controls should be invoked and considered before the onset of repair. The repair cavity size and configuration should be chosen so that the controlled deposition procedures can be properly implemented and low heat input welding techniques always should be used.

Summary of Program and Results of Testing and Evaluation

Introduction

This program was predicated on the obtaining and testing of 1¼Cr-½Mo materials which represented wide ranges in composition and thus would cover the majority of materials currently in use or those that are now offered in the marketplace for the construction of petroleum/refinery vessels. A total of 17 lots representing 17 different heats of 1¼Cr-½Mo materials were acquired from both foreign and domestic sources. The time span of the production of the materials was greater than 20 years. It was originally intended that materials from vessels that had experienced cracking problems would be used during the conduct of the program. Unfortunately, no such materials were made available. Nevertheless, it is felt that the range of compositions and behavior obtained within the 17 materials tested is sufficient to formulate approaches to vessel fabrication and repair that are meaningful and technically sound. However, partial compositions of four heats that were reported to have suffered severe service/fabrication problems were obtained. These partial compositions indicated that if the proposed MPC Factors had been used for screening, the materials would have been identified as susceptible to cracking.

The Appendixes that form the basis of this report contain detailed information on all aspects of the effort and provide support for the conclusions and recommendations offered. The report Appendix titles are shown in Table 1 and excerpts/conclusions from this data base are used in the following sections.

It is to be noted that a significant amount of highly complementary research was conducted under the auspices of the Welding Research Council (WRC) and the Pressure Vessel Research Council (PVRC). The results and benefits of that work are included here because of their importance to the conclusions and recommendations offered.

Section A. Literature Review

The literature review covers Cr-Mo steel vessel problem areas related to both reheat/PWHT cracking during fabrication and in-service cracking ("creep embrittlement") related to weld HAZs. It is believed that these phenomena are closely related and the same metallurgical and fabrication conditions apply to them. The literature review contained in Appendix A covers the physical metallurgy of the Cr-Mo steels together with the transformation characteristics pertaining to weld HAZs. The microstructural evaluation in the HAZ is addressed in terms of carbide evolution during PWHT and service exposure and the relationship between the metallurgical changes and the cracking potential of the material. The elemental effects are discussed together with the various theories for reheat/PWHT cracking and in-service HAZ cracking. Compositional factors found in the literature to characterize material behavior, based on chemistry, and the testing techniques to reveal sensitivity to cracking are discussed. This literature review

Table 1 - List of Appendices

A	Literature Survey - Cr-Mo Steels - Reheat and In-Service Cracking
B	Chemical Composition of 1¼Cr-½Mo API Materials
C	Coarse Grained HAZ Transformation Behavior and Associated Microstructures
D	Assessment of Reheat Cracking Susceptibility
D1:	Gleeble Simulation Smooth Bar Reheat Crack Testing
D2:	Spiral Notch Testing
D3:	Development of a New Reheat Cracking Test - PREVEW Test and Evaluation of Reheat Cracking in API Materials
E	Determination of Factors to Quantify Reheat Cracking Susceptibility Based on Chemical Composition
F	Toughness Study
G	Microstructural and Fractographic Evaluations
G1:	Fractographic Examination of Notched Creep and Gleeble Stress Rupture Samples of API Materials
G2:	SEM Metallographic Investigation and EDS Analyses of UT2 and UT3 Materials
G3:	High Resolution Electron Microscopic Evaluations on API Materials (Phase I&II)
G4:	Transmission Electron Microscopy Evaluation on API Materials
H	Creep Rupture Behavior of the HAZ
H1:	Notch Bar and Smooth Bar Creep/Stress Rupture Testing
H2:	Preparation of Extended Length HAZ Simulation Specimens by the Gleeble Technique
H3:	Sample Tests
I	Repair Welding Procedure - Behavior of Low Carbon Weld Metal and Repaired Weldments
J	Program Tasks

provides the background upon which the results of this program can be assessed and contrasted.

Section B. Materials

The materials employed in the program were obtained form both virgin heats and service exposed materials extracted from service piping and vessels. The service exposed materials were renormalized at 1650°F for 1 hour and tempered at 1150°F for 1 hour before being tested in this program. This return to the virgin state (RV) of the materials that were in the service exposed condition was considered very important. It had been thought that because the microstructure in the HAZ is changed (transformed and homogenized), during both the HAZ simulation cycles and actual weld tests, that all prior metallurgical (aging) changes that occur during service exposure would be erased. There were strong indications that this was not the case and, therefore, the RV treatment was utilized to provide a standard reference state.

The chemistry of all of the materials studied was obtained from the same laboratories and analysis for 23 elements was made. The analysis techniques and the 23 element chemistry for all materials tested is presented in Appendix B.

Section C. Weld HAZ Transformation Behavior

The transformation characteristics and the resultant microstructures in the coarse grained HAZ are important to the microstructural morphology changes during both PWHT and thermal exposure in-service. Thus, the continuous cooling transformation behavior was determined for two heats of the program materials which had significant differences in carbon content (0.10% vs. 0.18%). The remaining materials are expected to fall between these two extremes in hardenability.

The coarse grained HAZ was characterized because it is in this weld region that the cracking occurs for both the PWHT and in-service thermal exposure regimes. The thermal cycles for the coarse grained region spanned the heat input range of 12–120Kj/in. for a 1 in. plate preheated to 350°F. The CCT diagrams are presented in Appendix C together with representative microstructures for the UT4 and UT6 materials fully characterized. In addition, the microstructures for UT2, 3, 4, 5 & 8 are presented for the 12 and 120Kj/in. heat inputs only. It can be noted from the diagrams that the main constituents formed in the coarse grained region of the HAZ in the

$1\frac{1}{4}$Cr-$\frac{1}{2}$Mo system are principally martensite and bainite with the lower energy input welds in the higher carbon content material forming higher percentages of martensite than the lower carbon materials. Ferrite begins to form at high energy inputs especially primarily for the lower carbon materials. The range of hardness attendant in the coarse grained HAZ associated with each cooling condition is shown both on the CCT diagrams and in the bar graphs in Appendix C. These hardness levels are as expected with the lower carbon material showing lower hardness for all energy inputs and a greater change in hardness upon an equivalent increase in energy input than the higher carbon material. The optical micrographs clearly show the difference in the bainitic structures (carbide and ferrite) formed with higher energy inputs as contrasted to the martensitic (acicular and needle-like) constituent formed upon more rapid cooling. The transformation temperatures determined for the materials are also presented in a table in Appendix C for ready reference as additional data for use in evaluation of the test results.

Section D. Reheat/PWHT Cracking Assessment

In order to determine the reheat/PWHT cracking response of the 17 heats of $1\frac{1}{4}$Cr-$\frac{1}{2}$Mo materials three test methods were employed. These three tests are described in Appendix D. One of the tests has been used for many years in assessing reheat/PWHT cracking tendency while the other two tests were developed at the University of Tennessee to answer special needs in reheat/PWHT cracking assessments. The Spiral Notch test was developed in order to assess which zone in the HAZ is most susceptible to reheat/PWHT cracking and to define the effect of different weld metal deposition techniques on the sensitivity of the HAZ to reheat/PWHT cracking. The PREVEW (Petroleum Refinery Vessel Evaluation of Weldability) test was developed in the current program so that the reheat/PWHT cracking sensitivity could be determined from a scaled-up test that employs an actual weld deposit. The test overcomes an additional attribute of the Gleeble and Spiral Notch test in that the stress relaxes as a function of time at the test temperature in much the same manner as the residual stresses relax an actual weldment. Furthermore, the test incorporates natural weld contour conditions that introduce realistic stress concentrations for the initiation of reheat/PWHT cracking.

(a) The Gleeble stress rupture test employing a simulated HAZ has been used for over 15 years in assessing HAZ cracking during PWHT. The details of the test methodology have been defined by the work at The University of Tennessee and other researchers. Criteria have been established and significant correlations have been made with service performance. The test has been used as a basis for the determination of welding conditions necessary to minimize the occurrence of reheat/PWHT cracking, the ranking of a material's sensitivity to reheat/PWHT cracking and for fundamental studies of the mechanism of reheat/PWHT cracking. The method of conducting the Gleeble simulation test is shown in Appendix D1 along with the test results.

The Gleeble tests were carried out using energy inputs of 12 and 120Kj/in. to span the range of energy inputs utilized for a wide range of welding procedures. The testing was carried out as a function of stress at a temperature of 1150°F and as a function of PWHT over the range of 1150–1350°F. The service exposed and the renormalized conditions were used for the ex-service material heats and the virgin condition was used for the new material heats. The samples were used for fractographic studies and for the determination of the hardness of the HAZ and the hardness changes as a function of PWHT. The full range of data is presented in Appendix D1 together with bar graphs. In addition to the ductility measurements that allow a definition of the material's sensitivity to reheat/PWHT three additional important findings are:

1. the employment of PWHT temperatures below 1250°F have only a minimal effect on the rupture ductility indicating that the material retains its sensitivity to coarse grained HAZ cracking unless a PWHT in excess of 1250°F is employed during fabrication (a PWHT greater than 1300°F significantly improves rupture ductility);
2. the hardness of the coarse grained HAZ does not fall rapidly at temperatures to 1200°F and then falls at rate considered to be slower than that anticipated. This hardness retention was noted in the study on the creep behavior of the coarse grained region as a function of PWHT temperature as explained in a later section, and
3. the high energy input places the coarse grained HAZ in a condition that is more susceptible to reheat cracking than the low heat input.

The significance of this result will also be further amplified in and explained in subsequent sections. The ranking of the materials by means of the Gleeble test will be presented after the discussion of the results of the PREVEW test.

(b) The Spiral Notch test was introduced in order to more rapidly and better define the region of the HAZ that is susceptible to reheat/PWHT cracking in actual welds and to define the conditions which mitigate the occurrence of reheat/PWHT cracking. The test is conducted at a temperature of 1150°F at a constant stress that is indicative of the residual stress in a welded structure. The location of the cracking and rupture in the notched region defines the HAZ microstructure most sensitive to reheat/PWHT cracking and the stress range over which coarse grained cracking occurs is a secondary indication of a material reheat/PWHT cracking sensitivity. The Spiral Notch testing methodology and test results, together with macrostructural evidence to show the type of ruptures indicative of both sensitive and insensitive materials is presented in Appendix D2.

The Spiral Notch test results on materials UT1-UT11 were evaluated in terms of verification of the Gleeble assessment. This was a one-to-one correlation with the data from both tests.

A significant amount of work was conducted in a PVRC study on the efficacy of the use of controlled deposition procedures in mitigating reheat/PWHT cracking on the material designated UT6 in this study (it is to be noted that UT6 material is the most sensitive to reheat/PWHT cracking of all of the materials examined in this study). The PVRC (1) study defined the conditions necessary for the mitigation of reheat/PWHT cracking by controlled deposition techniques. This PVRC study revealed that if the coarse grained region of the HAZ is eliminated by grain refinement from successive weld passes the reheat/PWHT cracking sensitivity essentially disappears. The Spiral Notch test was instrumental in defining this behavior for 10 full scale weldments utilizing UT6 material. This same elimination of reheat/PWHT cracking by controlled deposition coarse grained HAZ refinement was also shown for a low carbon precipitation hardening steel by the utilization of the Spiral Notch test. Further, the Spiral Notch test was used in an other study to define the differences in HAZ structure for down-hand and out-of-position welds. Thus, the Spiral Notch test has an inherent utility in the testing of full scale weldments duplicating the procedures to be used in production, in addition to testing simulated HAZ's for sensitivity.

(c) The development of the PREVEW test was undertaken as a part of this program to provide a correlation with the Gleeble and Spiral Notch tests using a full scale weldment test. The development of the PREVEW test is presented in Appendix D3. This test has the advantage of the utilization of an actual weld with stress relaxation, during the PWHT duplication, which is similar to actual weldment behavior. The stainless steel fixture is simply constructed and no specialized equipment, except for a suitable furnace, is required to conduct the test. The specimen size 10 × 4 × 2 in. allows for actual welds using appropriate consumables and the employment of NDE methods for a rapid assessment of the test results. The tests were conducted on all materials whose configuration permitted the extraction of samples (thus not all materials were tested in this manner). A significant number of tests were conducted before the standardized procedures were defined and then utilized for all additional testing. Dye penetrant NDE is used after welding, after application of the test strain and after testing at elevated temperature to insure that the cracking found is representative of true reheat/PWHT cracking. The degree of cracking in a test sample is indicative of the relative sensitivity of the material. The test is recommended with a fillet weld configuration for which all of the tests were conducted in this study. However, a butt weld configuration with a broached notch was also evaluated and found to be appropriate to the assessment of controlled deposition weld procedures.

The tests also showed that the hardness of the base metal (original plate condition) was important to the extent of reheat/PWHT cracking, in that the harder the base plate material the more extensive the cracking, which occurred in the coarse grained HAZ. This is due to the fact that a softer base material allows for more ready relaxation of stresses and thus reduces the magnitude of stresses present as a function of PWHT time in the HAZ. The location of the cracking clearly showed the influence of the condition of the weld toes in exacerbating the initiation of cracking in sensitive material. The more abrupt the fillet weld contour the greater the cracking tendency (the change from the base metal to weld metal should be smooth and gradual).

It is felt that the development the PREVEW Test is significant as a verification test and as a test that can be utilized for the screening of materials and for the evaluation or selection of welding procedures which influence reheat/PWHT cracking.

The reheat/PWHT cracking sensitivity ranking of the program materials using the Gleeble and PREVEW test is shown in Table 2. The data is presented in three categories: high, intermediate and low. The correlations are considered quite adequate and while more materials were rated with the Gleeble test than the PREVEW the rankings are consistent. The Gleeble rankings are given separately for the low and high heat input evaluations and this further illustrates that at the high energy input conditions no material ranks in the low category. This ranking is of significant value when the assessment of the sensitivity based on chemistry of the base material is considered in the following section.

Section E. Development of Factors to Predict Reheat/PWHT Cracking

The literature presents more than 10 factors for predicting the behavior of the Cr-Mo materials based on heat chemistry. At least eight of these factors are in some way related to reheat/PWHT cracking. Appendix E, which describes the utility and determination of compositional factors for predicting behavior in the reheat/PWHT or in-service cracking regimes, presents the literature-derived factors (Appendix E, Table E2). These factors and the material chemistry for all 17 program materials are shown in the graphical presentations in Appendix E, Figs. E1–11. This assessment showed that the extent of scatter was too large to utilize any of the literature factors as an index of reheat/PWHT cracking sensitivity. Thus, a series of elemental factors based on multiple regression analy-

Table 2. Reheat Cracking Sensitivity Ranking

SENSITIVITY	PREVEW TEST*	GLEEBLE TEST**	
		12 KJ/in	120 KJ/in
HIGH			UT-8
			UT-14
			UT-6
			UT-15
	UT-3	UT-3	UT-12
	UT-14	UT-6	UT-16
	UT-4	UT-14	UT-4
	UT-8		UT-5
			UT-13
			UT-3
			UT-9
			UT-7
INTERMEDIATE		UT-5	
		UT-15	UT-2
	UT-5	UT-4	UT-1
		UT-8	UT-11
		UT-9	UT-10
		UT-17	UT-17
LOW	UT-2	UT-16	
	UT-11	UT-7	
	UT-12	UT-11	
	UT-13	UT-1	
	UT-15	UT-13	
	UT-16	UT-12	
	UT-17	UT-2	
		UT-10	

*PREVEW:	HIGH	CRACKING
	INTERMEDIATE	MINOR CRACKING
	LOW	NO CRACKING
**GLEEBLE:	HIGH	0-10% RA
	INTERMEDIATE	10-20% RA
	LOW	>20% RA

sis and mechanistically related criteria was undertaken. A statistician was employed to utilize the available ductility data and the 23 element analysis for 16 of the heats evaluated. The data were fitted and this resulted in MPC Factor 3 as shown in Fig. E12 in Appendix E. While the data treatment appeared to show a strong correlation it did not agree with accepted mechanistic-based models that consider elemental effects on behavior. Also, when the data from an additional heat, UT17, became available it did not fit the statistical regression analysis as shown in Fig. E12 in Appendix E. Thus, the majority of the work to derive a factor that could describe reheat/PWHT cracking sensitivity based on chemistry was directed toward an elemental regression approach and a mechanistic approach as described in this appendix. From these efforts MPC Factors 5 and 7 emerged as the most predictive factors for reheat/PWHT cracking sensitivity. These two Factors are shown in Figs. 3 and 4. MPC Factor-5 combines a carbon function

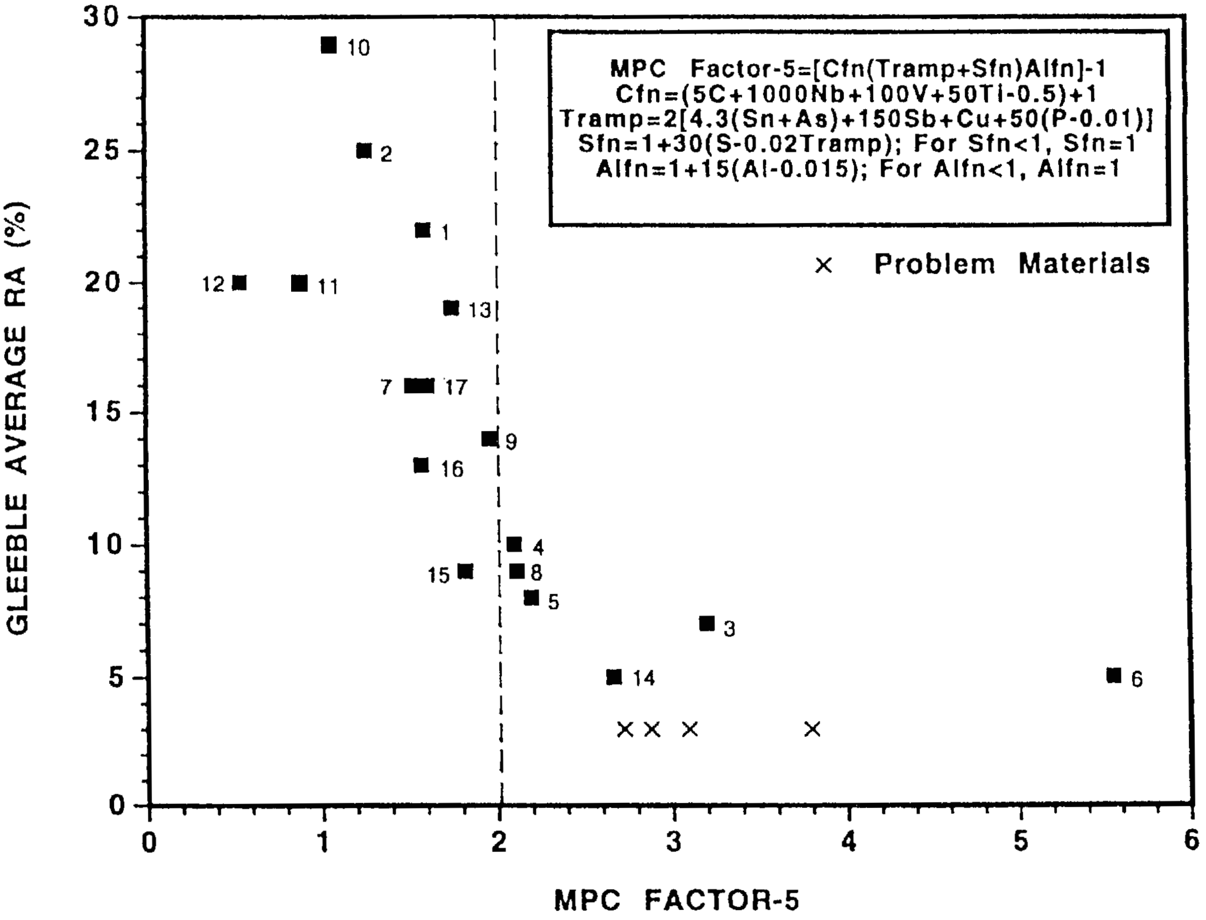

Fig. 3—Correlation of Gleeble reheat cracking results with MPC Factor 5

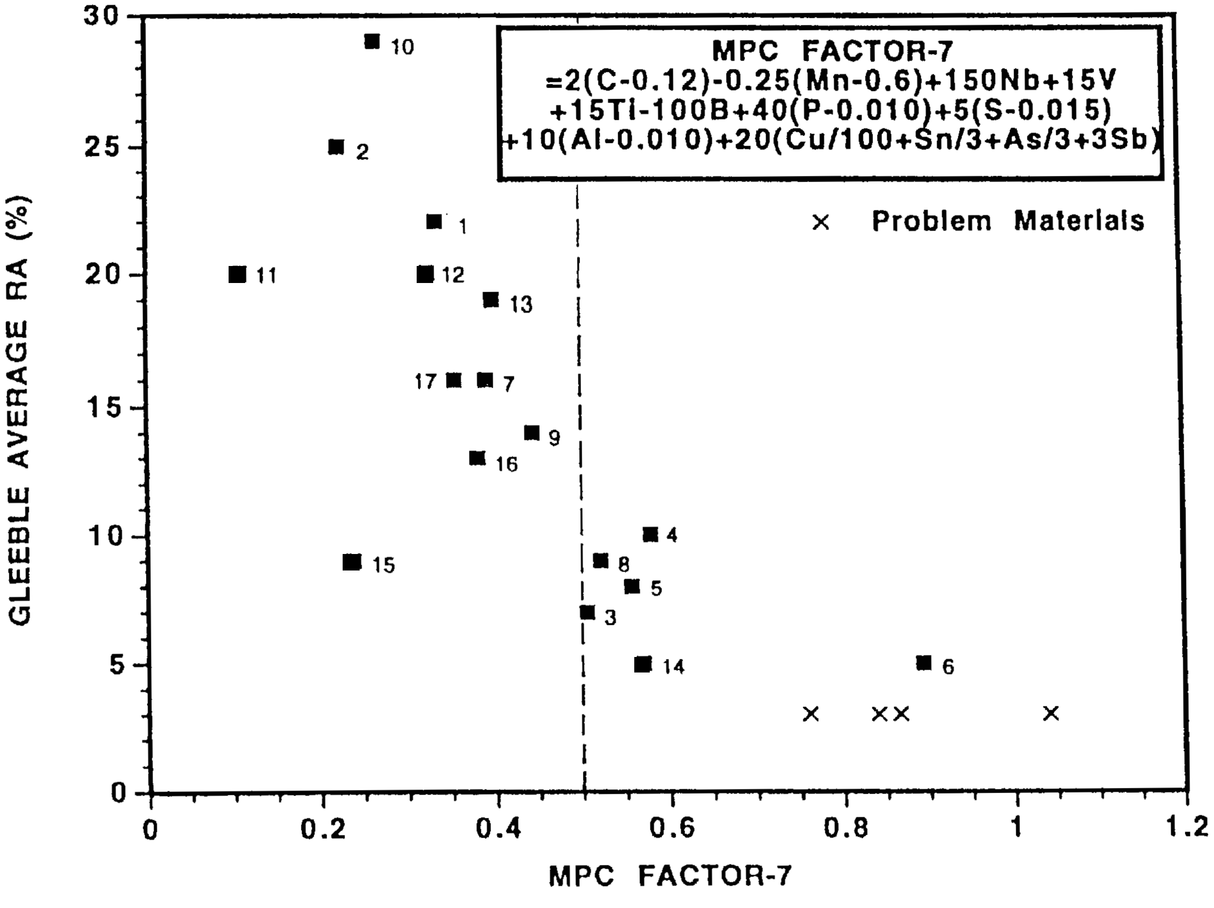

Fig. 4—Correlation of Gleeble reheat cracking results with MPC Factor 7

(strength), a tramp element function (embrittlement), a sulfur function (embrittlement) and an aluminum function. The combination of these functions is shown in the factor as stated in Fig. 3. MPC Factor-7 (Fig. 4) utilizes the concept of a lower limit cutoff as a basis for the effect of the elements in an additive fashion. It is felt that the sensitivity to reheat/PWHT cracking is assessed by either of these factors and a reasonable correlation exists with fabrication behavior. Using MPC Factor-5 the limiting value for the onset of a potential for reheat/PWHT cracking is 2.0 and for MPC Factor-7 the limiting value is 0.5. Thus, the evaluation of a material in regard to its reheat/PWHT cracking behavior can be made utilizing either of these factors. These are the factors to be employed with the recommendations for fabrication and repair presented previously in this report.

Since no problem materials were received from cracked vessels the literature description (5, 6) of four reactors that experienced HAZ cracking was used to provide a check on the factors described above. The elemental analysis for the 4 problem materials is shown in Table 3 and also in Appendix E. The entire spectrum of elements was not available in the literature reporting and for the elements that were not reported a value representing the lowest detectable limit was used in calculating the factor (Table 3). The problem materials are shown at an arbitrary selected reference ductility of 3% as Xs on Figs. 3 and 4. It is clear that these materials fall to the high side of the factors describing reheat/PWHT cracking behavior. Indeed, if the actual chemistry was available for the unreported elements in these problem heats, the points would fall at higher factor levels. Thus, the selected factors MPC Factor-5 and MPC Factor-7 appear to be relevant to practical cracking occurrences.

Section F. Toughness Evaluations as a Function of PWHT

The data obtained with regard to the effect of PWHT temperature on reheat/PWHT cracking potential clearly showed that PWHT at as high a PWHT temperature as possible is desirable in mitigating both reheat cracking and in-service low creep ductility (cracking). Thus, a limited evaluation of the changes in toughness attendant upon PWHT was made. Three materials from the 17 lots evaluated for reheat/PWHT cracking were selected spanning the full range of carbon content. Heats UT11 (0.086%C), UT12 (0.10%C) and UT5 (0.17%C) were PWHT over the range of 1250°F–1350°F for times to 8 hours. The full set of data obtained from the Charpy toughness evaluation as a function of PWHT is presented in Appendix F. Figs. 5, 6 and 7 summarize the toughness results for the three materials as a function of PWHT. It is clear by inspection of these figures that the low carbon (UT11) material showed little change in toughness as function of PWHT whereas the high carbon (UT5) heat showed a progressive deterioration with increasing in PWHT temperature. This effect is attributed to the precipitation and growth of carbides along the grain boundaries (not to embrittlement phenomena). The good initial toughness of the UT12 material enabled it to retain at least 40 ft-lbs at −40°F after a 1350°F 8 hour PWHT even though the as-received toughness was degraded by the PWHT.

These data are offered to illustrate the effect of PWHT temperature on toughness and the need to consider this aspect of material properties when selecting the proper material under all aspects of petroleum vessel fabrication and for optimum in-service performance.

Table 3. Chemical Composition of Problem Materials

Material	C	Si	Mn	P	S	Ni	Cr	Mo	Cu	Al	As	Sn	Sb	N	O
PM-1	0.15	0.67	0.57	0.014	0.012	0.15	1.28	0.53	0.25	0.018	0.024	0.025	NR*	NR	NR
PM-2	0.14	0.59	0.60	0.017	0.008	0.18	1.38	0.51	0.24	0.006	0.030	0.032	NR	NR	NR
PM-3	0.15	0.67	0.58	0.015	0.009	0.17	1.21	0.53	0.23	0.015	0.032	0.028	NR	NR	NR
PM-4	0.15	0.51	0.61	0.018	0.019	0.21	1.15	0.49	0.21	0.005	0.018	0.020	.0045	.0111	.0035

NR*: Not Reported

Values assigned to un-reported elements for factor calculations:

Ti - 0.0001%, V - 0.005%, Nb - 0.0001%, B - 0.000005%

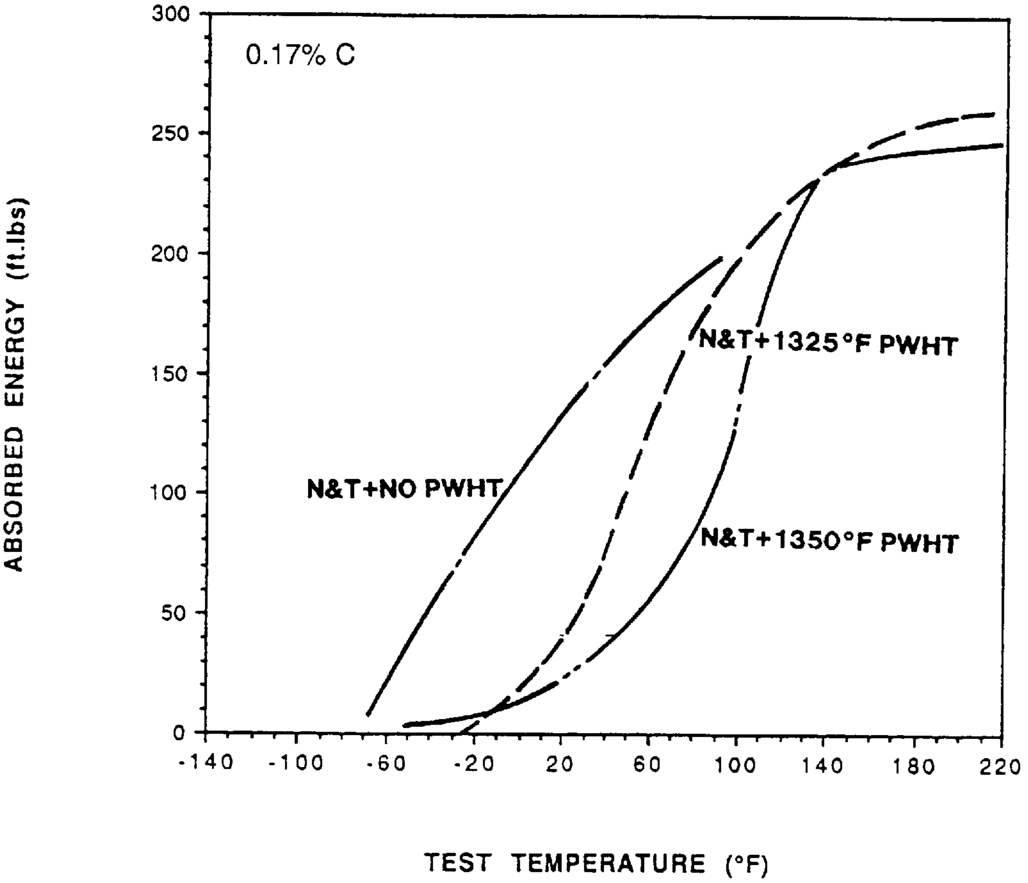

Fig. 5—UT5 CVN-ENERGY N(1650°F-40 min) & T(1320°F-86 min)

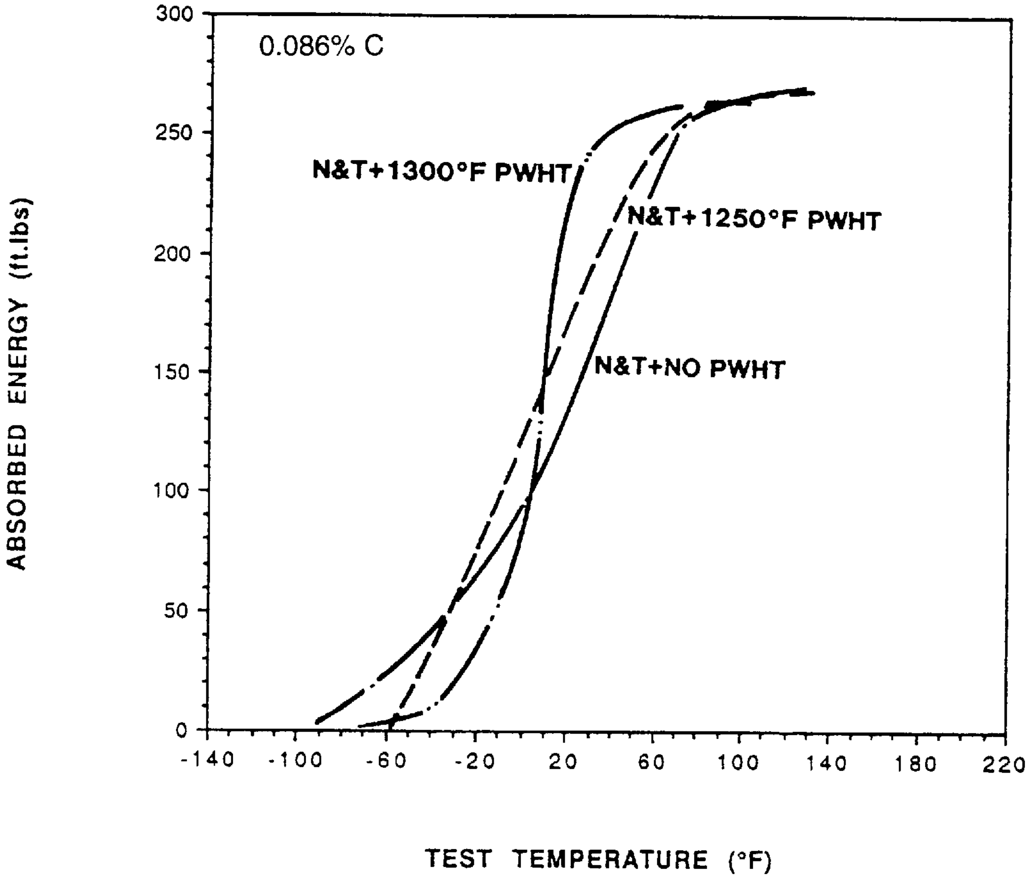

Fig. 6—UT11 CVN-ENERGY N(1650°F-1 hr) & T(1150°F-1 hr)

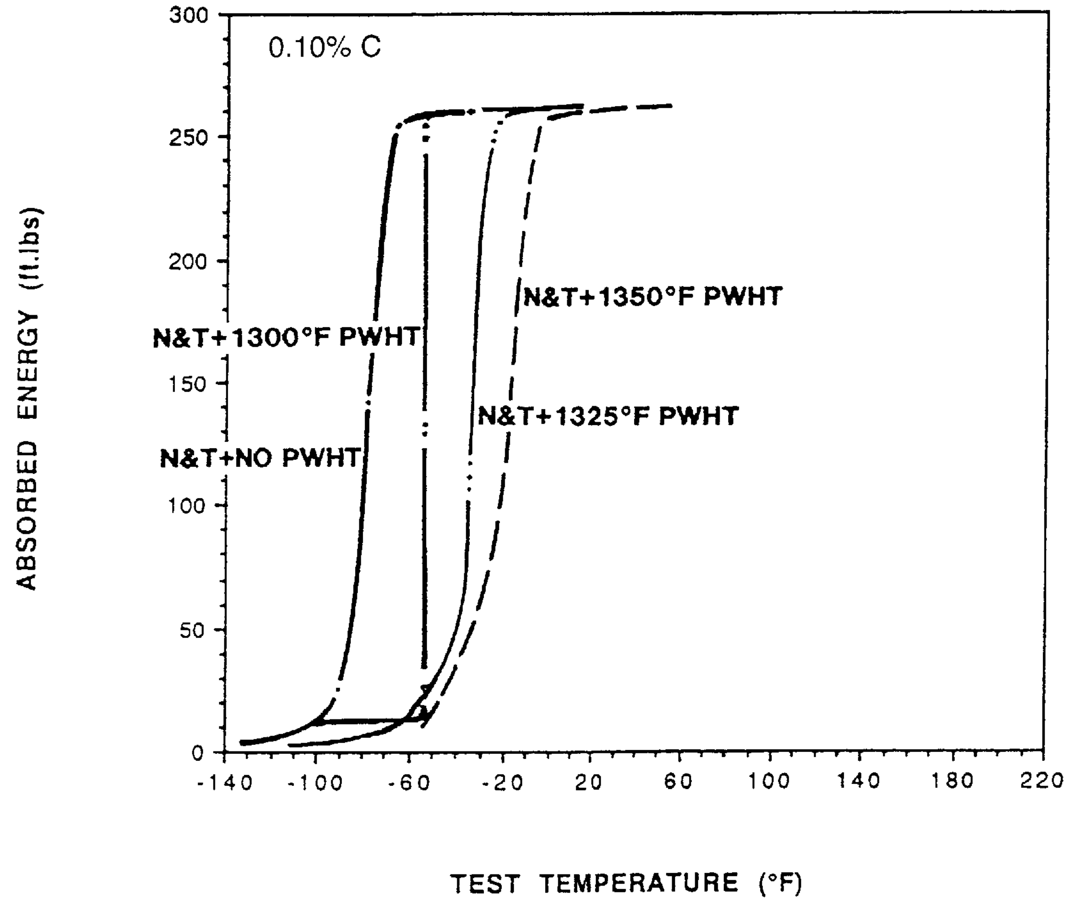

Fig. 7—UT12 CVN-energy, N(1700°F, ? hr) & T(1310°F, 30 min)

Section G. Microstructural and Fractographic Evaluations

Evaluation of the microstructural aspects of the behavior of the coarse grained HAZ was undertaken to provide the mechanistic aspects of the assessment of behavior and to provide a basis for the understanding of the test results. Fractographic examinations of tested reheat/PWHT cracking samples and creep rupture tested samples were also carried out to define the nature of the cracking and to relate fractographic features and elemental changes on the grain boundaries to rupture ductility. The full range of metallographic and fractographic studies is presented in Appendix G.

The reheat/PWHT cracking evaluations clearly showed that the high energy weld heat inputs resulted in lower rupture ductilities than the low weld heat input conditions. It was also found from the creep testing of the coarse grained HAZ that higher creep rates were evident for the low energy input conditions even though the initial HAZ hardness was high (indicating a stronger material). There are literature reports that indicate that higher temperature transformation products such as bainite result in a stronger material in the creep range than the lower temperature transformation product martensite. Extensive OLM, SEM, STEM and TEM work on the high and low heat input samples as a function of PWHT temperature clearly showed that the carbide evolutionary sequence is distinctly different for the two microstructures. For a martensitic structure the carbides evolve to the more stable forms such as M_7C_3, $M_{23}C_6$ and M_6C more rapidly as a function of time at equivalent temperature than does the initially bainitic HAZ characteristic of high weld heat input weld conditions. The high heat input weld conditions result in the formation of M_3C- and M_2C-type carbides that persist for long times and thus result in strengthening the material in the elevated temperature regime. The decrease in hardness, upon PWHT, for the coarse grained HAZ microstructures is less than anticipated from studies of normally heat treated base metal and thus the maintenance of strength at higher temperatures speaks to the need to PWHT at high temperatures to place the material in a more creep ductile condition.

These observations in several materials with widely differing reheat/PWHT cracking responses are not in conflict with the traditional assessment of reheat cracking tendency. The cause of reheat/PWHT cracking most likely does not lie in only one aspect of material behavior and thus the approach to the MPC Factors with the mechanistic approach, incorporating a variety of effects, including strengthening, tramp elements, effect of all elements on hardenability, carbide precipitation kinetics and creep rate differences are all important in the ultimate causation.

Elemental species such as manganese and boron appear to influence creep behavior (increase creep rate) by enhancing hardenability and martensite formation in the HAZ for equivalent levels of other elements. This effect on creep rate may be an important ancillary feature that leads to reduction of residual stress without the strain accumulation and rupture of grain boundaries which are the sites for segregation of the tramp elements, P and S.

Section H. Creep Rupture Behavior of the Coarse Grained HAZ—Notch Bar and Smooth Bar Creep/Stress Rupture Testing

An extensive matrix of smooth and notch bar creep and rupture testing established the fact that PWHT temperatures should be above 1275°F to improve the HAZ ductility (Tables H1–H5 in Appendix H). Also, these tests provided further justification for avoiding high heat input welds. Ductilities of equivalent zones were about twice as high at 45 Kj/in as at 120 Kj/in.

It was found that PWHT temperatures of 1350°F and above did not significantly reduce the rupture lives of the hard heat affected zone materials. The remarkably low ductilities and low creep rates observed for the hard portions of 1¼Cr-½Mo heat affected zones goes a long way to explaining the tendency for cracking in-service. There is no evidence that the materials become brittle in time (creep embrittlement). Instead it is concluded that brittleness is a consequence of the as-tempered microstructure that must be softened significantly before ductility can be observed. Some heats tended to show low ductility and notch sensitivity even after extensive tempering. Such persistent crack susceptibility appeared to be due to the same impurity factors that contributed to susceptibility to cracking during PWHT.

Section I. Repair Welding Procedures, Behavior of Low Carbon Weld Metal and Repaired Weldments

The subject of optimum repair procedures for 1¼Cr-½Mo materials have been addressed in a PVRC study (1) dealing with the considerations of the effects of both controlled deposition and PWHT on the efficacy and life of repaired weldments. The initial study was followed by an evaluation of the use of low carbon weld metal as an adjunct to repair for limited life or for repairs that do not employ PWHT.

The PVRC study, which was conducted with industrial involvement from the repair procedure development aspects, tested 10 full scale weldments made with program material UT6 (the most sensitive material to reheat/PWHT cracking) and clearly demonstrated that if the welding procedure used a controlled deposition approach, which was aimed at the elimination of the coarse grained HAZ, the potential sensitivity toward reheat/PWHT cracking was eliminated. In like manner, if a conventional welding procedure was employed which resulted in a significant amount of coarse grains in the HAZ, the reheat/PWHT cracking tendency was high.

The replacement of the coarse grained HAZ with a completely refined region adjacent to the weld in the HAZ causes some concern in terms of elevated creep rupture behavior. It is well known that a fine grained material creeps at a greater rate than a coarse grained material. Thus, the total creep life of a controlled deposition repaired weldment might be reduced over that of a conventional weldment. This concern was answered in the PVRC study by numerous creep rupture tests of the controlled deposition weldments. The creep rupture samples behaved in a ductile manner and the life of the weldment, based on a Larson-Miller approach, showed that the failure times fell within the virgin base metal data band (between the minimum and mean). The ductility revealed in these tests was good and thus the potential for in-service low ductility cracking is considered negligible. The PWHT weldments behaved in a similar manner, in the creep regime, provided that the PWHT temperature was above 1250°F. Thus, the controlled deposition methods produced elevated temperature behavior similar to the PWHT weldments. However, it is to be noted that the HAZ hardness in the controlled deposition weldments is significantly higher than in the PWHT weldments but it is below that of the conventional weldments. Therefore, in regard to repairs for which there is a significant consideration for cracking due to the presence of coarse grained regions, either during PWHT or after the structure is returned to service, the controlled deposition methodology should be strongly considered. Further, if the weld metal is to be used in an environment where hydrogen cracking is possible the hardness level attendant with the non-PWHT repair methods must be addressed.

The controlled deposition repair procedure, as stated in Appendix I, has been used to repair ex-service weldments from both petrochemical plants and steam power plants. Long seam welds in these components were repaired using low carbon (0.025%) SMAW filler (E8018-B2L) and tests have been conduced using full scale jumbo creep samples of full thickness, incorporating all of the service exposed material and the weld repair. The initial results of this work have been reported to the PVRC Committee on Welds. The behavior of these repaired weldments, based on a Larson-Miller approach, shows lives in at the mean of the virgin base metal data band. Comparison tests of the PWHT repairs and the original service-exposed weldments are currently in progress.

Testing of the low carbon weld metal is underway and the early results show that the weld metal creep rupture strength, in the as-welded condition, exceeds the minimum Larson-Miller expectations. PWHT weld metals are in test.

The toughness of the low carbon deposit was determined for the as-welded condition and after PWHT at 1350°F for 8 hours. Summary curves are shown in Figs. 8–10, which reveal that the 1350°F/8

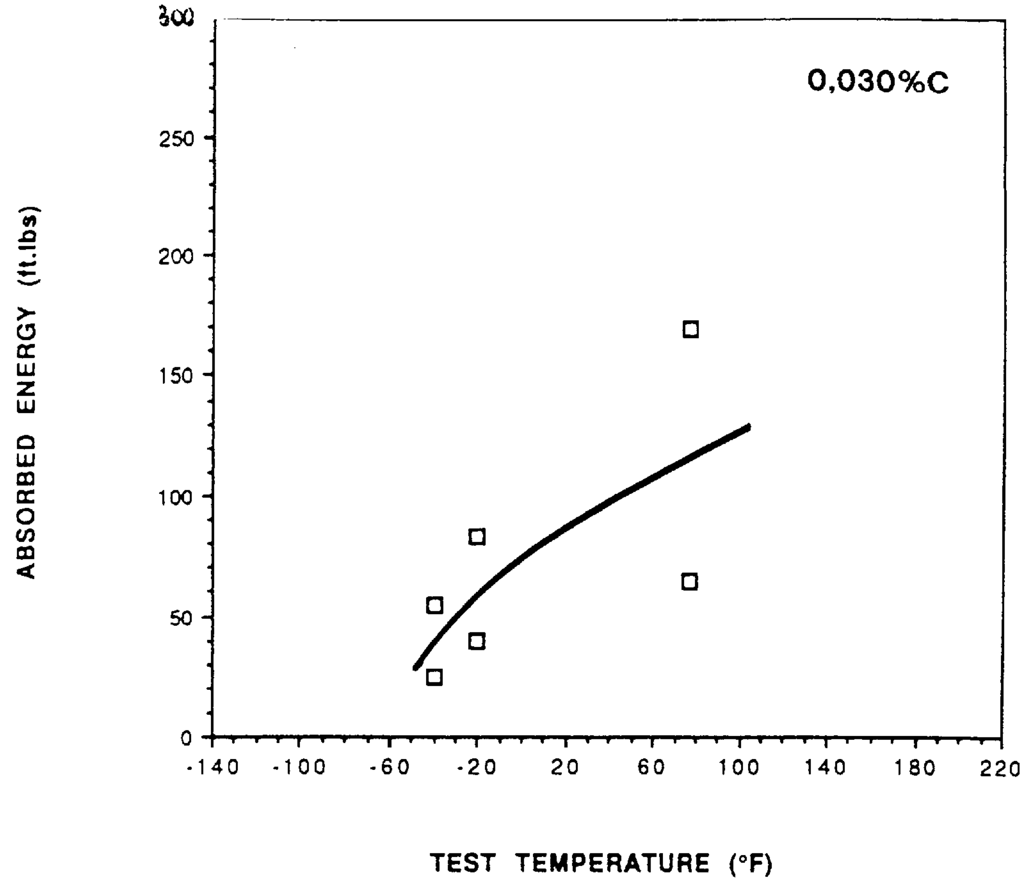

Fig. 8—CVN-absorbed energy, low C SMA repair weld metal (E8018 B2L) in as-welded condition

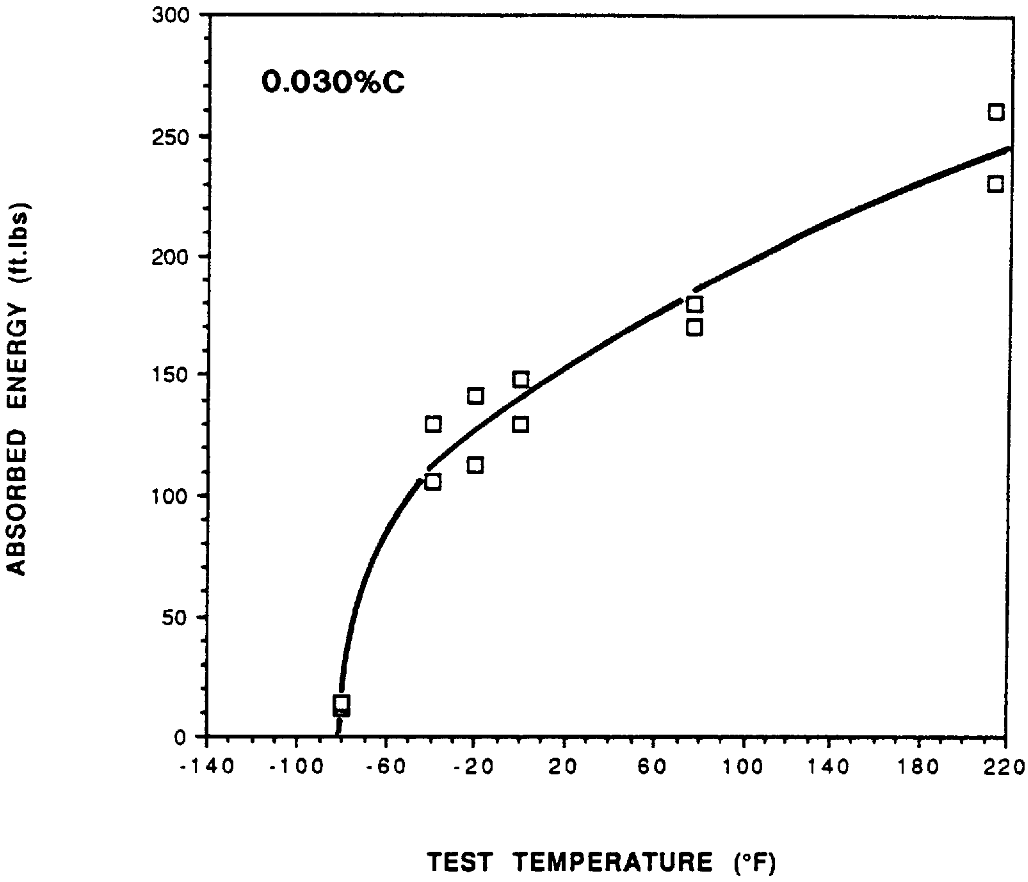

Fig. 9—CVN-absorbed energy, low C SMA repair weld metal (E8018 B2L) PWHT, 1350°F for 8 hrs

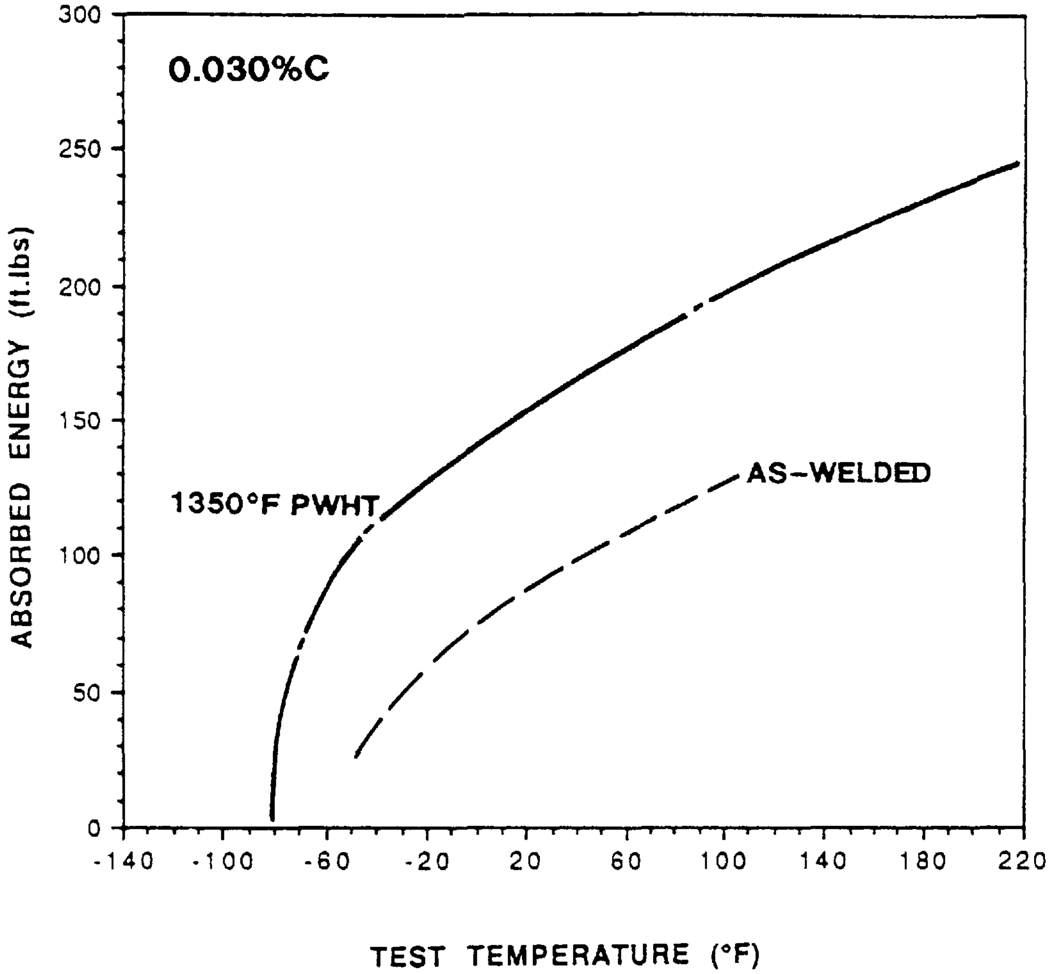

Fig. 10—CVN-absorbed energy low C SMA repair weld metal (8018 B2L) PWHT, 1350°F for 8 hrs/as-welded

hour PWHT significantly improved the weld metal toughness over that of the as-welded condition. The toughness levels for both conditions exceeded 40 ft-lbs at −40°F.

Thus, for short term repairs, the use of a low carbon filler metal, which should reduce residual stress and enable the weld to be made with less concern for hydrogen cracking, should be adequate from both the toughness and creep resistance standpoints. Therefore, this aspect of weld repair is to be considered in the repair methodology presented in the recommendations accompanying this report.

References

1. Lundin, C. D. and Wang, Y. "Half-Bead/Temper-Bead/Controlled Deposition Techniques for Improvement of Fabrication and Service Performance of Cr-Mo Steels," Draft Final Report Submitted to the Committee on Welds of the Pressure Vessel Research Council (December 1993).
2. Lundin, C. D. and Khan, K. K. "Fundamental Studies of the Metallurgical Causes for Reheat cracking in 2¼Cr-1Mo, 1¼Cr-½Mo and Copper Precipitation Hardenable Steels and Problem Mitigation," Final Report to the Weldability Committee of Welding Research Council (January 1993).
3. Lundin, C. D., Khan, K. K., Zhou, G. and Al-Ejel, K. A. "The Efficacy of the Utilization of Low Carbon Cr-Mo Weld Metal for Repairs in Cr-Mo Vessels and Piping," Progress Report Submitted to the Committee on Welds of the Pressure Vessel Research Council (January 1994).
4. Lundin, C. D., Khan, K. K., Zhou, G. and Liu, P. "The Efficacy of the Utilization of Low Carbon Cr-Mo Weld Metal for Repairs in Cr-Mo Vessels and Piping," Progress Report Submitted to the Committee on Welds of the Pressure Vessel Research Council (May 1994).
5. Nomura, T. et al. "Creep Embrittlement of Structural Components in Catalytic Reformer Reactor," Trans. Japan Soc. of Mechanical Engineers, 1993-9, pp. 2066–2073.
6. Cantwell, J., Private Communication to M. Prager of MPC (May 1993).

Appendix A—Literature Survey: Cr-Mo Steels—Reheat and In-Service Cracking

HAZ Transformation Behavior and Microstructure

The metallurgical transformations that occur during welding affect the final microstructure and therefore can influence many problems that can develop during and after welding. The coarse grained heat affected zone (CGHAZ) is the location of maximum susceptibility for reheat cracking, stress rupture/relief cracking (SRC) or postweld heat treatment (PWHT) cracking. It is also a primary region for reduction in toughness.

In a discussion of reheat cracking by Ito and Nakanishi,[8] they indicate that in 1Cr-½Mo alloys a HAZ microstructure consisting of martensite or lower bainite was more susceptible to PWHT cracking than upper bainite. In temper embrittlement, a related materials problem, it was found that a martensitic microstructure is more prone to a loss in ductility and toughness than a bainitic microstructure. Thus, the determination of HAZ transformation characteristics is a first step in determining the weldability of a material which may, in turn, provide the key to reducing or eliminating weld HAZ problems.

Easterling[9] has compared the microstructural regions of a weld with the equilibrium diagram (Fig. A1). However, such a representation is overly simplistic in that it ignores major differences between the weld thermal cycle and the conditions that are utilized in establishing the equilibrium diagram. Welding can induce rapid heating (3000°F/sec) and cooling (500°F/sec) rates resulting in conditions far from equilibrium. Furthermore, the complete homogenization, required for equilibrium, never exists upon welding. Also, equilibrium considerations do not include such nonequilibrium constituents as martensite or bainite.

Many of the objections to the use of the equilibrium diagram to predict weld HAZ transformations also extends to the use of standard continuous cooling diagrams.[10] These diagrams are developed starting with homogeneous austenite. In welding, inhomogeneity occurs due to the inability of alloying elements to diffuse uniformly throughout the austenite and the incomplete solution of carbides, nitrides and other constituents as a result of the rapidity of the welding thermal cycle and the concomitant short austenitizing times. In order to predict accurately the on-cooling transformation temperatures and microstructures, weld HAZ continuous cooling transformation diagrams must be derived using the heating and cooling conditions attendant upon welding.

Fig. A2 shows a conventional continuous cooling transformation diagram for 2¼Cr-1Mo and Fig. A3

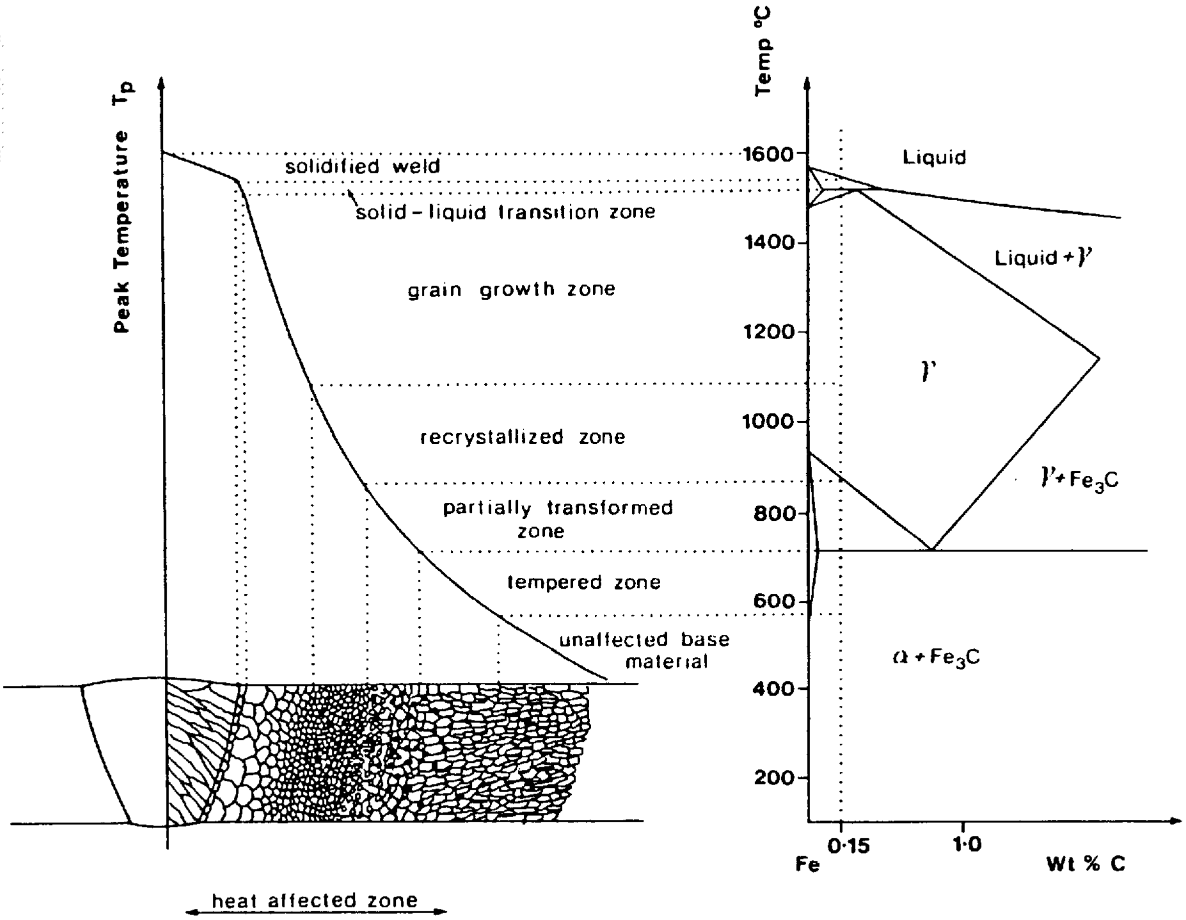

Fig. A1—Schematic diagram of the various regions of the HAZ approximately corresponding to the 0.15% carbon indicated on the Fe-Fe_3C equilibrium diagram. Source: Easterling, K., Introduction to the Physical Metallurgy of Welding, Butterworts, 1983

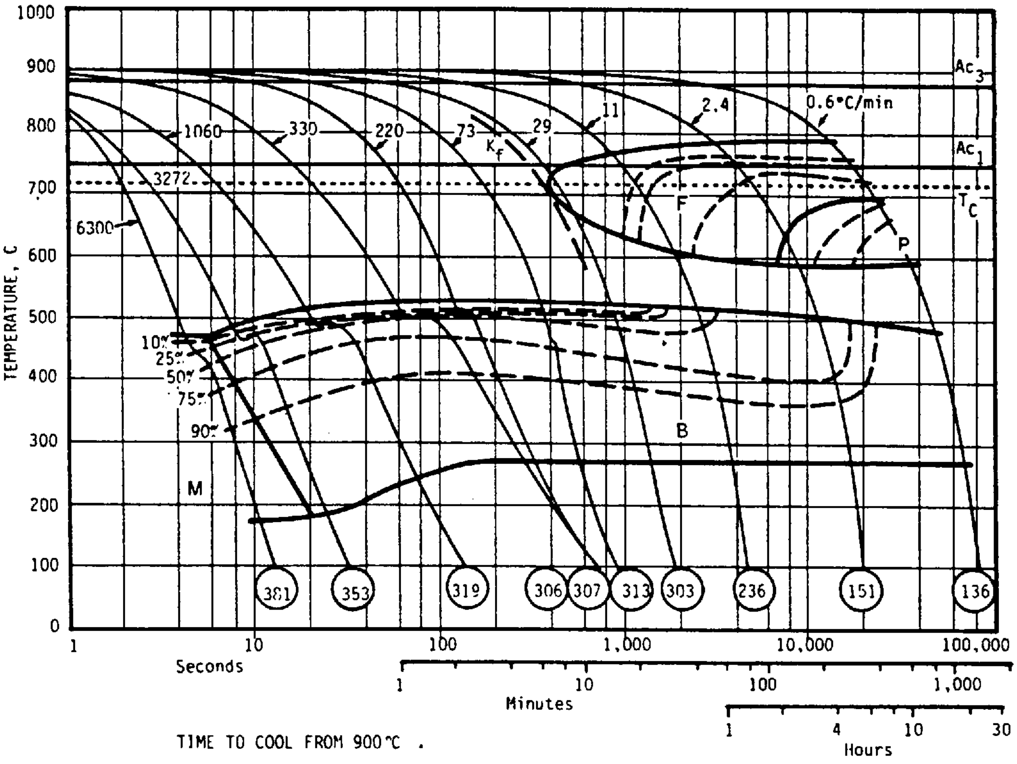

Fig. A2—CCT diagram for 2¼Cr-1Mo steel. Source: Wada, T. and Eldis, G. T., "Transformation Characteristics of 2¼Cr-1Mo Steel," Applications of 2¼Cr-1Mo Steel for Thick Wall Pressure Vessels, ASTM-STP 755, 1982, pp. 343–362

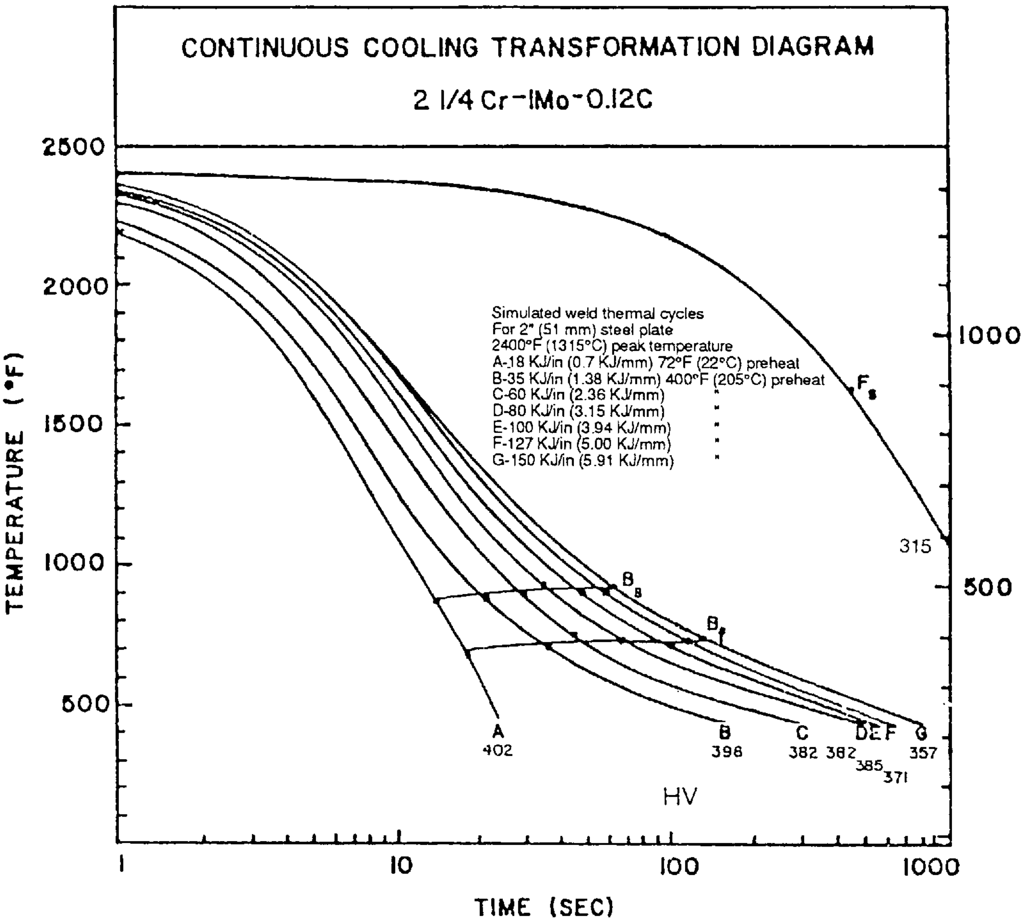

Fig. A3—CCT diagram for 2¼Cr-1Mo steel under simulated welding conditions. Source: Lundin, C. D., Richey, M. W. and Henning, J. A., "Transformation, Metallurgical Response and Behavior of the Weld Fusion Zone and Heat Affected Zone in Cr-Mo Steels for Fossil Energy Applications," AR&TD Final Technical Report, UT/CME-07685-03, September 1984 illustrates a diagram determined under simulated welding conditions for the CGHAZ in 2¼Cr-1Mo.[11] As may be seen by comparing Figs. A2 and A3, the depression of the on-cooling transformation temperatures (principally bainite) under welding conditions is approximately 90°F due to the rapid heating and cooling rates and short austenitizing times.

A literature review by Lundin *et al.*[11] revealed that only a few continuous cooling transformation diagrams have been determined under welding conditions for the Cr-Mo materials. However, conventional continuous cooling diagrams are available for many of the unmodified and modified Cr-Mo alloys. Continuous cooling transformation diagrams for various Cr-Mo steels are shown in Figs. A4, A5 and A6. The effects of the addition of vanadium, titanium and boron to the 2¼Cr-1Mo and 3Cr-1Mo alloys on the continuous cooling transformation behavior are shown in Figs. A4 and A5 by the superposition of the continuous cooling transformation diagrams for the unmodified and modified materials.

The 2¼Cr-1Mo and 3Cr continuous cooling transformation diagrams (Figs. A4, A5 and A6) give clues to the fact that the resulting microstructure under various welding conditions is complex. Depending on the degree of homogenization and the cooling rate (related to the heat input and preheat for a given process and material thickness), the on-cooling microstructures in the weld HAZ may consist of martensite, mixed martensite and bainite or bainite coupled with retained austenite.

The microstructure of the 2¼Cr and 3Cr steels may be further complicated by the formation of martensite-austenite islands (a martensite-austenite constituent).[12] The formation of a martensite-austenite constituent is due to the partitioning of carbon to the austenite during the bainite transformation reaction resulting in locking of dislocations which prevents the shear transformation from occurring[13] or the stabilization of austenite.[14,15] The last austenite present can be highly enriched in carbon. Carbon contents of the martensite-austenite constituent have been reported by Biss and Cryderman[14] to exceed 0.5 wt% in a nominal 0.15% C alloy and to be approximately 3 at % (approximately 0.7 wt%) in a series of 0.3C-3Cr-0.5Mo as shown by Thomas *et al.*[15]

Biss and Cryderman[14] found that slow cooling rates enhanced formation of the martensite-austenite constituent by allowing carbon to diffuse away from the ferrite-austenite interface into the austenite. However, rapid cooling rates resulted in higher ferrite-austenite interface carbon content due to carbon diffusion being slower than interface advancement. This results in enhanced cementite precipitation and

	C	Si	Mn	P	S	Cr	Mo	V	Ti	B	Austenitizing Temperature
2¼Cr-1Mo-V-Ti-B	.10	.02	.51	.005	.005	2.20	.94	.30	.022	.0023	950℃ (1742°F)
2¼Cr-1Mo	.10	.34	.48	.017	.013	2.16	.96	–	–	–	920℃ (1688°F)

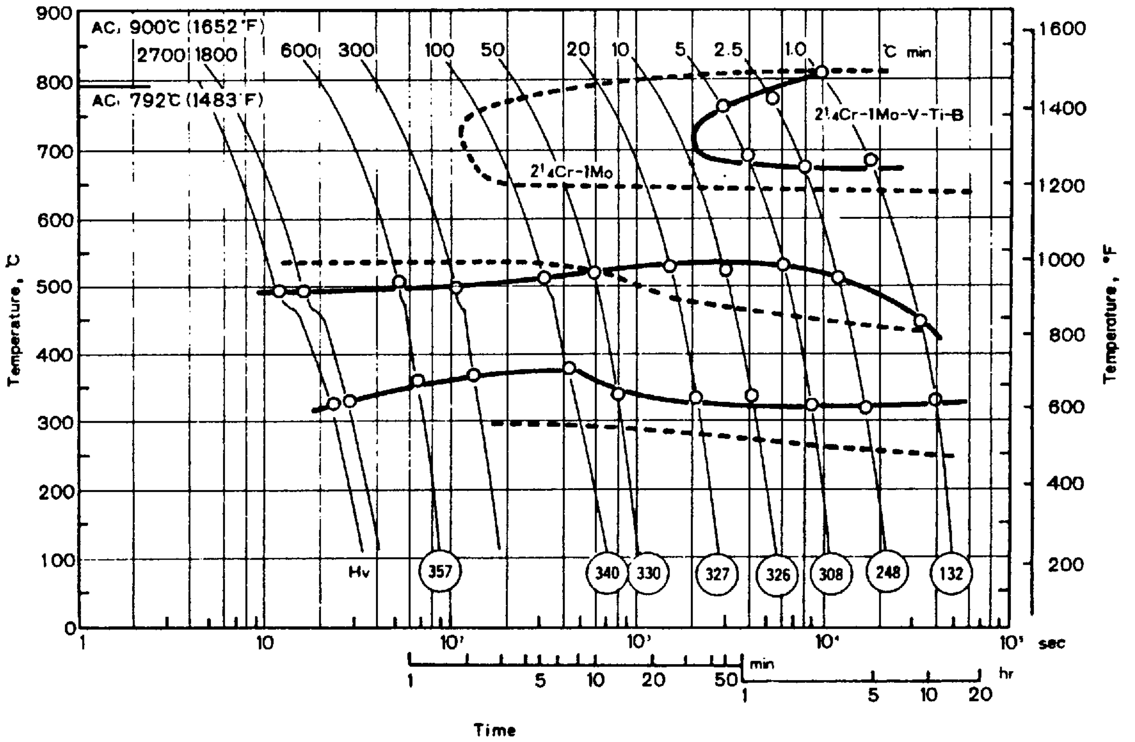

Fig. A4—CCT diagrams for V-Ti-B modified 2¼Cr-1Mo steel and standard 2¼Cr-1Mo steel. Source: Ishiguro, T., Murakami, Y., Ohnishi, K. and Watanabe, J., "A 2¼Cr-1Mo Pressure Vessel Steel with Improved Creep Rupture Strength," Applications of 2¼Cr-1Mo Steel for Thick Wall Pressure Vessels, ASTM-STP 755, 1982, pp. 129–147

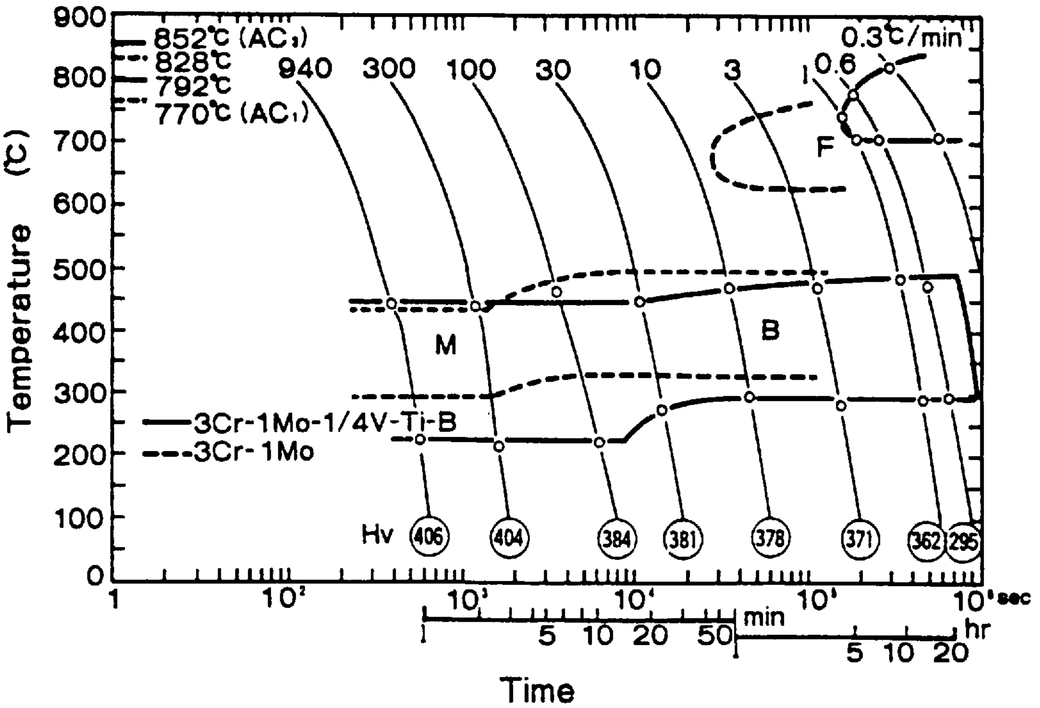

Fig. A5—CCT diagrams of a 3Cr-1Mo and a 3Cr-1Mo-¼V-Ti-B steels. Source: Ishiguro, T., Murakami, Y., Ohnishi, K. and Watanabe, J., "A 2¼Cr-1Mo Pressure Vessel Steel with Improved Creep Rupture Strength," Applications of 2¼Cr-1Mo Steel for Thick Wall Pressure Vessels, ASTM-STP 755, 1982, pp. 129–147

suppression of the martensite-austenite constituent. Economopoulos and Habraken[13] found that the presence of the martensite-austenite constituent was associated particularly with massive, or granular, bainitic structures formed at slow cooling rates. Wada and Eldis[12] found martensite-austenite islands in 2¼Cr-1Mo steel under a slow cooling rate of 4°C/sec. The cooling rate dependence of martensite-austenite

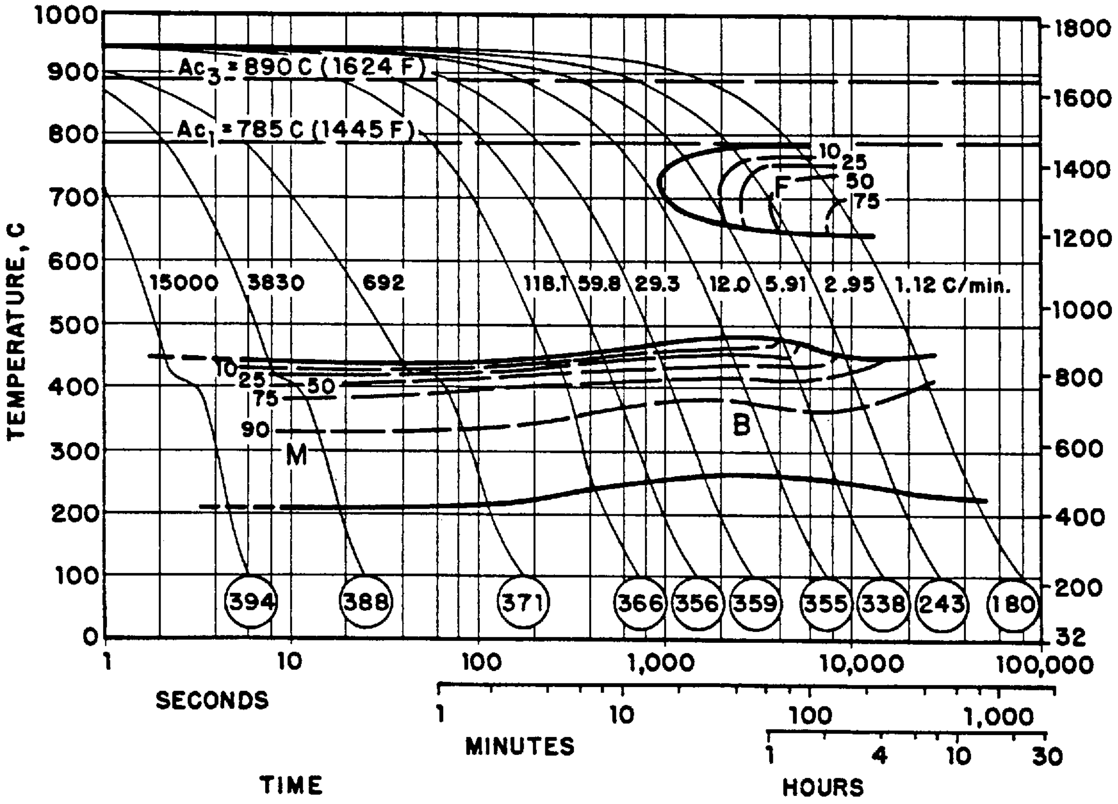

Fig. A6—CCT diagram for a commercial heat of 3Cr-1½Mo steel, Austenite grain Size: ASTM No. ⅚. Source: Wada, T. and Cox, T. B., "A New 3Cr-1½Mo Steel for Pressure Vessel Applications," MPC-21 Research on Chrome-Moly Steels, ASME, 1984, pp. 77–94 constituent formation probably accounts for the inability of Lundin *et al.*[11] to detect any martensite-austenite constituent in their study of the transformation characteristics of 2¼Cr-1Mo steels under simulated welding conditions. However, Thomas *et al.*[15] detected thin films of retained austenite along martensite laths by TEM examination. It was claimed that the retention of austenite was due to carbon redistribution during the martensite reaction and that this diffusion of carbon was possible due to the high M_s temperature (572°F (300°C) or higher) and the time to cool through the temperature range for martensite formation.

Apblett *et al.*[16] investigated the transformation behavior of the HAZ in 1¼Cr-½Mo and 2¼Cr-1Mo steels. They found that these two steels essentially transformed to proeutectoid ferrite and bainite and the extent of either constituent varied depending on the peak temperature experienced and the cooling rate. In regions containing homogeneous (or nearly so) austenite, that is, regions which have been heated to peak temperatures of 2000°F (1095°C) and above, the ferrite reaction is suppressed and only a bainitic reaction occurs. The reaction start temperatures are in the vicinity of 1000°F (540°C) depending on the peak temperature and grain size of the austenite. Regions heated between 1750–2000°F (955–1095°C) contain undissolved carbides. These carbides act as nucleating sites for the formation of proeutectoid ferrite in addition to bainite.

In the portions of the HAZ heated in a temperature range between 1450–1750°F (790–955°C), austenitization is limited only to those regions in the immediate vicinity of the grain boundaries. This continuous network of austenite may transform to martensite which can result poor impact toughness. In general, the same trends are found in 2¼Cr-1Mo steel as in the 1¼Cr-½Mo steel. An increase in alloy content only tends to reduce appreciably the amount of proeutectoid ferrite in the microstructure.

Two factors should be evident from the above discussion of transformation characteristics and resulting microstructure. Since the continuous cooling transformation diagrams are important to the understanding of properties and potential cracking susceptibility, there exists a need to determine the continuous cooling transformation diagrams for welding conditions as the development and understanding of the weldability of the Cr-Mo alloys continue. Also, since the possible role of partial austenite transformation on HAZ softening has not been previously addressed due to temperature excursions into the intercritical region, a need exists to evaluate the effect of partial transformation on HAZ softening.

Microstructural Evolution in the HAZ upon PWHT

A major function of PWHT is to restore ductility in the HAZ and weld metal in Cr-Mo weldments.[18] In addition, the PWHT also reduces the residual stresses in the weldment by a creep relaxation process.

Recommended practices for welding Cr-Mo steels are detailed in ANSI/AWS D10.8-86.[18] The recommended postweld heat treatment temperatures and holding times for the various grades of Cr-Mo steels are often given as follows. For 1¼Cr-½Mo the recommended temperatures for PWHT are 1175–1275°F (635–690°C); for components intended for creep service and 1275–1350°F (690–730°C) for components where resistance to corrosion and hydrogen embrittlement are the primary considerations. For 2¼Cr-1Mo the recommended temperature is 1275–1375°F (690–745°C). Holding times are generally one hour per in. of thickness up to two in. and 15 min for each additional inch of thickness.

During a weld thermal cycle all or part of the carbides are taken into solution depending upon the peak temperature experienced, the energy input and the material thickness. During subsequent cooling the transformed matrix (bainite/martensite/ferrite) remains supersaturated with respect to carbon as well as alloying elements that subsequently precipitate as carbides during tempering. The various types of carbides that occur in Cr-Mo steels are MC, M_2C, M_3C, M_4C_3, M_7C_3, and M_6C. The carbide types, size, distribution and morphology will depend on the chemical composition, microconstituents present and the tempering temperature and time. The niobium, titanium and vanadium carbides are more stable than the chromium, molybdenum or iron carbides.

Baker and Nutting[19] have shown that the types of carbides present in 2¼Cr-1Mo base metal are dependent on starting microstructure, heat treatment (tempering) and time at the tempering temperature. After normalizing, the microstructure is generally found to consist of a mixture of ferrite and bainite whereas after quenching the microstructure is mainly bainitic. They determined that the carbide evolution in the bainitic regions of both quenched and normalized material was similar, as shown below:

In bainite

$$\begin{array}{ccccccc} & & & & \multicolumn{3}{r}{|\longrightarrow M_7C_3} \\ \epsilon\text{-carbide} & & & & \text{cementile} & & | \\ + & \rightarrow & \text{cementile} & \rightarrow & + & \rightarrow M_{23}C_6 \rightarrow & M_6C \\ \text{cementile} & & & & Mo_2C & & \end{array}$$

However, in the ferritic regions the Mo_2C type carbides do not undergo all the transition carbides and transform directly to M_6C carbides. Mo_2C, the carbide conferring the greatest resistance to creep deformation, was found to be more stable in ferrite than in the initial microstructures consisting of martensite or bainite. In the martensitic and bainitic microstructures $M_{23}C_6$ grew at the expense of Mo_2C, resulting in a degradation of the creep properties with increasing tempering temperature or time at a tempering temperature.

Because of the stability of Mo_2C within the ferrite, Baker and Nutting[19] recommended the use of normalized and tempered 2¼Cr-1Mo rather than quenched and tempered 2¼Cr-1Mo. However, the presence of proeutectoid ferrite is generally regarded as unfavorable due to its lower strength and poorer toughness. Current alloy development reflects the need to avoid the formation of primary ferrite in the microstructure during cooling by making increased hardenability one of the principal criteria in alloy design.[20]

Modification of 2¼Cr by the addition of vanadium results in the precipitation of finely dispersed, slow growing V_4C_3 upon tempering or postweld heat treatment.[21] The precipitation of V_4C_3 occurs directly from the matrix and, unlike Mo_2C, is not dependent on the formation of other carbides. Vanadium has also been reported to be present in Mo_2C with a metal atom ratio of up to 0.3 in alloys that contain more than 0.1% V. Vanadium in Mo_2C results in stabilization of the Mo_2C.[22] The combined effects of precipitation and stabilization result in vanadium being one of the most potent elements in promoting creep resistance.

Similar investigations to determine the carbide evolutionary sequence in other Cr-Mo steels upon tempering have been conducted by several investigators.[23,24] However it is reasonable to believe that although the carbide evolutionary sequence in the CGHAZ may be similar to that in the base metal, the situation is complicated by the fact that some of the stable carbides (such as TiC, NbC, V_4C_3, etc.) although generally finer than the chromium-, molybdenum- or iron-containing carbides, may not dissolve upon weld thermal experience. Lundin *et al.*[110,140] have found that in the 2¼Cr and 3Cr alloys that contain modifying (stabilizing) elements such as vanadium, titanium and niobium the carbides do not completely dissolve upon a coarse grain HAZ simulation thermal cycle. However, in standard composition alloys all the carbides dissolve upon CGHAZ simulation. Thus, the subsequent reprecipitation of carbides will be affected. The carbide evolution sequence in the CGHAZ of 1CrMoV steel is shown in Fig. A7.[25] It can be seen from Fig. A7 that the carbides present in the CGHAZ on tempering will depend on the postweld heat treatment temperature.

Lundin *et al.*[110,140] have investigated the carbide evolutionary sequence in the CGHAZ of several standard and modified 2¼Cr-1Mo, 3Cr-1Mo and 3Cr-1½Mo alloys as a function of PWHT time at 1250°F (675°C). Their investigation revealed that in the alloys modified with vanadium, titanium and boron, the Mo_2C type carbides persist for longer times compared to the unmodified alloys.

Elevated Temperature Intergranular Cracking. Elevated temperature intergranular cracking, referred to as reheat, SRC/PWHT cracking, may occur in Cr-Mo steels containing less than 3 percent chromium.[27] However, reheat cracking has been occasionally observed in steels containing 3% and more chromium. Cracking is manifested by low rupture ductility and intergranular fracture along prior austenite grain boundaries, typically occurring in the coarse grained heat affected zone and occasionally in

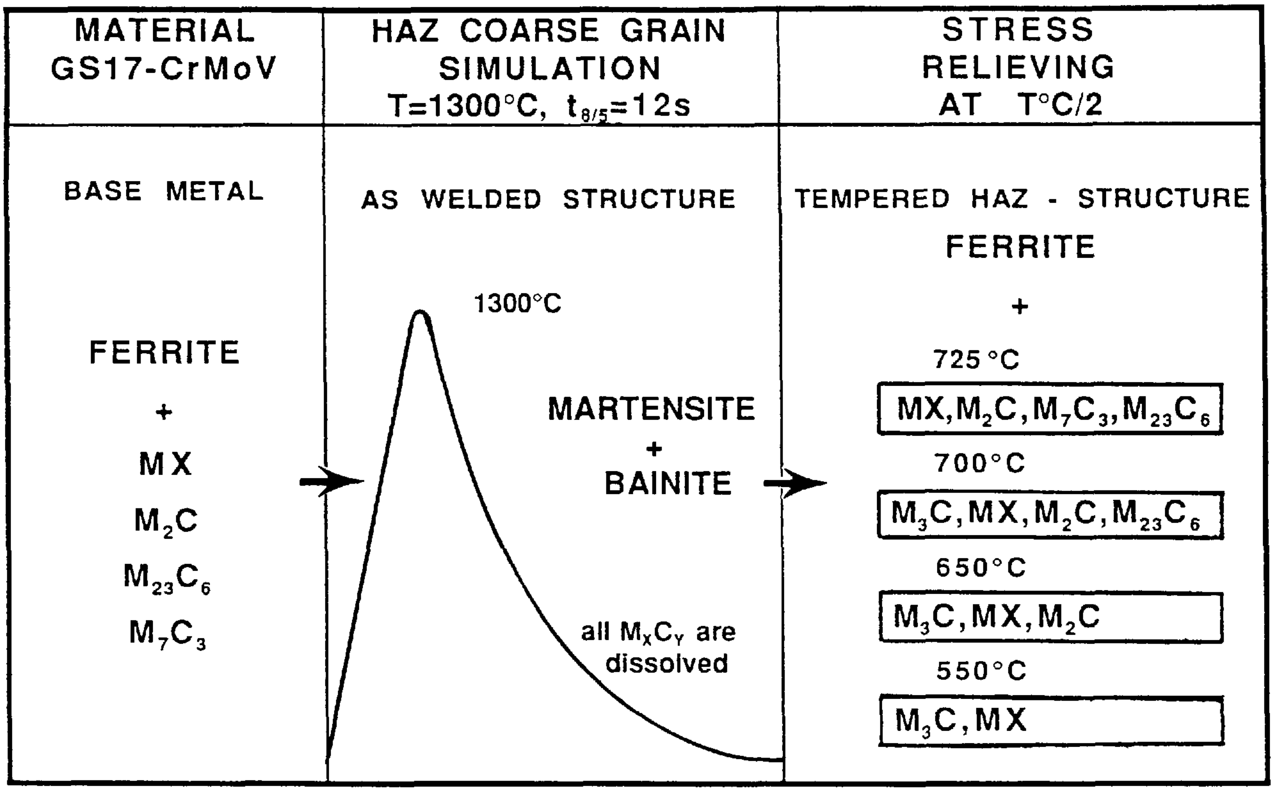

Fig. A7—Carbides in the coarse grained HAZ of 1CrMoV steel upon PWHT. Source: Buchmayr, B., Cerjak, H. and Fauland, H. P., "The Effect of the Precipitation Behavior on the HAZ-Properties of 1%Cr-Mo-V-Steel," 2nd International Conference on Trends in Welding Research, Gatlinburg, Tennessee, May 1989 the weld metal after an initially sound weldment has been subjected to PWHT or elevated temperature service.[4] Heat-to-heat variations in cracking susceptibility indicate a dependence on residual elements that adds to the worrisome nature of this problem as bulk chemistry of an alloy may not be a reliable predictor of cracking susceptibility.[5] If undetected this type of cracking may lead to failure of pressure vessels and piping in service.[6]

Large localized creep deformations may occur during PWHT to relax the residual stresses generated by the welding operation. Vinckier and Dhooge[28,29] state that the extent of plastic strain required to relax residual stresses is directly proportional not only to the level of residual stresses but also to the size of the component. Notches and sharp transitions that are under high residual tensile stresses will act as severe strain raisers once stresses begin relaxing at elevated temperature and can easily cause fissuring in susceptible material.

Examination of unoxidized fracture surfaces under the SEM reveals primarily smooth grain boundary facets with no definable fracture characteristics. Only with high resolution have some portions of the grain boundary fracture surface of cracks been shown to consist of numerous small dimples surrounded by ductile tear ridges. According to Debiez and Granjon[30] brittle intergranular fracture is characteristic of low temperatures and high stresses and the ductile intergranular dimpled fracture occurs under low stresses at high temperatures. TEM, using carbon extraction replicas of fresh fracture surfaces, reveals an almost complete absence of grain boundary precipitation and only in a few instances small carbide particles are detected in the small dimples on the grain faces (microcavitation).

There is no longer any doubt that the reheat/stress rupture cracks follow the prior austenite grain boundaries in those regions in the HAZ that have been heated to temperatures well in excess of 2000°F (~1100°C) and that have subsequently undergone plastic deformation either during deposition of subsequent beads or during PWHT. In some cases the grain boundaries show only a row of small voids and in other cases the cracks are well developed, readily visible under the optical microscope and extending for several grain boundaries.

Briant and Bannerji[31] in their review of the existing theories and mechanisms of intergranular failure in steel report that the circumstances under which steels exhibit intergranular fracture can be classified into four general categories:

1. the presence of certain secondary phases at the grain boundaries;
2. thermal treatments that cause impurity segregation to the grain boundaries without precipitation of an observable second phase;
3. the action of certain environments; and
4. combination of stress and high temperature.

It is well known that certain tramp elements at grain boundaries are a major cause of intergranular fracture. These elements are believed to lower the cohesive energy of the boundaries and at a given concentration, which depends on the yield strength, grain size and microstructure of the material, can change the fracture characteristics from cleavage to grain boundary separation. The most common embrittlers are from groups IV, V and VI in the periodic table presented below.

Common Grain Boundary Embrittlers

Group IVa	*Group VA*	*Group VIa*
Si	P	S
Ge	As	Se
Sn	Sb	Te

Segregation of the alloying elements can occur in any of three ways:

1. equilibrium segregation during tempering;
2. equilibrium segregation during austenitization; and
3. carbide rejection during tempering.

Elements such as sulfur, phosphorus, nitrogen, boron, etc. are known to segregate to the prior austenite grain boundaries during austenitization with the extent of segregation decreasing with increasing austenitization temperature. Carbide precipitation along the grain boundaries is also a possible mean of increasing the impurity concentration. Certain impurities are more soluble in ferrite than in carbides and thus they build up at the ferrite-carbide interface.

Alloying elements or impurity elements can be placed in five broad categories:

1. promoters of segregation that act by co-segregating with the impurities such as manganese, nickel, etc.;
2. promoters that do not themselves segregate, such as chromium;
3. scavengers prohibiting segregation such as titanium, molybdenum, etc.;
4. embrittling elements such as hydrogen, nitrogen, silicon, phosphorus, sulfur, germanium, arsenic, selenium, tin, antimony, tellurium, bismuth, etc.;
5. improve grain boundary cohesion, such as carbon.

Although mechanisms of reheat/stress rupture cracking are not completely understood, it is now generally believed that several conditions must be fulfilled: first, a susceptible microstructure such as a coarse prior austenite grain size as readily occurred in the CGHAZ of welds; second, the presence of residual stresses; and third, discontinuities or notches that act as stress concentrators, for example weld configuration, slag/lack of fusion, cracks, etc. It has been clearly demonstrated that if a material with a CGHAZ is postweld heat treated so that no plastic strain occurs during heat treatment, then it will show no loss in elevated temperature bend or tensile ductility. However, tests on simulated HAZ microstructures show that the impact transition temperature is raised even without plastic strain. PWHT and stress rupture cracks form because relaxation strains exceed the creep ductility of the CGHAZ at elevated temperature.

According to the existing theory of reheat cracking, carbides (vanadium, molybdenum, chromium, etc.) are taken into solution in the HAZ when the temperatures exceed 2200°F (1200°C). In addition, grain growth occurs in the HAZ. Due to rapid cooling from these high temperatures and the low temperatures at which transformation starts for such steels, the reprecipitation of carbides is almost completely suppressed and martensitic and lower bainitic transformation products are formed. PWHT or service cause the carbide forming elements to precipitate as carbides from the supersaturated solid solution in a manner similar to that which occurs in normal tempering. These precipitates form in the grain interior as submicroscopic platelets only a few Angstroms in diameter, causing considerable stiffening of the grain interior and, depending on temperature, produce an increase in hardness (secondary hardening). The grain boundaries, however, remain generally free of precipitates of sufficient size to prevent grain boundary sliding and it has been observed that areas adjacent to grain boundaries may be denuded (no precipitates).[32] Any relaxation of residual stresses or plastic deformation imposed upon such a microstructure will be resisted by the stronger grain interiors and deformation will be concentrated along the weaker grain boundaries or in the narrow denuded zones causing grain sliding. Although the overall strains are small, local high shear and tensile strains develop at the grain boundaries, especially if the grain size of the material is large (less grain boundary area). The resultant significant deformations lead to the formation of voids at steps or other discontinuities on the grain boundary interfaces. Such cavities, when linked up, form the final grain boundary cracks.

Another theory holds that precipitates or inclusions on the grain boundaries nucleate voids or promote boundary decohesion when grain boundary sliding occurs. According to Kanazawa *et al.*,[33,34] however, the stress relaxation characteristics and strength of the HAZ are more important for cracking susceptibility than the secondary hardening behavior. If the HAZ resists stress relaxation and if the fracture strength of the HAZ is low then the material will exhibit higher susceptibility to reheat cracking.

The type and morphology of precipitates occurring in the HAZ has been a topic of considerable research. Several investigators have contended that the most critical time at elevated temperature is during the formation of coherent or preprecipitate clusters at about 500–550°C (932–1022°F) which corresponds to the maximum in secondary hardening.[35,40] Orr *et al.*[39] have noted that due to the strong lattice correspondence of Mo_2C with bainite or martensite, the nucleation energy is relatively low and therefore Mo_2C forms quickly as a finely divided slow growing precipitate. Swift *et al.*[35–38] have proposed that coherent precipitates, Mo_2C or V_4C_3, nucleate in the matrix and at dislocation jogs and intersections. Coherent Mo_2C yields a nonuniform, highly strained matrix with decreased dislocation mobility and dislocation locking and results in a reduction of the ability of the grain interiors in the CGHAZ to plastically deform during PWHT or in-service.

Temperature is an important factor in that coherent Mo_2C persists for more than 500 hours at 1100°F (590°C) without decomposition to more complex carbides and has a correspondingly long coherency duration. However, at 1250°F (680°C) coherency is quickly lost as evidenced by the formation of incoherent Mo_2C within one-half hour at temperature.[38]

A carbide denuded zone has also been reported to exist adjacent to the grain boundaries.[22,41–44] These zones are apparently a result of the depletion of alloying elements due to carbide precipitation in the grain boundaries. Several researchers have considered the carbide denuded zones to be detrimental as they provide a narrow soft region in which strain can preferentially accumulate.[21,44] However, Meitzner and Pense[28] found the presence of denuded zones did not contribute to stress relief cracking. Swift[38] found that although denuded zones were present they formed only at times beyond those corresponding to a minimum in ductility. In investigations conducted by Lundin *et al.*[110,140] no correlation could be determined between the denuded zone width and the SRC/PWHT cracking susceptibility in a variety of modified and standard 2¼Cr and 3Cr alloys.

Thus, from the above theory it can be assumed that susceptibility to reheat/stress rupture cracking increases with an increase in the grain size in the CGHAZ and higher initial hardness of the HAZ before PWHT/service. Also, a higher strain hardening rate in the base metal, which forces deformation into the HAZ, may promote cracking. Slow strain rates, which allow grain boundary sliding, also may promote cracking unless they are slow enough to permit softening of the microstructure during elevated temperature exposure.

Another factor is the presence of notches, either surface irregularities or internal defects, at which cracking almost invariably initiates.[45] The notches in the CGHAZ are particularly detrimental, as they act as intense stress concentrators in the very region of the weld already under a high tensile stress and with a low rupture ductility microstructure.[28,41,42,46] The notch acuity further inhibits deformation by the creation of a triaxial stress state.[38]

Another theory deals with the effect of trace elements or impurities. Some investigators have shown that high purity heats of the same bulk chemistry do not show a ductility loss for simulated CGHAZ microstructures. It is known, however, that various interactions among alloying elements and trace elements exist and can affect ductility either by a direct influence in the nonmetallic inclusion content/chemistry/shape or by embrittlement caused by a segregation of trace impurities to grain boundary interfaces at high temperature. Thus, interest in the heat-to-heat variability and the development of new techniques, particularly Auger spectroscopy, to study grain boundary composition led to intense evaluation of residual element effects on cracking.[41,47] Segregation of residual elements (phosphorus, sulfur, tin and antimony) was found to play a critical role by causing embrittlement of grain boundaries.[29,48,49] The effects of grain boundary embrittlement due to impurity segregation and impurity interactions during precipitation are superposed on the matrix strengthening effects by coherent precipitation.[35] Hippsley *et al.*[50] have noted that grain boundary segregation of impurities can be due to equilibrium segregation from the grain matrix or may be due to solute rejection from grain boundary carbides, the solubility of impurities being higher in the matrix material than in the carbides. Vinckier and Dhooge[29,48] state that loss of ductility caused by segregation during elevated temperature is certainly a major factor in cracking but that the true mechanism is most likely a combination of these two ideas (segregation and precipitation strengthening) and is more complex.

Other researchers have proposed additional factors that increase the intricacy of the previous cracking mechanisms. Vinckier[6] proposed that the decomposition of martensite needles during heating creates high localized strains at the grain boundary interfaces. These strains plus external restraint can result in the formation of microcavities, particularly when the matrix is strengthened by intragranular precipitation. Hippsley *et al.*[51] have proposed that segregation of less mobile embrittling elements such as phosphorus, tin and antimony occurs at elevated temperatures in a fashion similar to that proposed by Troiano[52] for hydrogen. Segregation is locally enhanced in regions of maximum triaxial stresses, such as at the root of a notch or in the region of a crack tip, by diffusion along the strain gradient. Dislocation pile ups at grain boundaries and grain boundary carbides plus the strain induced segregation of impurities reduce the cohesive strength of the grain boundaries and carbide-matrix interfaces sufficiently to allow the development of microcracks. Thus, according to Hippsley *et al.*[51] the factors involved in cracking are not only segregation and precipitation but also the amount of plastic strain which, for a given load, increases as the yield strength falls with increasing temperature.

The necessary factors for cracking were summarized by Ito and Nakanishi:[8]

1. the material must have undergone a thermal cycle that results in solution of alloying elements and that retains the elements in solid solution after cooling;
2. grain growth must have occurred as a result of thermal cycling;
3. heat treatment between 850–1300°F (450–700°C) resulting in significant precipitation strengthening;
4. grain strength and internal stress must exceed the strength of the grain boundaries; and
5. a stress riser must be present to initiate cracking.

In addition, the material must be one that has a composition that is susceptible to cracking with regard to major alloy content and residual or impurity elements.

Origin of Residual Stresses

Residual stresses are developed in the weld HAZ and fusion zone during cooling due to restrained shrinkage and transformation volume changes as a result of austenite decomposition.[53,54] On cooling, those areas of the base metal that experienced thermal expansion due to heating must contract or plastically flow. The bulk of the base metal that has experienced no significant heating (and therefore no decrease in strength) prevents or restrains the contraction of the cooling material. Above approximately 1200°F (650°C) the weld fusion zone and those regions immediately adjacent to the weld accommodate the thermal contraction by plastic deformation without developing any significant stress as the yield strength is low above this temperature. Cooling below 1200°F (650°C) results in significant increases in yield strength with decreasing temperature. Plastic deformation only occurs when the stresses due to thermal contraction exceed the yield stress and therefore cooling to the preheat temperature results in increasing residual tensile stress concomitant with the increased yield strength in the fusion zone and the HAZ. The resultant residual tensile stresses occurring in the HAZ and fusion zone are in equilibrium with comprehensive stresses in the bulk of the base material.

Transformational stresses are a result of the volumetric expansion that occurs during the decomposition of austenite. The material being transformed attempts to expand but expansion is hindered by the cooler material not undergoing transformation. Therefore the material being transformed experiences a compressive stress and the cooler material a tensile stress. If the transformation temperature is high the transformation stresses will be overridden by the effects of subsequent bulk shrinkage. However, if the transformation temperature is low, the transformation stresses will lower the overall tensile stress in the HAZ and fusion zone.

Superposition of the components of the residual stress developed during welding leads to an extremely complex final residual stress state. The CGHAZ, that portion of the HAZ adjacent to the fusion zone, is under a significant tensile stress both in the direction of and perpendicular to the weld. This biaxial residual stress state as well as the unfavorable metallurgical characteristics of the CGHAZ exacerbates the susceptibility of this zone to reheat cracking.

Microstructural Effects

Meitzner and Pense[43] have found that martensite and lower bainite are more susceptible to cracking than upper bainite although the authors state that the difference is probably due to precipitation processes rather than optically resolved microstructure. Ito and Nakanashi[8] also found that martensite and lower bainite microstructures are more susceptible than upper bainite. They related the increased susceptibility to the supersaturation of the bainitic and martensitic microstructures with alloying elements and carbon which results in intense secondary precipitation. Debiez and Granjon[30] found that bainitic structures appear to be more susceptible to cracking than martensitic structures upon implant testing. However, they do not state whether the bainitic microstructure obtained was upper or lower bainite.

Effect of Composition

The composition obviously plays a major role in susceptibility to cracking. Alloying elements added to structural and pressure vessel steels to increase tensile and creep strength form carbide or carbonitride precipitates in ferrite. Widely used alloy additions to steels are chromium, molybdenum and vanadium in high temperature steels. According to many authors the presence of these elements increases the susceptibility of a steel to reheat cracking. However, the restriction of these elements as low-alloy additions, cannot be considered in practice, as their presence is vital to the hardenability, strength and creep resistance of these steels.

In extensive literature reviews Meitzner[41] and Dhooge *et al.*[48] defined the effects of specific alloying elements. The elements generally considered to be detrimental to cracking are: carbon, vanadium, molybdenum (individually and in concert with vanadium), niobium, aluminum, copper and the residual elements: phosphorus, sulfur, tin, antimony and arsenic. The effects of chromium, boron and titanium are not clearly defined. Nickel was found to be one element that appears to have no effect on cracking. In general, the elements found to be deleterious are either those that promote the formation of carbides of the M_2C or M_4C_3 type or those that are known to have general grain boundary embrittling effects.

Many investigators have tried to quantify the effects of alloying elements on the cracking susceptibility. Nakamura *et al.*[55] attempted to determine the effect of alloy additions on cracking susceptibility in Cr-Mo steels by development of a cracking susceptibility parameter (ΔG). Variations in the levels of chromium (0.1–1.5%), molybdenum (0.3–0.6%), nickel (0–3%) and vanadium (0–0.08%) resulted in the ΔG parameter relationship:

$$\Delta G = Cr + 3.3Mo + 8.1V - 2$$

when ΔG is greater than zero the material is considered to be susceptible to cracking. In 1972, Ito and Nakanishi[8] extended the work of Nakamura. The alloying elements (manganese (0.5–1.4%), nickel (0.5–1.5%), chromium (0.5–1.5%) and vanadium (0.05–0.12%)) were varied and additions of copper (0.15–0.26%), niobium (0.06%) and titanium (0.02–0.07%) were made to steels containing nominally 0.3% silicon and 0.5% molybdenum. This work resulted in the development of the cracking parameter, P_{SR}:

$$P_{SR} = Cr + Cu + 2Mo + 10V + 7Nb + 5Ti - 2$$

when P_{SR} is greater than zero the material is deemed to be susceptible to cracking. The applicable range of the P_{SR} parameter is limited to alloys that contain less than: 2% Mo, 1.5% Cr, 1% Cu and 0.15% V, Ti and Nb. However, Ito and Nakanashi found that chromium contents in excess of 2% eliminated cracking.

Subsequent to development of the P_{SR} and ΔG parameters several investigators have found poor correlation between the parameters and actual susceptibility of different alloys. Pense *et al.*[56] found that ΔG was a poor predictor of cracking in A 535-A, A 517-F and A 543 steels. McMahon *et al.*[57] found that both P_{SR} and ΔG did not accurately predict cracking susceptibility in multiple heats of SA 533-B and SA 508-2. Also, many investigators[26,36–38,51,58–61,110,140] have found that 2¼Cr-1Mo alloys are susceptible to cracking although a chromium content of 2% or greater was considered to eliminate cracking susceptibility by Ito and Nakanishi.[8]

McMahon *et al.*[57] have suggested an additional parameter, CERL, with the addition of chromium:

$$CERL + Cr = Cr + 0.2Cu + 0.44S + P + 1.8As + 1.9Sn + 2.7Sb.$$

The greater the CERL + Cr value the greater the cracking susceptibility. This parameter clearly emphasizes the effects of embrittling elements over the effect of carbide formers. The authors state that individual alloy content will affect the parameters and that increasing the former carbide content may necessitate their inclusion in a manner similar to that of the P_{SR} parameter. Similarly, in reviewing results of cracking susceptibility tests of 2¼Cr-1Mo weld metal, Boniszewski[62] recommended use of the metal composition factor (MCF) to rank cracking susceptibility. The metal composition factor:

$$MCF = Si + 2Cu + 2P + 10As + 15Sn + 20Sb$$

combines the relative overall potency of grain boundary embrittling elements present in a material. An increase in the MCF was found to correlate with a decrease in rupture ductility as measured by elongation in hot tensile tests.

Since the ΔG and P_{SR} parameters were published, several similar equations evolved for other steel compositions. T factor was developed for SA 508 Cl2 and SA 533 Gr B steels:

$$T = 20V + 7C + 4Mo + Cr + 1.5 \log X - 0.5Mn$$

where

$$X = Al \text{ for } Al \leq 2N$$

or

$$X = 2N \text{ for } Al > 2N.$$

Steels are susceptible if $T > 0.9$.

$\Delta G1$ parameter was formulated to consider the effect of carbon in the original ΔG parameter:

$$\Delta G1 = Cr + 3.3Mo + 8.1V + 10C - 2.$$

When the $\Delta G1$ parameter is greater than 2 the material is considered susceptible to cracking.

Considering the effect of tramp elements alone R value was developed for 0.5CrMoV steels:

$$R = P + 2.43As + 3.57Sn + 8.16Sb.$$

Susceptibility to PWHT cracking increases with increase in R value.

Bruscato[63] devised an embrittling factor relating weight percent of impurity elements (in ppm), based on 50% shear fracture appearance transition temperature:

$$\overline{X} = \frac{10P + 5Sb + 4Sn + As}{100}$$

where susceptibility increases with $\overline{X}$-values.

In the subsequent part of this section an attempt has been made to review the effect of some alloying elements individually and in combination with other elements.

Effect of Chromium and Molybdenum. In the ΔG and P_{SR} crack susceptibility parameters chromium is an element that increases the susceptibility to SRC/PWHT cracking. However, it has been pointed out by both Nakamura and Ito that steels that contain greater than 1.5% chromium are not susceptible to cracking. Published literature reveals that this is not true and that steels containing up to 3% chromium have been found susceptible to SRC/PWHT cracking. However, this may be because of the effect of other elements such as vanadium, niobium and titanium in the steels tested. Some results show that chromium between 0–2% decreases high temperature ductility and when above 2% increases it markedly.

Molybdenum increases the susceptibility to SRC/PWHT cracking and its effect is greater than that of chromium. In the early stages of tempering the Mo_2C type carbides precipitate and cause hardening of the grain interiors. Other carbide forming elements (such as vanadium, titanium, niobium) that have more affinity for carbon than molybdenum and tend to form more stable carbides. Even in such cases, molybdenum is a potent solid solution hardening element.

The recent work of Tamaki[27,64–68] attempts to determine the separate effects of chromium and molybdenum on SRC/PWHT cracking. His papers represent extensive work on materials of varying chromium (0–5%) and molybdenum (0.3–1.5%) content. The effects of chromium and molybdenum, independently and in concert, were studied using a modified implant test. The modified implant test was employed to determine the minimum stress that would cause a specimen to fracture within 20 hours while postweld heat treating the specimen at a temperature of 1112°F (600°C). The susceptibility to cracking was related to the magnitude of the critical stress to rupture ($\sigma_{AW-crit}$). The lower the minimum critical stress to cause rupture, the greater is the susceptibility to cracking.

Alloys containing chromium in the range tested but low in molybdenum (0.25%) were found to be susceptible to cracking. The 1%Cr-0.25%Mo alloy showed the lowest critical stress for failure and therefore the greatest susceptibility to cracking. Increasing molybdenum at any level of chromium increased susceptibility, but the lowest critical stress for any particular molybdenum level occurred for alloys containing 1% chromium. The data from Tamaki's studies are shown in Fig. A8. Note that for low molybdenum content (0.25% and 0.5%) when no chromium is present no cracking occurred over the range of stresses employed indicating that these materials are not susceptible.

When the results are expressed as a function of chromium and molybdenum for different stress levels the evaluation shown in Fig. A9 results. Susceptibility to SRC/PWHT cracking with a change in alloying element content is a maximum on these diagrams where the stress contours are closest together. Susceptibility for a particular alloy may be judged by the magnitude of the critical stress to failure ($\sigma_{AW-crit}$). The plotted data is divided into four regions labelled I, IIa, IIb and III (Fig. A9). The materials in region I, those with less than 1% Cr and less than 0.5% Mo, are relatively insensitive to cracking. Materials in region IIa, comprised of alloys with 0–1% Cr and 0.5–1% Mo, have rapidly increasing sensitivity to cracking with increasing chromium or molybdenum content based on relatively large decreases in the critical stress with small changes in alloy content. Region IIb, comprised of alloys with greater than 2% Cr and 0.5–1% Mo, characterizes behavior of decreasing sensitivity with increasing chromium content. Region III, comprised of alloys with approximately 1% Cr and greater than 1% Mo, represents the highest sensitivity to cracking. The Nakamura parameter[55] for PWHT cracking susceptibility, ($\Delta G > 0$), was found to predict cracking principally in fields IIa and III and extending somewhat into field IIb. The cracking parameter due to Ito[8] ($P_{SR} > 0$) predicted cracking principally in field IIa. These parameters are limited to chromium contents less than 1.5%. Since fields IIa and III indicate

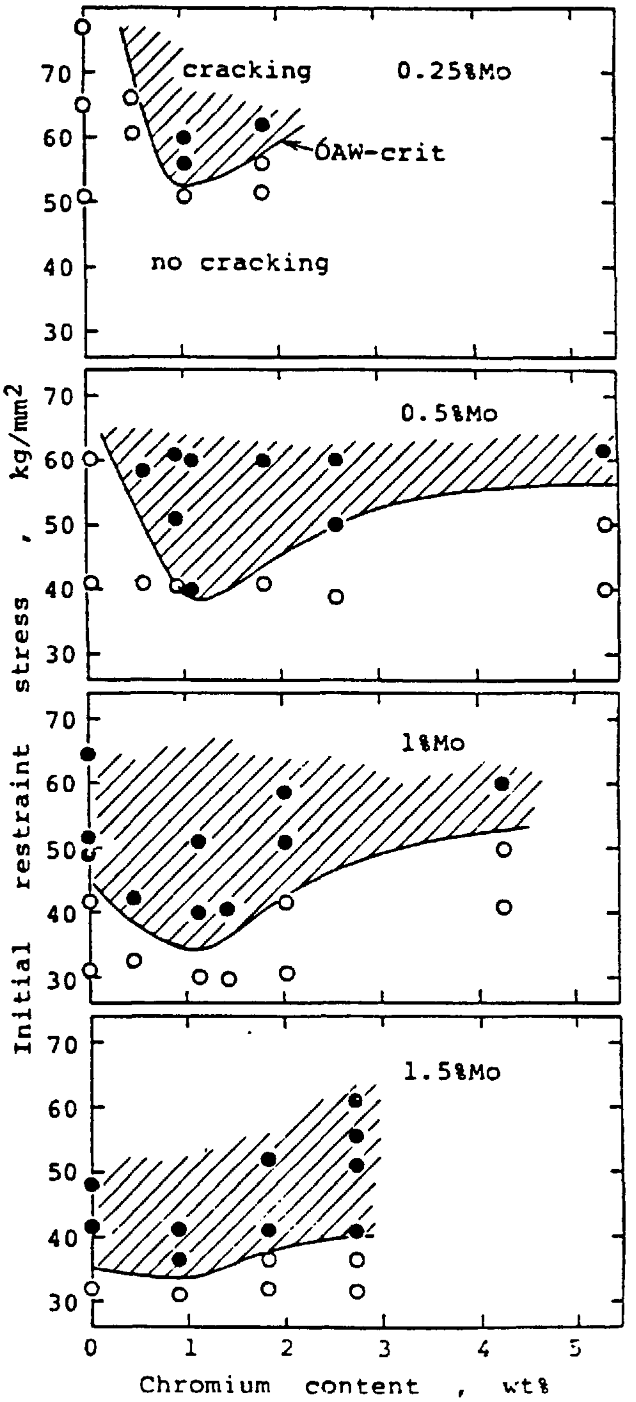

Fig. A8—Effect of chromium on the critical restraint stress, $\sigma_{AW\text{-}crit}$. Source: Tamaki, K. and Suzuki, J. "Effect of Chromium and Molybdenum on Reheat Cracking Sensitivity of Steels," Transactions on the Japan Welding Society, Vol. 14(2), October 1983, pp. 39–43

the alloys of maximum reheat cracking sensitivity, the agreement is excellent, with Tamaki's diagrams being more discriminating than either index (Fig. A10).

In order to discern the microstructural causes for the differences in cracking susceptibility for various materials, Tamaki[64] undertook an extensive study of the carbides in the alloys using X-ray diffraction techniques (extracted carbides) and transmission electron microscopy of carbide extraction replicas. It was found that the materials most susceptible to PWHT cracking showed the greatest fraction of M_2C type

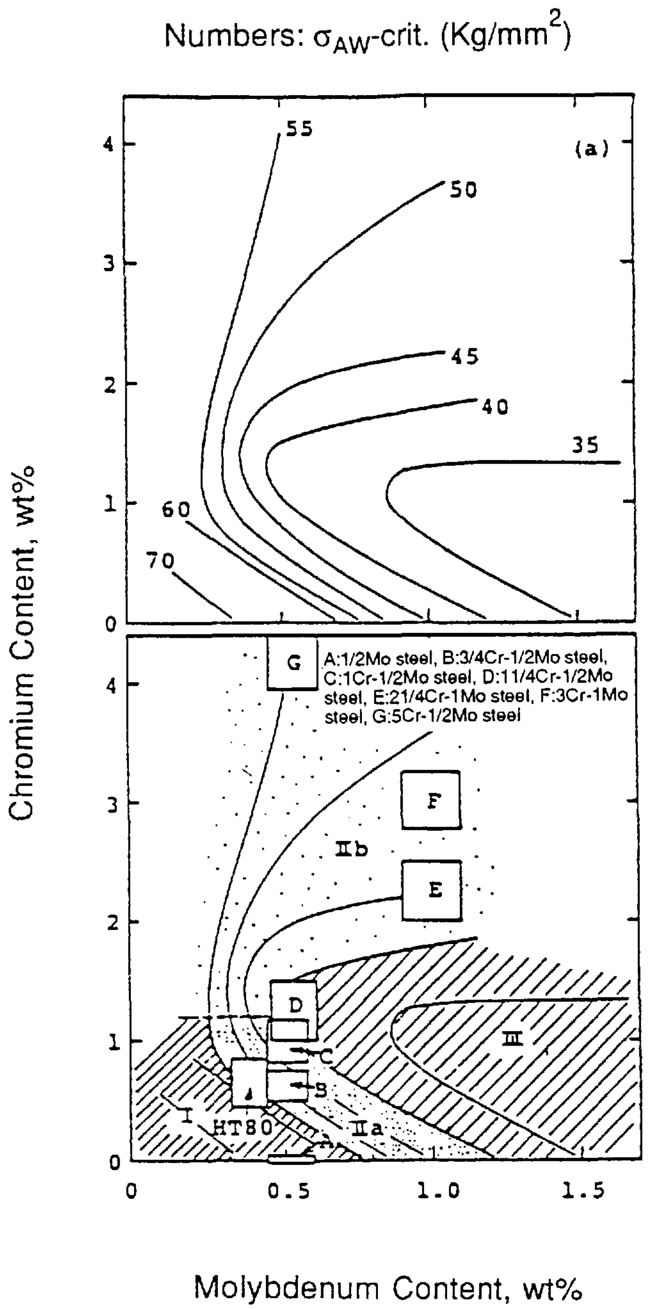

Fig. A9—Contour lines of critical restraint stress ($\sigma_{AW\text{-}crit}$) shown on the Cr-Mo content diagram. Source: Tamaki, K. and Suzuki, J. "Effect of Chromium and Molybdenum on Reheat Cracking Sensitivity of Steels," Transactions on the Japan Welding Society, Vol. 14(2), October 1983, pp. 39–43

carbides after PWHT. With a smaller amount of M_2C (or a larger amount of M_7C_3 or $M_{23}C_6$), the susceptibility to cracking decreased. Figs. A11 and A12 depict these results graphically. Fig. A11 shows the relative amount of carbides present for different alloys on a chromium vs. molybdenum content diagram with the curved lines being constant weight percent M_2C. Fig. A12 superimposes these constant weight percent M_2C lines (solid lines, Fig. A12) on the chromium vs. molybdenum content diagram of Fig. A9. Figs. A11 and A12 thus show that the greatest susceptibility to cracking coincides with the largest fraction of M_2C. The only exception noted is confined to below the a-a[1] line in Fig. A12 where, according to Tamaki, phospho-

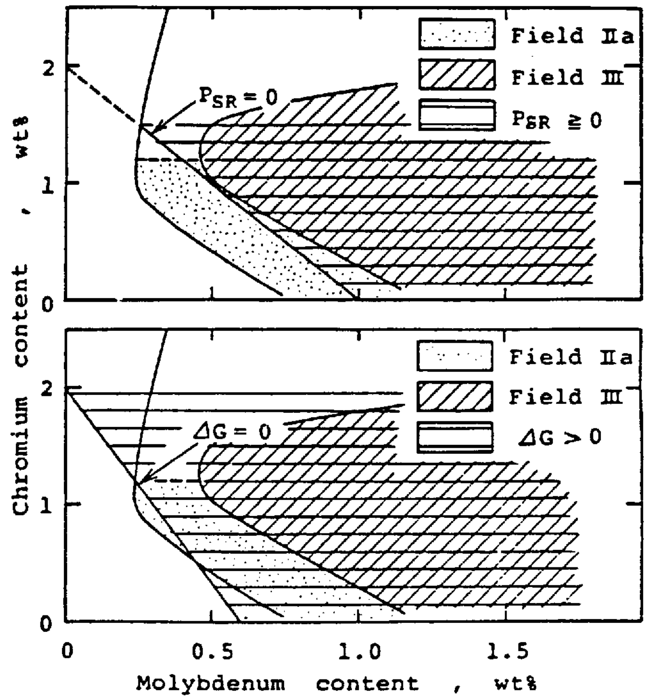

Fig. A10—Comparison between the critical restraint stress ($\sigma_{AW\text{-}crit}$) and cracking sensitivity indexes, P_{SR} and ΔG. Source: Tamaki, K. and Suzuki, J., "Effect of Chromium and Molybdenum on Reheat Cracking Sensitivity of Steels," Transactions on the Japan Welding Society, Vol. 14(2), October 1983, pp. 39–43

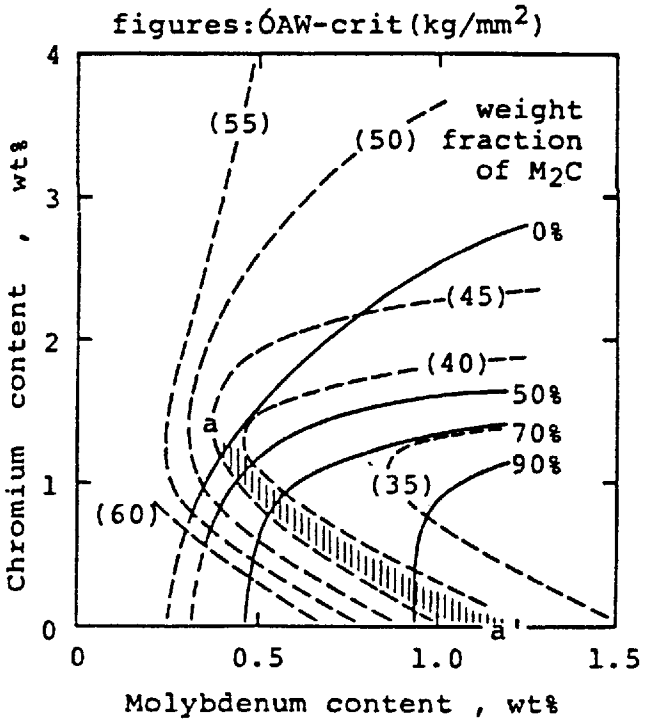

Fig. A12—Weight fraction of M2C shown on the $\sigma_{AW\text{-}crit}$ diagram. Source: Tamaki, K., Suzuki, J., Nakaseko, Y. and Tajiri, M., "Effect of Carbides on Reheat Cracking Sensitivity," Transactions on the Japan Welding Society, Vol. 15(1), April 1984

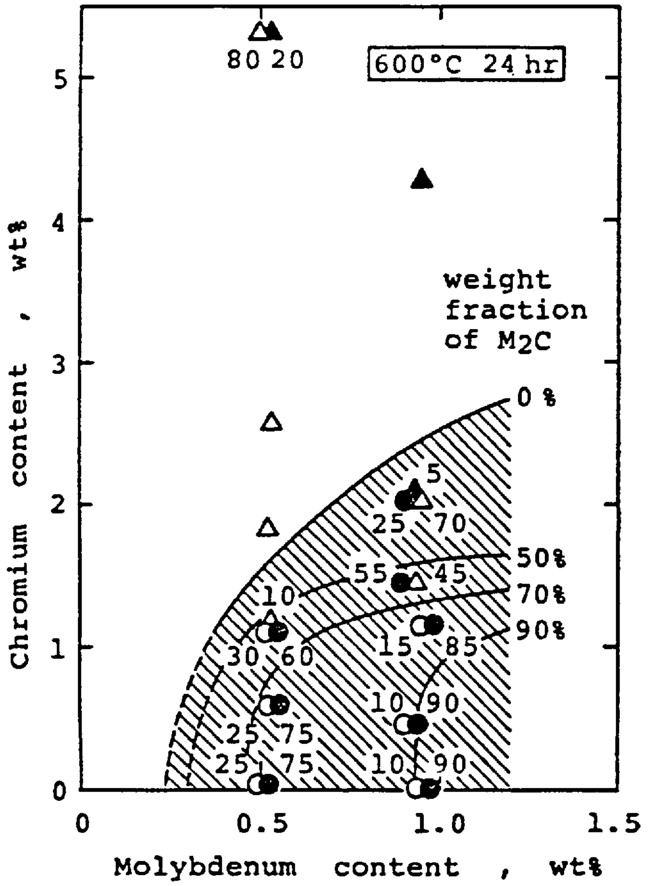

Fig. A11—Carbides present in Cr-Mo steels tempered at 600°C for 24 hours. ○ M_3C ● M_2C △ M_7C_3 ▲ $M_{23}C_6$. Source: Tamaki, K., Suzuki, J., Nakaseko, Y. and Tajiri, M., "Effect of Carbides on Reheat Cracking Sensitivity," Transactions on the Japan Welding Society, Vol. 15(1), April 1984

rus segregation is inhibited in alloys with less than 1% Cr and less than 1% Mo.

Since both M_2C and M_7C_3 strengthen the matrix by precipitation, Tamaki investigated the effects of secondary strengthening and high temperature hardness by making hardness measurements on samples held at temperature for one hour both at the holding temperature and at room temperature after cooling. While secondary hardening is manifested by an increase in hardness at room temperature, Tamaki found that at high temperature the phenomenon is represented only in a delay in softening. That is, softening continues to occur but at a lower rate than that which occurs at lower temperatures. Fig. A13 illustrates these results with the room temperature hardness shown as filled circles and the elevated temperature hardness as open circles. This is in accordance with the findings of Bauford.[69] In hot tensile tests Bauford found that at temperature there is no increase in strength with time but yield strength remains constant over a long period followed by a slow loss in strength.

It was found that in alloys in which the principal precipitate is M_7C_3, the delay in softening occurred at lower temperatures than for alloys in which the precipitate consists of large fractions of M_2C. Tamaki[67] postulated that the grain boundary embrittlement would be of a similar nature in either type of alloy and therefore embrittlement of the grain boundaries would initiate at the same temperature and proceed in a similar fashion for both types of alloys. As shown schematically in Fig. A14, if a delay in

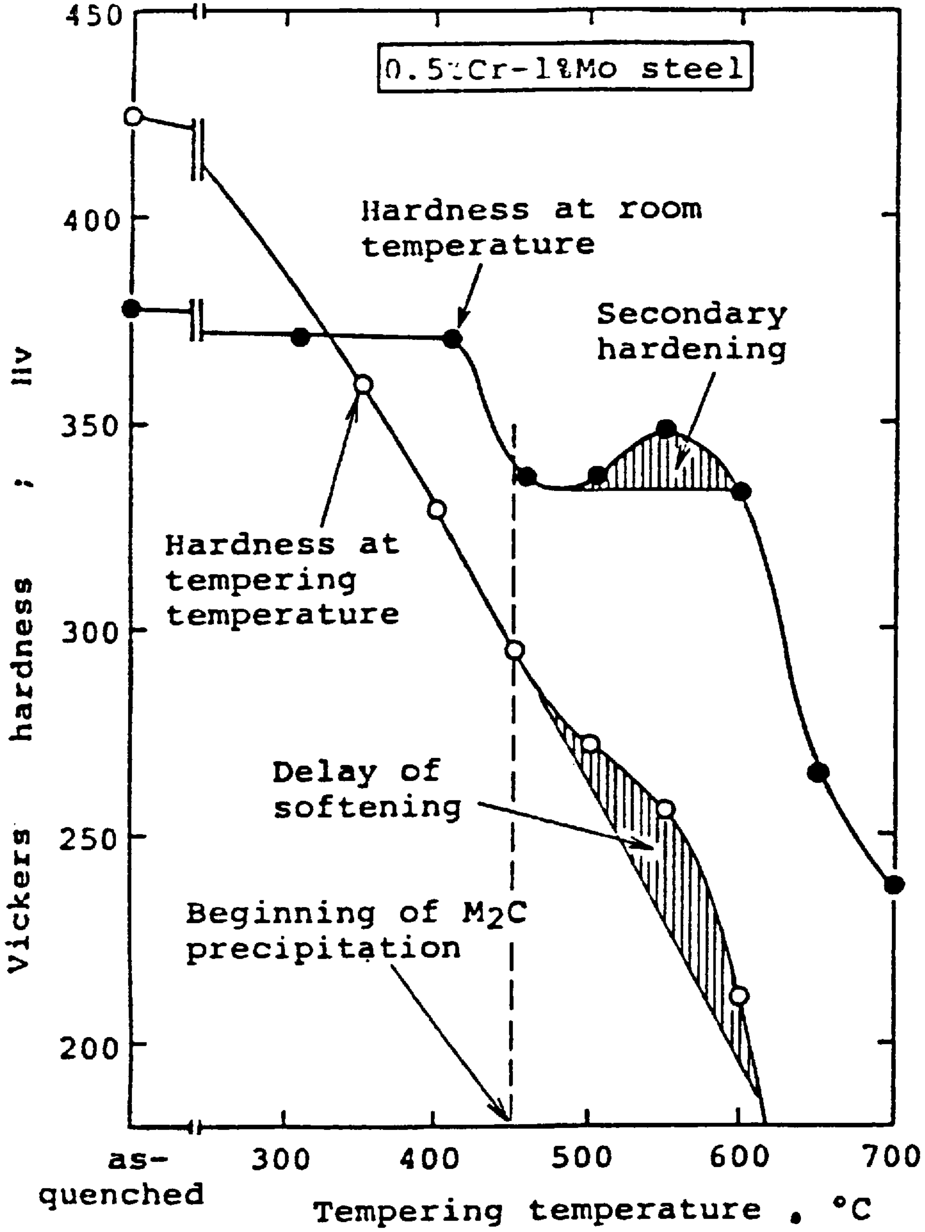

Fig. A13—Hot hardness and hardness at room temperature versus tempering temperature. Source: Tamaki, K., Suzuki, J., Nakaseko, Y. and Tajiri, M., "Effect of Carbides on Reheat Cracking Sensitivity," Transactions on the Japan Welding Society, Vol. 15(1), April 1984

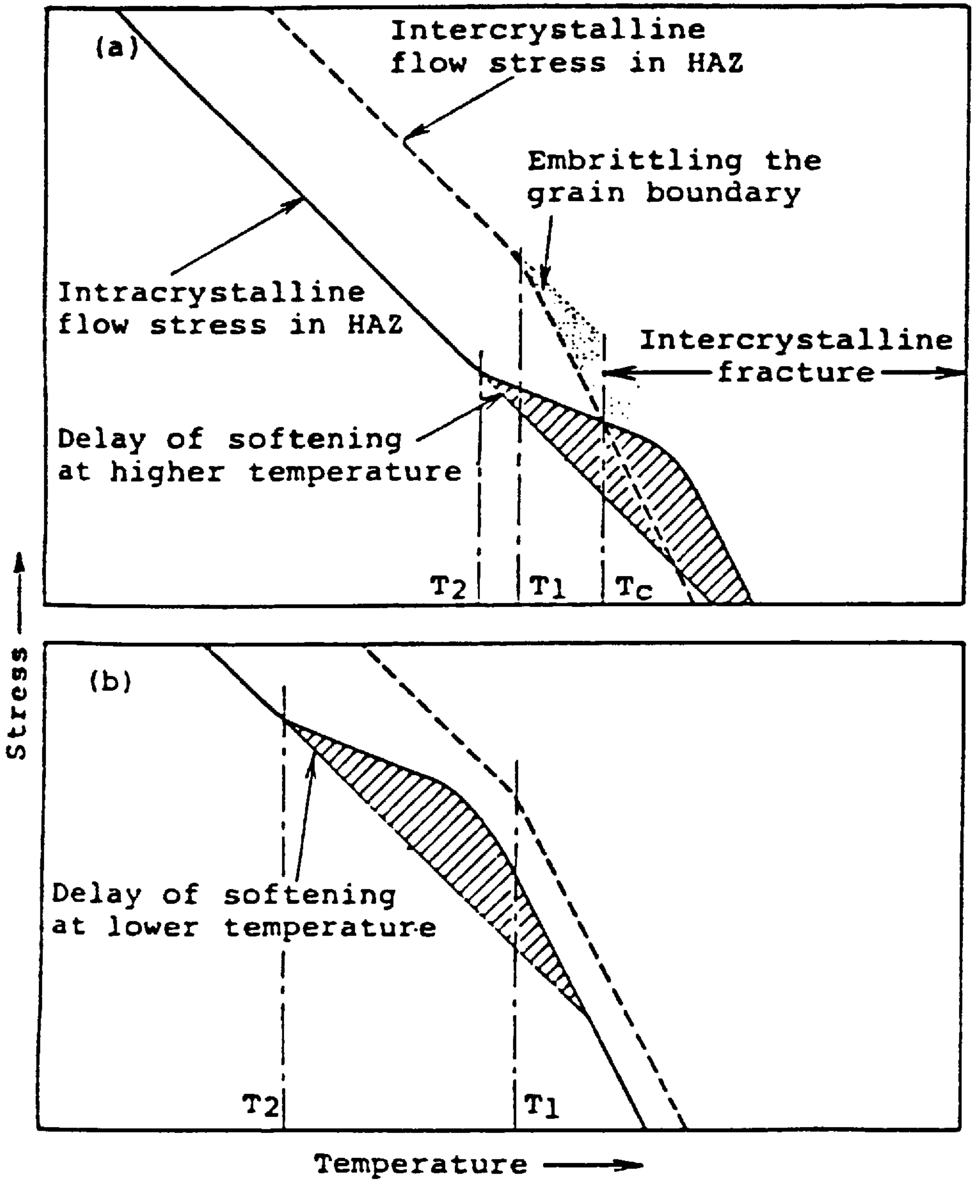

Fig. A14—Schematic representation of Tamaki's mechanism of reheat cracking. Source: Tamaki, K., Suzuki, J., Nakaseko, Y. and Tajiri, M., "Effect of Carbides on Reheat Cracking Sensitivity," Transactions on the Japan Welding Society, Vol. 15(1), April 1984 softening occurs at high temperatures, as in M_2C type precipitation, the embrittlement of the grain boundary may cause the intercrystalline flow stress to be less than the intracrystalline flow stress resulting in fracture. However, as shown in Fig. A14B, if a delay in softening occurs at lower temperatures as with M_7C_3 precipitation, the intercrystalline flow stress exceeds the intracrystalline flow stress at all temperatures and thus intercrystalline fracture does not occur.

Effect of Vanadium. In Cr-Mo alloys vanadium additions dramatically increase elevated temperature strength. Unfortunately, the addition of vanadium to Cr-Mo steels has been found almost universally to result in an equally dramatic increase in SRC/PWHT cracking susceptibility.[6,8,26,30,38,40,42,43,46,70] The importance of vanadium in increasing cracking susceptibility can be seen in the P_{SR} and ΔG parameters in that the multipliers for vanadium are the highest.[8,55]

The addition of vanadium results in a uniform and fine precipitation of V_4C_3 in the matrix, resulting in significant grain matrix strengthening and accumulation of strain in the grain boundaries.[46] Bently[40] has noted that early in the heat treatment cycle, intense V_4C_3 precipitation occurs at the ferrite-bainite interfaces due to segregation effects, the bainite having a higher carbon content and the ferrite having a higher vanadium content. At temperatures between 930–1020°F (500–550°C) coherent precipitation of V_4C_3 occurs in the ferrite similar to Mo_2C formation and is concurrent with the development of maximum hardness and strength. At higher temperatures (1300°F (700°C)) and longer time periods (10 hours) carbide precipitation occurs in the grain boundaries and large carbides and a grain boundary denuded zone are formed.

In a study of ½Cr-½Mo with varying vanadium content, Meyers[71] determined that vanadium below 0.22–0.27% did not appreciably increase cracking susceptibility. It was speculated that vanadium could be increased if residual elements were restricted in order to limit grain boundary embrittlement. However, Meyers noted that attention must also be paid to the effects of chromium, manganese and nickel, which increase initial hardness, and to the effect of molybdenum, which increases secondary hardening. Restrictions may have to be placed on them as well as vanadium.

Jones[72] noted that the vanadium-to-carbon ratio must be considered. In a study of welds in 1Cr-½Mo-1½V materials with vanadium-to-carbon ratios between 3.5–4.5, a high susceptibility to cracking was found. Stone and Murray[21] noted that a minimum in creep ductility was apparent at vanadium-to-carbon ratios of 3 to 4 and the reduction of this ratio to 1.5 markedly increased ductility. Thus, a vanadium-to-carbon ratio of 1.5 to 2 was recommended to mitigate cracking.

Tamaki *et al.*[68] found that small additions of vanadium (0.06%) reduced the critical stress to fracture in the implant test as shown in Fig. A15. The maximum effect was found to occur in low chromium and low-to-high molybdenum alloys. The increase in cracking susceptibility was said to be related to a decrease in the rate of stress relaxation in a similar fashion to that experienced in the Cr-Mo alloys previously studied. The decrease in the rate of stress relaxation due to a vanadium addition has been suggested to be brought about by the precipitation of vanadium carbides in addition to molybdenum carbides. Ito and Nakanishi[8] found that cracking in the Y-groove restraint test increased from 0–95% as vanadium was increased from 0–0.08%. They also showed that the

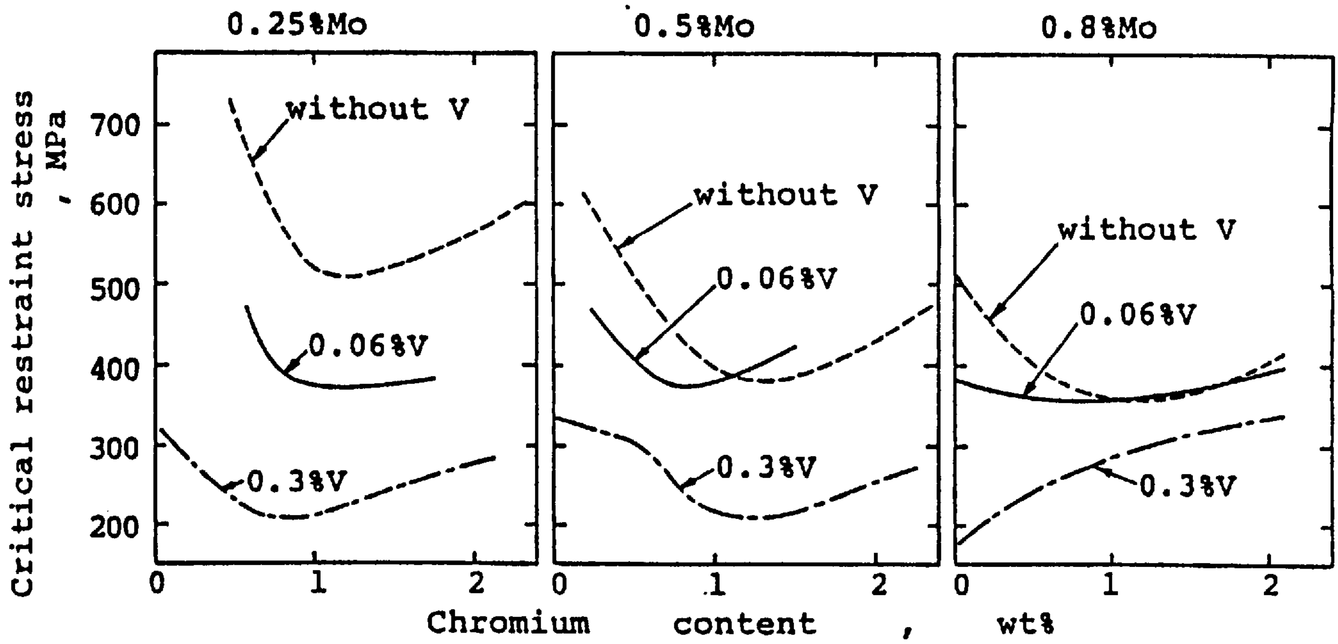

Fig. A15—Effect of vanadium additions on the critical restraint stress, $\sigma_{AW\text{-}crit}$ of Cr-Mo steels. Source: Tamaki, K., Suzuki, J. and Kojima, M., "Combined Influence of Chromium, Molybdenum and Vanadium on Reheat Cracking of Steels," IIW Document Ix-1518-88 base composition was important, in that no cracking was observed for several steels with up to 0.14% vanadium.

Fractographic examination of PWHT cracks in CrMoV steel (0.37% Cr, 0.56% Mo, 0.29% V) conducted by Boniszewski and Eaton[32] revealed that the grain boundary cavities were faceted and contained V_4C_3 type particles 200–600Å in diameter. This suggests a heterogeneous cavity nucleation mechanism. Nonmetallic inclusions were not found to be associated with cavity nucleation.

Effect of Nickel. Nickel is one element that appears to have the least detrimental effect on the Cr-Mo alloys with respect to SRC/PWHT cracking susceptibility. In establishment of the ΔG parameter nickel was varied between 0–3.4% without increasing susceptibility to cracking.[55] The same is true of the P_{SR} parameter where nickel was varied between 0–1.5%.[8] Thus nickel does not appear in either cracking susceptibility parameter. Tamaki and Suzuki[65] found that a nickel content below 1.5% had no effect on the critical stress to fracture but that above 1.5% nickel content greatly increased cracking susceptibility.

The effect of nickel is probably related to the fact that nickel alters the kinetics of carbide precipitation. In a study of the tempering characteristics of 3Cr-1½Mo-Ni alloys, Ritchie *et al.*[73] found that $M_{23}C_6$ replaces M_2C, M_3C and M_7C_3 after only one half hour at 1290°F (700°C) as compared to 400 hours for 2¼Cr-1Mo. In accordance with Tamaki's model,[67] carbides that cause the greatest strengthening of the matrix would form while the overall strength of the grain boundaries is high and before significant embrittlement could occur. The rapid formation of carbides at lower temperatures and the probable very short times of coherency would result in the lowering of SRC/PWHT cracking susceptibility.

Effect of Manganese and Silicon. The effect of manganese on the susceptibility to SRC/PWHT cracking is controversial. A high manganese-to-silicon ratio has been observed to decrease susceptibility of 2¼Cr-1Mo SA weld metal to PWHT cracking.[74] When the Mn:Si ratio was increased from 2.5 to 4, accelerated stress rupture tests revealed a fourfold increase in the elongation and a twofold increase in the reduction in area. Mullery and Cadman[46] found lower cracking susceptibility with increased manganese in CrMoV steels. However, according to Bodnar *et al.*[75] and Weng and McMahon[76] manganese cosegregates with phosphorus to prior austenite grain boundaries and thus manganese is also a potent embrittling element reducing intergranular fracture strength.

In nickel-bearing steels, silicon behaves as an embrittling element and cosegregates with nickel to prior austenite grain boundaries. In low nickel or nickel-free steels, silicon promotes segregation of phosphorus to austenite boundaries. Boniszewski[62] states the effect of silicon reduction is an increase in ductility and a lower cracking susceptibility. Vinckier[74] found that silicon has been reported to enhance Mo_2C formation in Cr-Mo materials.[70,77] Ratliff and Brown[78] state that increased silicon appears to enhance cementite dissolution and thereby precipitation of alloy carbides containing chromium, molybdenum and vanadium resulting in increased secondary strengthening which ultimately impairs stress rupture ductility. According to Yu[79] silicon appears to accelerate the precipitation of Mo_2C type carbides in 2¼Cr-1Mo steel.

Effect of Titanium. Titanium in steel is used as an alloying element in addition to its role as a deoxidizer and grain refiner. Research on the effects of titanium on SRC/PWHT cracking susceptibility have had mixed results. When titanium has been added for deoxidation purposes (Meyers,[80] 0.016–0.055% and Harris and Jones,[81] 0.021–0.030%) cracking susceptibility was reported to diminish in comparison to the same material deoxidized with other elements, particularly aluminum. Spaeder and Plodder[82] found that addition of 0.048% titanium to T-1 steel did not increase susceptibility while Ito and Nakanishi[8] found that additions of 0.03–0.07% titanium in 1Cr-½Mo alloys slightly increased susceptibility. Tamaki and Suzuki[64] found that the addition of a small amount of titanium, 0.07%, increased the critical stress to fracture in low chromium high molybdenum alloys. Harris[83] pointed out that, while small amounts of titanium may appear beneficial, larger amounts as deliberate alloying additions may increase cracking susceptibility due to matrix strengthening.

Effect of Niobium. The effect of niobium has not been investigated extensively in the constructional and ferritic creep resisting alloys, probably because it is not commonly used in many of the steels. However, the work of Ito and Nakanishi[8] shows that niobium in the range of 0.06–0.10% can have a strong detrimental effect in 1Cr-½Mo alloys. From a study to determine the effect of niobium and vanadium in 2¼Cr-1Mo steel[70,84] it was found that a steel with niobium (0.013%) and vanadium (0.005%) resisted PWHT cracking whereas another heat (Nb, 0.001%, V, 0.108%) exhibited cracking susceptibility in the Y-groove test.

Effect of Aluminum, Nitrogen and Boron. The presence of aluminum, used as a deoxidizer and grain refiner in Cr-Mo steels, has been found to enhance SRC/PWHT cracking susceptibility.[49,81] Meyers[80] found that increasing amounts of aluminum, up to 0.035%, used for deoxidation progressively lowered resistance to cracking in a ½Cr-½Mo-¼V alloy. Aluminum was thought to prevent grain boundary mobility by the presence of aluminum-nitrogen precipitate clusters rendering the grain boundaries unable to recrystallize local regions of strain induced shear. Ratliff and Brown[78] found that when aluminum content exceeded 0.010% in a 1Cr-½Mo-¼V alloy a marked degradation in stress rupture properties occurred. Viswanathan and Beck[85] have suggested that presence of aluminum in solid solution in CrMoV steel reduces the rupture ductility due to increased precipitation of vanadium carbides. Aluminum was proposed to reduce the stability of cementite thereby enhancing the formation of Mo_2C and V_4C_3. Edwards *et al.*[44] found segregation of aluminum, silicon and nitrogen occurred at the grain boundaries by Auger spectroscopy. They speculated that if the combined aluminum and silicon concentration exceeded the austenite solubility, formation of ferrite at the grain boundaries could result and cause the rejection of carbon and the creation of a soft, carbide denuded region.

Several researchers have found that the combination of boron and aluminum was particularly detrimental in promoting cracking.[5,44,49] Presser and McPherson[49,86] speculated that aluminum scavenges nitrogen, allowing boron to remain in solution and segregate to the grain boundaries. Boron, when segregated to the grain boundaries, forms $M_{23}(C,B)_6$ when held between 1100–1650°F (600–900°C) during cooling and upon reheating above 1200°F (659°C) results in de-embrittlement. Presser and McPherson[49,86] also speculated that other strong nitride formers such as titanium or zirconium could enhance embrittlement due to boron. Boron alone has been reported to cause a slight increase in cracking susceptibility.[15,43,49,86] However, Paju and Moller[87] suggest that boron reduces grain boundary embrittlement induced by phosphorus segregation during austenitization. This is due to boron occupying the grain boundary sites in preference to phosphorus.

Effect of Copper. Copper has been found to increase the HAZ SRC/PWHT cracking susceptibility of steels. Ito and Nakanishi[8] noted increased cracking as copper was increased to about 1% and Harris and Jones[81] report that higher-than-usual Cu + Sn trace levels significantly affect cracking in steels that represent a variety of deoxidation practices. Copper was also reported to increase susceptibility in ½Cr-½Mo-¼V alloy.[57,62] Konosu and Maeda[126] have found an increase in the susceptibility to creep embrittlement in the HAZ at 1022°F (550°C) when the copper content was raised to 0.2% in 1¼Cr-½Mo steel.

Copper also has a deleterious effect in promoting weld metal SRC/PWHT cracking. Hunter[88,89] and Wolstenholme[90] found a direct correlation between weld metal copper content in 2¼Cr-1Mo and cracking susceptibility. This susceptibility increased with increasing copper content. However, at a given copper content, weld metal deposited with a basic agglomerated flux was not as extensively embrittled as that deposited under less basic fused flux.

Effect of Carbon. Since carbide formation is involved in all elevated temperature phenomena, carbon obviously plays an important role in SRC/PWHT cracking. Few researchers seem to have paid any significant attention to the influence of carbon and thus carbon has not appeared in the crack susceptibility parameters. However, remember that carbon in solid solution is known to increase intergranular cohesion.[76] Dolet *et al.*[74] have determined that increasing carbon decreases ductility at 1112°F (600°C) for a steel with the same ΔG parameter. In an investigation of Cr-Mo steels with two vanadium levels, Ito and Nakanishi[8] found that cracking increased markedly as carbon was increased from 0.05–0.10% but was not changed by further increase to 0.25%.

Auger analysis of grain boundaries in an Fe-Ti-P alloy has shown that both titanium and phosphorus segregate to the grain boundaries.[94] An addition of 0.025% carbon in an Fe-0.26Ti-0.04P alloy showed 2.5 times more phosphorus at the grain boundaries than the alloy without carbon. Tamaki and Suzuki[95] have also suggested an increase in phosphorus segregation with an increase in carbon content.

Effect of Tramp Elements. Tramp elements have also been reported to affect SRC/PWHT cracking susceptibility. According to Drinnan *et al.* an increase in total percentage of trace elements (P + Cu + Sn + Sb + As) times a factor (considering the grain size) from 0.5–1.3 resulted in an increase in the percentage of cracking from 0–100%.

Tin was reported to increase susceptibility in ½Cr-½Mo-¼V.[81] Townsend[83] reported that the addition of tin to ½Cr-½Mo-¼V significantly lowered ductility in weld-simulated specimens. However, Meyers[80] determined that tin additions decreased susceptibility in ½Cr-½Mo-¼V while both copper and antimony additions increased cracking susceptibility.

Among the residual elements, phosphorus is the most potent in embrittling the grain boundaries and therefore in enhancing SRC/PWHT cracking susceptibility. Tamaki *et al.*[95] have found that the solubility of phosphorus in ferrite and austenite decreases markedly upon addition of chromium and molybdenum. Thus, chromium and molybdenum can enhance the segregation of phosphorus to grain boundaries and can even cause phosphide precipitation at grain boundaries. Auger analysis of fracture surfaces has provided significant evidence of phosphorus segregation in many studies.[51,58,76,77,96–99] Phosphorus segregation has been reported to be affected by carbide formation and element interaction,[51,77,99–102] microstructure,[100,102] and grain size.[100] Wilkinson *et al.*[103] have suggested that phosphorus, when segregated to prior austenite grain boundaries, enhances nucleation of cavities.

Phosphorus has been reported by Yu and McMahon,[77,99] Hippsley *et al.*,[51,101] Wada *et al.*[104] and Eyre *et al.*[100] to interact with molybdenum in solution in the matrix. Molybdenum in solution scavenges or ties up phosphorus in the form of Mo-P clusters or compounds preventing the segregation of phosphorus to the grain boundaries. Precipitation of Mo_2C during heat treatment releases phosphorus allowing segregation to the grain boundaries to occur. It has been suggested that the change in phosphorus concentration in ferrite is closely related to the formation of M_2C carbides.

Silicon enhances the formation of Mo_2C and has been reported to have a repulsive interaction with phosphorus similar to one that occurs with carbon. Silicon content was also shown by Auger analysis to be lower at the grain boundaries than within the grains.[77,99] Thus, silicon would appear to enhance grain boundary embrittlement by phosphorus.

Precipitation of alloy carbides has also been reported to decrease the activity of carbon in solution thus allowing greater phosphorus segregation.[98,100] The precipitation of molybdenum-rich carbides increases the relative amount of chromium in solution and appears to enhance phosphorus segregation through Cr-P cosegregation.[77,99,102] Also, the formation of carbides in the grain boundaries results in the rejection of phosphorus to the grain boundaries as phosphorus solubility in the carbides is less than the solubility in the matrix.[51,100,101]

Viswanathan and Joshi[105] and Eyre *et al.*[100] have found that phosphorus segregation is greater in martensitic microstructures than in bainitic microstructures. Viswanathan and Joshi[105] also reported that segregation increased with increasing hardness for a given microstructure in a 1¼Cr-½Mo-0.3V material. Eyre *et al.*[100] demonstrated that grain size also affected embrittlement in that increased grain size decreases the area available for segregation.

Tamaki also undertook a study of the effect of phosphorus in Cr-Mo alloys.[64,66,95,106] Several notable results were obtained from Tamaki's study.

1. Plots similar to those of Figs. A8 and A9 but made for alloys low in phosphorus (0.010–0.013%) and high in phosphorus (0.016–0.020%) showed that increased phosphorus moved the critical stress curve to lower molybdenum contents.
2. Phosphorus had already segregated, to some extent, in the HAZ during the weld thermal cycle.
3. For a particular alloy there exists a critical phosphorus level below which embrittlement is not apparent. The minimum critical value of phosphorus of 0.008% coincides with the 1Cr-½Mo composition.
4. For the range of alloys tested, (0–2%Cr, 0.5%Mo), as long as the phosphorus content was below a critical value for a particular alloy, the critical stress level remained approximately the same.

Thus, phosphorus did adversely affect the cracking susceptibility of the Cr-Mo alloys.

Tamaki surmised that the transformation to austenite played a vigorous role in the segregation of phosphorus as phosphorus did not segregate in materials subjected to heat treatment below the A_1 temperature but did segregate when heat treated in the austenite region. It was assumed that the equilibrium distribution of phosphorus was established at the ferrite/austenite interface during the course of transformation and that the diffusion rate is so low that it diffuses little from the ferrite/austenite interface.[95] These assumptions, combined with the knowledge that the solubility of phosphorus is approximately 2½ times greater in ferrite than in austenite, led Tamaki to conclude that phosphorus was carried along on the ferrite/austenite interface. This interface, which is the prior austenite grain boundary on cooling, is therefore enriched with the phosphoruous. The welding cycle thus initiates the segregation and embrittling processes.

An Auger electron spectroscopic study[94] revealed that grain boundary concentration of phosphorus was much lower in the Fe-C-P alloy than in the Fe-Cr-C-P alloy thus indicating that the addition of chromium to an Fe-C-P alloy considerably enhances grain boundary segregation of phosphorus. This is probably due to the fact that addition of chromium decreases the activity of carbon in Fe-Cr-C-P alloy thus influencing the segregation of phosphorus to grain boundaries.

Sulfur is another residual element that has been found to segregate on fracture surfaces by Auger analysis.[97,98,107] The segregation of sulfur is associated with dislocation tangles along the boundaries generated by impurity penetration.[108,109] Thus, impurity segregation to grain boundaries may be associated with the formation of dislocation tangles with which the impurities become interlocked. Such a grain boundary state will be conducive to sliding, will inhibit migration and thus cavity nucleation at suitable particles may occur. Further, the adsorption of embrittling elements on a cavity surface would have a stabilizing effect.

Imanaka *et al.*[61] and a study at Kawasaki Steel Corporation[84] of the effects of sulfur, rare earth metal (REM) and calcium additions in 2¼Cr-1Mo found that if free sulfur exceeded 25 ppm the material showed a high sensitivity to SRC/PWHT cracking but below 25 ppm exhibited no susceptibility. Free sulfur was calculated by the equation:

$$(\mathrm{S}) = [\%\mathrm{S} - (32/40)\ \%\ \mathrm{Ca} - (32/140)\ \%\ \mathrm{REM}] \times 10^4\ \mathrm{ppm}.$$

Ladle calcium treatments appear to improve susceptibility to SRC/PWHT cracking. Lundin *et al.*[110] have also found low susceptibility in a heat of modified 2¼Cr-1Mo steel treated with calcium compared to heats of similar composition not treated with calcium. Nikhitin and Kreshchanovsky[32] found that treatment of molten CrMoV steel with $BaCl_2$ and NaCl improved ductility and toughness and at the same time rendered the prior austenite grain boundaries resistant to etching.

Sulfur in the form of grain boundary sulfides has been linked with the initiation of cavitation on the grain boundaries.[58,111,112] Middleton and Fujii *et al.*[113] have suggested that submicron ($\sim 0.1\ \mu m$) α-MnS inclusions at prior austenite boundaries in HAZ regions could act as nucleation sites for cavitation in CrMoV steels. Similar observations were also made by Hippsley *et al.*[58,101] on 2¼Cr-1Mo steels. Ayres *et al.*[48] also report that MnS inclusions are responsible for SRC/PWHT cracking due to liquation. Thus, the cracking susceptibility is increased with increase in energy input and a decrease in Mn/S ratio especially at higher carbon levels. However, it is generally believed that while liquation cracks may help to initiate SRC/PWHT cracks, their presence is not a requirement for the formation of cracks.

Hippsley *et al.*[58,111] have shown that at PWHT temperatures in excess of 1110°F (600°C), materials susceptible to cracking exhibit a change from smooth intergranular fracture surfaces to fracture surfaces with extensive intergranular microvoid coalescence. The microvoids were said to have nucleated on sulfides which were thought to have low interfacial strength with the matrix. The presence of sulfides was thought to be the result of solution of MnS during the thermal cycle and subsequent preferential reprecipitation at grain boundary sites during cooling. Shin and McMahon[114] and Hippsley *et al.*[115,117] have also suggested stress induced segregation of sulfur to the grain boundaries ahead of the crack tip region during stress relief by grain boundary diffusion and also sulfide dissolution resulting in low crack growth energy requirements.

However, Dolby[112] reports that the relationship between grain boundary particles and SRC/PWHT cracking is unclear in that some researchers have found that grain boundary particles have no effect on cracking. Further, both Horn and Kunze[98] and Kikuchi and Nakao[97] have found that even in relatively high sulfur materials a reduction in the phosphorus content eliminated cracking in susceptible materials. Thus, the effect of sulfur is apparently minor in comparison to that of phosphorus.

Sun *et al.*,[107] in a study of ultra pure heats of A 508-2 type steel with controlled addition of various impurities, conclude that A 508-2 steel normally susceptible to SRC/PWHT cracking, a very high resistance to cracking was evident in high purity laboratory heat. Thus, SRC/PWHT cracking depends on trace impurities. They found that boron (2 ppm) increased susceptibility markedly even when the sulfur level was 10 ppm. They also suggest that in the presence of boron and sulfur, phosphorus additions decreased cracking susceptibility, which is generally considered to be contradictory to the popular belief.

In their study to investigate the PWHT cracking susceptibility of 2¼Cr-1Mo and ½Cr-Mo-V steel Batte and Murphy[118] conclude that by an appropriate choice of welding process and parameters PWHT cracking can be prevented. According to them it is unnecessary to reduce the residual element content below the levels generally obtained in current low-alloy steelmaking practice.

In summary, it is evident that composition is probably the most significant factor in SRC/PWHT cracking of the Cr-Mo alloys. Of the alloying elements, molybdenum and vanadium have the greatest effect due to the preferential formation of coherent or fine precipitates in the grain matrix which significantly increases the flow strength of the grain matrix over that of the grain boundaries. Of the residual elements, phosphorus has the greatest effect due to segregation to and embrittlement of the grain boundaries. The effect of composition is complicated by precipitation kinetics, element interactions and the superposition of the effects of other elements such as sulfur, titanium, tin and copper.

Testing Techniques for SRC/PWHT Cracking

To determine the susceptibility to SRC/PWHT cracking of a certain steel, a suitable test must be chosen or developed.[48,74] Preferably the specimen should incorporate a welded joint similar to, and made with the same heat inputs as, the joints used in the structure. Furthermore, the thermal treatment should duplicate as closely as possible the PWHT/service exposure. The complex interactions of residual stress and strain, their magnitude and distribution, triaxiality and relaxation together with the progressively changing microstructures during PWHT or service can hardly be integrated in a small weld sample. Baker[83] has enumerated some of the factors that should be included for the ideal PWHT cracking test. The specimen should include some defect or notch in a microstructure representative of the actual HAZ. The HAZ should be strained in a manner similar to that experienced in an actual weld. Finally, the test method employed should preferably incorporate stress relaxation since constant load testing may introduce misleading factors into the evaluation. Dhooge *et al.*[48] note that the incorporation of all the factors involved in an actual weld into a small specimen would be difficult.

A common theme among papers reviewing SRC/PWHT cracking is that there exists a multitude of tests that have been employed and therefore comparison of test results is difficult and sometimes confusing.[41,47,48,74] Dhooge *et al.*[48] cite the use of 26 different testing techniques prior to 1978. In order to simplify the overall number of tests three categories were proposed to classify the tests.

A. *Tests on complete weldments*
    (1) Lehigh restraint test
    (2) Restrained fillet weld test
    (3) Y-groove test
    (4) Stellite bead test
    (5) BWRA ring test
    (6) Steampipe butt-weld test
    (7) H-type restraint test
    (8) Circular patch restraint test
    (9) Strained root bead test
    (10) Restrained butt weld test
    (11) MRT test
    (12) NRC Regulatory Guide cladding test
B. *Tests on specimens containing a weld*
    (1) Jigged stress relaxation test
    (2) Isothermal constant load rupture test

   (3) Implant test
   (4) Controlled heating rate, constant load test
   (5) Vinckier test, Stainless backing bar test

C. *Tests on specimens containing a thermally simulated HAZ*
   (1) Isothermal stress relaxation test
   (2) Isothermal constant load rupture test
   (3) Isothermal slow strain rate tensile test
   (4) Controlled heating rate stress relaxation test
   (5) Controlled heating rate constant load test
   (6) Stainless sleeve test
   (7) Pre-cracked bend test
   (8) Slit tube test
   (9) Jigged stress relaxation test

Meitzner[41] in 1975 separated tests into only two categories: direct weldment tests (those containing an actual weld or portions of an actual weld) and simulated weld tests. Vinckier[47,74] in 1974 used three categories to divide some 17 different testing techniques.

1. Tests of a welded specimen: Specimens are welded with various degrees of restraint which depends on specimen geometry and subjected to PWHT followed by metallographic examination for cracks.
2. Tensile tests at high temperatures on welded or simulated specimens: The various parameters used to rank the susceptibility of materials in such tests are the rupture time, stress, reduction in area, elongation, etc.
3. Simulation of the PWHT cycle on simulated specimens: Time to rupture, temperature at failure, stress, reduction in area, etc. are the criteria in these tests to rank the susceptibility of materials.

The use of tests on complete weldments or direct weldment tests have the obvious advantage of being directly related to the actual weld and PWHT/service conditions as well as joint geometry. However, both Meitzner[41] and Dhooge *et al.*[48] note that reproducibility is a significant problem with Meitzner citing erratic results in which one specimen may crack extensively while another may not crack at all. Also, a small test specimen will experience a significantly smaller amount of creep strain than a large welded structure.[41,74]

Weld simulation tests have the advantage of reproducibility, known stress level and control of microstructure.[6,41] In simulated specimens it is also possible to locate accurately a notch in a well defined microstructure and that a number of such specimens can be reproduced. The disadvantages are that the strains associated with weld contractional stresses are not duplicated and in general, only one region of the HAZ is tested and the effects of adjacent weld metal and base metal are not present.[41,48] Therefore, the results of simulation tests must be evaluated carefully before being directly applied to full scale weldments.

Although no standard exists the most popular type of test is the tensile or stress rupture test.[48] Several means of evaluating this type of test have been proposed. Vinckier[6] suggested that in hot tensile tests the minimum acceptable reduction in area for an alloy to be considered not susceptible to cracking was 20%. Meyers and Price[119] suggested that, in constant load stress rupture testing HAZ, base metal and weld metal rupture strengths be compared. If the HAZ rupture strength was lower than the base metal and weld metal strength, the material was to be considered susceptible and the greater the difference the greater the susceptibility. Spaeder and Plodder[82] have proposed a stress rupture parameter in which the reduction in area was multiplied by the stress to rupture in 10 min. If the stress rupture parameter was less than 15×10^4 the material was determined susceptible to cracking. Vinckier and Pense[48,74] in extensive Gleeble simulation have determined the following criteria for simulated PWHT at 1110°F (600°C):

1. extremely susceptible if the reduction in area is less than 5% and peak temperature of the weld simulation exceeds 2190°F (1200°C);
2. highly susceptible if the reduction in area is below 10% and peak temperature exceeds 2370°F (1300°C);
3. slightly susceptible if the reduction in area is below 15% and the peak temperature exceeds 2460°F (1350°C); and
4. not susceptible if the reduction in area exceeds 20% at all peak temperatures.

Thus, tensile type or stress rupture tests have been shown to yield a general determination as to the susceptibility of a material to PWHT cracking and allow a ranking of various materials to be determined.[41]

In accordance with the factors enumerated by Baker[83] Lundin *et al.*[91,110,133] have developed a C-ring test that appears to incorporate all the factors for an ideal PWHT cracking test. For this test a square bar (1 in. × 1 in.) is machined with a flat bottomed groove at the center of one of the faces parallel to the plate surface. The groove geometry can be modified in order to accommodate different diameter SMAW electrodes. A single pass SMA weld metal of matching chemistry is used to fill the groove. The bar is then machined into hollow cylinder (1 in. outside diameter, wall thickness 0.125 in.). The cylinder is then sliced to obtain pieces 0.75 in. long. A V-notch is then broached in the CGHAZ and holes drilled at 90° from the notch axis. The back of the ring opposite to the notch is removed in order to allow compression of the ring by tightening of a bolt placed through the drilled holes. The rings are then stressed by tightening the bolt (an equation was developed to relate the reduction in diameter due to tightening the bolt and stress at the root of the notch) and postweld heat treated. To determine cracking the specimen is metallographically or fractographically examined after the test.

Thus, this test includes a weld, a discontinuity and stress relaxation during PWHT similar to that experienced in a weldment. In addition, this test is simple and requires no special equipment. They found that the results of this test correlated well with the Gleeble simulation test results in terms of ranking heats according to PWHT cracking susceptibility.

Another test developed at the University of Tennessee is the Spiral Notch Test. This test has been found to be very useful in evaluating a controlled deposition techniques in HSLA steel for successful prediction of in-service behavior. This test is described in detail in the following chapters.

The ideal test described by Baker[83] can perhaps be accomplished by the use of two or more tests that make more efficient use of materials and funds. Utilizing Gleeble simulation to make an initial ranking of a material's SRC/PWHT cracking susceptibility will determine if further testing is indicated. If the material is deemed susceptible to cracking further testing may be employed with specimens incorporating a weld or full scale weldments to determine if the material is susceptible under welding conditions employed in actual weldment fabrication.

Ways to Mitigate SRC/PWHT Cracking

The most obvious remedy for SRC/PWHT cracking, as suggested by Stout,[120] is to avoid the use of susceptible alloys. Murray[26] has recommended the use of alloys with limited molybdenum and vanadium. Mullary and Cadman[46] have recommended the use of materials in which the sulfur, phosphorus, and vanadium contents are minimized and manganese content is increased.

When the avoidance of susceptible alloys is not practical, process changes may be beneficial. Murray[26] and Pense *et al.*[56] have recommended using a low strength weld metal with high strength base metals to allow deformation to occur in the fusion zone rather than in the HAZ. Mullary and Cadman[46] have proposed buttering susceptible alloys to promote the formation of coarser carbides in the CGHAZ of the parent material. Muraki *et al.*[60] have suggested preferential welding of the larger side of unsymmetric, double-V grove butt joints.

Increasing heat input or preheat has been seen to bring about favorable microstructural changes in the HAZ.[56,60,83,121] Higher energy inputs and preheating results in slower cooling rates and softer transformation products.[120] Overaging of carbides in the HAZ during cooling,[8] or an autostress relief.[36] Preheating may also be beneficial in decreasing the temperature range over which internal stresses build up.[122] However, Vinckier[6] reported that higher heat input yielded mixed results. Higher heat input causes two competing effects to occur: a coarser grain structure results which increases intergranular embrittlement and a softer HAZ is formed which decreases intergranular embrittlement.

An alternative to increasing heat input is to decrease heat input in multiple pass welds. Miller and Batte[59] found that using small gas tungsten arc weld beads in a multiple pass weld increased the amount of grain refinement due to overlapping of the HAZs and that even highly susceptible materials could be welded with this technique with no evidence of cracking after PWHT. Similarly, the use of temper beads, small stringer beads placed over the last pass to refine the grain structure of the HAZ, have been found to benefit in eliminating stress relief cracking.[6]

Complete austenitization after welding[6,123] or normalizing[30,47] has been seen to increase the HAZ toughness and prevent cracking. Bentley[40] recommended using high PWHT temperatures and high heating rates to avoid prolonged coherent precipitate formation. Debiez and Granjon[30] also found that increasing the heating rate is effectual in reducing the risk of cracking. However, Hippsley[124] and Debeiz and Granjon[30] also indicate that high heating rates produce marginal benefits in reducing cracking but speculated that high heating rates might exacerbate cracking in actual weldments due to the introduction of additional tension stresses due to temperature gradient. Kanazawa *et al.*[121] have found no effect with a heating rate from 80°C/hour–400°C/hour on PWHT cracking susceptibility. Ueda[123] has suggested the use of higher temperature and longer time PWHT for the prevention of grain boundary embrittlement.

Weld dressing to remove discontinuities at weld toes has been found effective in reducing cracking by elimination of crack initiation sites.[26,46,60,120] Peening has also been suggested to eliminate residual tensile stresses at the surface of the weld.[120] Weld stresses can also be reduced by attention to weld sequencing, the use of techniques such as backstepping, the use of interstage PWHT, and simplification of the design of weldments to lower overall levels of restraint.[26]

Thus, it may be possible to mitigate SRC/PWHT cracking in susceptible alloys by utilizing the techniques described above. Perhaps the most economical means is to eliminate stress risers through careful dressing of the surface of the weld. If performed correctly, temper beading combined with weld dressing should provide a microstructure and surface unfavorable to the initiation and propagation of cracks. One important factor however, is that oxidation during PWHT/service may provide initiation sites by oxide penetration and wedging along grain boundaries.[30] Therefore inherently susceptible materials may not be prevented from cracking by simple measures and it becomes necessary to know the susceptibility of individual alloys to SRC/PWHT cracking in order to ascertain the usefulness of preventive measures.

Vinckier[6] has recommended the following checks if susceptible steels are to be used and thermal stress relieving must be carried out.

1. Tensile tests should be carried out at PWHT temperatures on weld simulation specimens

heated to 2462°F (1350°C). A minimum ductility of 20% reduction in area should be required.

2. The design should be checked to avoid as much as possible built in stress raisers and to allow adequate nondestructive inspection of all joints.
3. By modifying the welding procedure (weld dressing, temper beads, raising preheat temperature, etc.) cracking in susceptible microstructures can sometimes be avoided.
4. Careful nondestructive inspection should take place after stress relieving the structure and again after final pressure testing.

The complexity of SRC/PWHT cracking is demonstrated in Fig. A16 by the interrelationship of the many factors. As has been shown previously the superposition of several factors may result in the occurrence of cracking but when the same factors are considered alone cracking may not occur.

From the review presented thus far one very important point is that SRC/PWHT cracking susceptibility of a steel is a complex interaction of variables such as composition, residual element levels, welding parameters, joint design, etc. In addition, there are other factors to be taken into account such as the persistence of Mo_2C carbides or other similar carbides of vanadium, titanium and niobium that are in coherence with the matrix. Thus, higher chromium steels such as 5Cr and 9Cr steels even with high levels of residual elements are not susceptible since the carbides that form during PWHT/service do not cause secondary strengthening. Other factors are austenite grain growth and the extent of carbide dissolution during HAZ thermal excursion. For example, in case of incomplete dissolution of carbides it is possible that during PWHT/service additional carbides precipitate on the preexisting carbides such that there is no significant secondary hardening or it may be possible that secondary hardening behavior is completely eliminated. Thus, it is not possible to rate a steel or a heat of steel as susceptible based on the composition or tramp element concentration alone. According to many researchers it is possible to weld any steel without SRC/PWHT cracking if proper design and welding procedures are followed and that it is unnecessary to reduce the level of impurity elements below the levels that are achieved today with good steelmaking practices.

Creep Embrittlement/Stress Rupture Cracking

A variety of Cr-Mo steels operating in the temperature range of 850–1050°F (450–565°C) show low ductility intergranular failure similar to that seen in the case of PWHT cracking.[4,31,37,63,125–130] The term creep embrittlement has been used to describe this behavior. It has been suggested that creep embrittlement occurs when hardening mechanisms within the grains prevent relaxation of stress such that grain boundary sliding occurs. It is apparent that PWHT may not be adequate to relax the residual welding stresses and stabilize the microstructure so that microstructural evolution in the HAZ can be in progress at the operating temperature. System stresses and residual stresses can thus cause creep embrittlement/stress rupture cracking (SRC).

However, creep embrittlement should not be confused with temper embrittlement which is a loss in toughness associated with a shift in the transition temperature. The toughness is not necessarily low at the operating temperature in a temper embrittled material. Also, temper embrittlement is reversible unlike creep embrittlement. In a creep embrittled material the tensile ductility or fracture toughness may be adequate at ambient temperatures. It is only at elevated temperatures that a creep embrittled material shows low ductility intergranular fracture.

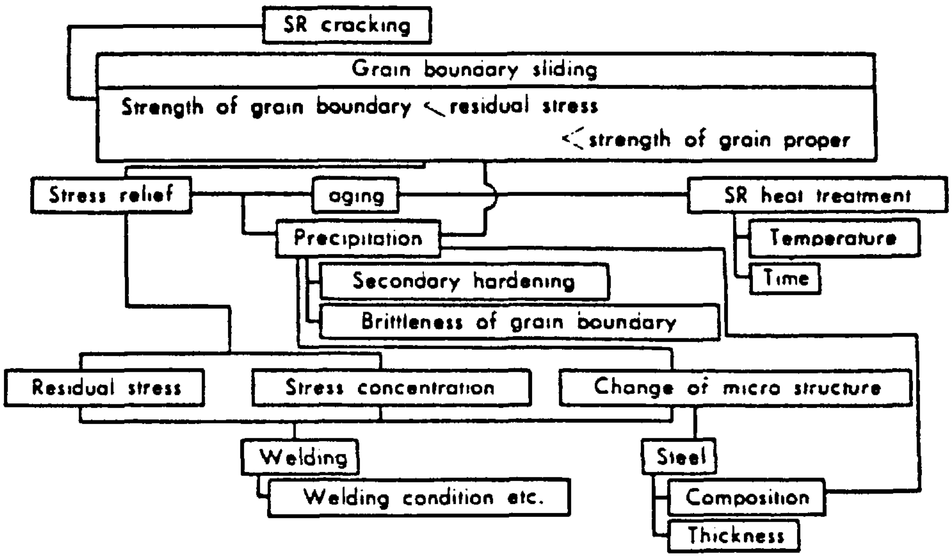

Fig. A16—Block diagram showing factors involved in stress relief cracking. Source: Ito, Y. and Nakanishi, M., "Study on Stress Relief Cracking in Welding Low Alloy Steels," The Sumitomo Search No. 7, May 1972, pp. 27–36

The term creep embrittlement as described by various researchers diverges somewhat depending on their particular experimental method of study or other circumstances. Some investigators apply the term creep embrittlement to stress rupture notch sensitivity, while some are describing actual observable creep damage (e.g., voids). Some researchers have used this term to describe simply low ductility creep failures (i.e., stress rupture cracking (SRC)). Such embrittlement may be due to weakened grain boundaries caused by either precipitation hardening of the grain interiors or by deleterious grain boundary segregates or both. Although creep embrittlement is a phenomenon that normally occurs in-service and is associated with metallurgical changes over time at operating temperature, it is important to remember that all microstructural changes occurring in Cr-Mo steels during service are not necessarily detrimental.

Emmer *et al.*[130] have suggested the following characteristics of creep embrittlement and parenthetical portions of the following are added to show the relevance to the HAZ.

1. Creep embrittlement is dependent on the strength level of the matrix, but is expected to be more severe for materials with high (> 110 ksi) tensile strength. (In Cr-Mo steels the coarse grained region of the HAZ in the as-welded condition exhibits tensile strength usually in excess of 200 ksi.)
2. Creep embrittlement is also dependent on grain size, microstructure, and austenitizing temperatures. A coarse grained material is more susceptible than a fine grained material. Use of unnecessarily high austenitizing temperatures tends to accentuate creep embrittlement. (In the HAZ close to the fusion boundary where the peak temperature experienced is of the order of the melting temperature of the alloy, grain growth cannot be avoided. Thus, in this region the combination of the high austenitizing temperature and coarser grain size presents ideal situations for susceptibility to creep embrittlement.)
3. Creep embrittlement can be most severe under conditions that permit small amounts of creep strain to occur over long periods of time. While creep embrittlement may occur in the temperature range 800–1100°F (425–595°C) it is more severe at lower temperatures. (The situation is even more complicated in welded structures. Different weld configurations such as nozzle welds, girth welds or longitudinal welds presents different degrees of restraint and residual stress states that tend to relax at the operating temperature. In addition, during start up and shut down cycles additional stresses are introduced into the structure. Because of the obvious mismatch between the strength levels (creep rate mismatch) of the various regions of the weld and even within the various regions of the HAZ the stress relaxation rates are different. As a result stresses may be concentrated at certain regions, especially in those regions that have higher strength and lower ability to accommodate creep strains to relax because of the low ductility.)
4. Creep embrittlement is manifested by a reduction in stress rupture ductility. When ductility is plotted as a function of time to rupture, there is typically a ductility minimum and then, with increasing time, an increase in rupture ductility. (In welded structures in addition to strength mismatch of the various regions as explained above, there is also ductility mismatch. Thus, if the ductility of various regions of welds is plotted as a function of time the ductility minimum in some regions may extend over the entire design life of the component.)

Swift and Rogers[37] have related the phenomenon of creep embrittlement to partially coherent precipitation of Mo_2C carbides that form during PWHT. Otoguro *et al.*[128,131] and Konosu and Maeda[126] have found segregation of antimony, copper and phosphorus at the prior austenite grain boundaries in CGHAZ of creep embrittled 1¼Cr-½Mo and 2¼Cr-1Mo weldments by Auger analysis. They have indicated that creep embrittlement is a premature transition from notch strengthening to weakening. They have also suggested the use of rare earth additions to mitigate this problem. In his study to determine effects of boron, antimony, tin and phosphorus on creep and temper embrittlement of normalized and tempered 1¼Cr-½Mo steel, Viswanathan[127] determined that boron additions cause an appreciable decrease in the rupture ductility compared to additions of large amounts of the other impurities. However, in the case of temper embrittlement the other elements were found to be more detrimental than boron. Nagae and Abe[125] found an increase in the tin and arsenic concentration along the prior austenite grain boundaries in a creep embrittled CGHAZ of a reactor vessel.

Rosenstein[132] has suggested an increase in the PWHT temperature resulting in tempering to a lower strength level to resist creep embrittlement. Ueda *et al.*[123] have also suggested decrease in the amounts of impurities, a full annealing treatment or an increase in the PWHT temperature to improve resistance to creep embrittlement. Konosu and Maeda[126] have found that an increase in the PWHT temperature considerably increased the ductility in small impurity content heats whereas in heats containing large amounts of impurities the effect of increasing PWHT temperature was small. However, a study at the University of Tennessee revealed improvements in short time stress rupture ductility of the CGHAZ if PWHT at higher temperatures even in heats containing higher-than-usual levels of impurities.

In general, little research has been done to determine creep embrittlement behavior in Cr-Mo steels. However, it is apparent that creep embrittlement is similar to PWHT cracking but occurs at lower (operating) temperatures over a longer period of time. If temperature and time dependence of stress relief cracking are considered C-curve as has been pointed out by various researchers, then creep embrittlement can be considered to be a form of PWHT cracking at low temperatures where the intersection with the C-curve is at longer times. Thus, creep embrittlement will most likely occur in structures not properly PWHT or in structures where PWHT has been omitted for various reasons. Thus, stress relaxation continues at the operating temperature and the situation is further worsened by the fact that during operation, system stresses add to the residual stresses.

Summary

From the literature review it is clear that although a significant amount of investigation has been carried out to determine reheat cracking susceptibility of various Cr-Mo, Cr-Mo-V and other pressure vessel steels, little information is available on the mechanism of SRC/PWHT cracking. In addition, conflicting ideas further complicate the available information.

As vanadium, titanium, niobium and boron are being used in the new generation of Cr-Mo alloys, with vanadium known to increase SRC/PWHT cracking susceptibility and the influence of titanium, niobium and boron unknown, it is evident that the susceptibility of these alloys to cracking needs to be investigated further.

It has been recognized that refinement of the prior CGHAZ by a subsequent weld pass improves the reheat cracking resistance of the HAZ in these steels which is usually taken advantage of during controlled deposition welding techniques such as temper-bead or half-bead techniques. However, no quantitative data or microstructural investigation in the published literature is available in this regard.

Therefore, it is necessary that the microstructural changes must be distinguished from segregation effects which may be occurring simultaneously if an understanding of the precise mechanism or mechanisms of reheat cracking is to be achieved.

References to Appendix A

1. "Welding Metallurgy," *Welding Handbook,* 7th Edition, Vol. 1, Chapter 4, American Welding Society, 1982.

2. Luther, G. G., Jackson, C. E., and Hartbower, C. E. "A Review of Weldability Test of Carbon and Low Alloy Steels," *Welding Journal, Research Supplement,* October 1949, pp. 376s–396s.

3. Coe, F. R. "The Avoidance of Hydrogen Cracking in Welding," The Welding Institute, 1973.

4. Erwin, W. E. and Kerr, J. G. "The Use of Quenched and Tempered 2 ¼Cr-1Mo Steel For Thick Wall Reactor Vessels in Petroleum Refinery Processes: An Interpretive Review of 25 Years of Research and Application," *WRC Bulletin 275,* February 1982.

5. McPherson, R. "Compositional Effects on Reheat Cracking of Low-Alloy Ferritic Steels," *Metals Forum,* Vol. 2(3), 1980, pp. 175–186.

6. Vinckier, A. "Use of Weld Simulation Tests to Study Susceptibility to Reheat Cracking," *Proceedings of International Conference on Welding Research Related to Power Plant,* University of Southampton, England, 17–21 September, 1972, pp. 336–355.

7. Weymueller, C. R. "Chrome-Moly Steel Builds Big Vessels," *Welding Design and Fabrication,* July 1983, pp. 47–52.

8. Ito, Y. and Nakanishi, M. "Study on Stress Relief Cracking in Welding Low Alloy Steels," *The Sumitomo Search,* No. 7, May 1972, pp. 27–36.

9. Easterling, K. *Introduction to the Physical Metallurgy of Welding,* Butterworths, Boston, 1983.

10. Harrison, P. L. and Farrar, R. A., "Application of Continuous Cooling Transformation Diagrams for Welding of Steels," *International Materials Reviews,* No. 1, Vol. 34, 1989, pp. 35–51.

11. Lundin, C. D., Richey, M. W., and Henning, J. A. "Transformation, Metallurgical Response and Behavior of the Weld Fusion Zone in Cr-Mo Steels for Fossil Energy Application," Final Technical Report No. ORNL/sub/81-7685/01&77, 1985.

12. Wada, T. and Eldis, G. T. "Transformation Characteristics of 2¼Cr-1Mo Steel," *Application of 2¼Cr-1Mo Steel for Thick-Wall Pressure Vessels, ASTM STP 755,* 1982, pp. 343–362.

13. Habraken, L. J. and Economopoulos, M. "Bainitic Microstructures in Low Carbon Alloy Steels and their Mechanical Properties," *Symposium on Transformation and Hardenability in Steels,* Climax Molybdenum Co., 1967, pp. 69–108.

14. Biss, V. and Cryderman, R. L. "Martensite and Retained Austenite in Hot-Rolled, Low-Carbon Bainitic Steels," *Metallurgical Transactions,* Vol. 2, August 1971, pp. 2267–2276.

15. Thomas, G., Sarikaga, M., Smith, G. D. W., and Barnard, S. J. "Microstructure, Retained Austenite and Mechanical Properties of Experimental 0.3%C Steels," *Proc. Conf. Advances in the Physical Metallurgy and Applications of Steel,* University of Liverpool, 21–24 September, 1981, Metals Society, London, pp. 259–265.

16. Apblett, W. R. Jr., Dunphy, R. P., and Pellini, W. S. "Transformation of Cr-Mo Steels During Welding," *Welding Journal, Research Supplement,* January 1954, pp. 57s–64s.

17. Deb, P., Challenger, K. D., and Burna, R. F. "Microstructural Characterization of Shielded Metal Arc Weldments of a Copper-Bearing HSLA Steel," *Materials Science and Technology,* November 1985, Vol. 1, pp. 1000–1006.

18. American Welding Society, Recommended Practices for Welding of Cr-Mo Steels, *ANSI/AWS D 10.8-86,* AWS, Approved November 18, 1985.

19. Baker, R. G. and Nutting, J. "The Tempering of 2¼%Cr-1%Mo Steel After Quenching and Normalizing," *Journal of Iron and Steel Institute,* July 1959, pp. 257–267.

20. Swindeman, R. W., Thomas, R. D., Nanstad, R. K., and Long, C. J. "Assessment of the need for an Advanced High-Strength Chromium-Molybdenum Steel for Construction of Third-Generation Gasifier Pressure Vessels," ORNL/TM-8873, ORNL Report for DOE Under Contract No. DE-AC05-840R21400, October 1984.

21. Stone, P. G. and Murray, J. D. "Creep Ductility of Cr-Mo-V Steels," *Journal of Iron and Steel Institute,* Vol. 203, November, 1965, pp. 1094–1107.

22. Woodhead, J. H. and Quarrel. "The Role of Carbides in Low-Alloy Creep-Resisting Steels," Climax Molybdenum Company Ltd.

23. Carruthers, R. B. and Collins, M. J. "Carbide Transformations in Microstructurally Unstable Low Alloy Ferritic Steel," *Metal Science,* Vol. 17, March 1983, pp. 107–110.

24. Todd, J. A. "The Early Stages of Tempering in a 3Cr-1.5Mo Steel," *Scripta Metallurgica,* Vol. 20, 1986, pp. 269–274.

25. Buchmayr, B., Cerjak, H., and Fauland, H. P. "The Effect of the Precipitation Behavior on the HAZ-Properties of 1%Cr-Mo-V-Steel," *2nd International Conference on Trends in Welding Research,* Gatlinburg, Tennessee, May 1989.

26. Murray, J. D. "Stress-Relief Cracking in Carbon and Low Alloy Steels," *British Welding Journal,* Vol. 14(8), August 1967, pp. 447–456.

27. Tamaki, K. and Suzuki, J. "Effect of Chromium and Molybdenum on Reheat Cracking Sensitivity of Steels," *Transactions on the Japan Welding Society,* Vol. 14(2), October 1983, pp. 39–43.

28. Vinckier, A. and Dooge, A. "Reheat Cracking in Welded Structures During Stress Relief Heat Treatments," *Journal Of Heat Treating,* Vol. 1(1), ASM, 1979, pp. 72–80.

29. Vinckier, A. and Dooge, A. "Reheat Cracking in Welded Structures During Stress-Relief Heat Treatments," *Proceedings of Conference on Residual Stresses in Welded Constructions and Their Effects,* London, 15–17 November, 1977, Welding Institute, Cambridge, 1978, pp. 375–385.

30. Debiez, S. and Granjon, H. "Work Carried out by the Institut de Soudure on Reheat Cracking," Paper 37 in *Proceedings of Conference on Residual Stresses in Welded Construction and Their Effects,* London, 15–17 November, 1977, Welding Institute, Cambridge, 1978, pp. 231–239.

31. Briant, C. L. and Banerji, S. K. "Intergranular Failure in Steel: The Role of Grain-Boundary Composition," *International Metals Reviews,* No. 4, Review 232, 1978, Vol. 23, pp. 164–199.

32. Boniszewski, T. and Eaton, N. F. "Electron Fractography of Weld-Reheat Cracking in CrMoV Steel," *Metal Science,* Vol. 3, 1969, pp. 103–110.

33. Kanazawa, S., Yamato, K., Takeda, T., and Hasimoto, K. "Study of Reheat Cracking in Weldment (Report 2)—Relation Between Cracking Susceptibility and Some Properties of HAZ at High Temperature," *Transactions of the Japan Welding Society,* Vol. 8(2), September 1977, pp. 39–45.

34. Kanazawa, S., Yamato, K., Takeda, T., and Hasimoto, K. "Study of Reheat Cracking in Weldment (Report 3)—Relation Between Cracking Susceptibility and Some Stress Relaxation Characteristics," *Transactions of the Japan Welding Society,* Vol. 9(1), April 1978, pp. 22–27.

35. Swift, R. A. and Rogers, H. C. "A Critical Review of Weld Metal Embrittlement," *Welding Journal, Research Supplement,* August 1971, pp. 357s–373s.

36. Swift, R. A. "The Mechanism of Stress Relief Cracking in 2¼Cr-1Mo Steel," *Welding Journal, Research Supplement,* May 1971, pp. 195s–200s.

37. Swift, R. A. and Rogers, H. C. "Embrittlement of 2¼Cr-1Mo Steel Weld Metal by Postweld Heat Treatment," *Welding Journal, Research Supplement,* April 1973, pp. 145s–153s.

38. Swift, R. A. "Creep-Rupture Tests on 2¼Cr-1Mo Simulated Heat-Affected Zone," Lukens Steel Company Research Division Report Serial No. RDR69-11, RP1008, June 1969.

39. Orr, J., Beckitt, F. R., and Fawkes, C. D. "The Physical Metallurgy of Cr-Mo Steels for Fast Reactor Boilers," Paper 16 of *Proceedings of Conference on Ferritic Steels for Fast Reactor Steam Generators,* British Nuclear Energy Society, London, 1978, pp. 91–109.

40. Bentley, K. P. "Precipitation During Stress Relief of Welds in Cr-Mo-V Steels," *British Welding Journal,* 11(10), 1964, pp. 507–515.

41. Meitzner, C. F. "Stress-Relief Cracking in Steel Weldments," *WRC Bulletin 211,* November 1975.

42. Nichols, R. W. "Reheat Cracking in Welded Structures," *Welding in the World,* 7(4), 1969, pp. 36–44, *Welding Research Abroad,* March 1970, pp. 36–44.

43. Meitzner, C. F. and Pense, A. W. "Stress-Relief Cracking in Low-

Alloy Steel Weldments," *Welding Journal, Research Supplement,* Vol. 48(10), 1969, pp. 431s–440s.

44. Edwards, R. H., Barbaro, F. J., and Gunn, K. W. "Stress Relief Cracking in Cr-Mo-V Steels," *Metals Forum,* Vol. 5(2), 1982, pp. 119–129.

45. Lundin, C. D. and Khan, K. K. "PWHT Cracking Susceptibility of 2¼Cr-1Mo MPC Materials, Report Submitted to MPC, June 1987.

46. Mullery, F. and Cadman, R. O. L. "Cracking of Welded Joints in Ferritic Heat-Resisting Steels," *British Welding Journal,* April 1962, pp. 212–220.

47. Vinckier, A. and Pense, A. W. "A Review of Underclad Cracking in Pressure-Vessel Components," *WRC Bulletin 197,* August 1974.

48. Dhooge, A., Dolby, R. E., Sebille, J., Steinmetz, R., and Vinckier, A. G. "A Review of Work Related to Reheat Cracking in Nuclear Reactor Pressure Vessel Steels," *International Journal of Pressure Vessels and Piping,* Vol. 6(5), September 1978, pp. 329–409.

49. Presser, R. I., McPherson, R. "The Role of Trace Elements in Reheat Cracking," *Proceedings of Conference on Residual Stresses in Welded Construction and Their Effects,* London, 15–17 November, 1977, Welding Institute, Cambridge, 1978, pp. 387–398.

50. Hippsley, C. A., King, J. E., and Knott, J. F. "Toughness Variations and Intergranular Fracture During the Tempering of Simulated HAZ Structures in a Mn-Mo-Ni Steel," *Proceedings of International Conference on Advances in the Physical Metallurgy and Application of Steels,* University of Liverpool, 21–24 September, 1981, Metals Society, London, England, pp. 147–155.

51. Hippsley, C. A., Knott, J. F., and Edwards, B. C. "A study of Stress Relief Cracking in 2¼Cr-1Mo Steel-II. The Effects of Multi-Component Segregation," *Acta Metallurgica,* Vol. 30, 1982, pp. 641–654.

52. Troiano, A. R. "The Role of Hydrogen and Other Interstitials in the Mechanical Behavior of Metals," *Trans. ASM,* Vol. 52, 1960, pp. 54–80.

53. Linnert, G. E. Welding Metallurgy, American Welding Society, Miami, Florida, 1983.

54. Udin, H., Funk, E. R., and Wulf, J. Welding for Engineers, John Wiley and Sons, New York, 1954.

55. Nakamura, H., Naiki, T., and Okabayashi, H. "Fracture in the Process of Stress-Relaxation Under Constant Strain," *1st International Conference on Fracture,* September 1965, Vol. 2, Sendai, Japan, pp. 863–878.

56. Pense, A. W., Galda, E. J., and Powell, G. T. "Stress Relief Cracking in Pressure Vessel Steels," *Welding Journal, Research Supplement,* August 1971, pp. 374s–378s.

57. McMahon, C. J. Jr., Dobbs, R. J., and Gentner, D. H. "Stress Relief Cracking in MnMoNi and MnMoNiCr Pressure Vessel Steels," *Materials Science and Engineering,* Vol. 37, 1979, pp. 179–186.

58. Hippsley, C. A., Knott, J. F., and Edwards, B. C. "A Study of Stress Relief Cracking in 2¼Cr-1Mo Steel-I. The Effects of P segregation," *Acta Metallurgica,* Vol. 28, 1980, pp. 869–885.

59. Miller, R. C. and Batte, A. D. "Reheat Cracking in ½CrMoV/2 ¼CrMo Welded Joints," *Metal Construction,* Vol. 7(11), November 1975, pp. 550–558.

60. "Reheat Cracking of 2¼Cr-1Mo Pressure Vessel Steel," Japan Steel Works Research Laboratory Internal Report, Ref No. PV 76-78, July 25, 1975.

61. Imanaka, T., Sato, S., Shimomura, J., and Aso, K. "Improvements in the Stress Relief Cracking of 2¼Cr-1Mo Steels," Kawasaki Steel Corporation, Mizushima, Japan, 1985.

62. Boniszewski, T. "Reheat Cracking in 2¼Cr-1Mo SA Weld Metal," *Metal Construction,* 14(9), 1982, pp. 495–496.

63. Bruscato, R. "Temper Embrittlement and Creep Embrittlement of 2¼Cr-1Mo Shielded Metal-Arc Weld Deposits," *Welding Journal, Research Supplement,* April 1970, pp. 148s–156s.

64. Tamaki, K. and Suzuki, J. "Assessment of Reheat Cracking Sensitivity of Steels from their Chemical Composition," *Metals/Materials Technical Series,* 85 ASM's International Welding Congress, Toronto, Canada, 14–17 October, 1985, pp. 1–8.

65. Tamaki, K. and Suzuki, J. "Reheat Cracking Test on High Strength Steels by a Modified Implant Test," *Transactions on the Japan Welding Society,* Vol. 14(2), October 1983, pp. 33–38.

66. Tamaki, K. and Suzuki, J. "Assessment of the Reheat Cracking Sensitivity of Cr-Mo Steels," *The fourth International Symposium of the Japan Welding Society,* November 1982, Osaka, 4JWS-II-17, pp. 467–472.

67. Tamaki, K., Suzuki, J., Nakaseko, Y., and Tajiri, M. "Effect of Carbides on Reheat Cracking Sensitivity," *Transactions on the Japan Welding Society,* Vol. 15(1), April 1984.

68. Tamaki, K., Suzuki, J., and Kojima, M. "Combined Influence of Chromium, Molybdenum and Vanadium on Reheat Cracking of Steels," *IIW Document* IX-1518-88.

69. Cadman, R. O. L. Discussion Session 4, Part 1, "Heat Treatment Cracking," Paper 11, *Metal Construction and British Welding Journal,* Vol. 1(2), 1969, pp. 125–128.

70. "Improvement in High Temperature Properties of Heavy Section 2¼Cr-1Mo Steel," Kawasaki Steel Corporation, January 1982.

71. Myers, J. "Influence of Alloy and Impurity Content on Stress-Relief Cracking in Cr-Mo-V Steels," *Metals Technology,* Vol. 5(11), November 1978, pp. 391–396.

72. Jones, K. E. "Stress-Relief Cracking of Welded Pipe/Casting Joints in Cr-Mo-V Steel," Paper 5 in *Proceedings of Conference on Welding Creep Resistant Steels,* The Welding Institute, Abington Hall, Cambridge, 17–18 February, 1970, pp. 66–78.

73. Ritchie, R. O., Parker, E. R., Spencer, P. N., and Todd, J. A. "A New Series of Advanced 3Cr-Mo-Ni Steels for Thick Section Pressure Vessels in High Temperature and Pressure Hydrogen Service," DOE/UC/07843-1, Topical Report No. UCB/RP/84/D1020, Feb. 1, 1980–Jan. 31, 1984, September 1984.

74. Anon. "Testing Techniques to Study the Susceptibility to Reheat Cracking of Carbon-Manganese and Low Alloy Steels," *Welding in the World,* Vol. 12(11/12), 1974.

75. Bodnar, R. L., Ohhashi, T., and Jaffee, R. I. "Effects of Mn, Si and Purity on the Design of 3.5NiCrMoV, 1CrMoV, and 2.25Cr-1Mo Bainitic Alloys," *Metallurgical Transactions A,* Vol. 20A, August 1989, pp. 1445–1460.

76. Weng, Y. Q. and McMahon, C. J. Jr. "Interaction of Phosphorus, Carbon, Manganese, and Chromium in Intergranular Embrittlement of Iron," *Materials Science and Technology,* Vol. 3, March 1987, pp. 207–216.

77. Yu, J. and McMahon, C. J. Jr. "The Effect of Composition and Carbide Precipitation on Temper Embrittlement of 2.25Cr-1Mo Steel: Part II. Effects of Mn and Si," *Metallurgical Transactions A,* Vol. 11A(2), February 1980, pp. 291–300.

78. Ratliff, J. L. and Brown, R. M. "The Deleterious Effect of Small Quantities of Aluminum on the Stress-Rupture Properties of a Cr-Mo-V Steel," *Transactions of the American Society of Metals,* Vol. 60, 1967, pp. 176–186.

79. Yu, J. "Carbide Stability Diagrams in 2.25Cr-1Mo Steels," *Metallurgical Transactions A,* Vol. 20A, August 1989, pp. 1561–1563.

80. Myers, J. "Effects of Deoxidants and Impurities on Simulated Stress Relief Cracking of ½Cr½Mo¼V Steel," *Proceedings of International Conference on Welding Research Related to Power Plant,* University of Southampton, England, 17–21 September, 1972, pp. 356–368.

81. Harris, P. and Jones, K. E. "The Effect of Composition and Deoxidation Practice on the Reheat Cracking Tendencies of ½Cr ½Mo ¼V Steel," *Proceedings of International Conference on Welding Research Related to Power Plants,* University of Southampton, England, 17–21 September, 1972, pp. 369–380.

82. Spaeder, G. J. and Plodder, G. "Stress-Rupture Properties of the Simulated Grain-Coarsened Weld-Heat-Affected Zone of USS "T-1" Steel," Technical Report, Project No. 40.02-004(1), Progress Report No. a-AS-IP-8.

83. Edmondson, B. Rapporteur's Remarks and Discussion of Paper 24-27 of *Proceedings of Conference on Welding Research Related to Power Plant,* University of Southampton, 17–21 September, 1972, CEGB, London, 1972, pp. 435–448.

84. "Developments of Advanced 2¼Cr-1Mo and 3Cr-1Mo Steels-On the Effects of Elements," Kawasaki Steel Corporation, May 13, 1985.

85. Viswanathan, R. and Beck, C. G. "Effect of Aluminum on the Stress Rupture Properties of Cr-Mo-V Steels," *Metallurgical Transactions A,* Vol. 6A, November 1975, pp. 1997–2003.

86. Presser, R. I. and McPherson, R. "Boron Segregation and Elevated Temperature Embrittlement of Ferritic Steel," *Scripta Metallurgica,* Vol. 11, 1977, pp. 745–749.

87. Paju, M. and Moller, R. "The Effect of Boron on Phosphorus Segregation in Austenite," *Scripta Metallurgica,* Vol. 18, August 1984, pp. 813–815.

88. Hunter, A. N. R. "Reheat Cracking in 2¼Cr-1Mo Submerged Arc Weld Metal—Part 1—Materials, Welding and Testing," *Metal Construction,* 14(4), 1982, pp. 198–201.

89. Hunter, A. N. R. "Reheat Cracking in 2¼Cr-1Mo Submerged Arc Weld Metal—Part 2—Results and Discussion," *Metal Construction,* 14(5), 1982, pp. 266–270.

90. Wolstenholme "Transverse Cracking and Creep ductility of 2CrMo Weld Metals," CEGB Research Division Report No. R/M/R266.

91. Menon, R., Lundin, C. D., and Chen, Z. "Postweld Heat Treatment Cracking in High Strength Low Alloy Steels," *WRC Bulletin 349,* December 1989, pp. 22–30.

92. Lundin, C. D., Khan, K. K., and Gill, T. P. S. "PWHT/Reheat/Stress Rupture Cracking and HAZ Toughness in Cu-Precipitation Hardenable Steel-ASTM A 710," *Proceedings of the International Conference on The Metallurgy, Welding, and Qualification of Microalloyed (HSLA) Steel Weldments,* Cosponsored by Microalloying International and AWS, Nov. 6–8, 1990, Houston, Texas, pp. 250–275.

93. Balaguer, J. P., Wang, Z., and Nippes, E. F. "Stress Relief Cracking of a Copper Containing HSLA Steel," *Welding Journal Research Supplement,* April 1989, pp. 121s–131s.

94. Ehart, H., Grabke, H. J., and Onel, K. "Grain Boundary Segregation of Phosphorus in Iron Base Alloys: Effects of Carbon, Chromium and Titanium," *Proceedings of Conference on Advances in the Physical Metallurgy and Application of Steels,* University of Liverpool, The Metals Society, London, England, 21–24 September, 1981, pp. 282–285.

95. Tamaki, K. and Suzuki, J. "Effect of Phosphorus on Reheat Cracking of Cr-Mo Steels," *Research Reports of the Faculty of Engineering, Mie University,* Vol. 9, December 1984, pp. 8–16.

96. Wittig, J. E., Sinclair, R., and Viswanathan, R. "Precipitation of Phosphorus and Tin in Temper Embrittled Low Alloy Steel," *Scripta Metallurgica,* Vol. 19(1), January 1985, pp. 111–116.

97. Kikuchi, T. and Nakao, Y. "Effects of Impurity Elements on the Reheat Cracking in the Weld Zones of Steels," 4JWS-II-15, *The Forth International Symposium of the Japan Welding Society,* November 1982, Osaka.

98. Horn, H. and Kunze, H. D. "Reheat Cracking Studies by Weld Simulation and Scanning Auger Investigation," 4JWS-II-14, *The 4th International Symposium of the Japan Welding Society,* November 1982, Osaka, pp. 449–454.

99. Yu, J. and McMahon, C. J. Jr. "The Effect of Composition and Carbide Precipitation on Temper Embrittlement of 2.25Cr-1Mo Steel: Part I. Effects of P and Sn," *Metallurgical Transactions A,* Vol. 11A(2), February 1980, pp. 277–289.

100. Eyre, B. L., Edwards, B. C., and Titchmarsh, J. M. "Physical Metallurgy of Reversible Temper Embrittlement," *Proceedings of International Conference on Advances in the Physical Metallurgy and Application of Steel,* University of Liverpool, 21–24 September, 1981, The Metals Society, London, England, pp. 246–258.

101. Hippsley, C. A. "Precipitation Sequences in Heat-Affected Zone of 2.25Cr-1Mo Steel During Stress-Relief Heat Treatment," *Metal Science,* Vol. 15(4), April 1981, pp. 137–147.

102. Muhammed, A. B., Szkopiak, Z. C., and Waldron, M. B. "Effect of Types of Carbides on Temper Embrittlement in Commercial 2.25Cr-1Mo Steel," *Proceedings of International Conference on Advances in the Physical Metallurgy and Applications of Steels,* University of Liverpool, 21–24 September, 1981, Metals Society, London, England, pp. 340–348.

103. Wilkinson, D. S., Abiko, K., Thyagarajan, N., and Pope, D. P. "Compositional Effects on the Creep Ductility of a Low Alloy Steel," *Metallurgical Transactions A,* Vol. 11A, November 1980, pp. 1827–1836.

104. Wada, M., Fukase, S., and Nishikawa, O. "Role of Carbides in the Grain Boundary Segregation of Phosphorus in a 2.25Cr-1Mo Steel," *Scripta Metallurgica,* Vol. 16(12), December 1982, pp. 1373–1378.

105. Viswanathan, R. and Joshi, A. "Effect of Microstructure on the Temper Embrittlement of Cr-Mo-V Steels," *Metallurgical Transactions A,* Vol. 6A(12), December 1975, pp. 2289–2297.

106. Tamaki, K. and Suzuki, J. "Recent Studies on Reheat Cracking of Cr-Mo Steels," *Proceedings of International Conference on Stress Relieving*

Heat Treatments of Welded Steel Constructions, 6–7 July, 1987, Sofia, Bulgaria, pp. 325–326.

107. Sun, J., Zaiss, R., Menyhard, M., and McMahon, C. J. Jr. "Impurity Effects in Stress Relief Cracking of a Mn-Cr-Mo-Ni Steel," *Materials Science and Technology*, Vol. 3, February 1987, pp. 139–145.

108. Ainslie, N. G., Hoffman, R. E., and Seybolt, A. V. "Sulfur Segregation at a-Iron Grain Boundaries—I," *Acta Metallurgica,* Vol. 8, August 1960, pp. 523–527.

109. Ainslie, N. G., Phillips, V. A., and Turnbull, D. "Sulfur Segregation at a-Iron Grain Boundaries—II." *Acta Metallurgica,* Vol. 8, August 1960, pp. 528–538.

110. Lundin, C. D., Henning, J. A., Menon, R., and Khan, K. K. "Transformation, Metallurgical Response and Behavior of the Weld Fusion Zone in Cr-Mo Steels for Fossil Energy Application," Final Technical Report No. ORNL/sub/81-7685/02&77, September 1987.

111. You, C. P., Hippsley, C. A., and Knott, J. F. "Stress Relief Cracking Phenomena in High Strength Structural Steel," *Metal Science,* Vol. 18, August 1984, pp. 387–394.

112. Dolby, R. E. "Advances in the Welding Metallurgy of Steel," *Proceedings of International Conference on Advances in the Physical Metallurgy and Applications of Steels,* University of Liverpool, 21–24 September 1981, The Metals Society, London, England, pp. 111–125.

113. Dhooge, A. and Vinckier, A. "Reheat Cracking—A Review of Recent Studies," *Welding in the World*, Vol. 24, No. 5/6, 1986, pp. 2–18.

114. Shin, J. and McMahon, C. J. Jr. "Mechanisms of Stress Relief Cracking in a Ferritic Steel," *Acta Metallurgica,* Vol. 32(9), 1984, pp. 1535–1552.

115. Hippsley, C. A. "Brittle Intergranular Fracture at Elevated Temperatures in Low-Alloy Steels," *Materials Science and Technology*, June 1985, Vol. 1, pp. 475–479.

116. Hippsley, C. A. and Lewandowski, J. J. "The Nucleation of High Temperature Brittle Intergranular Fracture in 2.25Cr-1Mo Steel," *Metallurgical Transactions A,* Vol. 19A, December 1988, pp. 3005–3011.

117. Hippsley, C. A., Rauh, H., and Bullough, R. "Stress-Driven Solute Enrichment of Crack-Tips During Low-Ductility Intergranular Fracture of Low-Alloy Steel," *Acta Metallurgica,* Vol. 32(9), September 1984, pp. 1381–1394.

118. Batte, A. D. and Murphy, M. C. "Reheat Cracking in 2.25Cr-Mo Weld Metal: Influence of Residual Elements and Microstructure," *Metals Technology,* Vol. 6(2), February 1979, pp. 62–68.

119. Meyers, J. and Price, A. T. "Stress-Relief Cracking Studies of 0.5Cr-Mo-V and 2Cr-Mo Steels Using HAZ Simulation," *Metals Technology,* 4(8), 1977, pp. 406–410.

120. Stout, R. D. "Postweld Heat Treatment of Pressure Vessels," *WRC Bulletin 302,* February 1985, pp. 1–14.

121. Kanazawa, S., Yamato, K., Takeda, T., and Hasimoto, K. "Study of Reheat Cracking in Weldment (Report 1)—Investigations on Testing Methods, Some Characteristics and Factors Contributing to Susceptibility of Reheat Cracking," *Transactions of the Japan Welding Society,* Vol. 7(1), April 1976, pp. 42–50.

122. Price, A. T. and Siverns, M. J. "Stress Relief Cracking in Low Alloy Ferritic Steels," *Metals Construction and British Welding Journal,* Vol. 2(6), June 1970, pp. 239–245.

123. Ueda, S., Sato, S., and Ishikawa "Grain Boundary Embrittlement and Cracking in Weldments of 1¼Cr-½Mo Steel Pressure Vessels," *The fourth International Symposium of the Japan Welding Society,* November 1982, Osaka, pp. 473–478.

124. Hippsley, C. A. "The Influence of Heating Rate on Reheat-Cracking in a Commercial 2¼Cr1Mo Steel," UKAEA Atomic Energy Research Establishment, AERE-R-10840 (DE83911013), March 1983.

125. Nagae, M. and Abe, N. "Creep Embrittlement of Heat Affected Zone and its Evaluation," *Proceedings of International Conference on Trends in Welding Research,* Gatlinburg, TN, 18–22 May, 1986, ASM, S. A. David, Editor, pp. 597–601.

126. Konosu, S. and Maeda, K. "Creep Embrittlement Susceptibility and Creep Crack Growth Behavior in Low-Alloy Steels: An Assessment of the Effects of Residual Impurity Elements and Postweld Heat Treatment Condition on Creep Ductility and Crack Growth," *Nonlinear Fracture Mechanics: Vol. 1—Time-Dependent Fracture, ASTM STP 995,* 1989, pp. 127–152.

127. Viswanathan, R. "Temper Embrittlement and Creep Embrittlement of 1.25Cr-0.5Mo Steels Containing Sb, Sn, P and B as impurities," *Scripta Metallurgica,* Vol. 8, 1974, pp. 1225–1230.

128. Otoguro, Y., Zaizen, T., Hasimoto, K., Kabasawa, W., and Takamatsu, T. "Embrittlement of 1¼Cr-½Mo Steels in High-Temperature Service," *Proceedings of the Joint Conf. of Pressure Vessels and Piping, Materials,* Nuclear Engineering and Solar Divisions, June 21–25, 1981, Denver, Colorado.

129. Materials Properties Council. "Preliminary Report to API on Prevention and Repair of Cracking in Cr-Mo Equipment," May 1990.

130. Emmer, L. G., Clauser, C. R., and Low, J. R. "Critical Literature Review of Embrittlement in 2¼Cr-1Mo Steel," *WRC Bulletin 183,* May 1973.

131. Otoguro, Y., Hasimoto, K., and Zaizen, T. "Embrittlement of Low-Alloy Steel During Service at Elevated Temperatures," Nippon Steel Technical Report No. 22, December 1983.

132. Rosenstein, A. H. "Phenomenological Investigations of Stress-Relief Embrittlement," *Welding Journal, Research Supplement,* March 1970, pp. 122s–131s.

133. Lundin, C. D., Henning, J. A., Menon, R. and Todd, J. A. "Postweld Heat Treatment Cracking in Chromium-Molybdenum Steels," *WRC Bulletin 349,* December 1989, pp. 1–21.

134. Bollinger, W., Varughese, R., Kaufmann, E., Qin, W. F., Pense, A. W., and Stout, R. D. "The Effect of Welding and Fabrication Operations on the Toughness of A710 Steel," *Microalloyed HSLA Steels,* Proceedings of Microalloying '88, 24–30 September, 1988, Chicago, Illinois, pp. 227–290.

135. Chen, I-W. and Yoo, M. H. "Creep Cavitation Under Interfacial Segregation," *Acta Metallurgica,* Vol. 32(9), 1984, pp. 1499–1508.

136. Dhooge, A. and Vinckier, A. "Reheat Cracking—Review of Recent Studies (1984–1990)," *IIW Doc. IX-1659-91.*

137. Lundin, C. D. "Evaluation of the Effect of Welding Procedure on Stress Relief/Reheat Cracking Sensitivity of ASTM A736 Weldments," Proprietary Report, June 1991.

138. Lewandowski, J. J., Hippsley, C. A., Ellis, M. B. D., and Knott, J. F. "Effects of Impurity Segregation on Sustained Load Cracking of 2¼Cr-1Mo Steels—I. Crack Initiation," *Acta Metallurgica,* Vol. 35(3), 1987, pp. 593–608.

139. Lewandowski, J. J., Hippsley, C. A., and Knott, J. F. "Effects of Impurity Segregation and Test Environment on Sustained Load Cracking of 2¼Cr-1Mo Steels—II. Crack Propagation," *Acta Metallurgica,* Vol. 35(8), 1987, pp. 2081–2090.

140. Shin, J. and McMahon, C. J. Jr. "Comparison of Stress Relief Cracking in A508 2 and A533 B Pressure Vessel Steels," *Metal Science,* Vol. 18, August 1984, pp. 403–410.

141. Lee, D. Y., Barrera, E. V., Stark, J. P. and Marcus, H. L. "The Influence of Alloying Elements on Impurity Induced Grain Boundary Embrittlement," *Metallurgical Transactions A,* Vol. 15A, July 1984, pp. 1415–1430.

142. Yu, J. and Grabke, H. J. "Effects of P Addition on Creep of 1Cr-Mo-V Steels," *Metal Science,* Vol. 17, August 1983, pp. 389–396.

143. Needham, N. G. and Gladman, T. "Intergranular Cavity Damage and Creep Fracture of 1Cr-0.5Mo Steels," Materials Science and Technology, Vol. 2, April 1986, pp. 386–373.

144. Needham, N. G. and Gladman, T. "Intergranular Creep Cavitation in 2¼Cr-1Mo Steels," *Proceedings of International Conference on Advances in the Physical Metallurgy and Applications of Steels,* University of Liverpool, 21–24 September 1981, The Metals Society, London, England, pp. 309–317.

145. Middleton, C. J. "Reheat Cavity Nucleation and Nucleation Control in Bainitic Creep-Resisting Low-Alloy Steels: Roles of Manganese Sulfide, Residual, and Sulfur-Stabilizing Elements," *Metal Science,* April 1981, pp. 154–167.

Appendix B—Chemical Composition of 1¼Cr-½Mo API Materials

The chemical composition of a steel is the most important factor determining the potential for achieving a set of properties for desired performance in a suitable environment. The 17 heats of 1¼Cr-½Mo steel in this investigation were accurately analyzed for all 23 elements. The trace elements that are believed to influence reheat cracking behavior were reanalyzed using modern techniques, some of which are capable of an accuracy of 0.1 ppm.

Initially, each heat was analyzed by Optical Emission Spectroscopy (OES) techniques for most of the major alloying and trace elements. The carbon and sulfur were analyzed by Leco C&S analyzer. The nitrogen and oxygen values were determined by using a Leco O&N analyzer. The C, S, O and N concentrations reported are an average of three determinations. Out of the 23 elements reported in Table B1, all except Ca was determined as above. This chemical analysis was conducted at the ABB-Combustion Engineering Metallurgical Laboratory at Chattanooga, Tennessee. It is to be noted that the OES technique has an accuracy of approximately 0.002% on most elements. Thus, to accurately determine the level of trace elements that were present at or below 0.002% other techniques were utilized.

To determine the level of Ca, an Atomic Absorption Spectroscopy (AA) technique was utilized which is capable of determining Ca to an accuracy of 1 ppm. The AA measurement of the level of Ca was conducted at the Herron Testing Laboratory in Cleveland, Ohio.

However, even the AA technique is not capable of determination of the low levels of Nb, Ti, B and Sb in some heats. Thus, these elements were reanalyzed by Inductively Coupled Plasma-Mass Spectroscopy (ICP-MS). The ICP-MS technique is capable of determining an accuracy of 0.1 ppm. The ICP-MS was conducted at Environment One of Valley View, Ohio. The suggested accuracy to which the MPC factor elements are to be measured is given in Table B2.

Table B1—Chemical Composition of 17 Heats of 1¼Cr-½Mo Steel (wt%)

MATERIALS	C	Mn	P	S	Si	Ni	Cr	Mo	V	Nb	Ti
UT1	0.15	0.58	0.006	0.022	0.71	0.13	1.27	0.58	0.002	0.00005	0.00035
UT2	0.10	0.45	0.010	0.013	0.65	0.18	1.30	0.53	0.004	0.00007	0.00173
UT3	0.15	0.50	0.007	0.017	0.61	0.21	1.27	0.47	0.010	0.00025	0.00238
UT4	0.18	0.79	0.009	0.003	0.52	0.20	1.33	0.53	0.005	0.00006	0.00149
UT5	0.17	0.50	0.008	0.004	0.64	0.08	1.41	0.50	0.004	0.00062	0.00250
UT6	0.103	0.53	0.013	0.013	0.58	0.25	1.31	0.48	0.014	0.00084	0.00122
UT7	0.14	0.62	0.013	0.011	0.64	0.26	1.25	0.50	0.004	0.00008	0.00031
UT8	0.13	0.42	0.010	0.015	0.62	0.17	1.22	0.58	0.003	0.00005	0.00313
UT9	0.14	0.41	0.012	0.025	0.58	0.06	1.25	0.61	0.003	<0.00001	0.00017
UT10	0.12	0.54	0.011	0.019	0.75	0.07	1.01	0.56	0.001	<0.00001	0.00010
UT11	0.086	0.42	0.010	0.016	0.49	0.01	1.04	0.54	0.003	<0.00001	0.00039
UT12	0.10	0.56	0.004	0.001	0.57	0.12	1.46	0.55	0.003	0.00001	0.00357
UT13	0.12	0.45	0.004	0.024	0.59	0.29	1.27	0.49	0.004	<0.00001	0.00015
UT14	0.17	0.51	0.015	0.012	0.66	0.09	1.16	0.49	0.002	0.00004	0.00137
UT15	0.096	0.46	0.010	0.027	0.62	0.01	1.27	0.54	0.005	<0.00001	0.00064
UT16	0.11	0.47	0.008	0.020	0.56	0.16	1.16	0.47	0.004	<0.00001	<0.00001
UT17	0.19	0.58	0.009	0.003	0.63	0.05	1.05	0.48	0.006	0.00011	0.00211

Table B1—Chemical Composition of 17 Heats of 1¼Cr-½Mo Steel (wt%) (Continued)

MATERIALS	Co	Cu	Al	B	W	As	Sn	Zr	Sb	Ca	N	O
UT1	0.013	0.13	0.005	<0.00001	<0.01	0.009	0.010	<0.001	0.00075	0.0005	0.0089	0.0094
UT2	0.010	0.05	0.004	<0.00001	0.008	0.007	0.007	<0.001	0.00041	0.0016	0.0155	0.0058
UT3	0.012	0.16	0.003	0.00003	<0.01	0.004	0.015	<0.001	0.00095	0.0011	0.0116	0.0048
UT4	0.015	0.15	0.017	<0.00001	0.001	0.016	0.014	0.005	0.00168	0.0001	0.0112	0.001
UT5	0.007	0.09	0.021	<0.00001	0.001	0.007	0.009	0.002	0.00055	0.0014	0.0083	0.002
UT6	0.011	0.15	0.031	<0.00001	<0.001	0.005	0.014	0.003	0.00086	0.0009	0.009	0.003
UT7	0.006	0.03	0.003	<0.00001	0.01	0.003	0.003	<0.001	0.00130	0.0009	0.008	0.0055
UT8	0.010	0.11	0.026	<0.00001	<0.01	0.008	0.012	<0.001	0.00146	0.0013	0.012	0.005
UT9	0.012	0.16	0.003	<0.00001	<0.01	0.005	0.013	<0.001	0.00125	0.0008	0.012	0.016
UT10	0.010	0.08	0.003	<0.00001	<0.01	0.008	0.009	<0.001	0.00100	0.0007	0.009	0.010
UT11	0.006	0.02	0.002	<0.00001	<0.01	0.004	0.002	<0.001	0.00016	0.0010	0.011	0.011
UT12	0.010	0.07	0.017	0.00005	<0.01	0.010	0.005	<0.001	0.00070	0.0012	0.007	0.002
UT13	0.014	0.17	0.002	<0.00001	<0.01	0.007	0.015	<0.001	0.00193	0.0010	0.008	0.007
UT14	0.009	0.13	0.003	0.00002	<0.01	0.007	0.012	<0.001	0.00105	0.0014	0.013	0.008
UT15	0.006	0.04	0.003	0.00001	<0.01	0.006	0.004	<0.001	0.00032	0.0002	0.014	0.010
UT16	0.012	0.17	0.001	<0.00001	<0.01	0.009	0.015	<0.001	0.00170	0.0013	0.007	0.003
UT17	0.011	0.01	0.018	0.00028	<0.01	0.003	0.003	<0.002	0.00032	0.0016	0.006	0.001

Table B2—Accuracy for Elemental Chemical Analysis Required for Discriminative Determination of MPC Factors 5 and 7

Elements	Accuracy Required (%)
C	0.001
Mn	0.01
P	0.001
S	0.001
V	0.001
Nb	0.00001
Ti	0.0001
Cu	0.01
Al	0.001
B	0.00001
As	0.001
Sn	0.001
Sb	0.0001

Appendix C—Coarse Grained HAZ Transformation Behavior and Associated Microstructures

The coarse grained HAZ transformation behavior was assessed using dilatometric techniques in the high speed time-temperature device called the Gleeble. A range of heat inputs (12–120 KJ/in) spanning the range for welding of 1¼Cr-½Mo materials for petrochemical applications was utilized on 2 heats of 1¼Cr steel in this investigation. The selection of the heats, UT4 and UT6, was based on carbon content. UT4 has a carbon content of 0.18% which is at the high end of the specification for 1¼Cr-½Mo and UT6 has a carbon content of 0.106% which is at the low end of carbon usually encountered in 1¼Cr materials. The thermal cycles were characteristic of the CGHAZ (peak temperature 2400°F) for welding a 1 in. thick plate at 350°F preheat temperature.

The results of this evaluation are presented in the following figures and tables. It is to be noted that the hardness (HV) of the CGHAZ in the simulated condition is presented on the CCT diagrams developed for these two heats of steel (Figs. C1 and C2) and in the accompanying bar graphs (Figs. C3 and C4). Microstructural examination of the CGHAZ was conducted to supplement the transformation results and is presented following the welding CGHAZ CCT diagrams.

In addition, the on-cooling transformation temperatures of 5 heats (UT2, UT3, UT4, UT5, and UT8) were determined for the 12 and 120 KJ/in heat inputs to assist explaining some of the differences in the creep rates observed in the notched and smooth bar creep rupture study of the CGHAZ. The on-cooling transformation temperatures determined are presented in Table C1 and the microstructures are presented for the CGHAZ of these materials at the 12 and 120 KJ/in heat input conditions in Figs. C5 through C26.

Table C1—On-cooling Transformation Temperatures for Selected API Materials

Material	Heat Input (KJ/in)	On-Cooling Transformation			Dilation
		Start (°C)	Intermediate (°C)	Finish (°C)	Arbitrary Units
UT2	12	M_s 435	--	M_f 380	6
UT2	50	B_s 575	--	B_f 450	8.5
UT2	120	F_s 605	B_s 570	B_f 455	5
UT2	120 (1/2)*	F_s 605	B_s 565	B_f 425	3
UT2	120 (1/4)*	F_s 605	B_s 565	B_f 445	1.5
UT3	12	M_s 445	--	M_f 330	10
UT3	50	B_s 470	--	M_f 285	4
UT3	120	F_s 575	B_s 520	B_f 420	6
UT4	12	M_s 410	--	M_f 270	9.5
UT4	50	M_s 430	--	M_f 260	8.5
UT4	120	B_s 525	--	B_f 345	7
UT4	120 (1/2)	F_s 550	B_s 515	B_f 405	5
UT5	12	M_s 445	--	M_f 280	9.5
UT5	50	B_s 520	--	B_f 375	8.5
UT5	120	F_s 575	B_s 520	B_f 435	4.5
UT8	12	M_s 485	--	M_f 310	6.5
UT8	50	B_s 515	--	B_f 405	6
UT8	120	F_s 555	B_s 525	B_f 435	8

* The cooling rate of the thermal cycle was multiplied by (XX)

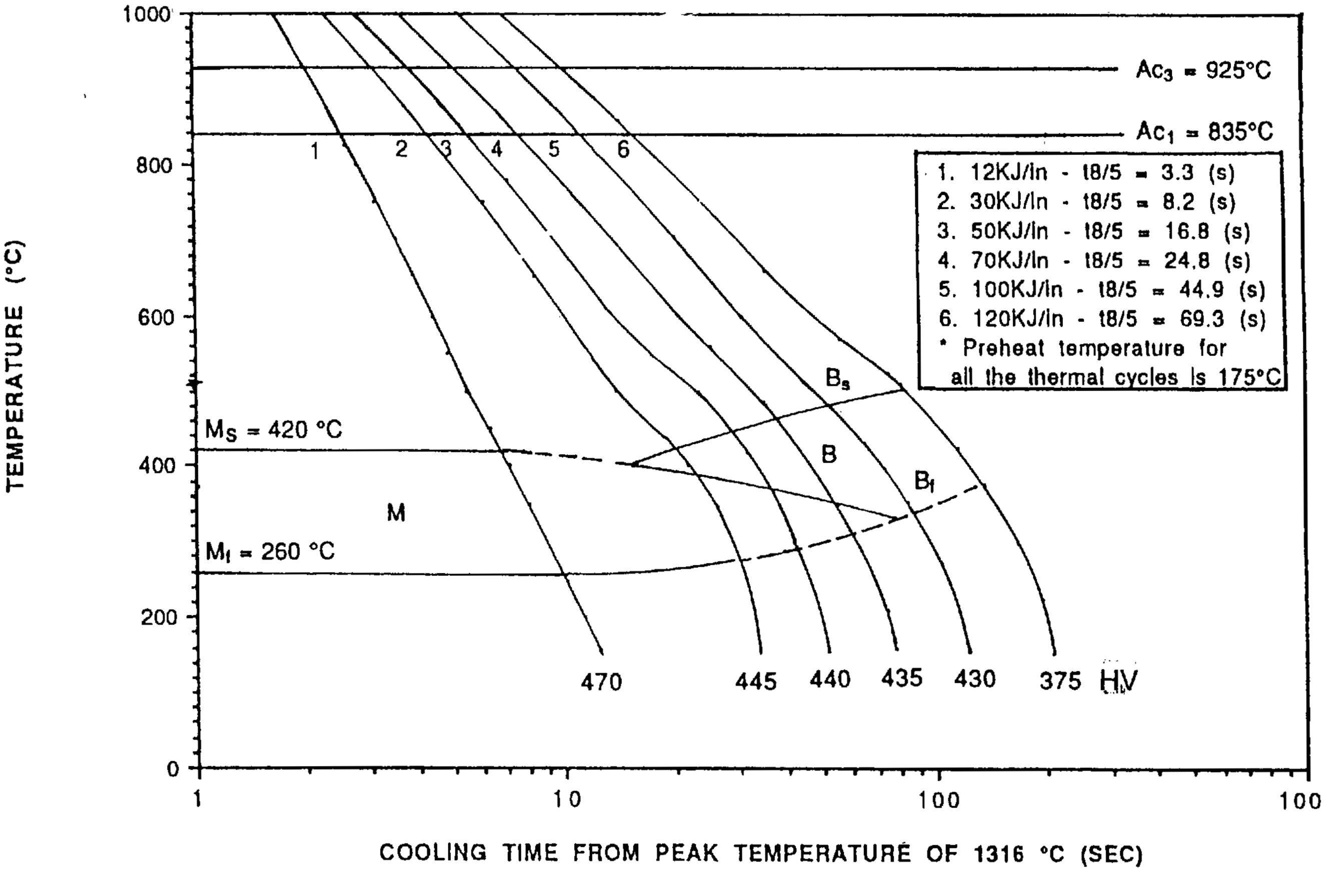

Fig. C1—Welding CCT diagram of coarse grained region for 1.25Cr-Mo steel (UT4). Major alloying element content: C: 0.18, Cr: 1.33, Mo: 0.53, Mn: 0.79, Ni: 20

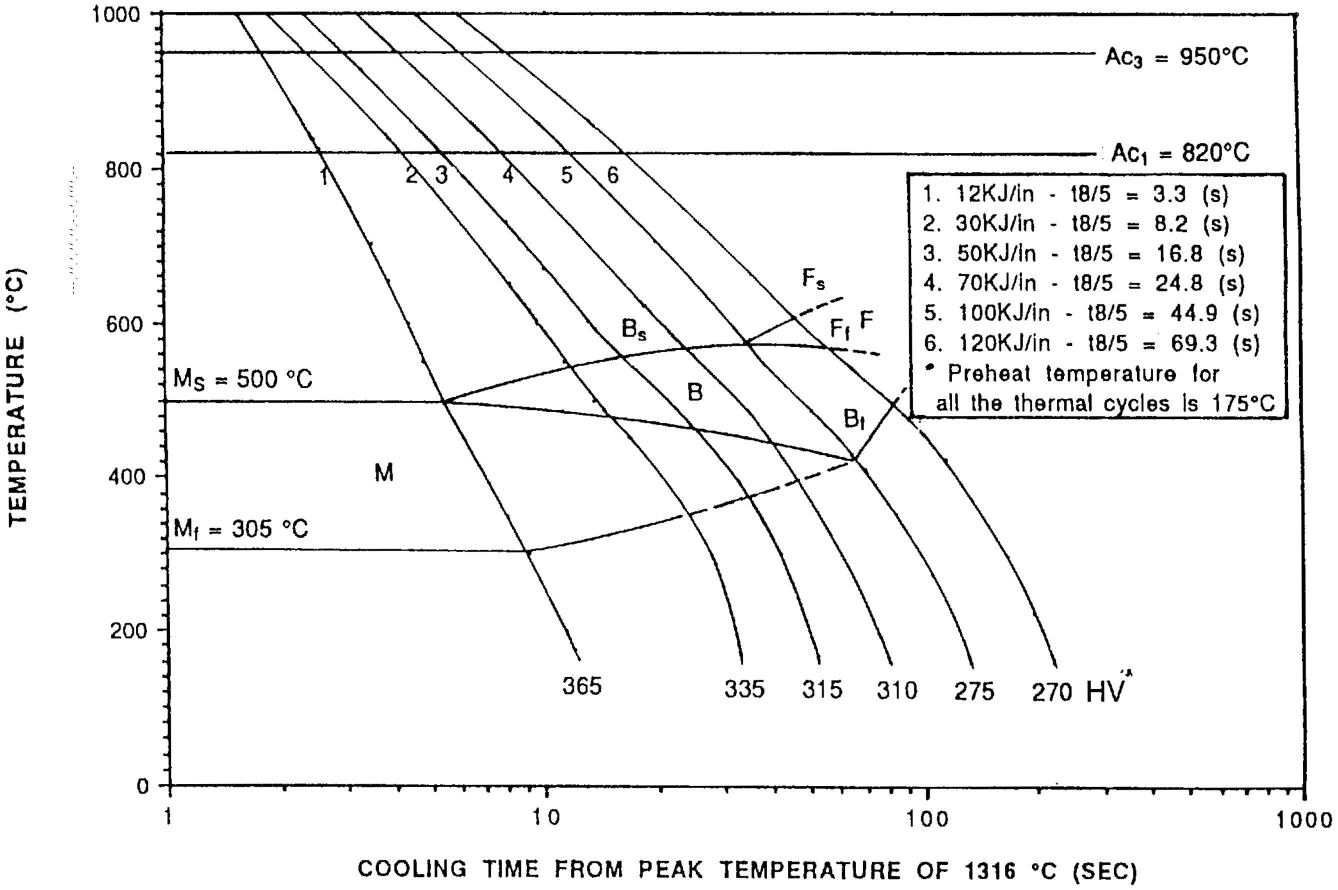

Fig. C2—Welding CCT diagram of coarse grained region for 1¼Cr-½Mo Steel (UT6). Major alloying element content: C: 0.103, Cr: 1.31, Mo: 0.48, Mn: 0.53, Ni: 0.25

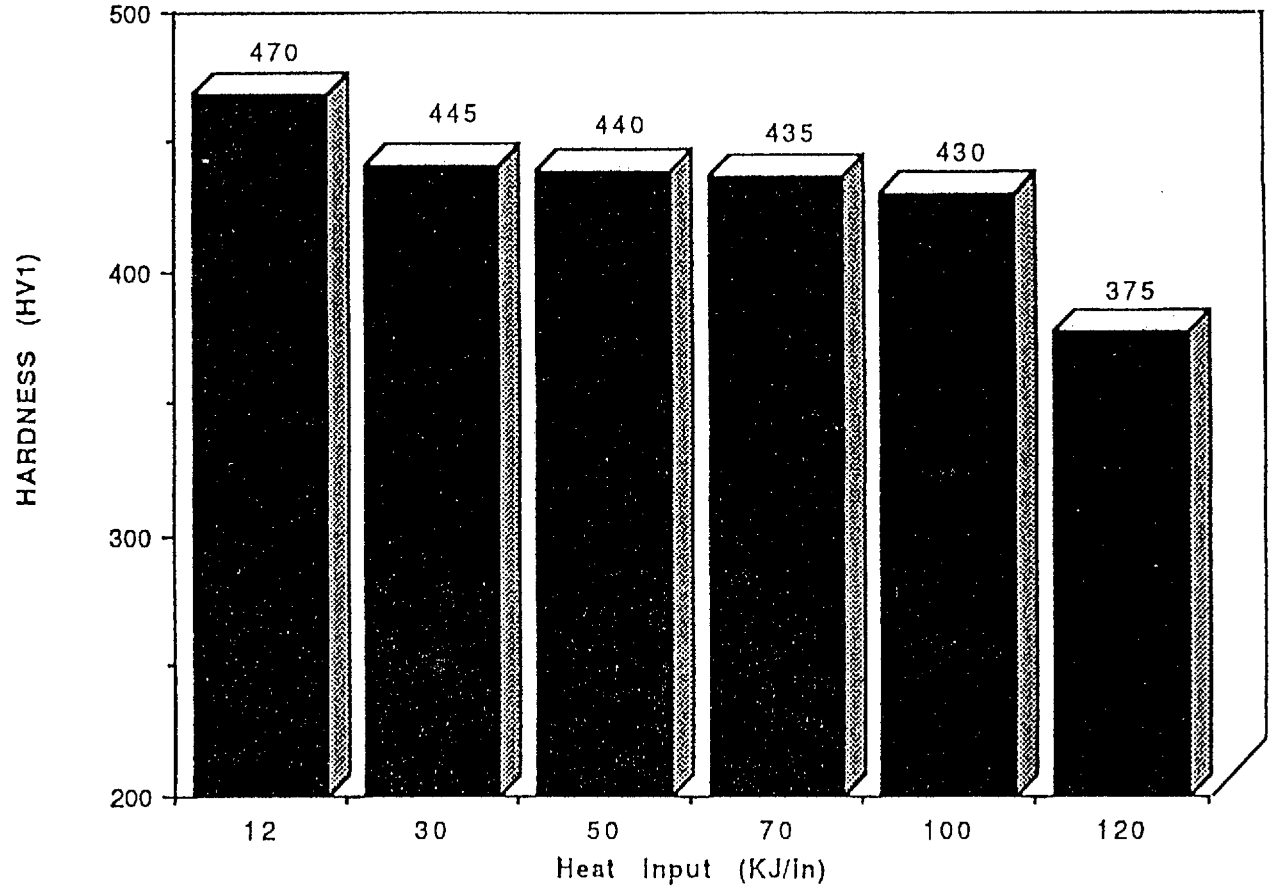

Fig. C3—Effect of heat input on the microhardness of the coarse grained HAZ of 1¼Cr-½Mo steel (UT4). Major alloying element content: C: 0.18, Cr: 1.33, Mo: 0.53, Mn: 0.79, Ni: 0.20

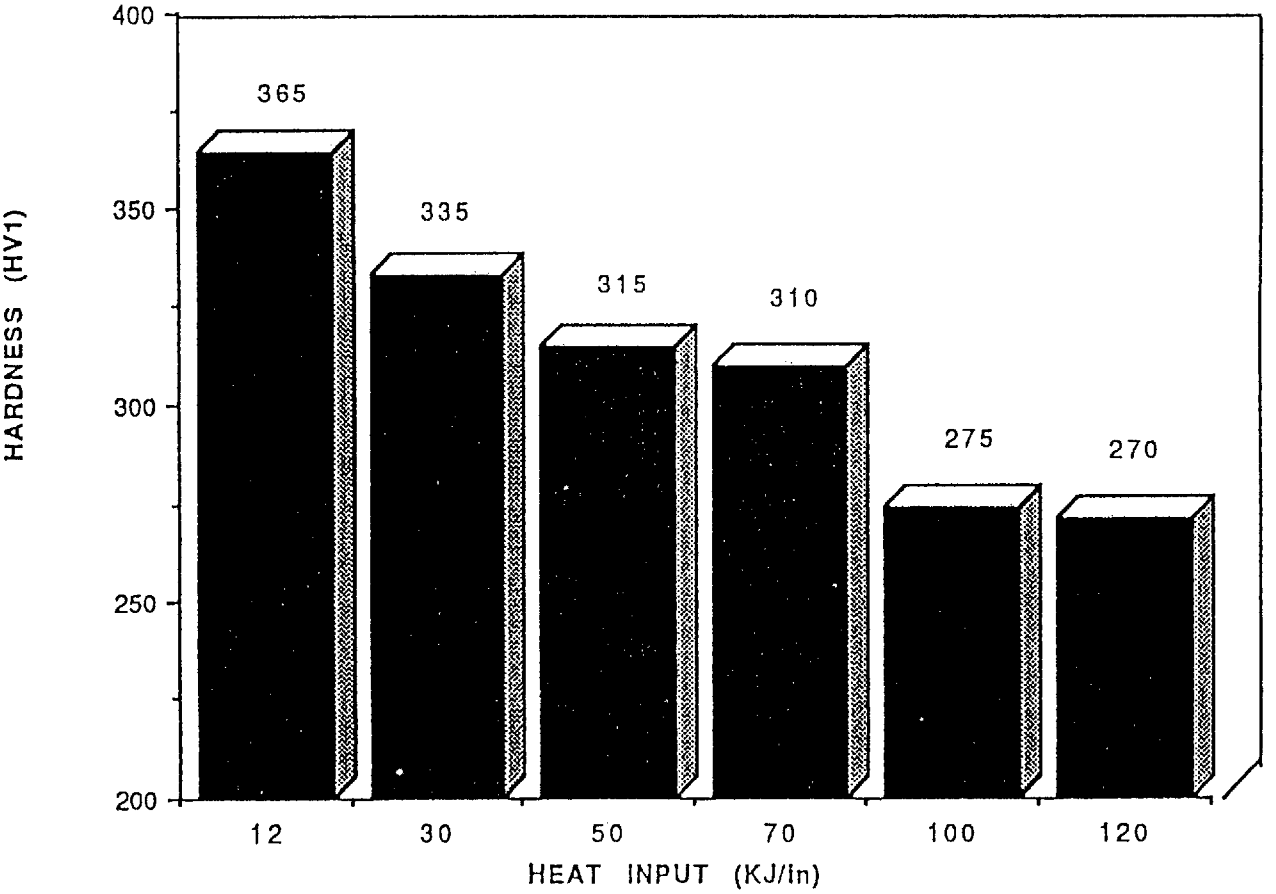

Fig. C4—Effect of heat input on the microhardness of the coarse grained HAZ of 1½Cr-½Mo steel (UT6). Major alloying element content: C: 0.103, Cr: 1.31, Mo: 0.48, Mn: 0.53, Ni: 0.25

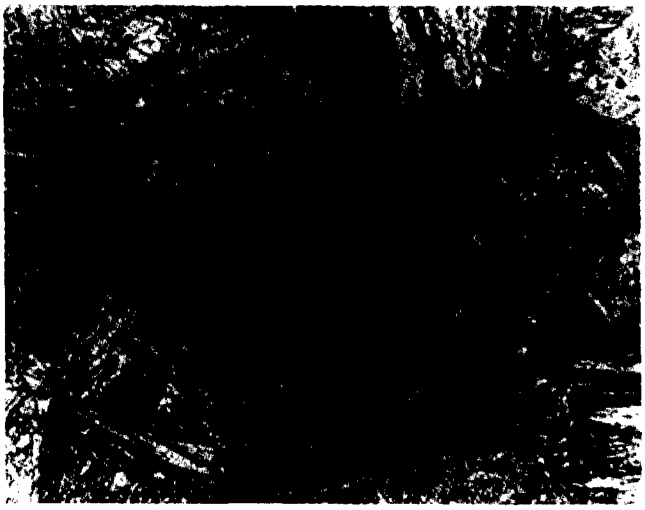

Fig. C5—UT4, 12 kJ/in. heat input, $t_{8/5}$ = 3.3 sec, 1316°C peak temperature, 1 in. plate and 175°C preheat, 400×

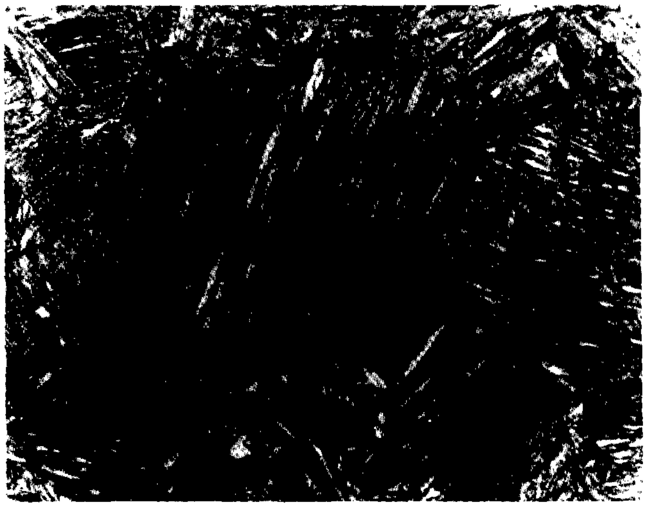

Fig. C8—UT4, 70 kJ/in. heat input, $t_{8/5}$ = 24.8 sec, 1316°C peak temperature, 1 in. plate and 175°C preheat, 400×

Fig. C6—UT4, 30 kJ/in. heat input, $t_{8/5}$ = 8.2 sec, 1316°C peak temperature, 1 in. plate and 175°C preheat, 400×

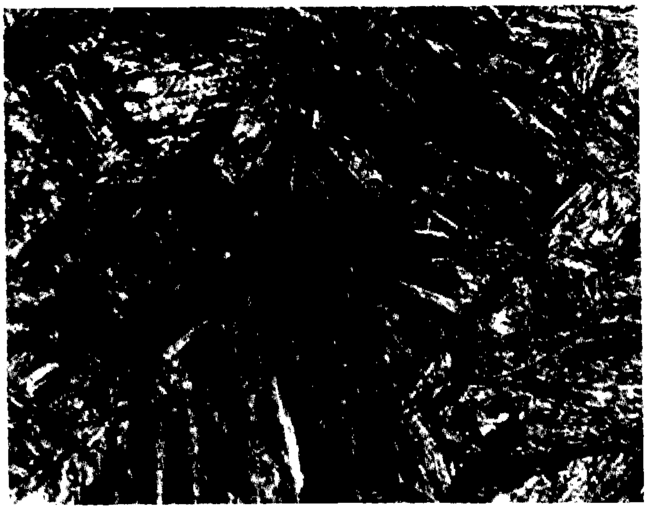

Fig. C9—UT4, 100 kJ/in. heat input, $t_{8/5}$ = 44.9 sec, 1316°C peak temperature, 1 in. plate and 175°C preheat, 400×

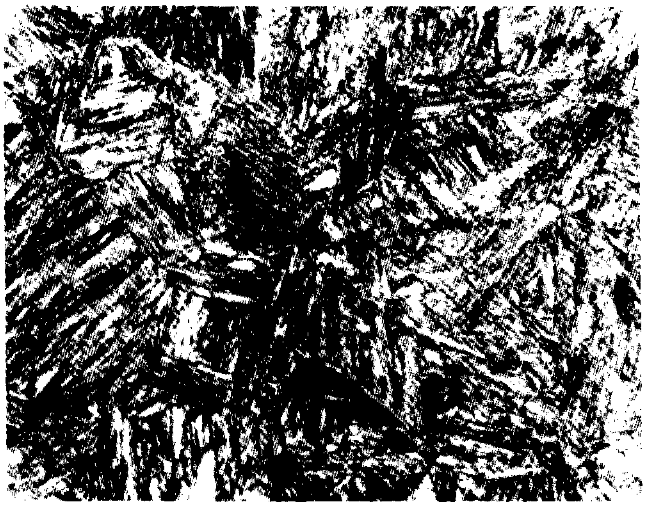

Fig. C7—UT4, 50 kJ/in. heat input, $t_{8/5}$ = 16.8 sec, 1316°C peak temperature, 1 in. plate and 175°C preheat, 400×

Fig. C10—UT4, 120 kJ/in. heat input, $t_{8/5}$ = 69.3 sec, 1316°C peak temperature, 1 in. plate and 175°C preheat, 400×

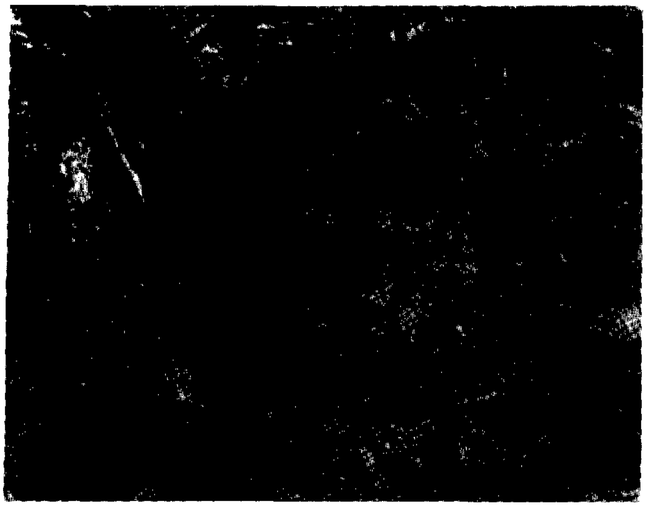

Fig. C11—UT6, 12 kJ/in. heat input, $t_{8/5}$ = 3.3 sec, 1316°C peak temperature, 1 in. plate and 175°C preheat, 400×

Fig. C12—UT6, 30 kJ/in. heat input, $t_{8/5}$ = 8.2 sec, 1316°C peak temperature, 1 in. plate and 175°C preheat, 400×

Fig. C13—UT6, 50 kJ/in. heat input, $t_{8/5}$ = 16.8 sec, 1316°C peak temperature, 1 in. plate and 175°C preheat, 400×

Fig. C14—UT6, 70 kJ/in. heat input, $t_{8/5}$ = 24.8 sec, 1316°C peak temperature, 1 in. plate and 175°C preheat, 400×

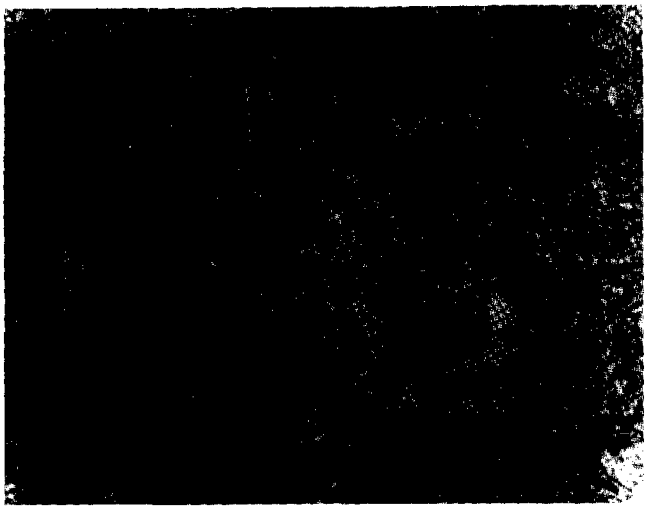

Fig. C15—UT6, 100 kJ/in. heat input, $t_{8/5}$ = 44.9 sec, 1316°C peak temperature, 1 in. plate and 175°C preheat, 400×

Fig. C16—UT6, 120 kJ/in. heat input, $t_{8/5}$ = 69.3 sec, 1316°C peak temperature, 1 in. plate and 175°C preheat, 400×

Fig. C17—UT2, 12 KJ/in. heat input, $t_{8/5}$ = 3.3 sec, 1316°C peak temperature, 1 in. plate and 175°C preheat, 400×

Fig. C18—UT3, 12 KJ/in. heat input, $t_{8/5}$ = 3.3 sec, 1316°C peak temperature, 1 in. plate and 175°C preheat, 400×

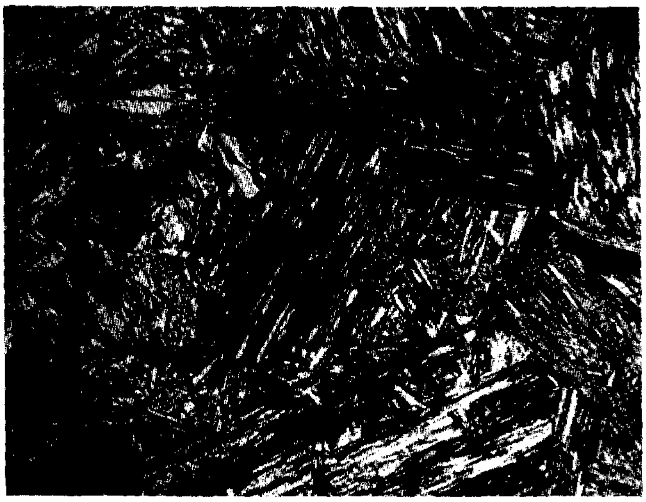

Fig. C19—UT4, 12 KJ/in. heat input, $t_{8/5}$ = 3.3 sec, 1316°C peak temperature, 1 in. plate and 175°C preheat, 400×

Fig. C20—UT5, 12 KJ/in. heat input, $t_{8/5}$ = 3.3 sec, 1316°C peak temperature, 1 in. plate and 175°C preheat, 400×

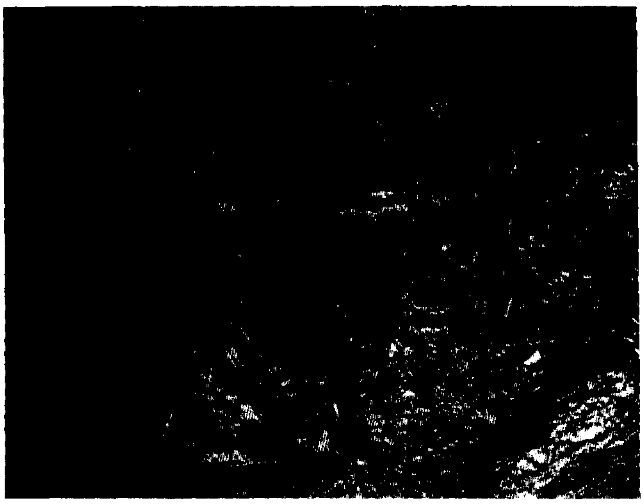

Fig. C21—UT8, 12 KJ/in. heat input, $t_{8/5}$ = 3.3 sec, 1316°C peak temperature, 1 in. plate and 175°C preheat, 400×

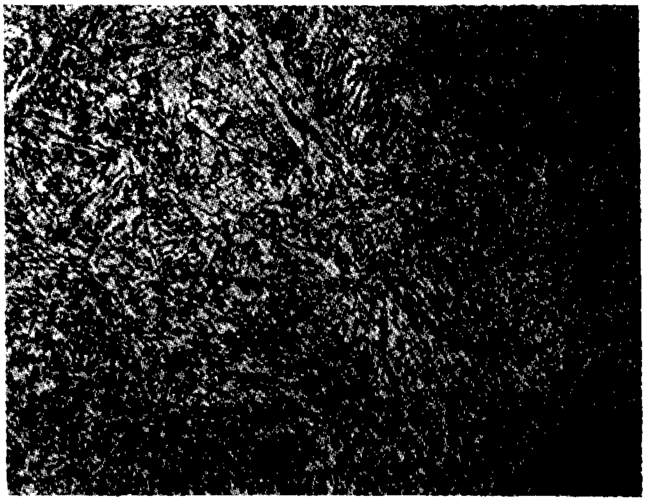

Fig. C22—UT2, 120 KJ/in. heat input, $t_{8/5}$ = 69.3 sec, 1316°C peak temperature, 1 in. plate and 175°C preheat, 400×

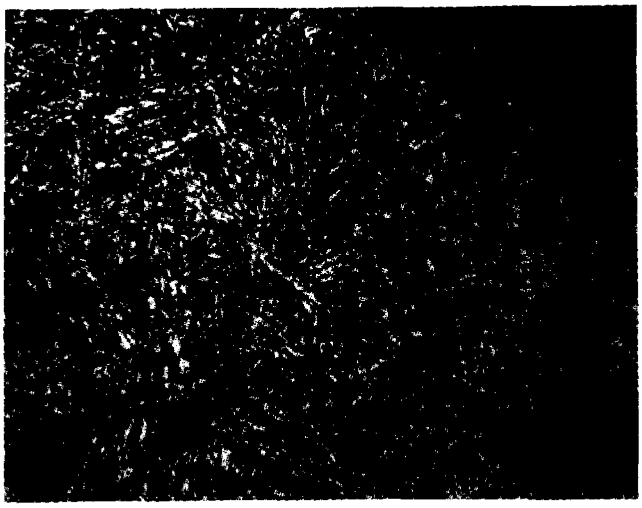

Fig. C23—UT3, 120 KJ/in. heat input, $t_{8/5}$ = 69.3 sec, 1316°C peak temperature, 1 in. plate and 175°C preheat, 400×

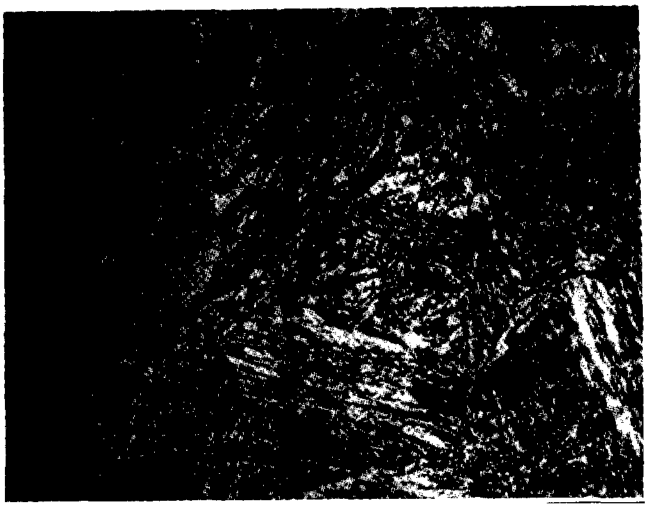

Fig. C25—UT5, 120 KJ/in. heat input, $t_{8/5}$ = 69.3 sec, 1316°C peak temperature, 1 in. plate and 175°C preheat, 400×

Fig. C24—UT4, 120 KJ/in. heat input, $t_{8/5}$ = 69.3 sec, 1316°C peak temperature, 1 in. plate and 175°C preheat, 400×

Fig. C26—UT8, 120 KJ/in. heat input, $t_{8/5}$ = 69.3 sec, 1316°C peak temperature, 1 in. plate and 175°C preheat, 400×

Appendix D—Assessment of Reheat Cracking Susceptibility

Appendix D1—Gleeble Simulation Smooth Bar Reheat Crack Testing

Introduction

The Gleeble reheat cracking test is a test that has evolved over a number of years and has been used extensively on a variety of steels. Criteria have been established based on the test for quantifying a material's susceptibility to reheat cracking. The test consists of the simulation of a CGHAZ in a small diameter specimen followed by a short time stress rupture test at a suitable temperature (normally in the PWHT range). Reduction in area of the tested ruptured specimen is used as an index to quantify the reheat cracking susceptibility. Based on fabrication/service cracking incidents and Gleeble reheat cracking test data it has been shown that a good correlation exists between this test and the susceptibility of material to reheat cracking.

It has been defined in the literature that if the Gleeble stress rupture test reduction in area is less than 5% then the material is extremely susceptible to reheat cracking. Between 5–10% the material is highly susceptible to reheat cracking, between 10–15% the material is slightly susceptible to reheat cracking; and above 20% the material is not susceptible to reheat cracking. Whether a material with a reduction in area (below 20%) in Gleeble reheat cracking test will actually reveal cracking in fabrication or service is a function of many variables such as PWHT temperature, welding procedure, restraint or residual stresses, service stress, design and presence of welding defects. However, it has been found that the Gleeble stress rupture reheat cracking test is a simple laboratory test that has the ability to screen and rank materials with respect to their reheat cracking potential.

Experimental Procedure

Reheat cracking susceptibility of all of the API steels was determined by the elevated temperature short time stress rupture test on simulated CGHAZ using the Gleeble. The samples are subjected to a CGHAZ thermal cycle (peak temperature of 2400°F, 1315°C). Subsequent to thermal cycling the specimen is simultaneously loaded in tension to simulate the weld restraint stress experienced by the CGHAZ in an actual weldment and heated to the PWHT test temperature. The stress is maintained constant for each specimen, and a range of stress levels are employed during evaluation of a material in order to obtain a range of times to rupture. A schematic representation of the CGHAZ simulation cycle followed by stress rupture testing is shown in Fig. D1.

In general, three test temperatures (1150, 1250 and 1325°F) are employed to determine the behavior of a material over the normal PWHT temperature range for 1¼Cr-½Mo. In addition, the effect of PWHT subsequent to CGHAZ simulation but prior to testing is also determined. After CGHAZ simulation the specimens are PWHT at 1150, 1250 and 1325°F for one hour and then tested at 1150°F using the procedure shown in Fig. D1. The ductility (RA) of the specimens tested is used as the criteria to quantify the material susceptibility to reheat cracking.

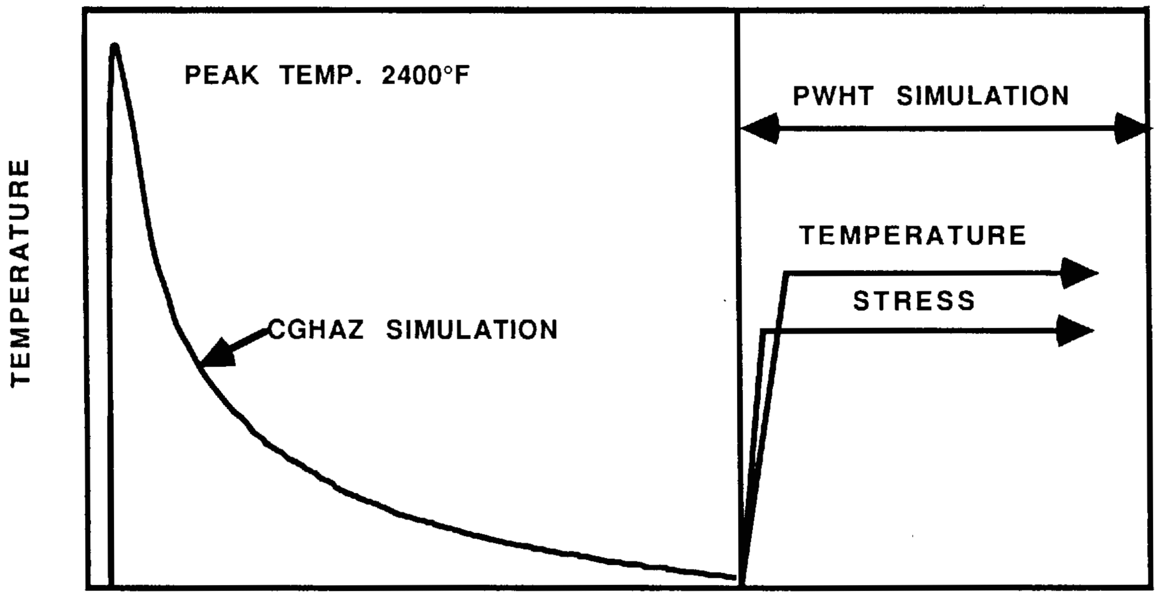

Fig. D1—Schematic representation of thermal and stress cycles for Gleeble reheat cracking studies

Gleeble Simulated HAZ Stress Rupture Test Results

Stress rupture tests were carried out on the simulated CGHAZ to determine the rupture time and the rupture ductility for all the API materials. The simulation condition used was representative of SMAW with heat inputs of both 12 KJ/in. and 120 KJ/in. at a preheat temperature of 350°F (175°C) for a 1 in. (25 mm) thick plate. A peak temperature of 2400°F (1315°C) was used. After CGHAZ simulation the specimens were loaded to the desired stress at the PWHT temperature. The samples were held at constant temperature until rupture. The reduction in area was determined.

The test results are presented in Table D1. It is to be noted in Figs. D2 & D3 that the rupture ductility of the CGHAZ is sensitive to the heat input. The RA is generally lower for the high heat input (120 KJ/in.) CGHAZ in comparison to the low heat input (12 KJ/in.) CGHAZ. However, for reheat crack susceptible heats the RA was not found to be strongly sensitive to heat input.

It was also found that an increase in the test temperature (1150, 1250 and 1325°F) generally resulted in an increase in reduction in area as shown in Fig. D4.

It was found that a PWHT after CGHAZ simulation but before stress rupture testing generally improves the stress rupture ductility in Figs. D2 and D3. The extent of improvement in the RA for PWHT at 1150°F is heat-to-heat sensitive. However, PWHT at 1250°F or 1325°F before stress rupture testing results in a significant improvement in the reduction in area and this is an indicative of an improvement of the CGHAZ to reheat cracking potential.

The hardness, micrographs, and froctographs are presented in Figs. D5 through D25.

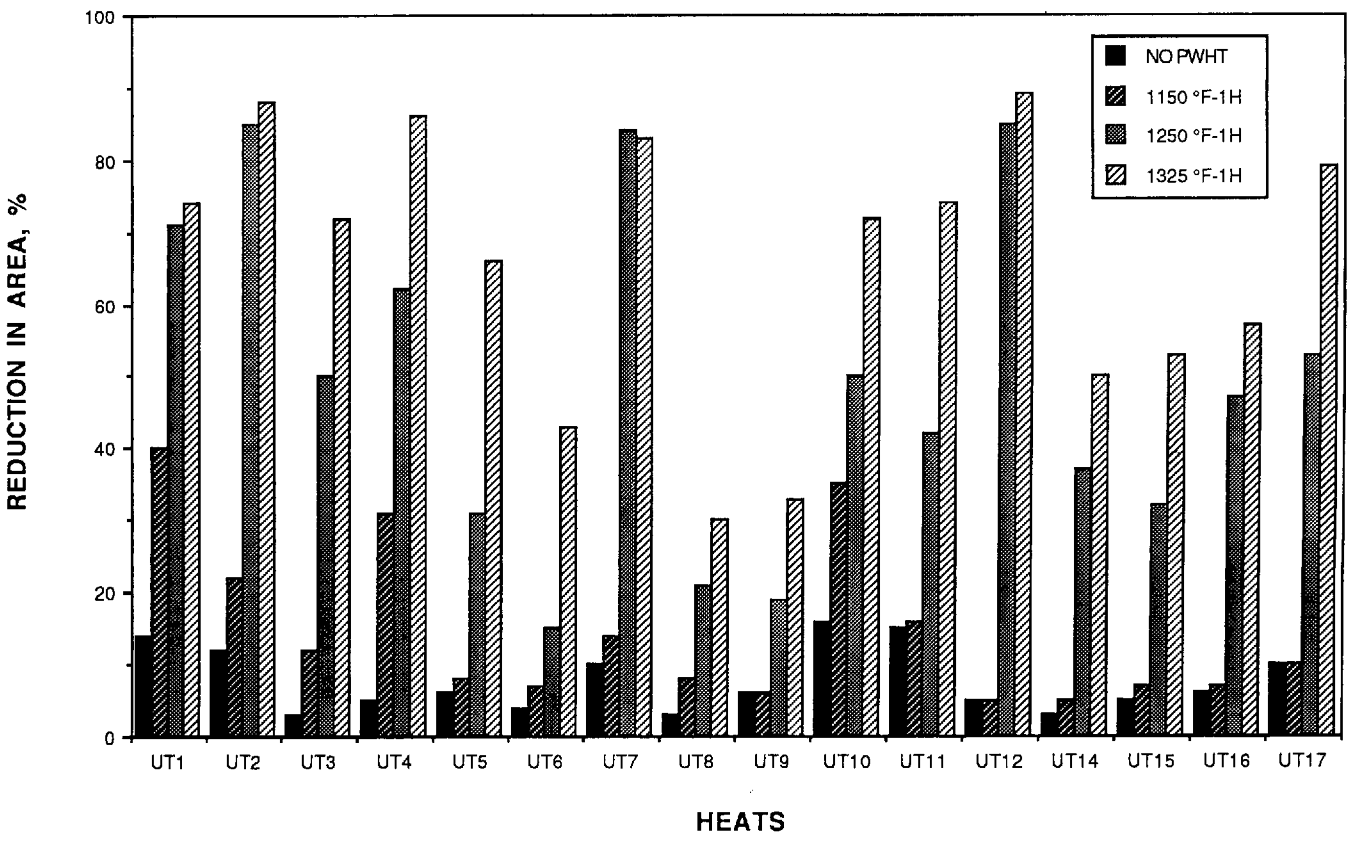

Fig. D2—Gleeble reheat cracking test results (N/T), 120 KJ/in.

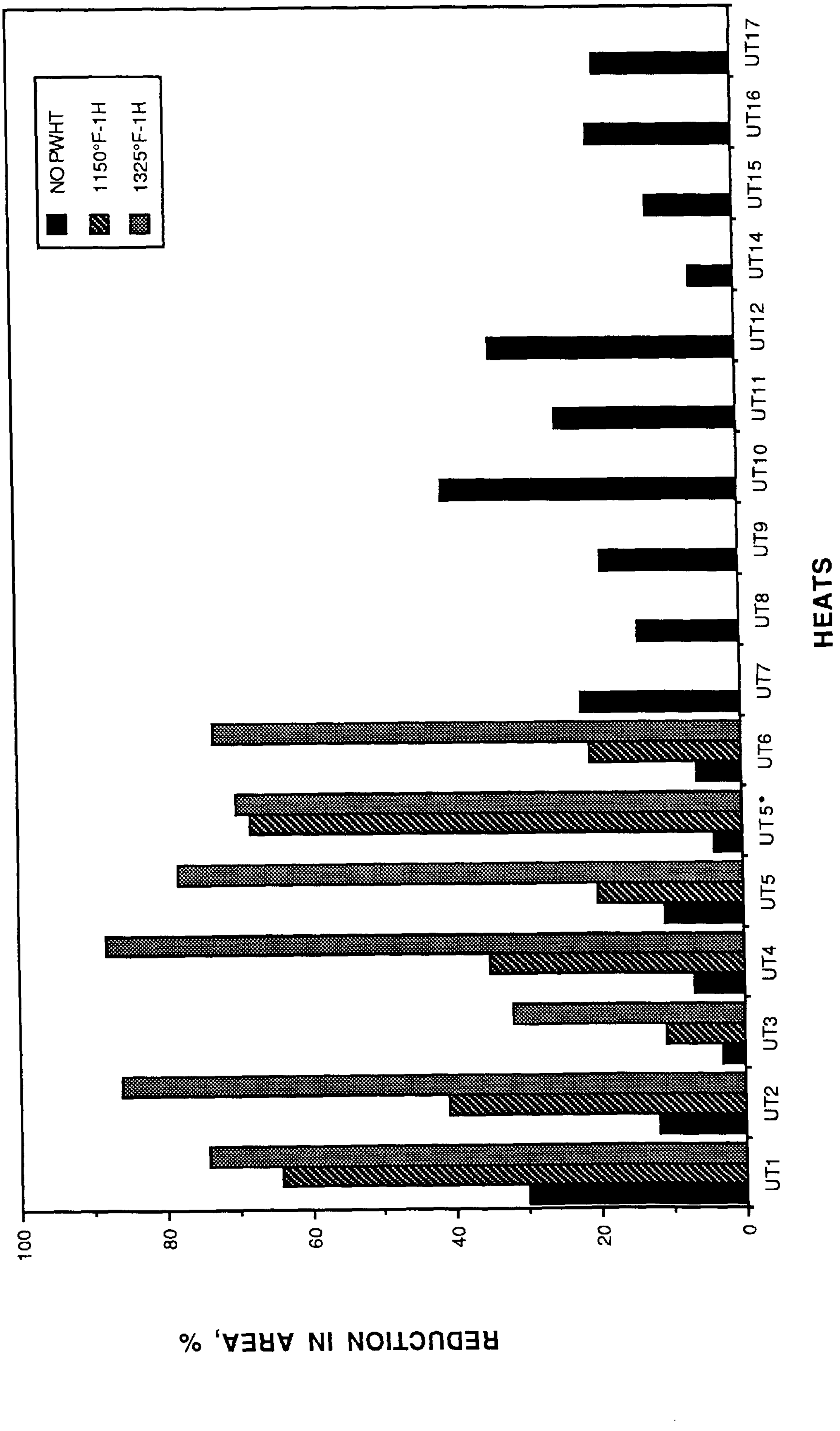

Fig. D3—Gleeble reheat cracking test results (N/T), 12 KJ/in. (*30 KJ/in.)

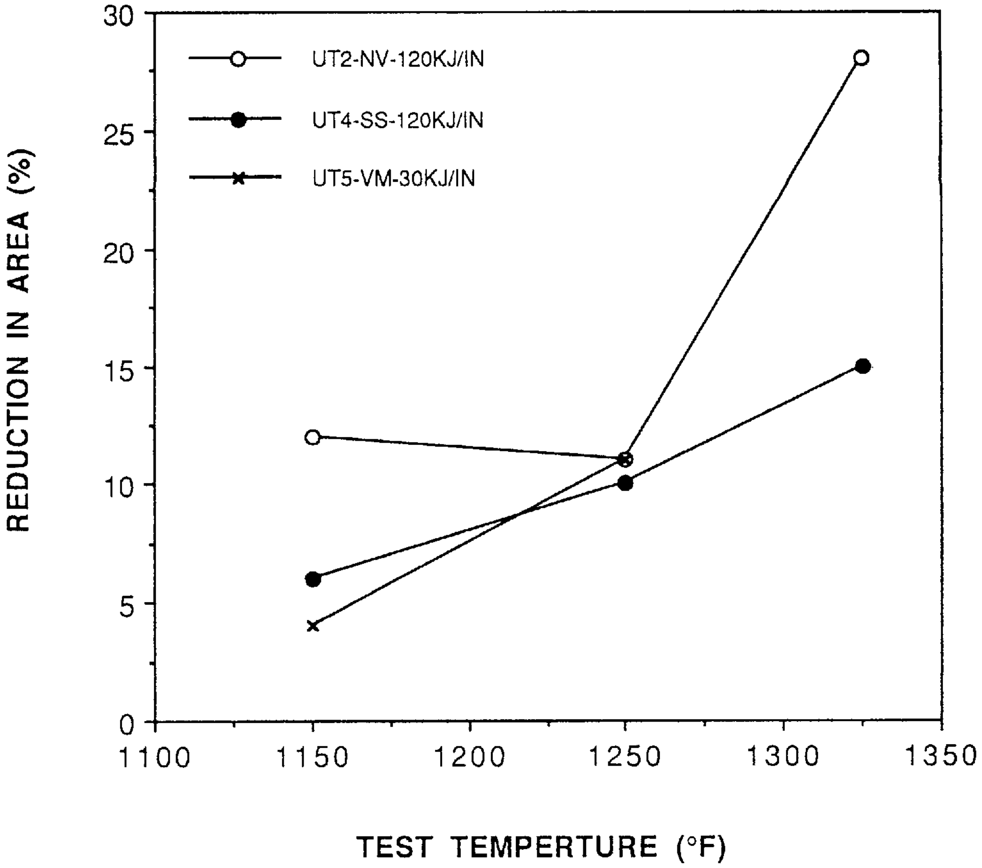

Fig. D4—Reduction in area in Gleeble reheat cracking test as a function of test temperature

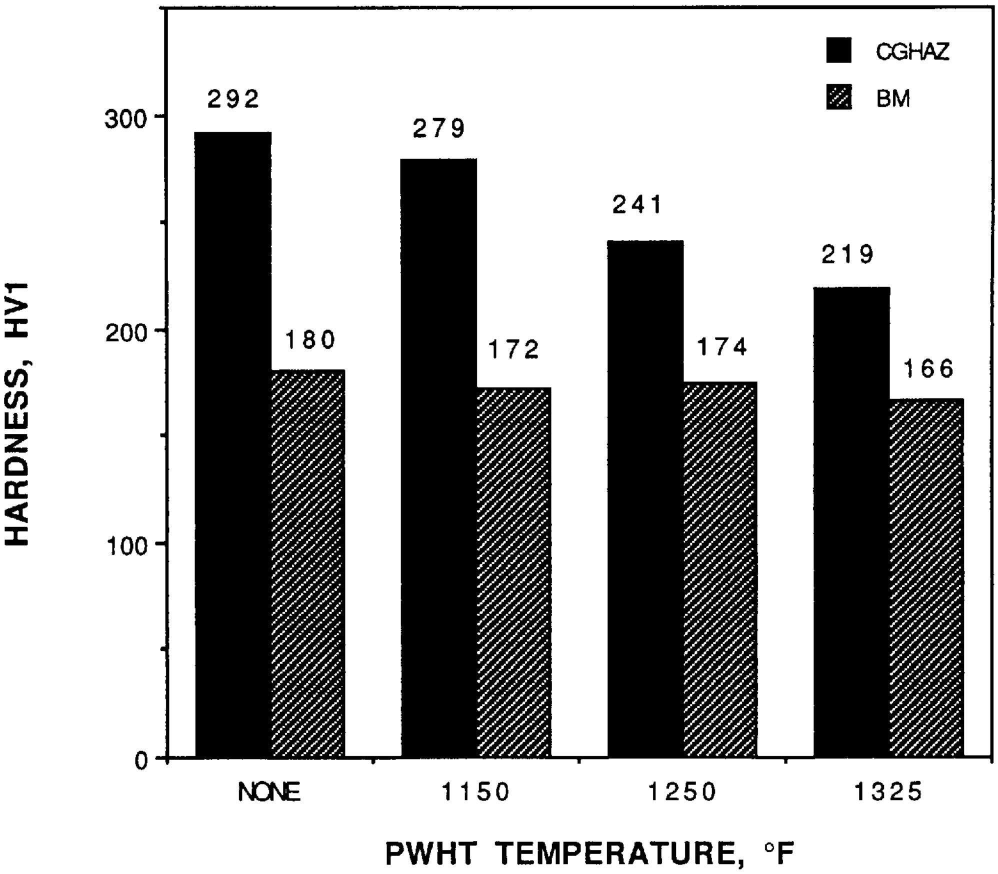

Fig. D5—UT12-VM hardness in Gleeble-simulated CGHAZ at heat input 120 KJ/in. and BM as a function of PWHT temperature

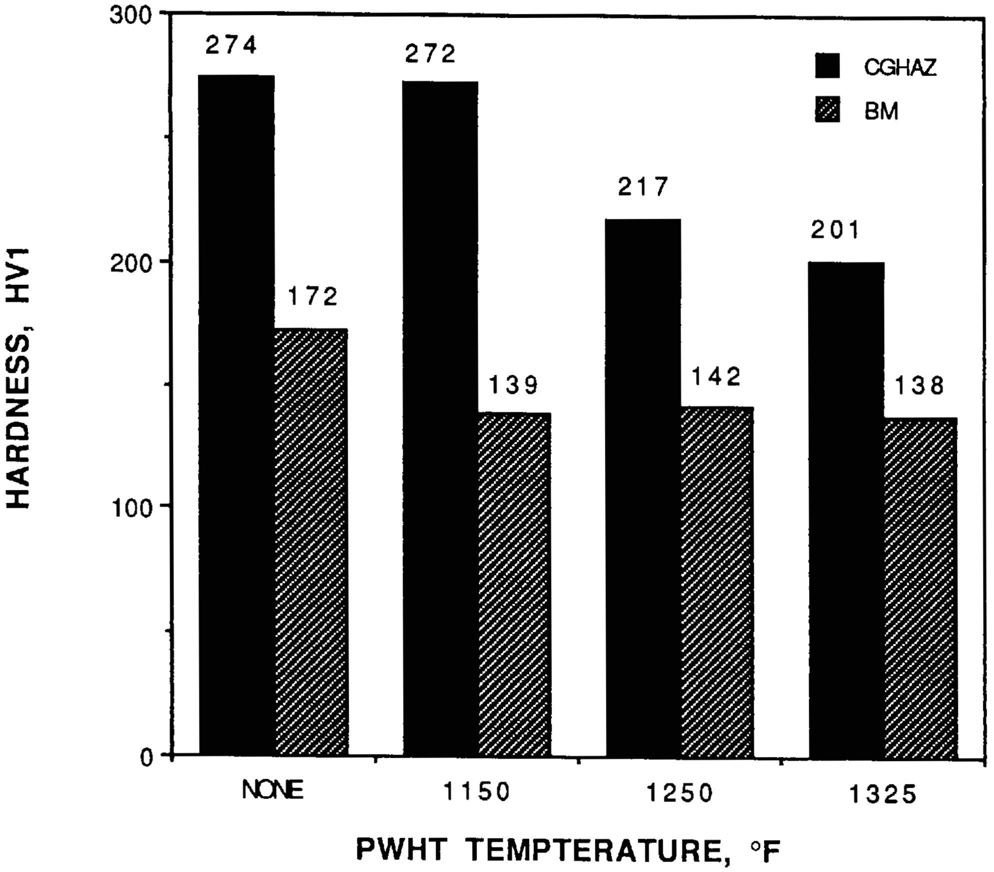

Fig. D6—UT13-SE hardness of Gleeble-simulated CGHAZ at heat input 120 KJ/in. and BM as a function of PWHT temperature

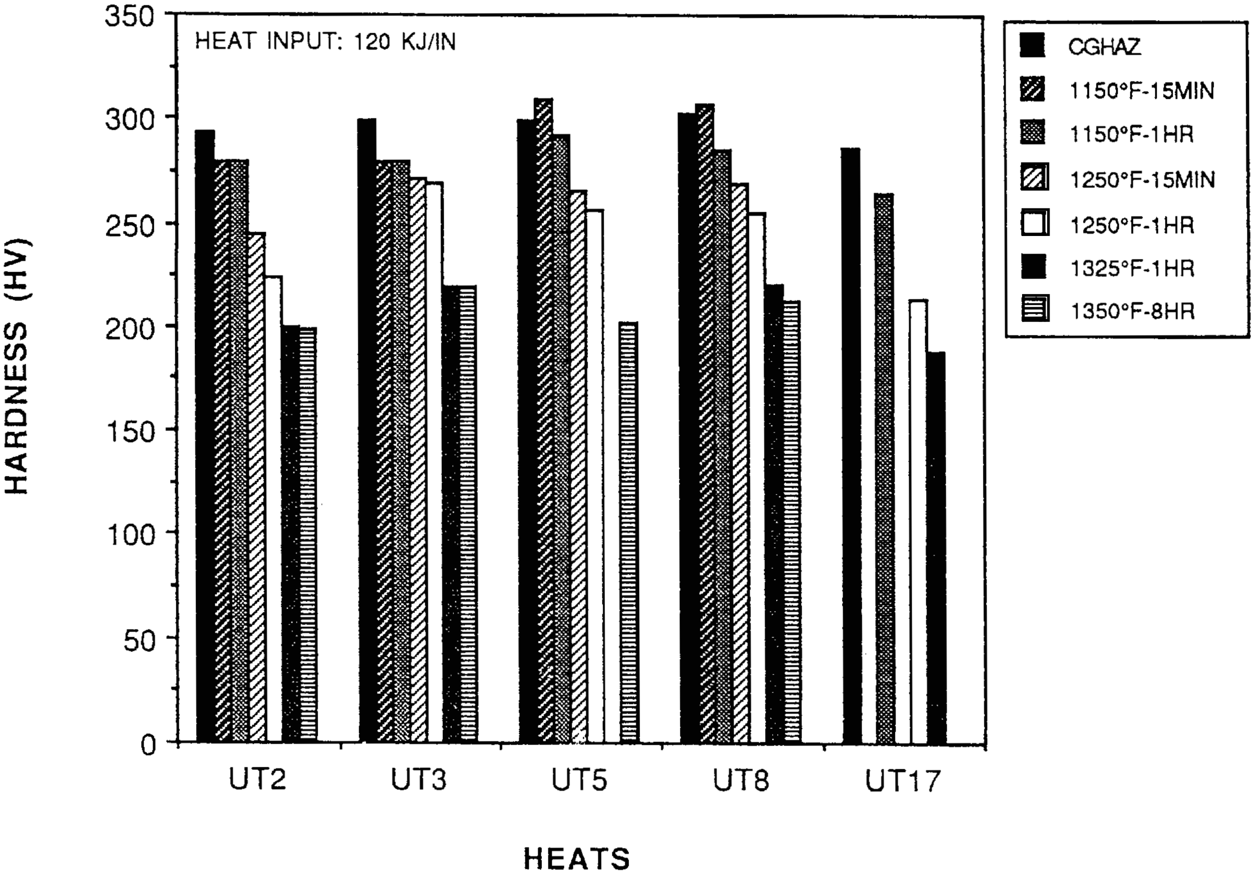

Fig. D7—Hardness of CGHAZ as a function of PWHT conditions

Fig. D8—UT1-NV microstructure of Gleeble reheat cracking test sample; heat input 12 KJ/in., 60 Ksi, 400×

Fig. D11—UT1-NV fractograph of Gleeble reheat cracking test sample; heat input 120 KJ/in., 60 Ksi, 300×

Fig. D9—UT1-NV fractograph of Gleeble reheat cracking test sample; heat input 12 KJ/in., 60 Ksi, 300×

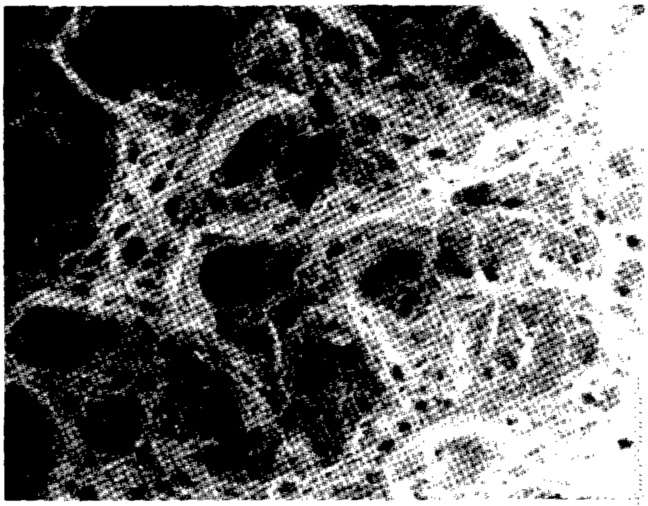

Fig. D12—UT2-SE microstructure of Gleeble reheat cracking test sample; heat input 12 KJ/in., 45 Ksi, 400×

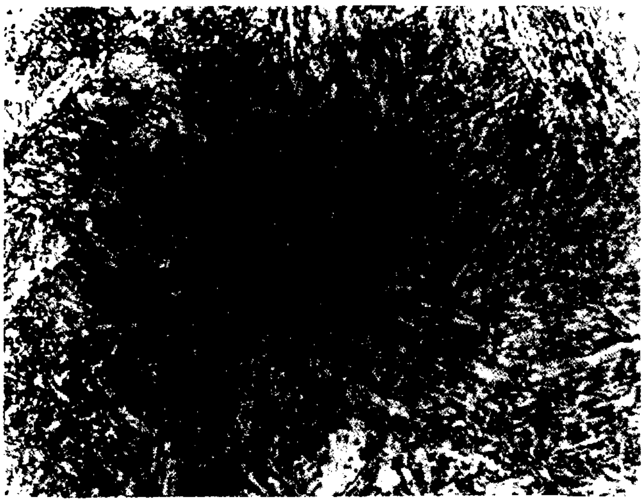

Fig. D10—UT1-NV microstructure of Gleeble reheat cracking test sample; heat input 120 KJ/in., 60 Ksi, 400×

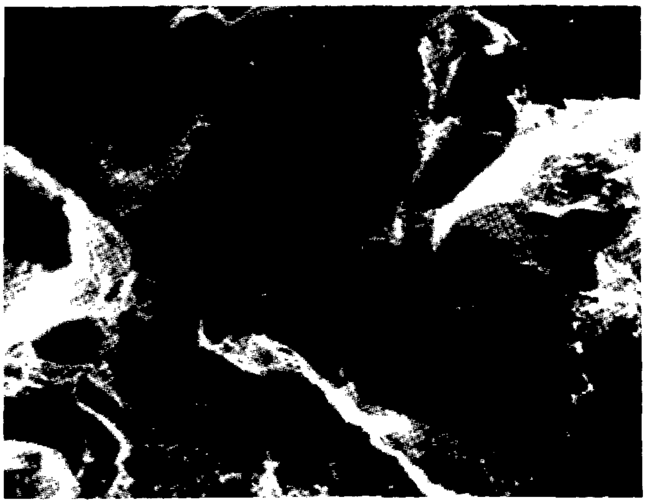

Fig. D13—UT2-SE fractograph of Gleeble reheat cracking test sample; heat input 12 KJ/in., 45 Ksi, 300×

Fig. D14—UT2-SE fractograph of Gleeble reheat cracking test sample; heat input 120 KJ/in., 50 Ksi, 300×

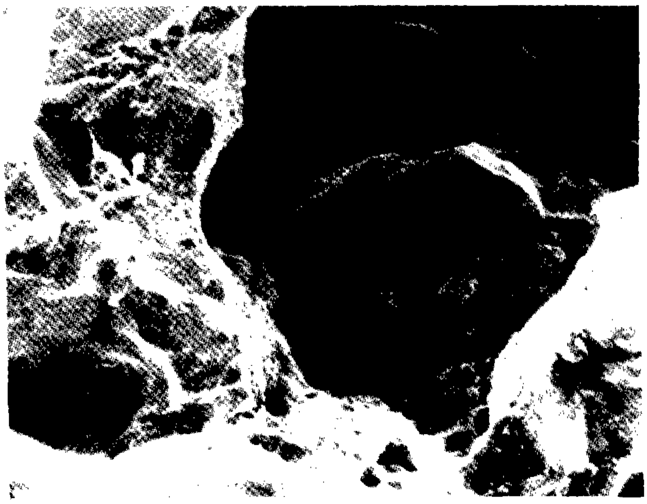

Fig. D17—UT2-NV fractograph of Gleeble reheat cracking test sample; heat input 120 KJ/in., 45 Ksi, 300×

Fig. D15—UT2-NV microstructure of Gleeble reheat cracking test sample; heat input 120 KJ/in., 45 Ksi, 400×

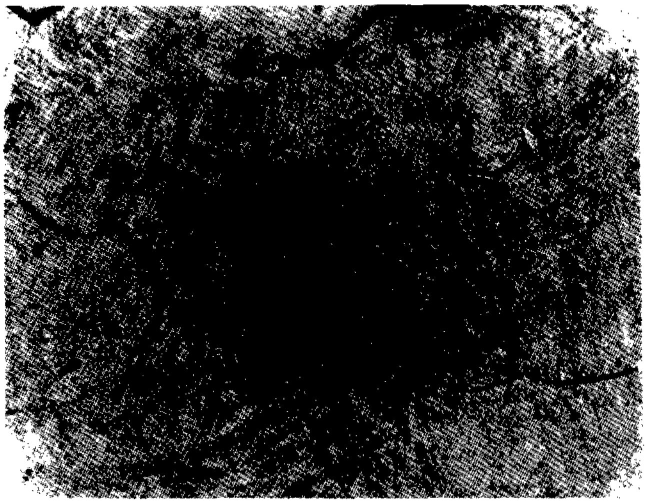

Fig. D18—UT3-SS microstructure of Gleeble reheat cracking test sample; heat input 12 KJ/in., 50 Ksi, 400×

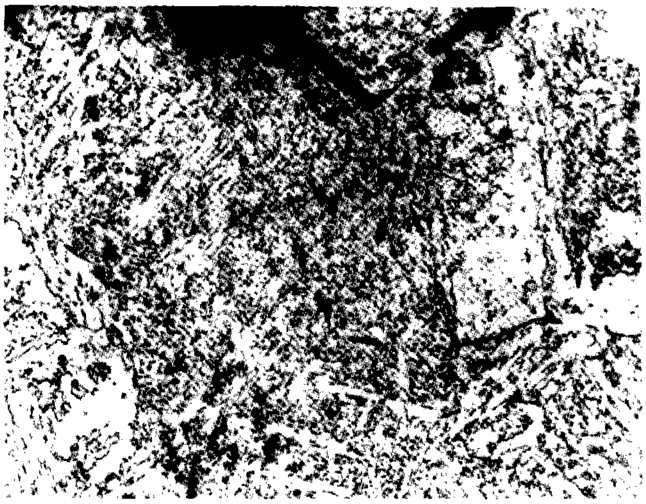

Fig. D16—UT2-NV fractograph of Gleeble reheat cracking test sample; heat input 12 KJ/in., 45 Ksi, 300×

Fig. D19—UT3-SS fractograph of Gleeble reheat cracking test sample; heat input 12 KJ/in., 50 Ksi, 300×

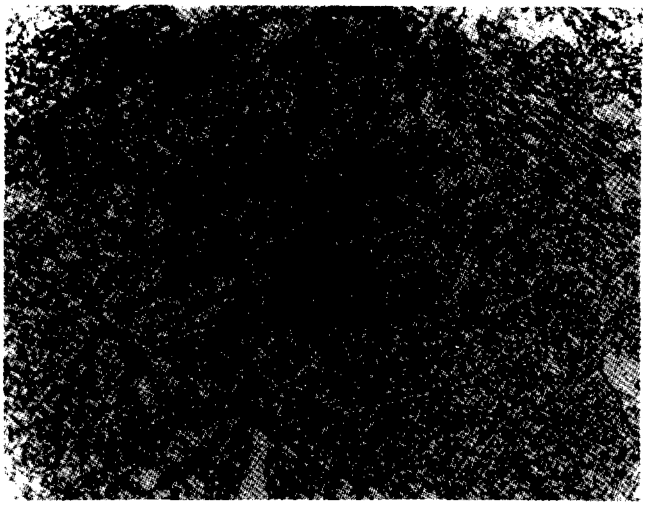

Fig. D20—UT3-SS microstructure of Gleeble reheat cracking test sample; heat input 120 KJ/in., 50 Ksi, 400×

Fig. D21—UT3-SS fractograph of Gleeble reheat cracking test sample; heat input 120 KJ/in., 50 Ksi, 300×

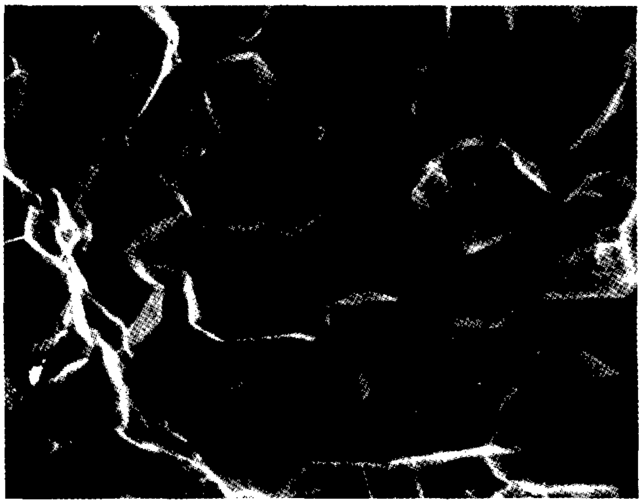

Fig. D22—UT4-VM microstructure of Gleeble reheat cracking test sample; heat input 12 KJ/in., 55 Ksi, 400×

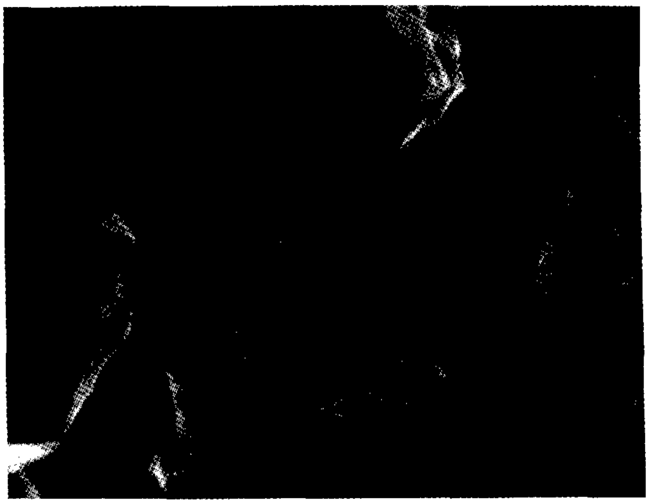

Fig. D23—UT4-VM fractograph of Gleeble reheat cracking test sample; heat input 12 KJ/in., 55 Ksi, 300×

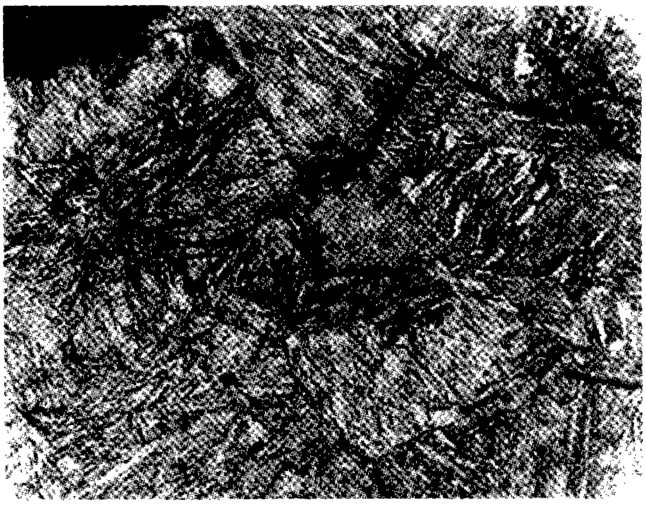

Fig. D24—UT4-SS fractograph of Gleeble reheat cracking test sample; heat input 12 KJ/in., 55 Ksi, 300×

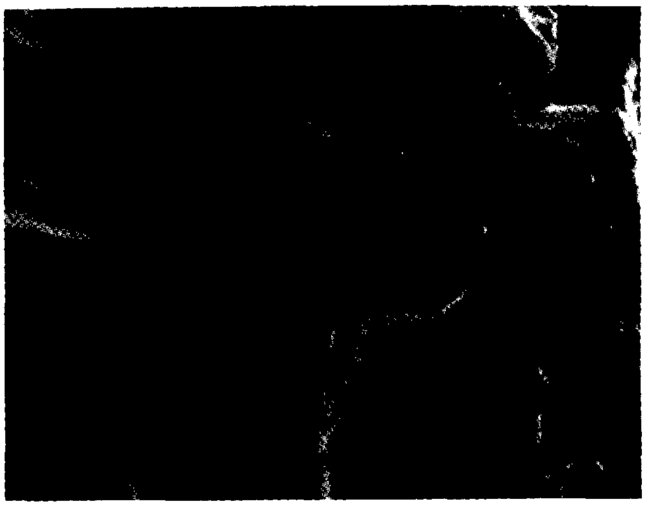

Fig. D25—UT4-SS fractograph of Gleeble reheat cracking test sample; heat input 120 KJ/in., 55 Ksi, 300×

Table D1—Data on 17 Heats Gleeble Reheat Cracking Test Results
Peak Temperature: 2400°F
Test Temperature: 1150°F

MATERIAL	HEAT INPUT (KJ/in)	STRESS (Ksi)	RA (%)	RUPTURE TIME (Minutes)
UT1-SE	120	35	32	30
UT1-SE	120	55	6	25
UT1-SE	120	60	26	8
UT1-SE	120	65	19	7
UT1-SE	12	55	33	12
UT1-SE	12	60	28	8
UT1-SE	12	65	54	1
UT1-NV	120	55	24	2
UT1-NV	120	60	14	8
UT1-NV	120	65	8	2
UT1-NV	12	55	35	18
UT1-NV	12	60	30	14
UT1-NV	12	65	18	3
UT2-SE	120	50	18	29
UT2-SE	120	55	70	1
UT2-SE	120	60	72	1
UT2-SE	12	45	64	20
UT2-SE	12	47.5	86	8
UT2-SE	12	50	36	12
UT2-NV	120	45	12	31
UT2-NV	120	50	11	28
UT2-NV	120	55	12	20
UT2-NV	12	45	73	12
UT2-NV	12	50	24	10
UT2-NV	12	55	14	6

VM - Virgin Materials
NV - Re-Normalized (Virgin)
SE - Service Exposed
SS - Service Simulated (SoCal Step Cooled)
12KJ/in = Martensite
120KJ/in = Coarse Bainite

Table D1—(Continued)

MATERIAL	HEAT INPUT (KJ/in)	STRESS (Ksi)	RA (%)	RUPTURE TIME (Minutes)
UT3-SS	120	40	8	24
UT3-SS	120	45	9	14
UT3-SS	120	50	8	8
UT3-SS	120	55	9	4
UT3-SS	12	40	8	13
UT3-SS	12	45	5	7
UT3-SS	12	50	8	2
UT3-SS	12	55	6	1
UT3-VM	120	45	13	10
UT3-VM	120	50	3	7
UT3-VM	120	55	9	4
UT3-VM	12	45	10	10
UT3-VM	12	50	3	3
UT3-VM	12	55	1	2
UT4-SS	120	35	5	24
UT4-SS	120	50	5	11
UT4-SS	120	55	6	5
UT4-SS	120	60	7	1
UT4-SS	12	35	14	20
UT4-SS	12	50	3	9
UT4-SS	12	55	6	8
UT4-SS	12	60	8	1
UT4-VM	120	35	7	40
UT4-VM	120	50	4	111
UT4-VM	120	55	5	4
UT4-VM	120	60	7	1
UT4-VM	12	35	26	20
UT4-VM	12	50	12	15
UT4-VM	12	55	7	7
UT4-VM	12	60	8	2
UT5-VM	120	55	6	31
UT5-VM	120	60	6	18
UT5-VM	12	55	11	31
UT5-VM	12	60	11	17

Table D1—(Continued)

MATERIAL	HEAT INPUT (KJ/in)	STRESS (Ksi)	RA (%)	RUPTURE TIME (Minutes)
UT5-VM	30	52	9	17
UT5-VM	30	55	4	52
UT5-VM	30	56	3	13
UT5-VM	30	60	3	8
UT5-VM	30	60	3	14
UT5-VM	30	65	5	6
UT5-VM	30	70	1	3
UT5-VM*	30	35	18	21
UT5-VM*	30	40	7	9
UT5-VM*	30	40	13	3
UT5-VM*	30	45	13	3
UT5-VM*	30	50	12	2
UT5-VM*	30	52	6	1
UT5-VM*	30	55	7	1
UT6-VM	120	40	4	43
UT6-VM	120	45	8	21
UT6-VM	120	50	4	10
UT6-VM	12	40	5	115
UT6-VM	12	45	4	54
UT6-VM	12	50	6	10
UT7-VM	120	50	7	90
UT7-VM	120	55	10	43
UT7-VM	120	60	10	5
UT7-VM	12	50	18	16
UT7-VM	12	55	25	35
UT7-VM	12	60	22	17

* Test temperature: 1250°F.

Table D1—(Continued)

MATERIAL	HEAT INPUT (KJ/in)	STRESS (Ksi)	RA (%)	RUPTURE TIME (Minutes)
UT8-SE	120	55	69*	2
UT8-SE	120	52	68*	3
UT8-SE	120	50	5	60
UT8-SE	120	45	5	74
UT8-SE	12	45	77*	40
UT8-SE	12	43	20	34
UT8-SE	12	40	No rupture	-
UT8-NV	120	55	3	8
UT8-NV	120	50	3	13
UT8-NV	120	45	3	61
UT8-NV	12	45	12	12
UT8-NV	12	40	15	106
UT8-NV	12	35	15	249
UT9-SE	120	60	8	17
UT9-SE	120	55	10	48
UT9-SE	120	50	2	109
UT9-SE	12	60	8	8
UT9-SE	12	55	20	65
UT9-SE	12	50	20	100
UT9-NV	120	55	6	30
UT9-NV	120	50	14	72
UT9-NV	120	45	8	155
UT9-NV	12	55	20	40
UT9-NV	12	50	20	43
UT9-NV	12	45	16	161

*Ruptured out of CGHAZ during test.

Table D1—(Continued)

MATERIAL	HEAT INPUT (KJ/in)	STRESS (Ksi)	RA (%)	RUPTURE TIME (Minutes)
UT10-SE	120	55	74*	2
UT10-SE	120	50	35	33
UT10-SE	120	45	27	72
UT10-SE	120	40	24	154
UT10-SE	12	50	72*	2
UT10-SE	12	45	78*	18
UT10-SE	12	40	41	67
UT10-SE	12	37	49	97
UT10-SE	12	35	49	190
UT10-NV	120	55	16	49
UT10-NV	120	50	16	82
UT10-NV	120	45	15	172
UT10-NV	12	50	44	151
UT10-NV	12	45	37	168
UT10-NV	12	40	No rupture	-
UT11-SE	120	55	71*	6
UT11-SE	120	52	73*	1
UT11-SE	120	50	12	44
UT11-SE	120	47	14	38
UT11-SE	120	45	No rupture	-
UT11-SE	12	50	63*	11
UT11-SE	12	45	40	145
UT11-SE	12	40	29	120
UT11-NV	120	60	19	30
UT11-NV	120	55	15	72
UT11-NV	120	50	11	155
UT11-NV	12	60	17	40
UT11-NV	12	55	25	43
UT11-NV	12	50	32	161

*Ruptured out of CGHAZ during test.

Table D1—(Continued)

MATERIAL	HEAT INPUT (KJ/in)	STRESS (Ksi)	RA (%)	RUPTURE TIME (Minutes)
UT12-VM	120	60	7	38
UT12-VM	120	55	5	38
UT12-VM	120	50	3	42
UT12-VM	12	60	35	64
UT12-VM	12	55	30	82
UT12-VM	12	50	37	126
UT13-SE	120	60	4	12
UT13-SE	120	55	11	19
UT13-SE	120	50	7	43
UT13-SE	12	60	28	30
UT13-SE	12	55	27	39
UT13-SE	12	50	35	89
UT14-NV	120	60	5	5
UT14-NV	120	55	3	35
UT14-NV	120	50	3	61
UT14-NV	12	60	6	1
UT14-NV	12	55	6	6
UT14-NV	12	50	5	9
UT15-NV	120	60	4	14
UT15-NV	120	55	5	34
UT15-NV	120	50	7	131
UT15-NV	12	60	12	20
UT15-NV	12	55	12	59
UT15-NV	12	50	13	111
UT16-NV	120	60	4	17
UT16-NV	120	55	6	23
UT16-NV	120	50	5	155
UT16-NV	12	60	20	27
UT16-NV	12	55	22	26
UT16-NV	12	50	18	73
UT17-VM	120	60	15	13
UT17-VM	120	55	10	107
UT17-VM	120	50	13	48
UT17-VM	12	60	15	5
UT17-VM	12	55	23	8
UT17-VM	12	50	19	3

Gleeble Reheat Cracking Test Results
Peak Temperature: 2400°F
Test Temperature: 1150°F

MATERIAL	HEAT INPUT (KJ/in)	PWHT (°F-1hr.)	STRESS (Ksi)	RA (%)	RUPTURE TIME (Min.)
UT1-SE	120	NONE	60	26	8
UT1-SE	120	1150	60	59	1
UT1-SE	120	1325	60	77	1
UT1-SE	12	NONE	60	28	8
UT1-SE	12	1150	60	54	1
UT1-SE	12	1325	55	75	1
UT1-NV	120	NONE	60	14	8
UT1-NV	120	1150	60	40	12
UT1-NV	120	1250	60	71	3
UT1-NV	120	1325	60	74	1
UT1-NV	12	NONE	60	30	14
UT1-NV	12	1150	60	64	4
UT1-NV	12	1325	60	74	1
UT2-SE	120	NONE	50	18	19
UT2-SE	120	1150	45	24	151
UT2-SE	120	1325	45	88	1
UT2-SE	12	NONE	50	36	10
UT2-SE	12	1150	50	81	6
UT2-SE	12	1325	50	85	2
UT2-NV	120	NONE	45	12	31
UT2-NV	120	1150	45	22	113
UT2-NV	120	1250	45	85	1
UT2-NV	120	1325	45	88	6
UT2-NV	12	NONE	45	12	12
UT2-NV	12	1150	45	41	43
UT2-NV	12	1325	45	86	4
UT3-SS	120	NONE	50	8	8
UT3-SS	120	1150	50	12	38
UT3-SS	120	1325	50	68	4
UT3-SS	12	NONE	50	8	2
UT3-SS	12	1150	50	10	11
UT3-SS	12	1325	50	33	4

Gleeble Reheat Cracking Test Results—(Continued)

MATERIAL	HEAT INPUT (KJ/in)	PWHT (°F-hr.))	STRESS (Ksi)	RA (%)	RUPTURE TIME (Min.)
UT3-VM	120	NONE	50	3	7
UT3-VM	120	1150	50	12	43
UT3-VM	120	1250	50	50	2
UT3-VM	120	1325	50	72	3
UT3-VM	12	NONE	50	3	3
UT3-VM	12	1150	50	11	13
UT3-VM	12	1325	50	32	5
UT4-SS	120	NONE	55	6	5
UT4-SS	120	1150	55	37	9
UT4-SS	120	1325	55	88	1
UT4-SS	12	NONE	55	7	8
UT4-SS	12	1150	55	37	12
UT4-SS	12	1325	55	81	1
UT4-VM	120	NONE	55	5	4
UT4-VM	120	1150	55	31	3
UT4-VM	120	1250	55	62	2
UT4-VM	120	1325	55	86	1
UT4-VM	12	NONE	55	7	7
UT4-VM	12	1150	55	35	7
UT4-VM	12	1325	55	88	1
UT5-VM	120	NONE	55	6	31
UT5-VM	120	1150	55	8	10
UT5-VM	120	1250	55	31	5
UT5-VM	120	1325	55	66	1
UT5-VM	12	NONE	55	11	31
UT5-VM	12	1150	55	20	7
UT5-VM	12	1325	55	78	3
UT6-VM	120	NONE	50	4	10
UT6-VM	120	1150	50	7	28
UT6-VM	120	1250	50	15	30
UT6-VM	120	1325	50	43	43
UT6-VM	12	NONE	50	6	10
UT6-VM	12	1150	50	21	12
UT6-VM	12	1325	50	73	1

Gleeble Reheat Cracking Test Results—(Continued)

MATERIAL	HEAT INPUT (KJ/in)	PWHT (°F-hr.)	STRESS (Ksi)	RA (%)	RUPTURE TIME (Min.)
UT7-VM	120	NONE	55	10	43
UT7-VM	120	1150	55	14	56
UT7-VM	120	1250	55	84	4
UT7-VM	120	1325	55	83	1
UT8-SE	120	NONE	45	5	74
UT8-SE	120	1150	45	11	94
UT8-SE	120	1325	45	29	47
UT8-SE	12	NONE	43	20	34
UT8-SE	12	1150	40	15	3
UT8-SE	12	1325	40	33	3
UT8-NV	120	NONE	55	3	8
UT8-NV	120	1150	55	8	32
UT8-NV	120	1250	55	21	19
UT8-NV	120	1325	55	30	21
UT9-SE	120	NONE	55	10	48
UT9-SE	120	1150	55	13	2
UT9-SE	120	1325	55	41	87
UT9-SE	12	NONE	55	20	65
UT9-SE	12	1150	55	28	29
UT9-SE	12	1325	55	50	46
UT9-NV	120	NONE	55	6	30
UT9-NV	120	1150	55	6	51
UT9-NV	120	1250	55	19	85
UT9-NV	120	1325	55	33	47
UT10-NV	120	NONE	55	16	49
UT10-NV	120	1150	60	35	3
UT10-NV	120	1250	55	50	17
UT10-NV	120	1325	55	72	1
UT11-SE	120	NONE	50	12	44
UT11-SE	120	1150	47	47	45
UT11-SE	120	1325	50	60	24
UT11-SE	12	NONE	45	40	145
UT11-SE	12	1150	45	70	27
UT11-SE	12	1325	45	79	11

Gleeble Reheat Cracking Test Results—(Continued)

MATERIAL	HEAT INPUT (KJ/in)	PWHT (°F-hr.)	STRESS (Ksi)	RA (%)	RUPTURE TIME (Min.)
UT11-NV	120	NONE	55	15	26
UT11-NV	120	1150	60	16	22
UT11-NV	120	1250	60	42	1
UT11-NV	120	1325	55	74	12
UT12-VM	120	NONE	55	5	38
UT12-VM	120	1150	55	5	64
UT12-VM	120	1250	55	85	6
UT12-VM	120	1325	55	89	2
UT13-SE	120	NONE	55	11	19
UT13-SE	120	1150	55	8	40
UT13-SE	120	1250	55	74	6
UT13-SE	120	1325	55	75	2
UT14-NV	120	NONE	55	3	35
UT14-NV	120	1150	55	5	55
UT14-NV	120	1250	55	37	12
UT14-NV	120	1325	55	50	3
UT15-NV	120	NONE	55	5	34
UT15-NV	120	1150	55	7	29
UT15-NV	120	1250	55	32	13
UT15-NV	120	1325	55	53	3
UT16-NV	120	NONE	55	6	23
UT16-NV	120	1150	55	7	24
UT16-NV	120	1250	55	47	10
UT16-NV	120	1325	55	57	2
UT17-NV	120	NONE	55	10	107
UT17-NV	120	1150	55	10	81
UT17-NV	120	1250	55	53	17
UT17-NV	120	1325	55	79	14

VM - Virgin materials; NV - Renormalized @ 1650°F for 1 hr/in thickness and tempered @ 1150°F for 1 hr/in thickness.

**Hardness and Grain Size of Gleeble Simulated CGHAZ
Peak Temperature 2400°F (No PWHT)**

MATERIALS	HEAT INPUT (KJ/in)	CG-HARDNESS (HV1)	BM-HARDNESS (HV1)	GRIAN SIZE IN CGHAZ ASTM No.
UT1-SE	120	310	190	3.5
UT1-NV	120	306	180	3.5
UT1-SE	12	430	-	5
UT1-NV	12	455	-	5
UT2-SE	120	260	155	4
UT2-NV	120	256	155	4
UT2-SE	12	360		6
UT2-NV	12	355		6
UT3-SS	120			3.5
UT3-VM	120	285	240	3.5
UT3-SS	12	-	240	5
UT3-VM	12	425		5
UT4-SS	120	-	195	3.5
UT4-VM	120	375	200	3.5
UT4-SS	12	-		4.5
UT4-VM	12	470		4.5
UT5-VM	120	298	155	3
UT5-VM	12	430		4
UT5-VM	30	410		3.5
UT6-VM	120	282	150	3
UT6-VM	12	391		3.5
UT6-VM	30	310		4
UT7-VM	120	285	160	3
UT7-VM	12	405		4
UT8-SE	120	260	150	4
UT8-NV	120	280	156	3.5
UT8-SE	12	380		5
UT8-NV	12	405		4

No PWHT—(Continued)

MATERIALS	HEAT INPUT (KJ/in)	CG-HARDNESS (HV1)	BM-HARDNESS (HV1)	GRIAN SIZE IN CGHAZ ASTM No.
UT9-SE	120	280	175	2.5
UT9-NV	120	289	162	3
UT9-SE	12	390		4
UT9-NV	12	372		4
UT10-SE	120	270	160	4
UT10-NV	120	259	167	3.5
UT10-SE	12	325		5.5
UT10-NV	12	417		4
UT11-SE	120	230	130	3
UT11-NV	120	233	159	3
UT11-SE	12	320		3.5
UT11-NV	12	298		3
UT12-VM	120	292	180	4
UT12-VM	12	372		4
UT13-SE	120	274	172	4
UT13-SE	12	393		4
UT14-NV	120	321	172	4
UT14-NV	12	464		4
UT15-NV	120	271	144	4
UT15-NV	12	345		4
UT16-NV	120	279	153	4
UT16-NV	12	413		4
UT17-VM	120	286	185	3
UT17-VM	12	485		3.5

Hardness and Grain Size of Gleeble Simulated CGHAZ
Peak Temperature 2400°F (No PWHT)

MATERIAL	HEAT INPUT (KJ/in)	PWHT (°F)-1H	CGHAZ (HV1)	CGHAZ GRAIN SIZE (ASTM NO.)
UT1-SE	120	NONE	310	3.5
UT1-SE	120	1150	300	3.5
UT1-SE	120	1325	210	3.5
UT1-SE	12	NONE	430	5
UT1-SE	12	1150	315	5
UT1-SE	12	1325	220	5
UT1-NV	120	NONE	306	3.5
UT1-NV	120	1150	300	3.5
UT1-NV	120	1325	205	3.5
UT1-NV	12	NONE	455	5
UT1-NV	12	1150	320	5
UT1-NV	12	1325	220	5
UT2-SE	120	NONE	260	4
UT2-SE	120	1150	240	4
UT2-SE	120	1325	200	4
UT2-SE	12	NONE	360	6
UT2-SE	12	1150	265	6
UT2-SE	12	1325	210	6
UT2-NV	120	NONE	256	4
UT2-NV	120	1150	255	4
UT2-NV	120	1325	200	4
UT2-NV	12	NONE	355	6
UT2-NV	12	1150	280	6
UT2-NV	12	1325	215	6
UT3-SS	120	NONE	-	-
UT3-SS	120	1150	290	3.5
UT3-SS	120	1325	220	3.5
UT3-SS	12	NONE	-	-
UT3-SS	12	1150	325	5
UT3-SS	12	1325	245	5

With PWHT—(Continued)

MATERIAL	HEAT INPUT (KJ/in)	PWHT (°F)-1H	CGHAZ (HV1)	CGHAZ GRAIN SIZE (ASTM NO.)
UT3-VM	120	NONE	285	3.5
UT3-VM	120	1150	285	3.5
UT3-VM	120	1325	220	3.5
UT3-VM	12	NONE	425	5
UT3-VM	12	1150	325	5
UT3-VM	12	1325	240	5
UT4-SS	120	NONE	-	-
UT4-SS	120	1150	310	3.5
UT4-SS	120	1325	230	3.5
UT4-SS	12	NONE	-	-
UT4-SS	12	1150	315	4.5
UT4-SS	12	1325	240	4.5
UT4-VM	120	NONE	375	3.5
UT4-VM	120	1150	310	3.5
UT4-VM	120	1325	230	3.5
UT4-VM	12	NONE	470	4.5
UT4-VM	12	1150	320	4.5
UT4-VM	12	1325	240	4.5
UT6-VM	120	NONE	282	3
UT6-VM	120	1150	286	3
UT6-VM	120	1250	250	3
UT6-VM	120	1325	217	3
UT8-SE	120	NONE	260	4
UT8-SE	120	1150	270	4
UT8-SE	120	1325	210	4
UT8-SE	12	NONE	380	5
UT8-SE	12	1150	320	5
UT8-SE	12	1325	220	5
UT8-NV	120	NONE	280	4
UT8-NV	120	1150	306	4
UT8-NV	120	1250	245	4
UT8-NV	120	1325	221	4

With PWHT—(Continued)

MATERIAL	HEAT INPUT (KJ/in)	PWHT (°F)-1H	CGHAZ (HV1)	CGHAZ GRAIN SIZE (ASTM NO.)
UT9-SE	120	NONE	280	2.5
UT9-SE	120	1150	270	2.5
UT9-SE	120	1325	205	2.5
UT9-SE	12	NONE	390	4
UT9-SE	12	1150	340	4
UT9-SE	12	1325	230	4
UT9-NV	120	NONE	289	3
UT9-NV	120	1150	294	3
UT9-NV	120	1250	255	3
UT9-NV	120	1325	221	3
UT10-NV	120	NONE	259	3.5
UT10-NV	120	1150	266	3.5
UT10-NV	120	1250	223	3.5
UT10-NV	120	1325	206	3.5
UT11-SE	120	NONE	230	3
UT11-SE	120	1150	235	3
UT11-SE	120	1325	190	3
UT11-SE	12	NONE	320	3.5
UT11-SE	12	1150	275	3.5
UT11-SE	12	1325	205	3.5
UT11-NV	120	NONE	233	3
UT11-NV	120	1150	250	3
UT11-NV	120	1250	210	3
UT11-NV	120	1325	194	3
UT12-VM	120	NONE	292	4
UT12-VM	120	1150	279	4
UT12-VM	120	1250	241	4
UT12-VM	120	1325	219	4
UT13-SE	120	NONE	274	4
UT13-SE	120	1150	272	4
UT13-SE	120	1250	217	4
UT13-SE	120	1325	201	4

With PWHT—(Continued)

MATERIAL	HEAT INPUT (KJ/in)	PWHT (°F)-1H	CGHAZ (HV1)	CGHAZ GRAIN SIZE (ASTM NO.)
UT14-NV	120	NONE	321	4
UT14-NV	120	1150	289	4
UT14-NV	120	1250	239	4
UT14-NV	120	1325	215	4
UT15-NV	120	NONE	271	4
UT15-NV	120	1150	245	4
UT15-NV	120	1250	210	4
UT15-NV	120	1325	191	4
UT16-NV	120	NONE	279	4
UT16-NV	120	1150	250	4
UT16-NV	120	1250	217	4
UT16-NV	120	1325	192	4
UT17-VM	120	NONE	286	3
UT17-VM	120	1150	264	3
UT17-VM	120	1250	214	3
UT17-VM	120	1325	188	3

Appendix D2—Spiral Notch Testing

Introduction

Reheat cracking (AKA PWHT cracking or stress rupture cracking) is intergranular cracking along prior austenite grain boundaries of the coarse grained HAZ observed in actual fabrications, either during PWHT or in-service, is virtually always associated with weld discontinuities such as slag or lack-of-fusion. Such defects act as a stress raiser (notch) and are considered a requisite for reheat cracking (cracking is not observed in sensitive weldments if no exacerbation of stress is evident).

To evaluate reheat cracking susceptibility of a particular steel or various heats of the same steel in the laboratory, a suitable test must be chosen. In the literature, some 30 different types of tests are available for testing reheat cracking susceptibility. The existing tests suffer from one or more of the following disadvantages:

1. poor reproducibility;
2. poor correlation with field experience;
3. difficulty in quantifying susceptibility;
4. one or more of the factors necessary for reheat cracking not included;
5. only one region of the HAZ is tested and the effects of weld metal, other HAZ regions and base metal not accounted for in the test; and
6. requirement of expensive instrumentation or elaborate testing facilities.

To overcome the deficiencies of the available tests, a new test utilizing a spiral notch (developed as a part of a WRC investigation) is used in this program. This test has the capability of simultaneous evaluation of reheat cracking in the various HAZ regions of a weldment (other test methods developed to date are not capable of this evaluation). The use of a notch is important for developing data on sensitivity to reheat cracking because it has been pointed out by many researchers that the effect of a stress raiser is paramount in the mechanism of cracking. A helical notch geometry similar to that used in the implant test (a hydrogen assisted cracking test) is employed. A schematic sketch of a specimen is shown in Fig. 1. This specimen has a major diameter of 0.165 in. (4.2 mm) and a minor diameter of 0.125 in. (3.2 mm). As shown in Fig. D2-1 every metallurgically different region of the weld HAZ is notched similarly and thus the stress concentration experienced by every region is virtually identical. The notch extends through the base metal and weld HAZ and the rupture time and notch strength of the different zones with respect to stress at different PWHT temperatures can be determined.

The test methodology is relatively simple and seeks to simulate a postweld heat treatment in the presence of discontinuity (stress raiser) and a HAZ microstructural spectrum. Specimens can be extracted from Gleeble-simulated HAZ specimens and actual weldments. In a Gleeble specimen a simulated CGHAZ is

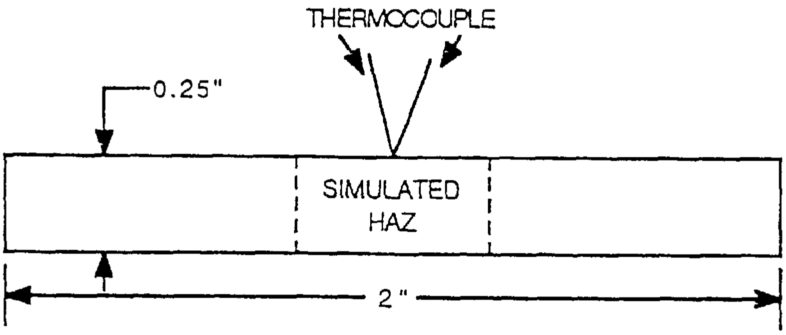

Specimen blank for HAZ simulation

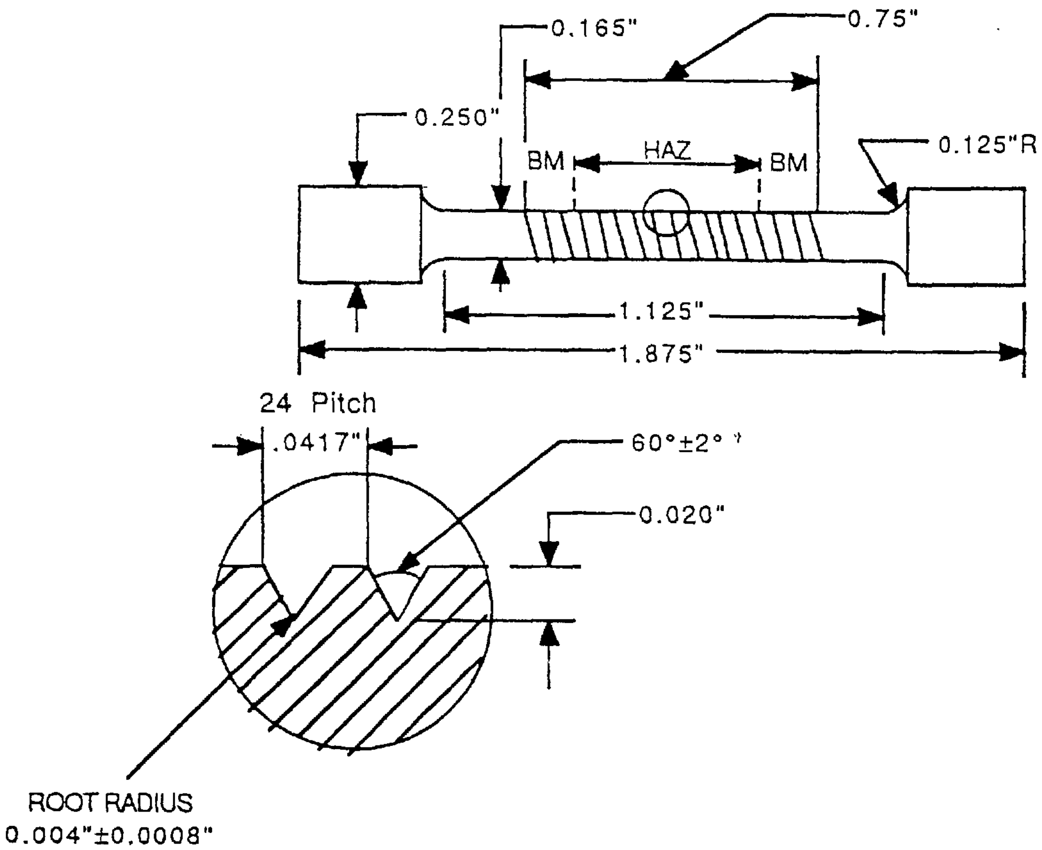

Fig. D2-1—Schematic sketch of 0.165 in. spiral notch specimen

created at the center and lower temperature HAZ microstructures exist on both sides of the CGHAZ. The specimen is loaded in a standard creep rupture frame at a given stress and heated under control to 1150°F in 1 hour and held at temperature until rupture. Spiral notch specimens with simulated CGHAZ at the center of the specimen gage lengths are tested in the as-simulated condition and subsequent to a PWHT exposure without stress. The rupture time and total specimen extension is recorded and the fracture surface examined to determine fracture mode. The specimen is normally reassembled and sectioned longitudinally to determine the specific location of fracture in the gage length, which encompasses the various regions of the HAZ including the base metal. The selection of the stress is based on the material and the fact that the residual stresses in a weldment approximate the yield strength at the PWHT temperature. The Spiral Notch Test can be utilized both as a screening test as well as a test to investigate the fundamental mechanisms of reheat cracking.

Spiral Notch Test Results

Spiral Notch Test results are presented in Table D2-1. At high stresses for most materials the specimen ruptures in the base metal. Upon reduction of the test stress the rupture location shifts to the

Table D2-1—Spiral Notch Test Results of Gleeble Simulated Samples
Peak Temperature: 2400°F, Test Temperature: 1150°F

MATERIALS	HEAT INPUT (KJ/in)	STRESS (Ksi)	RUPTURE TIME (hrs)	RUPTURE LOCATION
UT1-NV	120	30	24.1	BM
UT1-NV	120	25	57.6	CGHAZ
UT1-NV	120	20	99.1	CGHAZ
UT1-NV	120	17	177.4	FGHAZ
UT1-NV	12	30	12.9	FGHAZ
UT1-NV	12	25	34.3	FGHAZ
UT1-NV	12	20	60.0	FGHAZ
UT1-NV	12	17	77.4	FGHAZ
UT2-NV	120	30	7.9	BM
UT2-NV	120	25	14.5	BM
UT2-NV	120	20	112.7	BM
UT2-NV	120	17	150.8	BM
UT2-NV	12	30	7.5	BM
UT2-NV	12	25	30.6	ICHAZ
UT2-NV	12	20	36.0	BM
UT2-NV	12	17	102.4	ICHAZ
UT3-VM	120	30	2.7	CGHAZ
UT3-VM	120	25	7.7	CGHAZ
UT3-VM	120	20	25.7	CGHAZ
UT3-VM	120	15	51.8	CGHAZ
UT3-VM	12	25	4.9	CGHAZ
UT3-VM	12	20	11.6	CGHAZ
UT3-VM	12	15	30.4	CGHAZ
UT3-VM	12	12	117.2	CGHAZ

NV-Re-Normalized (Virgin)   VM-Virgin Materials

Table D2-1—(Continued)

MATERIALS	HEAT INPUT (KJ/in)	TEST TEMP (°F)	STRESS (Ksi)	RUPTURE TIME (hrs)	RUPTURE LOCATION
UT4-VM	30	1150	50	0.05	BM
UT4-VM	30	1150	50	0.05	CGHAZ
UT4-VM	30	1150	25	13.7	CGHAZ
UT4-VM	30	1150	25	5.2	CGHAZ
UT4-VM	30	1150	25	4.4	CGHAZ
UT4-VM	30	1150	20	36.7	CGHAZ
UT4-VM	30	1150	17	47.4	FGHAZ
UT4-VM	30	1250	25	0.5	CGHAZ
UT4-VM	30	1250	20	1.5	CGHAZ
UT4-VM	30	1250	17	3.2	FGHAZ
UT4-VM*	30	1150	25	10.5	CGHAZ
UT4-VM**	30	1150	25	10.2	FGHAZ
UT5-VM	30	1150	35	2.8	BM
UT5-VM	30	1150	25	21.8	BM
UT5-VM	30	1150	25	21.4	BM
UT5-VM	30	1150	20	72.4	CGHAZ
UT5-VM	30	1150	18	119	ICHAZ
UT5-VM	30	1250	20	2	BM
UT5-VM	30	1250	15	12.3	BM
UT5-VM	30	1250	13.5	17.8	FGHAZ
UT5-VM	30	1250	12	31.2	FGHAZ
UT5-VM*	30	1150	20	74.5	FGHAZ
UT5-VM**	30	1150	20	32.4	BM
UT6-VM	30	1150	35	2.3	CGHAZ
UT6-VM	30	1150	30	2.3	CGHAZ
UT6-VM	30	1150	25	10.0	CGHAZ
UT6-VM	30	1150	20	38.0	CGHAZ

*PWHT-1150°F-2Hrs.

**PWHT-1350°F-2Hrs.

Table D2-1—(Continued)

MATERIALS	HEAT INPUT (KJ/in)	STRESS (Ksi)	RUPTURE TIME (hrs)	RUPTURE LOCATION
UT7-VM	120	25	9.3	BM
UT7-VM	120	20	51.6	BM
UT7-VM	120	17	134.4	BM
UT7-VM	120	15	265.1	ICHAZ
UT7-VM	12	25	21.0	BM
UT7-VM	12	20	54.4	FGHAZ
UT7-VM	12	17	109.1	FGHAZ
UT7-VM	12	15	163.0	FGHAZ
UT8-SE	120	25	1.4	BM
UT8-SE	120	17	10.1	BM
UT8-SE	120	15	20.3	BM
UT8-SE	120	12	100.5	FGHAZ
UT8-SE	12	20	2.8	BM
UT8-SE	12	17	8.7	BM
UT8-SE	12	15	21.9	BM
UT8-SE	12	12	85.4	ICHAZ
UT8-NV	120	25	7.2	BM
UT8-NV	120	17	34.1	BM
UT8-NV	120	15	74.1	ICHAZ
UT8-NV	12	25	12.4	BM
UT8-NV	12	17	35.6	ICHAZ
UT8-NV	12	15	76.4	ICHAZ
UT9-SE	120	25	19.0	BM
UT9-SE	120	20	59.9	FGHAZ
UT9-SE	120	17	117.4	FGHAZ
UT9-SE	120	15	220.7	FGHAZ
UT9-SE	12	25	17.8	BM
UT9-SE	12	20	32.5	FGHAZ
UT9-SE	12	17	64.3	FGHAZ
UT9-SE	12	15	121.5	FGHAZ

Table D2-1—(Continued)

MATERIALS	HEAT INPUT (KJ/in)	STRESS (Ksi)	RUPTURE TIME (hrs)	RUPTURE LOCATION
UT10-SE	120	20	7.3	BM
UT10-SE	120	17	30.9	BM
UT10-SE	120	15	50.3	BM
UT10-SE	120	12	213.8	FGHAZ
UT10-SE	12	20	10.3	BM
UT10-SE	12	17	22.3	BM
UT10-SE	12	15	33.1	BM
UT10-SE	12	12	178.0	BM
UT11-SE	120	25	2.0	BM
UT11-SE	120	17	40.8	BM
UT11-SE	120	15	111.5	BM
UT11-SE	120	12	416.3	FGHAZ
UT11-SE	12	20	14.8	BM
UT11-SE	12	17	52.2	BM
UT11-SE	12	15	139.7	FGHAZ
UT11-SE	12	12	382.3	FGHAZ

CGHAZ for crack susceptible heats. Further reduction in stress results in a shift of the rupture location to the FGHAZ or ICHAZ. The range of stress over which the specimens rupture in the CGHAZ is an indicator of the relative susceptibility of a material to reheat cracking. However, it is to be noted that for heats resistant to reheat cracking the rupture location shifts directly from the base metal at high stresses to the FG/ICHAZ at low stresses. Thus, the narrower the stress range over which a specimen ruptures in the CGHAZ the more resistant the material/heat will be to reheat cracking at a particular PWHT temperature. If a specimen does not rupture in the CGHAZ the heat is not susceptible to reheat cracking. Macro-photos of typical fractured spiral notched specimens are shown in Fig. D2-2.

The Spiral Notch Test methodology has been extended to full scale weldment characterization to evaluate the behavior of controlled deposition weld methods. Proprietary work at the University of Tennessee utilizing spirally-notched specimens for evaluation of a controlled deposition technique in a A710 steel repair was successfully used in developing procedures to avoid cracking in the CGHAZ in service. Further, the use of the test aided in the development of repair techniques that have proven extremely successful in preventing cracking during PWHT. By extracting samples from actual welds that represent repaired or original weld deposition methods, a means of obtaining direct information on relative base metal-weld metal strengths, microstructure, and PWHT, is at hand. The sample size can be chosen to be representative of full scale weldments with deposition characteristics reflecting different welding processes. The Spiral Notch Test developed in the WRC funded program has been successfully used to evaluate welds in a PVRC funded program at the University of Tennessee to investigate controlled deposition techniques in Cr-Mo and HSLA steels.

The spiral notched specimen used in this program has a major diameter of 0.165 in. (4.2 mm) and a minor diameter of 0.125 in. (3.2 mm). This specimen has also been scaled-up to a major diameter of 0.350 in. (8.9 mm) and a minor diameter of 0.250 in. (6.35 mm) using almost identical notch acuity and has been successfully used in the PVRC program. The scaled-up spiral notch specimen is recommended for actual weld procedure evaluations and procedure qualification tests because it samples a larger volume of material. It was shown that susceptible materials show more consistent susceptibility responses to reheat cracking initiation when scaled-up specimens are utilized. The scaled-up specimen is shown schematically in Fig. D2-3 as applied to a weldment. The scaled-up sample can also be employed with a simulated HAZ.

Thus, it is evident that the Spiral Notch Test is very useful for investigating the fundamental mechanisms and relative reheat cracking susceptibility of materials. It has been demonstrated that the notch,

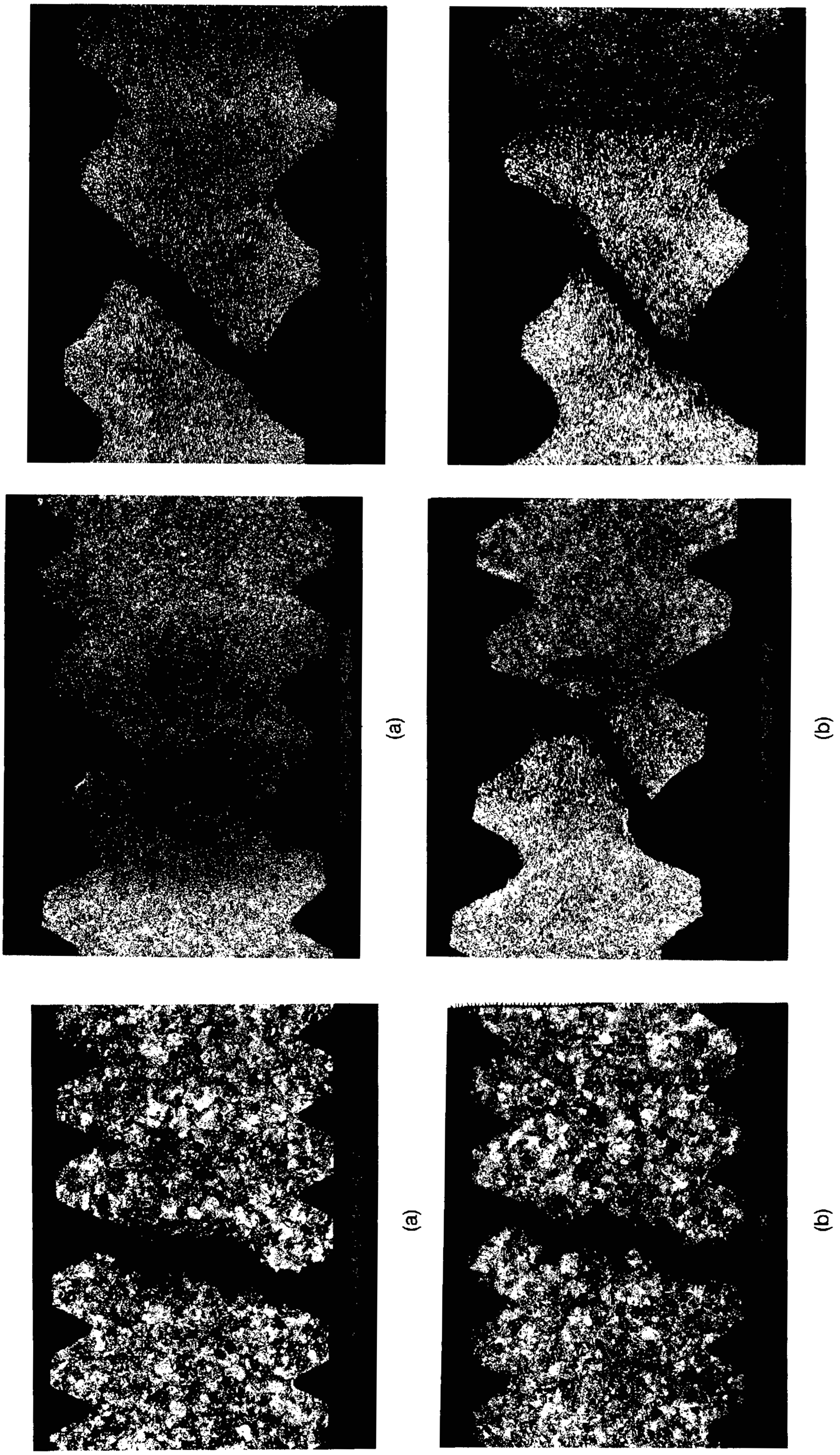

(a)

(b)

(a)

(b)

Fig. D2-2—Macrographs of typical fractured spiral notched specimens

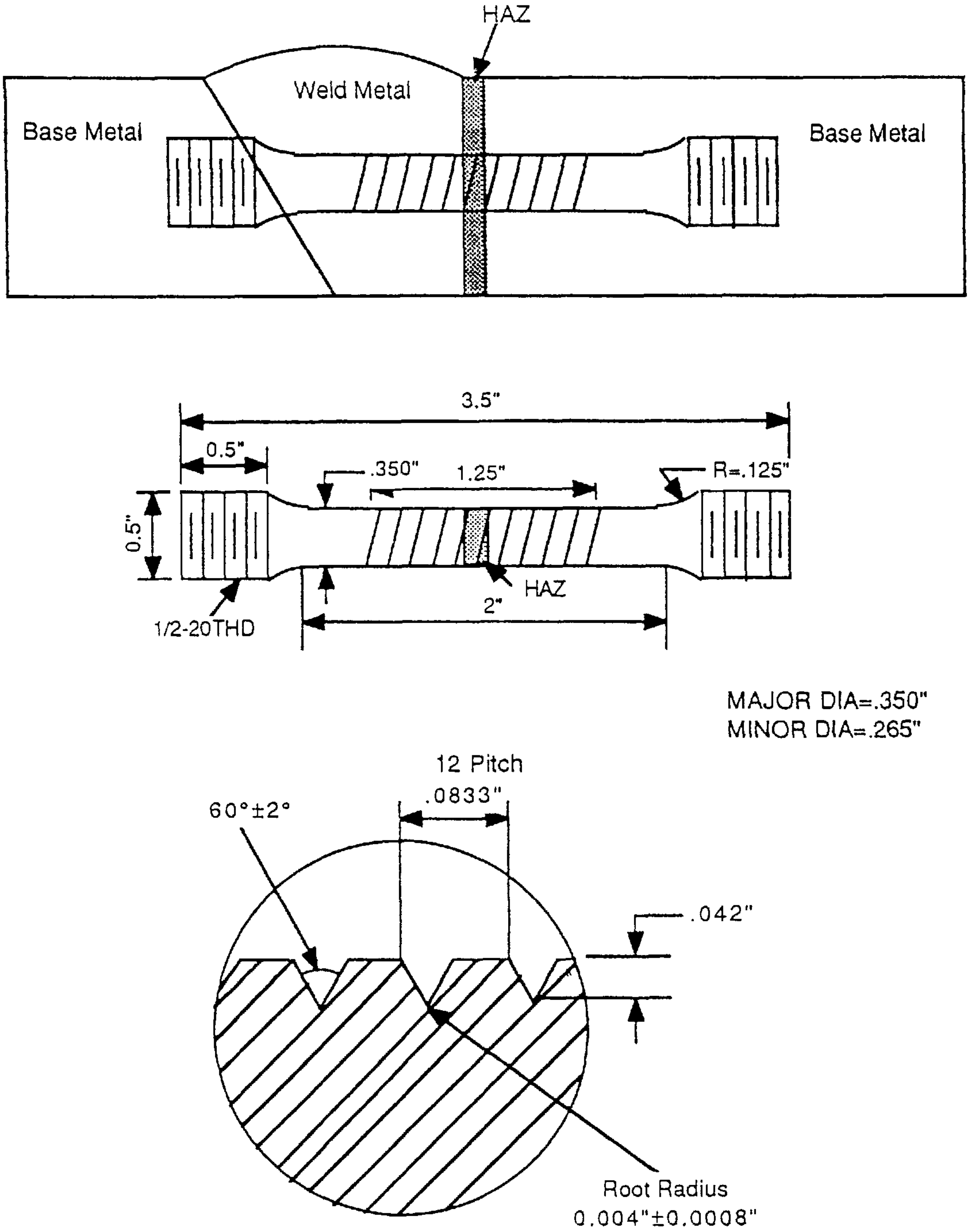

Fig. D2-3—Sketch of 0.350 in. spiral notch specimen

which encompasses all the metallurgically different regions of a weld, is an added advantage due to the fact that the effects of all regions are accommodated in the test. Because a notch is present in all regions itis possible to study the shift in notch sensitivity of each region as a function of PWHT time, temperature and stress. The test is also applicable to both simulated and actual weld samples. By this technique it is possible to determine the effect of overlapped HAZs and also the effect of prior PWHT as well as the effect of heating rate on the reheat cracking susceptibility. The lowest stress to avoid rupture in the CGHAZ and the range of stresses over which rupture occurs in the CGHAZ can be used as a criterion for quantifying the susceptibility of a material to reheat cracking susceptibility.

Appendix D3—Development of a New Reheat Cracking Test—PREVEW Test and Evaluation of Reheat Cracking in API Materials

Abstract

As a part of the API program to investigate reheat crack susceptibility of 1¼Cr-½Mo steels, it was necessary to develop a versatile large scale laboratory test to correlate with small scale tests (Gleeble and Spiral Notch) and with actual weld cracking behavior. Thus, a new test called the PREVEW test (Petroleum REfinery Vessel Evaluation of Weldability), was developed to investigate weld reheat cracking in 1¼Cr-½Mo steels. The advantages of this new test are.

1. the scale of the test is larger than most currently available tests and it employs an actual weld;
2. external stress can be applied quantitatively to simulate weld residual stress;
3. stress relaxation of the sample occurs in the same manner as it would occur in an actual fabrication weld;
4. both fillet weld joint and butt weld joint can be used;
5. the effect of welding procedures can be evaluated;
6. the susceptibility of materials can be quantified;
7. the effect of prior condition of the base metal (hardness/heat treatment, e.g., N&T or Q&T) can be evaluated; and
8. no expensive specialized equipment is required except for the simple restraining/stressing fixture.

The PREVEW test results were determined to have an excellent correlation with Gleeble reheat cracking and Spiral Notch Test results.

Introduction

Reheat cracking is intergranular cracking along prior austenite grain boundaries in the coarse grained heat-affected zone (CGHAZ) or weld metal (WM) that occurs during postweld heat treatment (PWHT) or subsequent service of welded assemblies at elevated temperatures. Usually, little or no evidence of deformation is associated with reheat cracking.[1,2]

In general, there are three types of reheat cracking tests:

1. self-restrained weldment tests such as the Y-groove and restrained butt weld tests;[3,4]
2. externally loaded weldment tests such as implant test;[5] and
3. simulated weld test such as the Gleeble stress rupture test.[6]

There are some advantages and disadvantages of both self-restrained weldment and simulated weld tests. The self-retrained weldment tests are desirable from the standpoint that they utilize actual welding conditions. Thus the thermal history and residual stress-strain patterns in the weld joint more closely typify real welding conditions. However, reproducibility is difficult and the actual stress and strain conditions are usually unknown. Finally, since the self-restrained weldment tests are difficult to use to evaluate quantitatively reheat cracking susceptibility, they can more readily serve as go-no go tests.

In terms of providing quantitative data for rating the relative susceptibilities of a material to reheat cracking, the basic advantages of the simulated tests are the stress and stress concentration effects are known and readily controlled and the ductility of the microstructure of interest is readily determined to assess the reheat cracking susceptibility. However, if such a test method is adopted, it is necessary to establish the relationship of the simulated test results to actual weldment conditions.

The external loading weldment tests were proposed to take advantage of both self-restrained tests and the simulated weld test variables. The actual welding procedure and geometry of the weld joint can be applied in the test. The strain can be applied externally and quantitatively.

A new external loading reheat cracking test technique was developed to evaluate the susceptibility of reheat cracking of 1¼Cr-½Mo steels at the University of Tennessee. Because this new test was developed for Petroleum Refinery Vessel Evaluation of Weldability, the test was named the PREVEW Test. The advantage of this test method is that both fillet and butt weld configurations can be used so that the thermal history of the tested samples is typical of real welding situation. Also, this test has the advantage of testing the entire joint: weld metal, heat-affected zone (HAZ) and base metal. In terms of providing quantitative test parameters for assessing the susceptibility of a material to reheat cracking, the pertinent variables relate the reheat cracking factors, such as stress, welding parameters and subsequent reheat temperature. The investigation of reheat cracking susceptibility of 1¼Cr-½Mo steel was conducted using this test method. A good correlation was found between PREVEW test results and the Gleeble stress rupture and Spiral Notch test results.

Test Device and Sample Design

A three point loading device was designed for the PREVEW test. Fig. D3-1 shows a schematic drawing of the device and a loaded fillet joint test sample. The sample can be loaded in bending by advancing the loading screw. The deflection of the sample can be measured accurately by a displacement gage attached to the sample while loading. The initial stress on the sample can be calculated using the displacement and simple beam equations. The fillet joint and butt joint were selected as the types of test specimens based on their common application in welding structures.

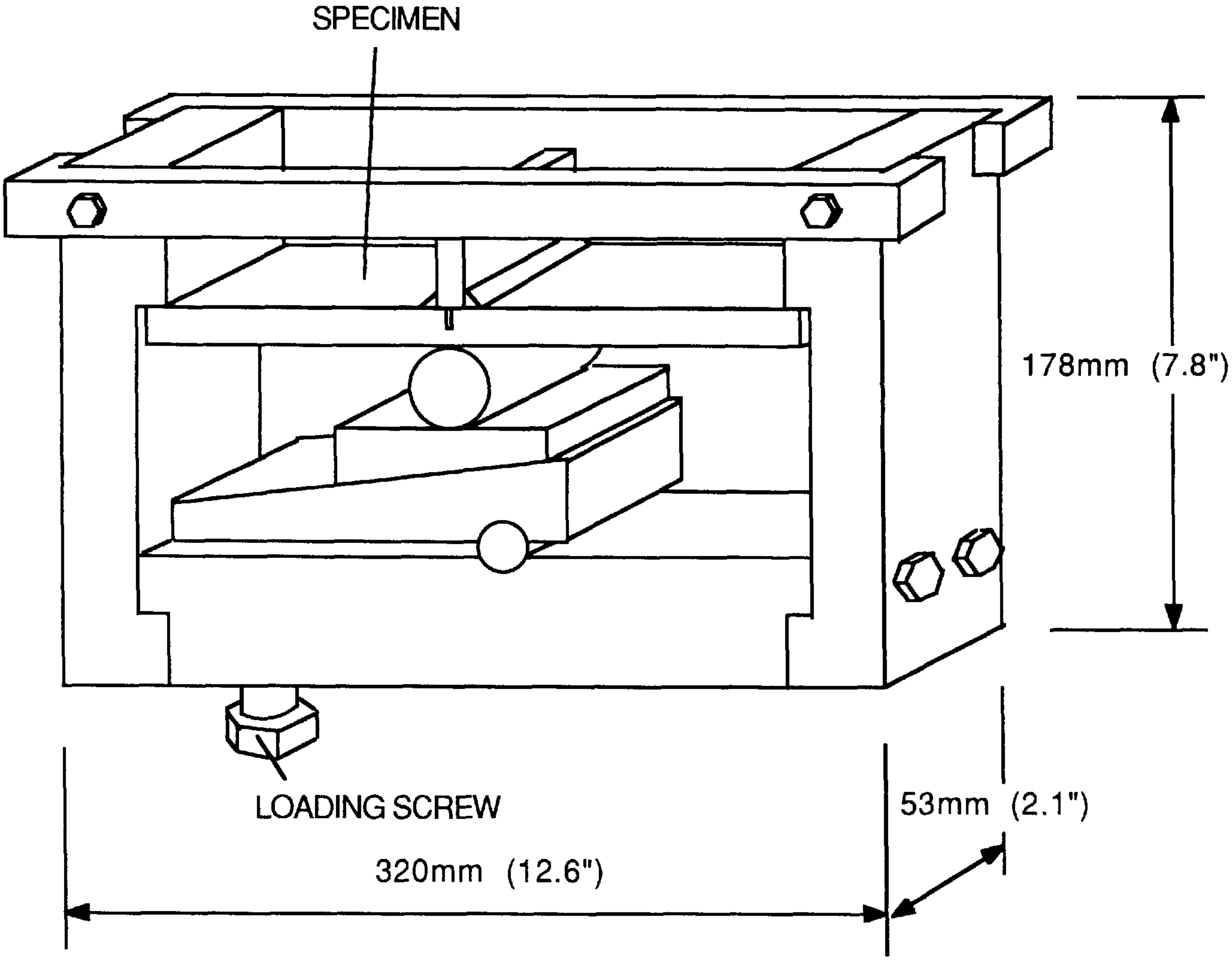

Fig. D3-1—Schematic of PREVEW test device

Fig. D3-2 shows a photograph of a fillet joint test sample loaded in the PREVEW test device. The postweld heat treatment or a simulated service exposure condition can be conducted by placing the fixture in furnace at the test temperature.

A schematic sketch of the fillet joint sample is shown in Fig. D3-3. The sample is 10 in. in length and 4 in. wide. However, the thickness of the sample may be chosen based on the actual weld configuration. For all the tests in this study the specimen used was ½ in. thick. A slot (¼ in. deep) is machined at the center of the base plate in order to produce a high stress concentration at the weld toes. Fig. D3-4 schematically shows the postulated distribution of isostress lines across the fillet joint.

The test described above can be modified for a butt joint configuration. The butt joint test sample for the PREVEW test is shown in Fig. D3-5. It may be noted that by using the butt joint configuration, weld deposition procedures may be evaluated. However, for reproducible results a notch (Charpy notch) is machined along the fusion line to introduce a stress concentration similar to that present in an actual weld due to discontinuities.

Materials

Eleven heats of 1¼Cr-½Mo steel were evaluated using the PREVEW reheat cracking test in the fillet configuration. In addition, limited tests were conducted with a butt weld configuration. The chemical composition of the heats evaluated by the PREVEW test is listed in Table D3-1.

Fabrication of Test Weldment Specimens

The test samples were welded using 5/32 in. SMA E8018-B2 electrodes for both fillet and butt joints with a preheat and interpass temperature of 150–180°C (300–350°F). The electrodes were baked at 350°C (660°F) for at least 2 hours to minimize hydrogen pick-up in weld metal and thus to avoid the possibility of hydrogen assisted cracking. Table D3-2 shows the welding parameters for fillet and butt joints. The welded sample is strained in the fixture to a specific deflection (usually representing the yield strength). Dye penetrant inspection is employed before and after straining to assure that the specimen is not cracked before heating the assembly to the test temperature of 621°C (1150°F). Heating and cooling conditions are controlled and recorded during the

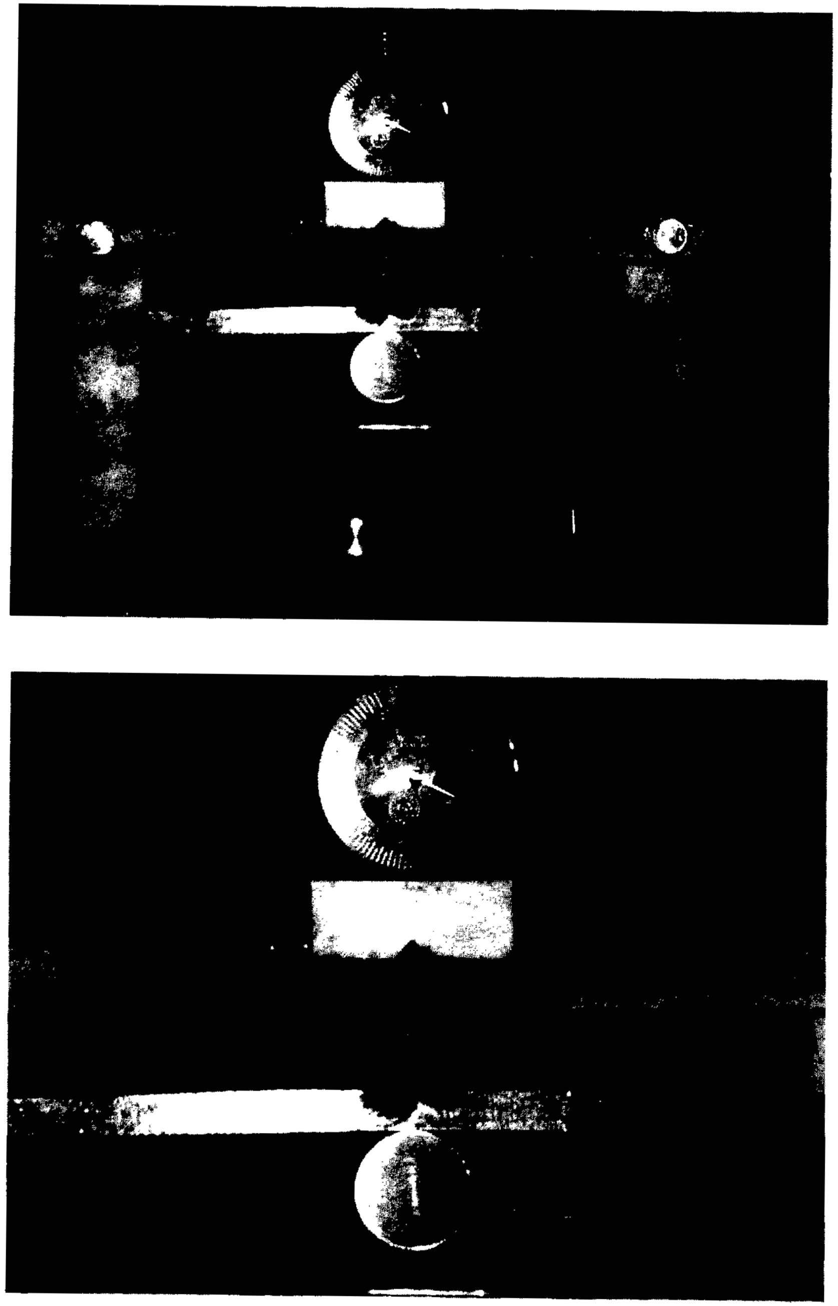

Fig. D3-2—PREVEW test device

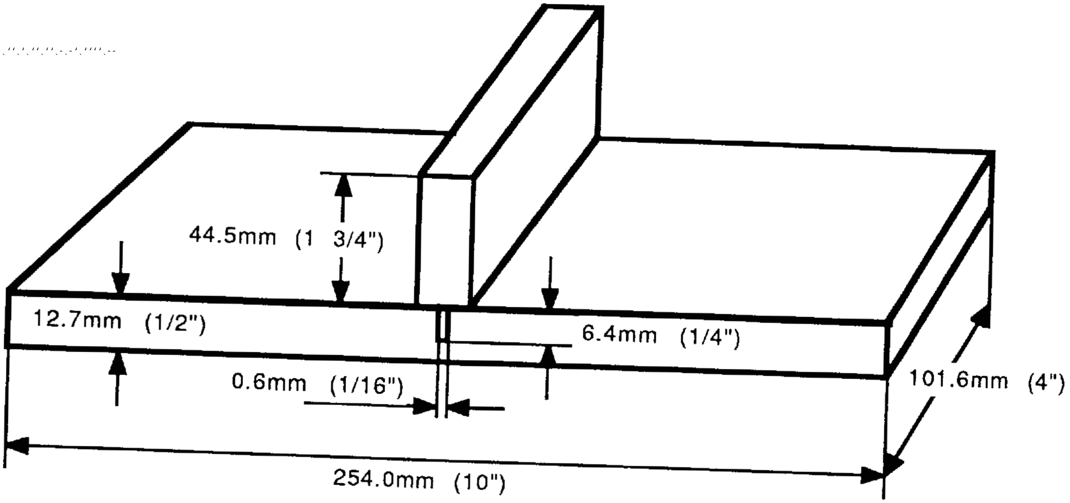

Fig. D3-3—Specimen dimensions for fillet weld

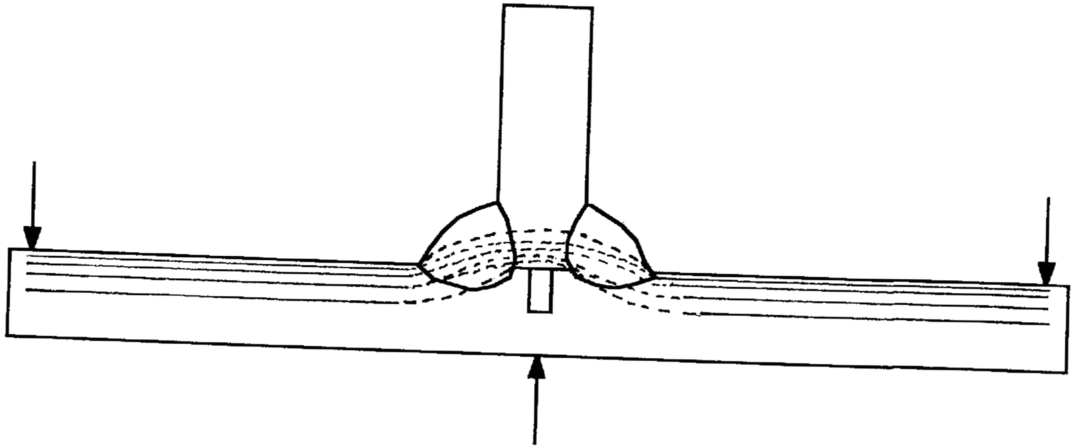

Fig. D3-4—Anticipated tensile stress distribution in a fillet weld

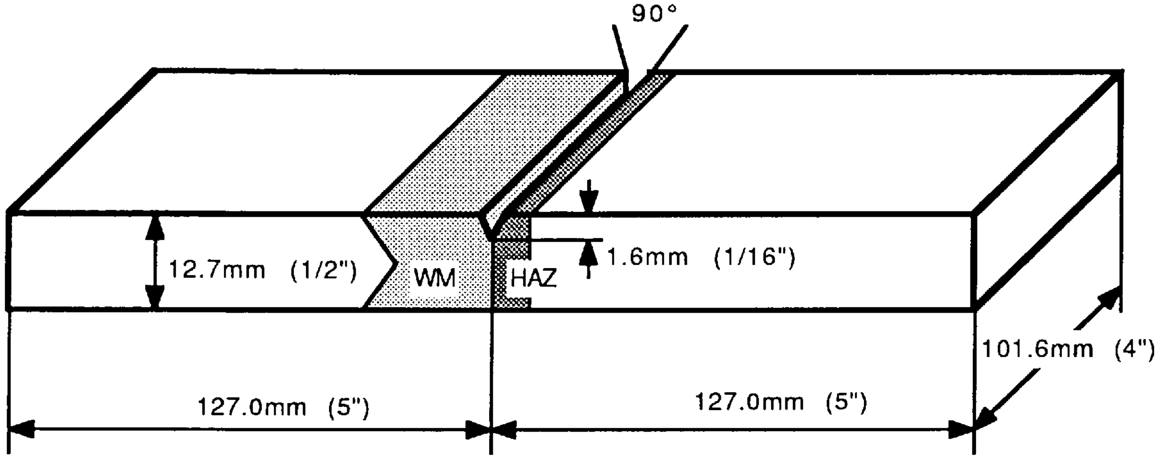

Fig. D3-5—Specimen dimensions for butt weld

Table D3-1—Chemical Composition of Materials Used for PREVEW Test (Wt%)

MATERIALS	C	Mn	P	S	Si	Ni	Cr	Mo	V	Nb	Ti
UT2	0.10	0.45	0.010	0.013	0.65	0.18	1.30	0.53	0.004	0.00007	0.00173
UT3	0.15	0.50	0.007	0.017	0.61	0.21	1.27	0.47	0.010	0.00025	0.00238
UT4	0.18	0.79	0.009	0.003	0.52	0.20	1.33	0.53	0.005	0.00006	0.00149
UT5	0.17	0.50	0.008	0.004	0.64	0.08	1.41	0.50	0.004	0.00062	0.00250
UT8	0.13	0.42	0.010	0.015	0.62	0.17	1.22	0.58	0.003	0.00005	0.00313
UT9	0.14	0.41	0.012	0.025	0.58	0.06	1.25	0.61	0.003	<0.00001	0.00017
UT11	0.086	0.42	0.010	0.016	0.49	0.01	1.04	0.54	0.003	<0.00001	0.00039
UT12	0.10	0.56	0.004	0.001	0.57	0.12	1.46	0.55	0.003	0.00001	0.00357
UT13	0.12	0.45	0.004	0.024	0.59	0.29	1.27	0.49	0.004	<0.00001	0.00015
UT14	0.17	0.51	0.015	0.012	0.66	0.09	1.16	0.49	0.002	0.00004	0.00137
UT15	0.096	0.46	0.010	0.027	0.62	0.01	1.27	0.54	0.005	<0.00001	0.00064
UT16	0.11	0.47	0.008	0.020	0.56	0.16	1.16	0.47	0.004	<0.00001	<0.00001
UT17	0.19	0.58	0.009	0.003	0.63	0.05	1.05	0.48	0.006	0.00011	0.00211

Table D3-1—Chemical Composition of Materials Used for PREVEW Test (Wt%) (Continued)

MATERIALS	Co	Cu	Al	B	W	As	Sn	Zr	Sb	Ca	N	O
UT2	0.010	0.05	0.004	<0.00001	0.008	0.007	0.007	<0.001	0.00041	0.0016	0.0155	0.0058
UT3	0.012	0.16	0.003	0.00003	<0.01	0.004	0.015	<0.001	0.00095	0.0011	0.0116	0.0048
UT4	0.015	0.15	0.017	<0.00001	0.001	0.016	0.014	0.005	0.00168	0.0001	0.0112	0.001
UT5	0.007	0.09	0.021	<0.00001	0.001	0.007	0.009	0.002	0.00055	0.0014	0.0083	0.002
UT8	0.010	0.11	0.026	<0.00001	<0.01	0.008	0.012	<0.001	0.00146	0.0013	0.012	0.005
UT11	0.006	0.02	0.002	<0.00001	<0.01	0.004	0.002	<0.001	0.00016	0.0010	0.011	0.011
UT12	0.010	0.07	0.017	0.00005	<0.01	0.010	0.005	<0.001	0.00070	0.0012	0.007	0.002
UT13	0.014	0.17	0.002	<0.00001	<0.01	0.007	0.015	<0.001	0.00193	0.0010	0.008	0.007
UT14	0.009	0.13	0.003	0.00002	<0.01	0.007	0.012	<0.001	0.00105	0.0014	0.013	0.008
UT15	0.006	0.04	0.003	0.00001	<0.01	0.006	0.004	<0.001	0.00032	0.0002	0.014	0.010
UT16	0.012	0.17	0.001	<0.00001	<0.01	0.009	0.015	<0.001	0.00170	0.0013	0.007	0.003
UT17	0.011	0.01	0.018	0.00028	<0.01	0.003	0.003	<0.002	0.00032	0.0016	0.006	0.001

Table D3-2—Typical Welding Parameters for Fillet and Butt Joints

Weld Joint	*Current (AMP)*	*Voltage (V)*	*Heat Input (KJ/in)*
Fillet joint	175	23	60
Butt joint	175	23	80

test. Both dye penetrant inspection and metallographic methods are utilized to evaluate the extent of cracking after test.

Calibration. In addition to stress estimation from material properties, Stresscoat was used to define the stress state in the PREVEW test.[7] Stresscoat is a strain-sensitive paint-like material which, after application and proper curing, cracks in a controlled fashion when a specimen is subjected to strain. Fig. D3-6 shows the coupon used for strain calibration. The density of coating cracks (when calibrated) is a good indication of the applied strain. The paint-like Stresscoat is uniformly sprayed on the top surface of the sample using an airbrush and allowed to cure for approximately 18–24 hours at room temperature before test loading. The cured coating is sensitive to cracking in the strain range of 0.05–0.5%. No cracking occurs if the strain is under 0.05% and the coating begins to flake if the strain is greater than 0.5%. The cracking pattern is an indication of the strain distribution on the sample surface and the crack density determines the strain or stress quantitatively. Fig. D3-7 gives the relationship of Stresscoat cracking intensity to material strain.

A fillet joint PREVEW sample of 1¼Cr-½Mo steel was coated on the top surface with Stresscoat following the procedure mentioned above. After curing for 24 hours, the sample was strained to a 0.3 mm (0.12

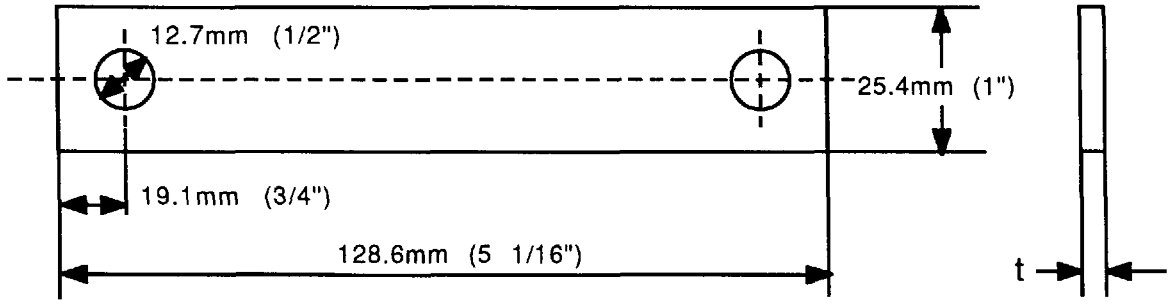

Fig. D3-6—Coupon for strain calibration

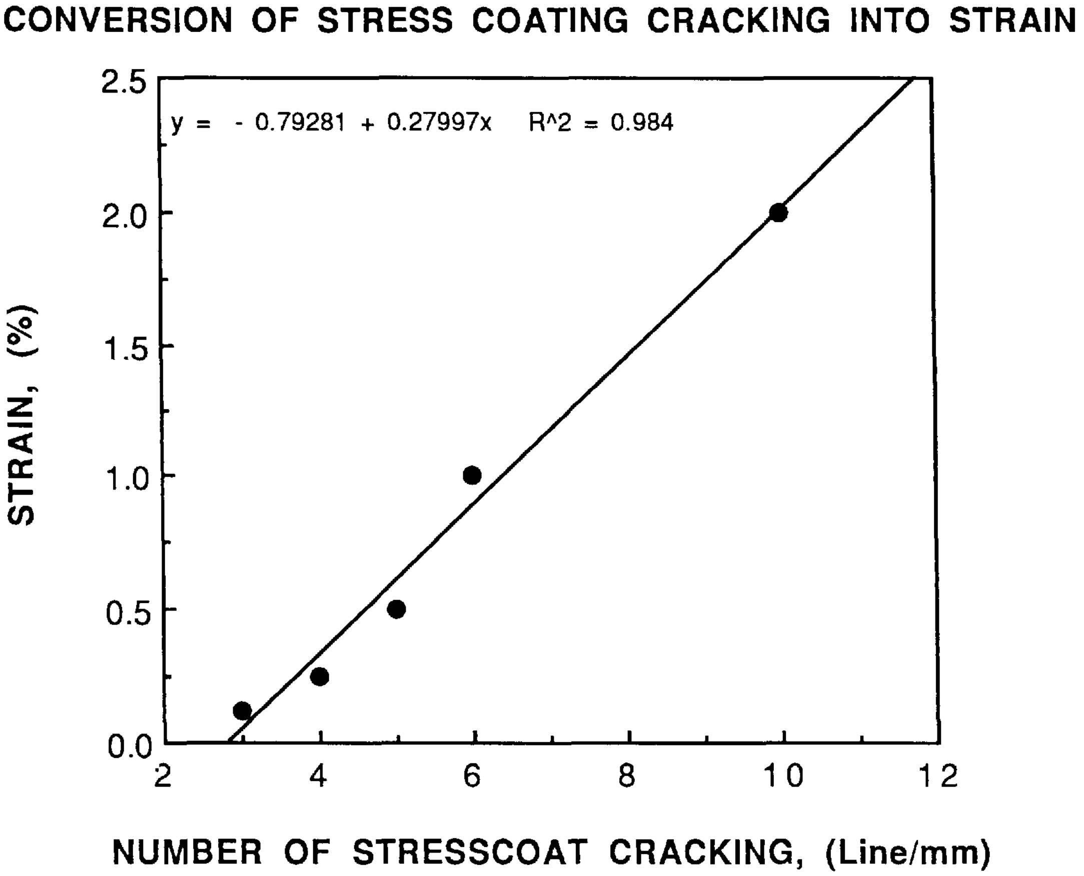

Fig. D3-7—Relationship of Stresscoat cracking intensity to material strain in.) in deflection in the test fixture and the number of cracks across a 10 mm length adjacent to the weldtoes were determined. The linear crack density was determined to be approximately 4.7/mm which is equivalent to 0.53% strain.

Considering only elastic deformation in the loaded PREVEW test sample, a strain of 0.53% can be calculated to be equivalent to a stress of approximately 1096 MPa (159 Ksi). Since the yield strength of 1¼Cr-½Mo steel is approximately 414 MPa (60 Ksi), an elastic-plastic theory must be used to calculate the resultant stress for 0.53% applied strain. The stress adjacent to the weld toe in the fillet joint is calculated to be approximately 483 MPa (70 Ksi) for 0.53% strain which corresponds to a deflection of 0.3 mm (0.12 in.). However, it must be recognized that the hardness or strength of the CGHAZ is significantly higher than that of the base plate. Thus, the stress in the CGHAZ region at the toe of the weld may be higher than 70 Ksi (considering most of the additional strain is relaxed by plastic deformation of the base plate).

Test Criteria

The following criteria were used to assess susceptibility to reheat cracking in the PREVEW test: maximum crack depth, average crack depth and crack length. The crack depth is measured in three metallographically-prepared transverse sections of both fillet welds or the butt joint (depending on the test configuration), at 100× to 400×. The average of the crack depth measured in the three transverse sections is used as a criterion.

Average crack depth (mm) = (Sum of crack/depth)/3

The maximum crack depth in three transverse sections can also be used as a criterion for assessment of reheat cracking susceptibility of a material using the PREVEW test.

The crack length criterion is defined as the percentage of crack length to the total weld bead length in two longitudinal sections along the fillet joint. The crack length is measured at 100× to 400× using an optical microscope

$$\text{Crack length (\%)} = \frac{100 \times \text{Sum of crack lengths at both toes}}{2 \times \text{Weld bead length}}$$

Test Time and Reheat Cracking Susceptibility

It has been suggested that reheat cracking is dependent on the time and temperature of the PWHT cycle. During PWHT or subsequent elevated temperature service, the welding residual stresses relax in a temperature range which also corresponds to the temperature range of reheat cracking susceptibility.

In this study, cracking initiation and propagation behavior was investigated by examining the crack depth in three transverse sections and crack length in two longitudinal sections of the fillet weld samples of UT3 tested at 621°C (1150°F) for various test times (Figs. D3-8, D3-9). It was found that heating to 621°C

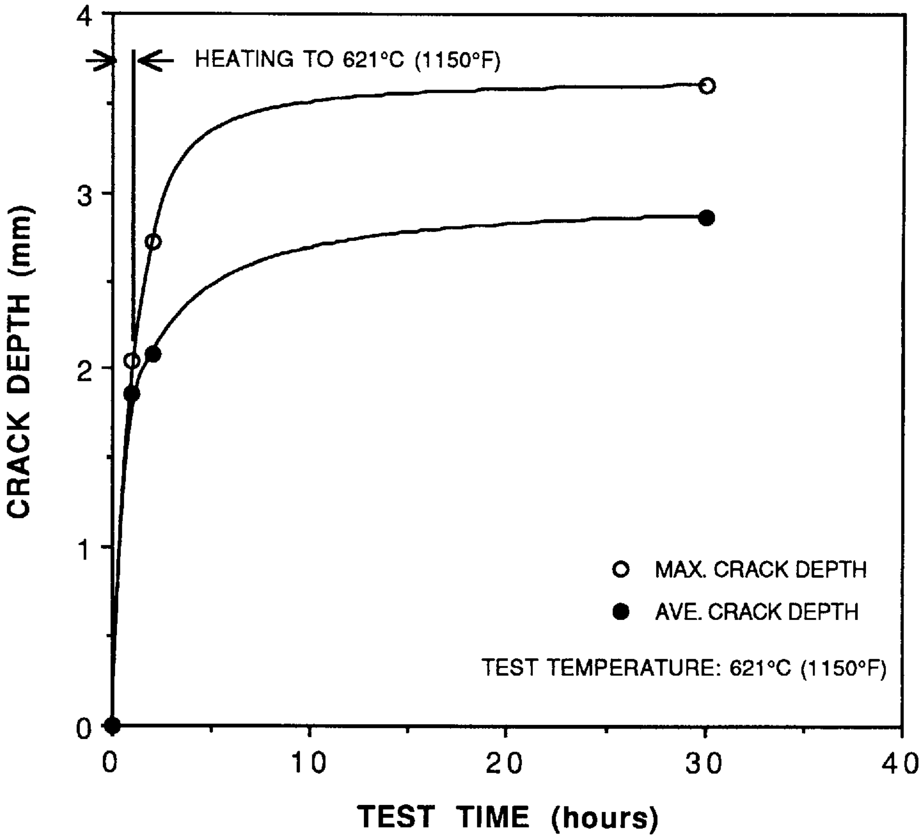

Fig. D3-8—Correlation of reheat crack depth with test time in fillet weld of UT3 using PREVEW test

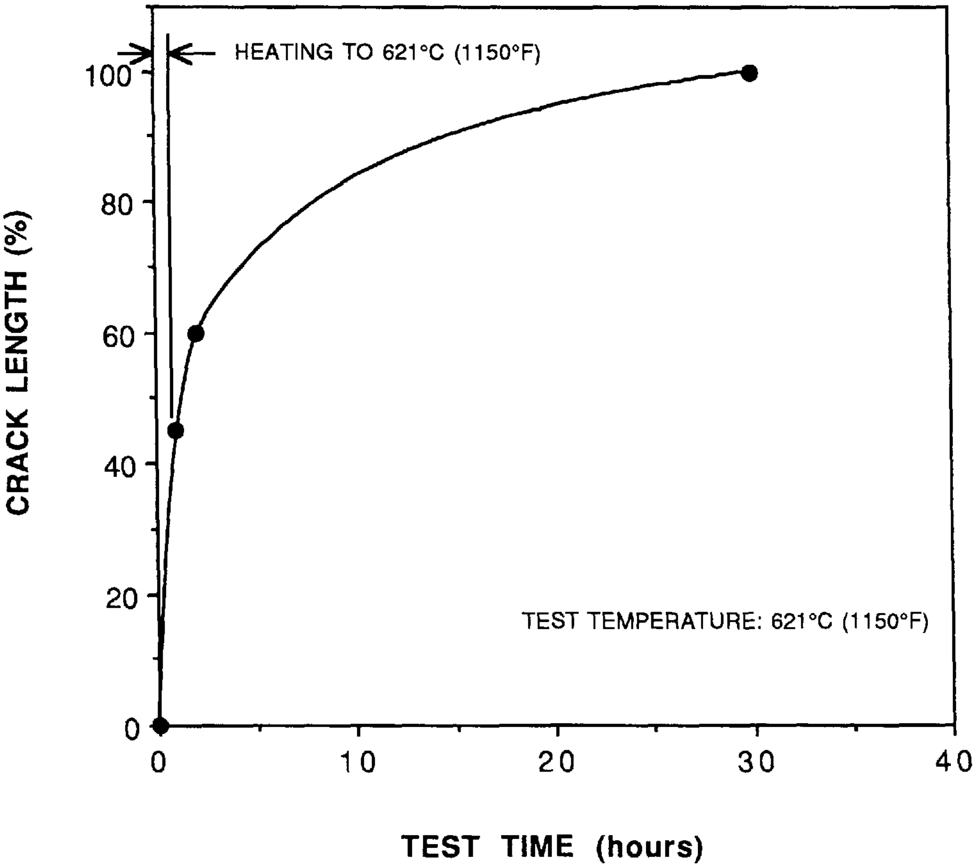

Fig. D3-9—Correlation of reheat crack length with test time in fillet weld of UT3 using PREVEW test

(1150°F) from room temperature in 1 hour, reheat cracking had already occurred in the PREVEW sample with a maximum crack depth of 2 mm and a crack length of 43%. With an increase in the test time the cracks propagated. Figure D3-8 shows that the extension of the reheat cracks does not occur beyond approximately 4 hours at 621°C (1150°F), which illustrates that most of the applied stress relaxes in approximately 4 hours.

A photograph of a dye penetrant inspection of a reheat cracked PREVEW specimen is shown in Fig. D3-10. Weld toe cracks along both weld beads are clearly revealed. The crack depth and crack length observed in the transverse and longitudinal sections of the fillet joint are shown in Figs. D3-11 and D3-12, respectively. It is clear that reheat cracks initiate at the weld toes and then propagate along the grain boundaries in CGHAZ, which is a typical reheat cracking morphology. Figure D3-13 shows a transverse section of the butt joint of UT3 with notch in CGHAZ tested at 621°C (1150°F) for 30 hours. It is clear that the crack initiated at the tip of notch and propagated approximately 2.5 mm along the grain boundaries in CGHAZ.

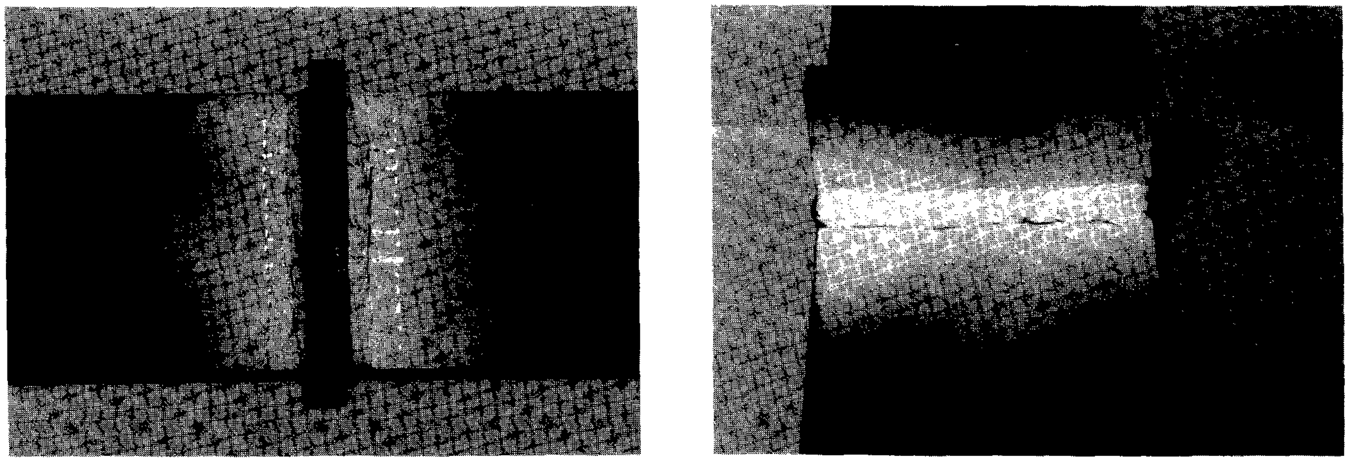

Fig. D3-10—Dye penetrant inspection of reheat cracking in fillet weld

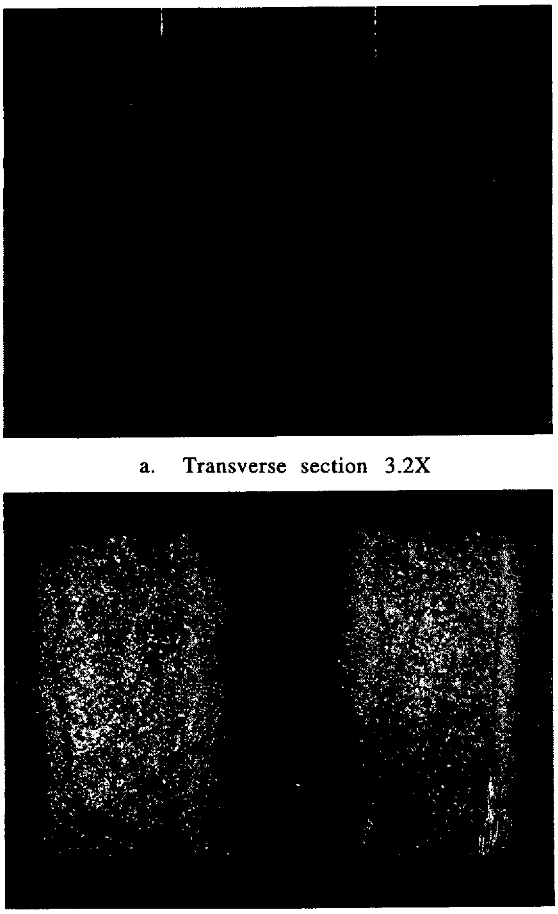
a. Transverse section 3.2X

b. Longitudinal section 1.8X

Fig. D3-11—Reheat cracking in fillet weld of UT3 tested at 1150°F for 30 hours

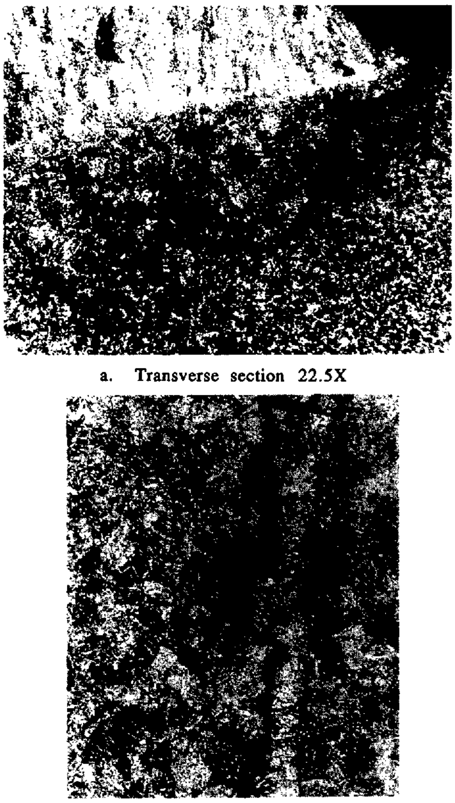
a. Transverse section 22.5X

b. Longitudinal section 50X

Fig. D3-12—Reheat cracking initiated at weld toes in HAZ of UT3

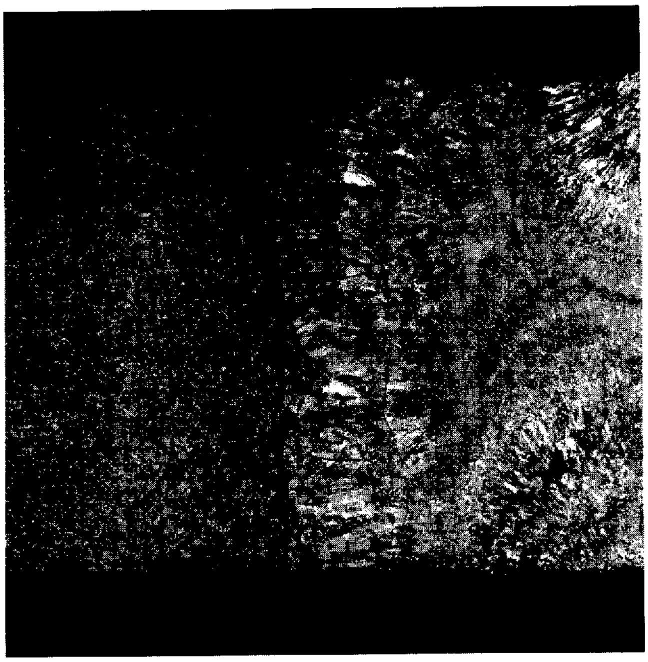
Fig. D3-13a—Transverse section of butt weld in UT3, 4.6×

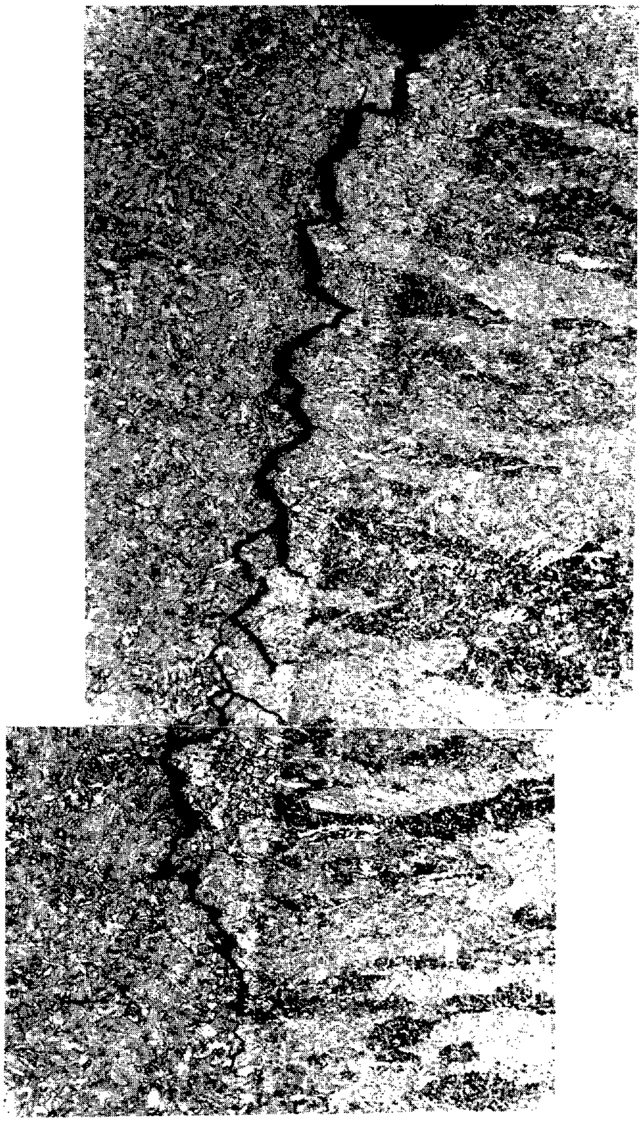
Fig. D3-13b—Reheat crack initiated at the notch tip. Propagated along CGHAZ of butt weld in UT3, 50×

Fig. D3-13c—Intergranular reheat crack in CGHAZ in butt weld of UT3, 200×

Correlation of PREVEW Test Results and Gleeble Rupture Test Results

The PREVEW test Results for samples UT2 thru UT17 are given in Table D3-3.

All of the heats tested in the PREVEW test were also investigated utilizing the Gleeble stress rupture test (described in Appendix D-1 of this report). The PREVEW test crack depth and length is plotted against the Gleeble reduction in area in Figs. D3-14, D3-15 and D3-16. If the Gleeble reduction in area is less than approximately 13% cracking occurs in the PREVEW test.

Vinckier and Pense[12] studied 18 steels using simulated specimens tensile tested at elevated temperature. A criterion for cracking based on the reduction in area of these materials previously subjected to simulated welding thermal cycles was established. The reheat cracking susceptibility was ranked as:

Susceptibility to reheat cracking	*Reduction in area (%)*
Extremely susceptible	<5
Highly susceptible	5–10
Slightly susceptible	10–15
Not susceptible	>20

The authors stated that any material capable of 20% RA in the CGHAZ at the specified PWHT temperature would not exhibit reheat cracking. The PREVEW test results are in agreement with this conclusion. However, the 20% RA as a criterion appears to beconservative based on the PREVEW reheat cracking test results.

Conclusions

The new reheat cracking test, the PREVEW test, has the advantages of both self-restrained weld tests and simulated weld tests. The PREVEW test can be applied in both fillet and butt weld configurations to typify closely the actual fabrication situations. The test conditions, such as welding parameters, restraint stress and test temperature, can be chosen identical to actual fabrication conditions.

The crack depth and length can be used as criteria to evaluate reheat cracking susceptibility of Cr-Mo steels. The test temperature and test time should be determined based on the PWHT or the in-service conditions.

The Stresscoat technique was successfully applied to determine the stress in the PREVEW test sample. The stress at the weld toes in fillet joint is about 483 MPa (70 Ksi) when the sample is loaded to 0.12 in. in deflection in severe restraint condition.

The PREVEW test results are satisfactorily reproducible and are in accordance with Gleeble reheat cracking test results. If the reduction in area of Gleeble stress rupture test is over 13% no reheat cracking occurs in the PREVEW test.

Table D3-3—Full-Scale Weld HAZ Cracking Test Results Using PREVEW Test (Test Temperature: 1150°F)

Samples	Base Metal Hardness (HV)	Joint Type*	Deflection (in)	Test Time (hrs)	Maximum** Crack Depth (mils)	Average** Crack Depth (mils)	Average*** Crack Length (%)
UT2-SE-T1	155	Fillet	0.12	30	0	0	0
UT2-Q/T-T2	228	Fillet 120KJ/IN	0.12	30	0	0	0
UT3-VM-T4	240	Fillet	0.12	0	81	73	45
UT3-VM-T3	240	Fillet	0.12	1	107	82	60
UT3-VM-T2	240	Fillet	0.12	30	142	113	100
UT3-VM/T-T5	172	Fillet	0.12	30	108	71	90
UT3-VM/T-T6	155	Fillet	0.12	30	28	14	30
UT3-VM/T-T8	153	Fillet	0.12	30	13	7	40
UT3-VM-T9	240	Fillet with temper beads	0.12	30	159	118	76
UT3-VM-T10	240	Fillet with clad temper beads	0.12	30	37	7	22
UT3-VM-T11	240	Fillet, temper in furnace****	0.12	30	0	0	0
UT3-VM-T12	240	Fillet	0.12	Heating to 1000°F	0	0	0
UT3-VM-T12	240	Fillet	0.12	1000°F 131 hrs.	60	10	18
UT3-VM-T7	240	Fillet(E7018)	0.12	30	20	3	5
UT3-VM-T1	240	Fillet	0.08	8	14	2	40
UT3-VM-B1	240	Butt	0.12	30	102	94	-

Table D3-3—Full-Scale Weld HAZ Cracking Test Results Using PREVEW (Continued)

Samples	Base Metal Hardness (HV)	Joint Type*	Deflection (in)	Test Time (hrs)	Maximum** Crack Depth (mils)	Average** Crack Depth (mils)	Average*** Crack Length (%)
UT3-VM-B2	240	Butt with temper bead	0.12	30	0	0	-
UT4-VM-T1	200	Fillet	0.12	30	42	40	25
UT4-VM-T2[a]	200	Fillet	0.12	30	40	37	19
UT5-Q/T-T2	264	Fillet	0.12	30	1	1	5
UT5-N/T-T3[b]	180	Fillet	0.12	30	2	1	<1
UT5-N/T-T4	169	Fillet	0.12	30	2	1	<1
UT5-VM-T1	155	Fillet	0.12	30	6	2	10
UT5-VM/T-T5	153	Fillet	0.12	30	0	0	0
UT5-VM-B1	155	Butt	0.12	30	0	0	-
UT8-SE-T1	150	Fillet	0.12	30	0	0	0
UT8-N/T-T2	159	Fillet	0.12	30	20	18	11
UT8-N/T-T3	159	Fillet 120KJ/in	0.12	30	16	14	12
UT11-Q/T-T2	195	Filet	0.12	30	0	0	0
UT11-SE-T1	130	Fillet	0.12	30	0	0	0
UT12-VM-T1	180	Fillet	0.12	30	0	0	0
UT12-VM-T2	180	Fillet 120KJ/in	0.12	30	0	0	0
UT13-SE-T1	172	Fillet	0.12	30	0	0	0
UT14-Q/T-T2[c]	266	Fillet	0.12	30	117	60	41
UT14-N/T-T1[c]	172	Fillet	0.12	30	20	6	11

Table D3-3—Full-Scale Weld HAZ Cracking Test Results Using PREVEW (Continued)

Samples	Base Metal Hardness (HV)	Joint Type*	Deflection (in)	Test Time (hrs)	Maximum** Crack Depth (mils)	Average** Crack Depth (mils)	Average*** Crack Length (%)
UT15-N/T-T1[c]	144	Fillet	0.12	30	0	0	0
UT16-N/T-T1	153	Fillet	0.12	30	0	0	0
UT17-N/T-T1	185	Fillet	0.12	30	0	0	0

* Heat input: Fillet joint: 50-60KJ/in.
Butt joint with weave bead:80 KJ/in.
Butt joint with temper bead: 11 KJ/in.
Electrode: E8018-B2 for UT2-UT13.

**Based on metallographic examination of 3 transverse sections, crack depth measured along the CGHAZ.

***Based on metallographic examination of 2 longitudinal sections.

****One side of the fillet was tempered at 1150°F for 1 hour and the other was furnace tempered at 1350°F for 1 hour prior to loading.

a). E8018-B2L-0.025%C (new data).

b). 1800°F normalization.

c). Ex-service-revirgined (new data).

CORRELATION OF MAXIMUM CRACK DEPTH IN PREVEW TEST WITH THE REDUCTION IN AREA IN GLEEBLE REHEAT CRACKING TEST

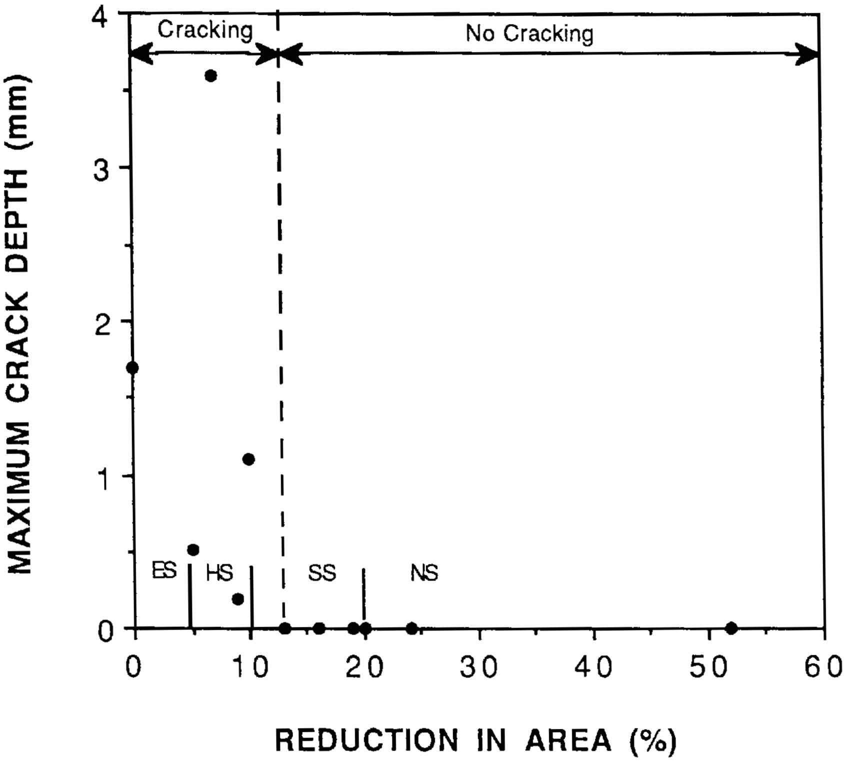

Fig. D3-14—Correlation of maximum crack depth in PREVEW test with the ductility of the HAZ from the Gleeble stress rupture test. Extremely susceptible (ES) <5%, Highly susceptible (HS) 5–10%, Slightly susceptible (SS) 10–15%, Not susceptible (NS) >20%.

CORRELATION OF AVERAGE CRACK DEPTH IN PREVEW TEST WITH THE REDUCTION IN AREA IN GLEEBLE REHEAT CRACKING TEST

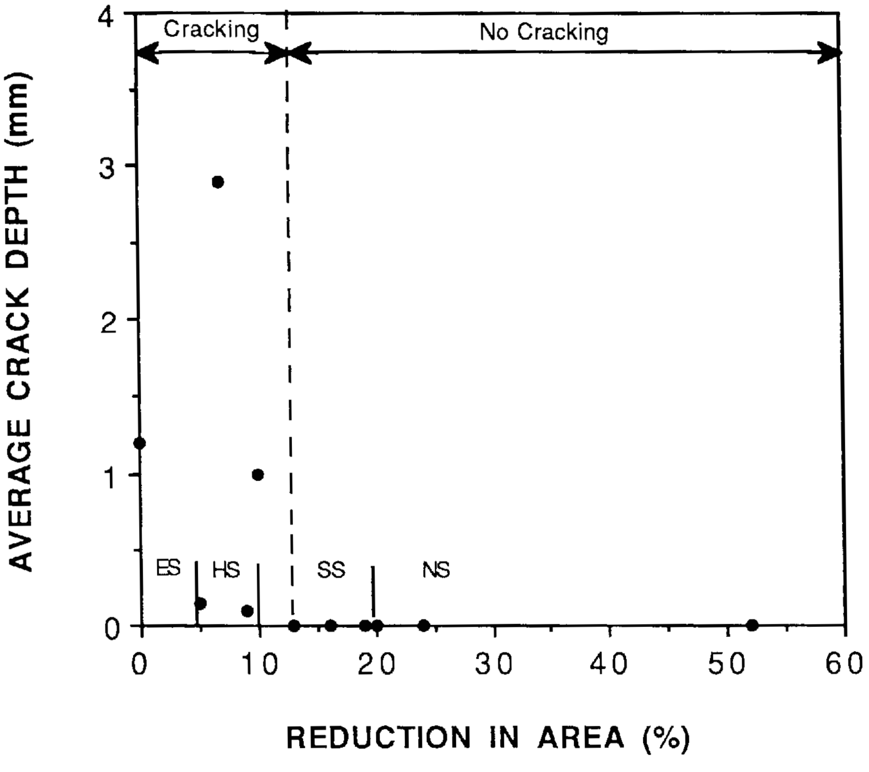

Fig. D3-15—Correlation of average crack depth in PREVEW test with the ductility of the HAZ from the Gleeble stress rupture test. Extremely susceptible (ES) <5%, Highly susceptible (HS) 5–10%, Slightly susceptible (SS) 10–15%, Not susceptible (NS) >20%.

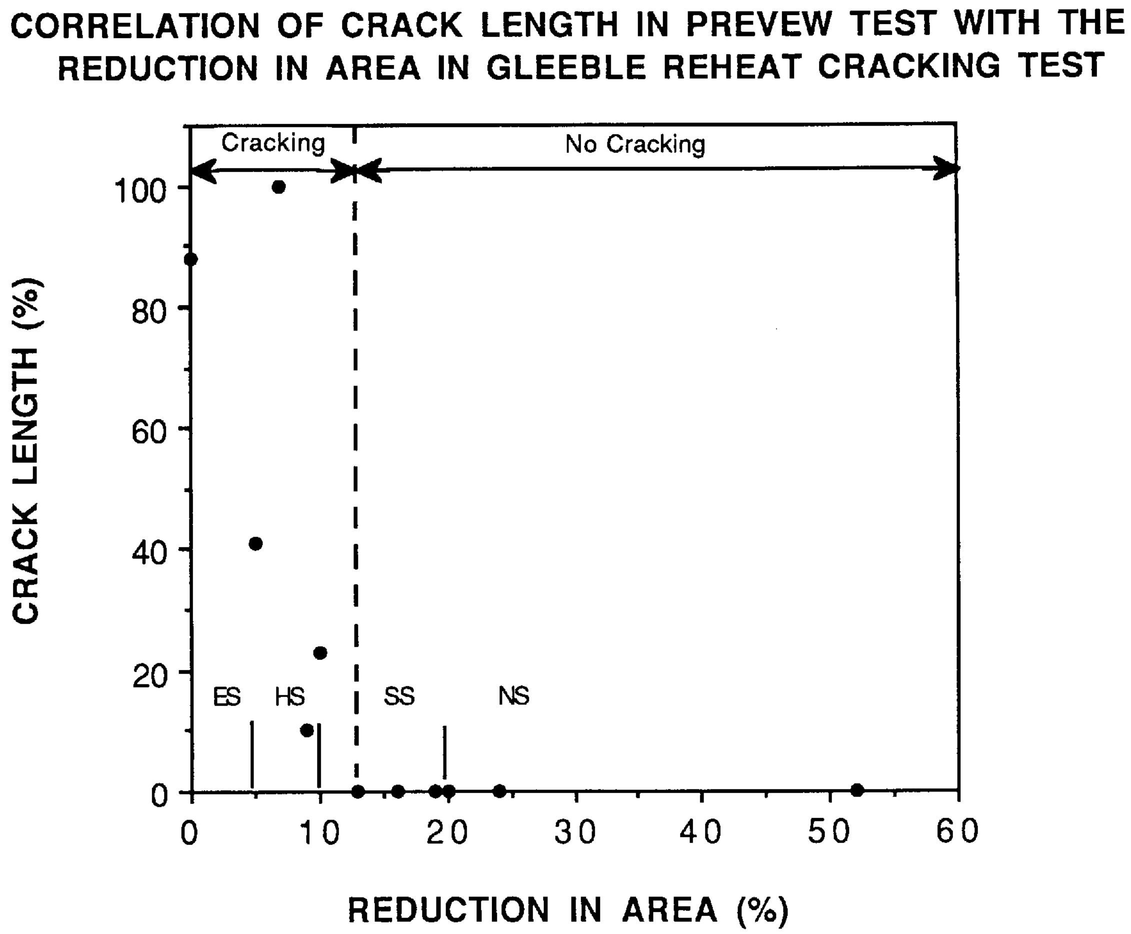

Fig. D3-16—Correlation of crack length in PREVEW test with the ductility of the HAZ from the Gleeble stress rupture test. Extremely susceptible (ES) <5%, Highly susceptible (HS) 5–10%, Slightly susceptible (SS) 10–15%, Not susceptible (NS) >20%.

References in Appendix D

1. Dhooge, A. and Vinckier, A. G. "Reheat Cracking—Review of Recent studies (1984–1990)," IIW Doc. IX-1659-91.
2. Vinckier, A. G. and Dhooge, A. "Reheat cracking in Welded Structures during Stress Relief Heat Treatments," Journal of Heat Treating, Vol. 1, No. 1, 1979, pp. 72–80.
3. JIS-3185. "Japanese Industrial Standard Method of Y-Groove Cracking Test."
4. Ito, Y. and Nakanishi, M. "Study on Stress Relief Cracking in Welded Low Alloy Steel," The Sumitomo Search, No. 7, May 1972, pp. 27–36.
5. Grajoin, H., Debiez, S., and Gaillard, R. "Implant Method at the Institute De Soudre," Met. Constr. Brit. Weld. J., No. 5, 1973, pp. 384–388.
6. Khan, K. K. "Fundamental Studies of the Metallurgical Causes for Reheat Cracking in 2¼Cr-1Mo, 1¼Cr-½Mo and Copper Precipitation Hardenable Steels and Problem Mitigration," Doctoral dissertation, the University of Tennessee, Knoxville, Dec. 1993.
7. Electrix Industries, Inc., "Application of Stresscoat," 1993.
8. Savage, W. F. and Lundin, C. D. "Application of the Varestraint Technique to the Study of Weldability," Welding Journal, No. 11, 1966, pp. 497s–530s.
9. Stout, R. D. "Weldability of Steels," Mack Printing Company, Easton, Pa., 1987, pp. 193–195.
10. ANSI/AWS D10.8-86. "Recommended Practices for Welding of Chromium-molybdenum Steel Piping and Tubing," 1986.
11. Meitzner, C. F. "Stress-Relief Cracking in Steel Weldments," WRC Bulletin, 211, Nov. 1975, pp. 1–18.
12. Vinckier, A. G. and Pense, A. W. "A Review of Underclad Cracking in Pressure Vessel Components," WRC Bulletin, 197, Aug. 1974, pp. 1–35.

Appendix E—Determination of Factors to Quantify Reheat Cracking Susceptibility Based on Chemical Composition

Many relationships have been developed in the past to relate reheat cracking susceptibility to chemical composition. These relationships have been primarily based on the assumption that reheat cracking is influenced by the effect of strengthening elements (such as Mo, Cr, V, Nb or C) or by the effect of tramp elements (such as P, S, Sn, Sb, As) or by both element groups.

One of the objectives of this study was to determine a relationship or validate a relationship (already published) between the chemical composition of the various 1¼Cr-½Mo heats and the reheat cracking susceptibility. It was considered that if one of the published formulas would fit the test data, this task would be simple. A list of approximately 10 such relationships were found in the literature. These are presented in Table E-2 (the chemical composition of all heats is presented in Table E-1). Unfortunately, the cracking susceptibility indexes calculated using these formulas did not fit the reheat cracking susceptibility levels determined from the three different test methods used in this study for the 17 heats of 1¼Cr-½Mo steel. The calculated susceptibility indexes for the API heats using the published formulas are presented in Table E-3 and graphically in Figs. E1 through E11 to illustrate the inappropriateness of the correlation.

Thus, an attempt was made to fit the reheat cracking susceptibility data (average Gleeble reduction in area) generated in this study to a chemical composition factor that would effectively relate the chemical composition to reheat cracking susceptibility. Four approaches were taken to derive proper relationships.

(1) The initial approach using the available data was to engage a statistician to perform multiple regression analyses. The chemical composition of 16 heats of API materials along with the Gleeble test average reduction in area was utilized. The analysis for 23 elements was utilized in chemical composition. The most suitable correlation derived from the statistician's analysis is presented in Fig. E-12 as MPC Factor-1. It may be noted that there is an excellent data fit. However, when data from an additional heat, UT17, became available and were plotted on same figure they did not fall along the defined curve. Thus, it was recognized that mathematical treatment of the data alone is not sufficient to derive a unique factor that is representative of reheat cracking behavior.

(2) The second approach was to derive approximate relations between each element and the reheat cracking susceptibility. The elements that did not appear to have any significant influence on reheat cracking susceptibility were dropped from consideration. The coefficients assigned to each of the important elements were then adjusted to reduce the data scatter. Although this procedure is not strictly statistical, two factors (MPC Factor-2 and MPC Factor-3) were derived based on this approach. The factor relationships showing calculated values for the API heats are presented in Table E3 and graphically in Figs. E-13 and E-14. Although the data do not fit wholly satisfactorily, the scatter is significantly less than that which resulted using the published formulas.

(3) The third approach was based on mechanistic effects of alloying elements on the potential for reheat cracking. A strength factor was devised that combined the effect of C and other strengthening elements such as V, Nb and Ti:

$$Cfn = (5C + 1000Nb + 100V + 50Ti - 0.5) + 1.$$

A tramp factor that combines the effect of trace elements that have been determined to affect reheat cracking by the mechanism of weakening the prior austenite grain boundaries was formulated:

$$\text{Tramp} = 2*[4.3(Sn + As) + 150Sb + Cu + 50(P - 0.01)].$$

A sulfur function was formulated that combined the detrimental effect of sulfur and other tramp elements recognizing the fact that if the sulfur concentration is high, it alone is a major overriding factor:

$$Sfn = 1 + (S - 0.02\text{Tramp})*30.$$

Thus, if Sfn is less than 1 it is to be considered as 1, indicating that if the sulfur concentration is low the tramp element concentration is a major factor in determining reheat cracking sensitivity.

Thus, the sum of the tramp factor and the sulfur function determines the effect of tramp elements and sulfur on reheat cracking susceptibility. An aluminum function was devised considering that if the steel is not aluminum treated there is no detrimental effect of aluminum:

$$Alfn = 1 + (Al - 0.015)*15.$$

The aluminum function is also a step function such that if the value of Alfn is <1, the function is to be considered equal to 1. Thus, the factor determining the reheat cracking susceptibility is the strength factor multiplied by sum of the tramp factor and the sulfur function multiplied by the aluminum function minus 1:

$$\text{New MPC Factor} = [Cfn(\text{Tramp} + Sfn)Alfn] - 1$$

MPC Factors-4, -5 and -6 are based on this principle. The coefficients assigned to different elements are different, but the basic principle behind these relationships is the same. Graphical representation of these three relationships is presented in Figs. E15 through E17. It may be noted that although there is some scatter present, the fit of the data should be acceptable for selection of heats of 1¼Cr-¼Mo steel to avoid

Table E1—Chemical Composition of 17 Heats of 1¼Cr-½Mo Steel (wt%)

MATERIALS	C	Mn	P	S	Si	Ni	Cr	Mo	V	Nb	Ti
UT1	0.15	0.58	0.006	0.022	0.71	0.13	1.27	0.58	0.002	0.00005	0.00035
UT2	0.10	0.45	0.010	0.013	0.65	0.18	1.30	0.53	0.004	0.00007	0.00173
UT3	0.15	0.50	0.007	0.017	0.61	0.21	1.27	0.47	0.010	0.00025	0.00238
UT4	0.18	0.79	0.009	0.003	0.52	0.20	1.33	0.53	0.005	0.00006	0.00149
UT5	0.17	0.50	0.008	0.004	0.64	0.08	1.41	0.50	0.004	0.00062	0.00250
UT6	0.103	0.53	0.013	0.013	0.58	0.25	1.31	0.48	0.014	0.00084	0.00122
UT7	0.14	0.62	0.013	0.011	0.64	0.26	1.25	0.50	0.004	0.00008	0.00031
UT8	0.13	0.42	0.010	0.015	0.62	0.17	1.22	0.58	0.003	0.00005	0.00313
UT9	0.14	0.41	0.012	0.025	0.58	0.06	1.25	0.61	0.003	<0.00001	0.00017
UT10	0.12	0.54	0.011	0.019	0.75	0.07	1.01	0.56	0.001	<0.00001	0.00010
UT11	0.086	0.42	0.010	0.016	0.49	0.01	1.04	0.54	0.003	<0.00001	0.00039
UT12	0.10	0.56	0.004	0.001	0.57	0.12	1.46	0.55	0.003	0.00001	0.00357
UT13	0.12	0.45	0.004	0.024	0.59	0.29	1.27	0.49	0.004	<0.00001	0.00015
UT14	0.17	0.51	0.015	0.012	0.66	0.09	1.16	0.49	0.002	0.00004	0.00137
UT15	0.096	0.46	0.010	0.027	0.62	0.01	1.27	0.54	0.005	<0.00001	0.00064
UT16	0.11	0.47	0.008	0.020	0.56	0.16	1.16	0.47	0.004	<0.00001	<0.00001
UT17	0.19	0.58	0.009	0.003	0.63	0.05	1.05	0.48	0.006	0.00011	0.00211

Table E1—Chemical Composition of 17 Heats of 1¼Cr-½Mo Steel (wt%) (Continued)

MATERIALS	Co	Cu	Al	B	W	As	Sn	Zr	Sb	Ca	N	O
UT1	0.013	0.13	0.005	<0.00001	<0.01	0.009	0.010	<0.001	0.00075	0.0005	0.0089	0.0094
UT2	0.010	0.05	0.004	<0.00001	0.008	0.007	0.007	<0.001	0.00041	0.0016	0.0155	0.0058
UT3	0.012	0.16	0.003	0.00003	<0.01	0.004	0.015	<0.001	0.00095	0.0011	0.0116	0.0048
UT4	0.015	0.15	0.017	<0.00001	0.001	0.016	0.014	0.005	0.00168	0.0001	0.0112	0.001
UT5	0.007	0.09	0.021	<0.00001	0.001	0.007	0.009	0.002	0.00055	0.0014	0.0083	0.002
UT6	0.011	0.15	0.031	<0.00001	<0.001	0.005	0.014	0.003	0.00086	0.0009	0.009	0.003
UT7	0.006	0.03	0.003	<0.00001	0.01	0.003	0.003	<0.001	0.00130	0.0009	0.008	0.0055
UT8	0.010	0.11	0.026	<0.00001	<0.01	0.008	0.012	<0.001	0.00146	0.0013	0.012	0.005
UT9	0.012	0.16	0.003	<0.00001	<0.01	0.005	0.013	<0.001	0.00125	0.0008	0.012	0.016
UT10	0.010	0.08	0.003	<0.00001	<0.01	0.008	0.009	<0.001	0.00100	0.0007	0.009	0.010
UT11	0.006	0.02	0.002	<0.00001	<0.01	0.004	0.002	<0.001	0.00016	0.0010	0.011	0.011
UT12	0.010	0.07	0.017	0.00005	<0.01	0.010	0.005	<0.001	0.00070	0.0012	0.007	0.002
UT13	0.014	0.17	0.002	<0.00001	<0.01	0.007	0.015	<0.001	0.00193	0.0010	0.008	0.007
UT14	0.009	0.13	0.003	0.00002	<0.01	0.007	0.012	<0.001	0.00105	0.0014	0.013	0.008
UT15	0.006	0.04	0.003	0.00001	<0.01	0.006	0.004	<0.001	0.00032	0.0002	0.014	0.010
UT16	0.012	0.17	0.001	<0.00001	<0.01	0.009	0.015	<0.001	0.00170	0.0013	0.007	0.003
UT17	0.011	0.01	0.018	0.00028	<0.01	0.003	0.003	<0.002	0.00032	0.0016	0.006	0.001

Table E2—Chemical Composition Factors-1

$J = (Mn+Si) \times (P + Sn) \times 10^4$

$X = (10\ P + 5\ Sb + 4\ Sn + As) \times 100$

$\Delta G = Cr + 3.3\ Mo + 8.1\ V - 2$

$P_{SR} = Cr + Cu + 2\ Mo + 10\ V + 7\ Nb + 5\ Ti - 2$

$CERL = 0.2\ Cu + 0.44\ S + P + 1.8\ As + 1.9\ Sn + 2.7\ Sb$

$CERL + Cr = 0.2\ Cu + 0.44\ S + P + 1.8\ As + 1.9\ Sn + 2.7\ Sb + Cr$

$MCF = Si + 2\ Cu + 2\ P + 10\ As + 15\ Sn + 20\ Sb$

$\Delta G1 = Cr + 3.3\ Mo + 8.1\ V + 10\ C - 2$

$R = P + 2.43\ As + 3.57\ Sn + 8.16\ Sb$

$MPF = C + 10\ V + Al$

SI - Susceptibility Index:

- %RA < 5% - Extremely Susceptible (ES);
- %RA between 5 - 10% - Highly Susceptible (HS);
- %RA between 10 - 15% - Slightly Susceptible (SS);
- %RA > 20% - Not Susceptible (NS).

All elements are expressed in Wt.%.

Table E3—Composition Factors

MATERIALS	J	$\overline{X}$	ΔG	PSR	CERL	CERL+Cr	MCF	ΔG1	R	MPF	SI*	
											120 KJ/IN	12 KJ/IN
UT1	206.4	11.3	1.200	0.582	0.079	1.349	1.237	2.700	0.069	0.175	NS	NS
UT2	187.0	13.7	1.081	0.459	0.053	1.353	0.953	2.081	0.055	0.144	NS	NS
UT3	244.2	13.9	0.902	0.483	0.085	1.355	1.228	2.402	0.078	0.253	HS	HS
UT4	301.3	17.0	1.120	0.598	0.100	1.430	1.242	2.920	0.112	0.247	HS	SS
UT5	193.8	12.6	1.092	0.556	0.059	1.469	1.052	2.792	0.062	0.231	HS	SS
UT6	299.7	19.5	1.007	0.572	0.087	1.397	1.183	2.037	0.082	0.274	HS	HS
UT7	201.6	15.15	0.932	0.322	0.038	1.288	0.827	2.332	0.042	0.183	HS	NS
UT8	228.8	16.33	1.158	0.536	0.079	1.299	1.149	2.458	0.084	0.186	ES	NS
UT9	247.5	18.3	1.287	0.661	0.092	1.342	1.194	2.687	0.081	0.173	HS	NS
UT10	258.0	15.9	0.866	0.221	0.069	1.079	1.167	2.066	0.071	0.133	NS	NS
UT11	109.2	11.3	0.846	0.172	0.032	1.072	0.623	1.706	0.028	0.118	SS	NS
UT12	101.7	7.4	1.299	0.678	0.048	1.508	0.907	2.299	0.052	0.147	HS	NS
UT13	197.6	11.7	0.919	0.461	0.095	1.365	1.271	2.119	0.090	0.162	HS	NS
UT14	315.9	21.0	0.793	0.297	0.085	1.245	1.221	2.493	0.083	0.193	ES	HS
UT15	151.2	12.4	1.093	0.443	0.049	1.319	0.846	2.053	0.041	0.149	HS	SS
UT16	236.9	15.75	0.743	0.310	0.100	1.260	1.265	1.843	0.097	0.151	HS	NS
UT17	145.2	10.66	0.683	0.091	0.024	1.074	0.749	2.583	0.029	0.268	SS	NS

* SI = Susceptibility Index

** Heat input: 30 KJ/in.

%RA < 5% - Extremely Susceptible (ES); %RA between 5 - 10% - Highly Susceptible (HS);

%RA between 10 - 15% - Slightly Susceptible (SS); %RA > 20% - Not Susceptible (NS).

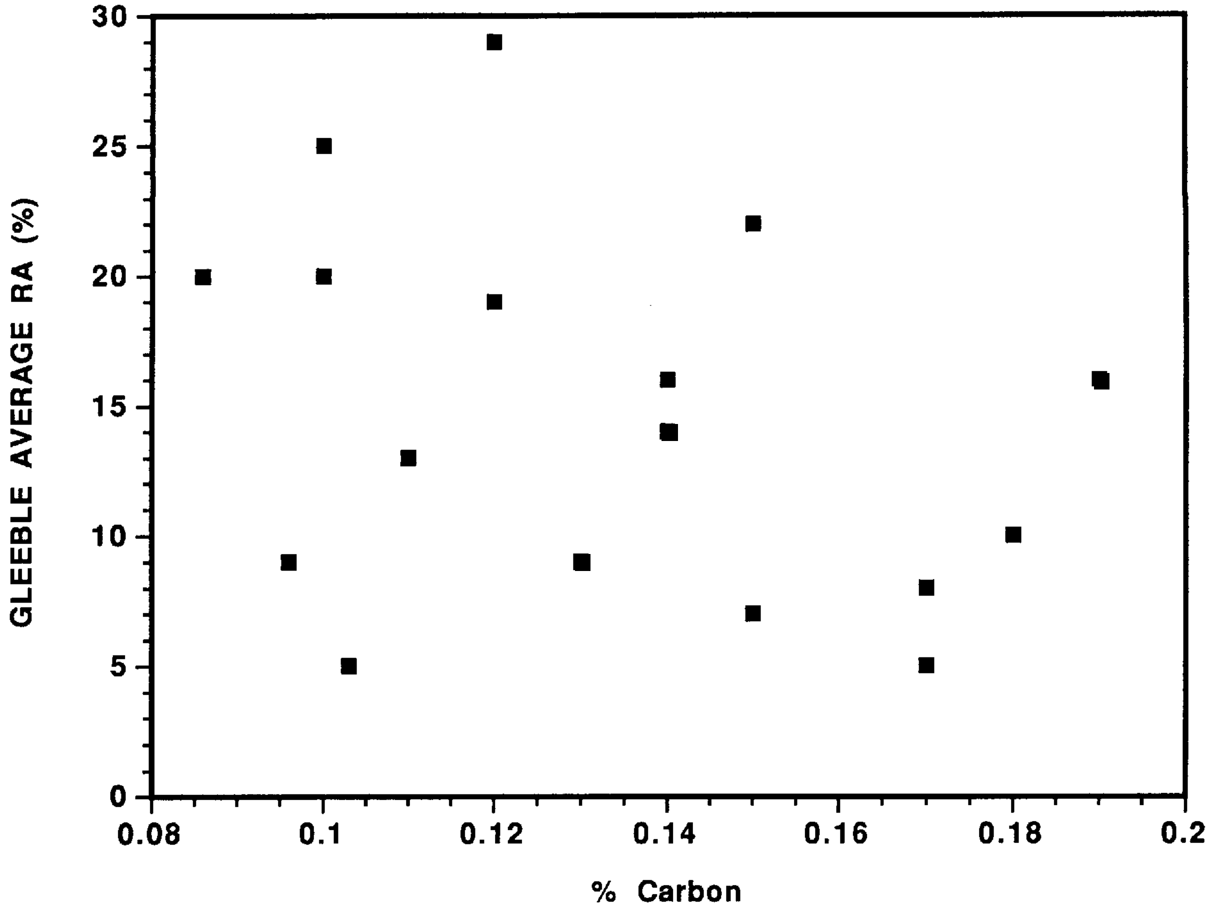

Fig. E1—Correlation between Gleeble reheat cracking test results and carbon content

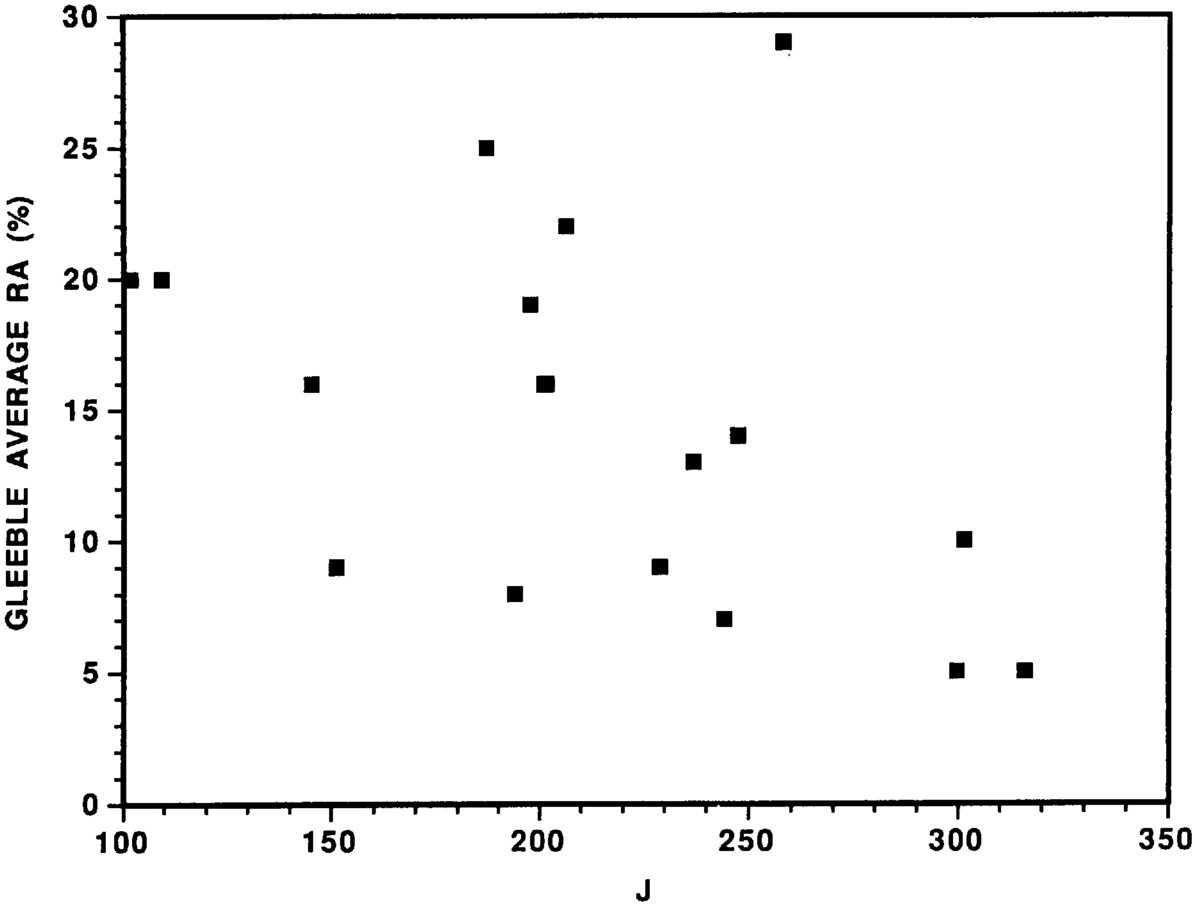

Fig. E2—Correlation between Gleeble reheat cracking test results and J-factor

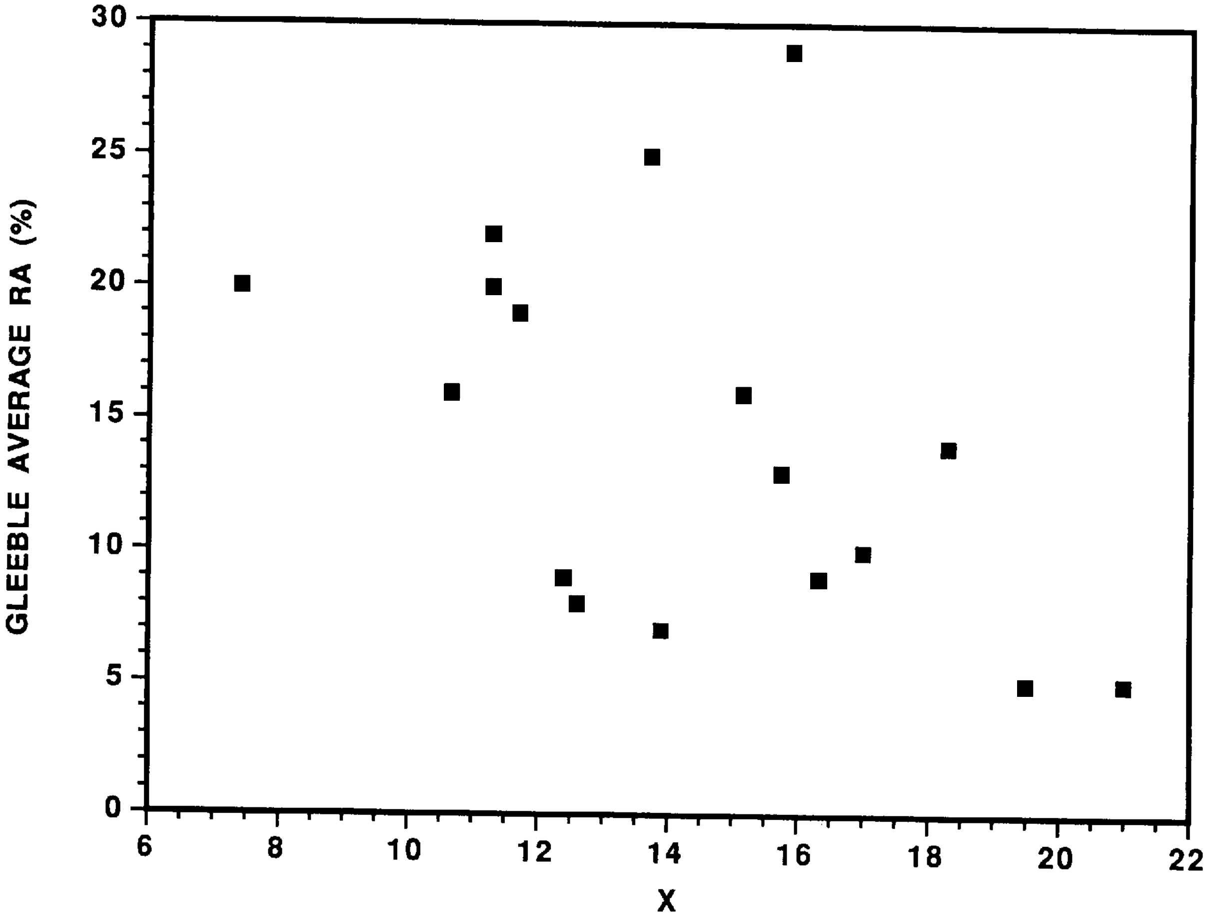

Fig. E3—Correlation between Gleeble reheat cracking test results and $\overline{X}$ factor

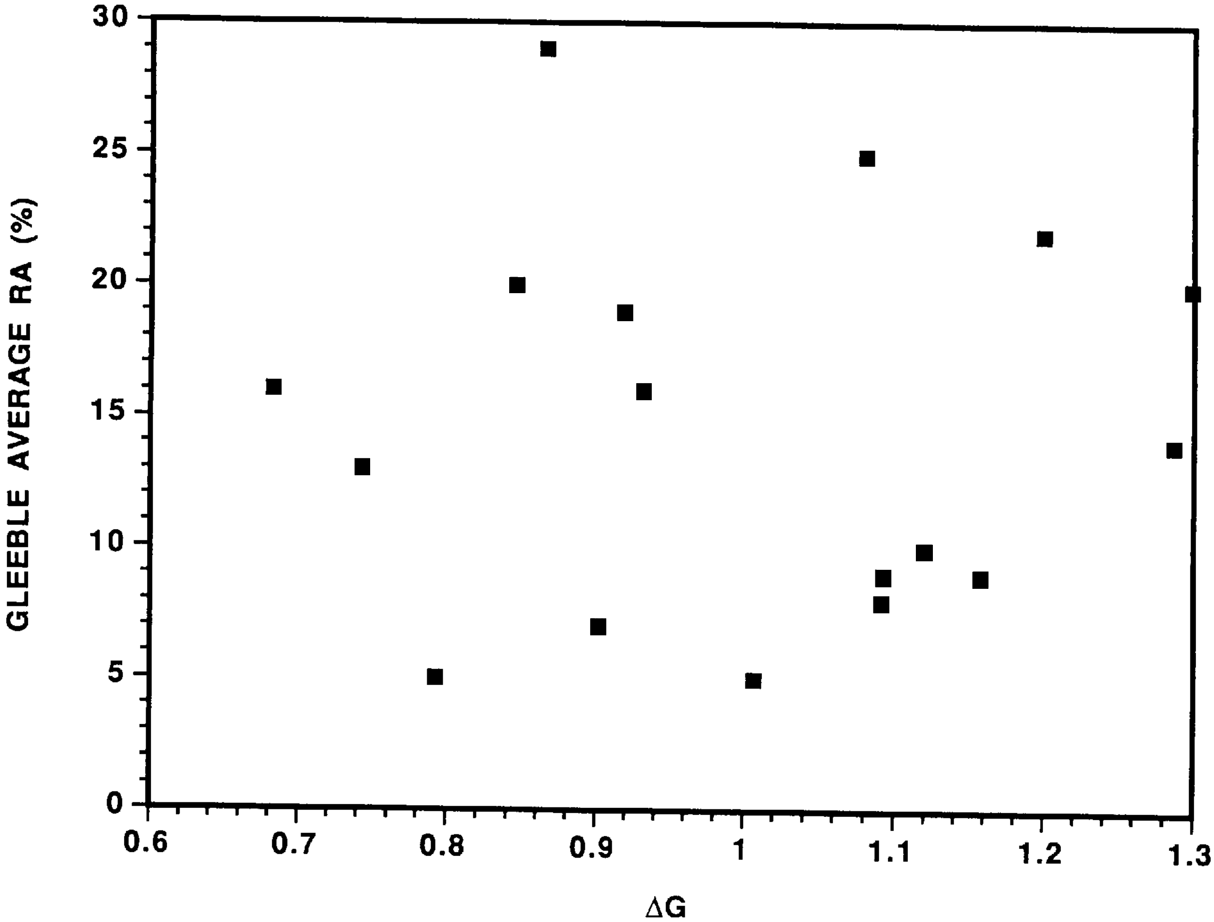

Fig. E4—Correlation between Gleeble reheat cracking test results and a G factor

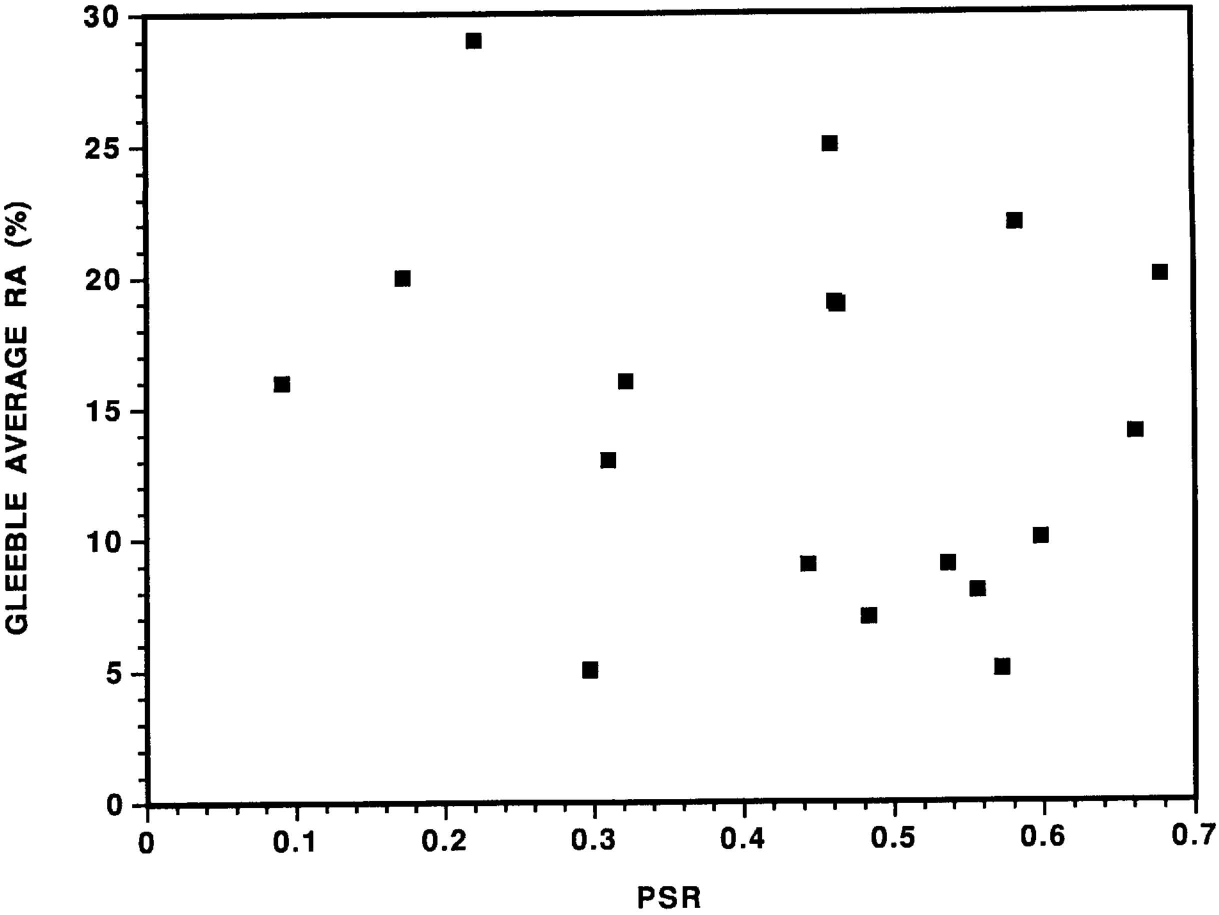

Fig. E5—Correlation between Gleeble reheat cracking test results and PSR

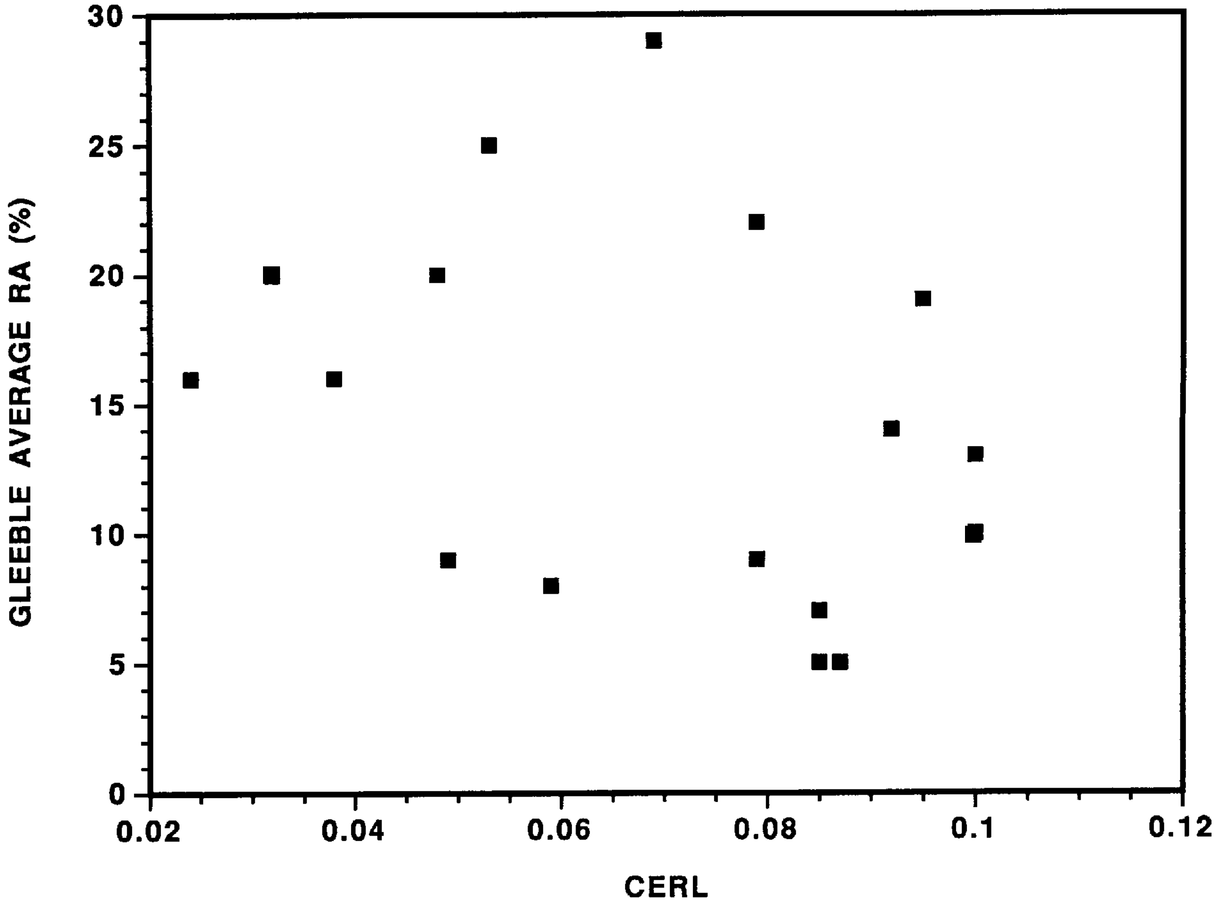

Fig. E6—Correlation between Gleeble reheat cracking test results and CERL

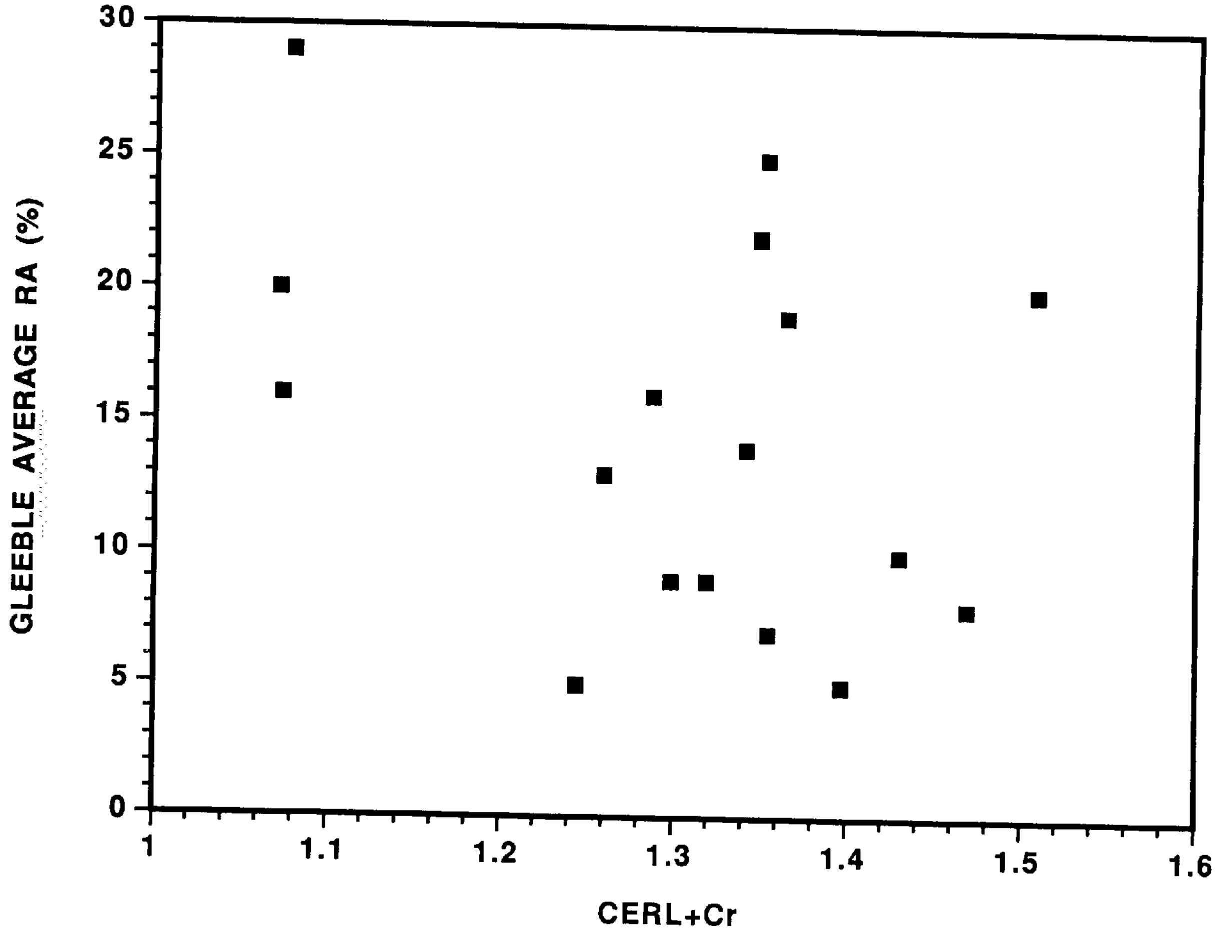

Fig. E7—Correlation between Gleeble reheat cracking test results and CERL + Cr

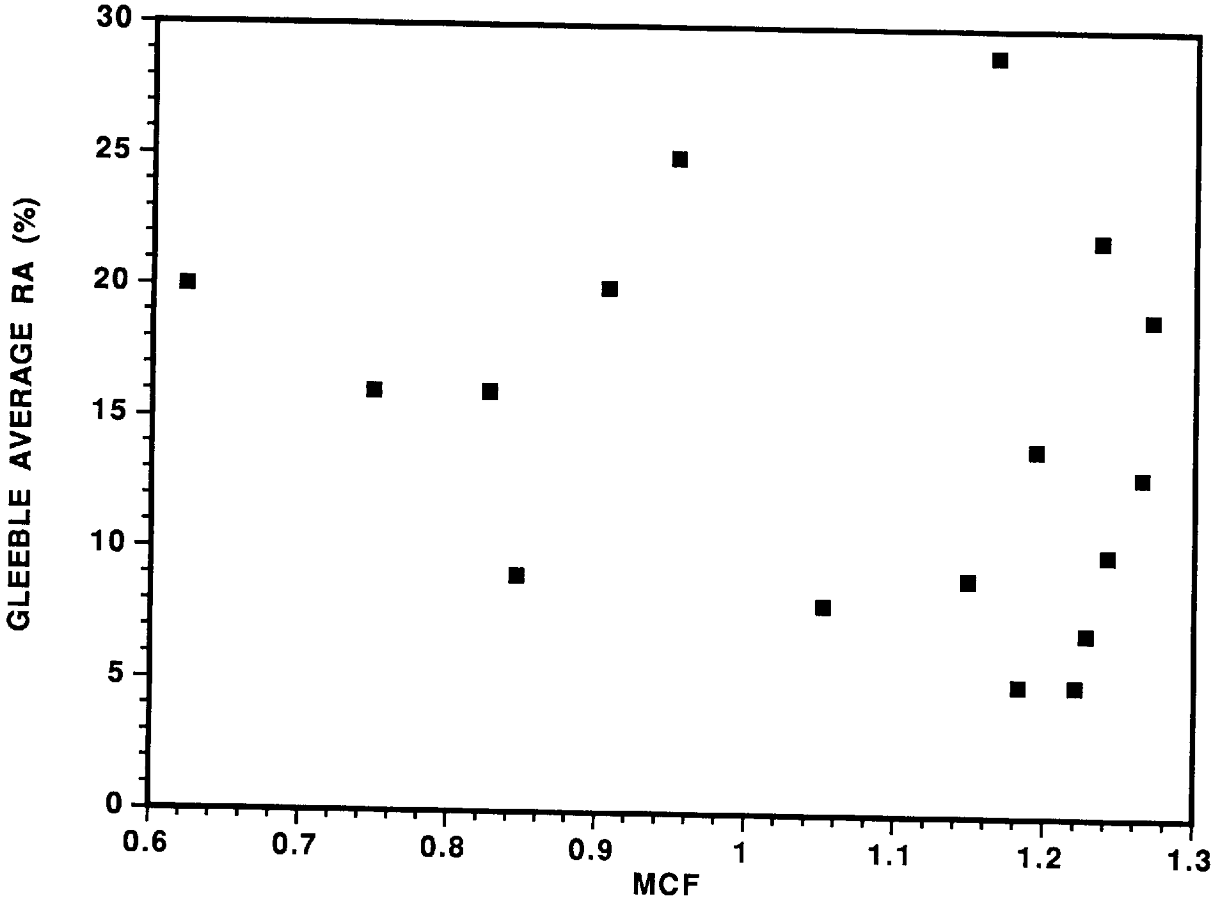

Fig. E8—Correlation between Gleeble reheat cracking test results and MCF

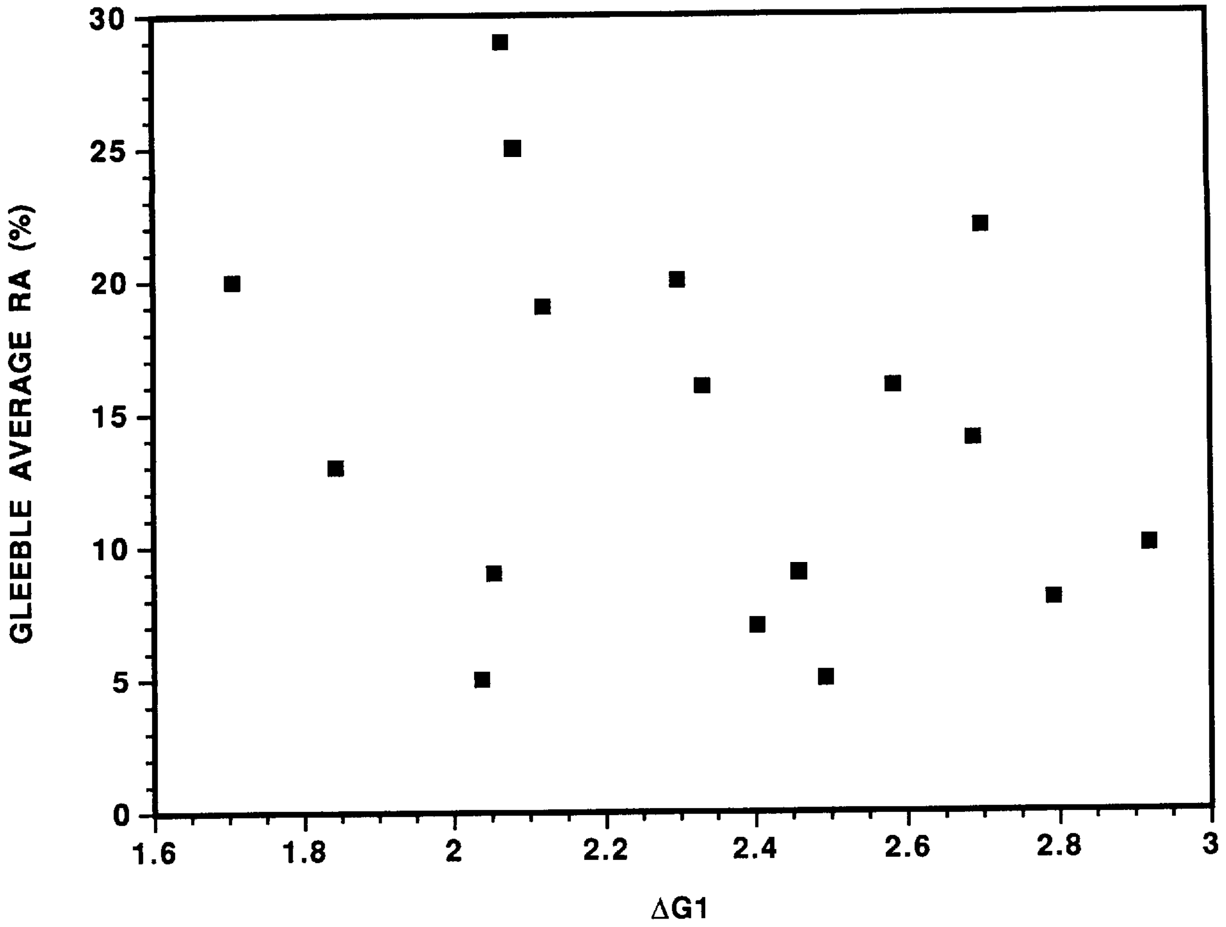

Fig. E9—Correlation between Gleeble reheat cracking test results and ΔG1

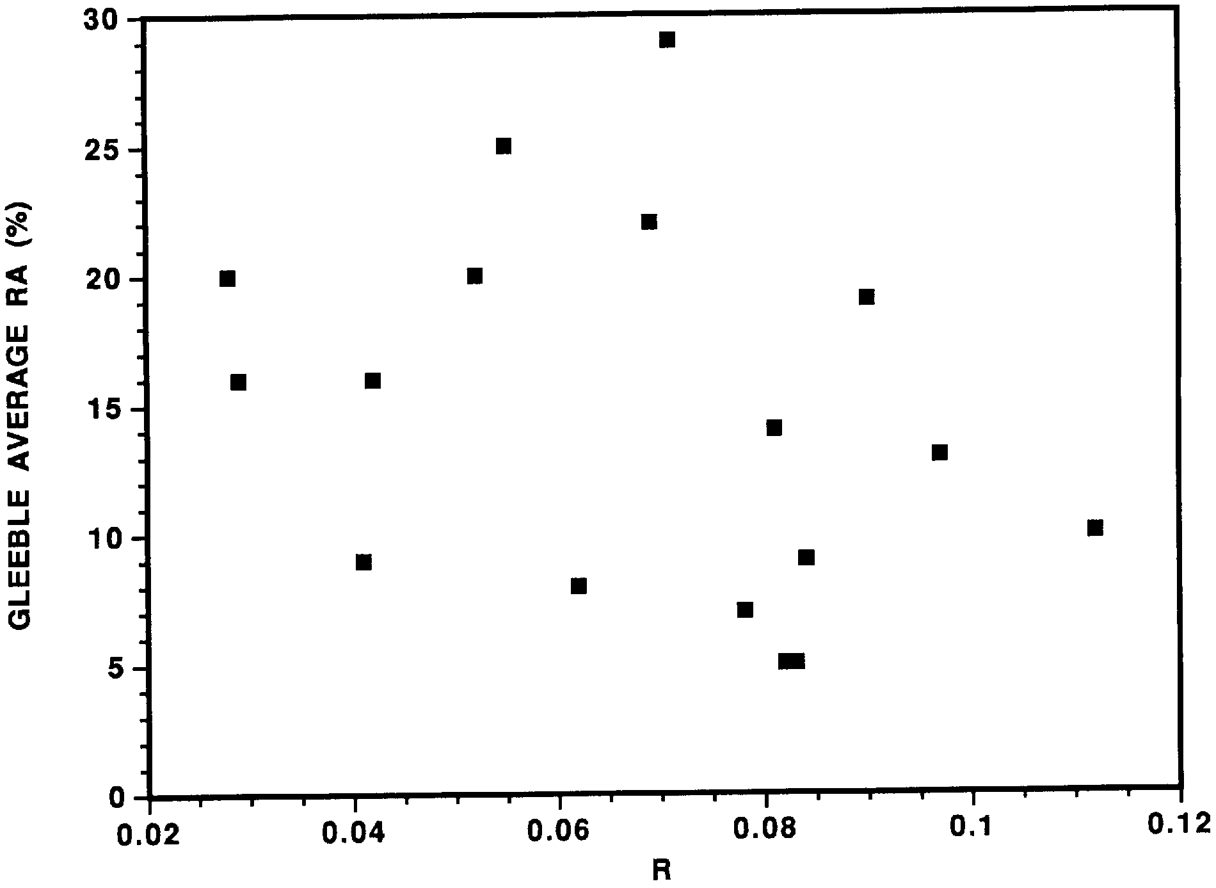

Fig. E10—Correlation between Gleeble reheat cracking test results and R factor

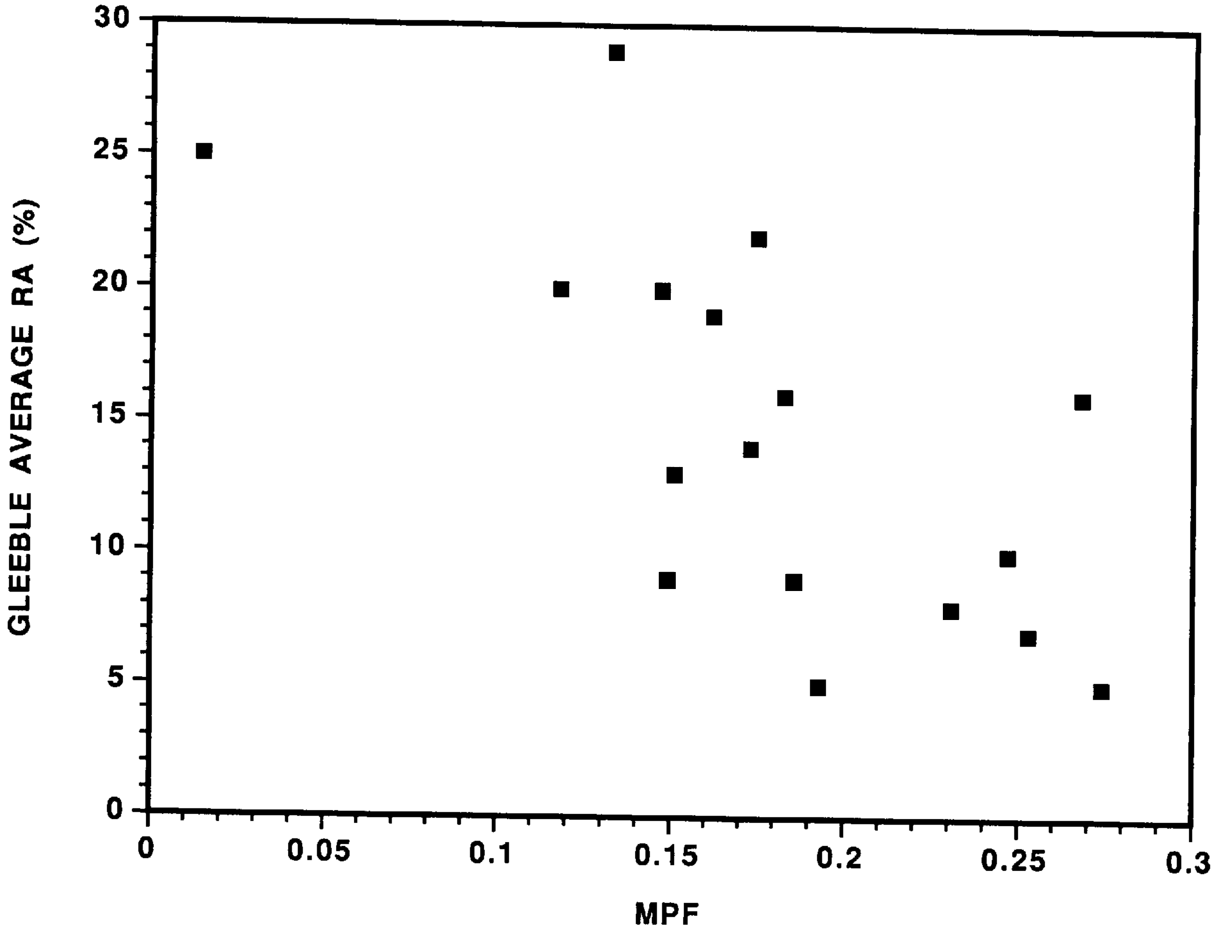

Fig. E11—Correlation between Gleeble reheat cracking test results and MPF

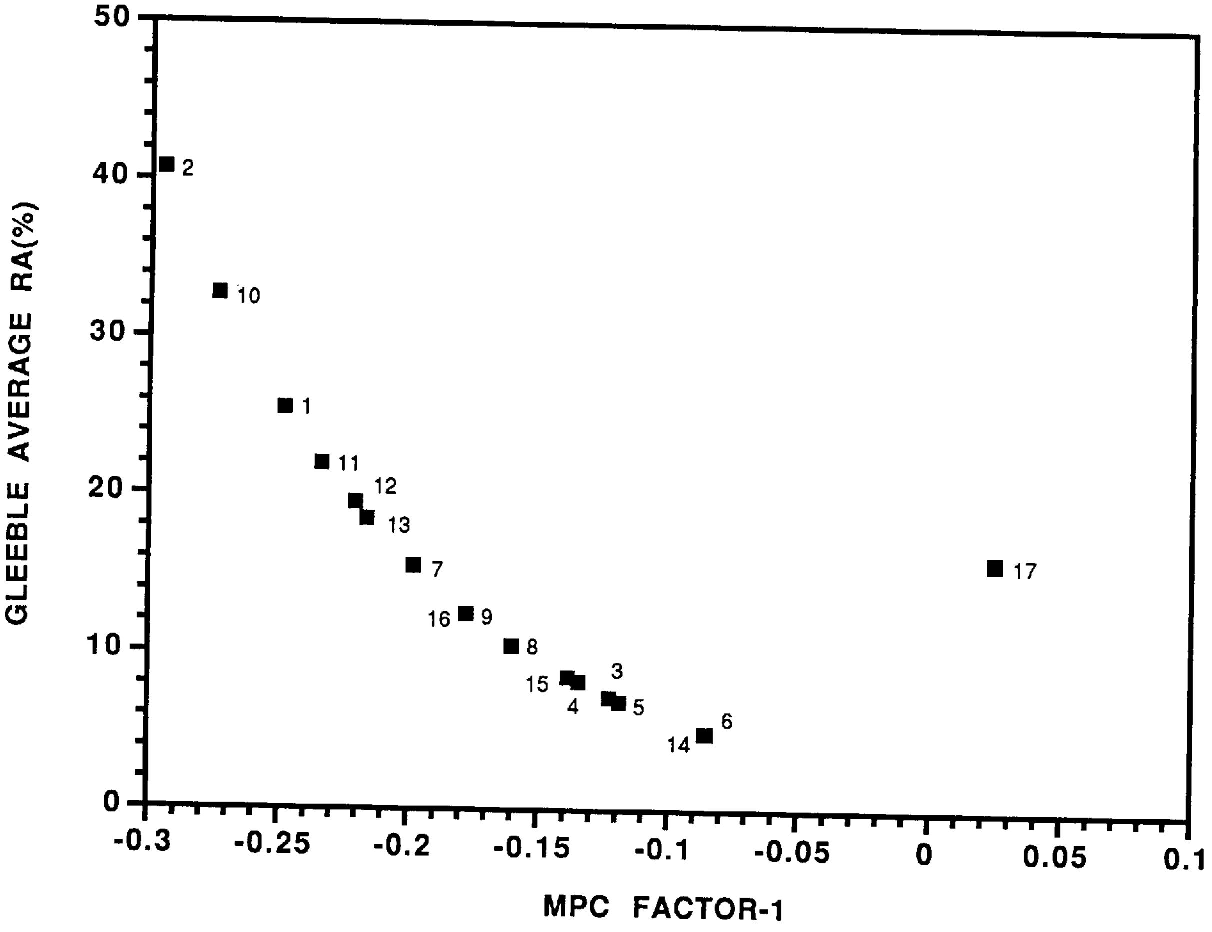

Fig. E12—Correlation between Gleeble reheat cracking test results and MPC factor-1

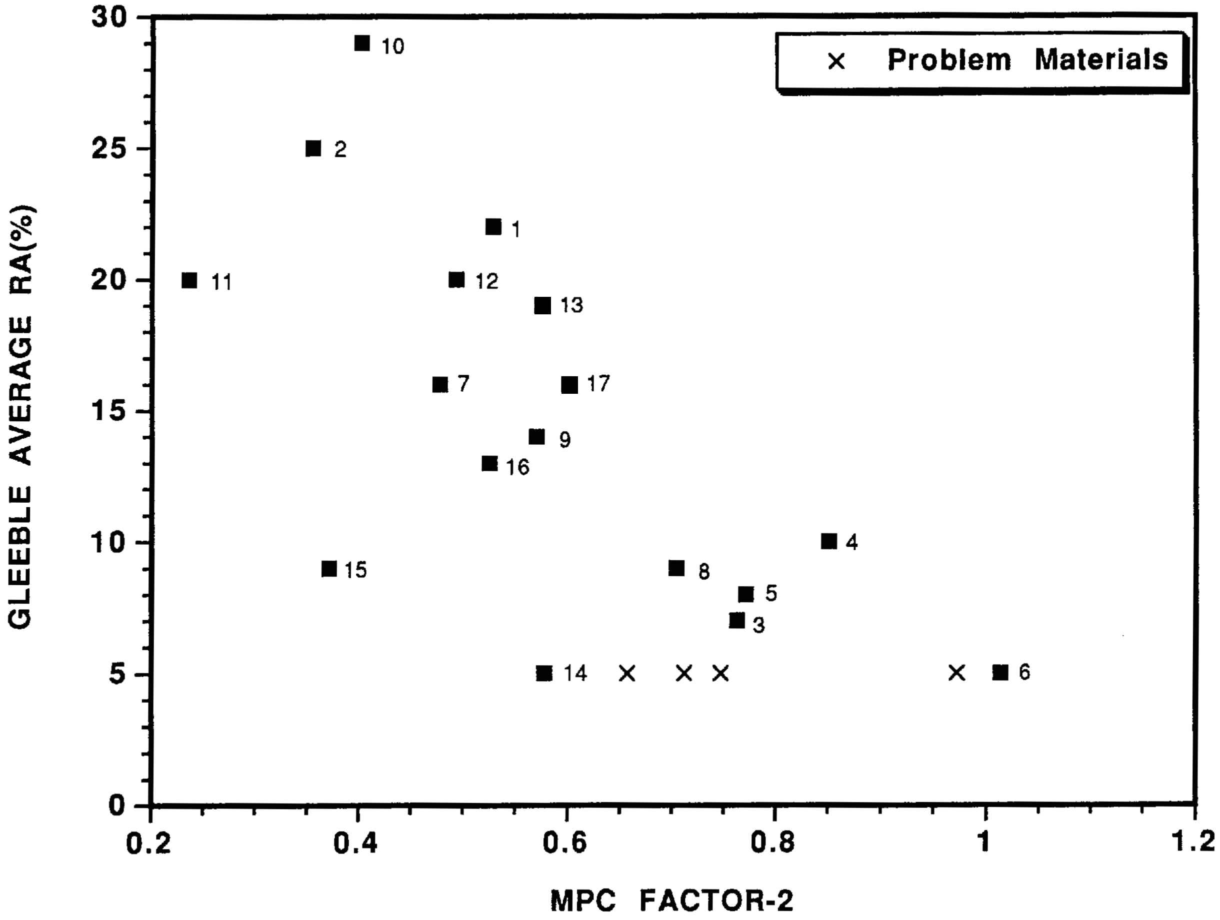

Fig. E13—Correlation between Gleeble reheat cracking test results and MPC factor-2

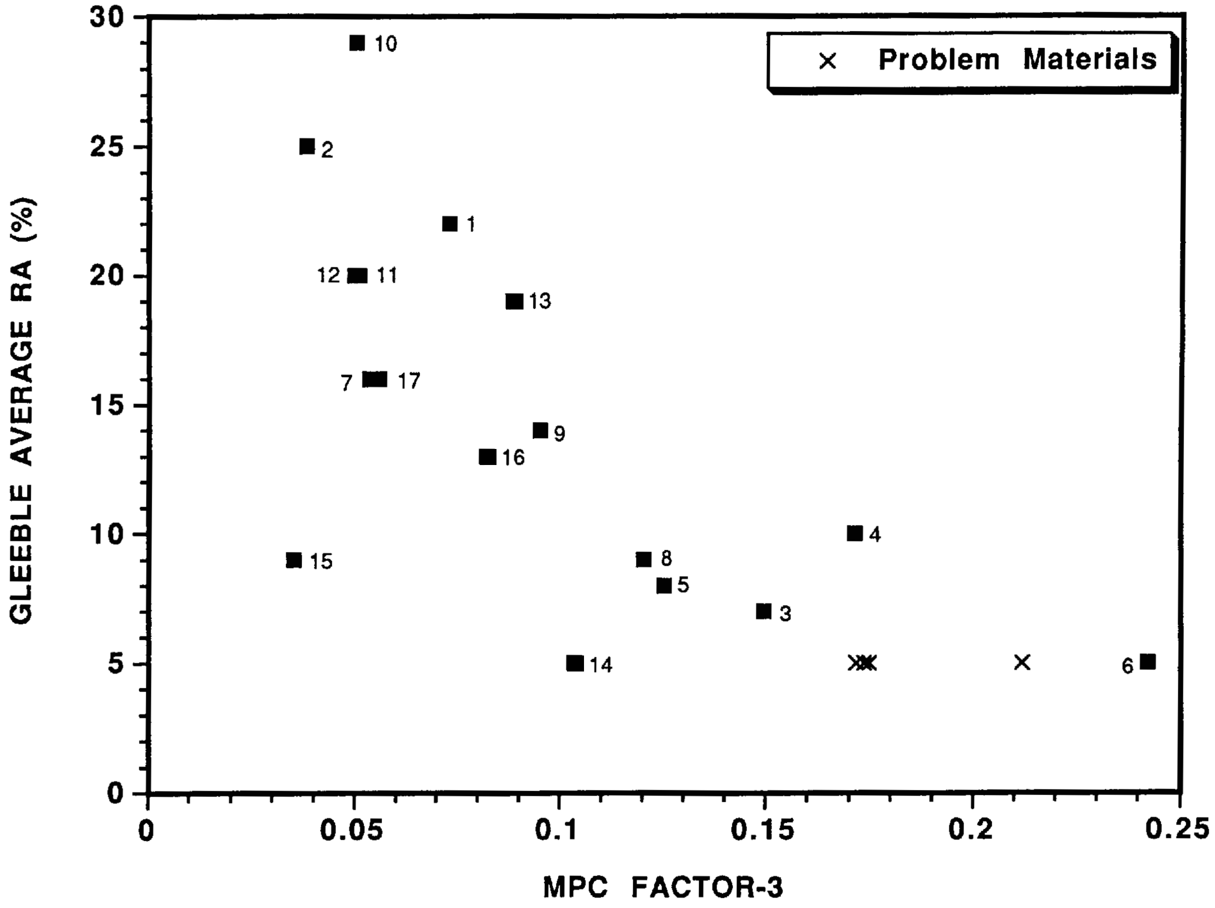

Fig. E14—Correlation between Gleeble reheat cracking test results and MPC factor-3

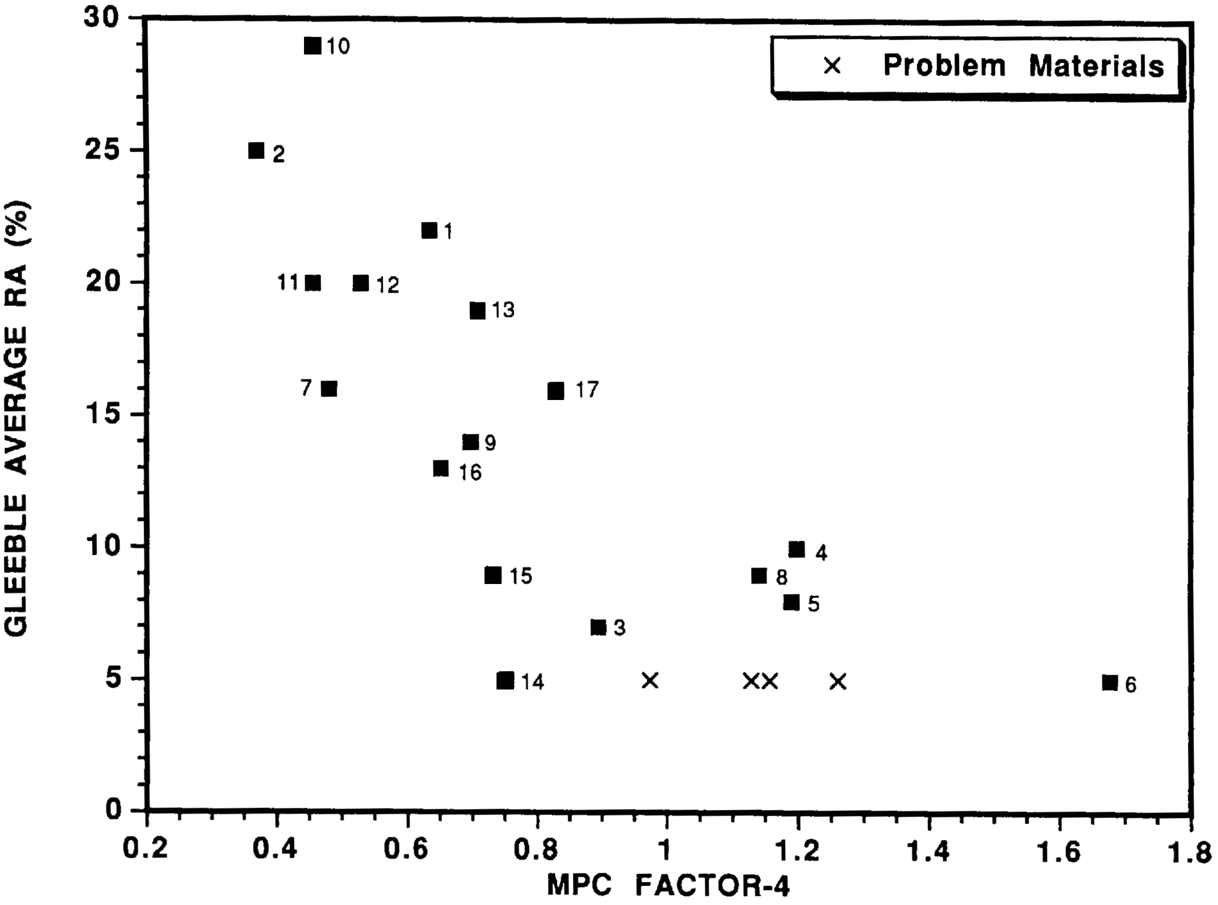

Fig. E15—Correlation between Gleeble reheat cracking test results and MPC factor-4

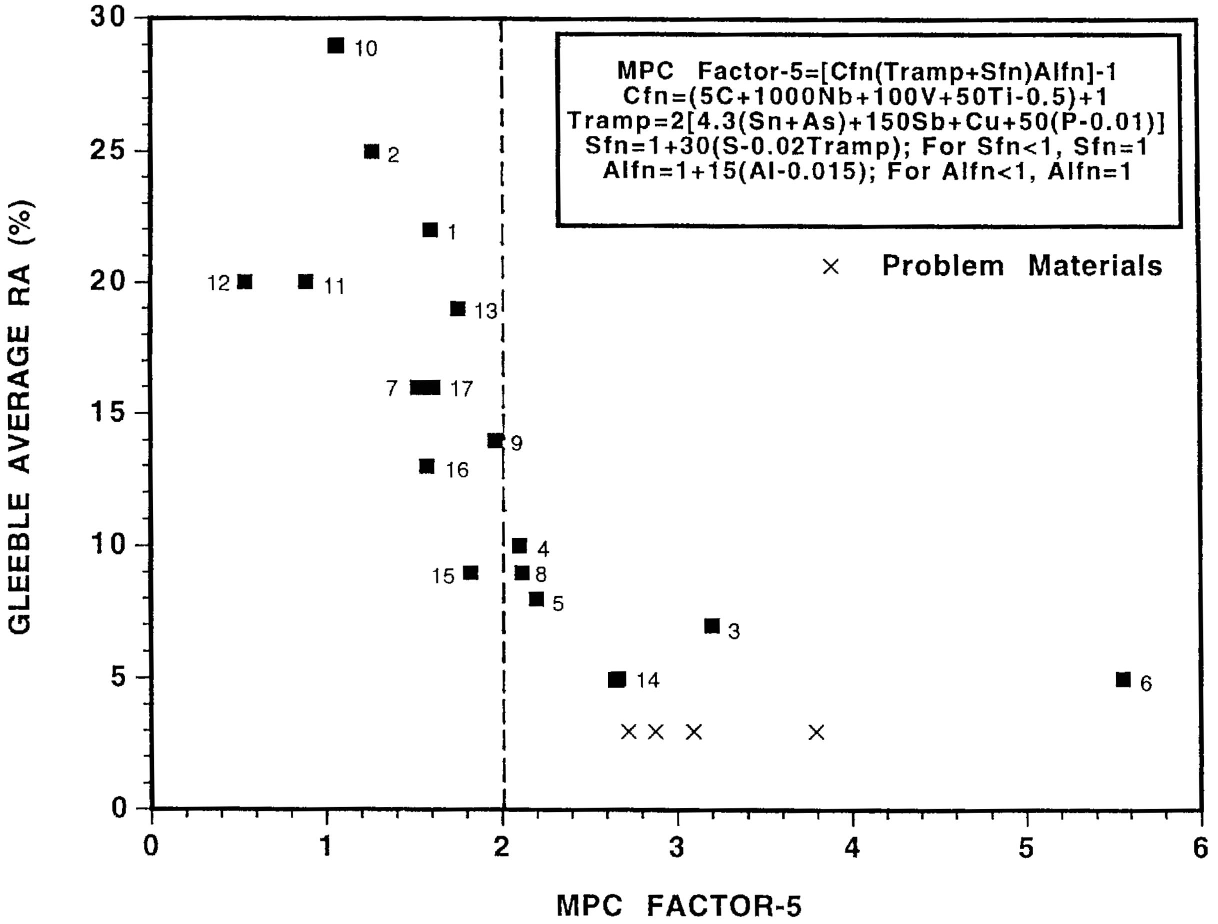

Fig. E16—Correlation between Gleeble reheat cracking test results and MPC factor-5

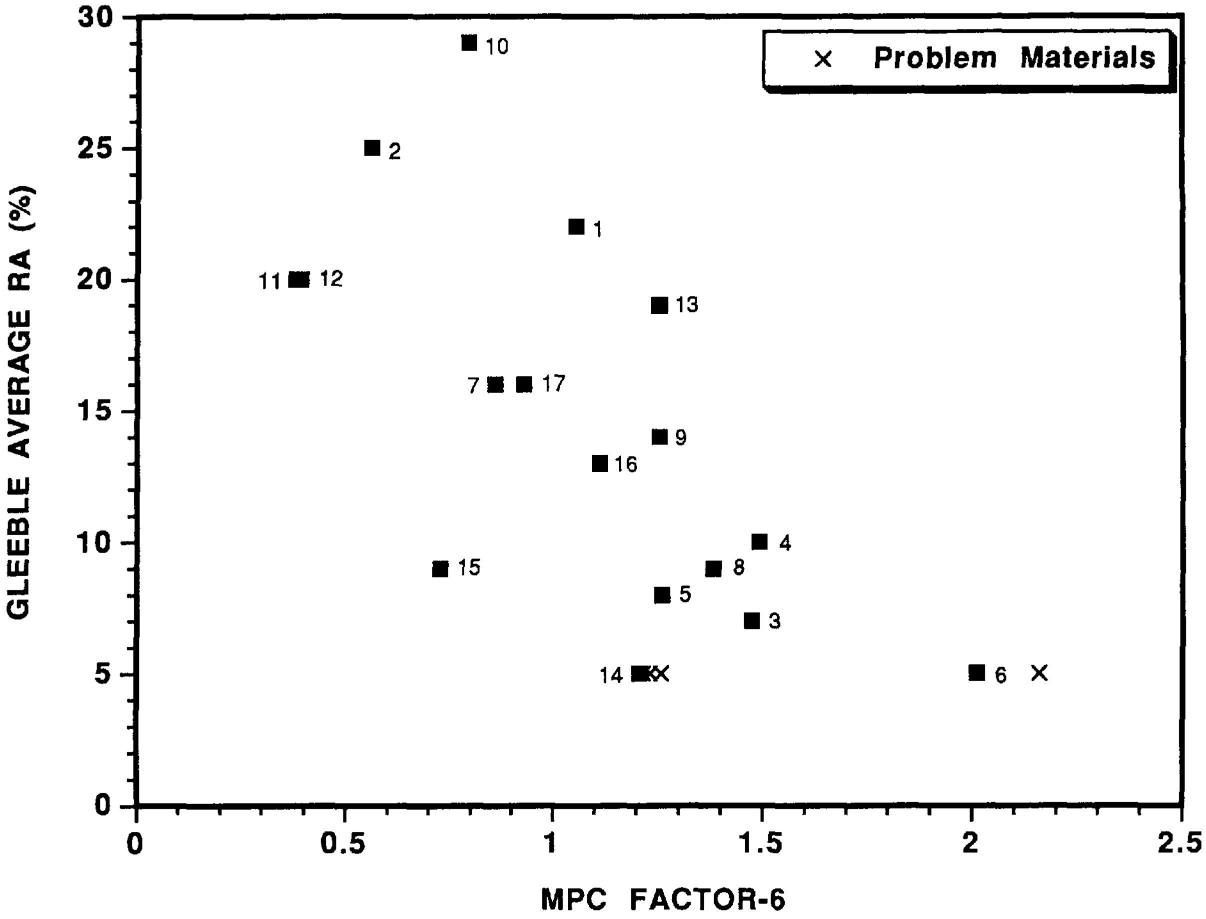

Fig. E17—Correlation between Gleeble reheat test results and MPC factor-6

susceptibility to cracking during PWHT or service. It may be noted that, to determine the level of sensitivity, a heat should be tested using one or more of the various techniques described in this report.

(4) Although the concept behind development of MPC Factors-4, -5 and -6 are sound, it was felt that the procedure to determine whether a heat may be sensitive to reheat cracking based on the chemical composition alone must be simple to use. The concept that if an alloying (or tramp) element is less than a certain value, that element would not be significantly responsible for rendering the heat susceptible to reheat cracking was utilized in the development of MPC Factor-7. It was considered that if the level of C is less than or equal to 0.12%, carbon will not be considered a contributor to reheat cracking. Similar thresholds were placed on Mn, P, S and Al and MPC Factor-7 was thus derived. If the amount of these threshold elements is less than the threshold level, a value of zero is assigned to the factor. The equation and the numerical values of MPC Factor-7 for the API materials are presented in Table E4 and graphically in Fig. E18.

It is suggested that MPC Factors-5 or -7 be employed for heat characterization based on cracking sensitivity with a factor of 2.0 and 0.5 respectively, being the cutoff level for high-low considerations.

Problem materials identified in the literature based on cracking incidences were considered based on the chemistry available (not all elemental amounts were reported). These problem materials are discussed in the text and are designed by an X in the factor plots.

Sources for Problem Materials Composition

1. Nomura, T., *et al.* "Creep Embrittlement of Structural Components in Catalytic Reformer Reactor," Trans. Japan Soc. of Mechanical Engineers, 1993-9, pp. 2066–2073.
2. Cantwell, J. *Private Communication to* M. Prager of MPC, May 1993.

Table E4—Chemical Factors For MPC-API Heats

Materials	Gleeble	MPC Factors						
	Av. RA (%)	MPC-1	MPC-2	MPC-3	MPC-4	MPC-5	MPC-6	MPC-7
UT1	22	-0.2483	0.5288	0.0732	0.6346	1.5994	1.0548	0.33490
UT2	25	-0.2951	0.3553	0.0382	0.3707	1.2704	0.5621	0.22390
UT3	7	-0.1227	0.7626	0.1496	0.8943	3.2000	1.4742	0.50590
UT4	10	-0.1344	0.8510	0.1713	1.1978	2.1035	1.4921	0.57920
UT5	8	-0.1190	0.7716	0.1252	1.1902	2.1996	1.2627	0.55770
UT6	5	-0.0851	1.0131	0.2424	1.6771	5.5554	2.0126	0.89210
UT7	16	-0.1980	0.4777	0.0534	0.4817	1.5268	0.8602	0.35520
UT8	9	-0.1601	0.7046	0.1202	1.1409	2.1186	1.3828	0.52190
UT9	14	-0.1776	0.5701	0.0951	0.6975	1.9664	1.2551	0.44480
UT10	29	-0.2740	0.4024	0.0504	0.4571	1.0706	0.7943	0.26610
UT11	20	-0.2340	0.2356	0.0510	0.4562	0.89170	0.3805	0.10970
UT12	20	-0.2207	0.4933	0.0498	0.5299	0.54200	0.3936	0.32560
UT13	19	-0.2163	0.5748	0.0886	0.7081	1.7552	1.2554	0.39950
UT14	5	-0.0860	0.5775	0.1035	0.7514	2.6663	1.2078	0.57020
UT15	9	-0.1385	0.3713	0.0353	0.7323	1.8253	0.7285	0.23820
UT16	13	-0.1774	0.5255	0.0822	0.6525	1.5776	1.1113	0.38130
UT17	16	+0.0248	0.6008	0.0560	0.8302	1.6125	0.9300	0.39140

MPC-1=(753.07B+11.57Ti+11.21P+2.93Al+2.53S+2.25V+1.22As+0.78C+0.59Cu+0.26Sn+0.14Cr+0.08Mn)
-(45.59Nb+45.05Ca+22.06Zr+9.31Co+6.06Sb+4.54W+1.93O+0.78N+0.66Mo+0.3Si+0.19Ni)

MPC-2=1.8C+2.6P+16.8V+213Nb+25Ti+Cu+5.8Al+75Sb-50Ca

MPC-3=(1.5C+14.3V+170Nb+18.4Ti)*(6.6P+0.8Cu+4Al+8.6Sn+52Sb-32Ca)

MPC-4=[Cfn*(Tramp+Sfn)*Alfn]-1; Cfn=(3C+200Nb+10V-0.15)+1; Tramp=8.6Sn+52Sb+0.8Cu;
Sfn=1+(S-0.1Tramp)*20, For Sfn<1, Sfn=1; Alfn=1+(Al-0.01)*20, For Alfn<1, Alfn=1

MPC-5=[Cfn*(Tramp+Sfn)*Alfn]-1; Cfn=(5C+1000Nb+100V+50Ti-0.5)+1; Tramp=2*[4.3(Sn+As)+150Sb+Cu+50(P-0.01)]; Sfn=1+(S-0.02Tramp)*30, For Sfn<1, Sfn=1; Alfn=1+(Al-0.015)*15, For Alfn<1, Alfn=1

MPC-6=[Cfn*(Tramp+Sfn)*Alfn]-1; Cfn=(5C+200Nb+20V+5Ti-0.5)+1; Tramp=8.6Sn+150Sb+Cu+5P;
Sfn=1+(1.5S/C), For Sfn<1, Sfn=1; Alfn=1+(Al-0.01)*20, For Alfn<1, Alfn=1

MPC-7=2(C-0.12)-0.25(Mn-0.6)+150Nb+15V+15Ti-100B+40(P-0.010)+5(S-0.015)+10(Al-0.010)+20(Cu/100+Sn/3+As/3+3Sb)

Table E4—Chemical Factors For other MPC Problem Heats* (Continued)

Materials	Gleeble	MPC Factors						
	Av. RA (%)	MPC-1	MPC-2	MPC-3	MPC-4	MPC-5	MPC-6	MPC-7
PM-1	ND**	+0.0632	0.9719	0.2119	1.1280	3.7936	2.1608	1.0403
PM-2	ND	+0.0550	0.7469	0.1735	1.2599	2.8774	1.2587	0.76020
PM-3	ND	+0.0867	0.6571	0.1716	0.9740	2.7245	1.2154	0.86480
PM-4	ND	+0.0358	0.7121	0.1748	1.1576	3.0940	1.2327	0.83950

*Note: Full chemical analysis of these heats were not available.
**ND: Not Determined

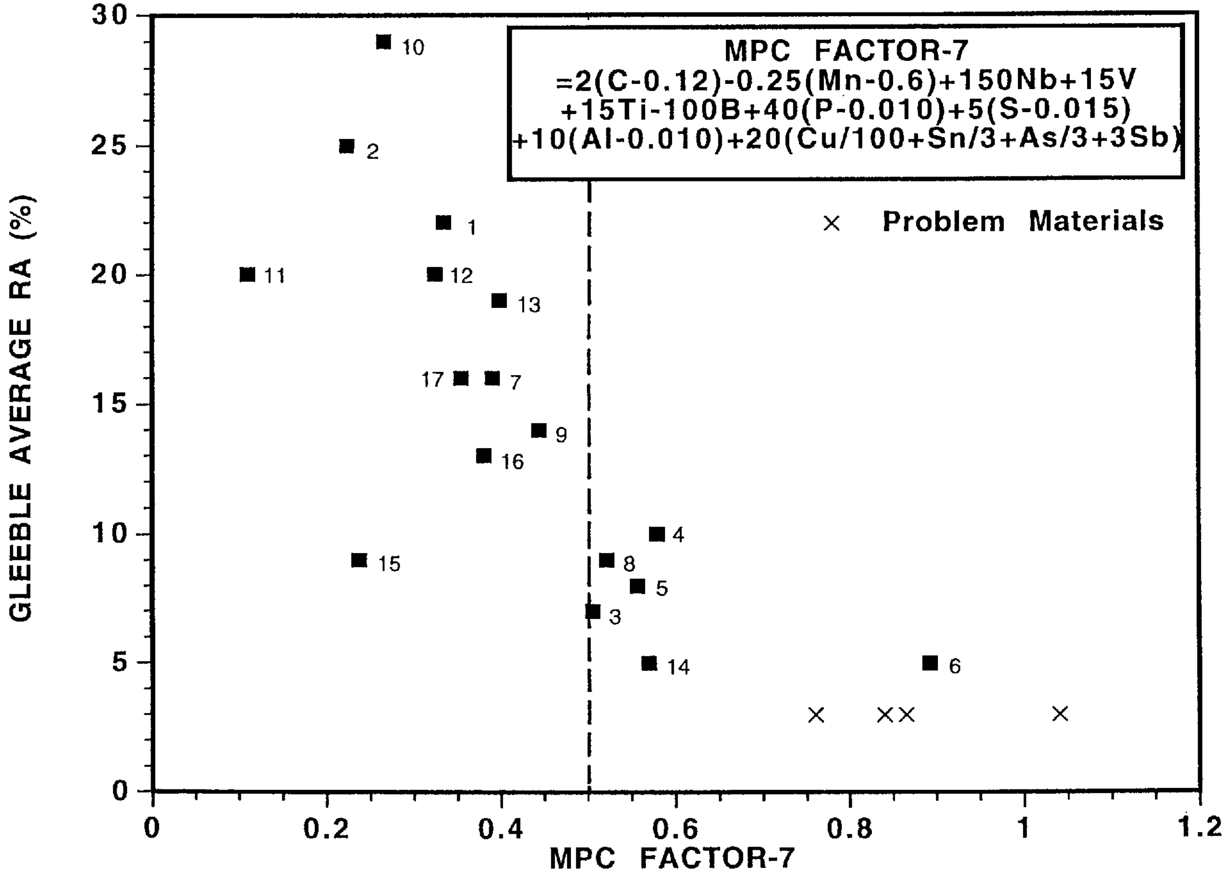

Fig. E18—Correlation between Gleeble reheat cracking test results and MPC factor-7

Appendix F—Toughness Study

It has been reported by some investigators that prolonged PWHT at high temperatures results in degradation of the impact toughness of the base metal. The reheat cracking study revealed that PWHT at higher than normal temperatures (e.g., 1325°F+) is necessary to mitigate reheat cracking and in-service cracking in susceptible heats. Thus, before suggesting that fabricators PWHT structures at higher than the currently employed temperatures, it was considered necessary to determine the extent of degradation of toughness of the base metal due to high temperature PWHT.

Three heats (UT5, UT11 and UT12) were utilized to determine the PWHT response on the toughness behavior of the base metal. The selection of these three heats was primarily based on carbon content. UT5 has high carbon (0.17%) and UT11 and UT12 have low and intermediate carbon (0.086 and 0.10%), respectively. UT11, which was obtained in the service exposed condition, was renormalized and tempered (N at 1650°F & T at 1150°F) so that the starting condition of all heats would be similar before the application of PWHT. In addition, to determine the impact toughness behavior as a function of PWHT after N&T for the three heats, UT12 was also assessed for impact toughness in the PWHT condition after a Q&T.

The test matrix used is shown in Table F-1. The entries in Table F-1 correspond to the conditions at which the toughness behavior was assessed, whereas the values are the hardnesses for the base metal under the particular condition of PWHT. It may be noted that, even for the low carbon material, (UT11) the hardness decrease upon PWHT is nominal and the strength level after PWHT will meet Class 1 properties.

Table F-1—Hardness of 1¼Cr-½Mo Steels Used for PWHT Toughness Study*

Materials	*No PWHT*	*1250°F, 8 h*	*1300°F, 8 h*	*1325°F, 8 h*	*1350°F, 8 h*
UT5-N/T	175	—	—	161	151
UT11-N/T	145	140	138	—	—
UT12-N/T	179	—	165	161	160
UT12-Q/T	203	—	—	164	—

*Hardness HV scale by conversion from HRB

Note: UT5-N/T: Received as a normalized (1650°F, 40 min) and tempered (1320°F, 86 min) condition.

UT11-N/T: Normalized at 1650°F for 1 h and tempered at 1150°F for 1 h.

UT12-N/T: Received as a normalized (1700°F, ? hr) and tempered (1310°F, 30 min) condition.

UT12-Q/T: Water quench cooling rate simulated by forced air cooling of ½ in. thick piece cut at ¼ t from 2⅜ in. thick plate.

The Charpy V-notch specimens were extracted in the LT-orientation after PWHT. A full impact energy curve was determined for the highest PWHT temperature for each material in the test matrix and for the lower PWHT temperature impact tests were conducted at selected temperatures.

In addition, the toughness behavior of low carbon (0.025%) weld metal was determined in the as-welded and PWHT (1350°F 8 hours) condition. The reason for the assessment of the toughness of low carbon weld metal is that low carbon filler metal may be a more viable choice for a successful repair. The stress rupture properties of the low carbon weld metal are addressed in Appendix I. The Charpy V-notch specimens from the low carbon weld metal were extracted transverse to the welding direction and notched in the thickness direction.

The test results are presented in tabular form and graphically at the end of the text for Appendix F. In the N&T condition UT12 exhibits a superior toughness when compared to UT11 and UT5. The toughness of UT11 was found to be improved with PWHT. However, a degradation of the toughness of UT12 was found with an increase in the PWHT temperature for both the N&T and Q&T condition. It is to be noted that UT12 revealed a sharp transition behavior after each PWHT. Even though the toughness of UT12 in the N&T condition revealed degradation upon PWHT, the toughness after the most severe PWHT (1350°F 8 hours) is considered acceptable (hammer stopper behavior at −20°F). The same is true for UT12 in the Q&T condition, after PWHT of 1325°F for 8 hours, the average absorbed energy is approximately 160 ft-lbs at −20°F. Thus, for heats UT11 and UT12, the toughness requirement that is usually specified as 40 ft-lbs at −20°F is met for all PWHT conditions.

The toughness of UT5, which is the high carbon heat (0.17%), was found to suffer significant degradation upon PWHT. In the N&T condition, the energy absorbed is approximately 75 ft-lbs at −20°F. After PWHT at 1325°F for 8 hours the toughness dropped significantly and the 40 ft-lbs transition occurred at approximately +20°F. A more severe PWHT at 1350°F for 8 hours resulted in further degradation of toughness, and the 40 ft-lbs transition temperature increased to approximately +50°F. Thus, it can be concluded that the higher the carbon (1¼Cr-½Mo materials) the greater the possibility of degradation in toughness as a result of PWHT. However, it may be recalled that UT5 also revealed a high to intermediate susceptibility to reheat cracking and thus a high temperature PWHT is necessary to avoid reheat cracking or low ductility creep. In such situations, it is recommended that controlled deposition techniques be utilized to refine the CGHAZ completely, such that reheat cracking problems may be avoided.

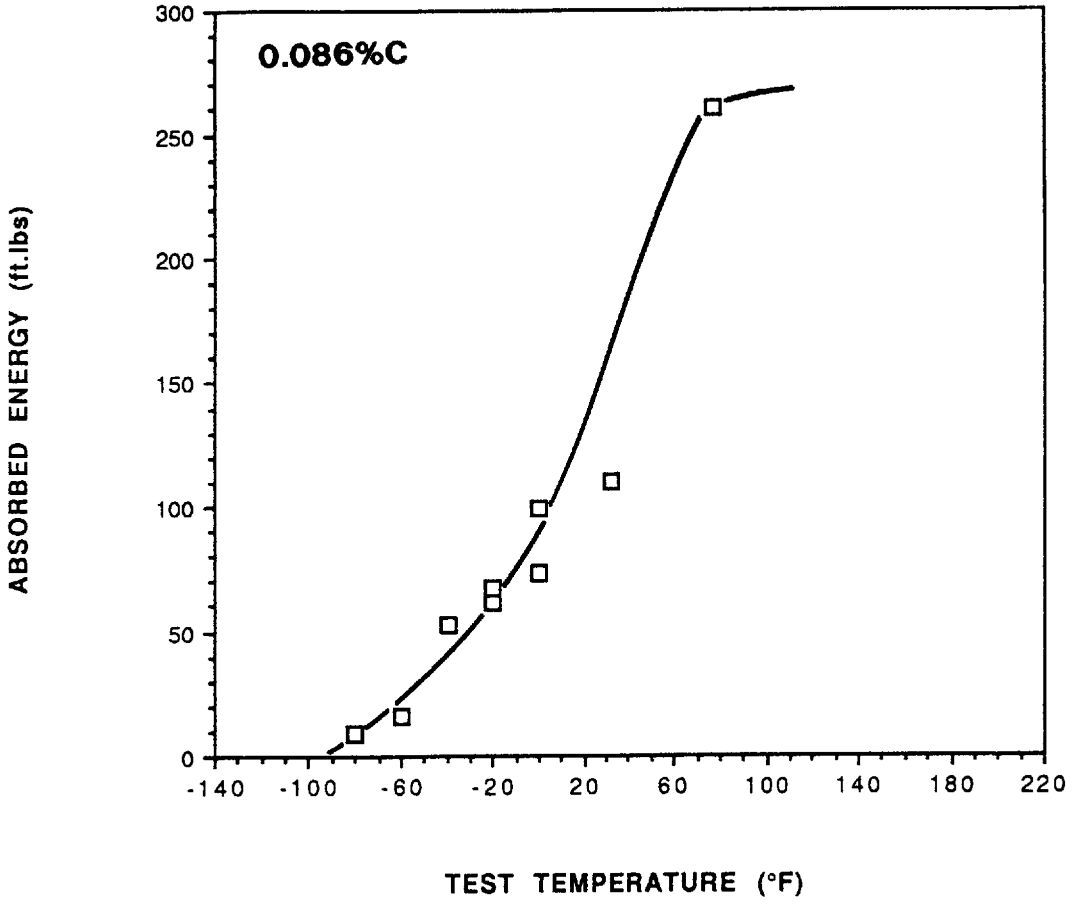

Fig. F1—UT11 CVN-energy N(1650°F, 1 hr) & T(1150°F, 1 hr)-NO PWHT

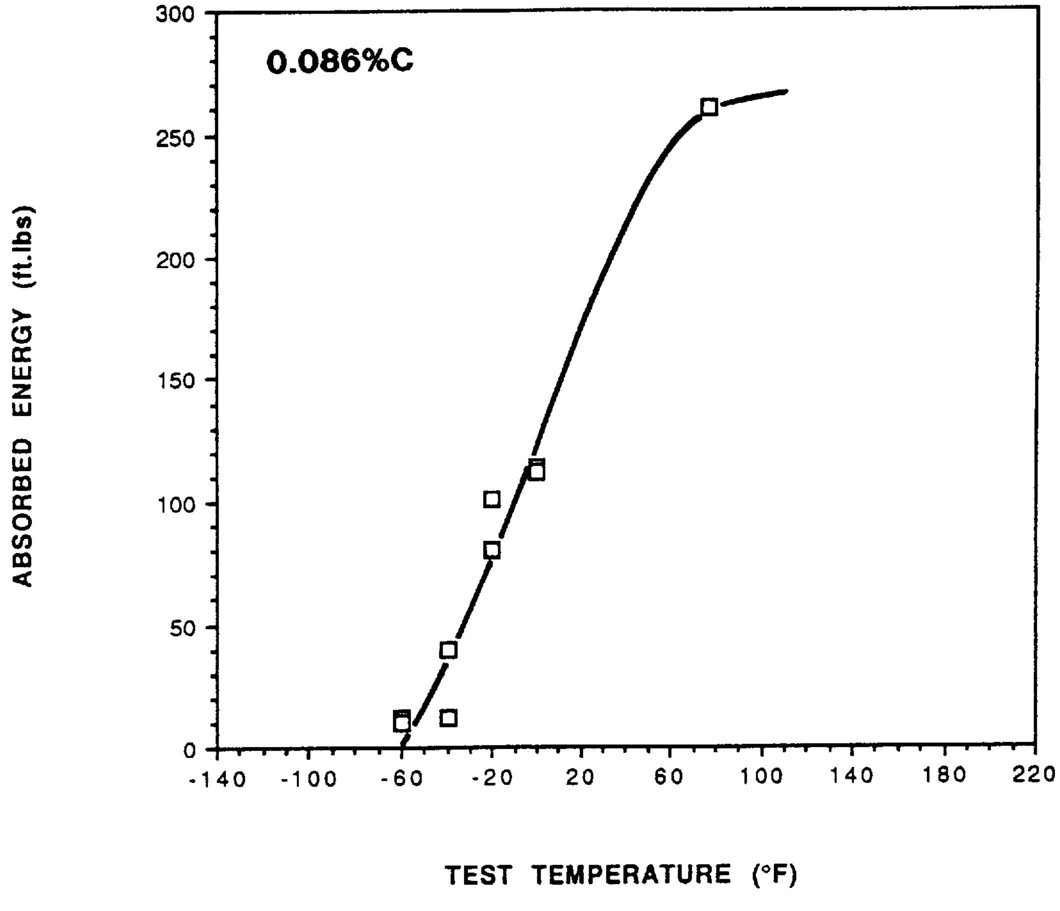

Fig. F2—UT11 CVN-energy N(1650°F, 1 hr) & T(1150°F, 1 hr), 1250°F, 8 hrs PWHT

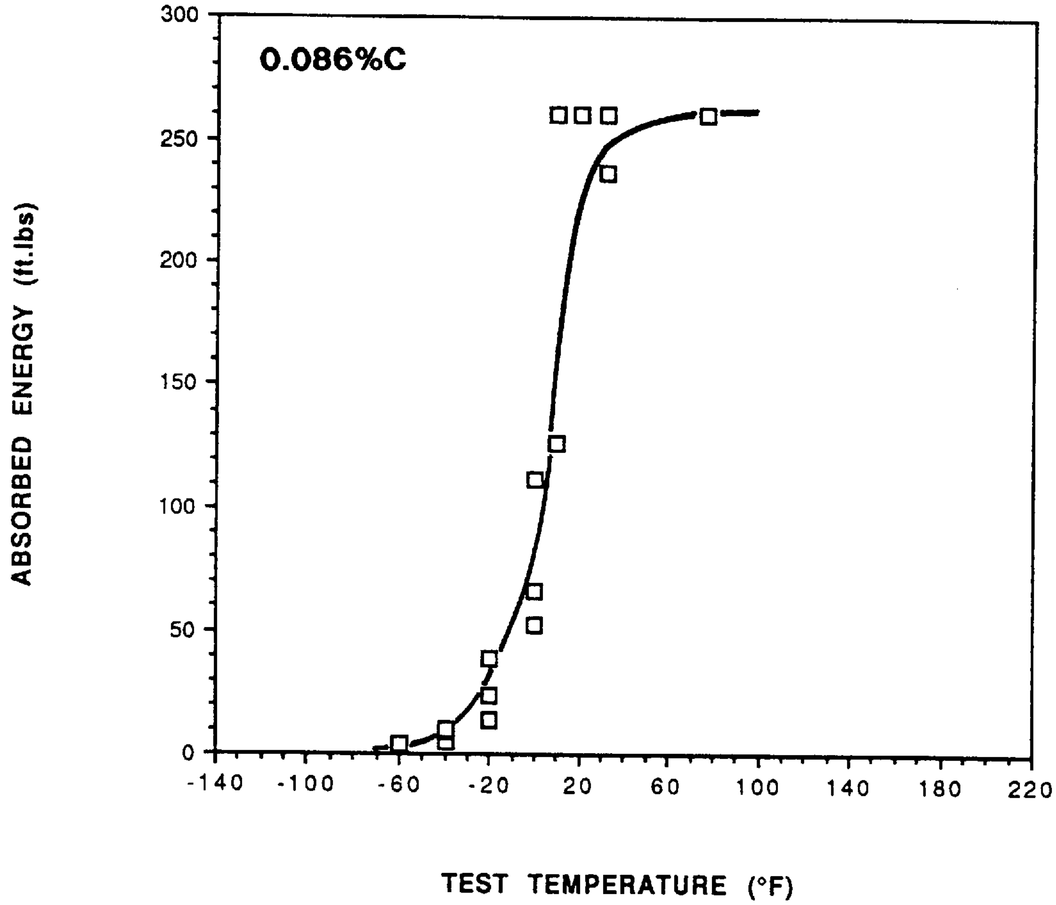

Fig. F3—UT11 CVN-energy N(1650°F, 1 hr) & T(1150°F, 1 hr) 1300°F, 8 hrs PWHT

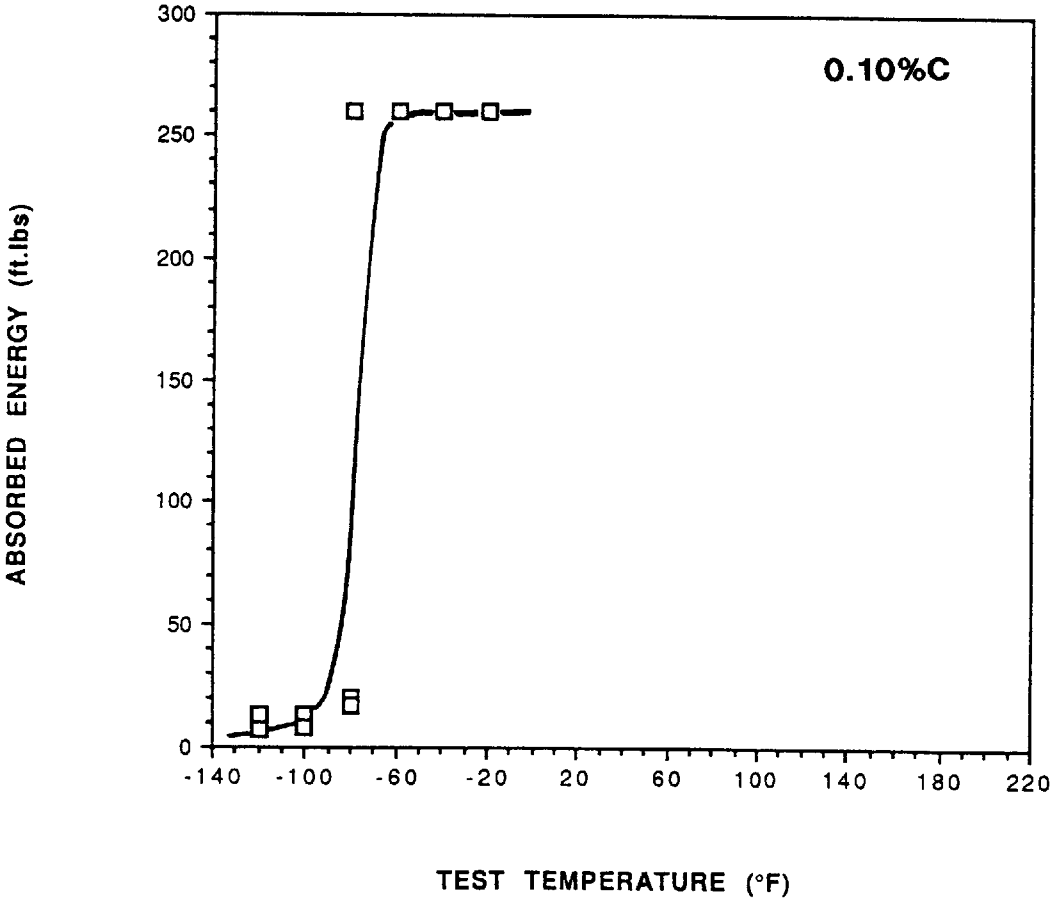

Fig. F4—UT12 CVN-energy N(1700°F, ?) & T(1310°F, 30 min) no PWHT

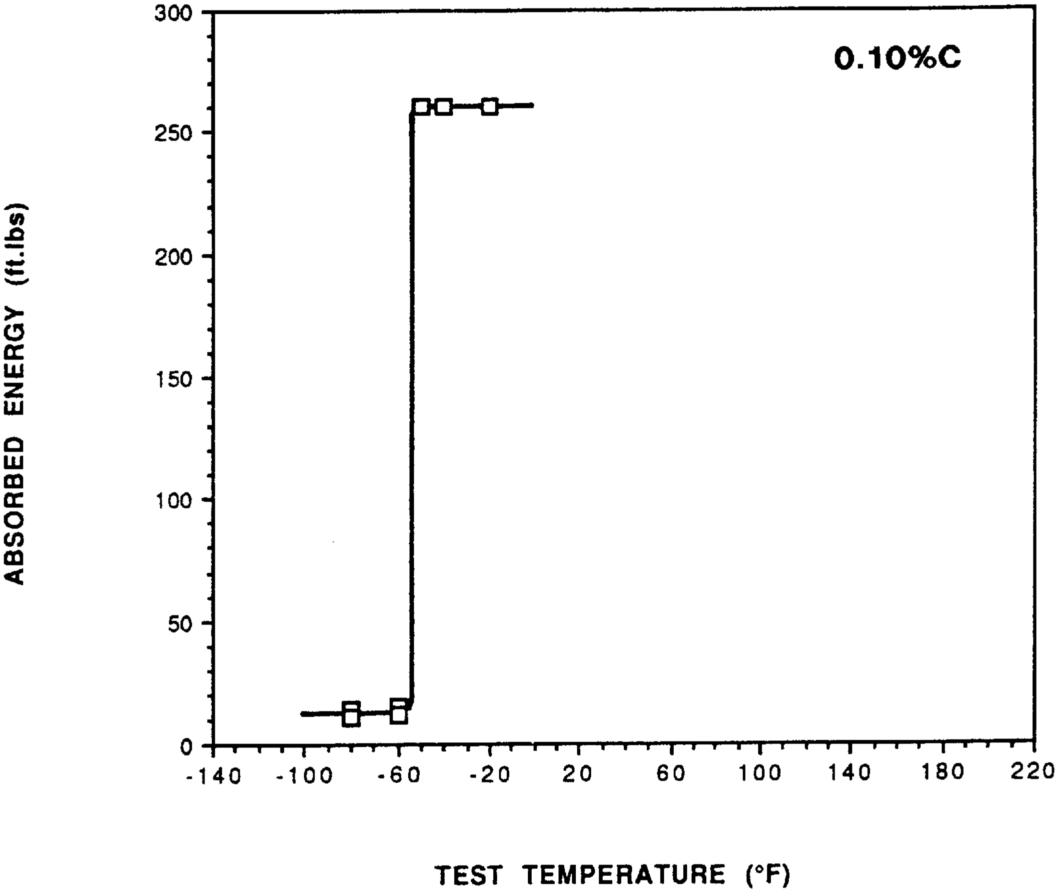

Fig. F5—UT12 CVN-energy N(1700°F, ?) & T(1310°F, 30 min) 1300°F, 8 hrs PWHT

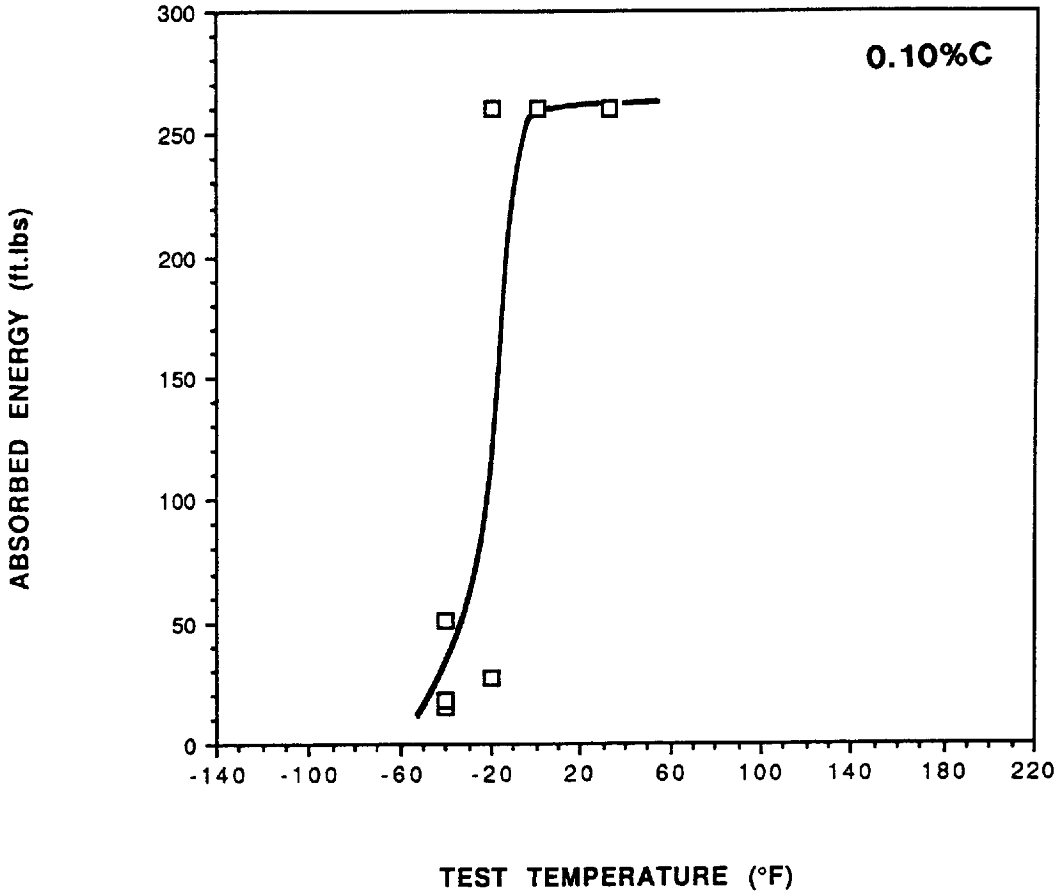

Fig. F6—UT12 CVN-energy N(1700°F, ?) & T(1310°F, 30 min) 1325°F, 8 hrs PWHT

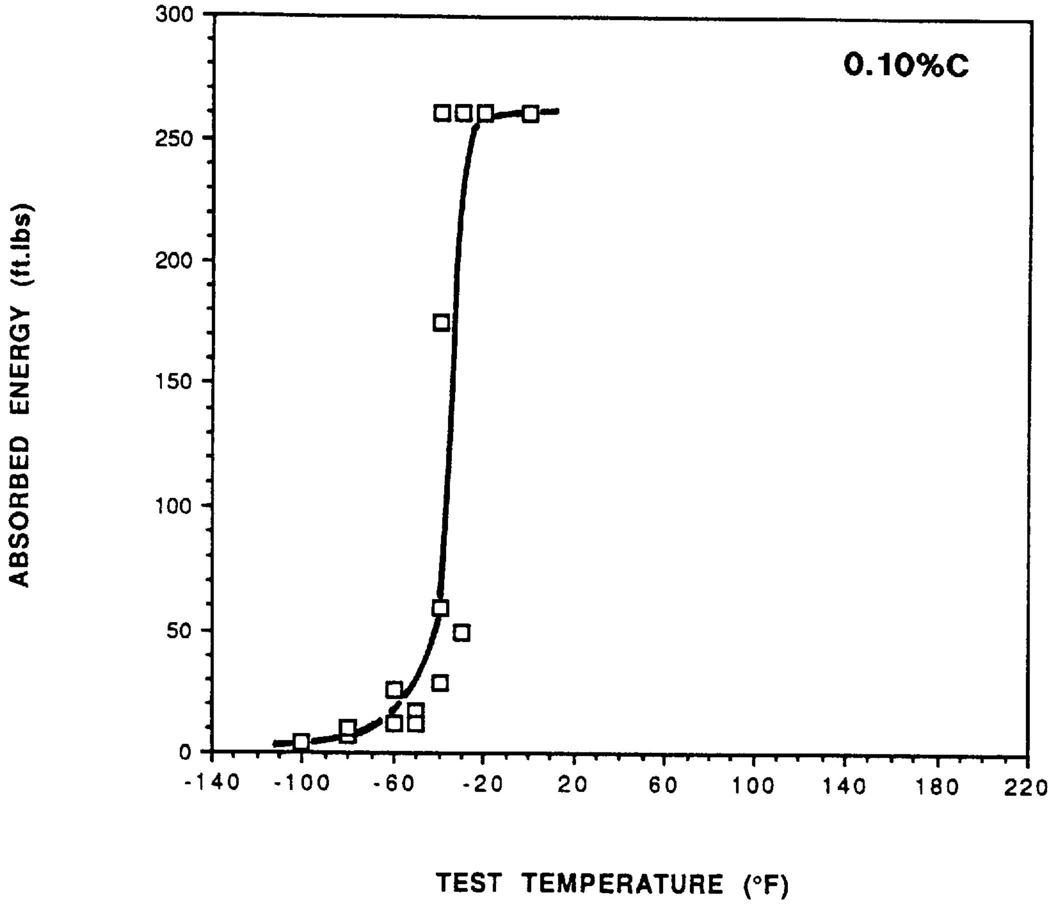

Fig. F7—UT12 CVN-energy N(1700°F, ?) & T(1310°F, 30 min) 1350°F, 8 hrs PWHT

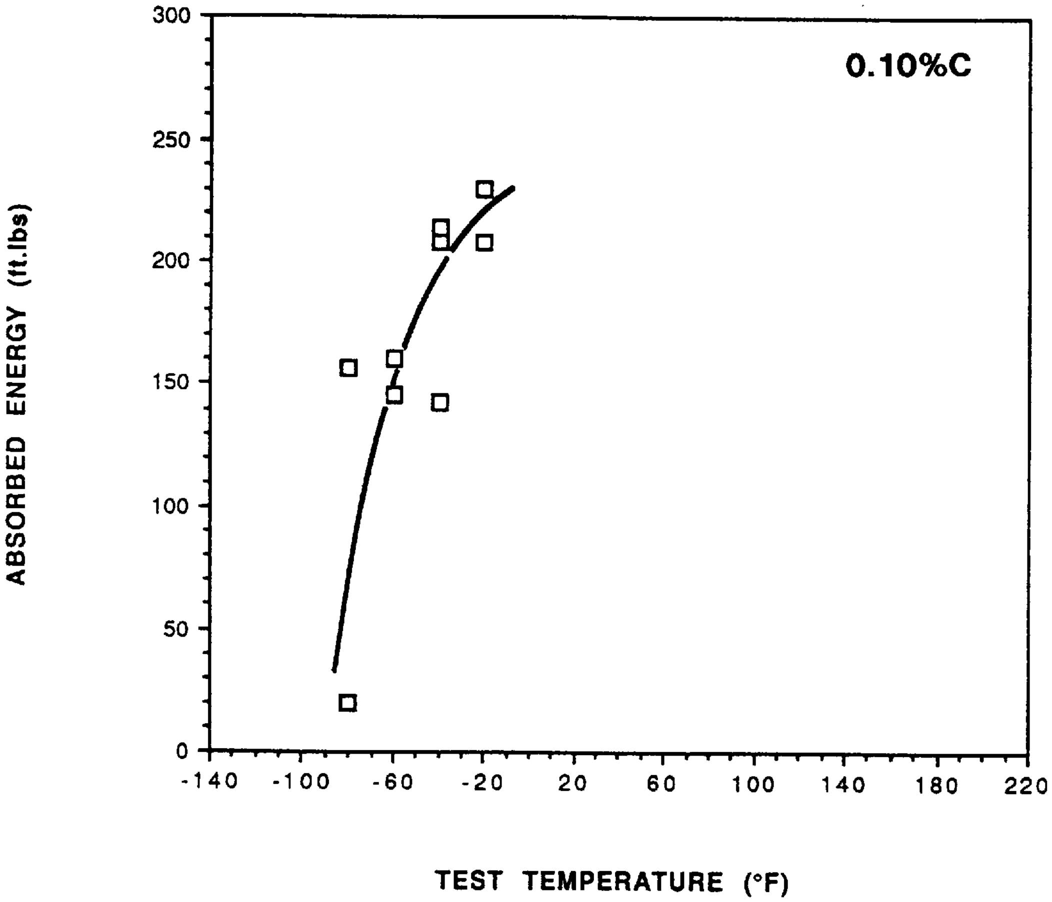

Fig. F8—UT12 CVN-energy Q(1650°F, 1 hr + simulated water quench) & T(1150°F 1 hr) no PWHT

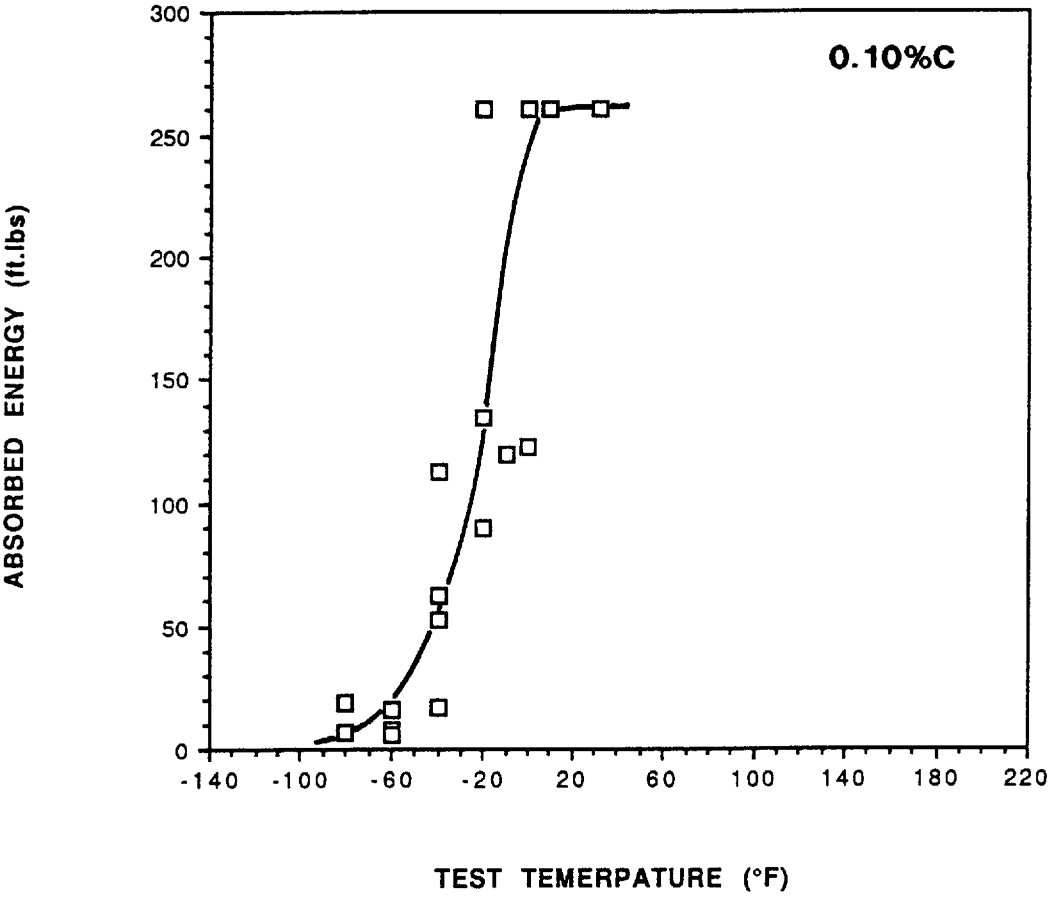

Fig. F9—UT12 CVN-energy Q(1650°F, 1 hr + simulated water quench) & T(1150°F, 1 hr) 1325°F, 8 hr PWHT

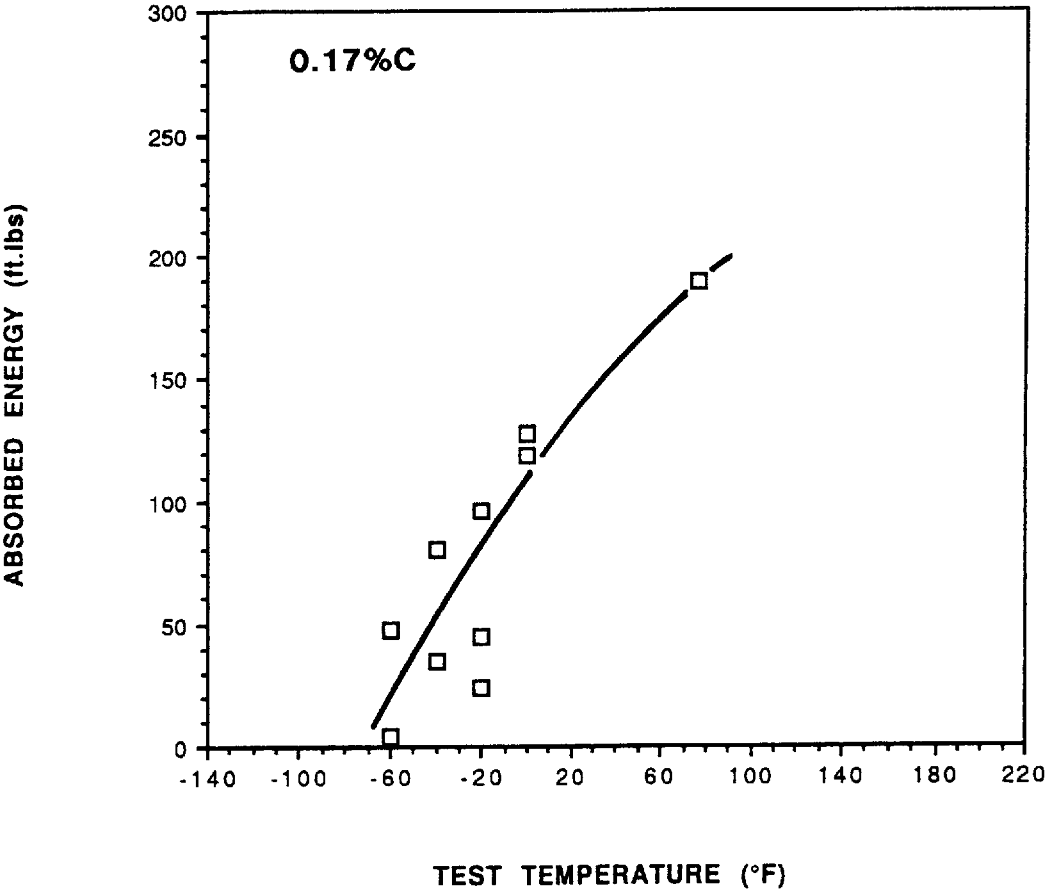

Fig. F10—UT5 CVN-energy N(1650°F, 40 min) & T(1320°F, 86 min) no PWHT

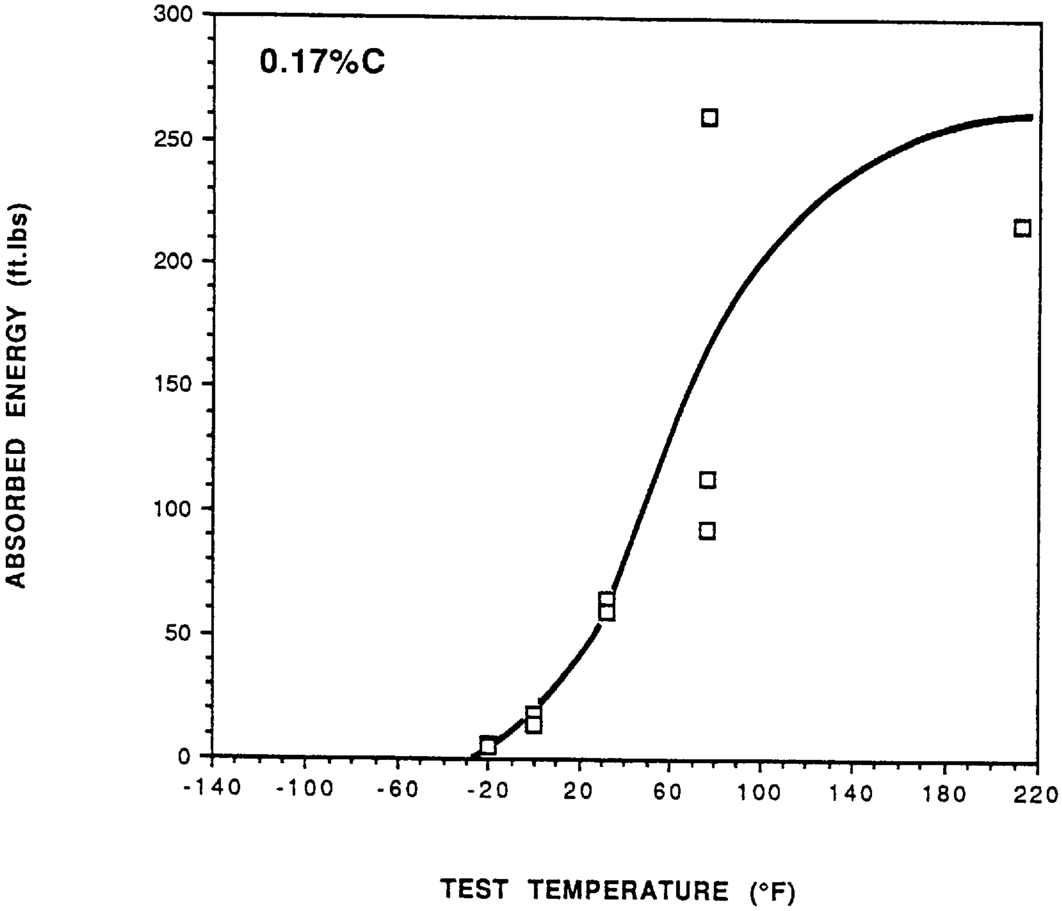

Fig. F11—UT5 CVN-energy N(1650°F, 40 min) & T(1320°F, 86 min) 1325°F, 8 hrs PWHT

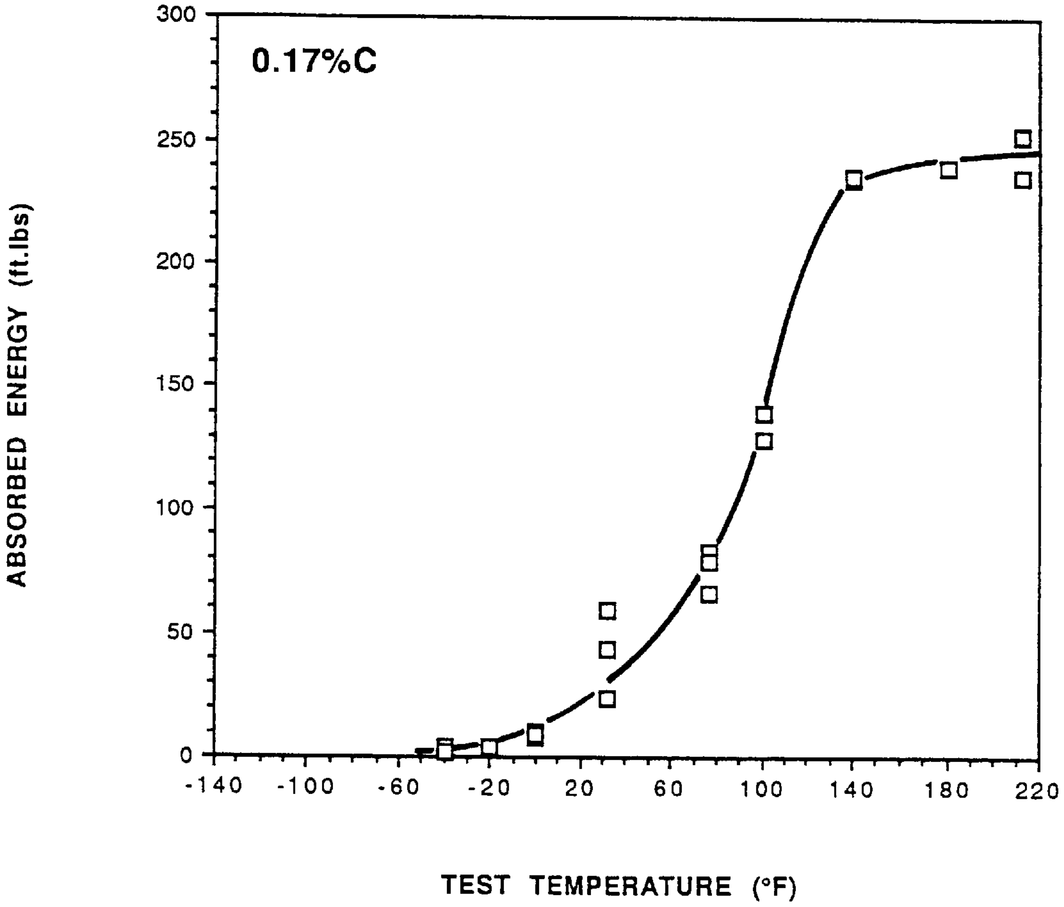

Fig. F12—UT5 CVN-energy N(1650°F, 40 min) & T(1320°F, 86 min) 1350°F, 8 hrs PWHT

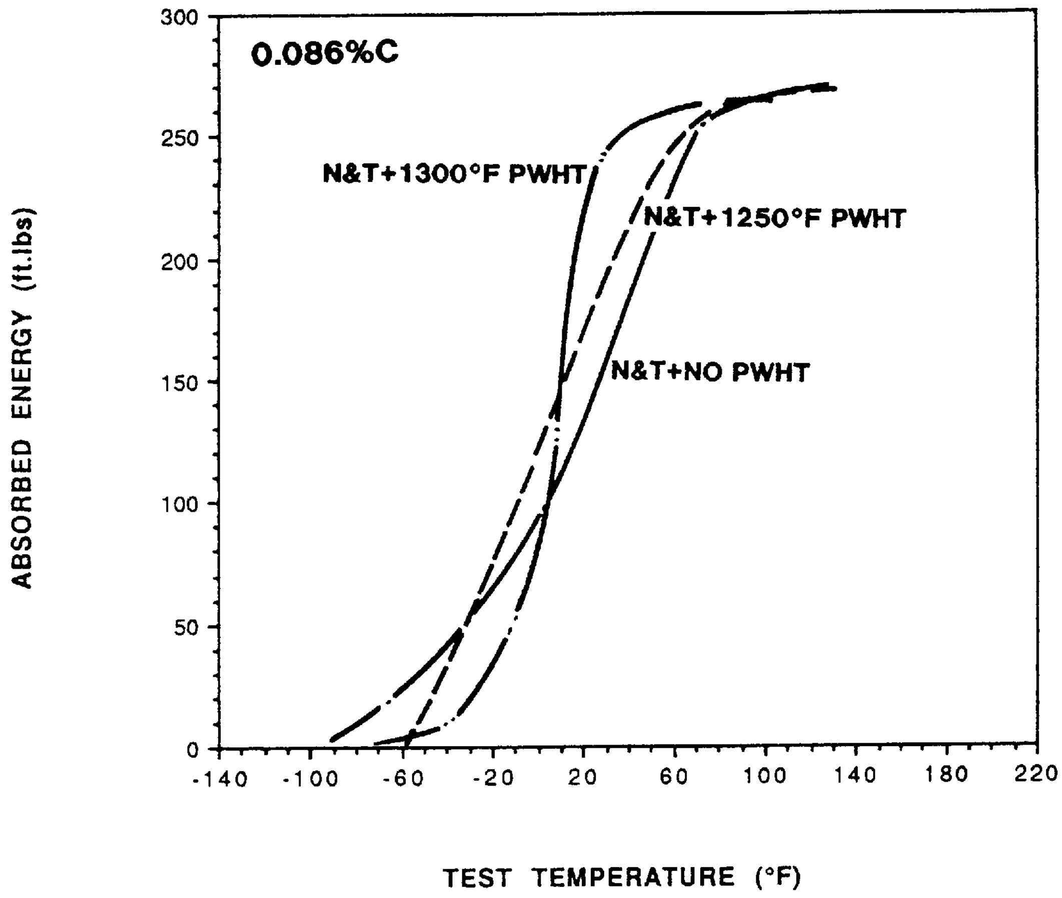

Fig. F13—UT11 CVN-energy N(1650°F, 1 hr) & T(1150°F, 1 hr)

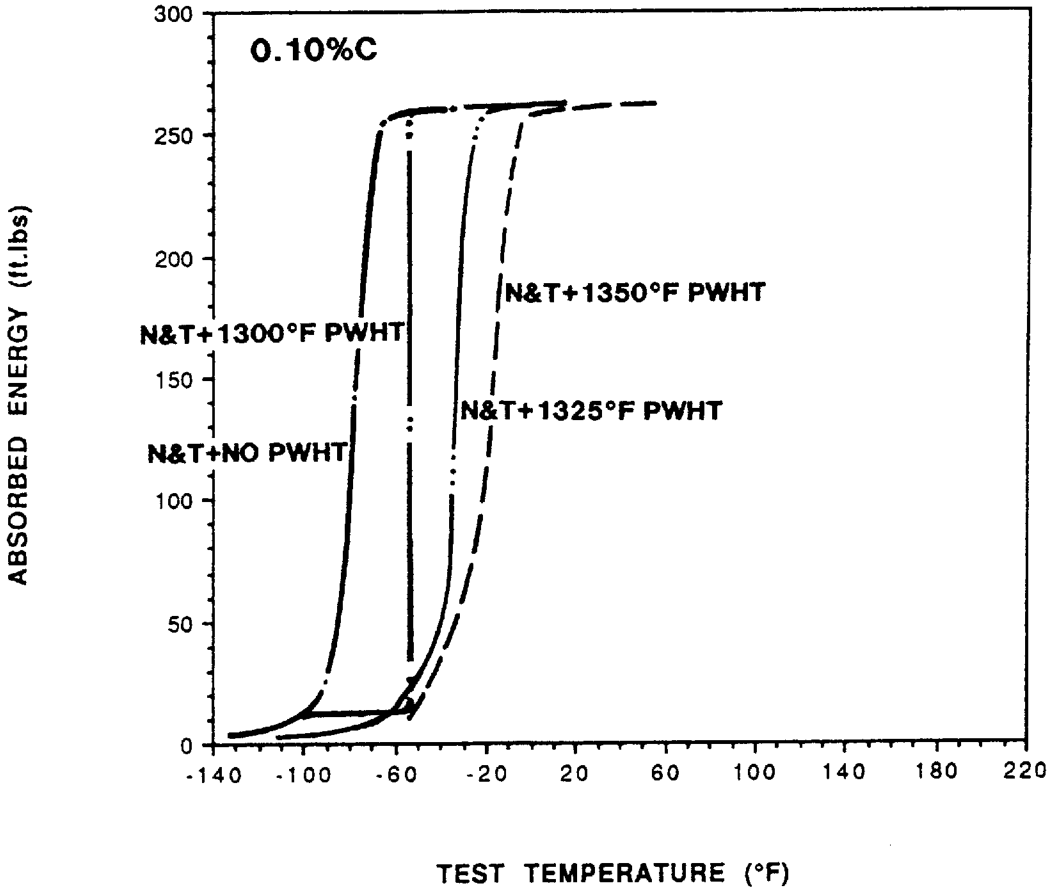

Fig. F14— UT12 CVN-energy N(1700°F, ? hr) & T(1310°F, 30 min)

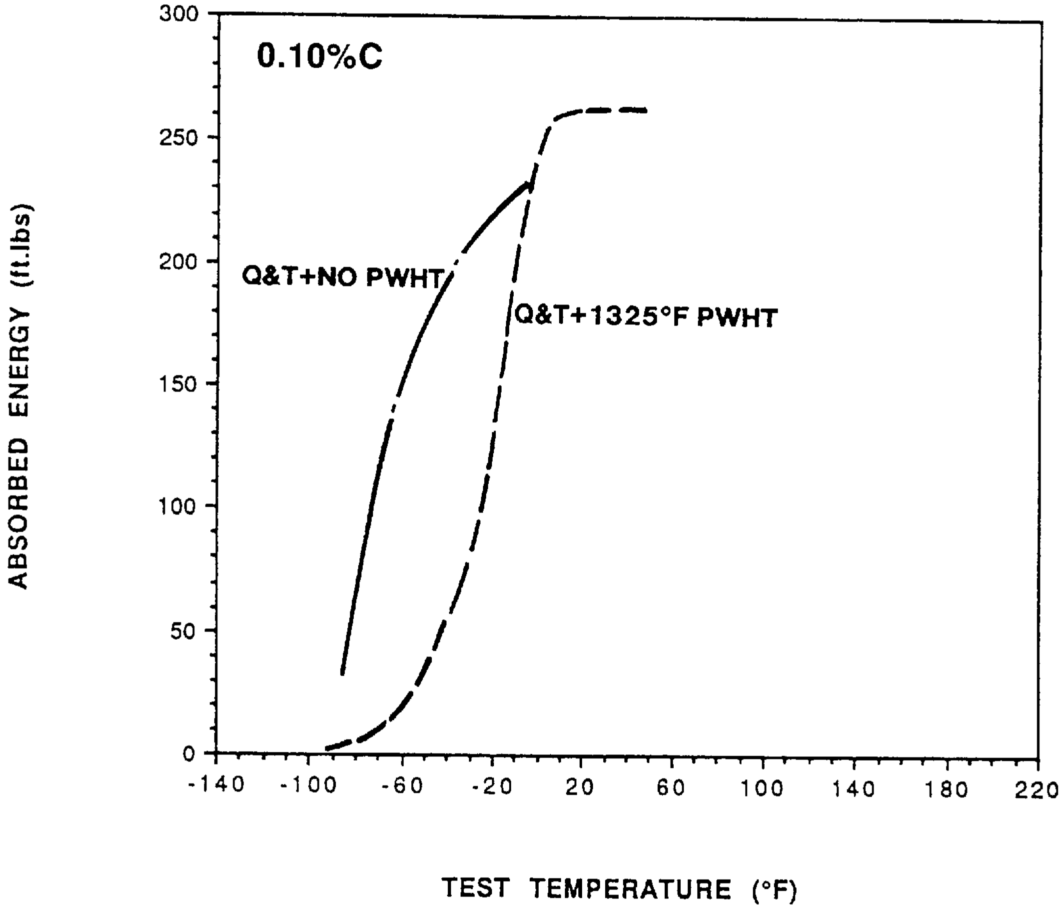

Fig. F15—UT12 CVN-energy Q(1650°F, 1 hr + simulated water quench) & T(1150°F, 1 hr)

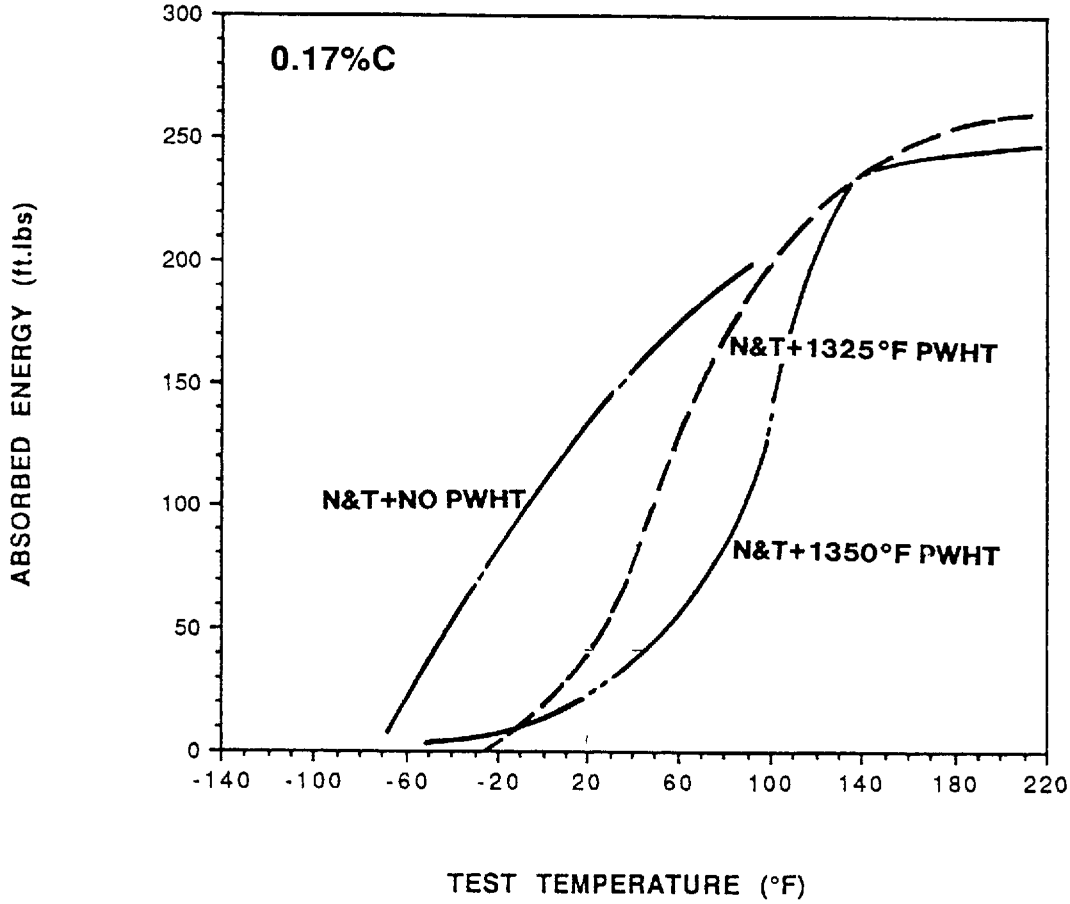

Fig. F16—UT5 CVN-energy N(1650°F, 40 min) & T(1320°F, 86 min)

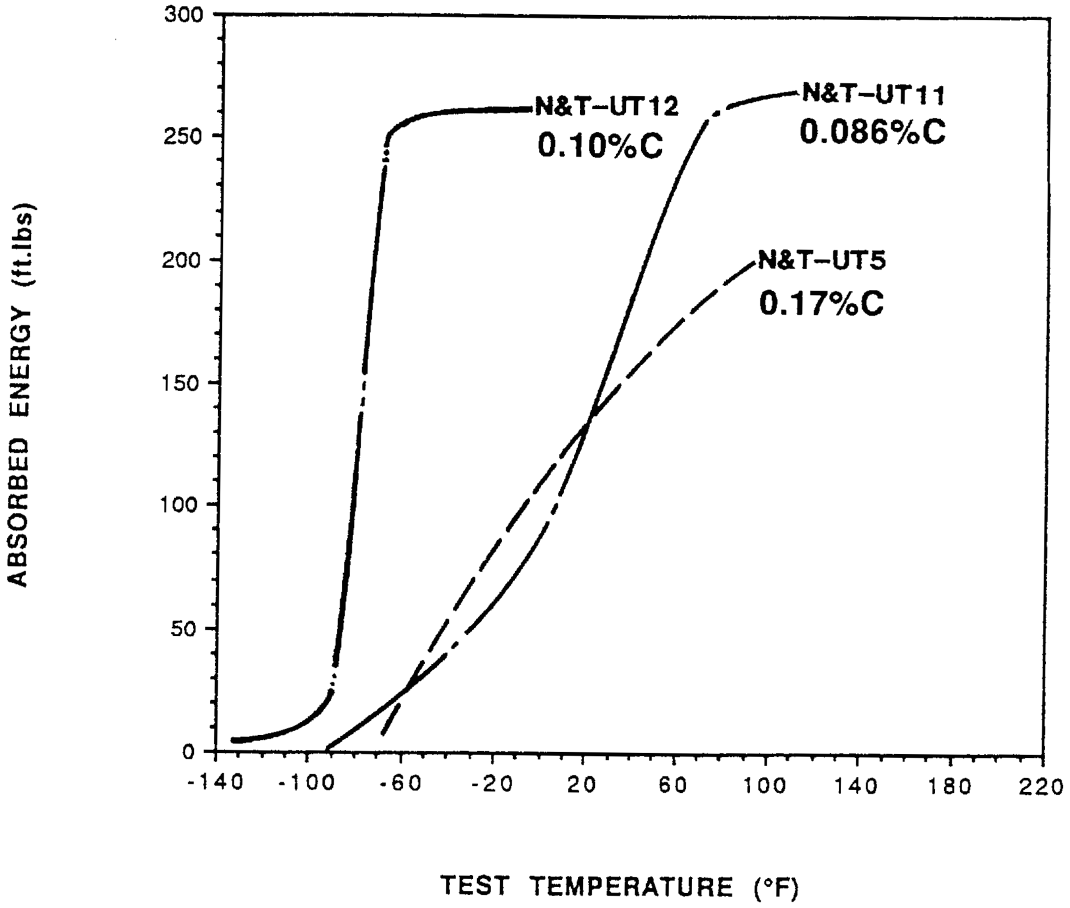

Fig. F17—UT5, UT11, UT12 CVN-energy, N & T

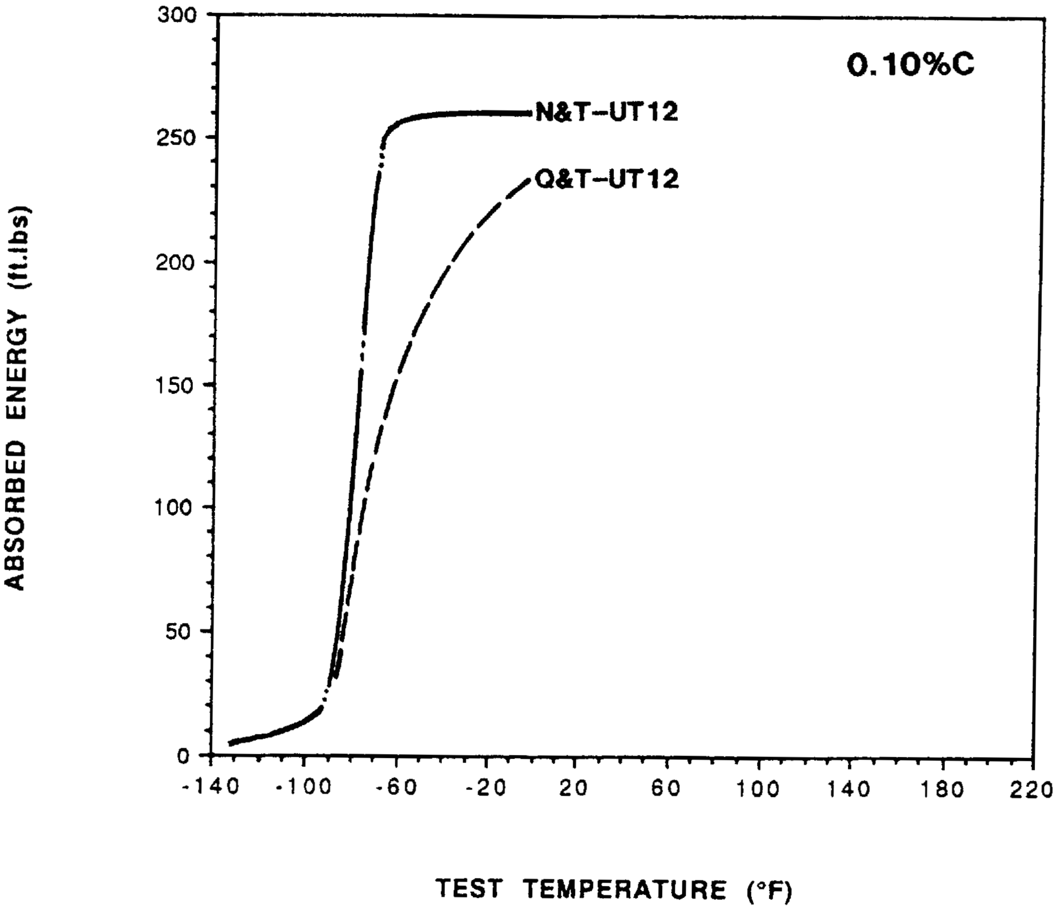

Fig. F18—UT12 CVN-energy N & T, Q & T

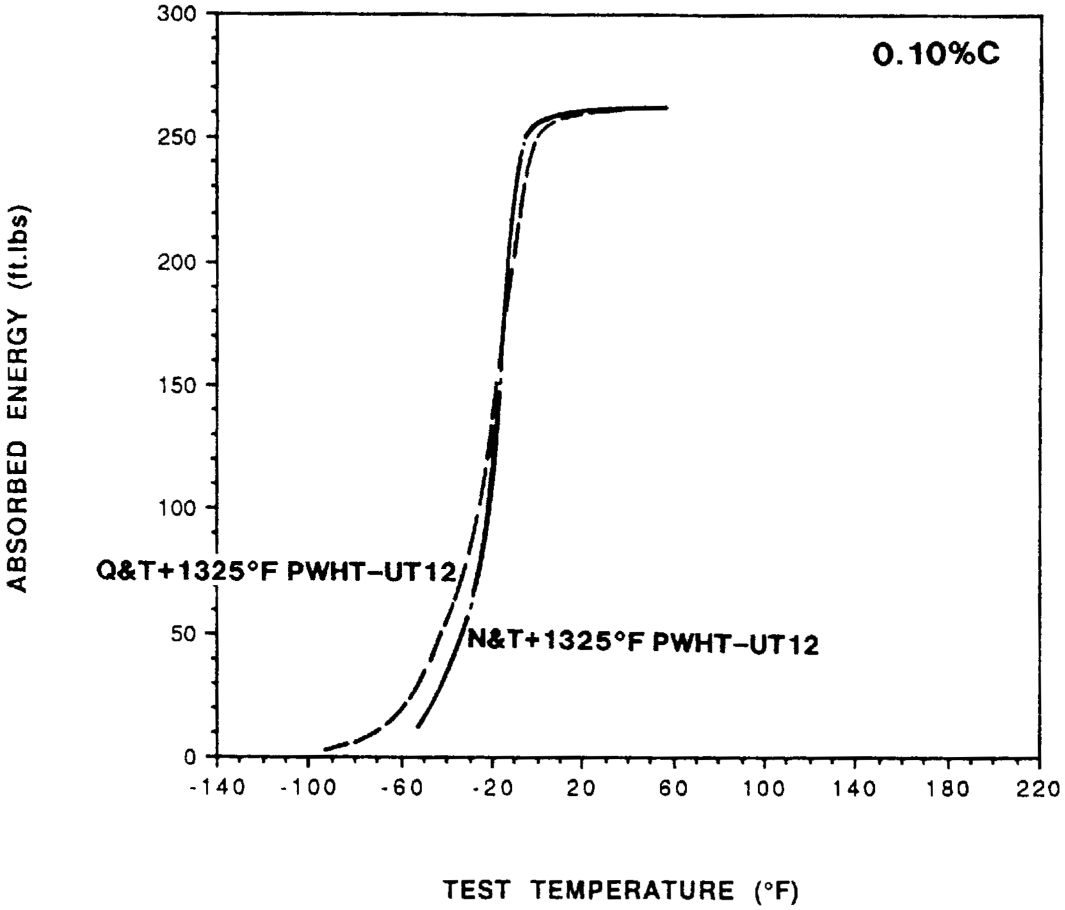

Fig. F19—UT12 CVN-energy N & T + 1325°F-Q & T + 1325°F

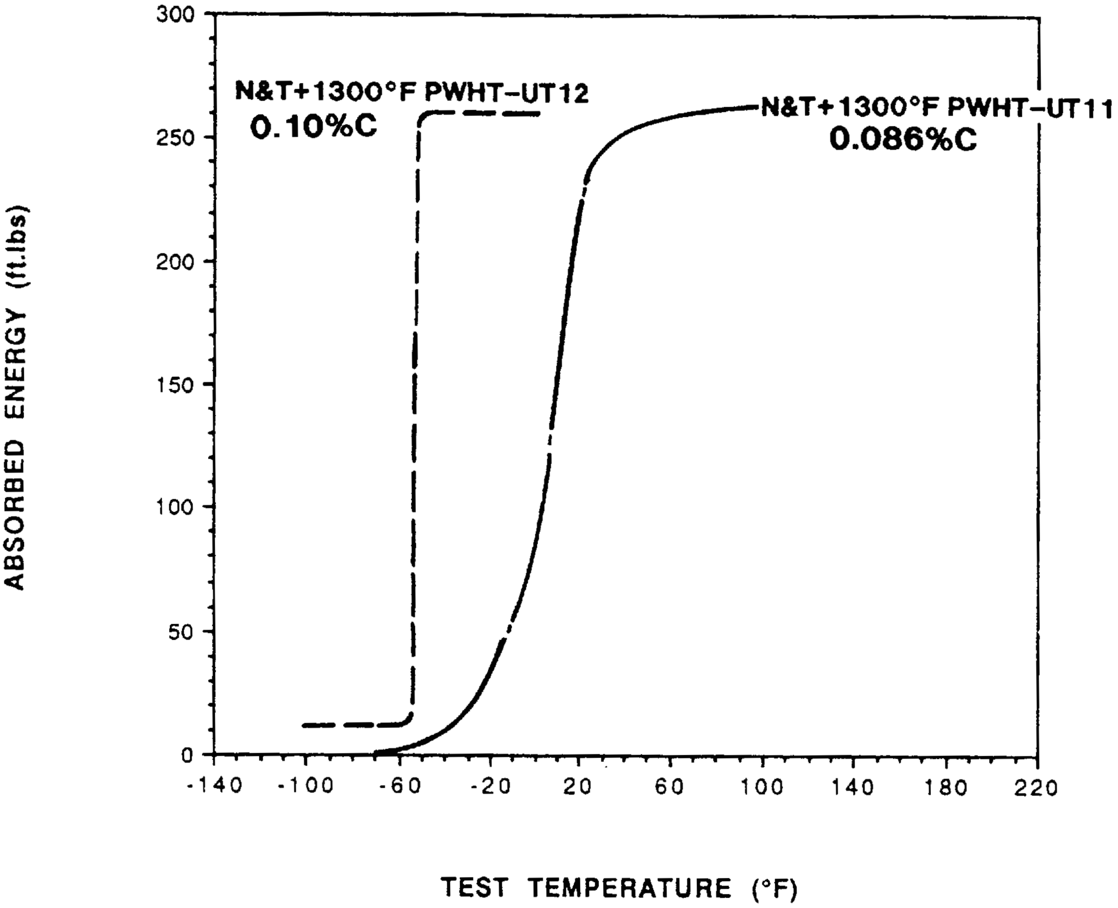

Fig. F20—UT11, UT12 CVN-energy N & T + 1300°F

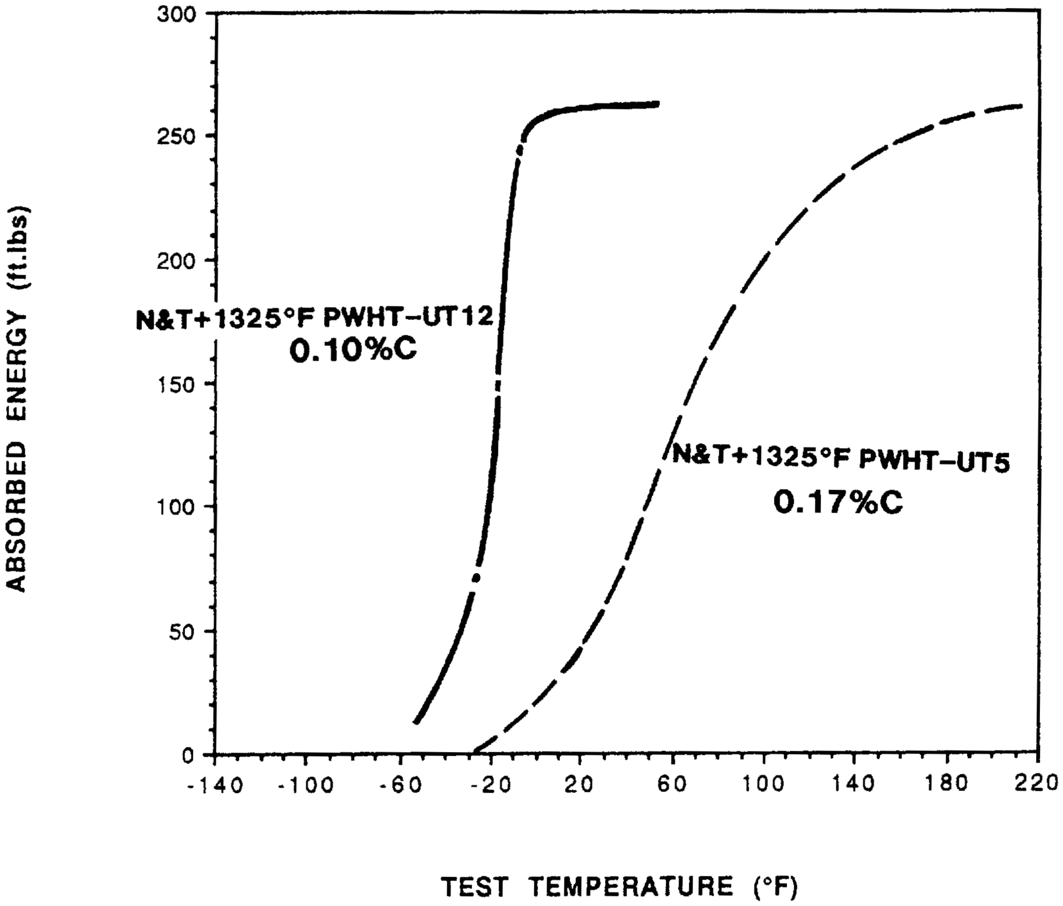

Fig. F21—UT5, UT12 CVN-energy, N & T + 1325°F

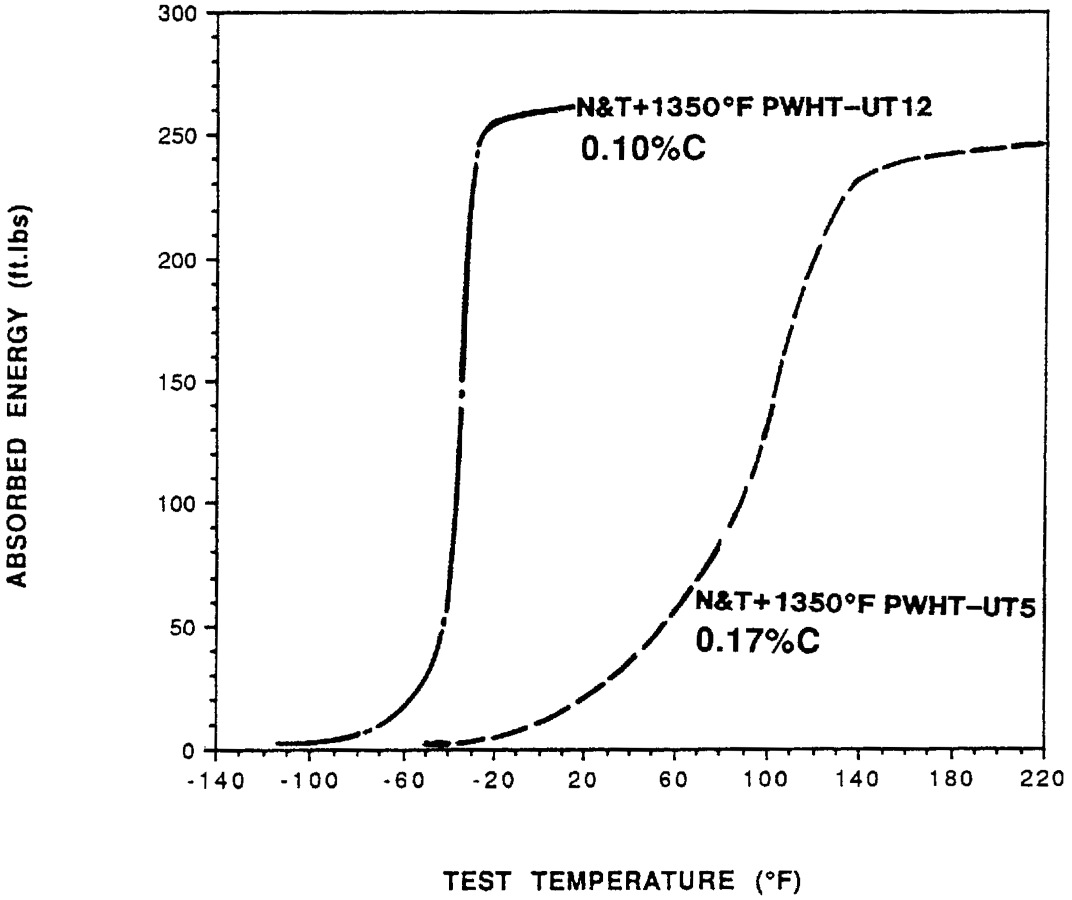

Fig. F22—UT5, UT12 CVN-ENERGY, N & T + 1350°F

Results of Charpy V-Notch Toughness Study

UT-5, N&T, No PWHT

Test Temperature (°F)	*Energy Absorbed (ft-lbs)*
RT	189
0	119
0	128
−20	45
−20	24
−20	96
−40	35
−40	80
−60	48
−60	4

UT-5, N&T, 1325°F-8 hrs. PWHT

Test Temperature (°F)	*Energy Absorbed (ft-lbs)*
212	217
RT	253
RT	93
RT	114
32	64
32	59
0	14
0	18
−20	5
−20	6

UT-5, N&T, 1350°F-8 hrs. PWHT

Test Temperature (°F)	*Energy Absorbed (ft-lbs)*
212	236
212	252
180	240
140	235
140	236
100	140
100	129
RT	79
RT	66
RT	83
32	59
32	44
32	24
0	8
0	10
0	9
−20	4
−20	4
−40	2
−40	4

UT-11, N&T, No PWHT

Test Temperature (°F)	*Energy Absorbed (ft-lbs)*
RT	237
32	110
0	99
0	73
−20	61
−20	67
−40	52
−40	52
−60	16
−80	9

UT-11, N&T, 1250°F-8 hrs. PWHT

Test Temperature (°F)	*Energy Absorbed (ft-lbs)*
RT	260
RT	260
0	112
0	114
−20	101
−20	80
−40	40
−40	12
−60	10
−60	12

UT-11, N&T, 1300°F-8 hrs. PWHT

Test Temperature (°F)	*Energy Absorbed (ft-lbs)*
RT	250
RT	254
32	237
32	260
10	127
10	260
20	260
0	66
0	52
0	112
−20	24
−20	9
−20	39
−20	14
−40	5
−40	10
−60	4
−60	4

UT-12, N&T, No PWHT

Test Temperature (°F)	*Energy Absorbed (ft-lbs)*
−20	260
−40	260
−60	260
−80	20
−80	260
−80	17
−100	13
−100	8
−120	7
−120	13

UT-12, N&T, 1300°F-8 hrs. PWHT

Test Temperature (°F)	*Energy Absorbed (ft-lbs)*
−20	260
−20	260
−40	260
−40	260
−50	260
−50	260
−60	12
−60	15
−80	14
−80	11

UT-12, N&T, 1325°F-8 hrs. PWHT

Test Temperature (°F)	*Energy Absorbed (ft-lbs)*
32	260
32	260
0	260
0	260
−20	27
−20	260
−20	260
−40	51
−40	15
−40	18

UT-12, N&T, 1350°F-8 hrs. PWHT

Test Temperature (°F)	*Energy Absorbed (ft-lbs)*
0	260
0	260
−20	260
−20	260
−30	260
−30	50
−40	260
−40	29
−40	59
−40	175
−50	17
−50	12
−60	12
−60	26
−80	10
−80	7
−100	4
−100	3

UT-12, Q&T, No PWHT

Test Temperature (°F)	*Energy Absorbed (ft-lbs)*
−20	208
−20	230
−20	208
−40	214
−40	208
−40	143
−60	160
−60	146
−80	20
−80	156

UT-12, Q&T, 1325°F-8 hrs. PWHT

Test Temperature (°F)	*Energy Absorbed (ft-lbs)*
32	260
32	260
10	260
10	260
0	123
0	123
0	260
−10	120
−20	135
−20	260
−20	90
−40	17
−40	52
−40	62
−40	113
−60	16
−60	8
−60	6
−80	7
−80	19

Appendix G—Microstructural and Fractographic Evaluations

G1: Fractographic Examination of Notched Creep and Gleeble Stress Rupture Samples of API Materials
G2: SEM Metallographic Investigation and EDS Analyses of UT2 and UT3 Materials
G3: High Resolution Electron Microscopic Evaluations on API Materials (Phase I&II)
G4: Transmission Electron Microscopy Evaluation on API Materials

Appendix G1—Fractographic Examination of Creep and Gleeble Stress Rupture Samples of API Materials

Introduction

In order to define differences in fracture/ductility characteristics between heats of 1¼Cr-½Mo in the API grouping, detailed fractographic examinations were performed. Two types of test specimens were employed. Fracture samples were extracted from double-notched HAZ creep bars. It was postulated that pristine intergranular fracture surfaces existed beneath the surface of the notch that were affected by the final rupture. Fracture samples were also prepared using constant strain rate stress rupture testing (Gleeble) under an argon atmosphere. Therefore, it should be kept in mind that different specimen types were tested under different conditions. First, lower stress level and longer test time were experienced by the creep rupture test samples as compared to constant strain rate rupture test samples. Secondarily, the PWHT for the creep samples was 1350°F for 3 hours while the Gleeble stress rupture samples were not PWHT. The test temperature was 1150°F and all Gleeble stress ruptured samples ruptured within one hour. Fresh fracture surfaces from all samples provided good surfaces for fractographic examination.

Fracture Surfaces of Notched Bar Creep Test Samples

The double-notched creep tested samples were fractured at low temperature at the second notch location, the one that did not completely fracture at the elevated temperature. The notch locations were noted by optical microscopy to show subsurface cracking at the root of the notch and thus offered an opportunity to examine the pristine intergranular fracture surfaces (unexposed to air) that were opened for examination by cooling the sample to liquid nitrogen temperature and impact fracturing through the notch. The crack surfaces thus exposed contained cleavage facets produced by the low temperature overload and the intergranular elevated temperature separated grain boundaries.

Fig. G1-1 shows the SEM fracture surface morphology of the notched bar creep test sample of UT2. The interface region between intergranular (creep) and intragranular (cleavage during fracture) fractures was chosen for fractographic study and EDS examination because it was free of oxidation products. In fact,

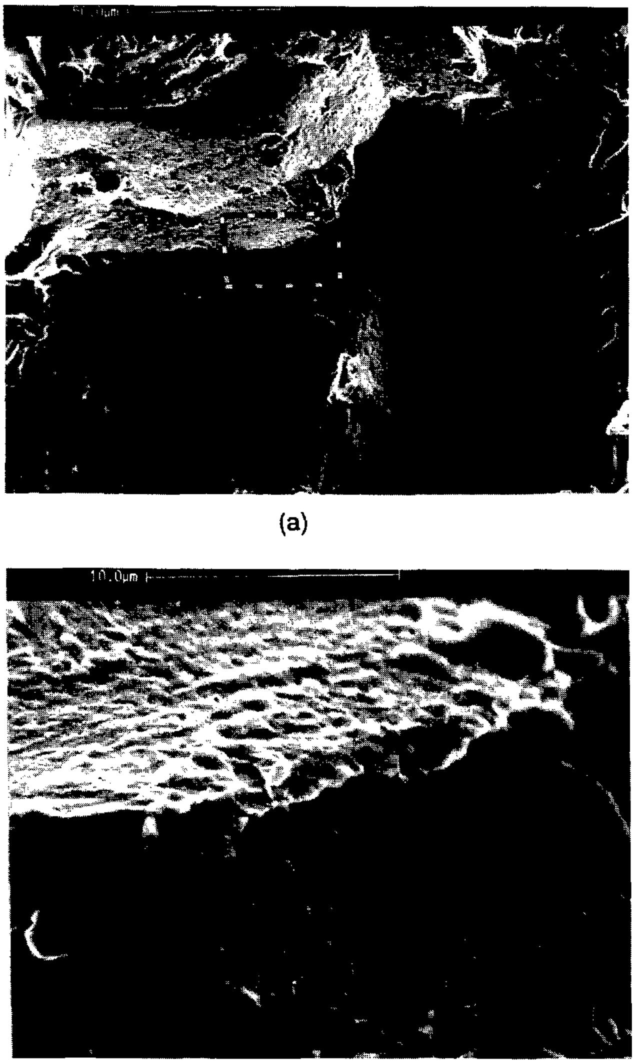

(a)

(b)

Fig. G1-1—SEM fracture morphology of fracture surface in notched bar creep tested sample of UT2. (a) 500×; (b) 4,000×

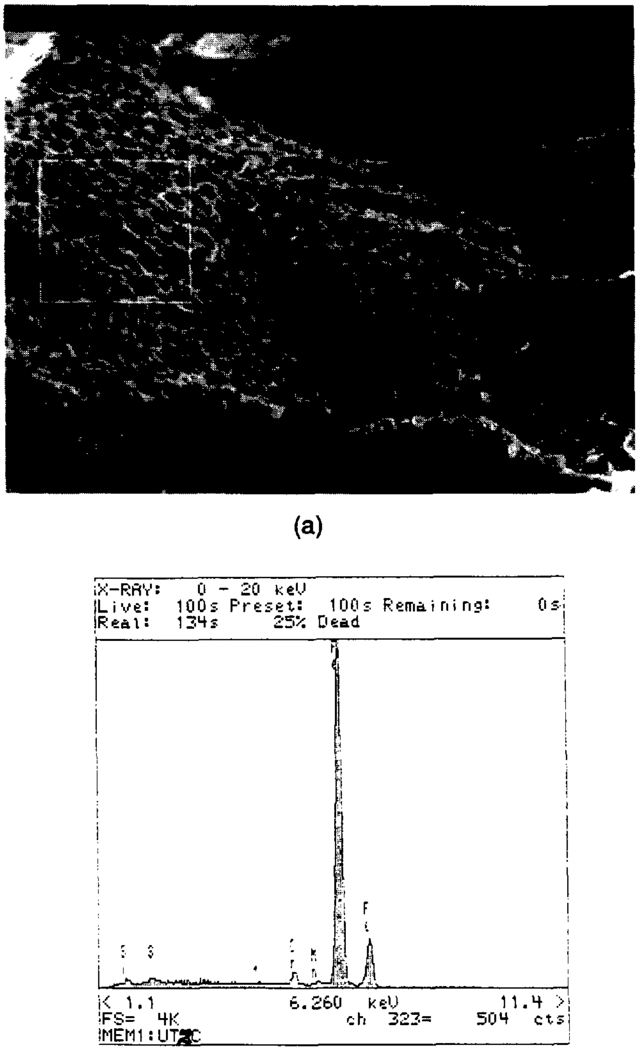

(a)

(b)

Fig. G1-2—(a) Another example of creep rupture surface morphology of UT2; 2,000×. (b) Partial field EDS result from the area indicated in (a)

the intergranular fracture region (in this figure) is surrounded by cleavage rupture and this creep-induced cracking was isolated from the air environment during creep testing. Another example of creep damaged fracture surface in a UT2 notched bar creep tested sample is shown in Fig. G1-2(a) while Fig. G1-2(b) shows partial field EDS results for the area indicated in Fig. G1-2(a). Under higher magnification, fine particles were found in the creep cavities (Fig. G1-3(a)). EDS analysis was performed on these particles and the EDS results for particle A in Fig. G1-3(a) are presented in Fig. G1-3(b). From Fig. G1-3(b) it is revealed that the particles in the creep cavities in the notched bar creep sample are primarily carbides.

Fig. G1-4 shows the UT3 intergranular fracture surface with creep and cleavage features. Clearly, the grain boundary region (indicated by the square) exhibits creep damaged with fine creep cavities. A higher magnification of area 1 in Fig. G1-4 is shown in Fig. G1-5(a). Fig. G1-5(b) shows that particle A is a sulfide. Fig. G1-6(a) is another example and the area where partial field EDS was performed is indicated. Fig. G1-6(b) shows the EDS results for this area. Comparing Fig. G1-3(a) and Fig. G1-6(a), clearly different fracture surfaces are evident in terms of the number and shape of the cavities. More ductile tearing (plastic deformation) evidence was observed in UT2 than in UT3. This is another factor supporting fact that UT2 possesses a lower reheat cracking susceptibility than UT3. No significant S segregation was detected in either material. However, a slightly higher S content was found in UT3 contrasted to UT2 possibly revealing that the S segregation level along the grain boundaries in UT3 is slightly higher than that in UT2.

An intergranular ruptured surface surrounded by cleavage facets in the creep tested sample of UT5 is indicated in Fig. G1-7. At a higher magnification the intergranular fracture surface appearance of UT5 has the combined topographic features of UT2 and UT3. However, the average size of the cavities is larger compared to those in UT2 and UT3. Another example of the creep damage related fracture surface in UT5 is shown in Fig. G1-8. The particles pointed

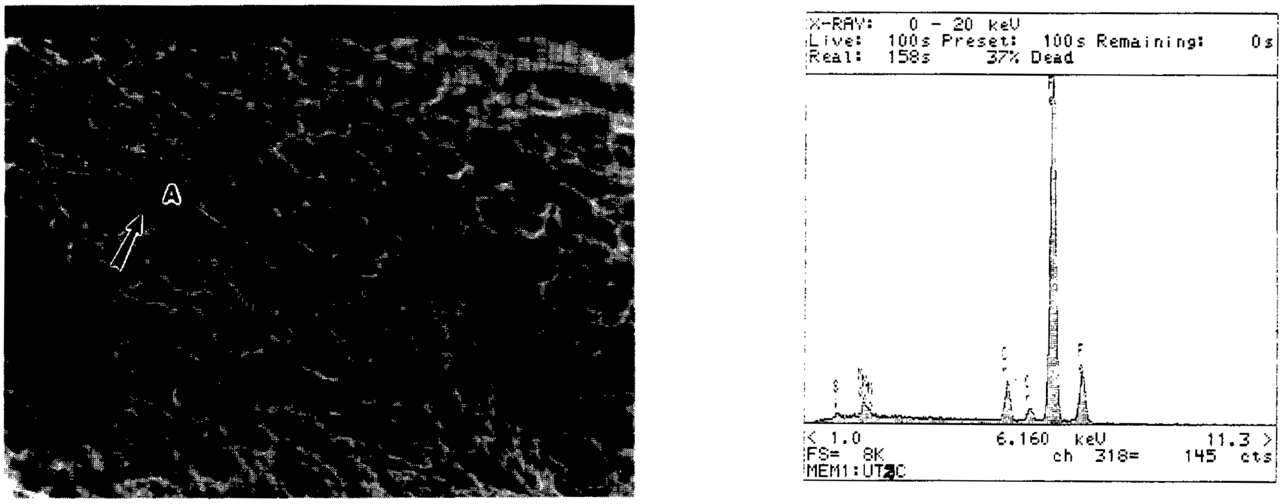

(a) (b)

Fig. G1-3—(a) Higher magnification of SEM morphology of intergranular rupture surface in the notched bar creep tested sample of UT2; 4,000×. (b) EDS result from particle A indicated in (a)

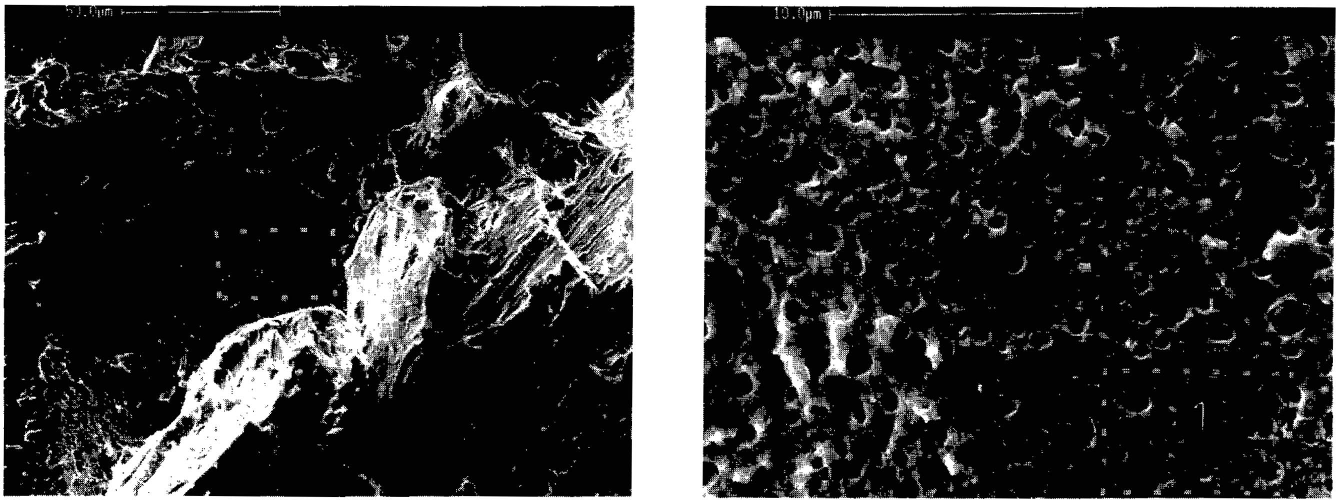

(a) (b)

Fig. G1-4—SEM fracture surface appearance in notched bar creep tested sample of UT3. (a) 500×; (b) 4,000×

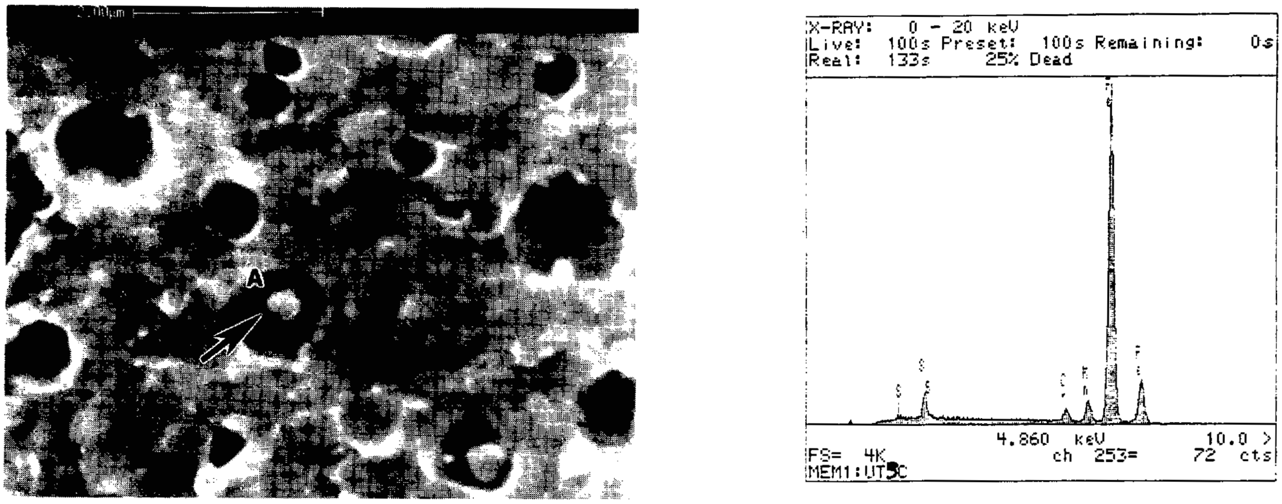

(a) (b)

Fig. G1-5—(a) Higher magnification of fracture surface on the area indicated in Figure G1-4 for UT3; 15,000×. (b) EDS spectrum of the particle A in (a)

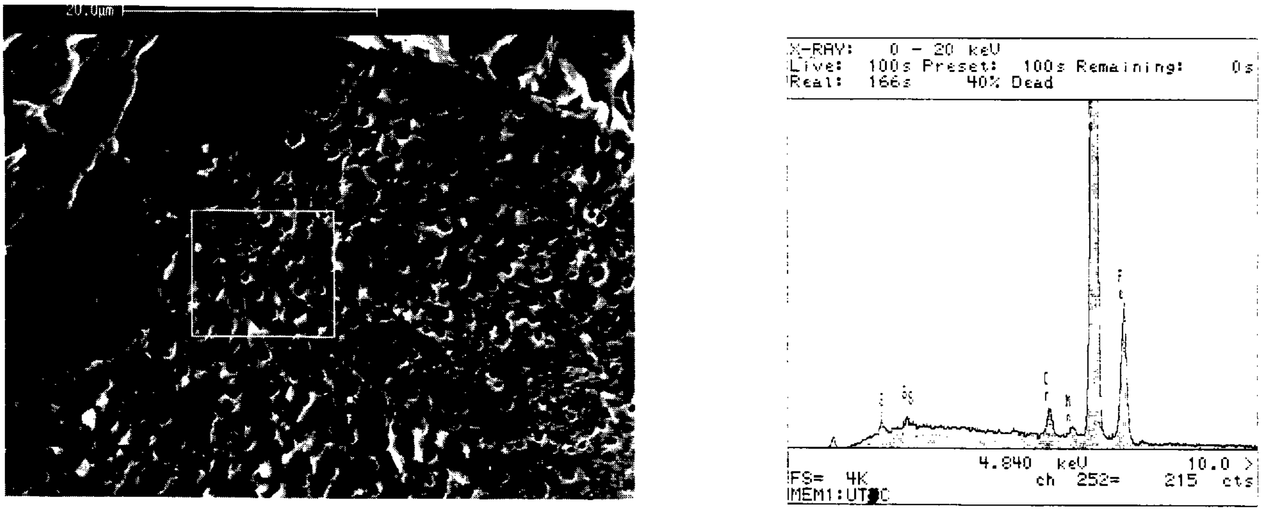

(a) (b)

Fig. G1-6—(a) The fractography photograph showing the fracture surface where partial field EDS examination was performed on notched bar creep tested sample of UT3, 2,000×. (b) EDS result from the area indicated in (a)

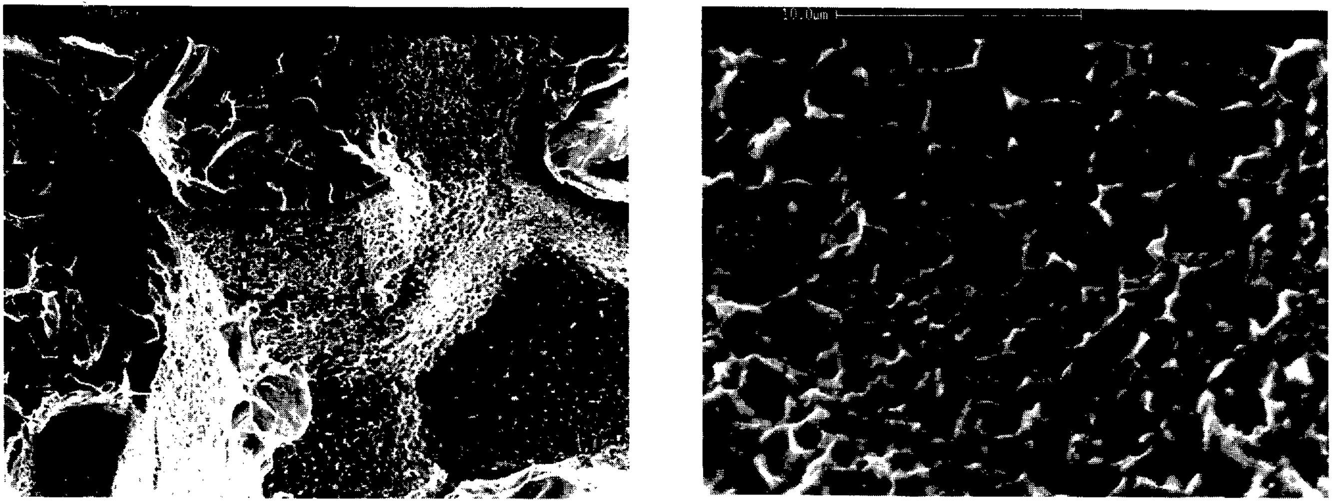

(a) (b)

Fig. G1-7—(a) SEM fracture morphology of notched bar creep tested sample of UT5. (a) 500×; (b) 4,000×

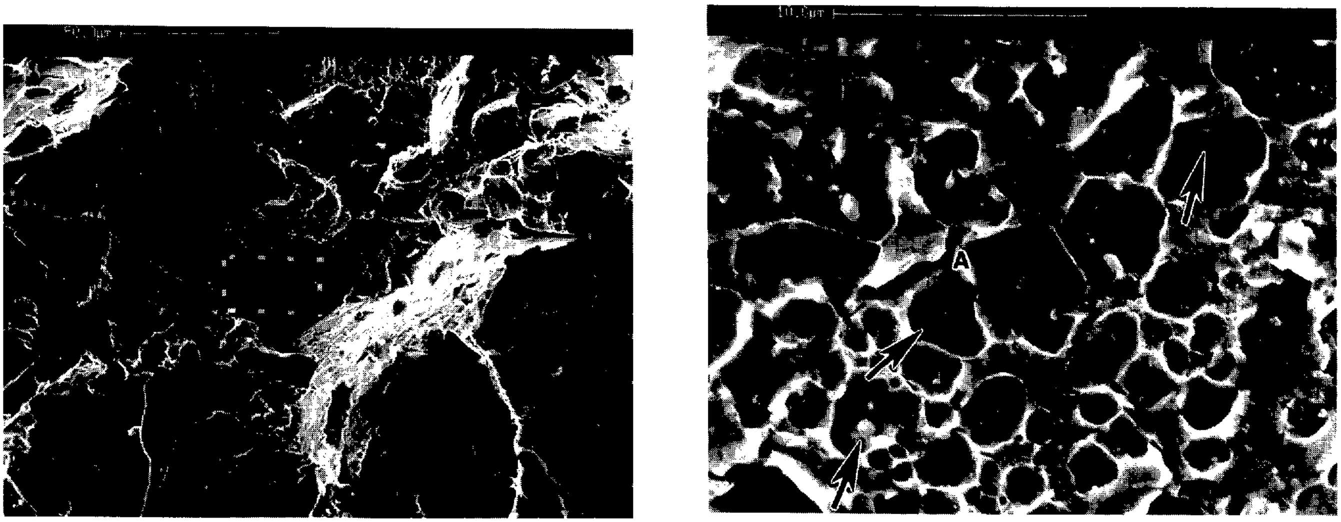

(a) (b)

Fig. G1-8—Another example of fracture surface appearance in the notched bar creep tested sample of UT5. (a) 500×; (b) 4,000×

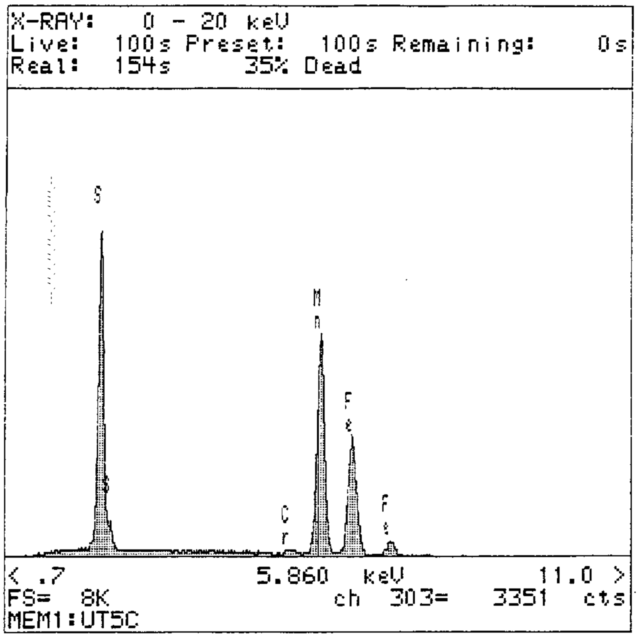

Fig. G1-9—EDS results from particle A indicated in Fig. 8

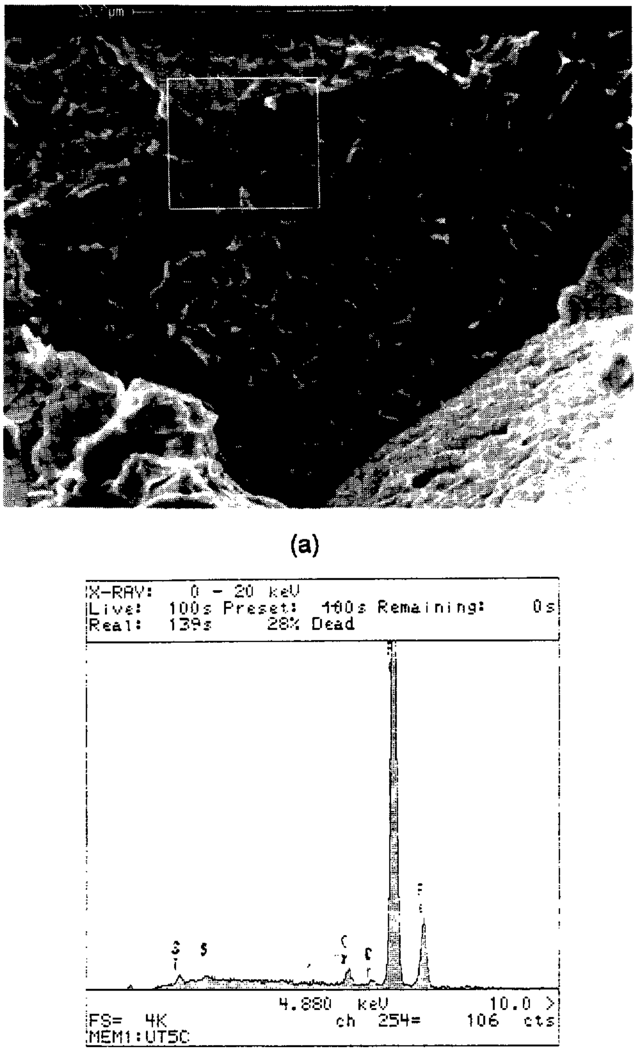

(a)

(b)

Fig. G1-10—(a) A photograph showing the area where partial field EDS examination was performed for UT5; 2,000×. (b) EDS results for the area indicated in (a)

out by arrows are sulfides and the EDS spectrum of particle A is exhibited in Fig. G1-9. Fig. G1-10(a) shows the area where a partial field EDS check was performed on UT5 while Fig. G1-10(b) shows the EDS result from this area. The spectra (Figs. G1-2(b), G1-6(b) & G1-10(b)) show little difference in fracture surface S level among UT2, UT3 and UT5 although UT3 may be slightly greater in S on the fracture.

Fracture Surfaces of Gleeble Stress Rupture Tested Samples

Fig. G1-11 shows the typical morphology of the fracture surface of a Gleeble stress rupture test sample of UT2 that reveals essentially a fully intergranular fracture. Ductile fracture features can be found at the corners or edges of the grains. Clear evidence of ductile tearing indicates that a certain amount of plastic deformation occurred causing the dimple features. It is also noted that particles exist in approximately 90% of the dimples. The EDS analysis results for the particles indicates that the particles are manganese sulfides.

Fig. G1-12 shows the typical morphology of the fracture surface of a Gleeble stress rupture test sample from UT3. It is clear that the dominant fracture mode is intergranular with a small amount of ductile tearing in certain regions of the fracture surface. However, the percent ductile tearing is much less than that in UT2. Most of particles on the fracture surface were identified as Mn-, S- or Si-rich inclusions. It should be pointed out that secondary intergranular cracks also occurred in the Gleeble stress rupture test samples of UT3 and this is a further indication of the brittle rupture tendency.

Fig. G1-13 shows the typical fracture morphology in a stress rupture test of UT4. The fracture morphology in this rupture sample is similar to UT3. A mixed fracture mode with intergranular low ductility creep fracture was dominant in this sample. Evidence of small percent of ductile fracture can be observed at the corners and edges of the grains. The ductile fracture region morphology is shown at higher magnification in Fig. G1-13(b). The particles in the dimples were found to be rich in Mn, S or Si.

Partial field EDS analysis on the fracture surfaces did not show any strong segregation for particular elements. Partial field EDS examinations were performed on the areas without visible particles (1,000× magnification) on the fracture surface.

Comparison of Fracture Appearances of Creep Test Samples and Gleeble Stress Rupture Test Samples

For all materials, intergranular-type fractures were revealed for samples tested by both the notched bar creep rupture and constant strain rate Gleeble stress rupture test. However, the extent and size of the cavities on the intergranular fracture surfaces are remarkably different. In general, the size of the cavities on the notched bar creep fracture surface is larger than those on the fracture surface of Gleeble

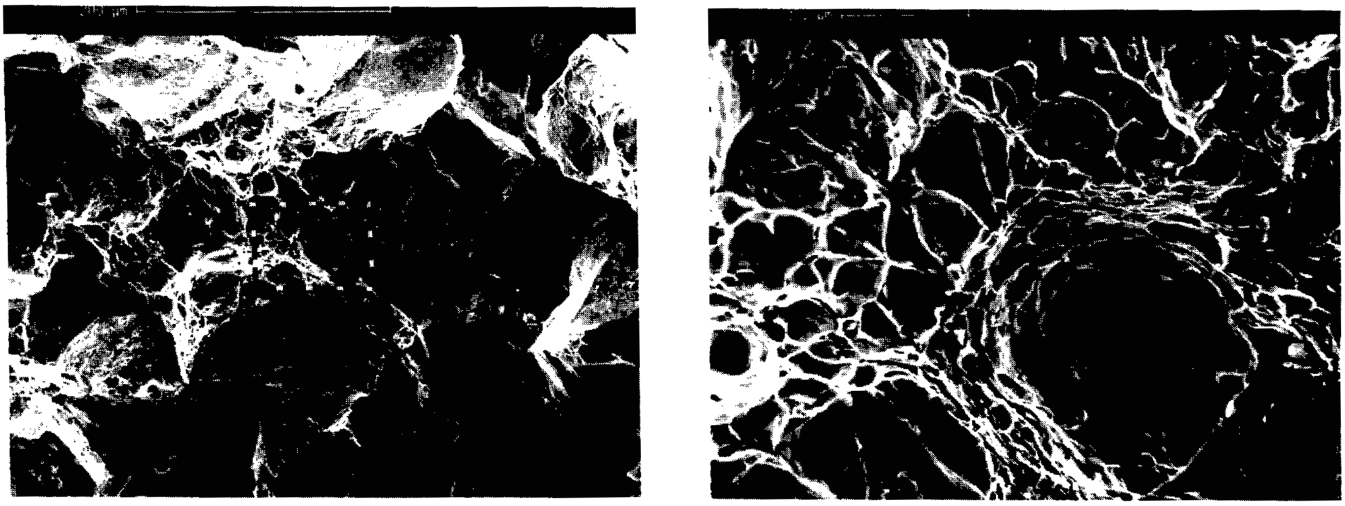
(a) (b)

Fig. G1-11—General fracture surface appearance of the Gleeble stress rupture tested sample of UT2. (a) 200×; (b) 1,000×

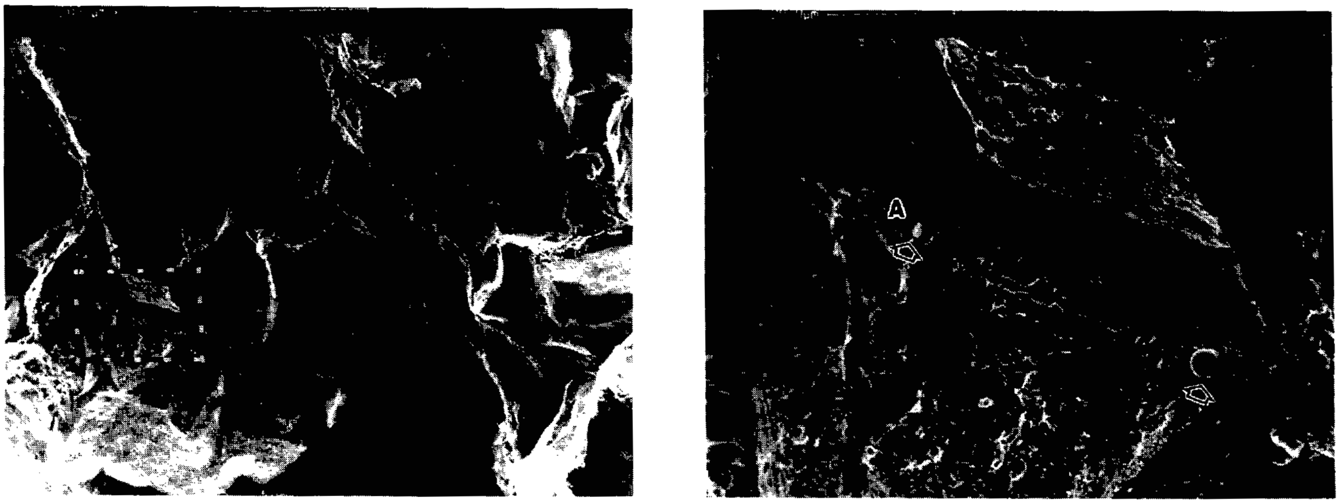

(a) (b)

Fig. G1-12—General fracture surface appearance of the Gleeble stress rupture tested sample of UT3. (a) 200×; (b) 1,000×

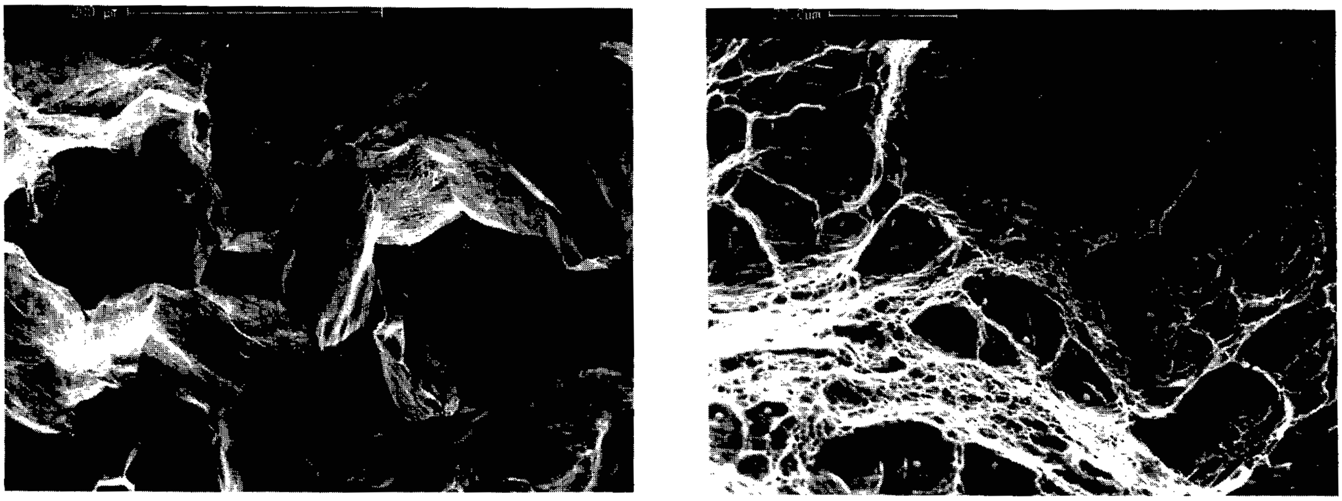
(a) (b)

Fig. G1-13—General fracture surface appearance of the Gleeble stress rupture tested sample of UT4. (a) 200×; (b) 1,000×

stress rupture tested sample. More ductile tearing evidence was observed at the edges of the cavities on the fracture surface of the Gleeble stress rupture tested samples than for the creep notched bar samples. This is to be somewhat expected due to fact that the notched bar creep test samples had a longer term elevated temperature thermal exposure.

No significant extent of particles was observed on the fracture surface of the UT2 notched bar creep test sample while Mn- and S-rich particles were found in the cavities on the Gleeble stress ruptured tested sample for UT2.

Appendix G2—SEM Metallographic Investigation and EDS Analyses of UT2 & UT3 Materials

Introduction

Two heats of 1¼Cr-½Mo steel (UT2 and UT3) were selected to conduct a detailed SEM investigation because of distinct differences in reheat cracking tendency. UT2 is insensitive while UT3 is significantly sensitive to reheat cracking. According to classical reheat cracking theories, grain boundary embrittlement of the CGHAZ is one of the factors that enhances the reheat cracking propensity. Therefore, this study of grain boundary segregation was undertaken to better define the mechanisms of reheat cracking in these heats of steels.

Gleeble thermal simulation techniques were employed to prepare the CGHAZ samples for metallographic and SEM/EDS examination. A 120 kJ/in. weld energy input was used. Two PWHT conditions were selected for the UT2 samples (1150°F for 15 min and 1350°F for 8 hours) and one PWHT condition (1150°F for 15 min) was used for UT3.

An automated EDS program was employed for a semi-quantitative analysis to define the pattern of alloying element distribution across grain boundaries. Both secondary imaging and back-scattered imaging techniques were used to reveal the distribution of inclusions.

Results and Discussions

Typical SEM microstructural morphologies (using both secondary electron and back-scattered electron imaging) of the CGHAZ microstructure in UT2 after a PWHT of 1150°F for 15 min are shown in Fig. G2-1. The dark spots (particles) in the back-scattered image (shown by arrows) were verified by EDS to be manganese sulfides. The EDS results from particle A are presented in Fig. G2-2.

Fig. G2-3 shows the SEM microstructural morphology in a UT2 Gleeble simulated CGHAZ sample after a PWHT of 1150°F for 15 min. EDS analyses were performed across a typical grain boundary using 2 μm intervals between spots. The grid intersections define the locations where the EDS spot checks were performed along each of the lines ab and cd. Figs. G2-4 and G2-5 show the elemental profiles along lines ab and cd for P, S, Cr, Mo, Ni, Si, Mn, Cu, V, Ti and Nb,

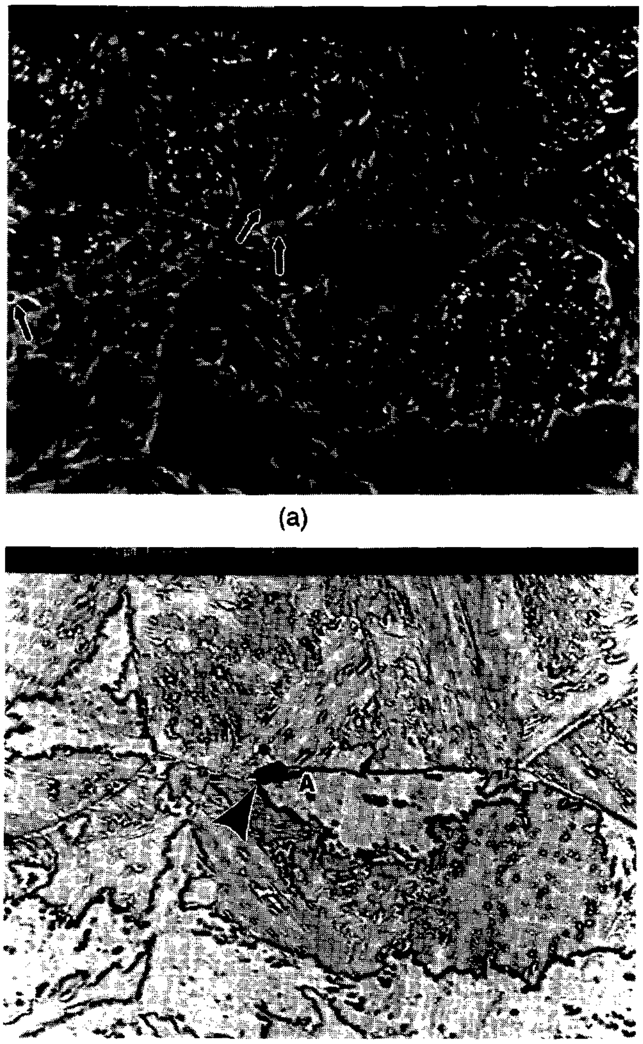

(a)

(b)

Fig. G2-1—SEM morphologies of secondary electron image (a) and back-scattered electron image (b) for the Gleeble simulated CGHAZ sample of UT2 after a PWHT at 1150°F for 15 minutes; 1,000×

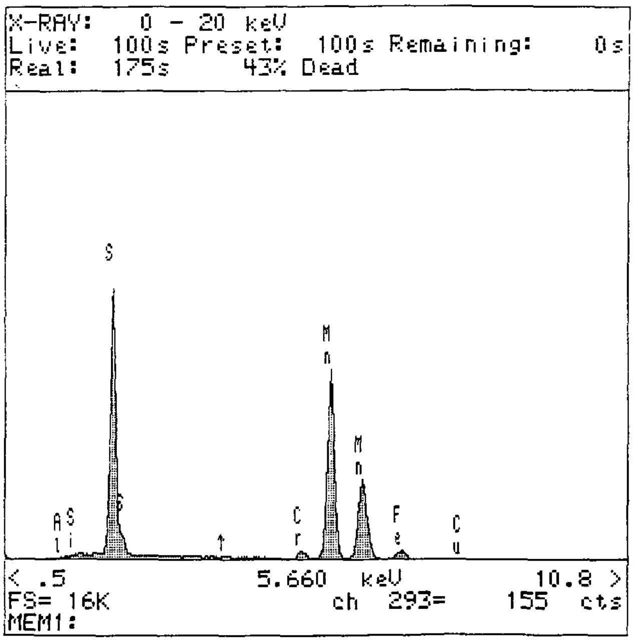

```
X-RAY:    0 - 20 keV
Live:  100s Preset:  100s Remaining:     0s
Real:  175s      43% Dead
```

```
< .5              5.660  keV          10.8 >
FS= 16K                 ch  293=     155  cts
MEM1:
```

Fig. G2-2—EDS result for particle A indicated in Fig. G2-1 (b)

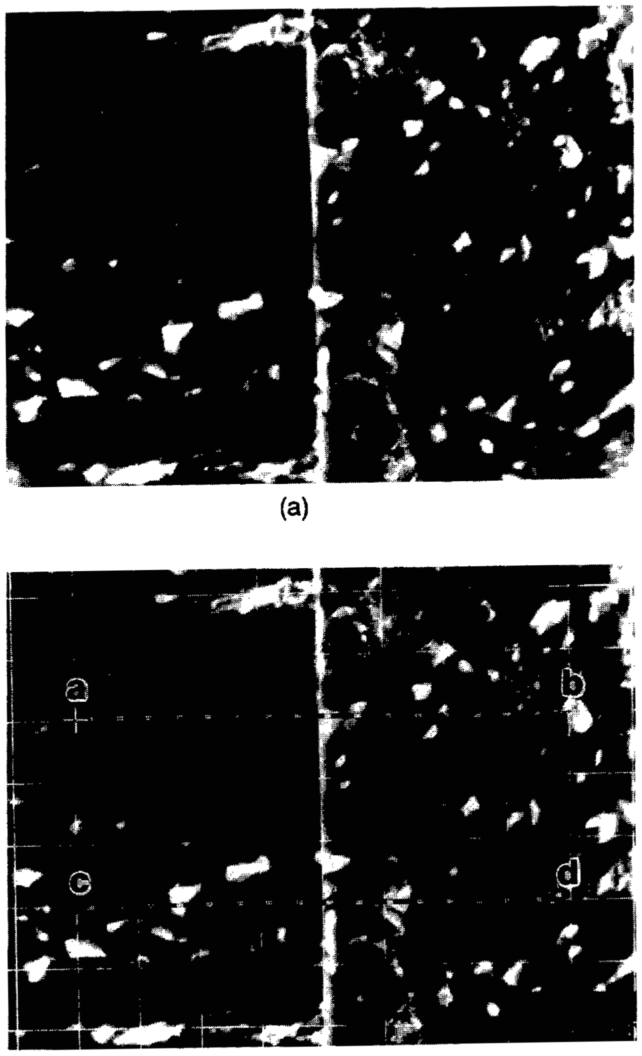

Fig. G2-3—(a) SEM microstructural morphology on the Gleeble simulated CGHAZ sample of UT2 after a PWHT at 1150°F for 15 min (5,000×) and (b) indication of the locations were the EDS analysis were performed

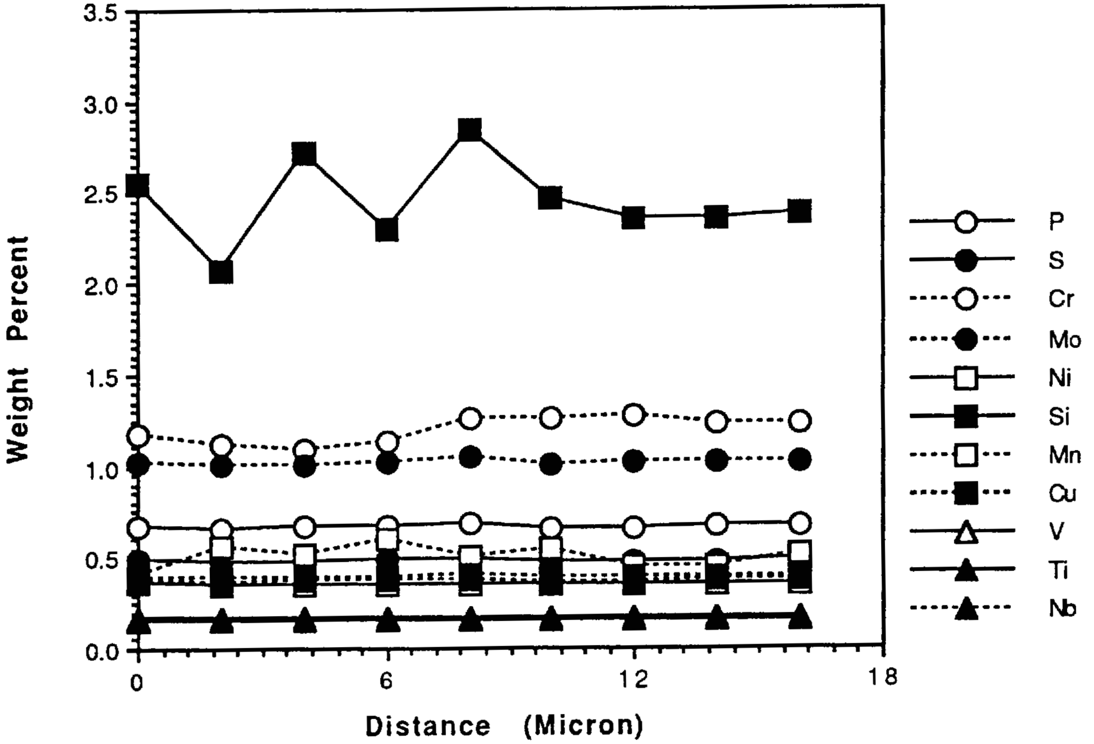

Fig. G2-4—Elemental profile of alloying elements along line ab in Gleeble simulated CGHAZ sample of UT2 after a PWHT at 1150°F for 15 min

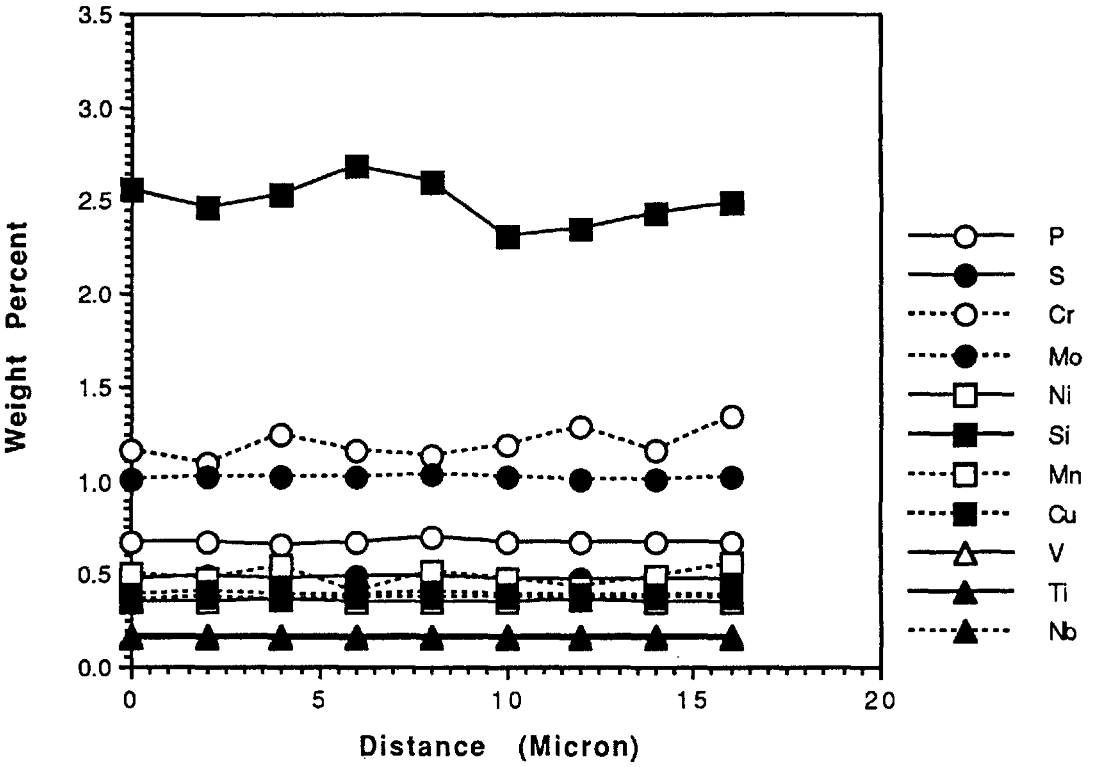

Fig. G2-5—Elemental profile of alloying elements along line cd in Gleeble simulated CGHAZ sample of UT2 after a PWHT at 1150°F for 15 min

respectively. From Figs. G2-4 and G2-5 it is clear that Si, Cr and Mn show variations across the grain boundary while the other elements remain constant at the matrix levels.

Fig. G2-6 shows the SEM microstructural morphology of the UT2 Gleeble simulated CGHAZ sample after a PWHT of 1350°F for 8 hours. The elemental profiles across the grain boundaries (lines ab and cd) are exhibited in Figs. G2-7 and G2-8, respectively, except for Si, Cr and Mn which are elevated at the grain boundary. The levels of the other alloying elements show essentially no change along lines ab and cd.

The SEM microstructure morphology with both secondary electron and back-scattered electron images of a Gleeble simulated UT3 CGHAZ sample after a PWHT of 1150°F are shown in Fig. G2-9. The dark spots (indicated by arrows) in the back-scattered electron image are manganese sulfides and a typical EDS result from particle A in Fig. G2-9(b) is shown in Fig. G2-10. The SEM microstructural morphology of the grain boundary region in a UT3 Gleeble simu-

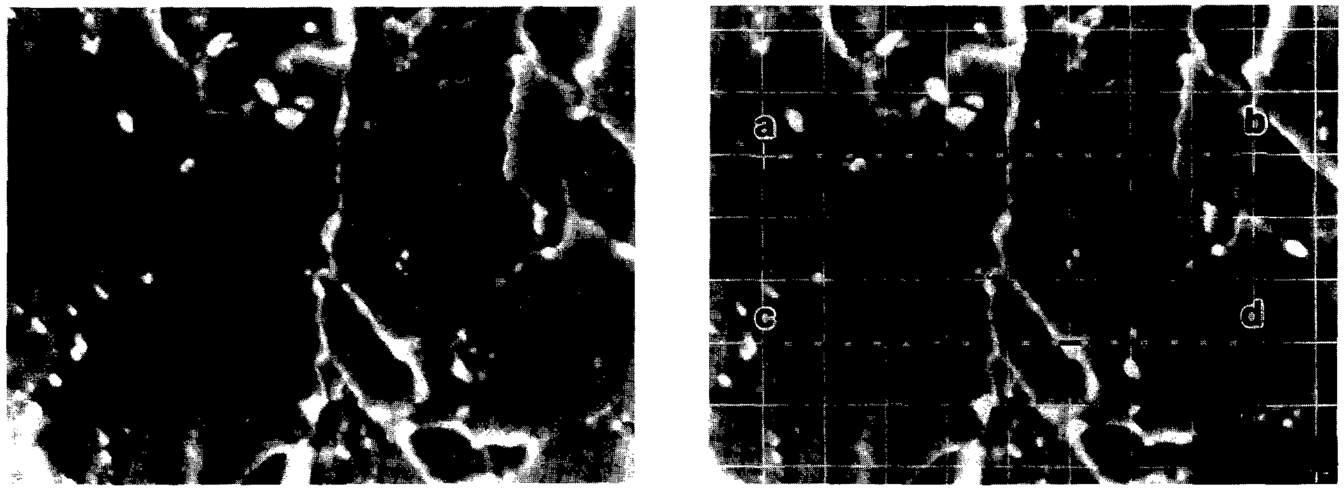

(a)

(b)

Fig. G2-6—(a) SEM microstructural morphology on the Gleeble simulated CGHAZ in UT2 after a PWHT at 1350°F for 8 min (5,000×) and (b) indication of the locations were the EDS analysis were performed

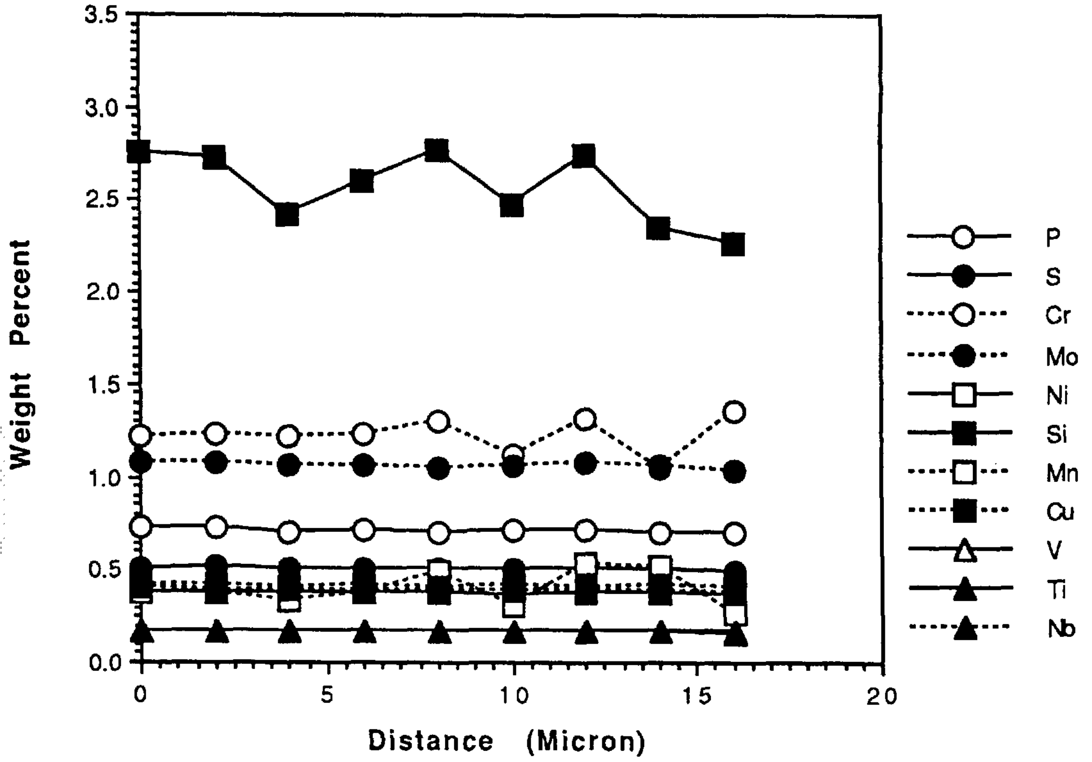

Fig. G2-7—Elemental profile of alloying elements along line ab in the Gleeble simulated CGHAZ sample of UT2 after a PWHT at 1350°F for 8 hours

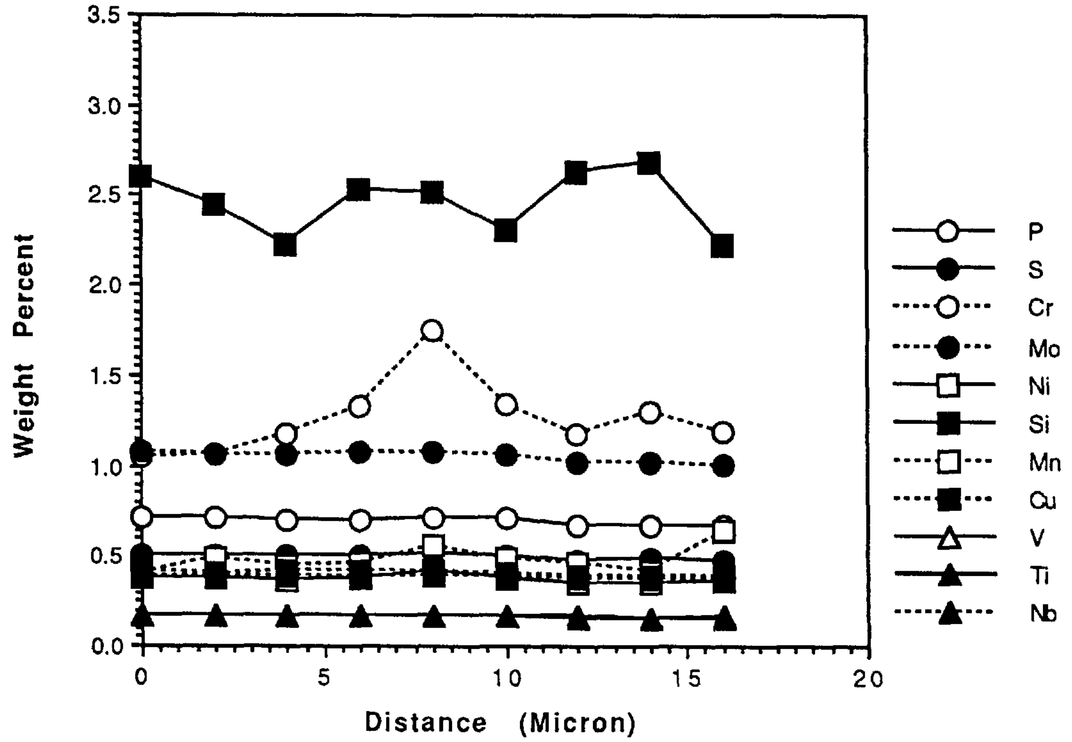

Fig. G2-8—Elemental profile of alloying elements along line cd in the Gleeble simulated CGHAZ sample in UT2 after a PWHT at 1350°F for 8 hours

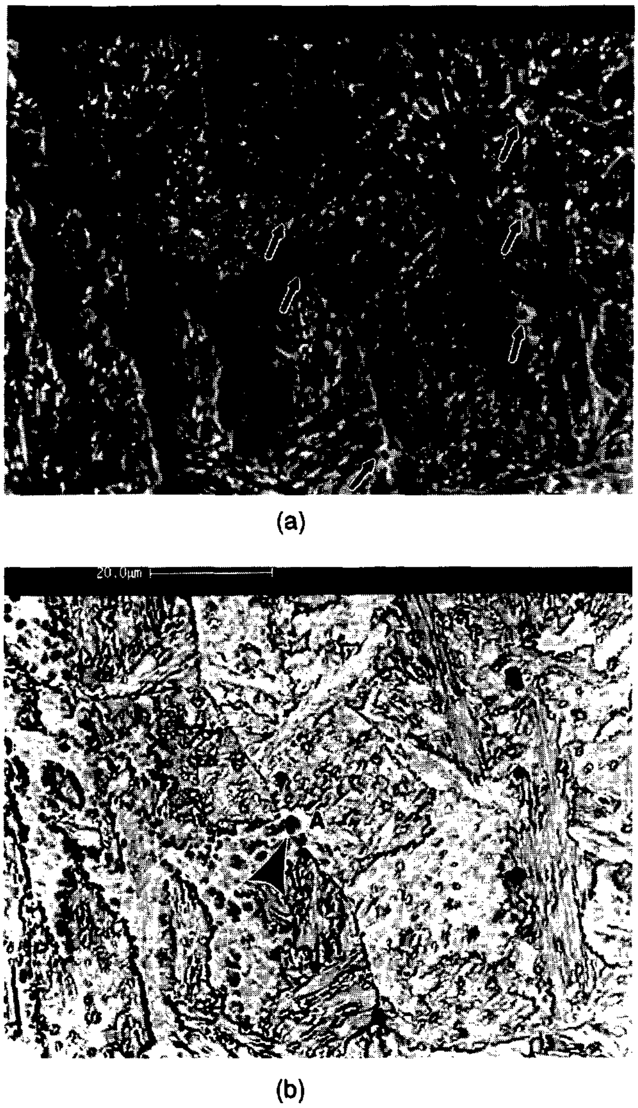

(a)

(b)

Fig. G2-9—SEM morphologies of secondary electron imaging (a) and back-scattered imaging (b) for the Gleeble simulated CGHAZ samples of UT3 after a PWHT at 1150°F for 15 min; 1,000×

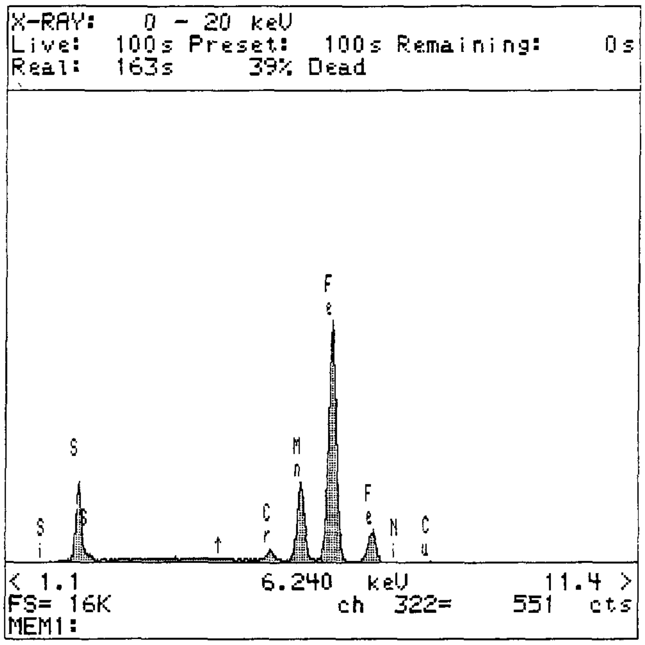

```
X-RAY:    0 - 20 keV
Live:   100s Preset:   100s Remaining:     0s
Real:   163s     39% Dead
```

```
< 1.1               6.240   keV          11.4 >
FS= 16K                ch  322=     551   cts
MEM1:
```

Fig. G2-10—EDS result from particle A in Fig. 9 (b)

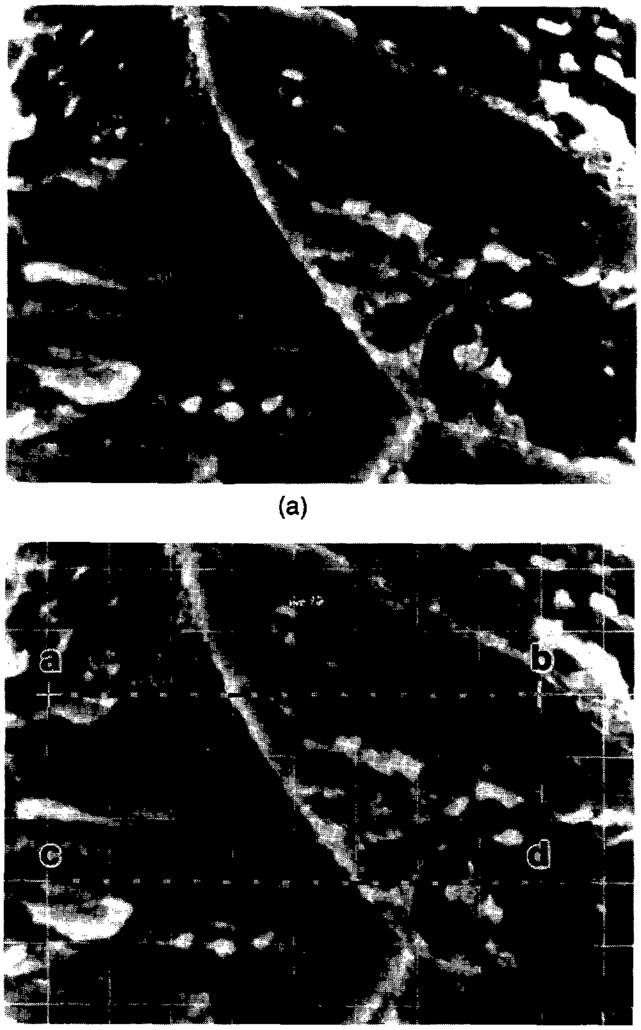

(a)

(b)

Fig. G2-11—(a) SEM microstructural morphology on the Gleeble simulated CGHAZ sample of UT3 after a PWHT at 1150°F for 15 min (5,000×) and (b) indication of the locations where the EDS analyses were performed

lated CGHAZ is exhibited in Fig. G2-11 at 5,000×. Grid lines on the micrograph in Fig. G2-11 were used to assist in defining the locations where the EDS spot examinations were performed. The elemental profiles for lines ab and cd are shown in Figs. G2-12 and G2-13, respectively. It is clear that Si, Cr and Mn show variations along lines ab and cd while the other elements do not.

Comparing the metallographic and EDS examination results obtained from UT2 (two PWHT conditions) and UT3, it is evident that more manganese sulfides exist in the Gleeble simulated CGHAZ of UT3 (both intergranularly and intragranularly) than in UT2. This may be one of the factors resulting in the fact that UT2 possesses a higher reheat cracking resistance than UT3. Increasing the tempering parameter (both temperature and time) varies the chemical profiles across the grain boundaries especially for Cr. A higher chromium content in the grain boundary vicinity was found in the 1350°F, 8 hours PWHT when compared to the short term PWHT condition (1150°C for 15 min).

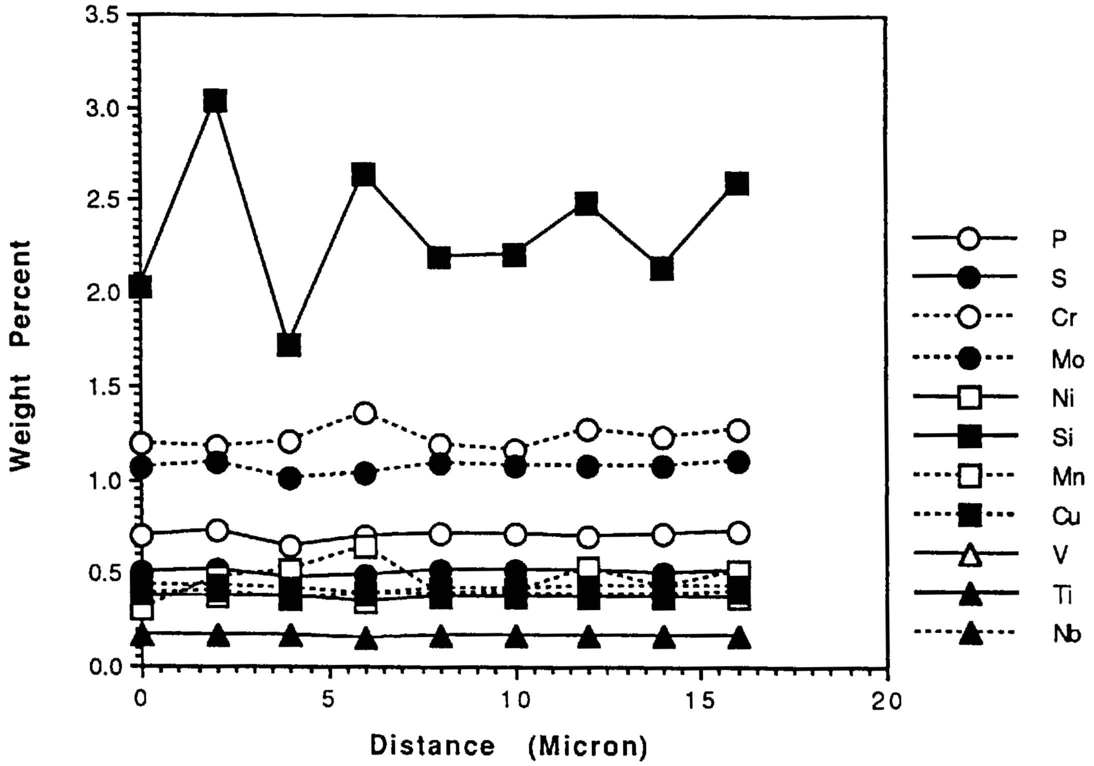

Fig. G2-12—Elemental profile of alloying elements along line ab in the Gleeble simulated CGHAZ sample of UT3 after a PWHT at 1150°F for 15 min

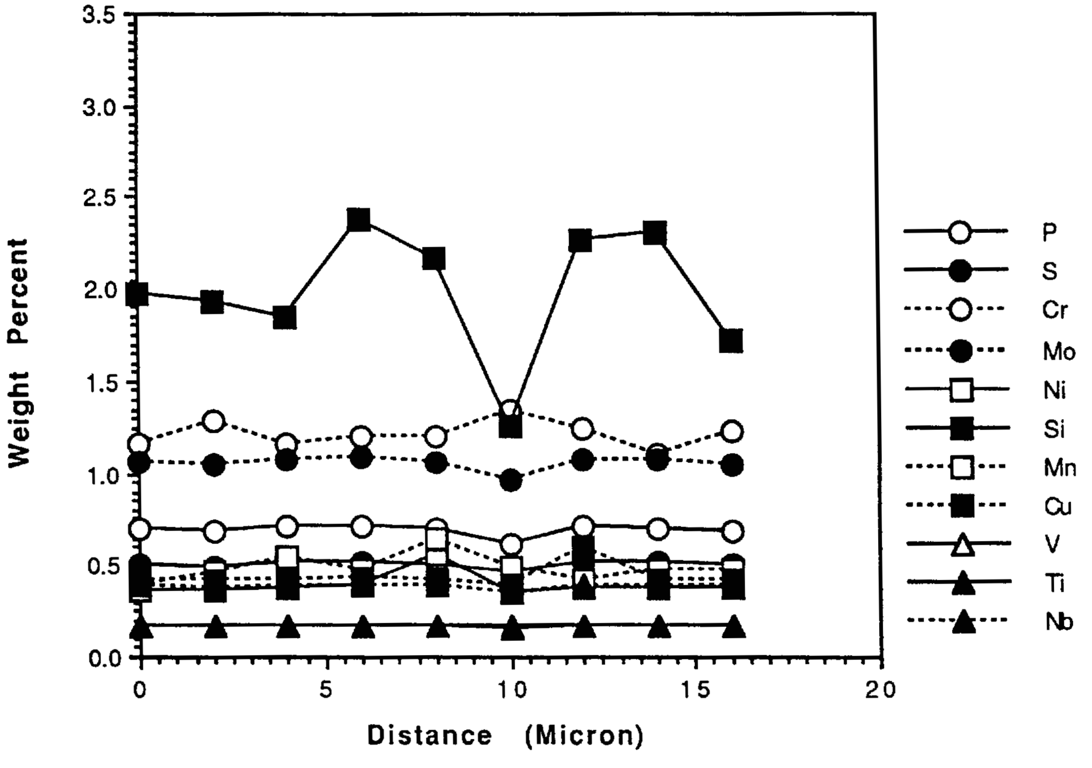

Fig. G2-13—Elemental profile of alloying elements along line cd in the Gleeble simulated CGHAZ sample of UT3 after a PWHT at 1150°F for 15 min

Appendix G3—High Resolution Electron Microscopic Evaluations on API Materials

Introduction

The evaluation of all 17 heats of the API 1¼Cr-½Mo materials revealed widely differing reheat cracking susceptibilities that could not be explained adequately based solely on chemical composition, hardness and microstructure. Thus, it was deemed necessary to determine differences in the fine scale microstructural evolution in the CGHAZ upon PWHT of heats with differing reheat cracking susceptibility so as to possibly explain the observed reheat cracking differences. High resolution electron microscopic techniques (TEM/STEM and SEM) were employed.

The study was conducted in two phases. The first phase was aimed at determination of the carbide evolution kinetics in the CGHAZ upon PWHT and to determine differences between the reheat crack susceptible and resistant heats. In addition, SEM evaluations of the prior austenite grain boundaries and the bainite/martensite lath characteristics was conducted. The results of this study are presented as Phase I of this Appendix.

The second phase of this investigation was directed toward a more comprehensive analysis of the data generated from the first phase. No additional experimentation was conducted. The data on carbide morphology, type, size and distribution were evaluated to determine differences between reheat crack susceptible and resistant heats. The results of this study are presented as Phase II of this Appendix.

G3 Phase I—High Resolution Electron Microscopic Evaluations on API Materials

Materials

Four heats of 1¼Cr-½Mo steel (UT2, UT3, UT5 and UT8) were selected to study the carbide evolution kinetics in the CGHAZ upon PWHT by TEM/STEM techniques. The primary focus of the TEM/STEM investigation was to determine the carbide type, size, distribution and morphology at various locations in the different microconstituents formed directly upon cooling of the CGHAZ and after subsequent PWHT. Another major emphasis of this study was to determine differences in carbide evolution kinetics in the CGHAZ of the heats which revealed different degrees of reheat cracking susceptibility (Gleeble reheat cracking tests and PREVEW tests).

Of these four heats UT2 and UT3 were selected for detailed microstructural characterization using SEM. The SEM investigation was conducted primarily to determine changes in the general microstructure of the CGHAZ as a function of PWHT with major emphasis on the appearance of the prior austenite grain boundaries and bainite/martensite lath coarsening.

The chemical composition data from the four heats are shown in Table G3-1. UT3 and UT5 are virgin materials in the normalized and tempered condition. UT2 and UT8 originally in the service-exposed condition were renormalized and tempered in order to bring them to the same "virgin" condition (as heats UT3 and UT5). The base metal microstructure of all four heats was ferrite and bainite. Of the four heats, UT3 and UT5 were susceptible to reheat cracking based on the Gleeble tests for both high and low heat input and the PREVEW test (Tables G3-2 and G3-3). UT2 is not susceptible at any heat input and the other heats show different degrees of sensitivity.

Postweld Heat Treatment of CGHAZ

Two heat inputs, 12 KJ/in. and 120 KJ/in. were used to simulate the CGHAZ with a 2400°F peak temperature. Five PWHT conditions were utilized to study the carbide evolution kinetics (early stages of PWHT as well as for prolonged PWHT). The PWHT conditions are: 1150°F, 15 minutes and 1 hour; 1250°F, 15 minutes and 1 hour; and 1350°F, 8 hours.

The tempering parameters, LMP = $(T + 460)(20 + \log t) \times 10^{-3}$, are:

1150°F-15 min	31	1150°F-1 hour	32
1250°F-15 min	33	1250°F-1 hour	34
1350°F-8 hours	37		

Figs. G3-1 and G3-2 show the base metal hardness and CGHAZ hardness as functions of PWHT at both heat inputs (12 KJ/in. and 120 KJ/in.). The hardness data are also shown in Table G3-4. The relationship between hardness and temper parameter is shown in Fig. G3-3 to G3-11. For comparison of the different heats, the hardness data for the CGHAZ are plotted together as a function of LMP for heat inputs of 12 and 120 KJ/in. as shown in Figs. G3-12 and G3-15.

Results

The initial microstructure of the four heats (N&T condition) was ferrite and bainite. Carbides at the grain boundaries and bainite lath boundaries were of the $M_{23}C_6$ and M_3C types whereas in the interior of the bainite laths and ferrite grains the carbides were M_2C. The $M_{23}C_6$ and M_3C carbides exhibit globular and rod-like morphologies whereas the M_2C carbides are acicular. Optical and SEM micrographs of the base metal of two representative heats (UT2 and UT3) are illustrated in Figs. G3-16 and G3-17 where the ferritic and bainitic regions in the microstructure are clearly revealed.

During on-heating to the peak temperature (2400°F) for CGHAZ simulation all preexisting carbides dissolve in the austenite. Upon cooling, transformation and carbide precipitation occurs. The CGHAZ microstructure for the 120 KJ/in. heat input is bainite + ferrite whereas for the 12 KJ/in. heat input the CGHAZ microstructure is martensite as shown in the optical and SEM micrographs presented in Fig. G3-18 for the UT2 material. In the as-simulated condition (no PWHT) for the 120 KJ/in. heat input, M_3C carbides are found primarily in bainitic regions. These carbides precipitated during and subsequent to the transformation of austenite to bainite. In the case of the 12 KJ/in. CGHAZ the microstructure is marten

Table G3-1—Chemical Composition of Materials for Carbide Evolution Study (Wt%)

Materials	*C*	*Mn*	*P*	*S*	*Si*	*Ni*	*Cr*	*Mo*	*V*	*Nb*	*Ti*
UT2	0.10	0.45	0.010	0.013	0.65	0.18	1.30	0.53	0.004	0.00007	0.00173
UT3	0.15	0.50	0.007	0.017	0.61	0.21	1.27	0.47	0.010	0.00025	0.00238
UT5	0.17	0.50	0.008	0.004	0.64	0.08	1.41	0.50	0.004	0.00062	0.00250
UT8	0.13	0.42	0.010	0.015	0.62	0.17	1.22	0.58	0.003	0.00005	0.00313

Materials	*Co*	*Cu*	*Al*	*B*	*W*	*As*	*Sn*	*Zr*	*Sb*	*Ca*	*N*	*O*
UT2	0.010	0.05	0.004	<0.00001	0.008	0.007	0.007	<0.001	0.00041	0.0016	0.0155	0.0058
UT3	0.012	0.16	0.003	0.00003	<0.01	0.004	0.015	<0.001	0.00095	0.0011	0.0116	0.0048
UT5	0.007	0.09	0.021	<0.00001	0.001	0.007	0.009	0.002	0.00055	0.0014	0.0083	0.002
UT8	0.010	0.11	0.026	<0.00001	<0.01	0.008	0.012	<0.001	0.00146	0.0013	0.012	0.005

Table G3-2—Gleeble HAZ Ductility Test Results

Material	*Heat Input (KJ/in)*	*RA (%)*	*Stress (Ksi)*
UT2-SE	120	53	50–60
UT2-SE	12	61	45–50
UT2-NV	120	12	45–55
UT2-NV	12	37	45–55
UT3-SS	120	9	40–55
UT3-SS	12	7	40–55
UT3-VM	120	8	45–55
UT3-VM	12	5	45–55
UT4-SS	120	6	35–60
UT4-SS	12	8	35–60
UT4-VM	120	6	35–60
UT4-VM	12	13	35–60
UT5-VM	120	6	55–60
UT5-VM	30	4	52–70
UT5-VM	12	11	55–60
UT8-SE	120	5	45–55
UT8-SE	12	20	40–45
UT8-NV	120	3	45–55
UT8-NV	12	14	35–45

Peak Temperature: 2400°F
Test Temperature: 1150°F
Abbreviations: VM, Virgin Materials; NV, Re-Normalized (Virgin); SE, Service Exposed; SS, Service Simulated (SoCal Step Cooled); 12KJ/in., Martensite; 120KJ/in., Coarse Bainite.

Table G3-3—Full-Scale Weld HAZ Cracking Test Result Using PREVIEW Test

Samples	*Base Metal Hardness (HV)*	*Joint Type**	*Deflection (in.)*	*Test Time (hrs)*	*Maximum** Crack Depth (mils)*	*Average** Crack Depth (mils)*	*Average** Crack Length (%)*
UT2-SE-T1	155	Fillet	0.12	30	0****	0	0
UT2-Q/T-T2	228	Fillet, 120KJ/in.	0.12	30	0	0	0
UT3-VM-T2	240	Fillet	0.12	30	142	113	100
UT3-VM/T-T5	172	Fillet	0.12	30	108	71	90
UT3-VM/T-T6	155	Fillet	0.12	30	28	14	30
UT3-VM/T-T8	153	Fillet	0.12	30	13	7	40
UT4-VM-T1	200	Fillet	0.12	30	42	40	25
UT4-VM-T2	200	Fillet	0.12	30	40	37	19
UT5-Q/T-T2	264	Fillet	0.12	30	1	1	5
UT5-N/T-T3	180	Fillet	0.12	30	2	1	<1
UT5-N/T-T4	169	Fillet	0.12	30	2	1	<1
UT5-VM-T1	155	Fillet	0.12	30	6	2	10
UT5-VM/T-T5	153	Fillet	0.12	30	0	0	0
UT8-SE-T1	150	Fillet	0.12	30	0	0	0
UT8-SE-T2	159	Fillet	0.12	30	20	18	11
UT8-SE-T3	159	Fillet, 120KJ/in.	0.12	30	16	14	12

*Heat input: 50–60KJ/in.
Electrode: E8018-B2.
**Based on metallographic examination of 3 transverse sections, crack depth measured along the CGHAZ.
***Based on metallographic examination of 2 longitudinal sections.
****No cracking.
Test Temperature: 1150°F

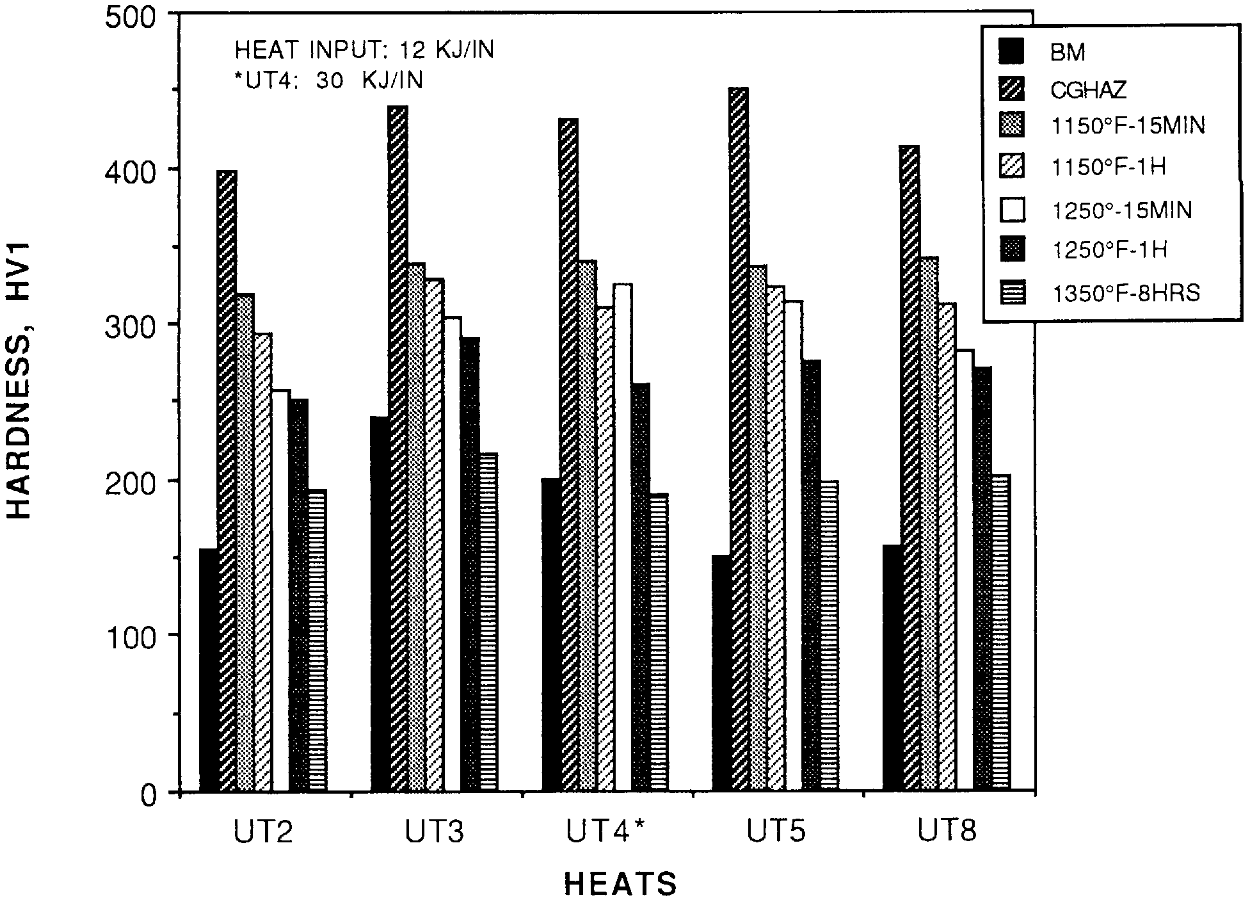

Fig. G3-1—Hardness of Gleeble simulated CGHAZ at heat input of 12 KJ/in. (*UT4: 30 KJ/in.) and with PWHT

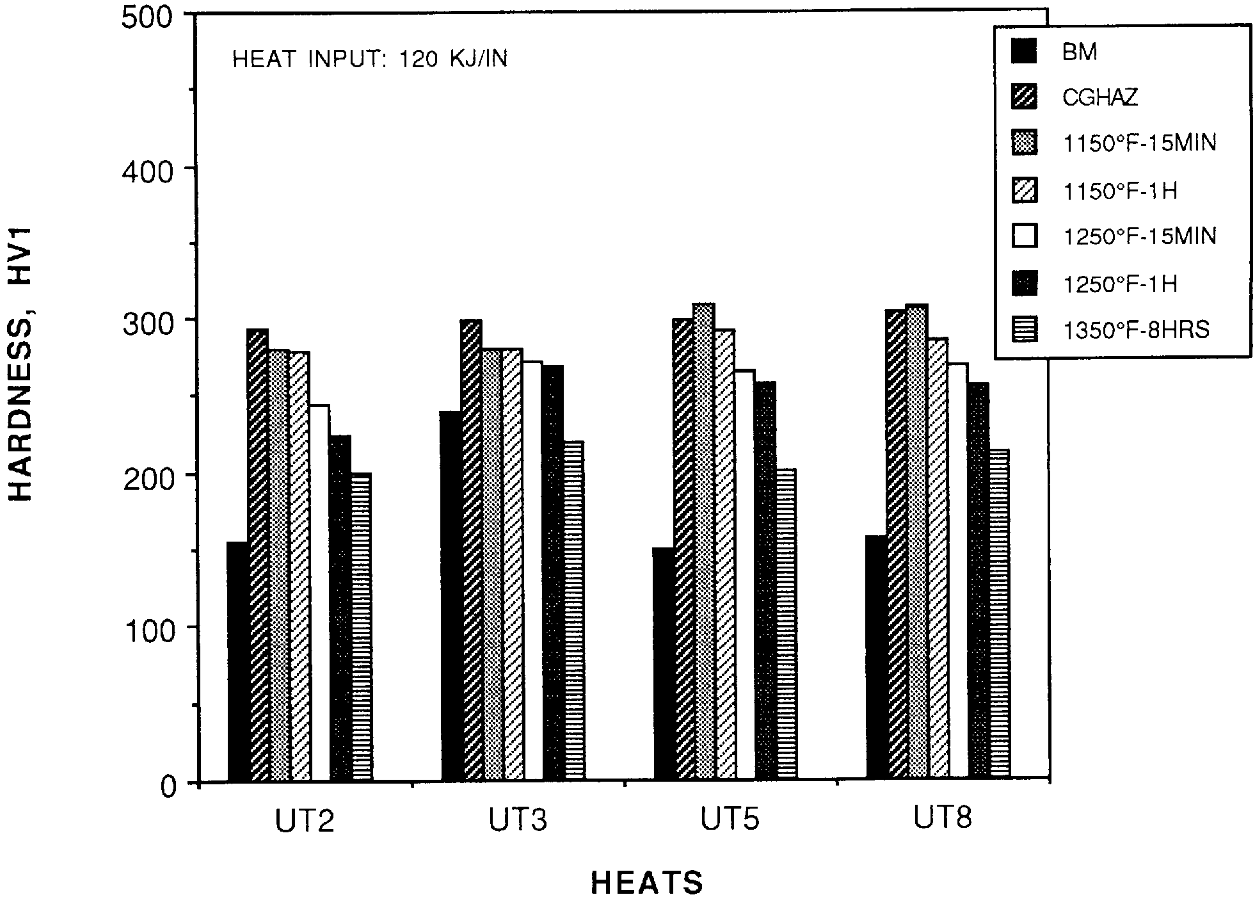

Fig. G3-2—Hardness of Gleeble simulated CGHAZ at heat input 120 KJ/in. and CGHAZ with PWHT

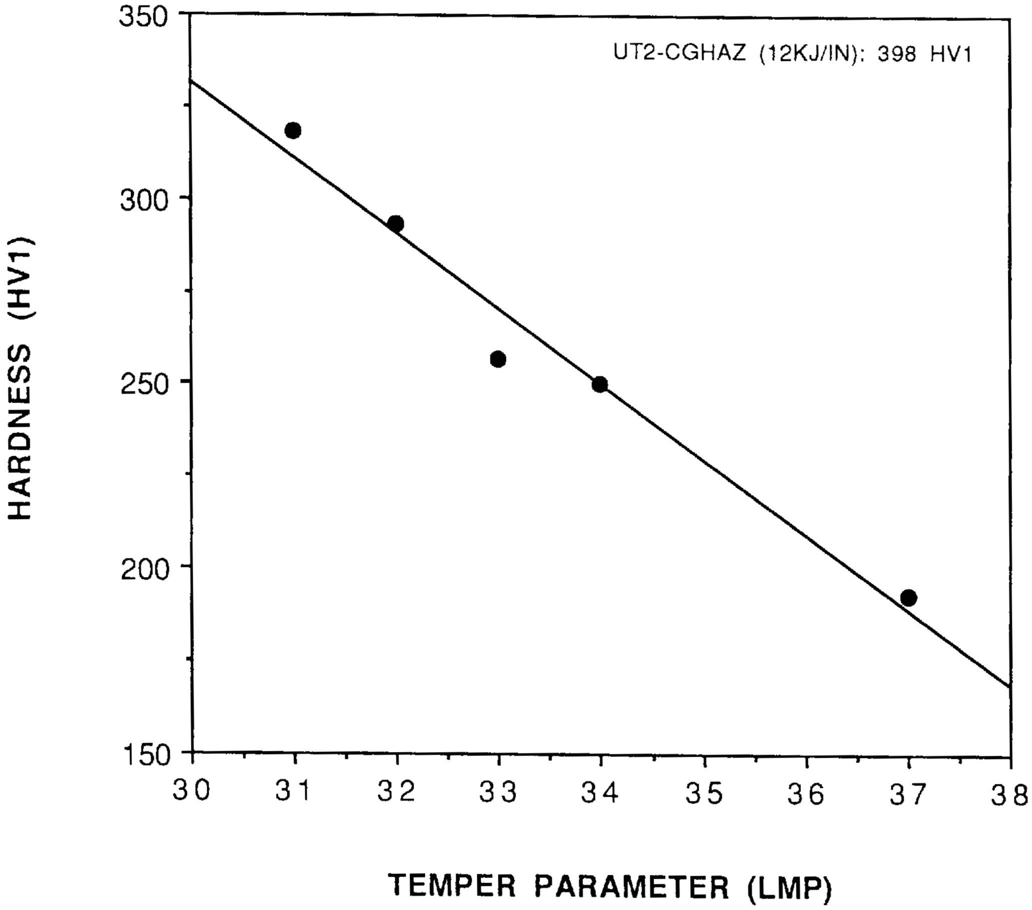

Fig. G3-3—Hardness of CGHAZ of UT2 with heat input 12 KJ/in. during PWHT

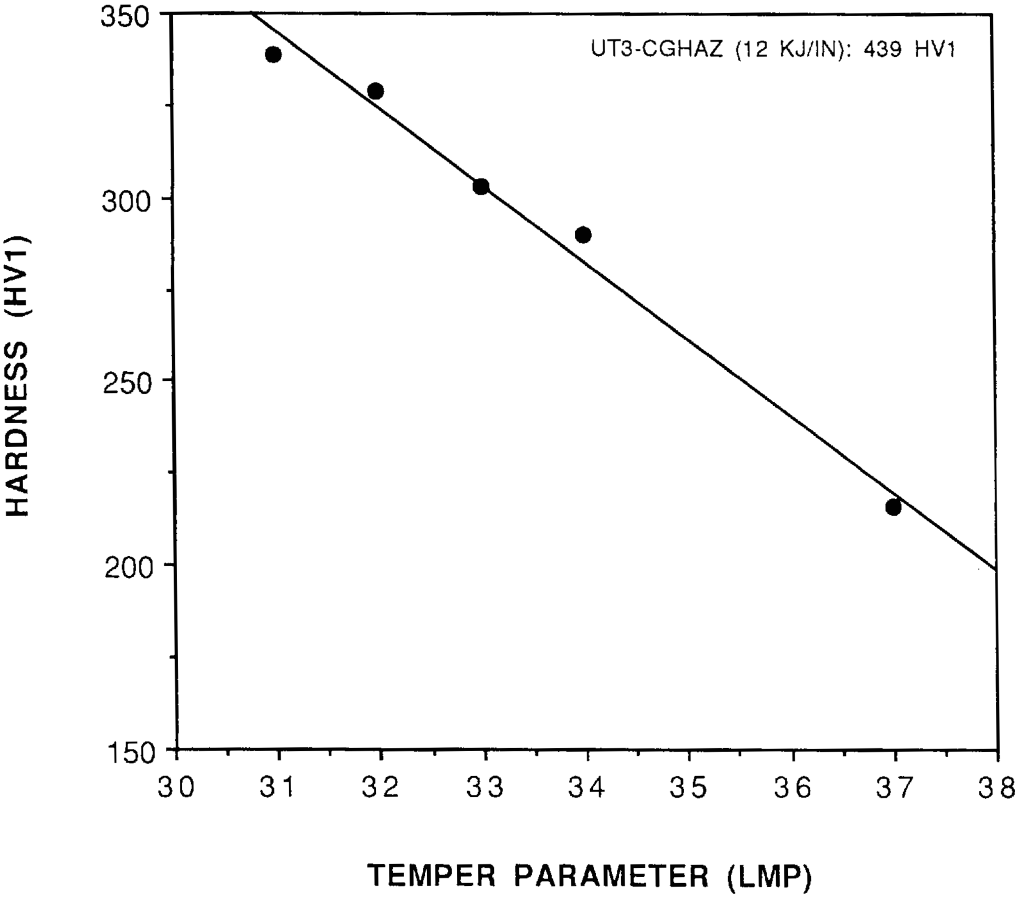

Fig. G3-4—Hardness of CGHAZ of UT3 with heat input 12 KJ/in. during PWHT

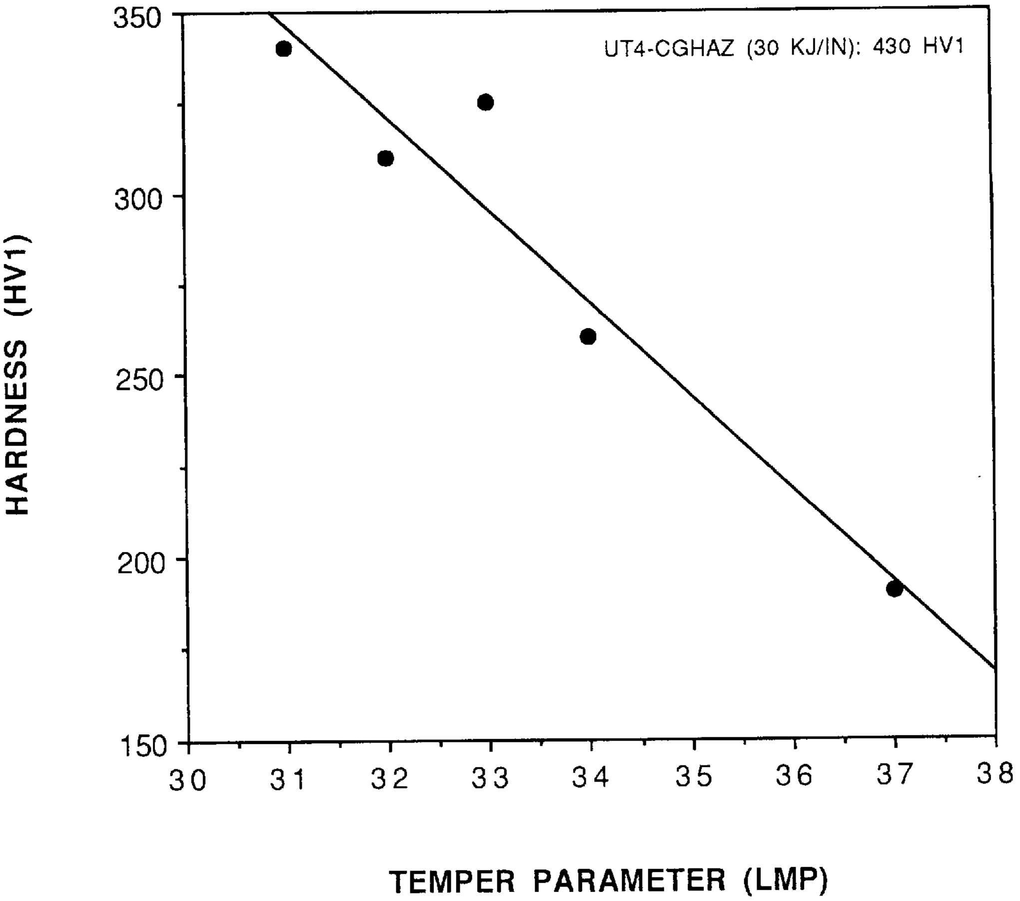

Fig. G3-5—Hardness of CGHAZ of UT4 with heat input 30 KJ/in. during PWHT

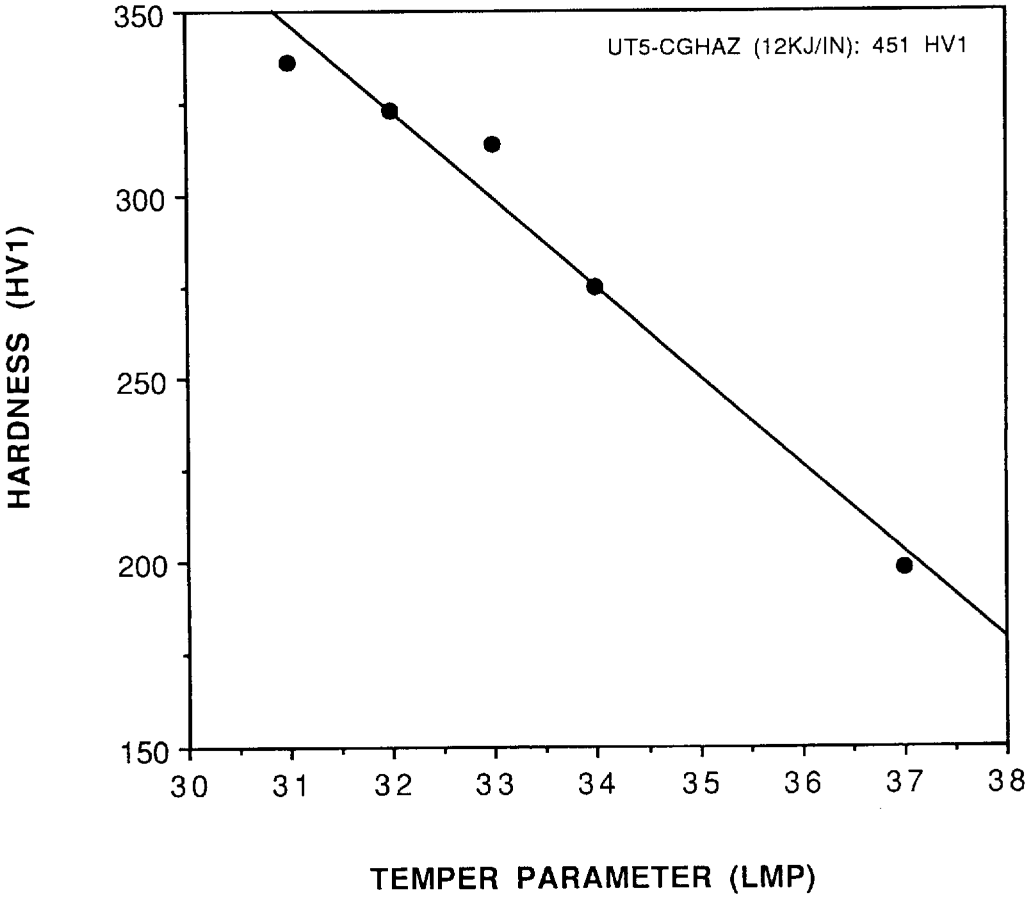

Fig. G3-6—Hardness of CGHAZ of UT5 with heat input 12 KJ/in. during PWHT

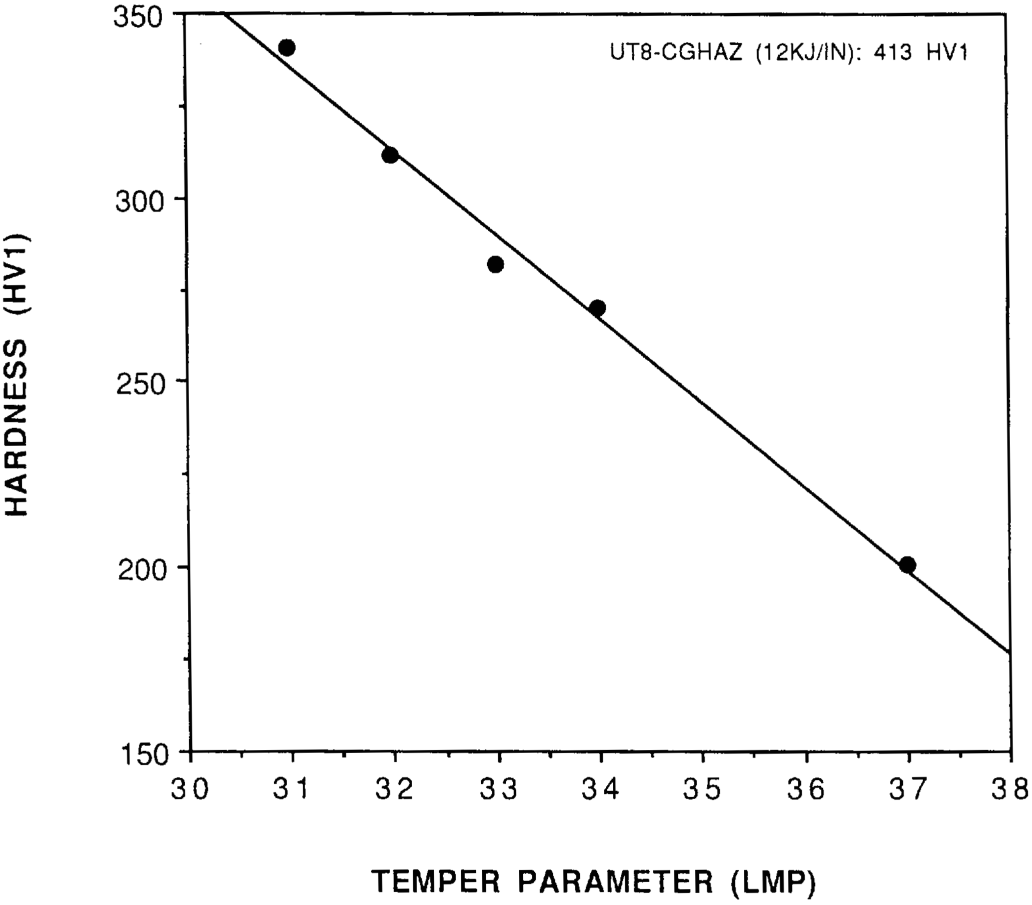

Fig. G3-7—Hardness of CGHAZ of UT8 with heat input 12 KJ/in. during PWHT

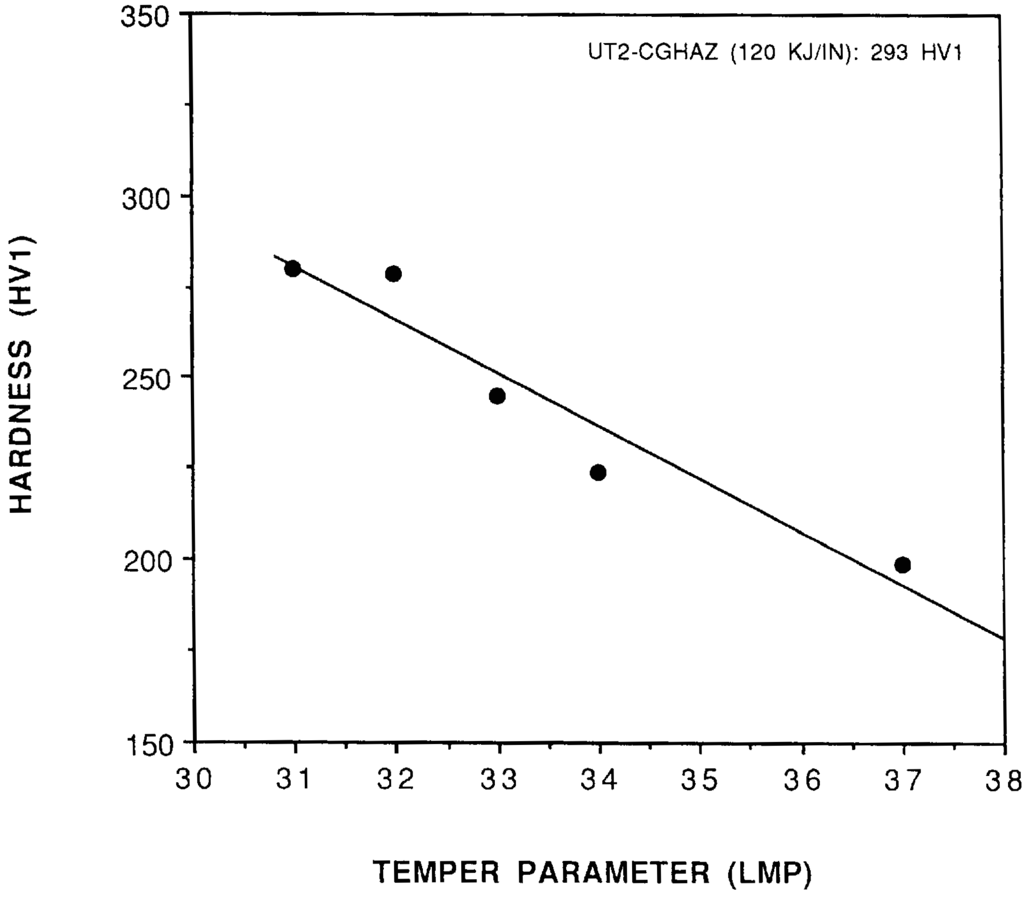

Fig. G3-8—Hardness of CGHAZ of UT2 with heat input 120 KJ/in. during PWHT

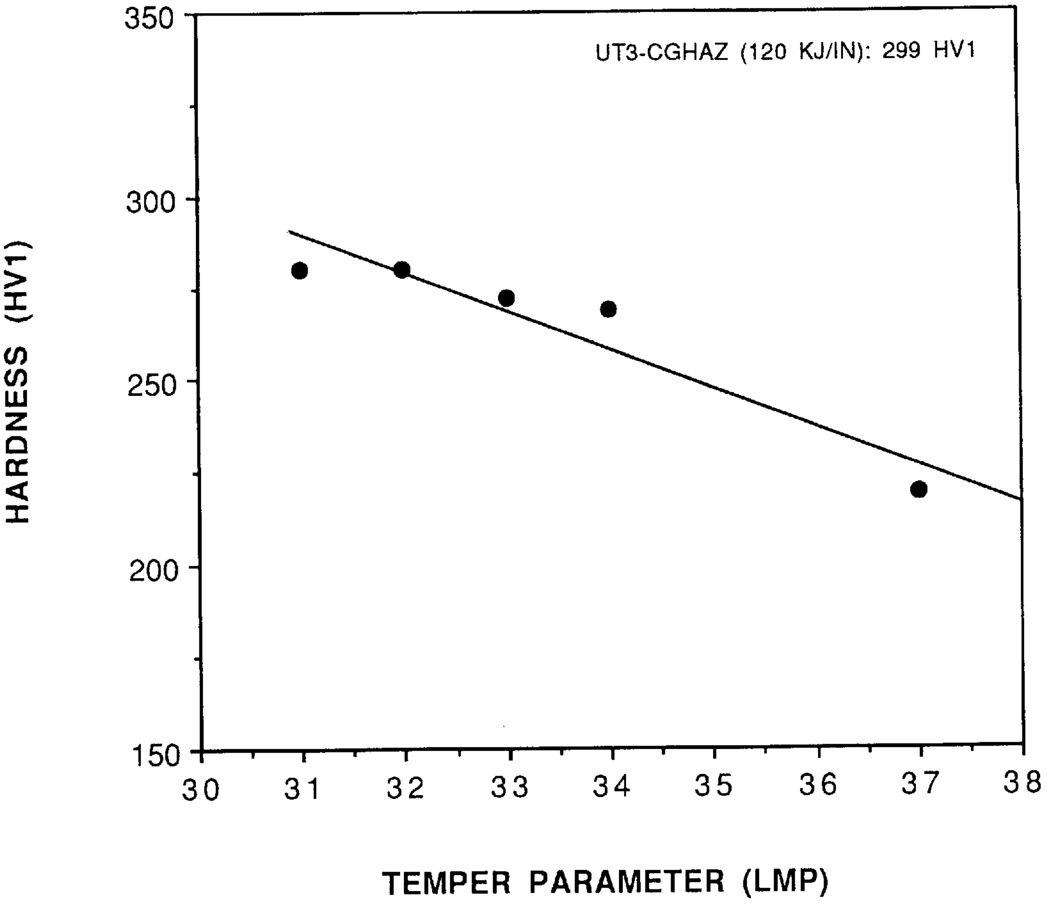

Fig. G3-9—Hardness of CGHAZ of UT3 with heat input 120 KJ/in. during PWHT

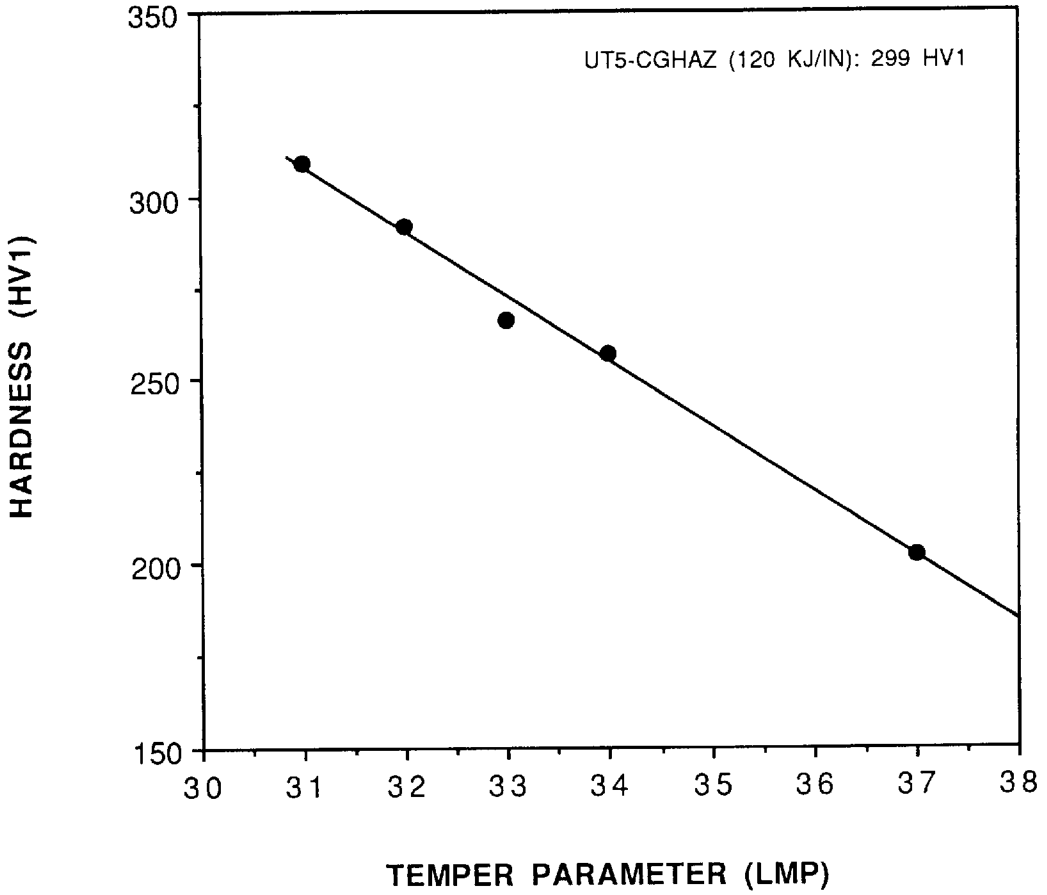

Fig. G3-10—Hardness of CGHAZ of UT5 with heat input 120 KJ/in. during PWHT

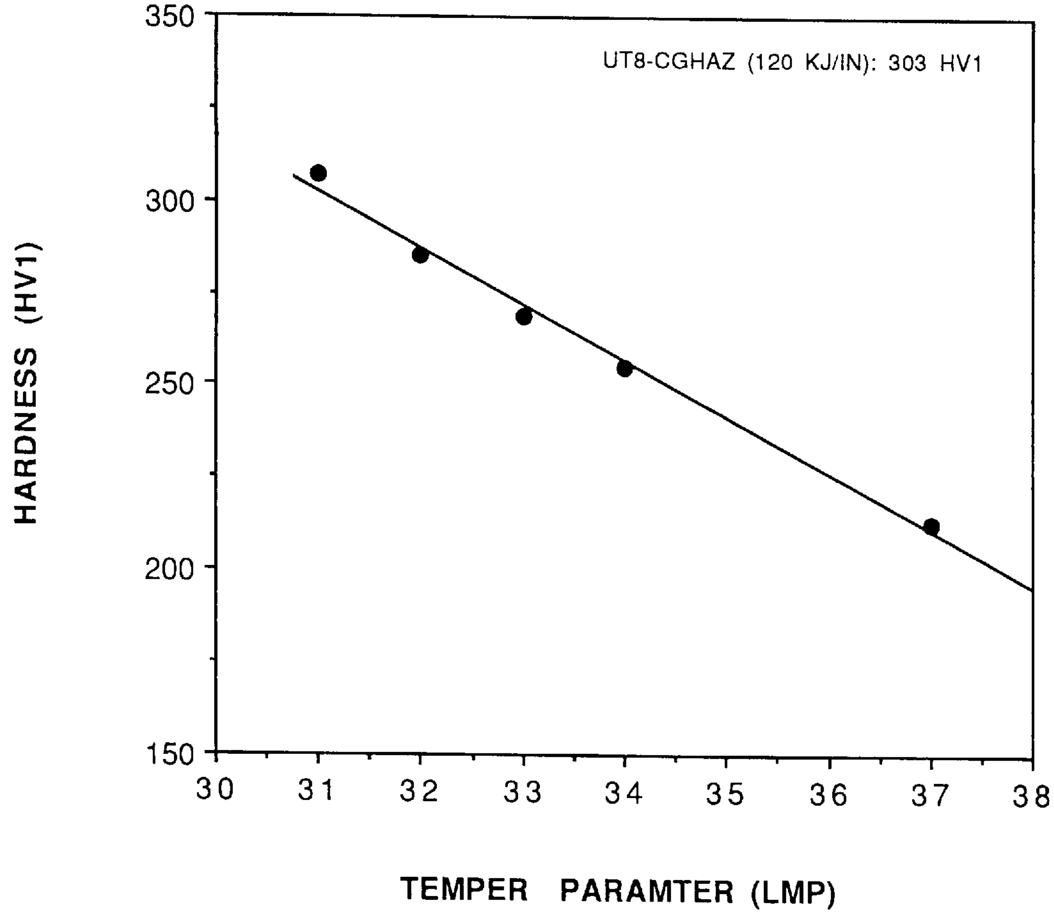

Fig. G3-11—Hardness of CGHAZ of UT8 with heat input 120 KJ/in. during PWHT

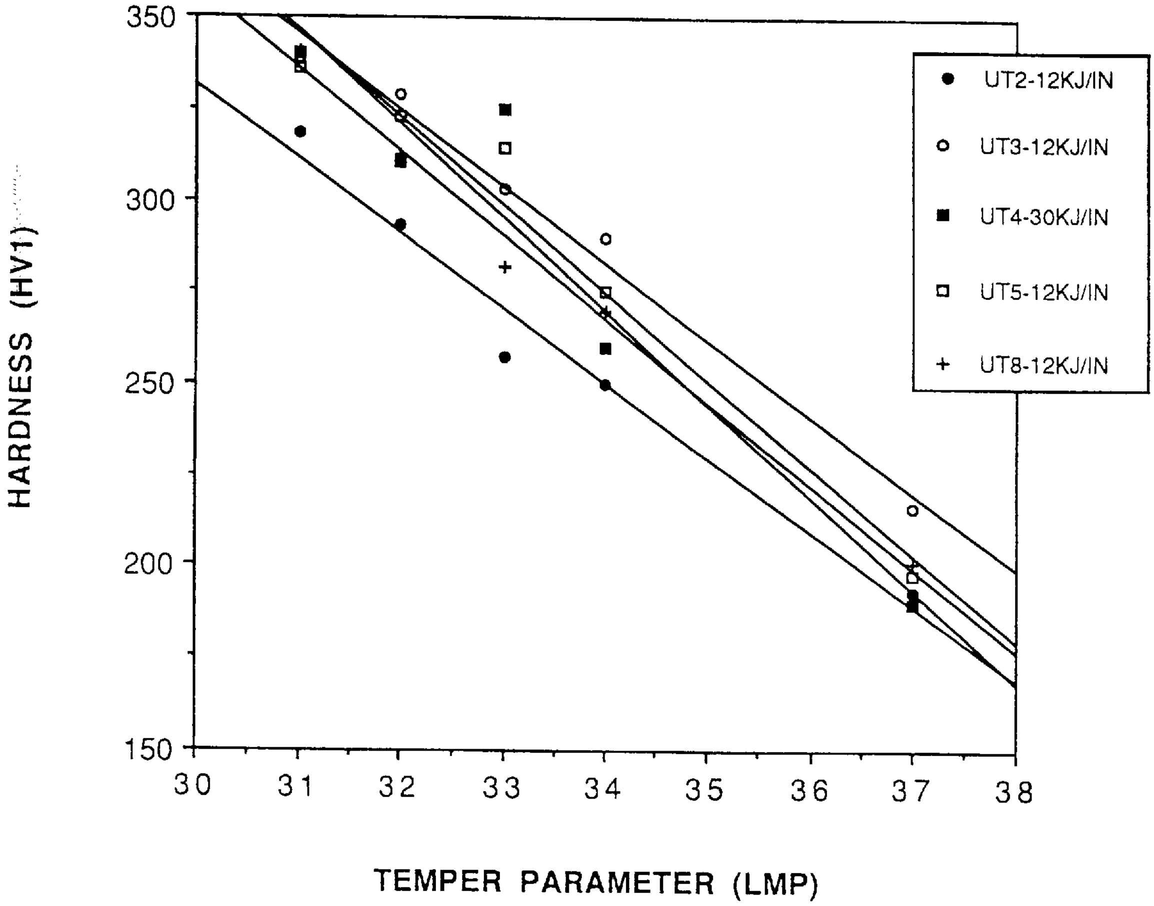

Fig. G3-12—Hardness of CGHAZ with heat input 12 KJ/in. (*30 KJ/in. for UT4) during PWHT

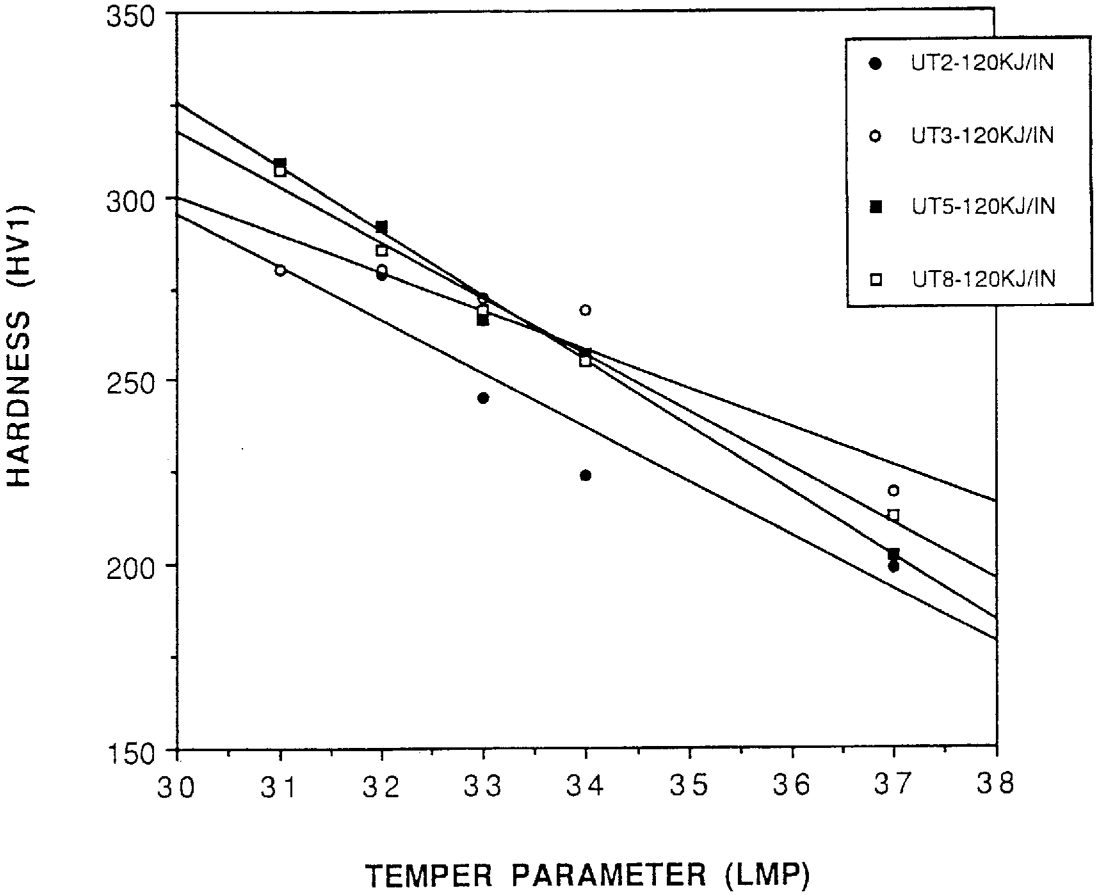

Fig. G3-13—Hardness of CGHAZ with heat input 120 KJ/in. during PWHT

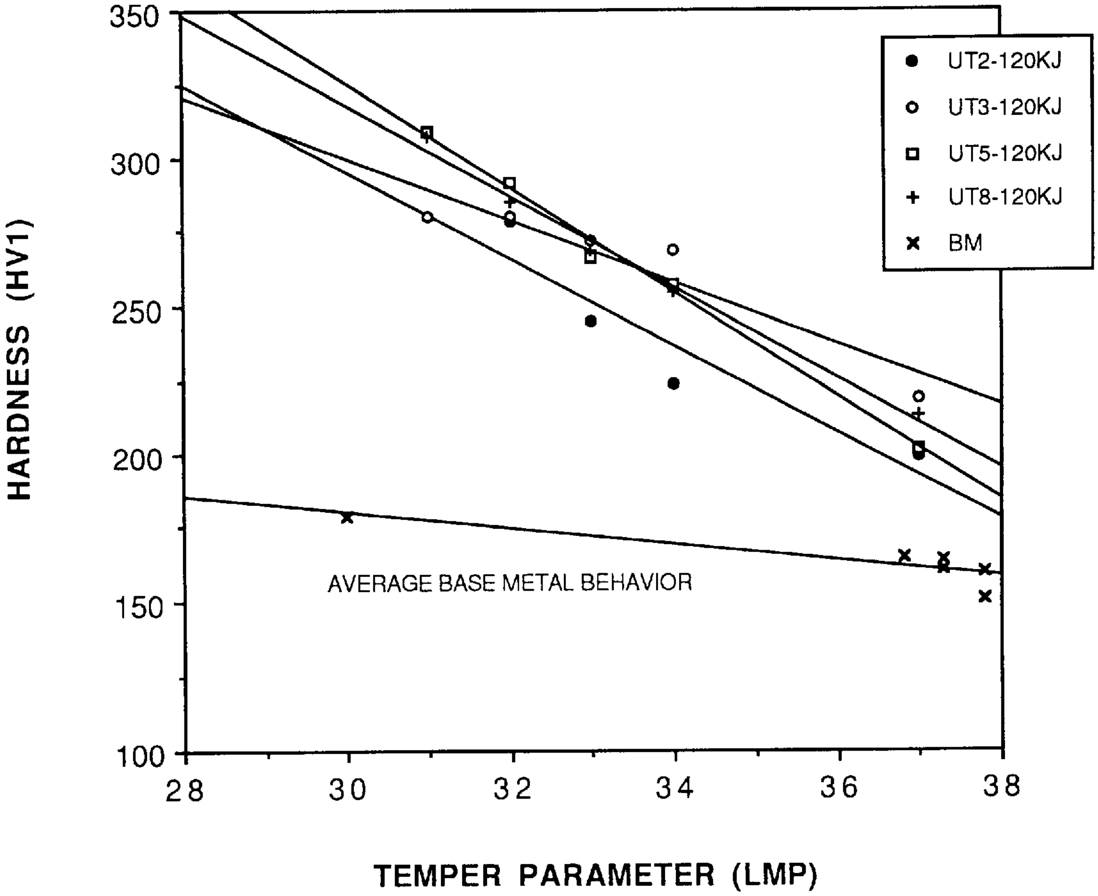

Fig. G3-14—Hardness of CGHAZ with heat input 120 KJ/in. and base metals during PWHT

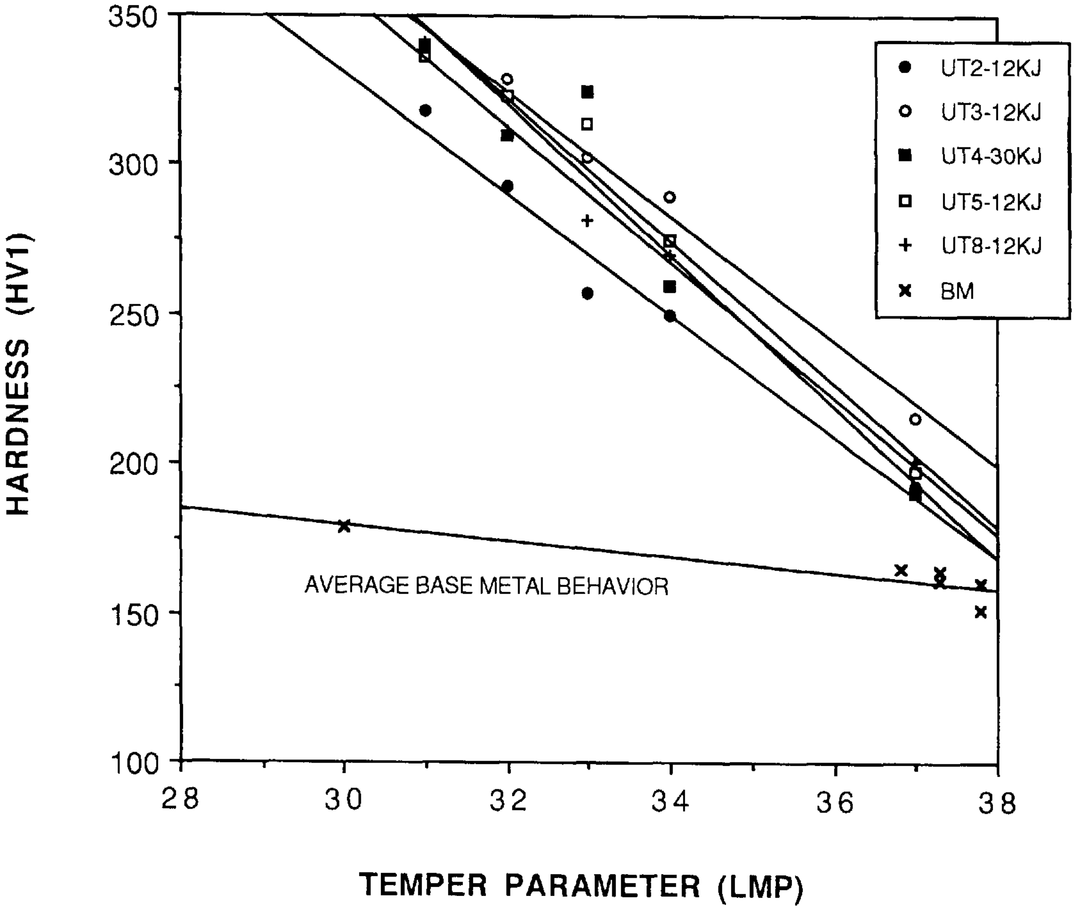

Fig. G3-15—Hardness of CGHAZ with heat input 12 KJ/in. (30 KJ/in. for UT4) and base metals during PWHT

Table G3-4—Hardness of CGHAZ as a Function of PWHT

Materials	*No PWHT*	*1150°F/ 15 min*	*1150°F/ 1 hr*	*1250°F/ 15 min*	*1250°F/ 1 hr*	*1350°F/ 8 hrs*
UT2 12KJ/in.	360	318	293	257	250	193
UT2 120KJ/in.	285	279	280	272	269	219
UT3 12KJ/in.	439	339	329	303	290	216
UT3 120KJ/in.	299	279	280	272	269	219
UT5 12KJ/in.	430	336	323	314	275	198
UT5 120KJ/in.	298	309	292	266	257	202
UT8 12KJ/in.	413	341	312	282	270	201
UT8 120KJ/in.	303	307	285	269	255	213

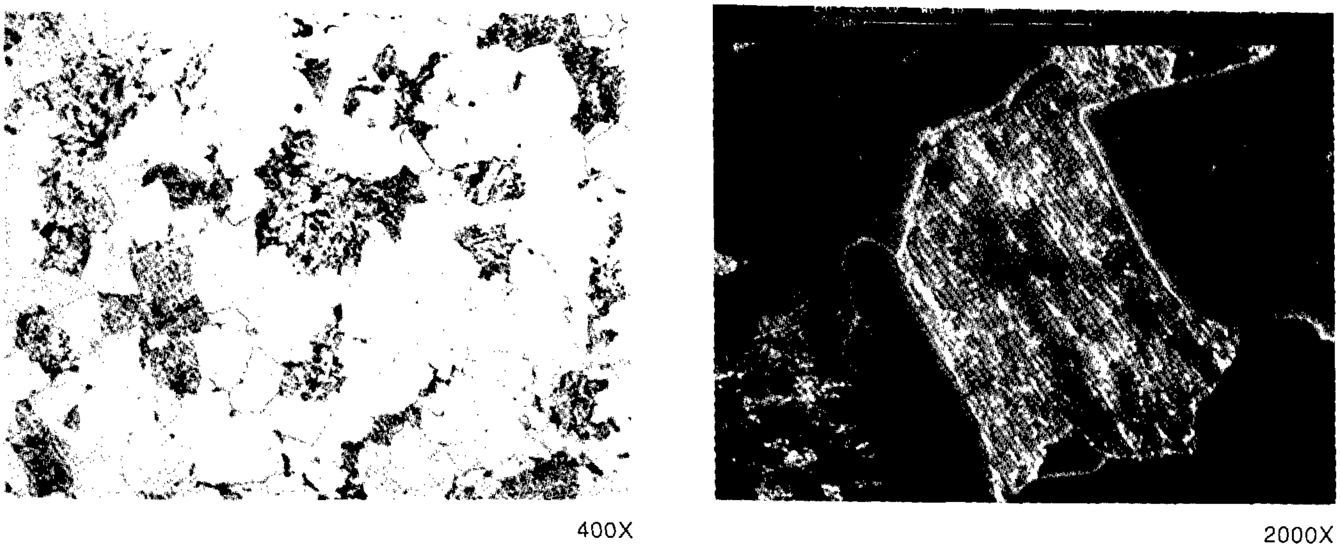

Fig. G3-16—Optical and SEM micrographs of base metal of UT2

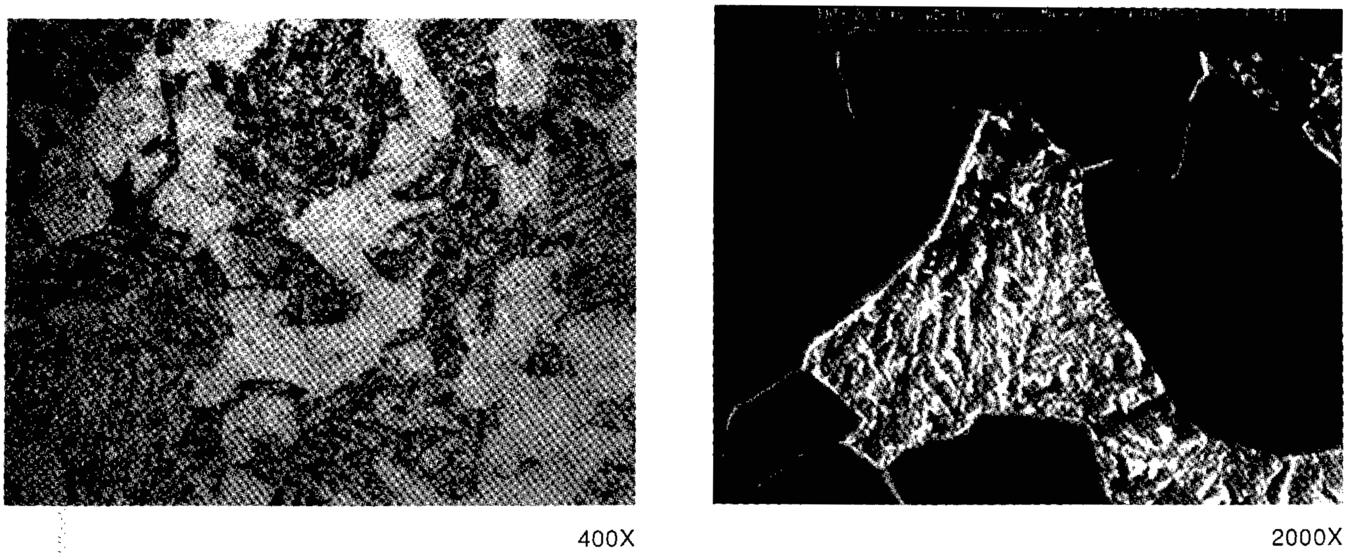

Fig. G3-17—Optical and SEM micrographs of base metal of UT3

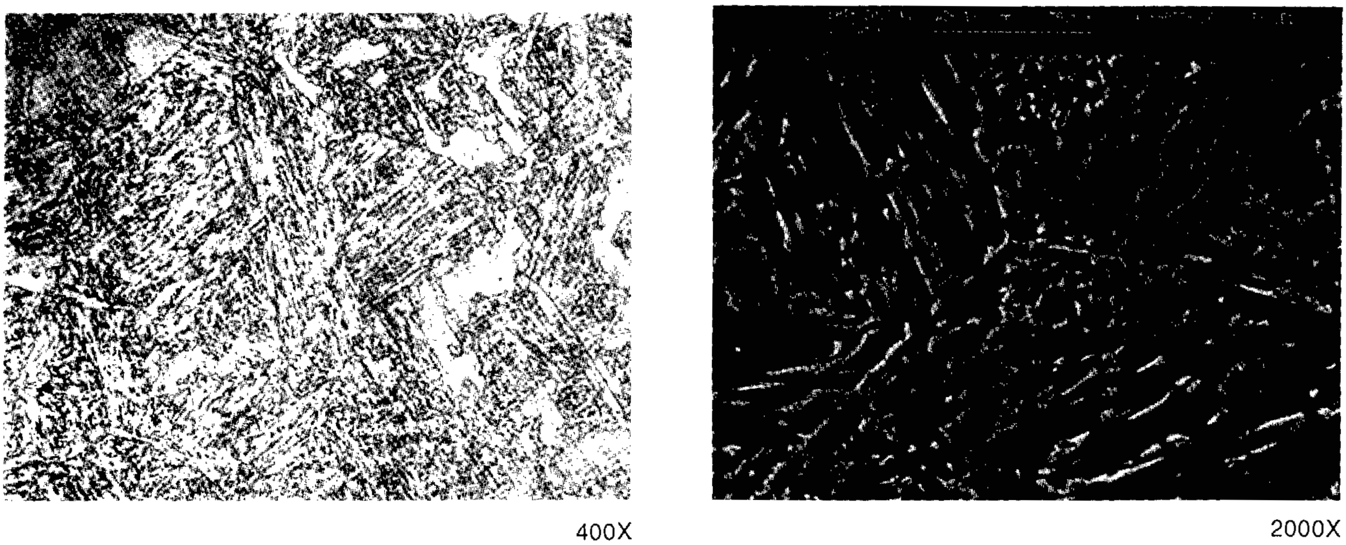

Fig. G3-18(a)—Optical and SEM micrographs of 120 KJ/in. CGHAZ of UT2

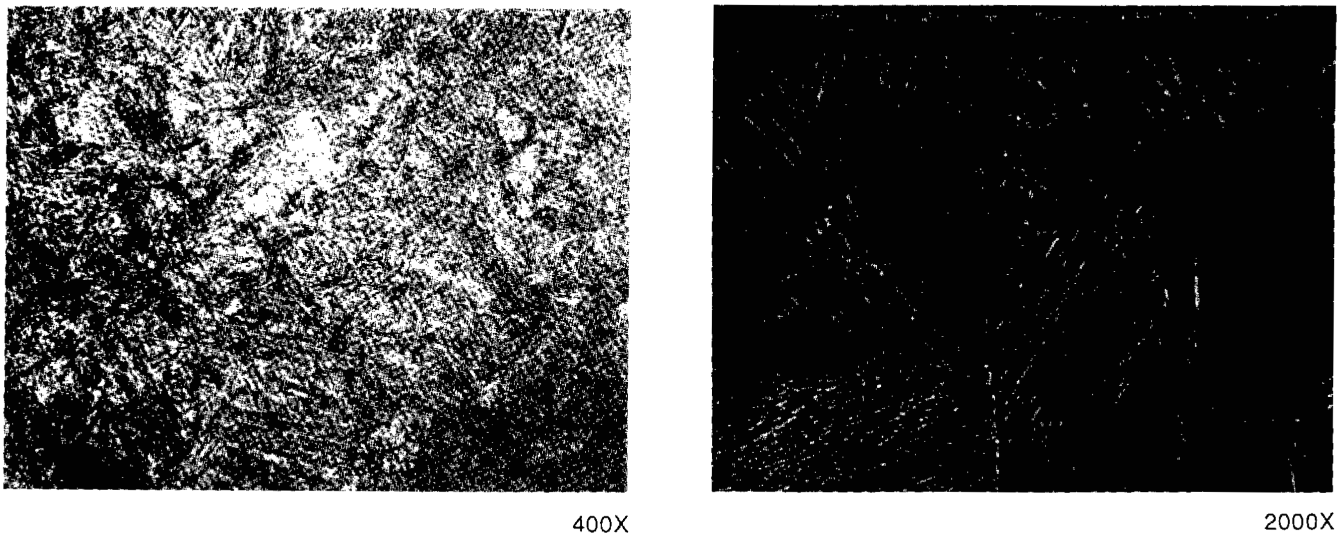

Fig. G3-18(b)—Optical and SEM micrographs of 12 KJ/in. CGHAZ of UT2 site, and only a few fine carbides (M_3C) are observed that precipitate due to auto-tempering of the martensite. Although there were no differences in the carbide type between heats in both the 12 and 120 KJ/in. CGHAZs (as-simulated), the fraction of ferrite and granular bainite was greater in UT2 (120 KJ/in.) compared to UT3 (120 KJ/in.) (owing to the difference in carbon content) as shown in Figs. G3-18 and G3-19a and G3-19b.

The STEM study revealed that during PWHT, additional M_3C carbides precipitate predominantly at prior austenite grain boundaries and bainite lath boundaries with elongated, rod-like and globular morphologies. With an increase in PWHT temperature and PWHT time the more stable types of carbides (M_2C, $M_{23}C_6$ and M_7C_3) are formed. The M_2C carbides are found only in the 120 KJ/in. CGHAZs. No M_2C carbides were found in the 12 KJ/in. CGHAZ over the entire PWHT range examined. The fine and acicular M_2C carbides are located in the bainite lath interiors and within the ferrite grains. Figures G3-20 and G3-21 illustrate (UT3 material) the carbide distribution at the prior austenite grain boundaries, bainite lath boundaries and lath interiors for 12 KJ/in. Fig. G3-22 shows carbide distribution in the proeutectoid ferrite regions for 120 KJ/in. in UT2.

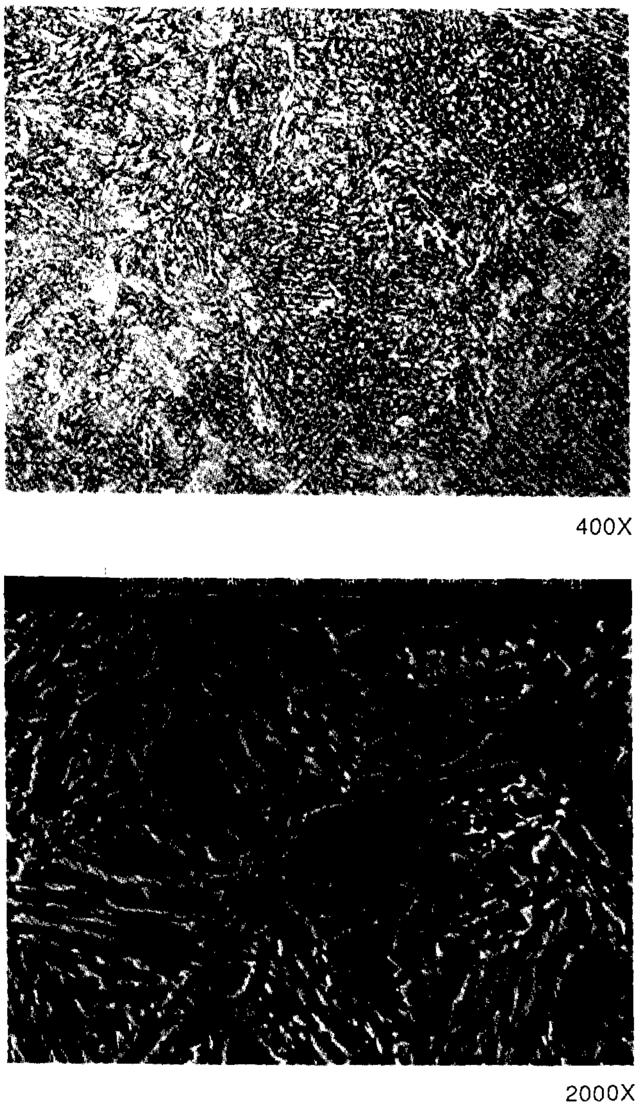

Fig. G3-19(a)—Optical and SEM micrographs of 120 KJ/in. CGHAZ of UT3

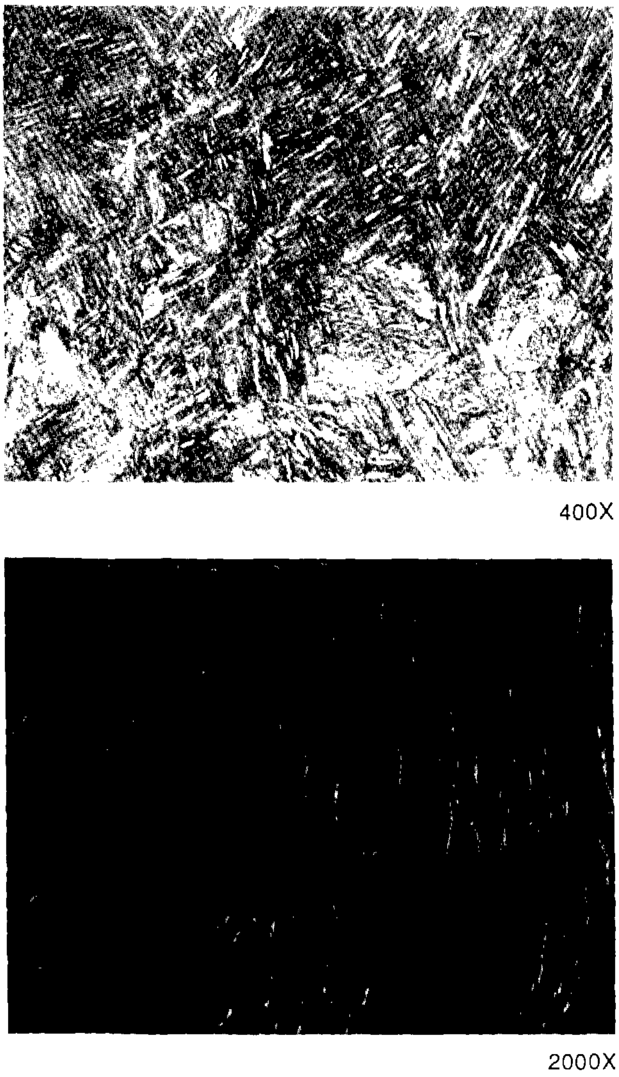

Fig. G3-19(b)—Optical and SEM micrographs of 12 KJ/in. CGHAZ of UT3

In general, the sequence of carbide evolution in the CGHAZ during PWHT can be summarized as follows:

High heat input (120 KJ/in.):

$$M_3C \rightarrow M_3C + M_2C \rightarrow M_3C + M_{23}C_6 + M_2C \rightarrow M_{23}C_6 + M_7C_3 + M_2C$$

Low heat input (12 KJ/in.):

$$M_3C \rightarrow M_3C + M_{23}C_6 \rightarrow M_{23}C_6$$

In another study of the UT4 material in which the CGHAZ was simulated with a 30 KJ/in. heat input, the sequence of carbide evolution was identical to that for the low heat input (12 KJ/in.) in this study.

In the low heat input (12 KJ/in.) CGHAZ, more stable carbides ($M_{23}C_6$) form at shorter time-temperature PWHT combinations than in the high heat input (120 KJ/in.) CGHAZ. The first $M_{23}C_6$ type carbides form in the interiors of the bainite laths followed by formation of $M_{23}C_6$ carbides at the prior austenite

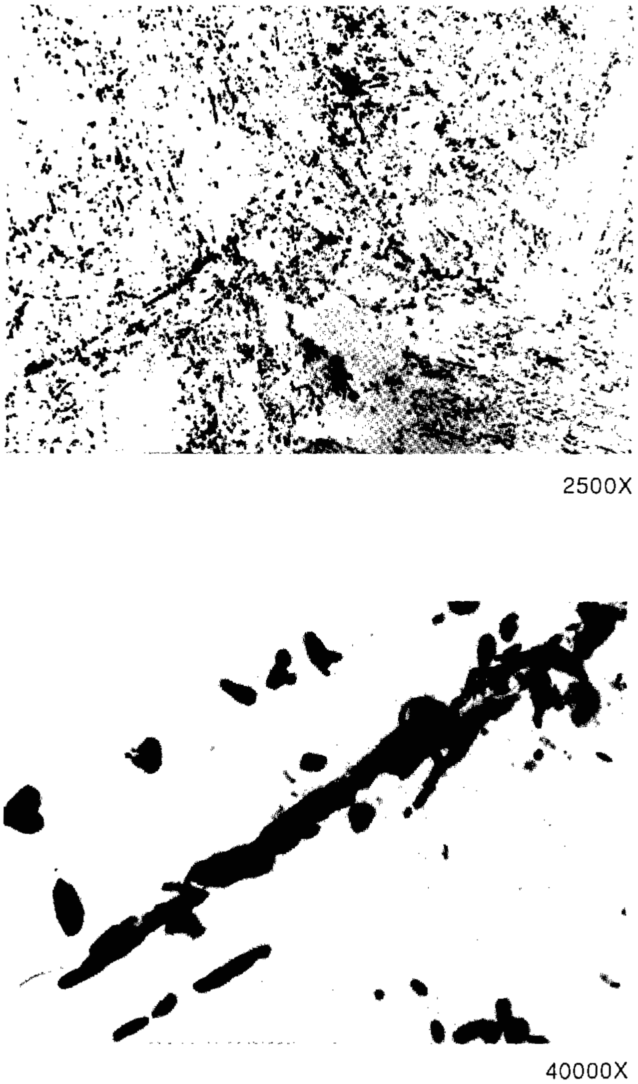

Fig. G3-20—Carbide structure at prior austenite grain boundaries in the CGHAZ of UT3 with heat input of 12 KJ/in. and PWHT of 1250°F, 15 min

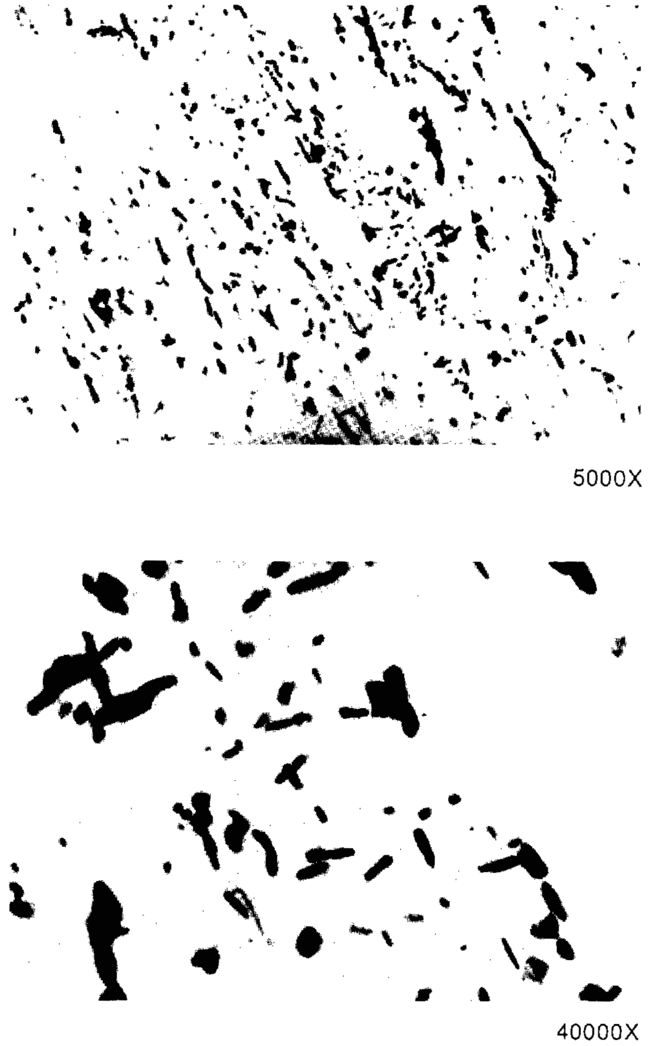

Fig. G3-21—Carbide structure at bainite lath boundaries and interiors in the CGHAZ of UT3 with heat input of 12 KJ/in. and PWHT of 1250°F, 15 min

grain boundaries. In addition, in the high heat input CGHAZ M_2C carbides form in the interior of the bainite laths and in the ferrite grains during PWHT. A distinct resistance to a decrease in hardness upon PWHT is observed for high heat input (in fact, for UT5 and UT8 during the initial stages of PWHT a slight secondary hardening is observed). These observations correlate with the fact that the high heat input CGHAZ is more susceptible to reheat cracking than the low heat input CGHAZ (Gleeble reheat cracking tests).

During PWHT of the CGHAZ the stable carbide $M_{23}C_6$ is formed at shorter time-temperature PWHT combinations in heats which are more resistant to reheat cracking (UT2 & UT8) as compared to the heats which are susceptible to reheat cracking (UT3, UT4 & UT5).

SEM study of UT2 and UT3 materials revealed that the bainite laths in the CGHAZ coarsen during PWHT. For the 120 KJ/in. as-simulated CGHAZ the bainite laths in UT2 material were found to be coarser than in UT3 (Fig. G3-23). This is probably

Fig. G3-22—Carbides precipitated in preutectoid ferrite regions of the CGHAZ of UT2 with heat input of 120 KJ/in. and PWHT of 1250°F, 15 min

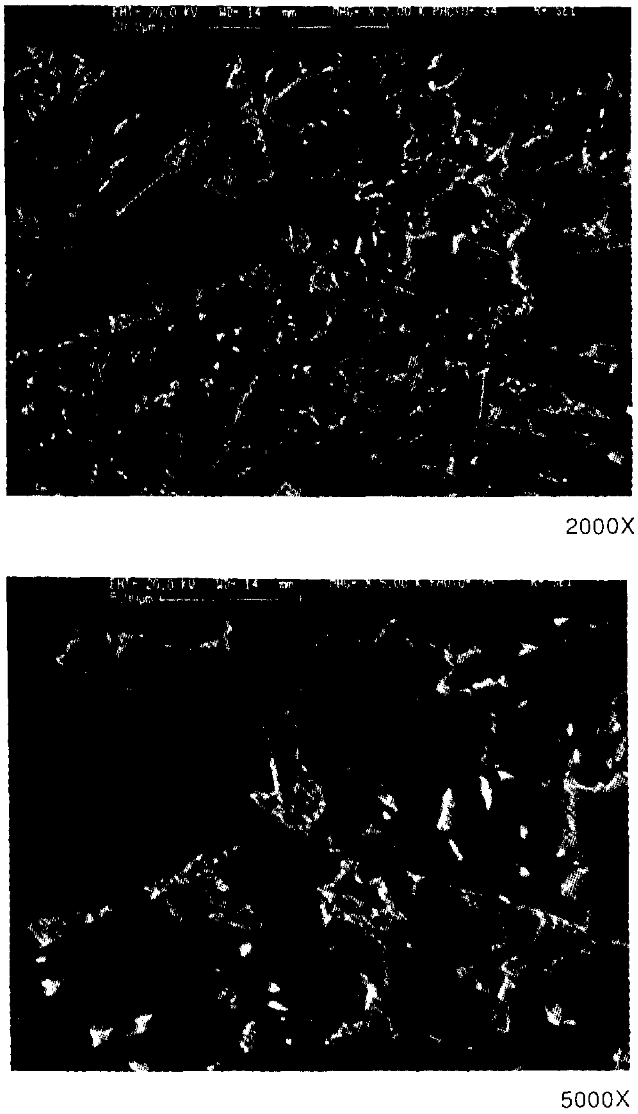

Fig. G3-23—Bainite lath morphology in the CGHAZ of UT2 with heat input of 120 KJ/in. and PWHT of 1150°F, 1 hour

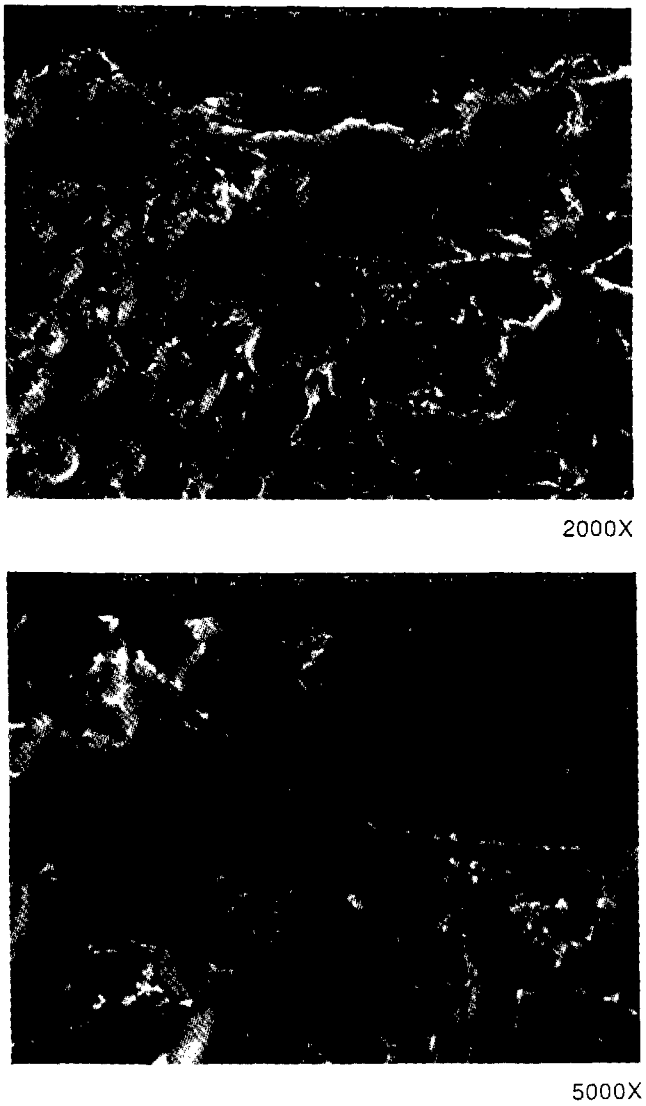

Fig. G3-24—Bainite lath morphology in the CGHAZ of UT3 with heat input of 120 KJ/in. and PWHT of 1250°F, 1 hour

because of the lower carbon in UT2 compared to UT3. The bainite laths become virtually indistinguishable in the CGHAZ after a PWHT of 1150°F, 1 hour for UT2 (Fig. G3-23) and after a PWHT of 1250°F, 1 hour for UT3 (Fig. G3-24). For the 12 KJ/in. as-simulated CGHAZ (martensite) the laths in both UT2 and UT3 were similar in width (Fig. G3-25). Although the laths coarsened during PWHT, distinct appearance of the laths was evident even for the most severe PWHT of 1350°F, 8 hours.

The examination of the appearance of the prior austenite grain boundaries in the UT2 and UT3 heats revealed that for UT3, the grain boundaries appear diffuse and wider with a higher density of carbides for 1150°F, 15 min PWHT. They remained diffuse until a PWHT of 1250°F, 1 hour were reached at which point the grain boundaries appeared sharp. In contrast, a diffuse nature of grain boundaries was noted in UT2 at PWHT of 1250°F, 15 min (the extent of the diffuse nature being much less compared to UT3) and the grain boundaries became sharp after PWHT at 1250°F, 1 hour. This phenomenon was observed for both heat inputs and is illustrated by the SEM micrographs presented in Figs. G3-26 and G3-27 for the UT2 and UT3, respectively.

For all heats upon PWHT the carbide evolution sequence is similar for equivalent energy inputs. For the low heat input (martensite) a PWHT of 1250°F, 1 hour results in $M_{23}C_6$ and M_3C carbides. For the high heat input (ferrite + bainite) a PWHT of 1250°F, 1 hour results in $M_{23}C_6$, M_2C and M_3C carbides. In addition the prior austenite grain boundaries become distinct after a PWHT of 1250°F, 1 hour. This observation may point to an indication that for a PWHT of 1250°F, 1 hour reheat cracking sensitivity may be minimized. Thus, weldments PWHT at temperatures greater than 1250°F for time in excess of 1 hour will tend to reduce reheat cracking sensitivity. These results correlate well with the Gleeble studies where a recovery of ductility is evident after 1250°F, 1 hour PWHT for all materials.

Discussion

Based on the observations presented above it may be noted that a persistence of M_3C carbides in the

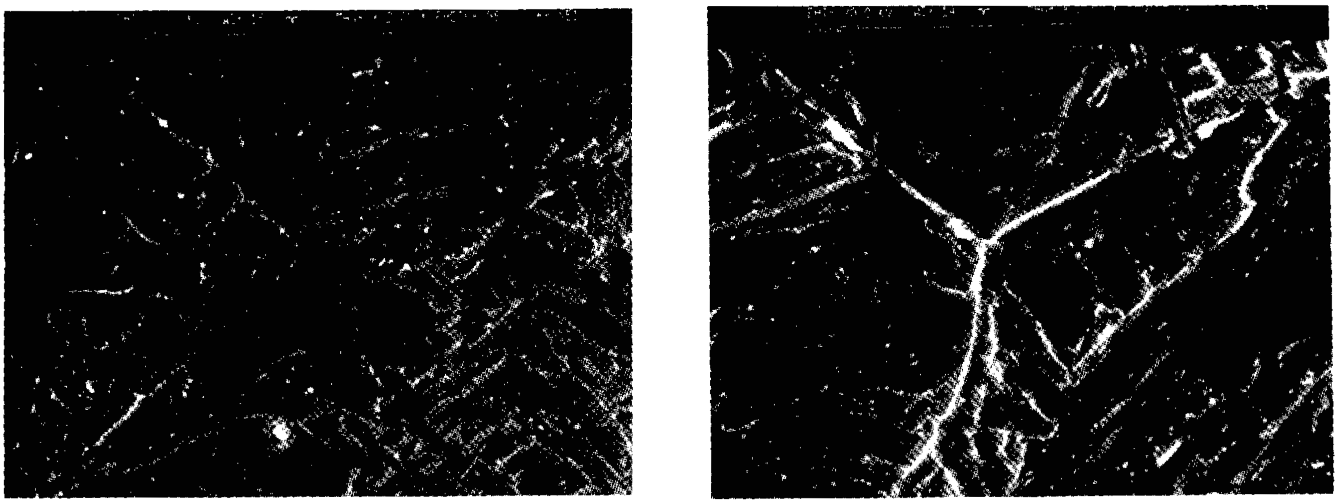

UT2 2000X UT3 2000X

Fig. G3-25—Bainite lath morphology in the CGHAZ of UT2 and UT3 with heat input of 12 KJ/in. and PWHT of 1350°F, 8 hours

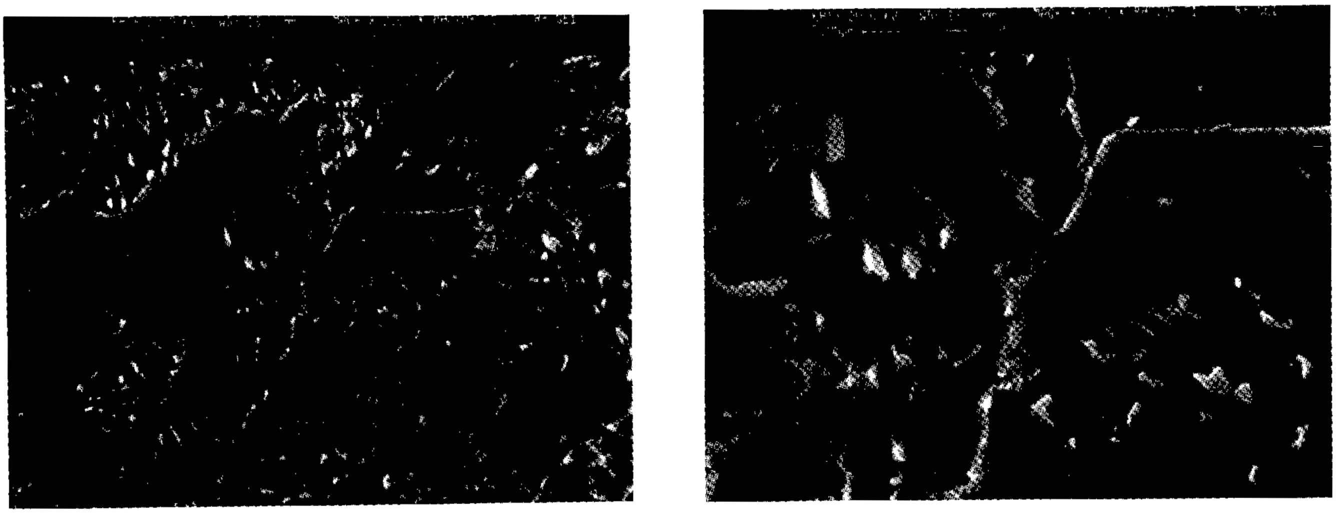

2000X 5000X

Fig. G3-26—Carbide precipitation at prior austenite grain boundaries in the CGHAZ of UT2 with heat input of 120 KJ/in. and PWHT of 1150°F, 15 min

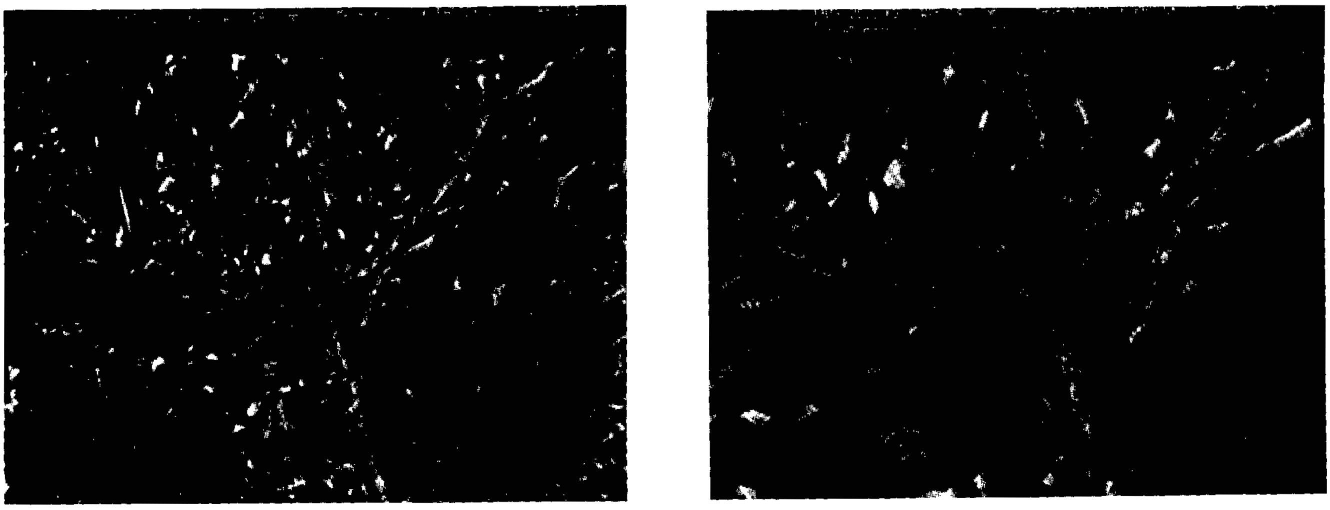

2000X 5000X

Fig. G3-27—Carbide precipitation at prior austenite grain boundaries in the CGHAZ of UT3 with heat input of 120 KJ/in. and PWHT of 1150°F, 15 min

CGHAZ upon PWHT is an indication that the heat is susceptible to reheat cracking. This conclusion cannot be derived from the chemical composition. However, it may be postulated that segregation of trace elements may be responsible for this behavior. Trace elements have been suggested by other authors to alter the carbide evolution kinetics. This trace element behavior has not been investigated fully and thus cannot be tied directly to material reheat cracking sensitivity at this time.

A WRC sponsored investigation at the University of Tennessee found a few atomic layers of high P concentration on the prior austenite grain boundaries in the CGHAZ in the reheat crack susceptible heat UT5 by Scanning Auger Spectroscopy. In a 2¼Cr heat resistant to reheat cracking, the P segregation was minimal, although these heats contained identical amounts of P.

Conclusions

M_3C carbides persist in the CGHAZ for greater PWHT time-temperature combinations in heats susceptible to reheat cracking. The reheat cracking susceptibility of higher heat input CGHAZs is apparently related to the formation of M_2C carbides in addition to the persistence of the M_3C carbides.

In all heats, the carbide evolutionary sequence upon PWHT is similar for equivalent energy inputs. However, the kinetics are different for heats susceptible and not susceptible to reheat cracking. For low heat input (martensite) a PWHT of 1250°F, 1 hr results in $M_{23}C_6$ and M_3C carbides. For high heat input (ferrite + bainite) a PWHT of 1250°F, 1 hour results in $M_{23}C_6$, M_2C and M_3C carbides. Thus, a weld successfully PWHT without cracking at temperatures greater than 1250°F for time longer than 1 hour will not likely show low ductility cracking in the CGHAZ in service.

For high heat input the presence of ferrite + bainite in the CGHAZ may be the necessary condition for the alteration of the carbide evolutionary sequence (leading to M_2C formation) which renders the HAZ somewhat more susceptible to reheat cracking.

Results of carbide analysis are tabulated on the following page.

Results of Carbide Analysis

UT2-N/T		
BM	FERRITE + BAINITE	$M_{23}C_6 + M_3C + MO_2C$
120 KJ/IN	BAINITE + FERRITE	Dissolved in matrix
120 KJ/IN-1150°F-15 min	BAINITE + FERRITE	M_3C
120 KJ/IN-1150°F-1 hr	BAINITE + FERRITE	$M_3C + MO_2C + M_{23}C_6$
120 KJ/IN-1250°F-15 min	BAINITE + FERRITE	$M_{23}C_6 + M_3C + (MO, CR)_2NC$
120 KJ/IN-1250°F-1 hr	BAINITE + FERRITE	$M_{23}C_6 + M_3C + (MO, CR)_2NC$
120 KJ/IN-1350°F-8 hrs	BAINITE + FERRITE	$M_{23}C_6 + M_3C + (MO, CR, V)_2NC + M_7C_6$
12 KJ/IN	MARTENSITE + BAINITE	Dissolved in matrix
12 KJ/IN-1150°F-15 min	MARTENSITE + BAINITE	$M_3C + M_{23}C_6$
12 KJ/IN-1150°F-1 hr	MARTENSITE + BAINITE	$M_3C + M_{23}C_6$
12 KJ/IN-1250°F-15 min	MARTENSITE + BAINITE	$M_{23}C_6 + M_3C + (MO, CR)_2NC$
12 KJ/IN-1250°F-1 hr	MARTENSITE + BAINITE	$M_{23}C_6 + M_3C$
12 KJ/IN-1350°F-8 hr	MARTENSITE + BAINITE	$M_{23}C_6$
UT3-VM		
BM	FERRITE + BAINITE	$M_3C + M_{23}C_6 + MO_2C$ in bainite
120 KJ/IN	BAINITE + FERRITE	Dissolved in matrix
120 KJ/IN-1150°F-15 min	BAINITE + FERRITE	$M_3C + (CR, MO)_2NC$
120 KJ/IN-1150°F-1 hr	BAINITE + FERRITE	$M_3C + (CR, MO)_2NC$
120 KJ/IN-1250°F-15 min	BAINITE + FERRITE	$M_3C + (CR, MO)_2NC$
120 KJ/IN-1250°F-1 hr	BAINITE + FERRITE	$M_{23}C_6 + (CR, MO)_2NC + M_3C$
120 KJ/IN-1350°F-8 hrs	BAINITE + FERRITE	$M_{23}C_6 + (CR, MO)_2NC + M_3C$
12 KJ/IN	MARTENSITE + BAINITE	Dissolved in matrix
12 KJ/IN-1150°F-15 min	MARTENSITE + BAINITE	M_3C
12 KJ/IN-1150°F-1 hr	MARTENSITE + BAINITE	M_3C
12 KJ/IN-1250°F-15 min	MARTENSITE + BAINITE	$M_{23}C_6 + M_3C$
12 KJ/IN-1250°F-1 hr	MARTENSITE + BAINITE	$M_{23}C_6 + M_3C$
12 KJ/IN-1350°F-8 hrs	MARTENSITE + BAINITE	$M_{23}C_6 + M_3C$
UT5-VM		
BM	FERRITE + BAINITE	$M_3C + M_{23}C_6 + MO_2C$
120 KJ/IN	BAINITE + FERRITE	Dissolved in matrix
120 KJ/IN-1150°F-15 min	BAINITE + FERRITE	M_3C
120 KJ/IN-1150°F-1 hr	BAINITE + FERRITE	$M_3C + (MO, CR)_2NC + M_{23}C_6$
120 KJ/IN-1250°F-15 min	BAINITE + FERRITE	$M_3C + M_{23}C_6 + (MO, CR)_2NC$
120 KJ/IN-1250°F-1 hr	BAINITE + FERRITE	$M_3C + M_{23}C_6 + (MO, CR)_2NC$
120 KJ/IN-1350°F-8 hr	BAINITE + FERRITE	$M_{23}C_6 + (MO, CR)_2NC$
12 KJ/IN	MARTENSITE + BAINITE	Dissolved in matrix
12 KJ/IN-1150°F-15 min	MARTENSITE + BAINITE	M_3C
12 KJ/IN-1150°F-1 hr	MARTENSITE + BAINITE	M_3C
12 KJ/IN-1250°F-15 min	MARTENSITE + BAINITE	$M_3C + M_{23}C_6$
12 KJ/IN-1250°F-1 hr	MARTENSITE + BAINITE	$M_{23}C_6 + M_3C$
12 KJ/IN-1350°F-8 hr	MARTENSITE + BAINITE	$M_{23}C_6$

Results of Carbide Analysis—(Continued)

UT8-N/T		
BM	FERRITE + BAINITE	$M_3C + M_{23}C_6 + MO_2C$
120 KJ/IN	BAINITE + FERRITE	Dissolved in matrix
120 KJ/IN-1150°F-15 min	BAINITE + FERRITE	M_3C
120 KJ/IN-1150°F-1 hr	BAINITE + FERRITE	M_3C + (MO, CR)$_2$NC + $M_{23}C_6$
120 KJ/IN-1250°F-15 min	BAINITE + FERRITE	M_3C + (MO, CR)$_2$NC + $M_{23}C_6$
120 KJ/IN-1250°F-1 hr	BAINITE + FERRITE	$M_3C + M_{23}C_6$ + (MO, CR)$_2$NC
1350 KJ/IN-1325°F-8 hr	BAINITE + FERRITE	$M_{23}C_6$ + (MO, CR)$_2$NC
12 KJ/IN	MARTENSITE + BAINITE	Dissolved in matrix
12 KJ/IN-1150°F-15 min	MARTENSITE + BAINITE	M_3C
12 KJ/IN-1150°F-1 hr	MARTENSITE + BAINITE	$M_3C + M_{23}C_6$
12 KJ/IN-1250°F-15 min	MARTENSITE + BAINITE	$M_3C + M_{23}C_6$
12 KJ/IN-1250°F-1 hr	MARTENSITE + BAINITE	$M_{23}C_6 + M_3C$
12 KJ/IN-1350°F-8 hr	MARTENSITE + BAINITE	$M_{23}C_6$

G3 Phase II—High Resolution Electron Microscopic Evaluation on API Materials

Introduction

Metallographic investigation of carbide behavior in 1¼Cr-½Mo steel was conducted using a Hitachi 800 scanning transmission electron microscope (STEM). The carbon replica technique was used to extract the carbides for determining carbide evolution sequence, carbide size, amount of carbides and carbide type. EDS was employed for the identification of particles. The combined results from this study (examination of carbon replica specimens) and the transmission electron microscopy examination (thin foil specimens) provide a relatively complete picture of carbide behavior as a function of postweld heat treatment (PWHT) parameters in the coarse grained HAZ (CGHAZ) and enhances the understanding of reheat cracking mechanisms.

Materials and Experiments

Four heats of 1¼Cr-½Mo steels (UT2, UT3, UT5 and UT8) were used for this evaluation. Among the materials, UT2 has the lowest carbon content (0.10 wt.%) while the UT5 has the highest carbon content (0.17 wt.%).

The carbon replica specimens were extracted from the cross section of Gleeble simulated CGHAZ samples. The procedures used to prepare the carbon replica specimens are described briefly as follows.

First, the mounted sample is mechanically polished and then chemically etched in nital. Then, the carbon film layer is deposited on the etched surface using a carbon evaporation technique. The thickness of the carbon film is controlled to 100–200Å for best results in terms of ease of replica floatation. Carbon coated samples are electrolytically etched using a 10 vol.% solution of hydrochloric acid in methanol for 30 sec followed by floating the replica in distilled water. The floated replicas are collected using 200 mesh copper grids. Limited quantitative imaging analysis was applied for obtaining area fraction of carbides.

Results

CGHAZ Samples Simulated with a Weld Energy Input of 120 kJ/in. A summary of the relative amount, shape, type and distribution of the carbides in the Gleeble simulated CGHAZs for all four selected materials with a weld energy input of 12KJ/in. is listed on the upper portion of Tables G3-1 to G3-4. Starting with the as-simulated CGHAZ condition

Table G3-1—Summary of Carbide Behavior in CGHAZ of UT2

Sample Identification ((kJ/in)F°/mins)	*Relative Amount (area %)*	*Shape & Size (μm)*	*Type & Distribution*
120/as-simulated	0.01–0.02	spherical; (ave. dia. 0.2) (A)	Fe_3C, M_2C GB (P)
120/1150/15	1–3	spherical (P); (ave. dia. 2.5); rod (S); (dia. 2.0, length 5)	Fe_3C, $M_{23}C_6$ GB (P)
120/1150/60	3–5	spherical (P), (ave. dia. 3.5) rod (S) (dia. 2.0, length 5)	Fe_3C, $M_{23}C_6$ GB (P)
120/1250/15	2–3	rod like (H) (ave. dia. 2.5, length 5); spherical (H) (ave. dia. 5)	Fe_3C, $M_{23}C_6$ GB (P)
120/1250/60	5–8	spherical (H) (ave. dia. 7.5); rod like (H) (dia. 2, length 15); needle like (1 × 4).	Fe_3C, $M_{23}C_6$ GB (P)
120/1350/480	6–9	spherical (H) (ave. dia. 15); rod like (H) (ave. 2.5, length 15)	$M_{23}C_6$ GB (P)
12/as-simulated	0.01–0.02	spherical, (A) (ave. dia. 0.2) (A)	Fe_3C, M_2C GB (P)
12/1150/15	3–5	spherical, (P) (ave. dia. 2)	Fe_3C, $M_{23}C_6$ GB & BLB (P)
12/1150/60	5–8	cluster of spherical (P) (ave. dia. of sigle spherical 2.5); rod like type (S) (dia. 2.5, length 10)	Fe_3C, $M_{23}C_6$ GB & BLB (P)
12/1250/15	5–8	spherical (P) (ave. dia. 2); needle like (F) (0.1 × 1)	$M_{23}C_6$, M_2C GB & BLB (P)
12/1250/60	5–8	rod like (H) (dia. 1.5, length 3); spherical (H) (ave. 1.5)	$M_{23}C_6$ GB (P)
12/1350/480	5–8	spherical (ave. dia. 3)	$M_{23}C_6$ (UD)

*GB: along GB; BLB: bainite lath boundary. **Dendrite-like carbides were observed along the grain boundary; in which rod-like carbides along the grain boundary while the spherical carbides along bainite lath boundary. UD: carbides uniformly distributed.

Abbreviations: A, 100%; P, Predominant; H, Approximately 50%; S, Some; F, Few.

Table G3-2—Summary of Carbide Behavior in CGHAZ of UT3

Sample Identification ((kJ/in)F°/mins)	*Relative Amount (area %)*	*Shape & Size (μm)*	*Type & Distribution*
120/as-simulated	0.1–0.2	spherical (A) (ave. dia. 0.1)	Fe_3C, M_2C GB (P)
120/1150/15	5	rod like (H) (dia. 1, length 4); spherical (H) (ave. dia. 1)	Fe_3C, $M_{23}C_6$ GB & BLB (P)
120/1150/60	5	spherical (P) (ave. dia. 2.0), rod like (S) (dia. 2.5, length 5)	Fe_3C, $M_{23}C_6$ GB & BLB (P)
120/1250/15	10	spherical (P) (ave. dia. 2.5); needle like (s) (0.1 × 2); rod like (dia. 1, length 3)	Fe_3C, $M_{23}C_6$ GB & BLB (P)
120/1250/60	12	spherical (H) (ave. dia. 2.0), rod like (H) (dia. 2.0, length 5); needle like (F) (0.1 × 2)	Fe_3C, $M_{23}C_6$ GB & BLB (P)
120/1350/480	18	spherical (P) (ave. dia. 3.5); rod like (S) (dia. 1, length 7.5); needle like (S) (0.3 × 4)	$M_{23}C_6$, M_2C UD
12/as-simulated	< 0.05	spherical (A) (ave. dia. 0.05)	Fe_3C GB (P)
12/1150/15	10	spherical (P) (ave. dia. 0.5); rod (F) (dia. 2, length 5); needle like (S) (0.1 × 0.2)	$M_{23}C_6$, M_2C GB & BLB (P)
12/1150/60	10	rod like (F) (dia. 2.0, length 7.5), spherical (P) (ave. dia. 2.0)	$M_{23}C_6$, M_2C
12/1250/15	15	spherical (S) (ave. dia. 2.5); rod like (F) (dia. 1.5, length 5.5); needle like (S) (0.1 × 2.5)	$M_{23}C_6$, M_2C GB & BLB (P)
12/1250/60	20	spherical (P) (ave. dia. 2.5), rod like (S) (dia. 1.5, length 4.5); needle like (S), (0.2 × 2.0)	Fe_3C, $M_{23}C_6$, M_2C
12/1350/480	20	spherical (H) (ave. dia. 3); needle like (H) (0.2 × 2.5); rod like (F) (dia. 0.5, length 5)	$M_{23}C_6$, M_2C UD

*GB: along GB; BLB: bainite lath boundary. **Dendrite-like carbides were observed along the grain boundary; in which rod-like carbides along the grain boundary while the spherical carbides along bainite lath boundary. UD: carbides uniformly distributed.

Abbreviations: A, 100%; P, Predominant; H, Approximately 50%; S, Some; F, Few.

Table G3-3—Summary of Carbide Behavior in CGHAZ of UT5

Sample Identification ((kJ/in)F°/mins)	*Relative Amount (area %)*	*Shape & Size (μm)*	*Type & Distribution*
120/as-simulated	0.01–0.02	spherical; (ave. dia. 0.2) (A)	Fe_3C, $M_{23}C_6$ GB (P)
120/1150/15	≈ 5	spherical (P); (ave. dia. 1.5); irregular shape	$M_{23}C_6$ GB & BLB [P]
120/1150/60	8–10	spherical (S), (ave. dia. 3.5); rod (P) (dia. 2.0, length 5); needle like [F]**	Fe_3C, $M_{23}C_6$ GB & BLB (P)
120/1250/15	10–15	rod like (H) (ave. dia. 2.5, length 5); spherical (H) (ave. dia. 2.5); irregular shape	Fe_3C, $M_{23}C_6$ GB & BLB (P)
120/1250/60	12–16	spherical (P) (ave. dia. 5); rod like (S) (dia. 2, length 20); needle like (S) (0.01 × 0.1).	Fe_3C, $M_{23}C_6$, M_2C GB (P)
120/1350/480	18–20	spherical (H) (ave. dia. 15); rod like (H) (ave. 2.5, length 15)	Fe_3C, $M_{23}C_6$,** M_2C UD
12/as-simulated	0.01–0.02	spherical, (A) (ave. dia. 0.2);	Fe_3C, M_2C GB (P)
12/1150/15	5–6	spherical, (S) (ave. dia. 1), rod like (S) (dia. 1, length 8), needle like (F) 0.1 × 1	Fe_3C, $M_{23}C_6$, M_2C GB & BLB (P)
12/1150/60	5–6	spherical, (P) (ave. dia. 1.5), rod like (S) (dia. 1.5, length 3), needle like (S) 0.05 × 0.2	Fe_3C, $M_{23}C_6$, M_2C GB & BLB (P)
12/1250/15	6–8	spherical, (H) (ave. dia. 1.5), rod like (H) (dia. 1.5, length 6), needle like (S) 0.05 × 4	Fe_3C, $M_{23}C_6$, M_2C GB & BLB (P)
12/1250/60	6–8	spherical, (H) (ave. dia. 1), rod like (H) (dia. 1, length 8), needle like (S) 0.5 × 2	Fe_3C, $M_{23}C_6$, M_2C GB & BLB (P)
12/1350/480	6–8	spherical, (S) (ave. dia. 5), rod like (S) (dia. 4, length 6), needle like (F) 0.5 × 3	$M_{23}C_6$, M_2C UD

*AGB: along GB; BLB: bainite lath boundary. **Dendrite-like carbides were observed along the grain boundary; in which rod-like carbides along the grain boundary while the spherical carbides along bainite lath boundary. UD: carbides uniformly distributed.

Abbreviations: A, 100%; P, Predominant; H, Approximately 50%; S, Some; F, Few.

Table G3-4—Summary of Carbide Behavior in CGHAZ of UT8

Sample Identification ((kJ/in)F°/mins)	*Relative Amount (area %)*	*Shape & Size (μm)*	*Type & Distribution*
120/as-simulated	≈0.01	spherical (A) (ave. 1)	Fe_3C, M_2C
120/1150/15	6–8	rod like (H) (dia. 1, length 4); spherical (H) (ave. dia. 1).	Fe_3C, $M_{23}C_6$ GB (P)
120/1150/60	6–8	spherical (P) (ave. dia. 2), rod like (S) (dia. 2, length 10)	Fe_3C, $M_{23}C_6$ GB & BLB (P)
120/1250/15	12–14	spherical (P) (ave. dia. 1.5); needle like (S) (0.1 × 2); rod like (S) (dia. 1.5, length 3)	Fe_3C, $M_{23}C_6$, M_2C GB & BLB
120/1250/60	12–14	spherical (H) (ave. dia. 2), rod like (H) (dia. 2, length 5); needle like (F) (0.4 × 5)	Fe_3C, $M_{23}C_6$, M_3C GB & BLB
120/1350/480	14–16	spherical (P) (ave. dia. 3); rod like (S) (dia. 3, length 10); needle like (S) (0.8 × 7.5)	$M_{23}C_6$, M_2C UD
12/as-simulated	≈0.01	spherical (A) (ave. dia. 1)	Fe_3C, M_2C
12/1150/15	4–6	spherical (P) (ave. dia. 0.5); rod (F) (dia. 2, length 5); needle like (S) (0.05 × 0.1)	Fe_3C, M_2C GB & BLB (P)
12/1150/60	6–7	rod like (S) (dia. 2.0, length 7.5), spherical (S) (ave. dia. 2.0); needle like (S) (0.8 × 8)	Fe_3C, $M_{23}C_6$, M_2C GB & BLB (P)
12/1250/15	6–8	spherical (S) (ave. dia. 2.5); rod like (F) (dia. 1.5, length 5.5); needle like (S) (0.1 × 2.5)	Fe_3C, $M_{23}C_6$, M_2C GB & BLB (P)
12/1250/60	8–10	spherical (P) (ave. dia. 2.5), rod like (S) (dia. 1.5, length 4.5); needle like (S), (0.2 × 2.0)	Fe_3C, $M_{23}C_6$, M_2C GB & BLB (P)
12/1350/480	10–12	spherical (A) (ave. dia. 3); needle like (F) (0.05 × 2.5)	$M_{23}C_6$, M_2C UD

*AGB: along GB; BLB: bainite lath boundary. **Dendrite-like carbides were observed along the grain boundary; in which rod-like carbides along the grain boundary while the spherical carbides along bainite lath boundary. UD: carbides uniformly distributed.

Abbreviations: A, 100%; P, Predominant; H, Approximately 50%; S, Some; F, Few.

UT3, UT5 and UT8 have essentially the same carbide precipitation rate while UT2 has the slowest carbide precipitation rate during PWHT. This result may be related to the reheat cracking behavior. This is a reasonable expectation since UT2 has the lowest carbon content while all four materials have essentially the same level of carbide reaction elements.

Figures G3-1 to G3-4 show the morphologies of the carbides and their distributions for an as-simulated CGHAZ condition in UT2, UT3, UT5 and UT8, respectively. In the as-simulated condition, almost all preexisting carbides were dissolved into the grain matrix (all four materials). Small amounts of fine carbides (mainly along the prior austenite grain boundaries) can be observed in these figures. These carbides were formed during the on-cooling portion of the simulated welding thermal cycle or are remnants of incompletely dissolved carbides.

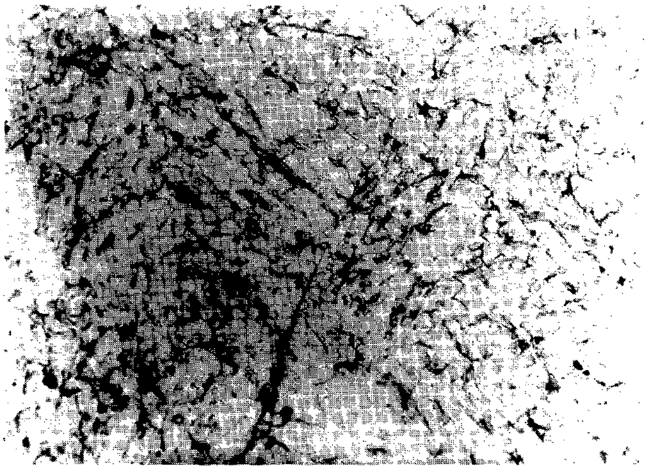

Fig. G3-2—Carbide morphology and distribution in the simulated CGHAZ sample of UT3 (weld energy input 120 kJ/in.), 2500×

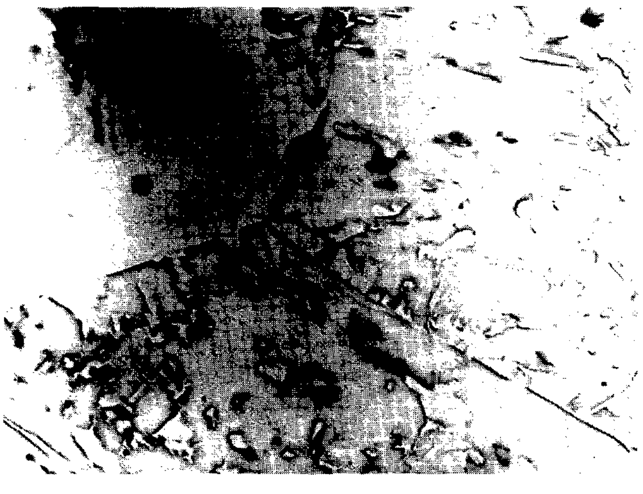

Fig. G3-1—Carbide morphology and distribution in the simulated CGHAZ sample of UT2 (weld energy input 120 kJ/in.), 2500×

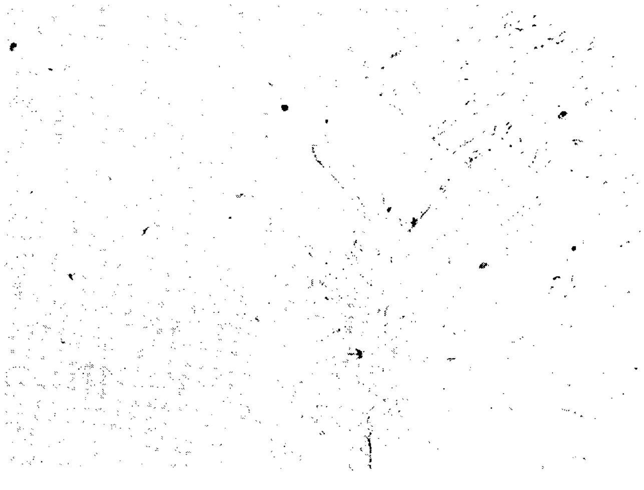

Fig. G3-3—Carbide morphology and distribution in the simulated CGHAZ sample of UT5 (weld energy input 120 kJ/in.), 2500×

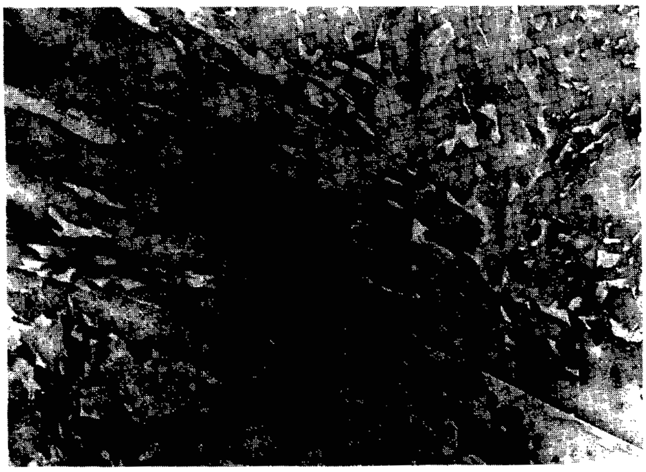

Fig. G3-4—Carbide morphology and distribution in the simulated CGHAZ sample of UT8 (weld energy input 120 kJ/in.), 2500×

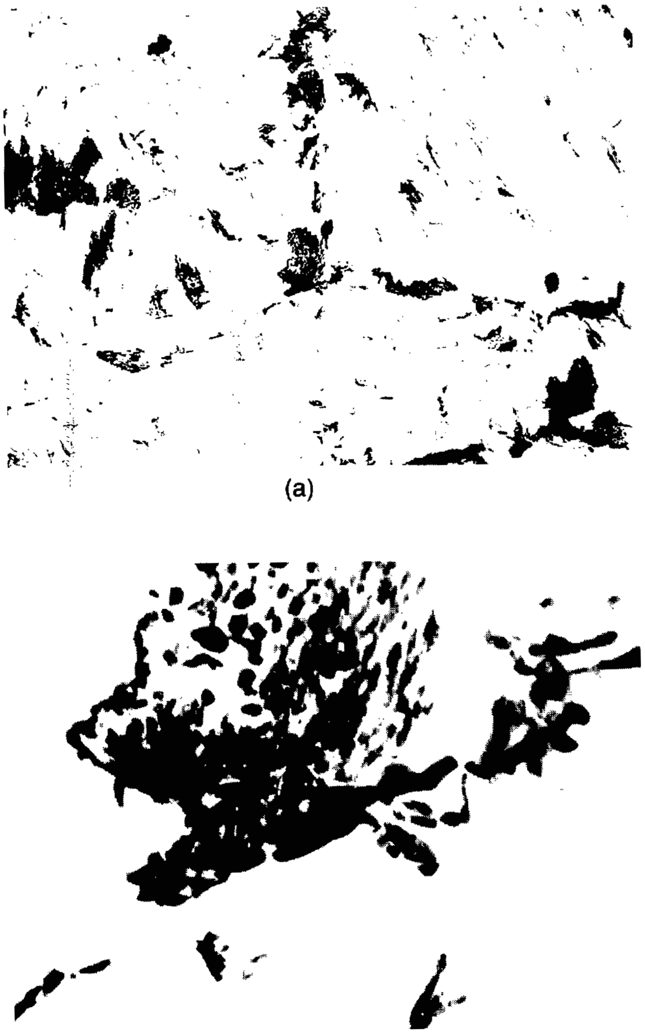

(a)

(b)

Fig. G3-5—Carbide morphology and distribution in the simulated CGHAZ sample heat treated at 1150°F for 15 min of UT2 (weld energy input 120 kJ/in.), (a) 2,500×; (b) 20,000×

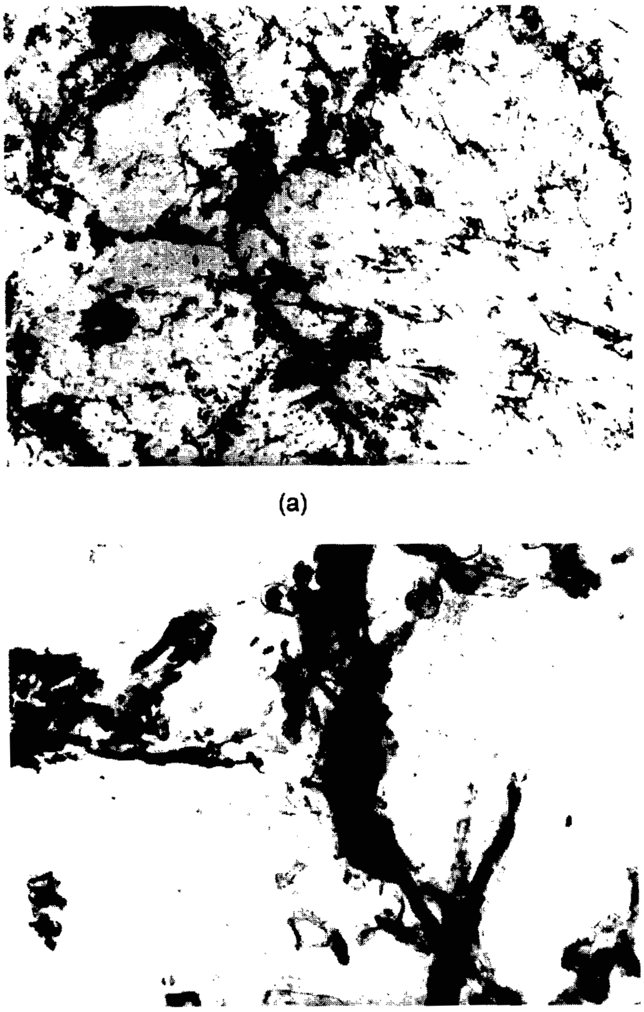

(a)

(b)

Fig. G3-6—Carbide morphology and distribution in the simulated CGHAZ sample heat treated at 1150°F for 15 min of UT3 (weld energy input 120 kJ/in.), (a) 2,500×; (b) 20,000×

Figs. G3-5 to G3-8 show the morphology of carbides and their distribution in the simulated CGHAZs after a PWHT at 1150°F for 15 min. For this PWHT condition, a significant amount of the fine carbides were formed. A slightly greater amount of carbide precipitate was observed in UT3 than in the other materials in the same PWHT condition. An even more important observation is that needle-like carbides (Mo_2C) were found in UT3, UT5 and UT8 with this PWHT condition but not in UT2.

Figs. G3-9 to G3-12 show the morphology of carbides and their distribution in the simulated CGHAZs after a PWHT at 1150°F for 60 min. In general, the amount of carbides in the samples with this PWHT is greater compared to the samples after a PWHT at 1150°F for 15 min. However, UT2 showed a smaller increase compared to the other three materials. Additionally, for the CGHAZ in UT2 after a PWHT at 1150°F for 60 min, the predominant carbides are along the grain boundaries. In general, amount of needle-like carbides decreased in the samples after a PWHT at 1150°F for 60 min compared to samples with a PWHT at 1150 for 15 min.

Figs. G3-13 to G3-16 show the morphology of carbides and their distribution in the simulated CGHAZs after a PWHT at 1250°F for 15 min. For UT2 the size and quantity of carbides in the Gleeble

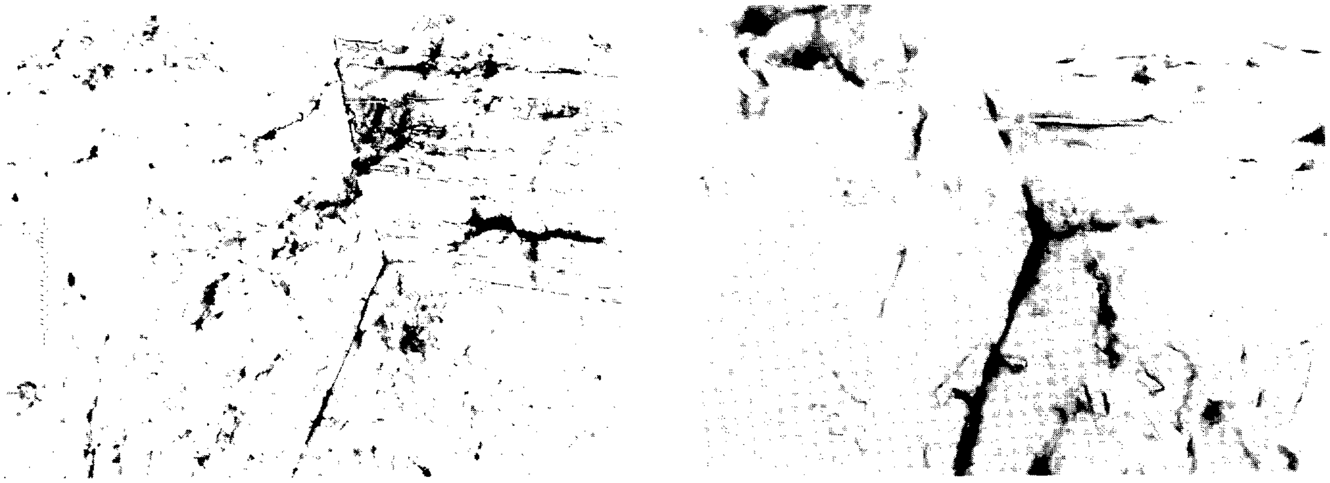

(a) (b)

Fig. G3-7—Carbide morphology and distribution in the simulated CGHAZ sample heat treated at 1150°F for 15 min of UT5 (weld energy input 120 kJ/in.), (a) 2,500×; (b) 10,000×

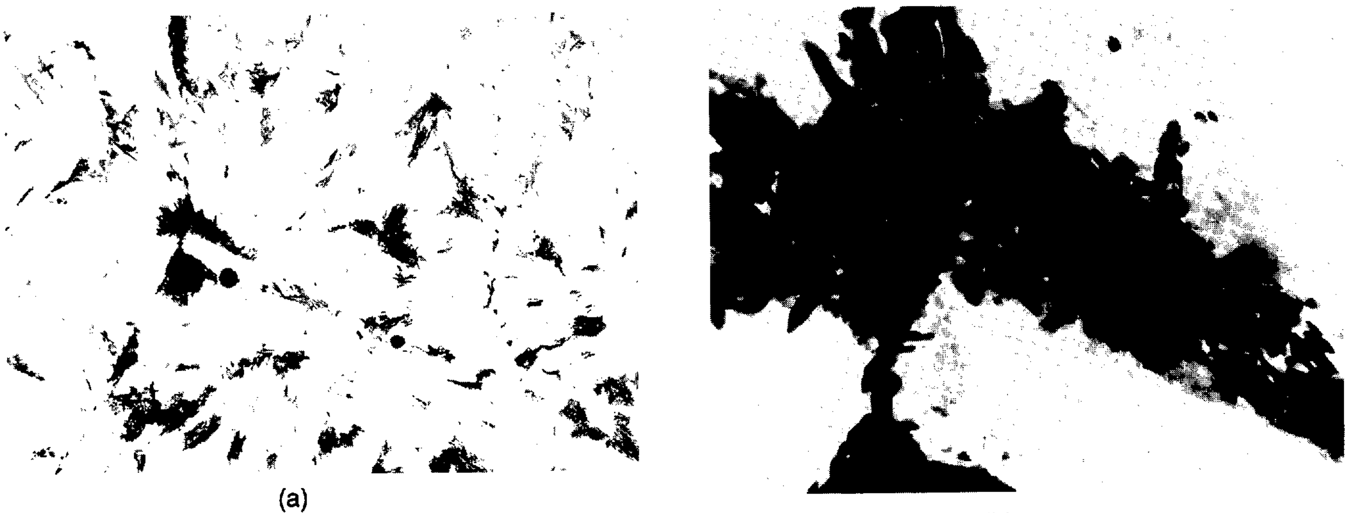

(a) (b)

Fig. G3-8—Carbide morphology and distribution in the simulated CGHAZ sample heat treated at 1150°F for 15 min of UT8 (weld energy input 120 kJ/in.), (a) 2,500×; (b) 20,000×

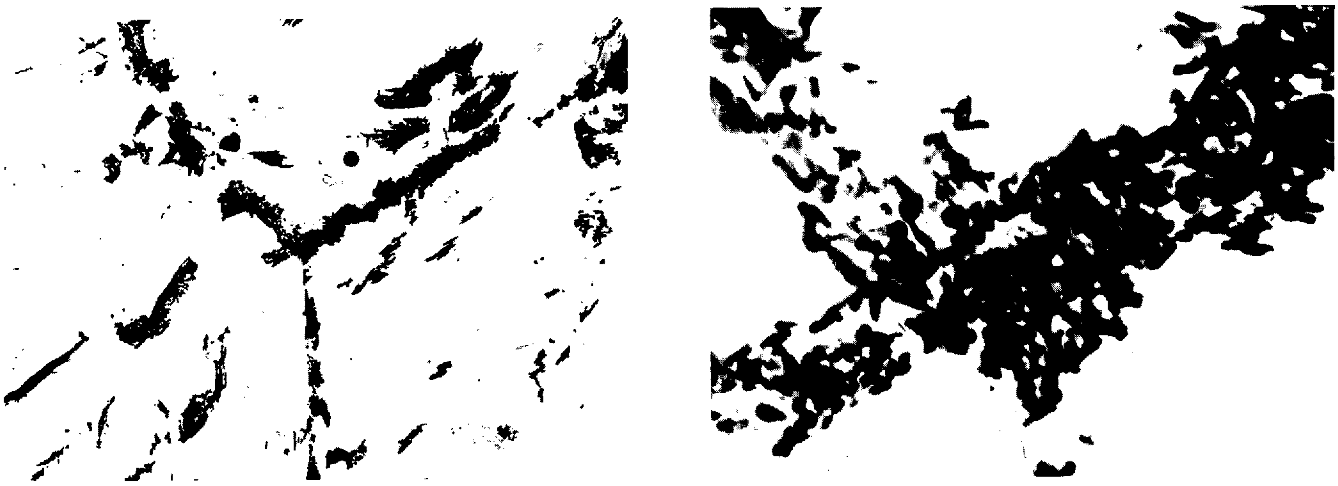

(a) (b)

Fig. G3-9—Carbide morphology and distribution in the simulated CGHAZ sample heat treated at 1150°F for 60 min of UT2 (weld energy input 120 kJ/in.), (a) 2,500×; (b) 20,000×

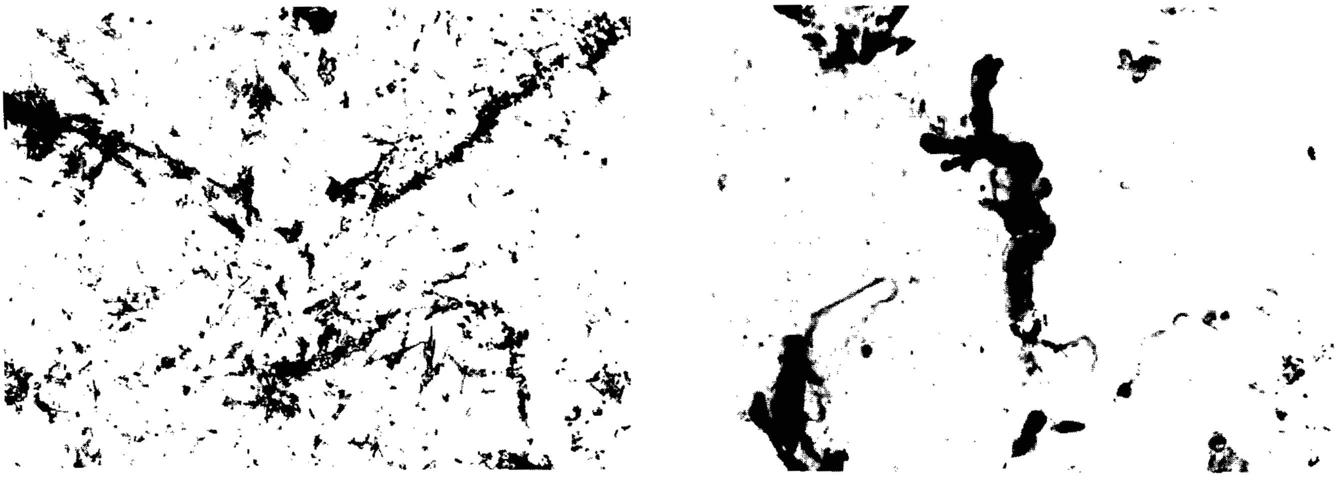

(a)

(b)

Fig. G3-10—Carbide morphology and distribution in the simulated CGHAZ sample heat treated at 1150°F for 60 min of UT3 (weld energy input 120 kJ/in.), (a) 2,500×; (b) 20,000×

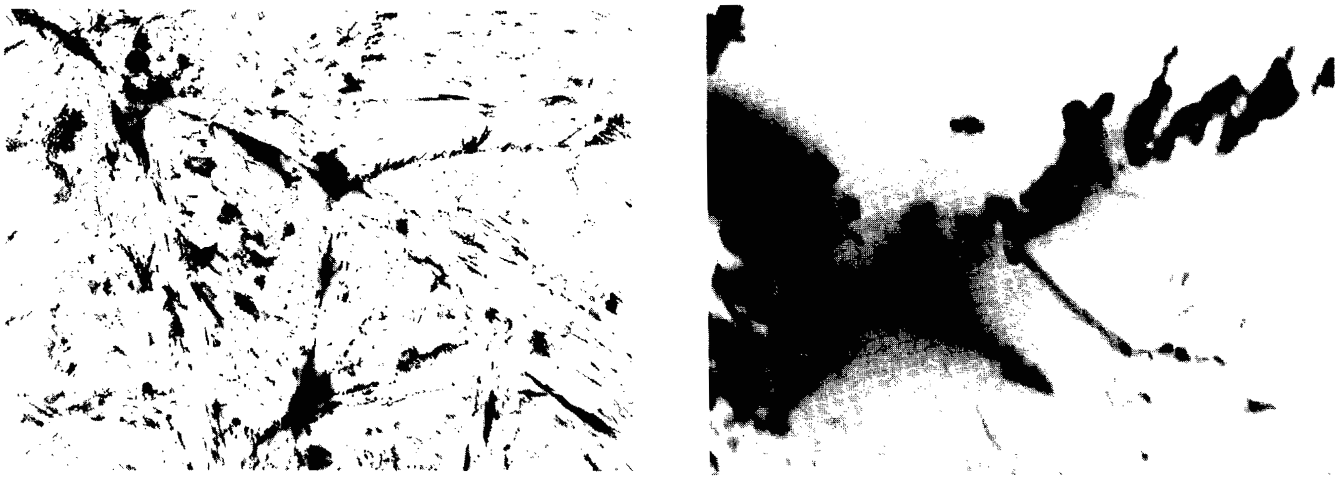

(a)

(b)

Fig. G3-11—Carbide morphology and distribution in the simulated CGHAZ sample heat treated at 1150°F for 60 min of UT5 (weld energy input 120 kJ/in.), (a) 2,500×; (b) 20,000×

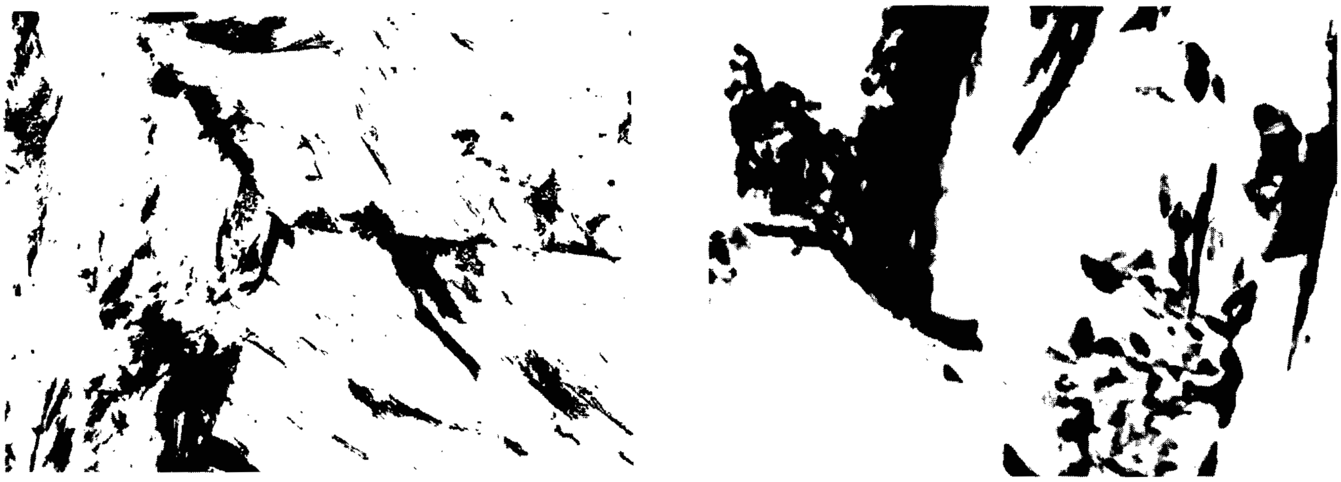

(a)

(b)

Fig. G3-12—Carbide morphology and distribution in the simulated CGHAZ sample heat treated at 1150°F for 60 min of UT8 (weld energy input 120 kJ/in.), (a) 2,500×; (b) 20,000×

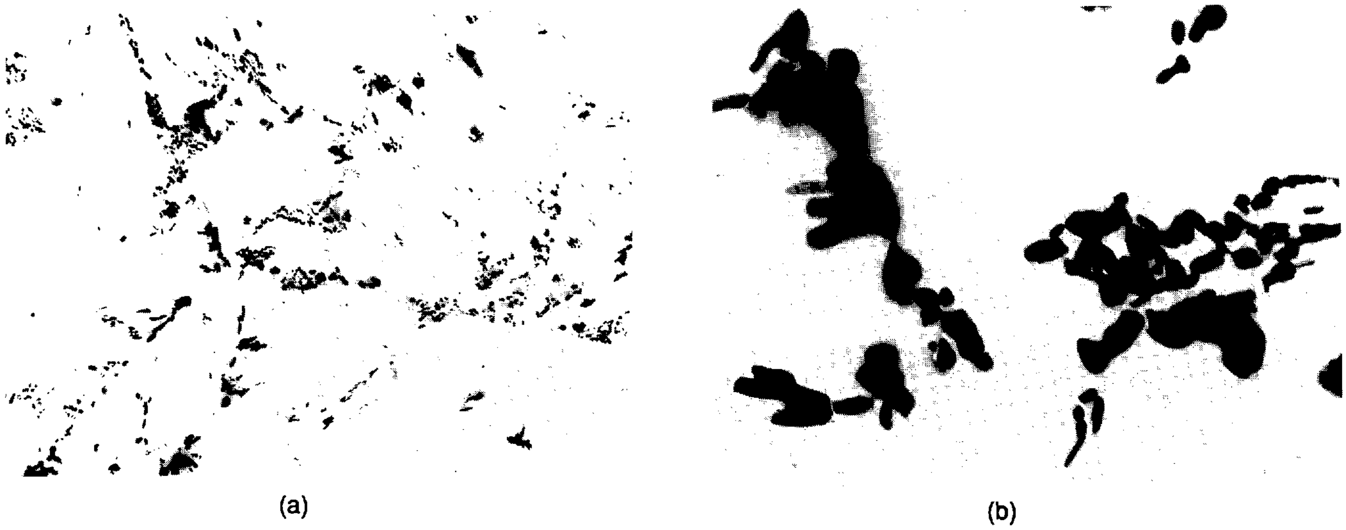

Fig. G3-13—Carbide morphology and distribution in the simulated CGHAZ sample heat treated at 1250°F for 15 min of UT2 (weld energy input 120 kJ/in.)

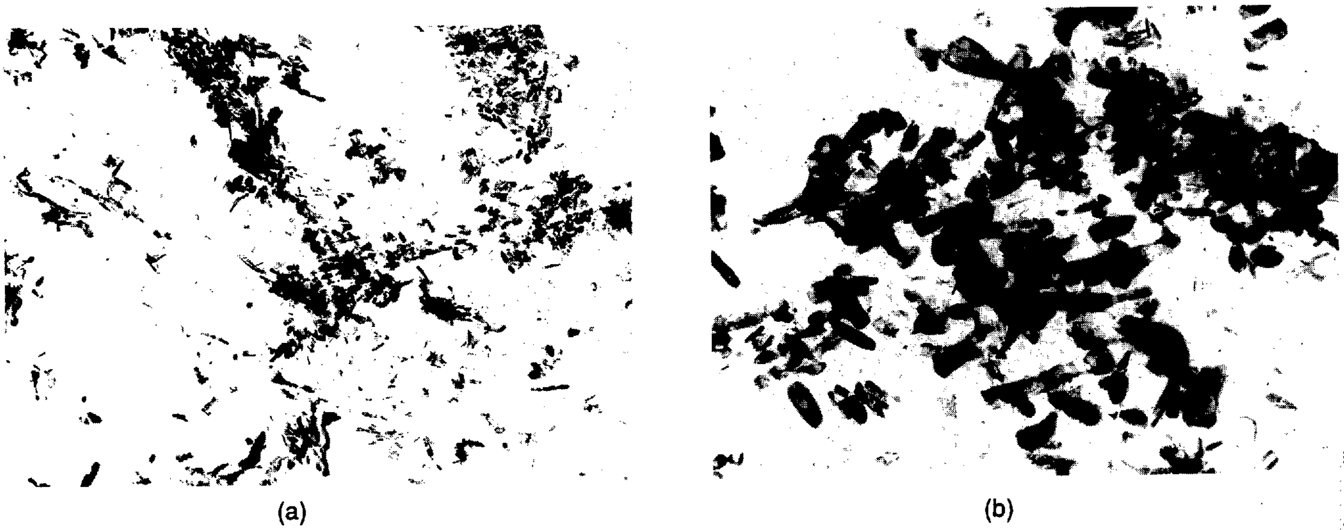

Fig. G3-14—Carbide morphology and distribution in the simulated CGHAZ sample heat treated at 1250°F for 15 min of UT3 (weld energy input 120 kJ/in.)

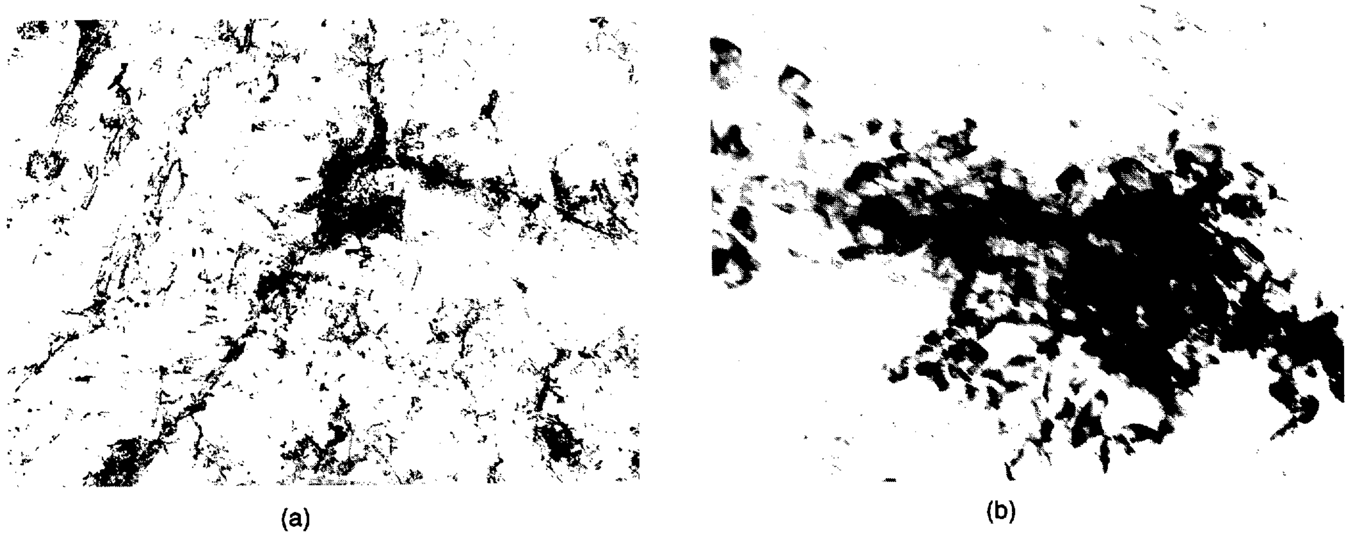

Fig. G3-15—Carbide morphology and distribution in the simulated CGHAZ sample heat treated at 1250°F for 15 min of UT5 (weld energy input 120 kJ/in.), (a) 2,500×; (b) 20,000×

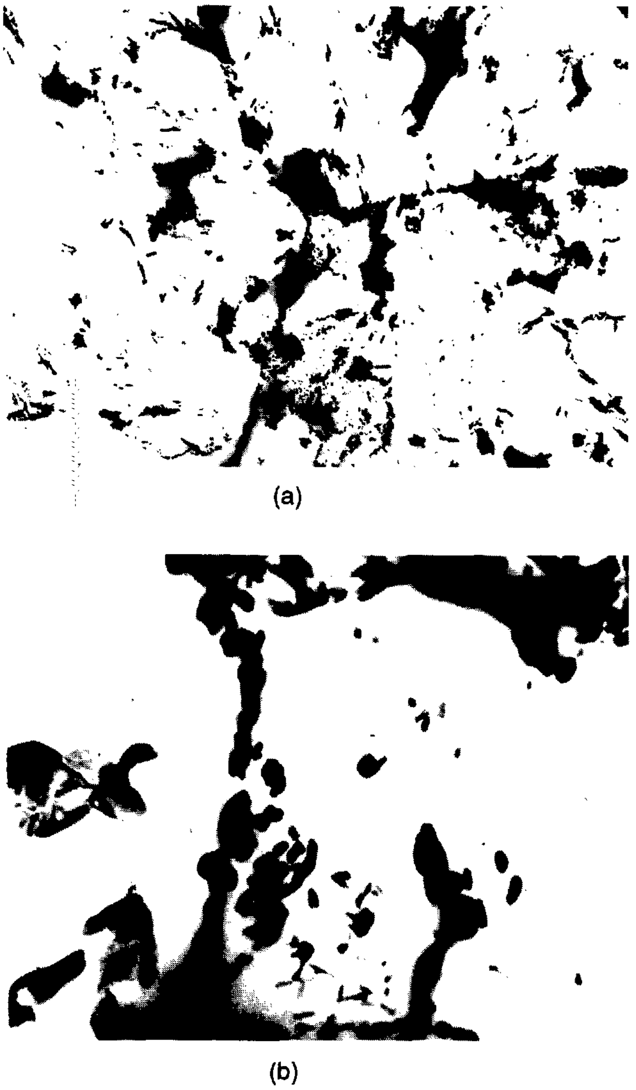

Fig. G3-16—Carbide morphology and distribution in the simulated CGHAZ sample heat treated at 1250°F for 15 min of UT8 (weld energy input 120 kJ/in.), (a) 2,500×; (b) 20,000×

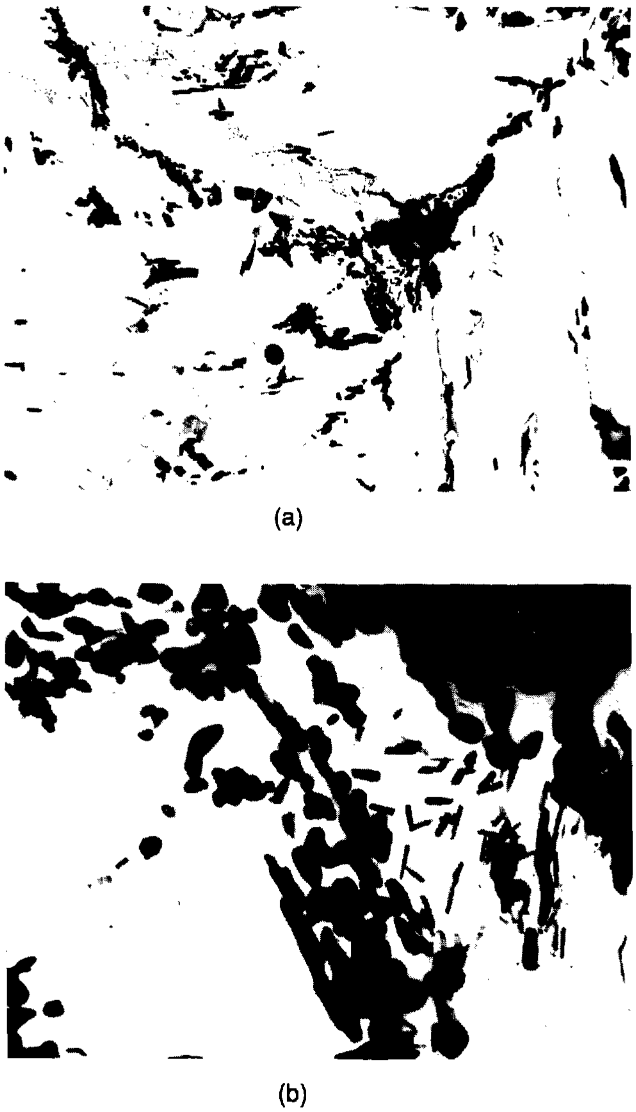

Fig. G3-17—Carbide morphology and distribution in the simulated CGHAZ sample heat treated at 1250°F for 60 min of UT2 (weld energy input 120 kJ/in.), (a) 2,500×; (b) 20,000×

simulated HAZ sample with a PWHT 1250°F for 15 min are similar to those in the sample with a PWHT at 1150°F for 15 min. However for heats UT3, UT5 and UT8 the amount of carbides in the samples after this PWHT is greater than that in the sample with the PWHT at 1150°F for 15 min.

Figs. G3-17 to G3-20 show the morphology of carbides and their distribution in the simulated CGHAZs after a PWHT at 1250°F for 60 min. On this PWHT condition, the size and quantity of carbides is significantly increased and the needle-like carbides are clearly observed. For heats UT3, UT5 and UT8 there was no significant increase in terms of the amount of precipitation after this PWHT compared to that with a PWHT at 1250°F for 15 min. However, the size of the carbides increased remarkably compared to that in the same material with a lower tempering parameter.

Figs. G3-21 to G3-24 show the morphologies of carbides and their distribution in the simulated CGHAZs after a PWHT at 1350°F for 8 hours. Although no significant increase in terms of the amount of carbide precipitation was found, the size of the carbides (such as rod-like, irregular and spherical) was significantly greater for all materials.

CGHAZ Samples Simulated with a Weld Energy Input of 12 kJ/in. A summary of carbide precipitation behavior including type, size, quantity and distribution in the Gleeble simulated CGHAZ samples with a weld energy input of 12 kJ/in. and different PWHT is documented in the lower portion of Tables G3-1 to G3-4 shown previously. In general, the carbide precipitation evolution behavior in the samples with a weld energy input of 12 kJ/in. are similar to those in the samples with weld energy input of 120 kJ/in. In general, it was observed that slightly enhanced carbide precipitation was found for the CGHAZ samples with weld energy input of 12 kJ/in. compared to that in the samples with weld energy input of 120 kJ/in.

Figs. G3-25 to G3-28 show the morphology of carbides and their distribution in the as-simulated

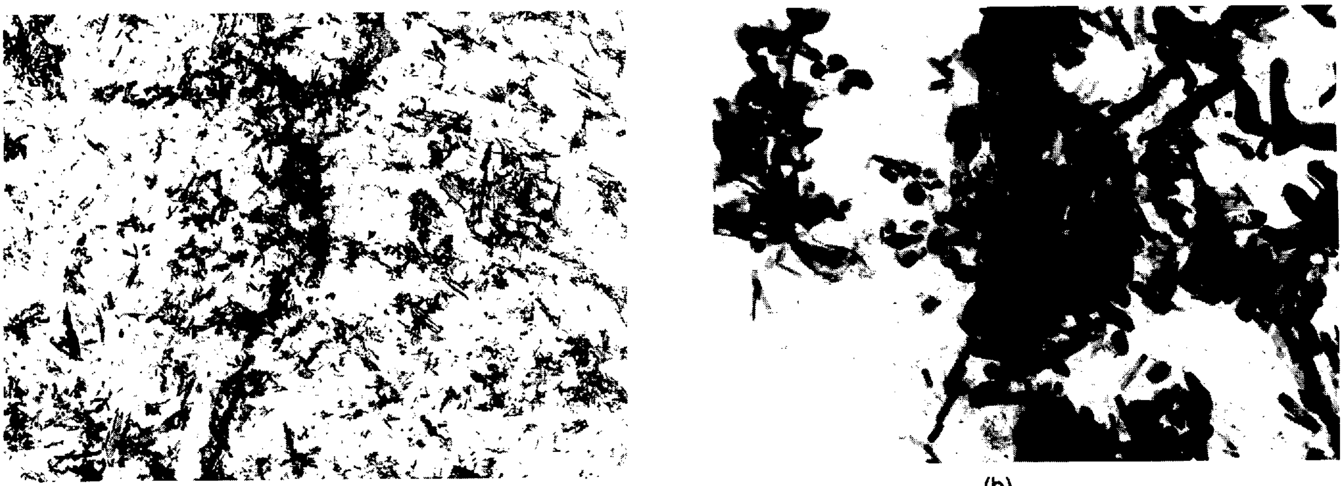

(a)

(b)

Fig. G3-18—Carbide morphology and distribution in the simulated CGHAZ sample heat treated at 1250°F for 60 min of UT3 (weld energy input 120 kJ/in.), (a) 2,500×; (b) 20,000×

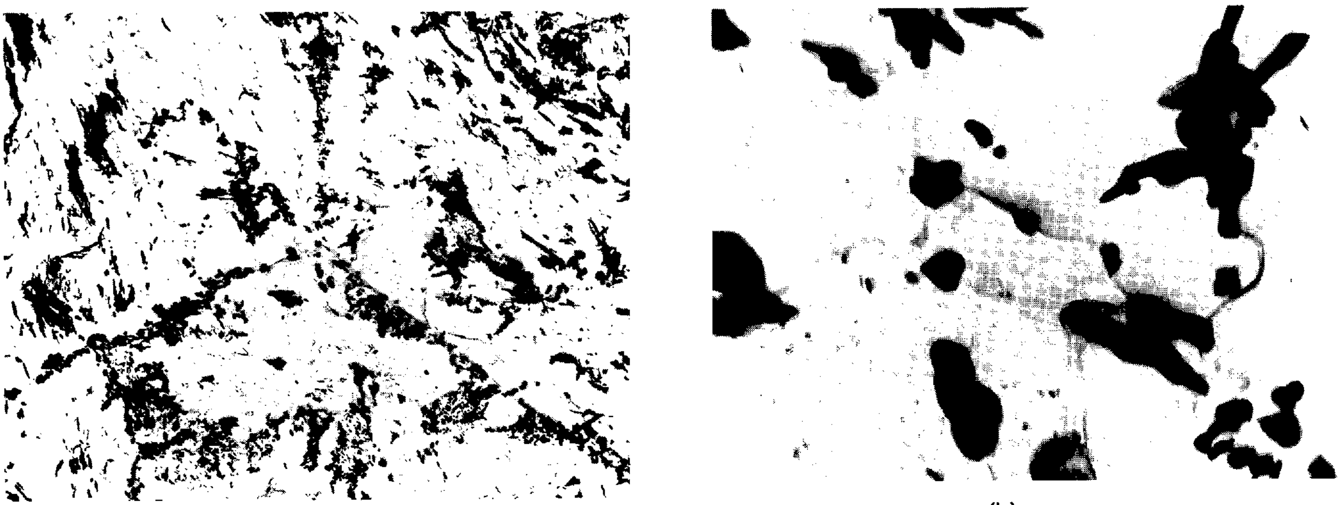

(a)

(b)

Fig. G3-19—Carbide morphology and distribution in the simulated CGHAZ sample heat treated at 1250°F for 60 min of UT5 (weld energy input 120 kJ/in.), (a) 2,500×; (b) 20,000×

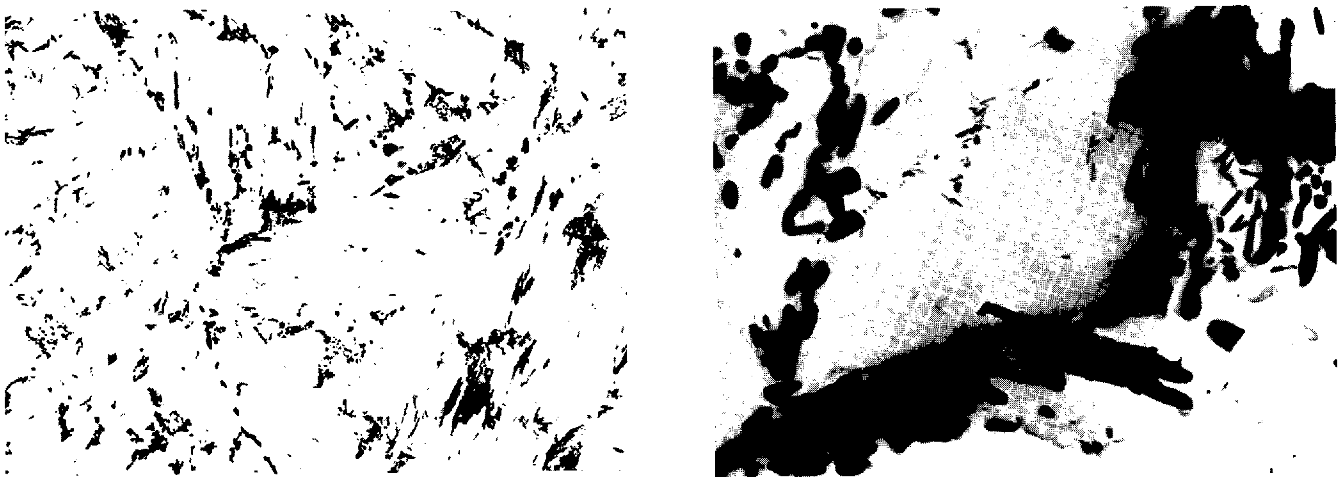

(a)

(b)

Fig. G3-20—Carbide morphology and distribution in the simulated CGHAZ sample heat treated at 1250°F for 60 min of UT8 (weld energy input 120 kJ/in.), (a) 2,500×; (b) 20,000×

Fig. G3-21—Carbide morphology and distribution in the simulated CGHAZ sample heat treated at 1350°F for 8 hours of UT2 (weld energy input 120 kJ/in.), (a) 2,500×; (b) 20,000×

Fig. G3-22—Carbide morphology and distribution in the simulated CGHAZ sample heat treated at 1350°F for 8 hours of UT3 (weld energy input 120 kJ/in.), (a) 2,500×; (b) 20,000×

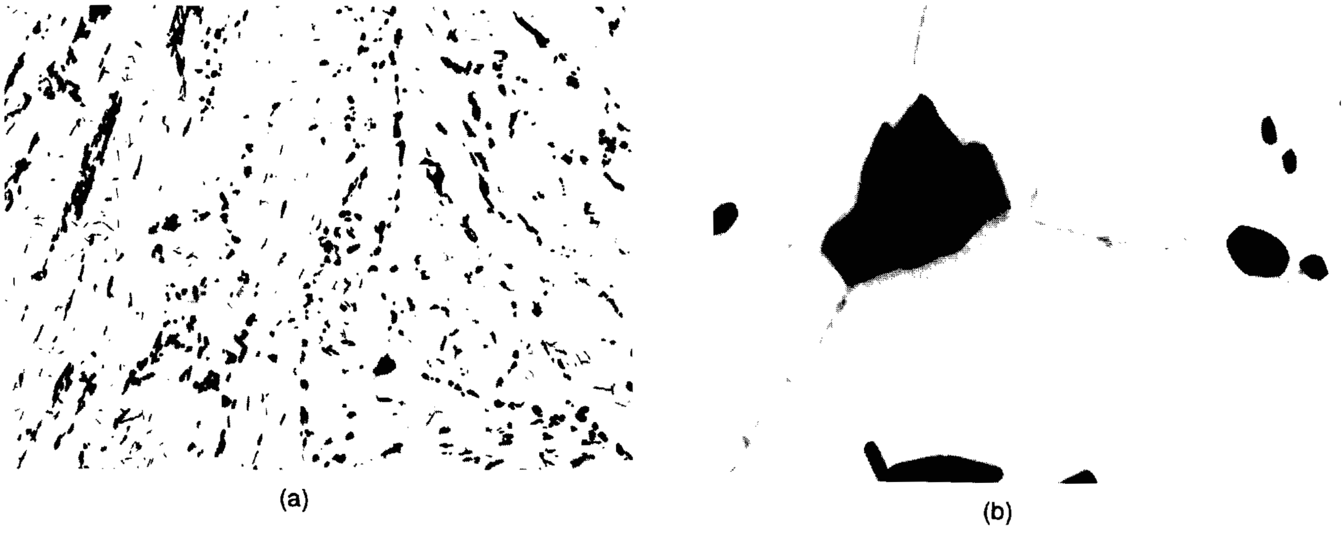

Fig. G3-23—Carbide morphology and distribution in the simulated CGHAZ sample heat treated at 1350°F for 8 hours of UT5 (weld energy input 120 kJ/in.), (a) 2,500×; (b) 20,000×

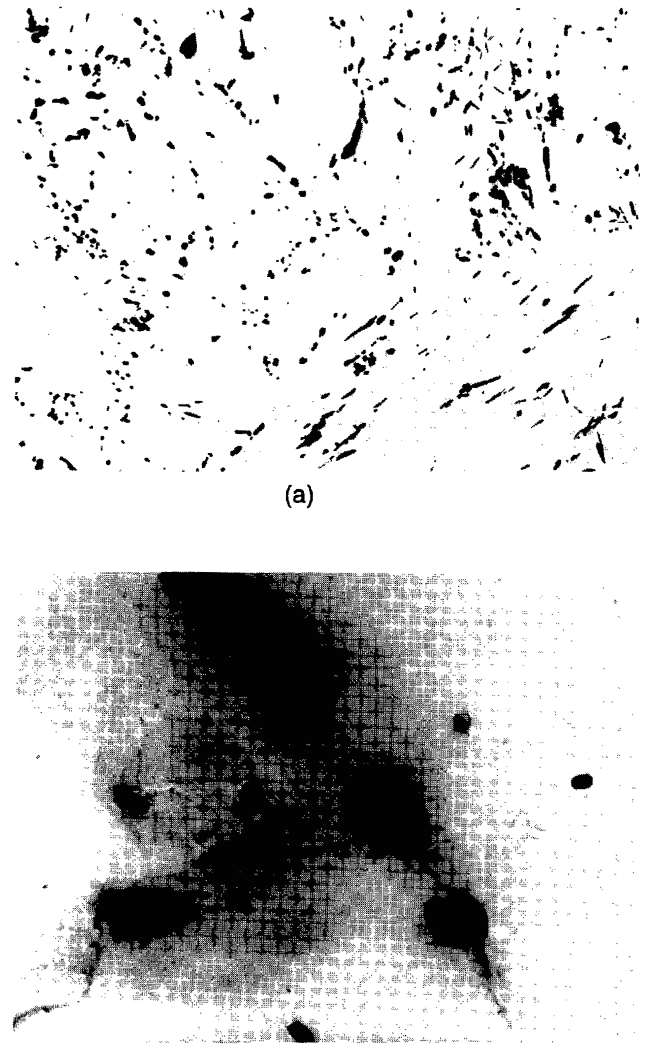
(a)

(b)

Fig. G3-24—Carbide morphology and distribution in the simulated CGHAZ sample heat treated at 1350°F for 8 hours of UT8 (weld energy input 120 kJ/in.), (a) 2,500×; (b) 20,000×

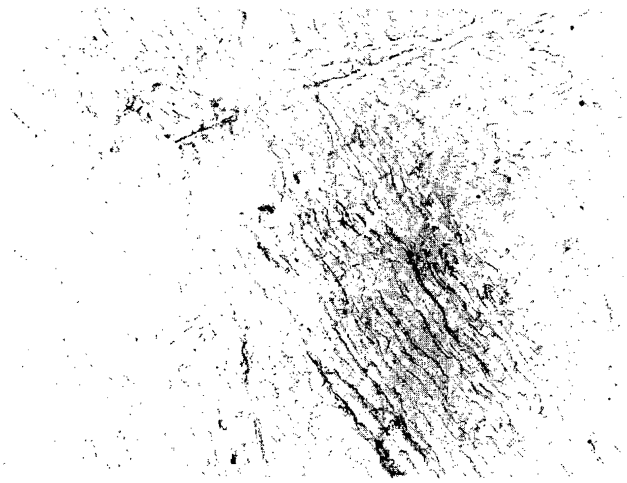

Fig. G3-25—Carbide morphology and distribution in the assimulated CGHAZ sample of UT2 (weld energy input 12 kJ/in.), 2500×

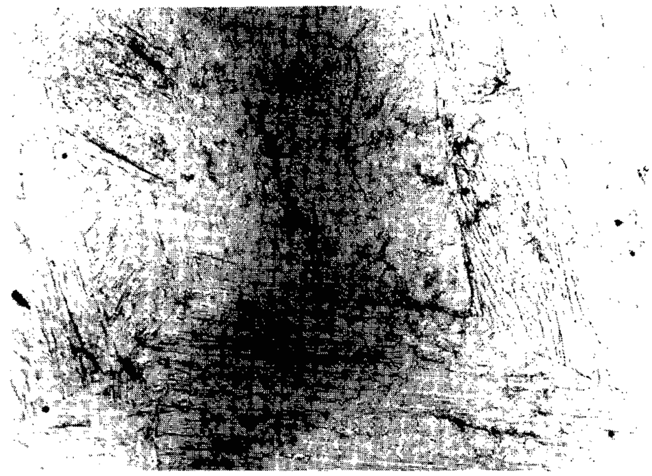

Fig. G3-26—Carbide morphology and distribution in the assimulated CGHAZ sample of UT3 (weld energy input 12 kJ/in.), 2500×

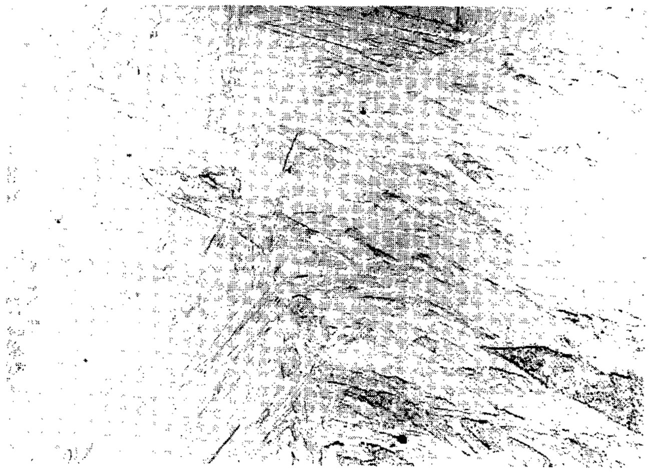

Fig. G3-27—Carbide morphology and distribution in the assimulated CGHAZ sample of UT5 (weld energy input 12 kJ/in.), 2500×

Fig. G3-28—Carbide morphology and distribution in the assimulated CGHAZ sample of UT8 (weld energy in put 12 kJ/in.), 2500×

CGHAZ samples. It is clear that the dominant carbides in the CGHAZ samples were dissolved into the matrix during the weld thermal simulation. However, some fine carbides remained along the grain boundaries or lath martensite boundaries. The above observation is true for all the heats with this energy input.

Figs. G3-29 to G3-32 show the morphology of carbides and their distribution in the CGHAZ samples after a PWHT of 1150°F for 15 min. With this PWHT, a significant amount of carbide precipitates were observed for all heats. The amount of carbide precipitation in UT2 is approximately at the same level as the other three heats. However, the carbide distribution in these materials is different. The carbides in heat UT2 showed an aggregate morphology and they were distributed along the prior austenite grain boundaries and lath martensite boundaries. In heat UT3, a significant fraction of the carbides was distributed within the grain matrix, although intergraular carbides were still dominant. For heat UT5 and UT8 the carbide distribution morphology is intermediate between UT2 and UT3.

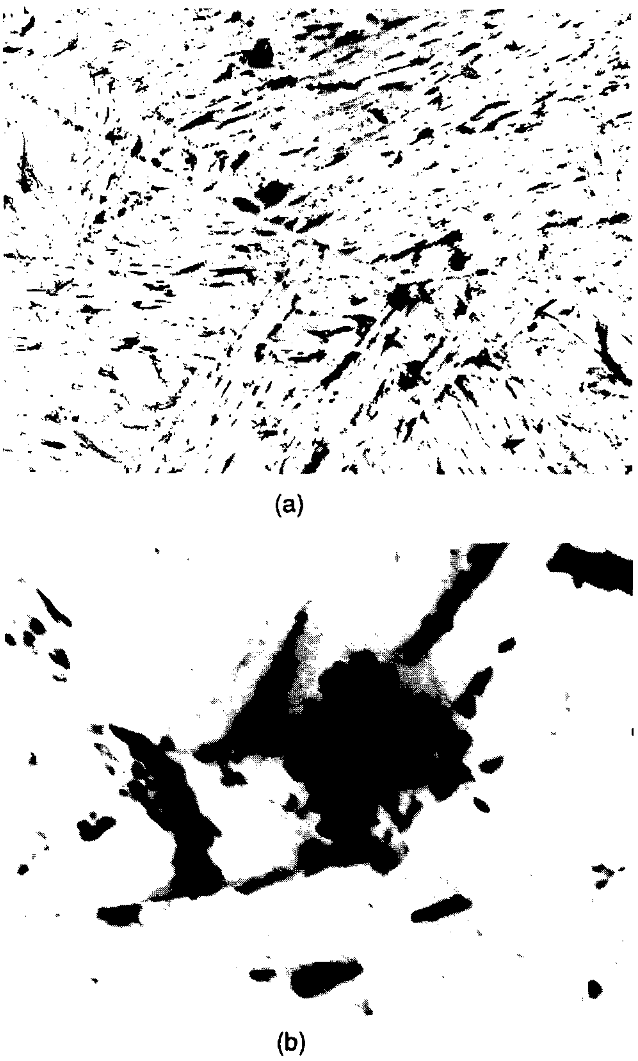
(a)

(b)

Fig. G3-29—Carbide morphology and distribution in the simulated CGHAZ sample heat treated at 1150°F for 15 min of UT2 (weld energy input 12 kJ/in.), (a) 2,500×; (b) 20,000×

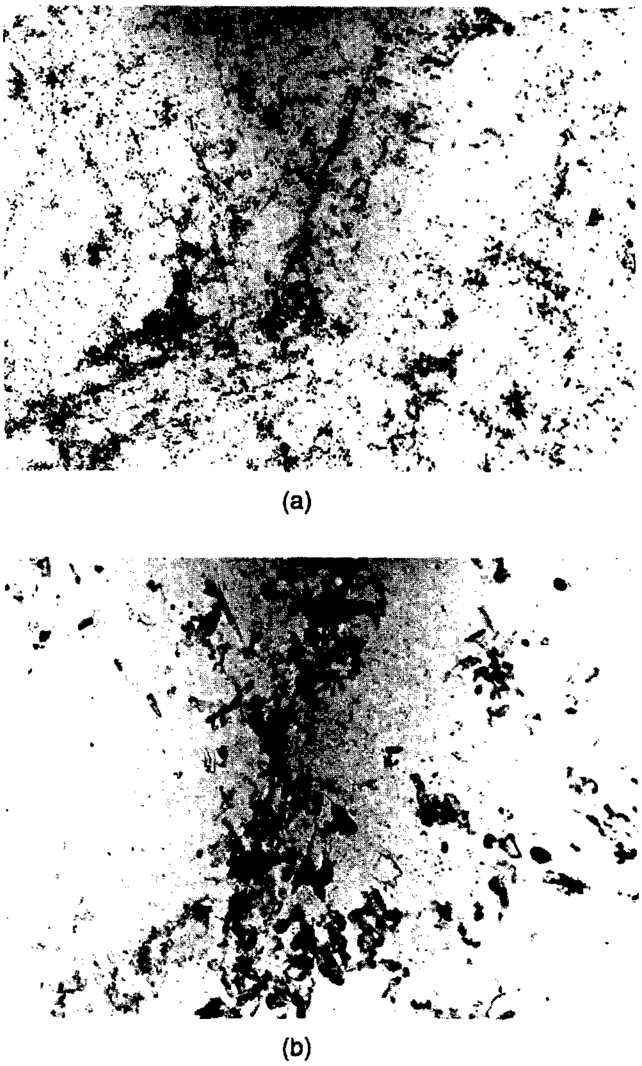
(a)

(b)

Fig. G3-30—Carbide morphology and distribution in the simulated CGHAZ sample heat treated at 1150°F for 15 min of UT3 (weld energy input 12 kJ/in.), (a) 2,500×; (b) 20,000×

Figs. G3-33 to G3-36 show the morphology of carbides and their distribution in the Gleeble simulated CGHAZs after a PWHT of 1150°F for 60 min. The amount of carbides increased for all four materials. The carbide distribution in the samples with a PWHT of 1150°F for 60 min is similar to that in the samples with a PWHT of 1150°F for 15 min.

Figs. G3-37 to G3-40 show the morphologies of carbides and their distribution in the Gleeble simulated CGHAZs after a PWHT of 1250°F for 15 min. The size and quantity of carbides in these samples is similar to that in the samples with a PWHT of 1150°F for 60 min.

Figs. G3-41 to G3-44 show the morphology of carbides and their distribution in the Gleeble simulated CGHAZs after a PWHT of 1250°F for 60 min. In general, the amount of carbides in this group of samples is similar to those with a PWHT of 1200°F for 15 min. However, the size of the carbides increased in the samples simulated with a PWHT of 1250°F for 60 min.

Figs. G3-45 to G3-48 show the morphology of

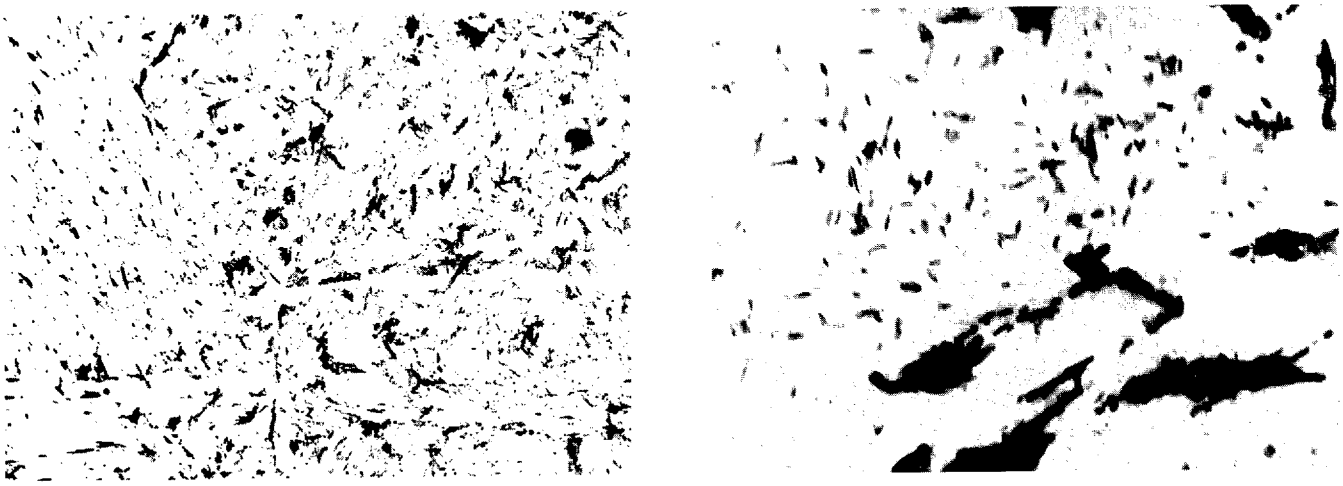
(a) (b)

Fig. G3-31—Carbide morphology and distribution in the simulated CGHAZ sample heat treated at 1150°F for 15 min of UT5 (weld energy input 12 kJ/in.), (a) 2,500×; (b) 20,000×

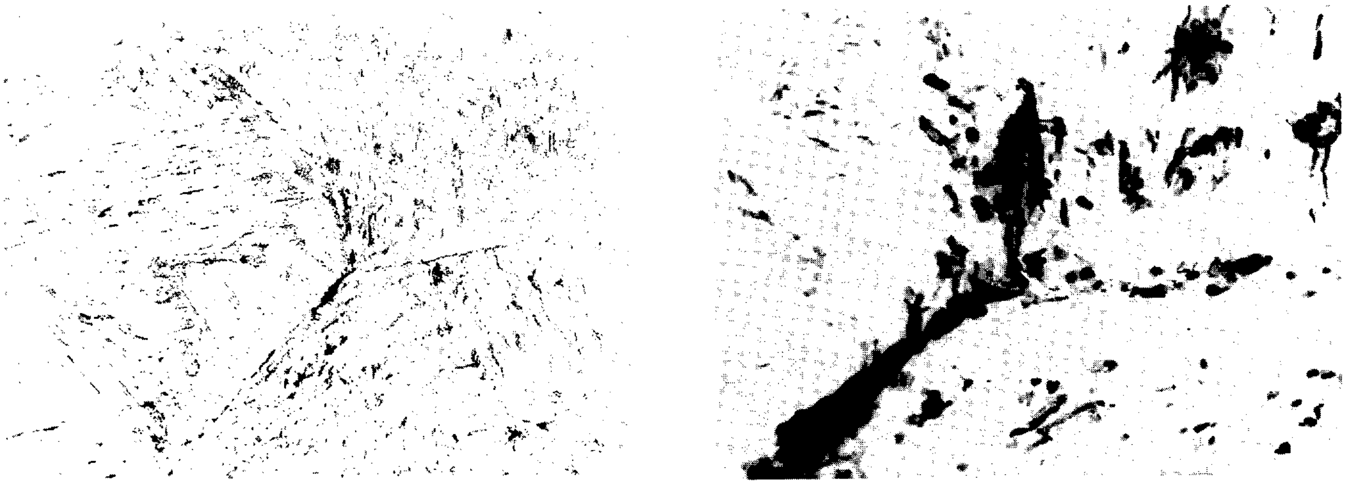
(a) (b)

Fig. G3-32—Carbide morphology and distribution in the simulated CGHAZ sample heat treated at 1150°F for 15 min of UT8 (weld energy input 12 kJ/in.), (a) 2,500×; (b) 20,000×

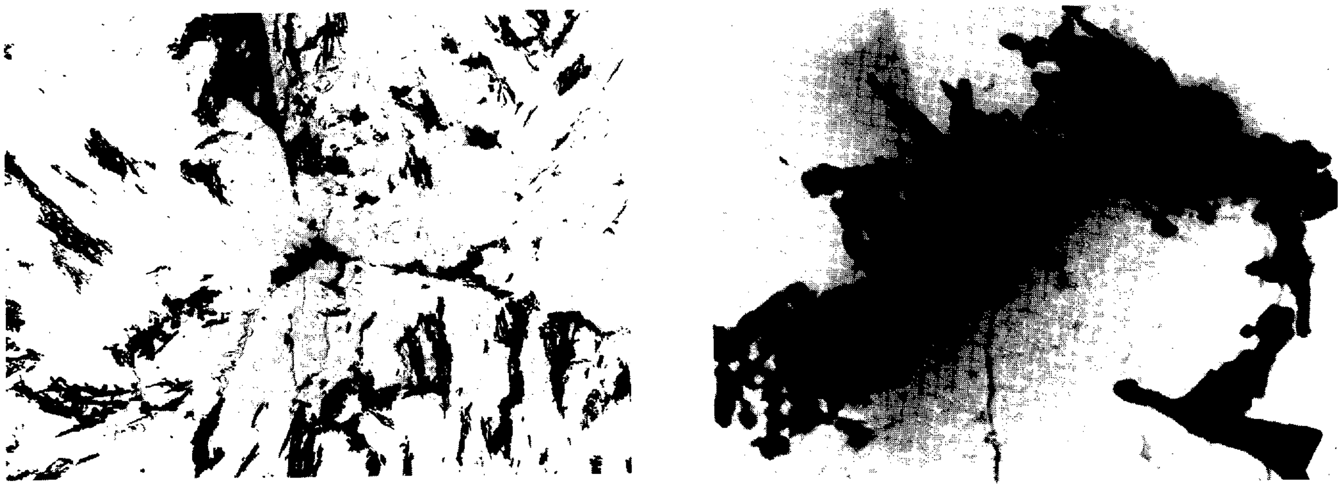
(a) (b)

Fig. G3-33—Carbide morphology and distribution in the simulated CGHAZ sample heat treated at 1150°F for 60 min of UT2 (weld energy input 12 kJ/in.), (a) 2,500×; (b) 20,000×

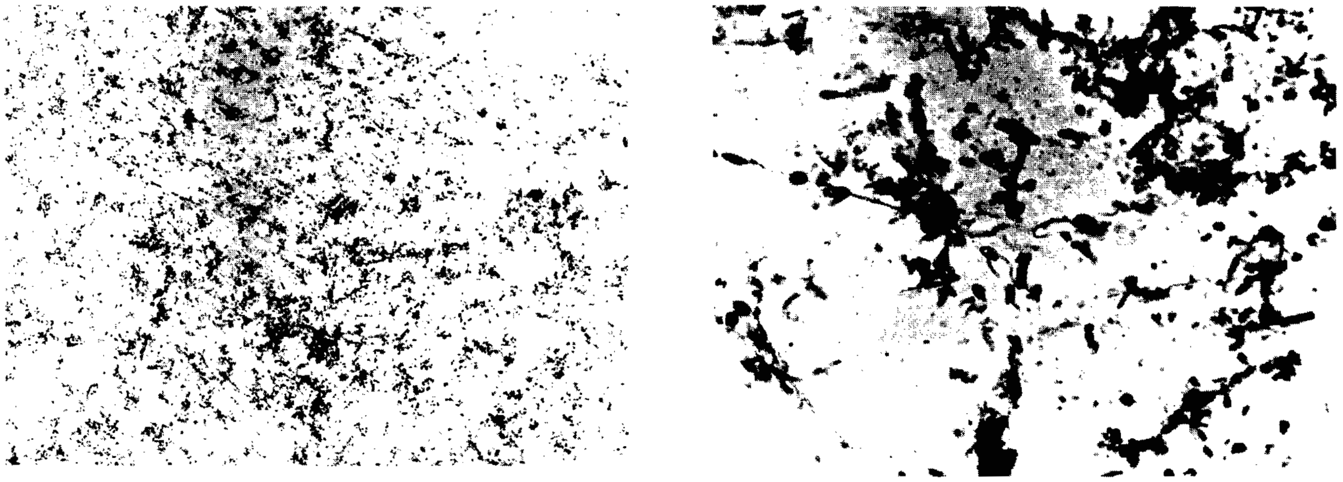

(a) (b)

Fig. G3-34—Carbide morphology and distribution in the simulated CGHAZ sample heat treated at 1150°F for 60 min of UT3 (weld energy input 12 kJ/in.), (a) 2,500×; (b) 20,000×

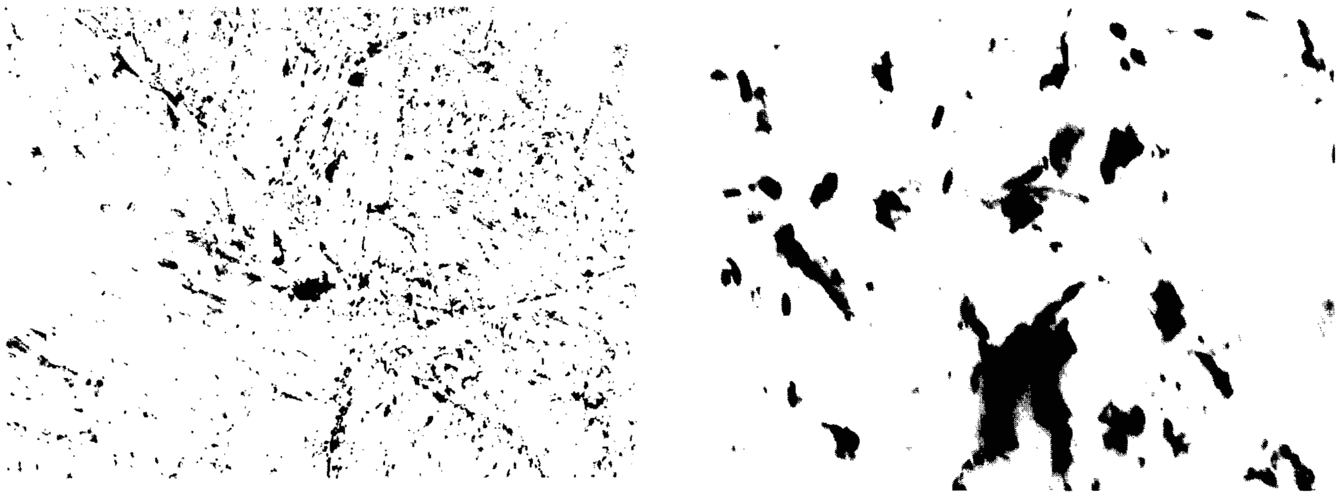

(a) (b)

Fig. G3-35—Carbide morphology and distribution in the simulated CGHAZ sample heat treated at 1150°F for 60 min of UT5 (weld energy input 12 kJ/in.), (a) 2,500×; (b) 20,000×

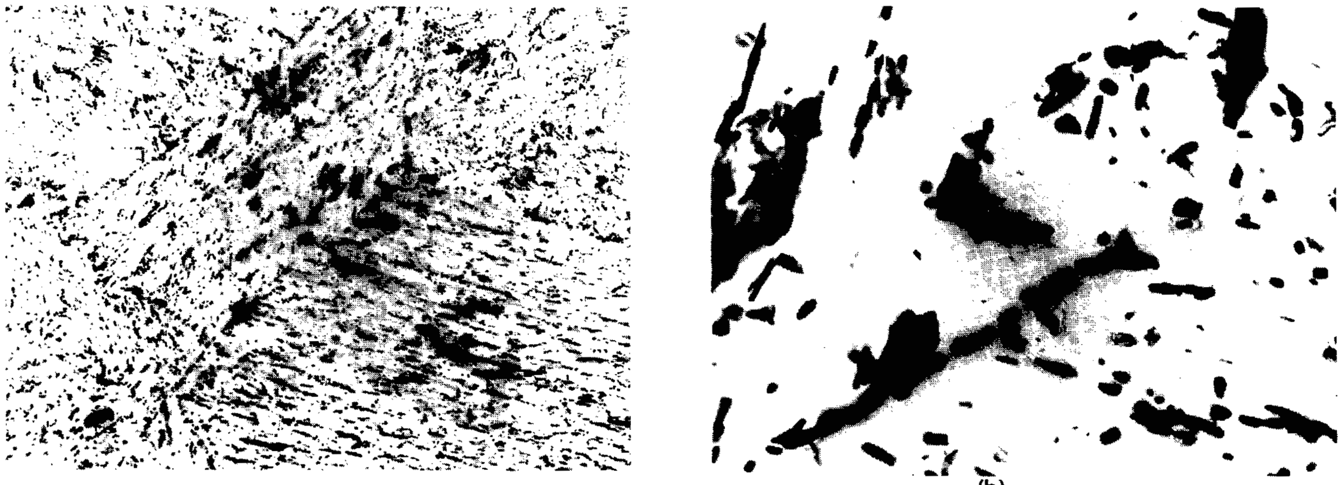

(a) (b)

Fig. G3-36—Carbide morphology and distribution in the simulated CGHAZ sample heat treated at 1150°F for 60 min of UT8 (weld energy input 12 kJ/in.), (a) 2,500×; (b) 20,000×

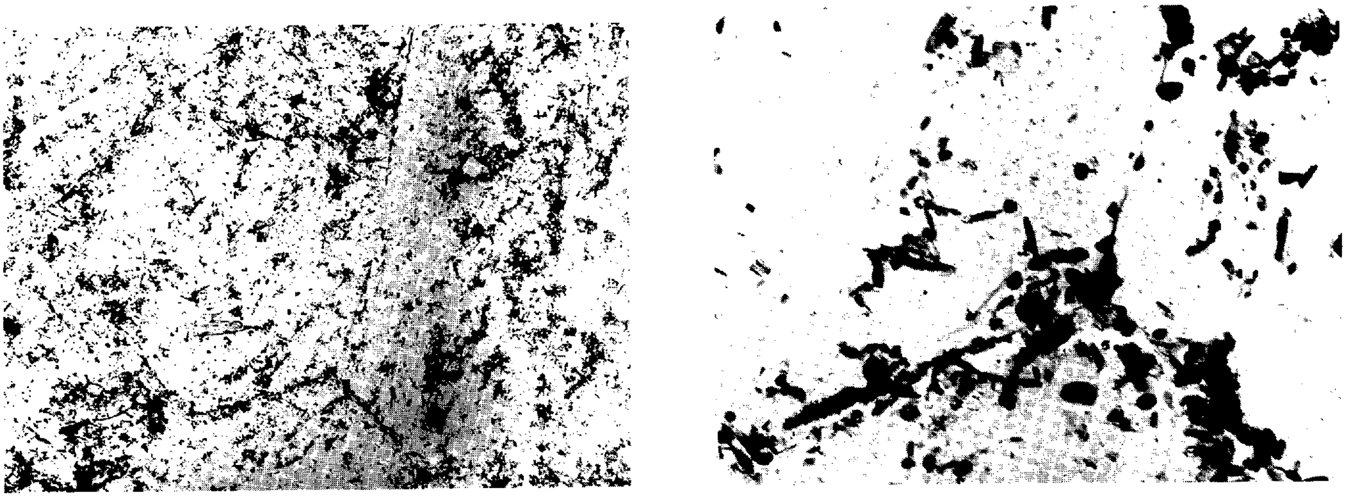

(a) (b)

Fig. G3-37—Carbide morphology and distribution in the simulated CGHAZ sample heat treated at 1250°F for 15 min of UT2 (weld energy input 12 kJ/in.), (a) 2,500×; (b) 20,000×

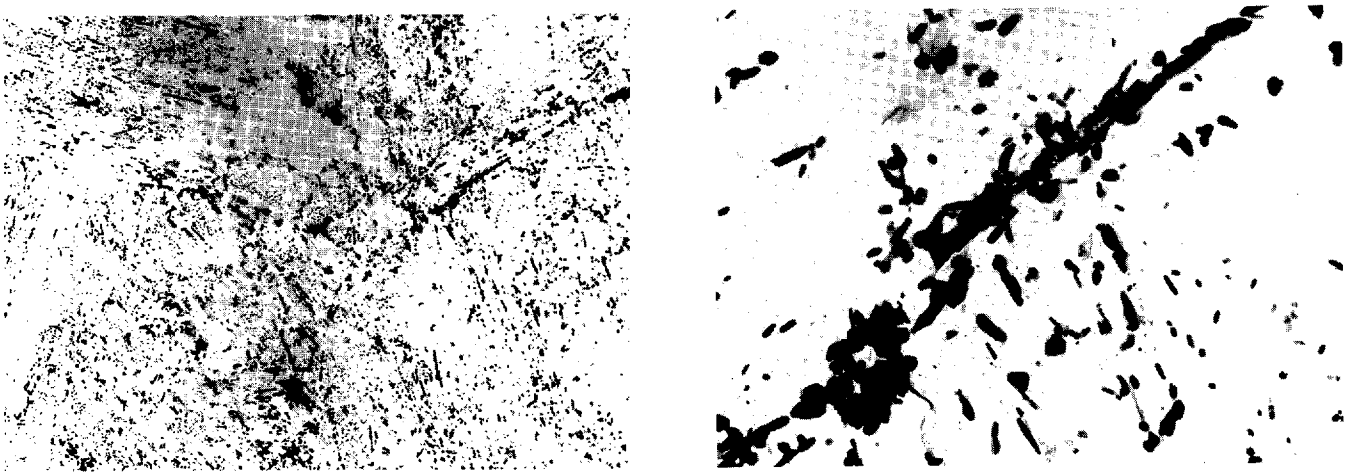

(a) (b)

Fig. G3-38—Carbide morphology and distribution in the simulated CGHAZ sample heat treated at 1250°F for 15 min of UT3 (weld energy input 12 kJ/in.), (a) 2,500×; (b) 20,000×

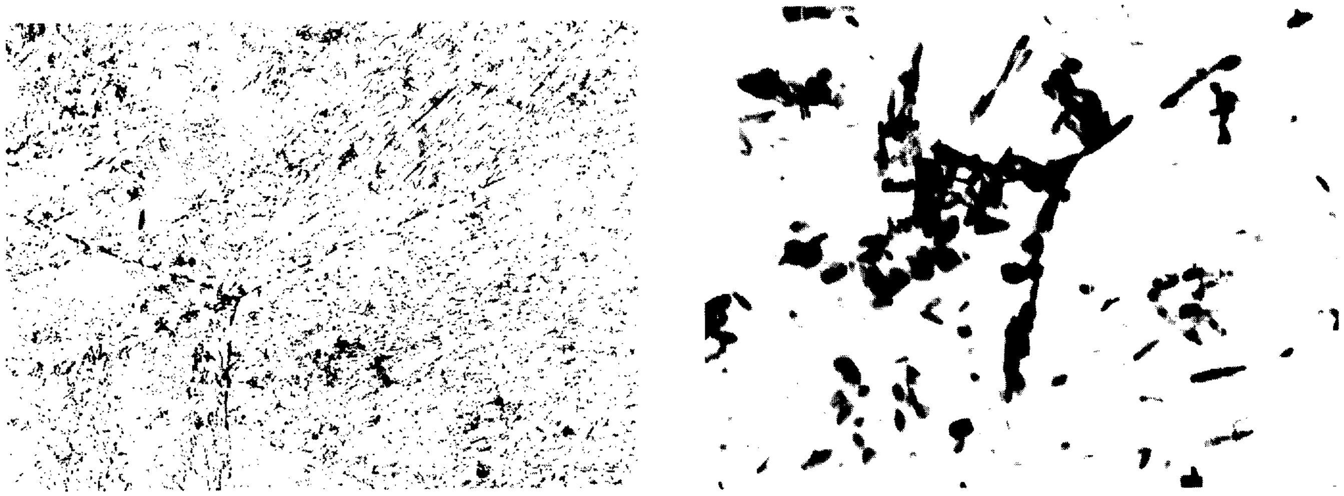

(a) (b)

Fig. G3-39—Carbide morphology and distribution in the simulated CGHAZ sample heat treated at 1250°F for 15 min of UT5 (weld energy input 12 kJ/in.), (a) 2,500×; (b) 20,000×

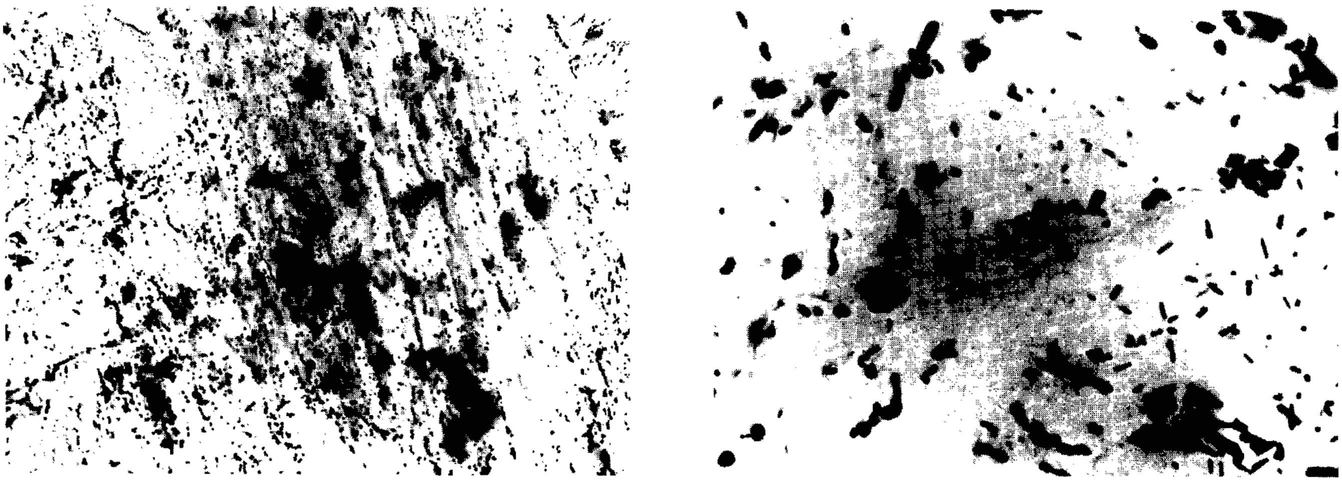

(a) (b)

Fig. G3-40—Carbide morphology and distribution in the simulated CGHAZ sample heat treated at 1250°F for 15 min of UT8 (weld energy input 12 kJ/in.), (a) 2,500×; (b) 20,000×

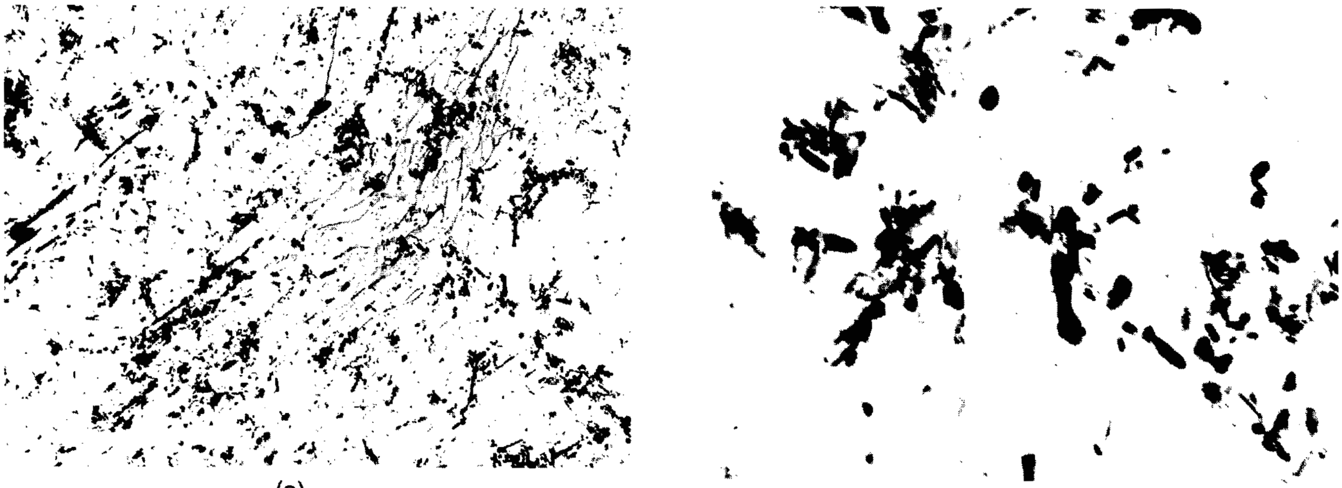

(a) (b)

Fig. G3-41—Carbide morphology and distribution in the simulated CGHAZ sample heat treated at 1250°F for 60 min of UT2 (weld energy input 12 kJ/in.), (a) 5,000×; (b) 20,000×

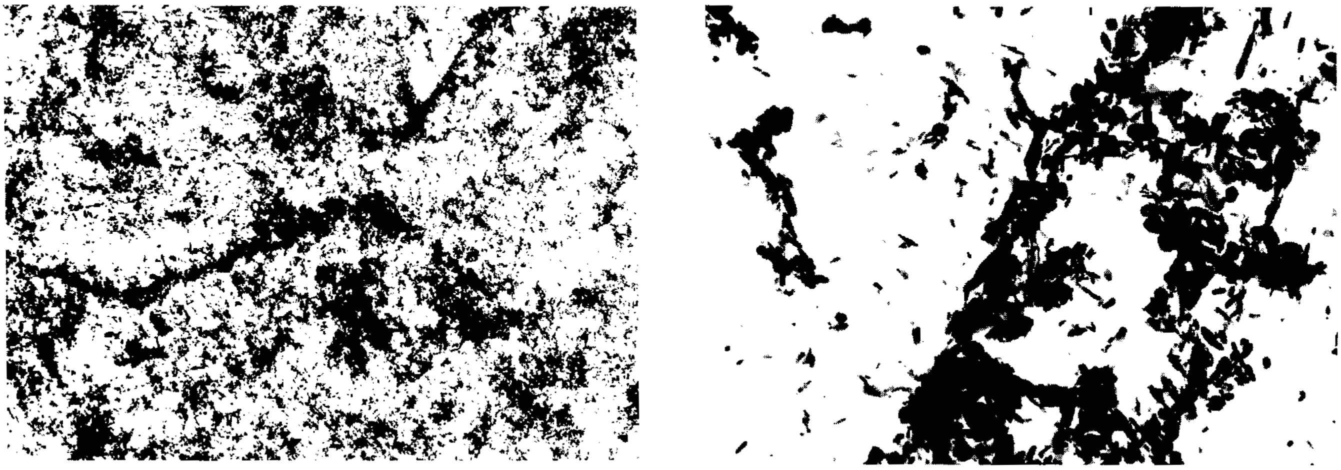

(a) (b)

Fig. G3-42—Carbide morphology and distribution in the simulated CGHAZ sample heat treated at 1250°F for 60 min of UT3 (weld energy input 12 kJ/in.), (a) 2,500×; (b) 20,000×

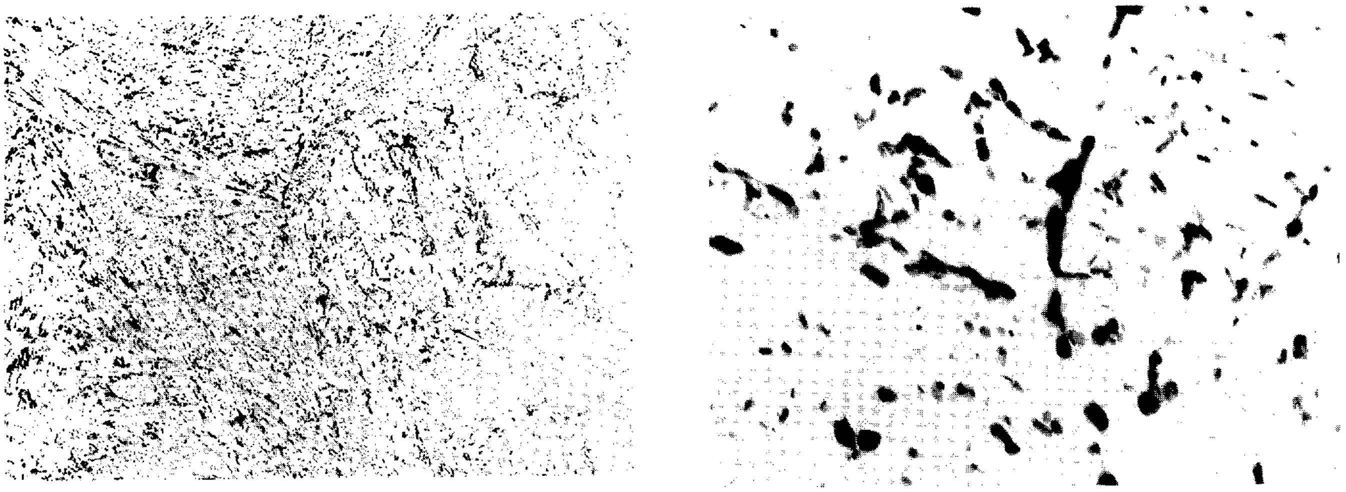
(a) (b)

Fig. G3-43—Carbide morphology and distribution in the simulated CGHAZ sample heat treated at 1250°F for 60 min of UT5 (weld energy input 12 kJ/in.), (a) 2,500×; (b) 20,000×

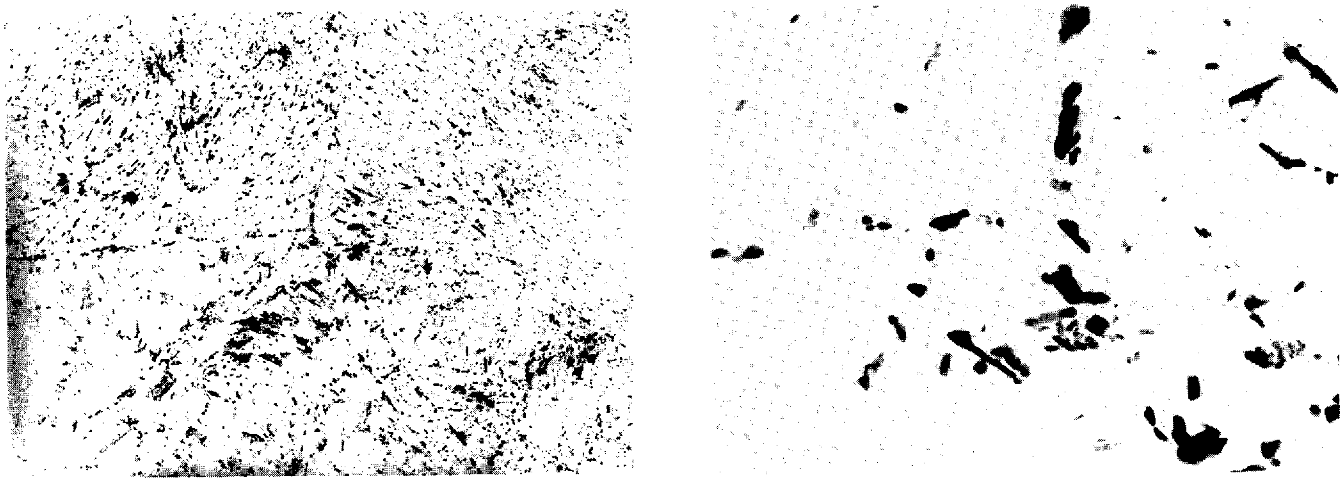
(a) (b)

Fig. G3-44—Carbide morphology and distribution in the simulated CGHAZ sample heat treated at 1250°F for 60 min of UT8 (weld energy input 12 kJ/in.), (a) 2,500×; (b) 20,000×

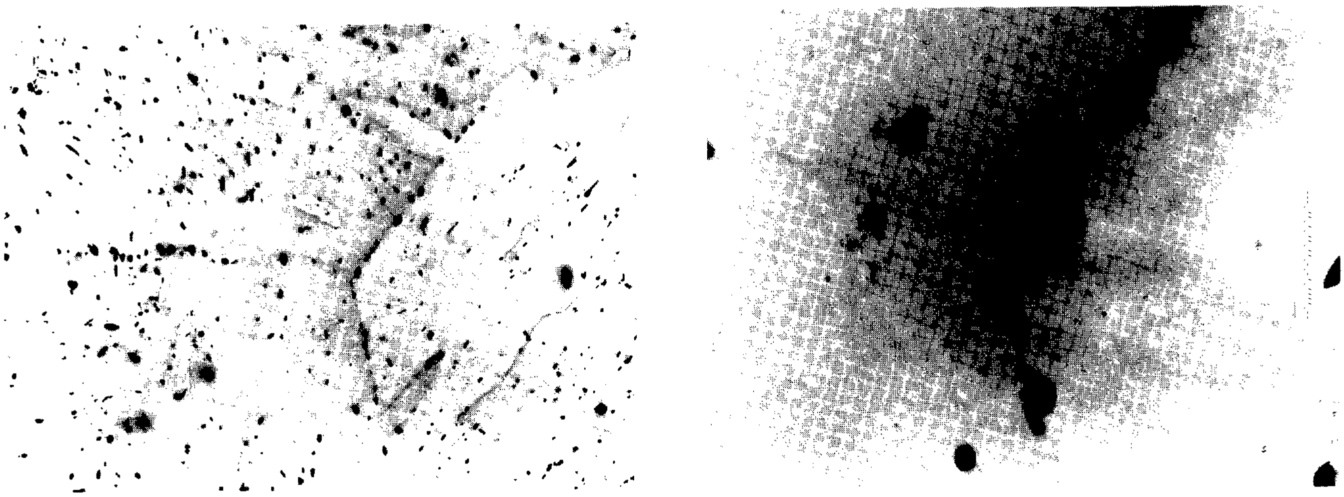
(a) (b)

Fig. G3-45—Carbide morphology and distribution in the simulated CGHAZ sample heat treated at 1350°F for 8 hours of UT2 (weld energy input 12 kJ/in.), (a) 2,500×; (b) 20,000×

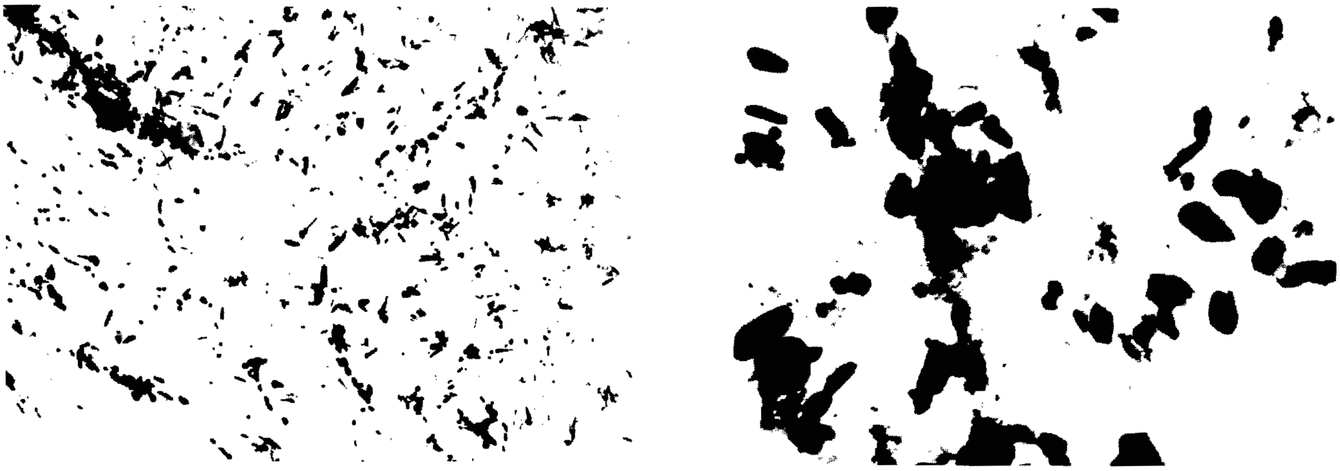

(a) (b)

Fig. G3-46—Carbide morphology and distribution in the simulated CGHAZ sample heat treated at 1350°F for 8 hours of UT3 (weld energy input 12 kJ/in.), (a) 2,500×; (b) 20,000×

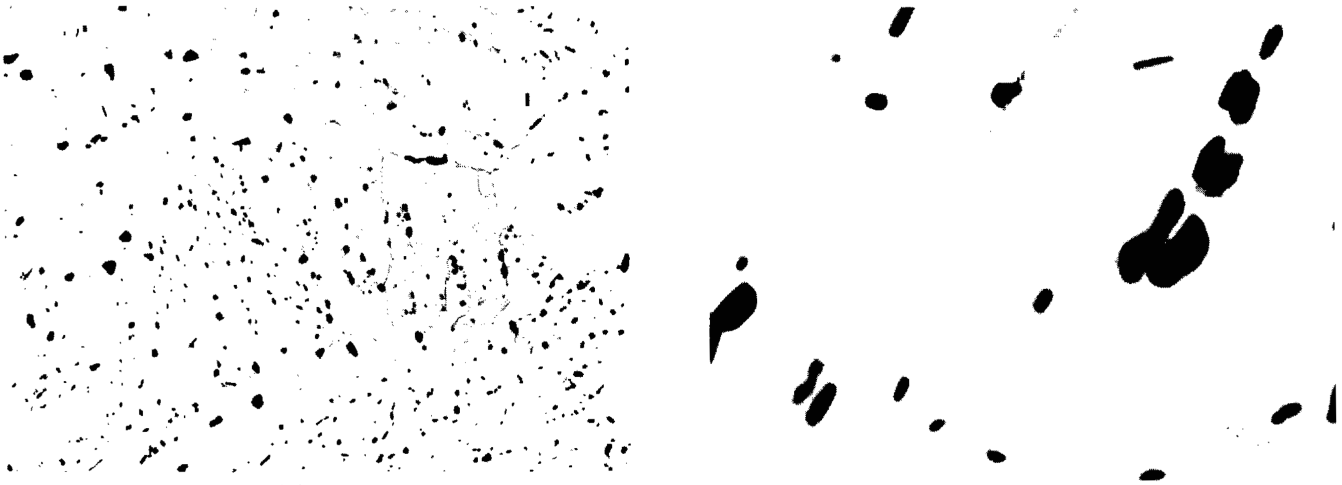

(a) (b)

Fig. G3-47—Carbide morphology and distribution in the simulated CGHAZ sample heat treated at 1350°F for 8 hours of UT5 (weld energy input 12 kJ/in.), (a) 2,500×; (b) 20,000×

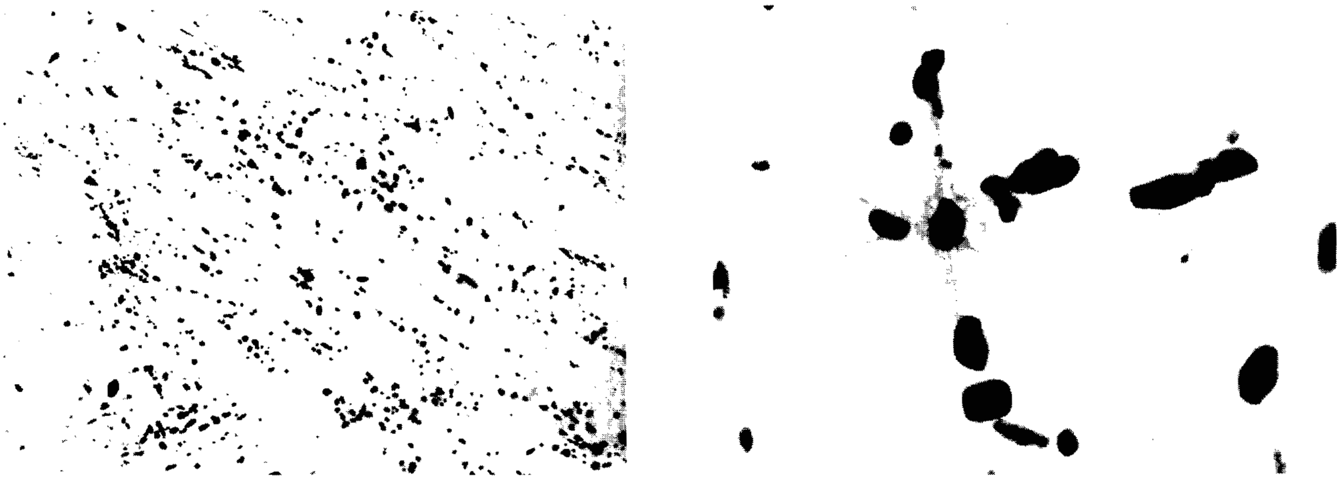

(a) (b)

Fig. G3-48—Carbide morphology and distribution in the simulated CGHAZ sample heat treated at 1350°F for 8 hours of UT8 (weld energy input 12 kJ/in.), (a) 2,500×; (b) 20,000×

carbides and their distribution in the Gleeble simulated CGHAZs after a PWHT of 1350°F for 8 hours. In general, the extent of carbide precipitate is similar to those samples with a lower tempering parameters. However, the size of the carbides in these samples is significantly increased.

Discussion

UT2 possesses an excellent reheat cracking resistance according to the PREVEW test results whereas heats UT3, UT5 and UT8 showed a tendency for reheat cracking. UT3 exhibited the highest reheat cracking tendency among the materials studied. An important conclusion from the above investigation is that the reheat cracking behavior of this group of materials is related to the carbide evolution behavior in the weld CGHAZ. Since carbide precipitation behavior is significantly dependent on the chemical composition, the development of an approach using carbide morphology and distribution for ranking the materials in terms of reheat cracking tendency may become necessary. The results of the study of the carbide precipitation behavior in the CGHAZ are correlated with the results obtained from stress rupture tests and PREVEW tests. Further, the carbide evaluation studies provide more direct physical evidence for interpreting the mechanisms of reheat cracking. It was shown by study on thin foil samples that the interaction between fine carbides and dislocations in the initial stage of PWHT significantly enhances the grain matrix strengthening. Therefore, both carbide nucleation and growth kinetics will significantly affect the reheat cracking behavior. If the carbide precipitation initiation time has been slightly delayed, then reheating cracking tendency will be reduced. Since the density of the intralath dislocations decreases rapidly during PWHT and strain relaxation is enhanced, the interaction between carbides and dislocations is reduced. In other words, controlling intralath fine carbide precipitation is important to minimizing reheat cracking tendency.

Carbon content is certainly the most important factor in the kinetics of carbide formation. Since UT2 has the lowest carbon content both the carbide precipitation initiation time and growth are delayed during PWHT. Thus, the material has excellent reheat cracking resistance. In addition, the carbide formation in UT2 preferentially takes place along the prior austenite grain boundary or interlath boundaries of bainite and martensite. Mo and Cr should be the second most important alloying elements in reheat cracking propensity for Cr-Mo steel, not only due to the fact that Mo and Cr have a great affinity for carbon but also because of the relative level of Mo and Cr. Thus, increasing the Mo and Cr content increases the tendency for carbide formation. The combined influence of Mo and Cr is usually used to interpret the reheat cracking behavior in Cr-Mo steels. However, other factors such as high temperature strength and oxidation resistance should be considered for making the decision of optimum Mo and Cr contents.

All of the MC, M_4C_3 and $M_{23}C_6$ type carbide forming alloying elements have a similar influence to Cr and Mo however, the magnitude of the other alloying elements such as V, Nb and Ti, is less when compared to Cr and Mo. These carbide forming elements also can delay and reduce the formation of Fe_3C-type carbides (which are thought to have a strong intralath strengthening effect in Cr-Mo steels as does Mo_2C). Therefore, a balance in the alloy element content is important to obtain an optimum reheat cracking resistance. Nickel has a slight influence on the reheat cracking tendency by enhancing C solubility. Nitrogen is another important element that can be used to replace some of the carbon. Since both nitrides and carbonitrides have a higher dissolution temperature and are relatively stable compared to the same alloying element, carbide replacement of some C by N should be a benefit to reheat cracking resistance. Trace elements such as P and S have a high tendency to segregate along the grain boundaries and reduce the strength and ductility of the grain boundary, thus increasing the reheat cracking tendency.

UT2:

$$M_3C \rightarrow M_{23}C_6 \rightarrow M_2C + M_{23}C_6 \rightarrow M_7C_3 + M_{23}C_6$$

UT5:

$$M_3C \rightarrow M_2C + M_{23}C_6 \rightarrow M_7C_3 + M_{23}C_6 + M_2C$$

Summary

From the investigation of carbide evolution in the Gleeble simulated CGHAZ samples it is revealed that UT2 showed a slower carbide evolution rate for the Mo_2C-type carbides during the initial stages of PWHT when compared to UT3, UT5 and UT8. This is considered a most important factor affecting the relative reheat cracking behavior.

The carbide distribution of UT2 also showed some differences compared to those of the other three heats. In UT2, the carbides are predominantly located along the prior austenite grain boundaries and lath boundaries of martensite or bainite whereas UT3 has significant grain interior precipitation. This behavior may also provide a significant contribution to the reheat cracking sensitivity.

The carbide evolution in the CGHAZ during PWHT is dependent on the contents of carbon and carbide forming elements. Increases in the content of carbon and carbide-forming elements enhances the carbide nucleation rate, hence the reheat cracking tendency.

Appendix G4—Transmission Electron Microscopy Evaluation on API Materials

Introduction

Three API lots of 1¼Cr-½Mo steels (UT2, UT3 and UT5) were employed. Base metal and coarse grained HAZ (CGHAZ) samples were examined using a Hitachi 800 scanning transmission electron microscope (STEM). Five postweld heat treatment conditions in addition to the as-simulated condition were utilized: 1150°F for 15 min, 1150°F for 60 min, 1250°F for 15 min, 1250°F for 60 min and 1350°F for 8 hours. The purpose of this study is to reveal the relationship between the occurrences and preserve of carbide (evolutionary process, distribution, quantity, type and interaction with dislocation) and the reheat cracking resistance of this group of materials and also to promote a more basic understanding of the reheat cracking mechanism in Cr-Mo steels.

Among the materials, UT2 possesses the highest reheat cracking resistance (previous study) and UT3 and UT5 have a relatively low reheat cracking resistance.

Experimental Procedures

Gleeble simulated CGHAZs were used to characterize the fine scale microstructure. A weld energy input of 120 kJ/in. was used with a peak temperature of 2400°F for the CGHAZ simulation.

Thin foil samples (approximately 25 micron discs) were carefully sectioned from the Geeble simulated bars (1/4 in. in diameter) using a slow speed diamond blade cutoff machine. No mechanical polishing was involved in order to avoid any plastic deformation. HCl diluted in methanol (30 vol. % HCl) was used as the polishing solution. A dual-jet electropolishing unit (Tenupol) was utilized for final thinning. The operational parameters for electrolytic polishing were varied for different samples to obtain optimum thinning.

The samples are ferromagnetic so extra care is required in TEM examination. Beam tilting and stigmator corrections were frequently employed during operation in order to obtain maximum resolution.

Several regions were examined in each specimen and two or more images, reflecting general base metal and CGHAZ TEM microstructural morphologies, were recorded. Representative TEM microstructural morphologies for the different PWHT conditions for all materials are exhibited in this report.

Results

CGHAZs in UT2. Fig. G4-1 shows the base metal TEM microstructural morphology (boundary region between ferrite and bainite) in UT2. The carbides are clearly shown along the lath structures of the bainite.

Figs. G4-2 and G4-3 show the TEM microstructural morphologies of two locations in the as-simulated CGHAZ sample of UT2. It is evident that only small particles exist in the grain matrix and at grain boundaries. Almost all carbides dissolve into grain matrix during the on-heating and high temperature on-cooling portion of the HAZ thermal cycle. However, at lower temperatures upon cooling carbides nucleate and grow. In general, little particle growth occurs for the as-simulated condition. Dislocations are observed in the CGHAZ for the as-simulated condition although the density is not significant.

Fig. G4-1—Base metal TEM microstructural morphology in UT2; 20,000×

(a)

(b)

Fig. G4-2—TEM microstructural morphologies in Gleeble simulated CGHAZ sample of UT2 with as-simulated condition; (a) 20,000×; (b) 100,000×

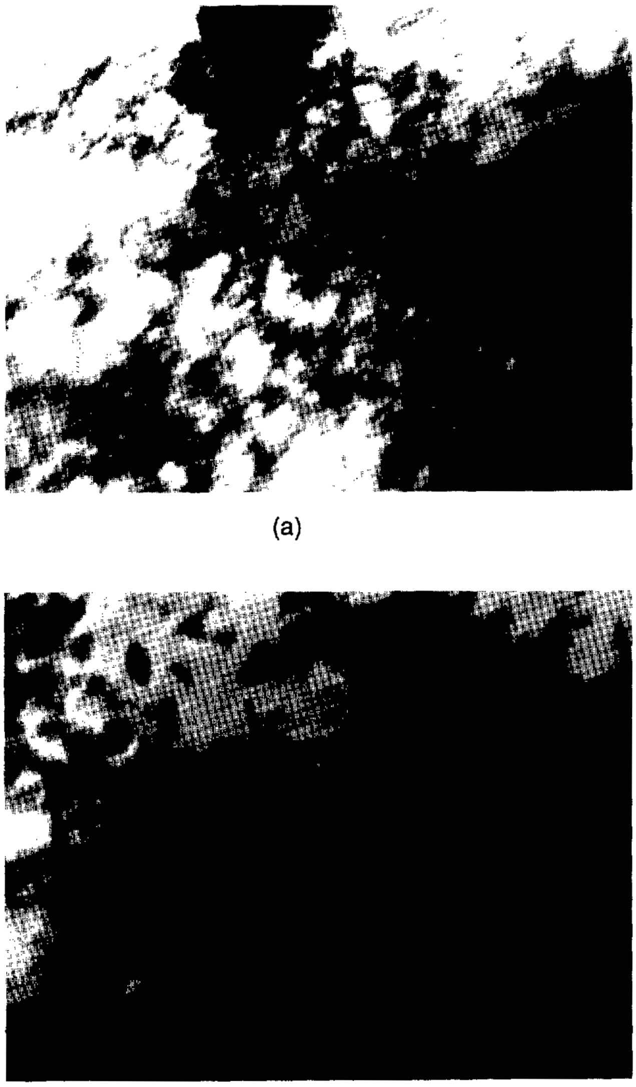

(a)

(b)

Fig. G4-3—TEM microstructural morphologies in Gleeble simulated CGHAZ sample of UT2 with as-simulated condition; (a) 20,000×; (b) 100,000×

Fig. G4-4 shows the TEM microstructural morphology in the CGHAZ of UT2 after a PWHT of 1150°F for 15 min. Clearly, the size of carbides has increased as contrasted to those in the as-simulated CGHAZ sample.

Fig. G4-5 shows the TEM microstructural morphologies at two different locations in the CGHAZ of UT2 after a PWHT treatment at 1150°F for 60 min. The carbides have grown along the grain boundaries and along the bainite laths. The dislocation density in this condition is less than that in the as-simulated CGHAZ sample.

Figs. G4-6 and G4-7 show the TEM microstructural morphologies of two different locations in the CGHAZ of UT2 after a PWHT of 1250°F for 15 min. In general, the size and amount of the carbides in this sample are similar to those in the CGHAZ after PWHT at 1150°F for 60 min. There is a reduction in dense dislocation as a function of PWHT.

Fig. G4-4—TEM microstructural morphologies in Gleeble simulated CGHAZ sample of UT2 after a PWHT at 1150°F for 15 min; 50,000×

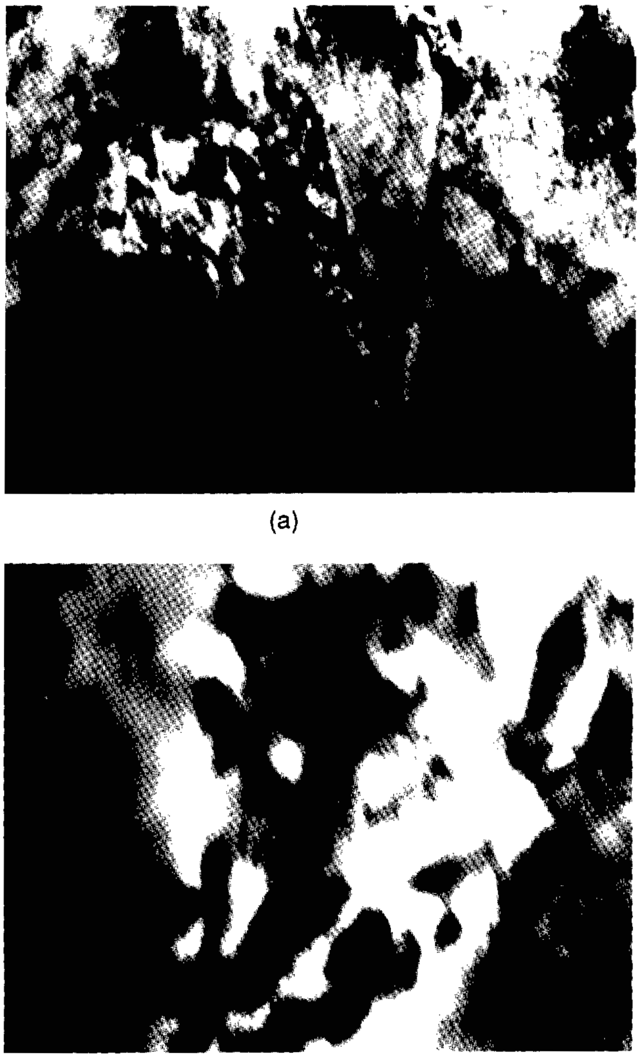

(a)

(b)

Fig. G4-5—TEM microstructural morphologies in Gleeble simulated CGHAZ sample of UT2 after a PWHT at 1150°F for 60 min as-simulated condition, (a) 20,000×; (b) 100,000×

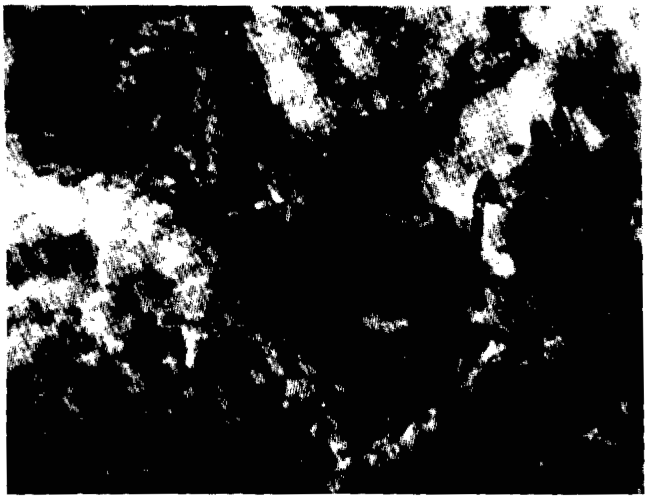

Fig. G4-6—TEM microstructural morphologies in Gleeble simulated CGHAZ sample of UT2 after a PWHT at 1250°F for 15 min; 20,000×

Figs. G4-8 and G4-9 show the TEM microstructural morphology at two different locations in the CGHAZ of UT2 after a PWHT of 1250°F for 60 min. Needle-like carbides (Mo_2C)-type appear in microstructure after this heat treatment.

Fig. G4-10 shows the TEM microstructural morphology at two different locations in the CGHAZ of UT2 after a PWHT at 1350°F for 8 hours. Clearly, the carbides grow significantly during this PWHT.

CGHAZs in UT3

The typical TEM microstructures of base metal of UT3 are shown in Figs. G4-11 and G4-12, respectively. The carbide distributed along the grain boundary (Fig. G4-11) and bainite lath boundaries (Fig. G4-12) are dominantly $M_{23}C_6$-type. Clearly, the size of the carbides in base metal of UT3 is larger than that of UT2.

Fig. G4-13 shows the TEM microstructural morphology in the CGHAZ after a PWHT at 1150°F for 15

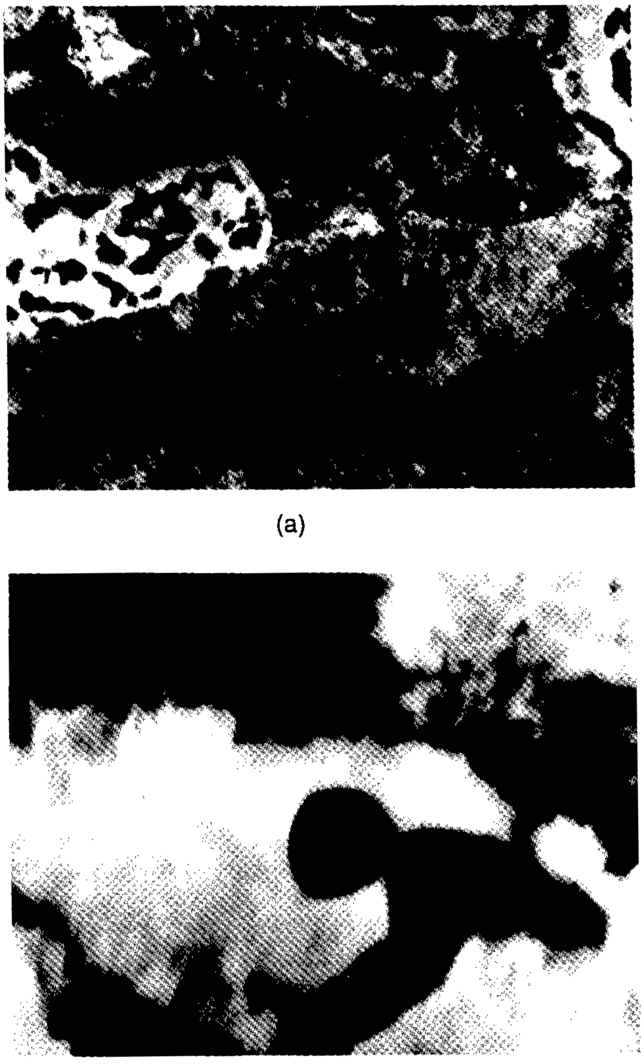

(a)

(b)

Fig. G4-7—TEM microstructural morphologies in Gleeble simulated CGHAZ sample of UT2 after a PWHT at 1250°F for 15 min; (a) 20,000×; (b) 100,000×

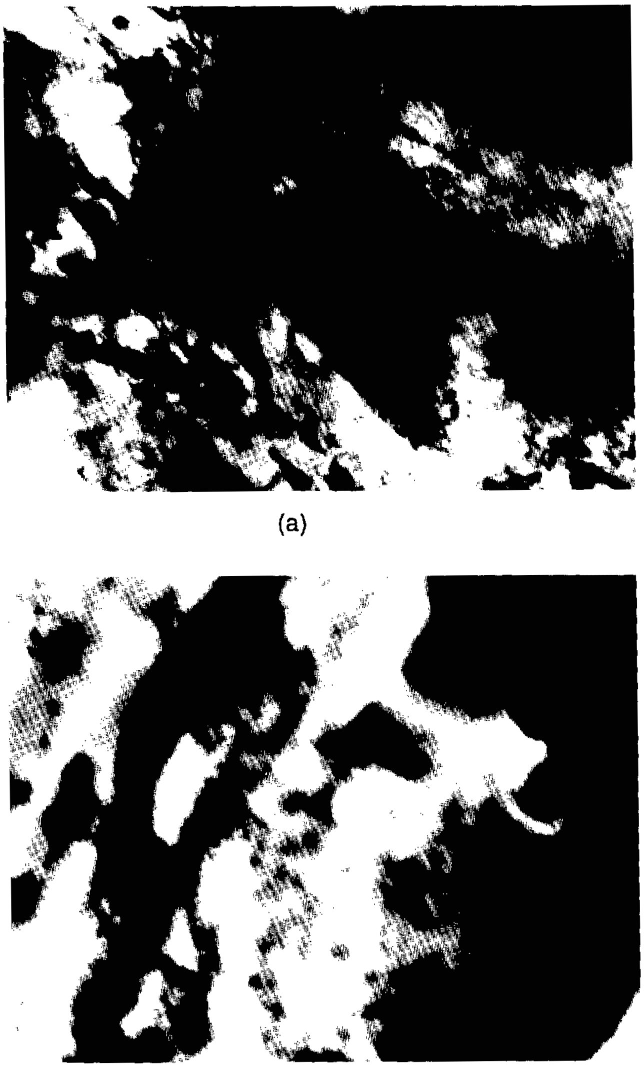

(a)

(b)

Fig. G4-8—TEM microstructural morphologies in Gleeble simulated CGHAZ sample of UT2 after a PWHT at 1250°F for 60 min; (a) 20,000×; (b) 100,000×

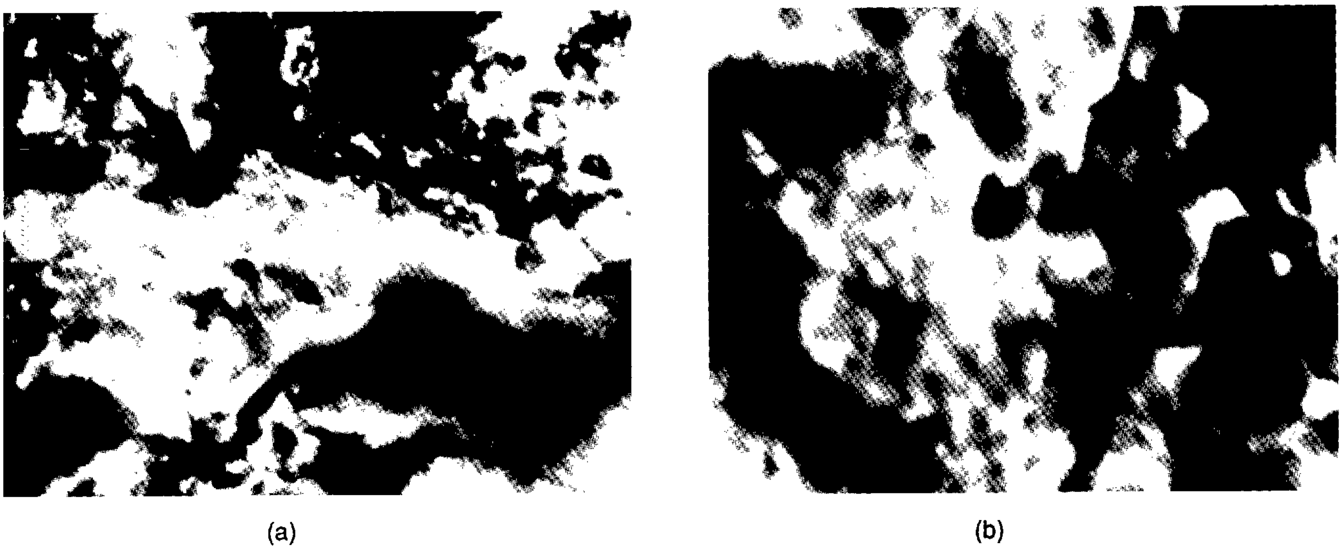

Fig. G4-9—TEM microstructural morphologies in Gleeble simulated CGHAZ sample of UT2 after a PWHT at 1250°F for 60 min; (a) 20,000×; (b) 100,000×

Fig. G4-10—TEM microstructural morphologies in Gleeble simulated CGHAZ sample of UT2 after a PWHT at 1350°F for 8 hours; (a) 20,000×; (b) 100,000×

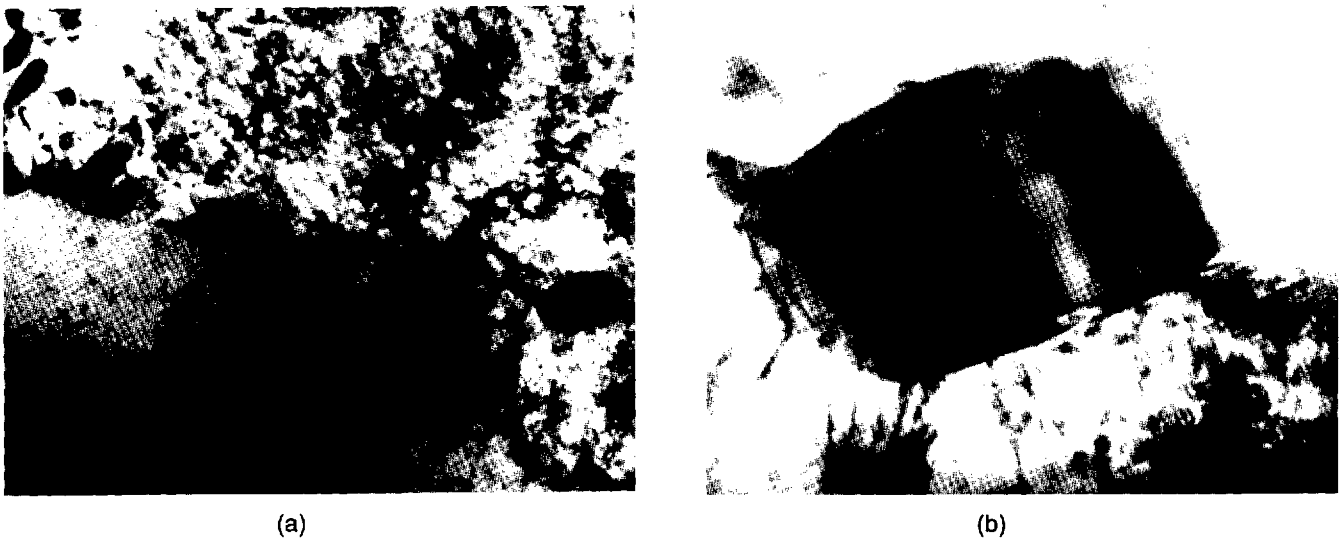

Fig. G4-11—TEM microstructural morphology of base metal of UT3 showing carbide distribution along the grain boundary; (a) 20,000×; (b) 100,000×

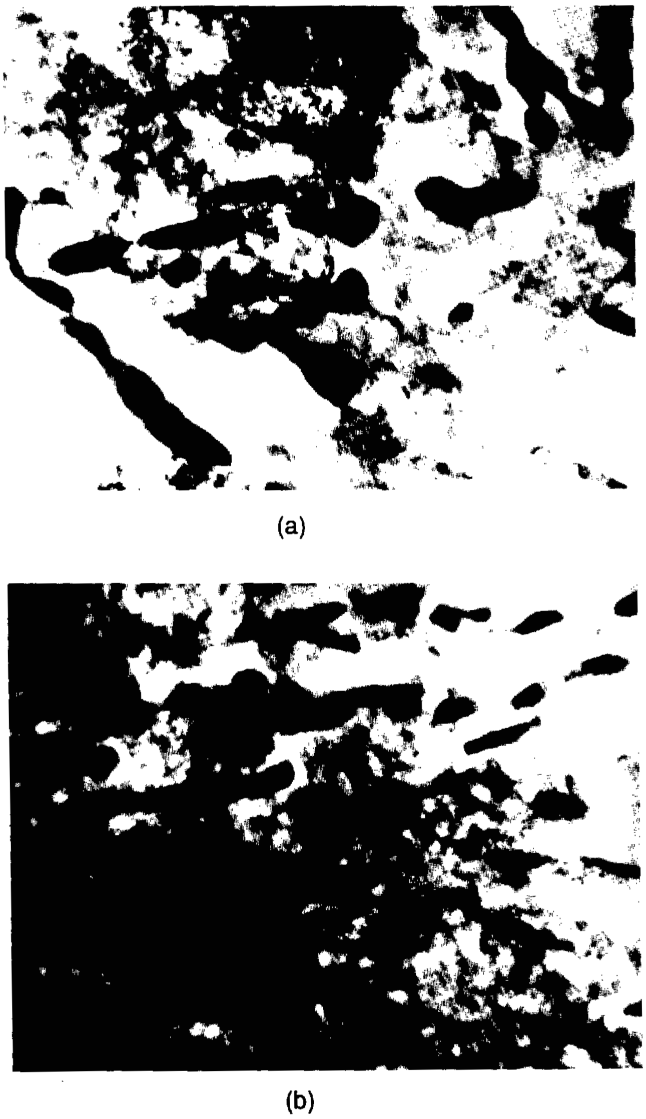
(a)

(b)

Fig. G4-12—TEM microstructural morphology in the base metal of UT3 showing the carbide distribution along the bainite lath boundaries; (a) 20,000×; (b) 20,000×

Fig. G4-13—TEM microstructural morphology in CGHAZ sample of UT3 after a PWHT at 1150°F for 15 min; 50,000×

min for UT3. In general, the size of the carbides is smaller than in the base metal.

Figs. G4-14 and G4-15 show the TEM microstructural morphology in the CGHAZ after a PWHT of 1150°F for 60 min for UT3. A significant carbide growth has occurred with this PWHT. The size and distribution of these carbides are similar to those in UT5 with the same PWHT condition.

Fig. G4-16 shows the TEM microstructural morphology in the CGHAZ after a PWHT at 1250°F for 60 min. Two locations showing different types of carbides are exhibited in the figure.

Fig. G4-17 shows the TEM microstructural morphology in the CGHAZ after a PWHT of 1350°F for 8 hours. It is evident that there is a reduction in dislocation density and significant carbide growth during this PWHT.

CGHAZs in UT5. Fig. G4-18 shows the TEM Microstructural morphology of the base metal of UT5. Coarser carbides are evident in UT5 compared

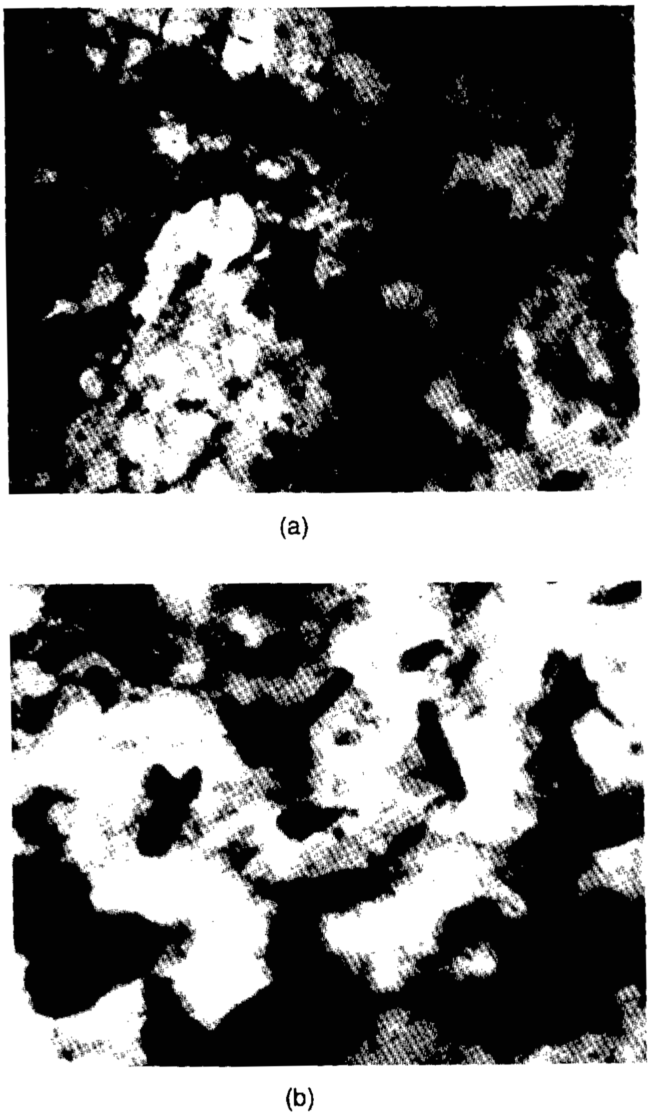
(a)

(b)

Fig. G4-14—TEM microstructural morphologies in Gleeble simulated CGHAZ sample of UT3 after a PWHT at 1150°F for 60 min; (a) 20,000×; (b) 100,000×

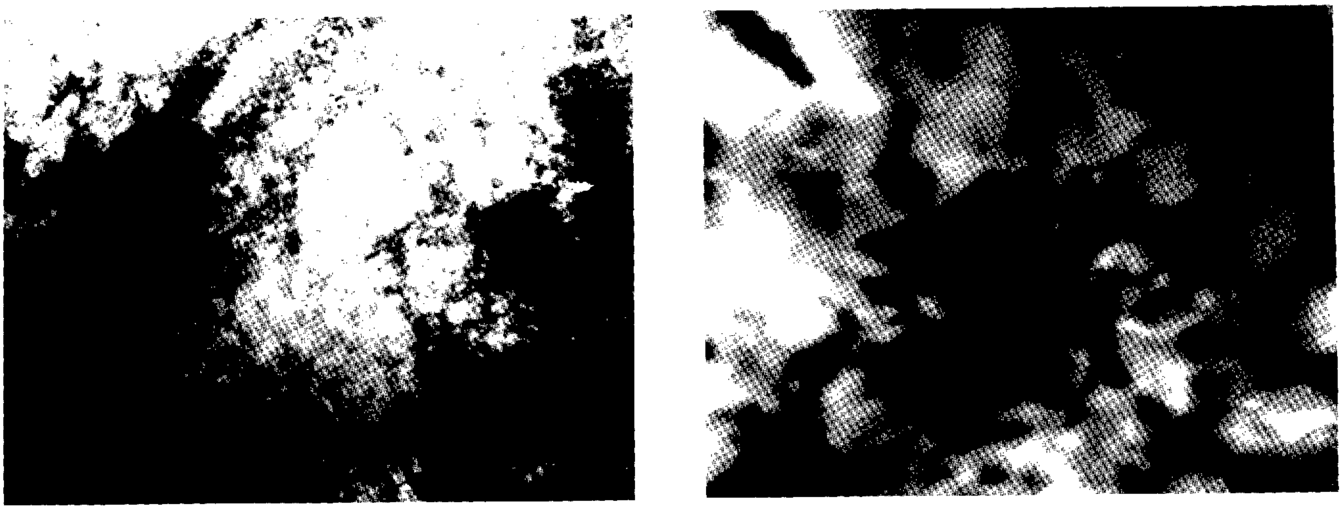

(a) (b)

Fig. G4-15—TEM microstructural morphologies in Gleeble simulated CGHAZ sample of UT3 after a PWHT at 1150°F for 60 min; (a) 20,000×; (b) 100,000×

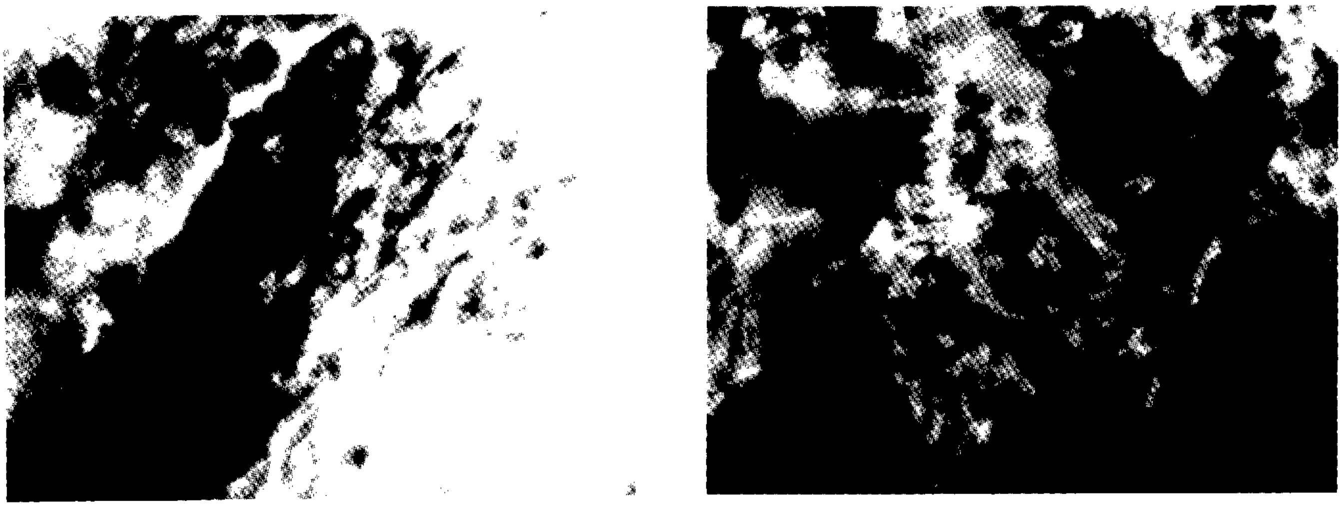

(a) (b)

Fig. G4-16—TEM microstructural morphologies in the CGHAZ sample of UT3 after a PWHT at 1250°F for 60 min; (a) 100,000×; (b) 100,000×

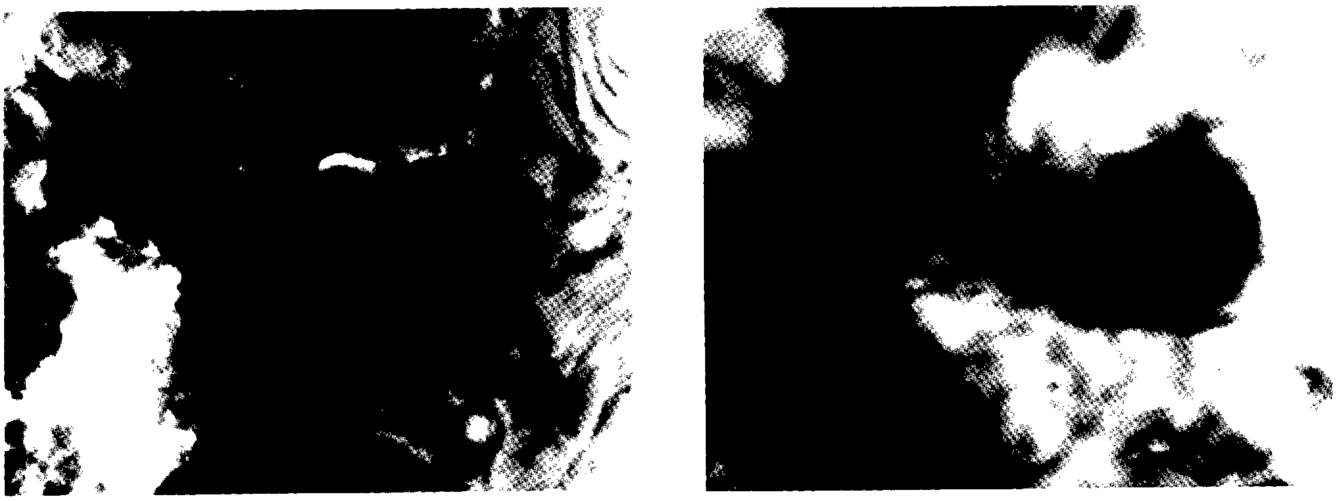

(a) (b)

Fig. G4-17—TEM microstructural morphologies in Gleeble simulated CGHAZ sample of UT3 after a PWHT at 1350°F for 8 hours; (a) 20,000×; (b) 100,000×

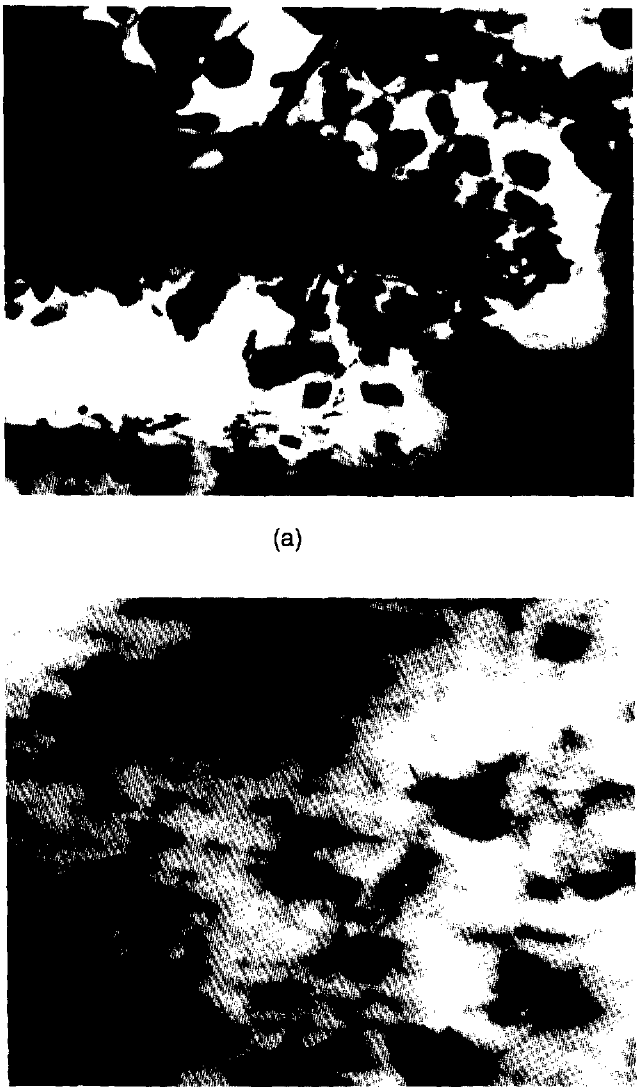
(a)

(b)

Fig. G4-18—TEM microstructural morphology in base metal of UT5; (a) 20,000×; (b) 100,000×

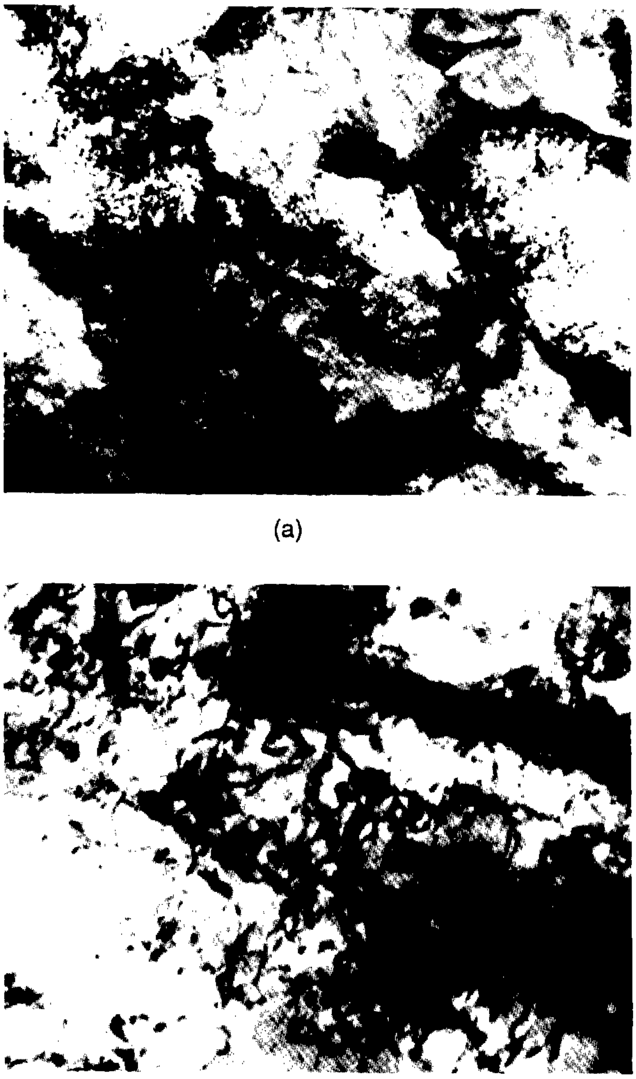
(a)

(b)

Fig. G4-19—TEM microstructural morphologies in as-simulated CGHAZ sample of UT5; (a) 20,000×; (b) 100,000×

to the base metal of UT2 (Fig. G4-1). At higher magnification fine carbides are evident uniformly distributed in the interlath bainite regions (Fig. G4-11(b)).

Figs. G4-19 and G4-20 show the TEM microstructural morphology at two locations in UT5 in the as-simulated condition. It is clear that a dense dislocation network is located along the bainite interlath regions. Most base metal carbides were dissolved during simulation. At a higher magnification, very fine carbides can be observed in the region of high dislocation density. These particles were formed mainly during the on-cooling portion of simulated welding thermal cycling (remnants of incompletely dissolved particles also exist). Based on the knowledge of the kinetics of carbide formation and the EDS results from previous carbon replica examination, these fine particles are considered to be Mo_2C- and Fe_3C-type carbides.

Figs. G4-21 and G4-22 show the TEM microstructural morphology in the CGHAZ of UT5 after a PWHT of 1150°F for 15 min. The density of intralath dislocations has clearly decreased. The number of intralath particles has increased slightly and they were preferentially located in the jot centers of the dislocations. The interaction between the dislocations and fine particles enhances intralath (grain matrix) strength.

Figs. G4-23 and G4-24 show the TEM microstructural morphology of the CGHAZ of UT5 after a PWHT of 1250°F for 15 min. The size of the intralath precipitate is increased and the intralath dislocation density is significantly reduced as contrasted to the as-simulated CGHAZ and the CGHAZ after a PWHT of 1150°F for 15 min.

Figs. G4-25 and G4-26 show the TEM microstructural morphology of the CGHAZ of UT5 after a PWHT of 1350°F for 8 hours. It is evident that the size, amount and shape of the carbides in the CGHAZ after the PWHT are significantly different from those in the samples of less severe PWHT. Rod-like and spherical carbides are predominant after this PWHT.

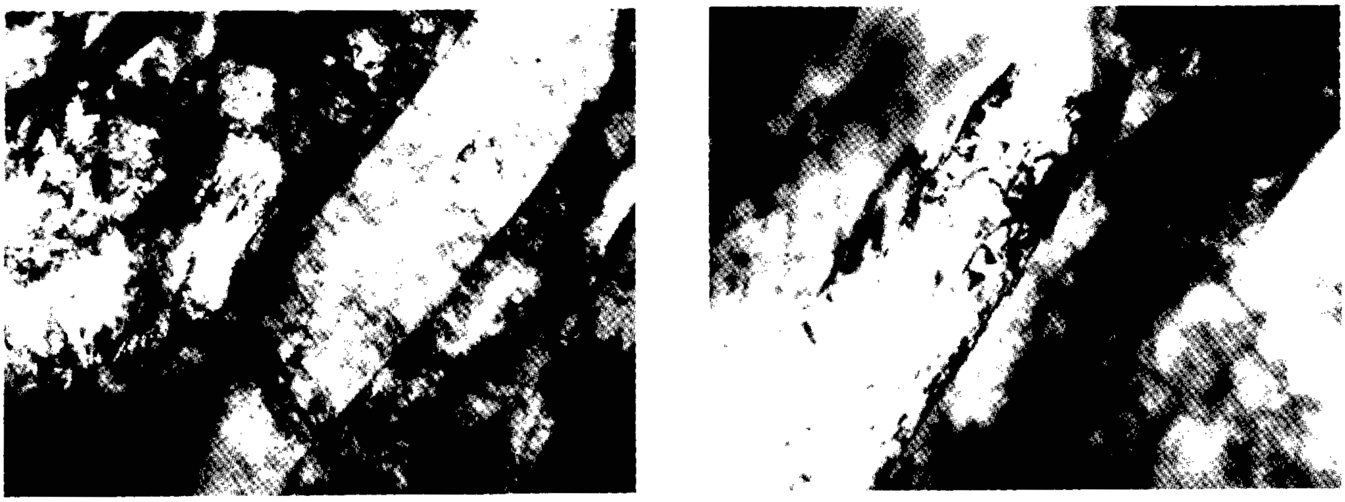

(a) (b)

Fig. G4-20—TEM microstructural morphologies in as-simulated CGHAZ sample of UT5; (a) 20,000×; (b) 100,000×

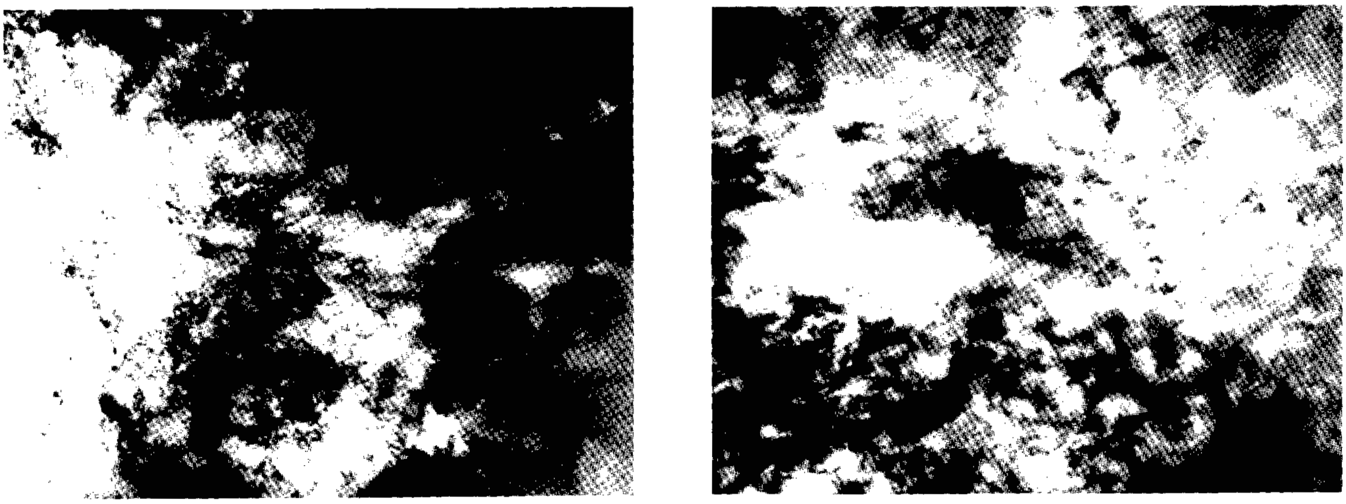

(a) (b)

Fig. G4-21—TEM microstructural morphologies in Gleeble simulated CGHAZ sample of UT5 after a PWHT at 1150°F for 15 min; (a) 20,000×; (b) 100,000×

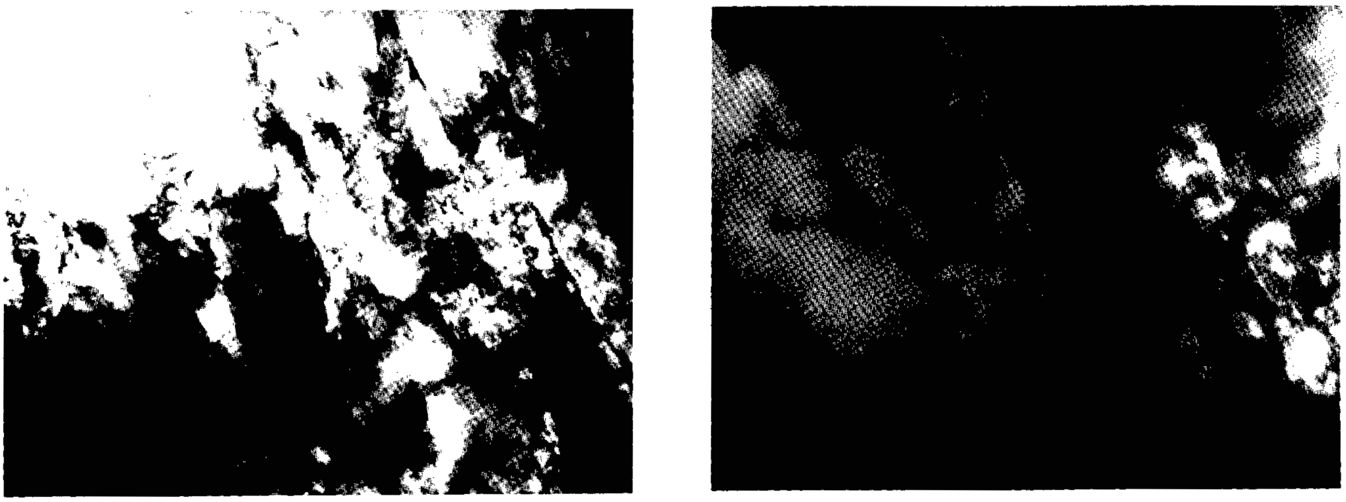

(a) (b)

Fig. G4-22—TEM microstructural morphologies in Gleeble simulated CGHAZ sample of UT5 after a PWHT at 1150°F for 15 min; (a) 20,000×; (b) 100,000×

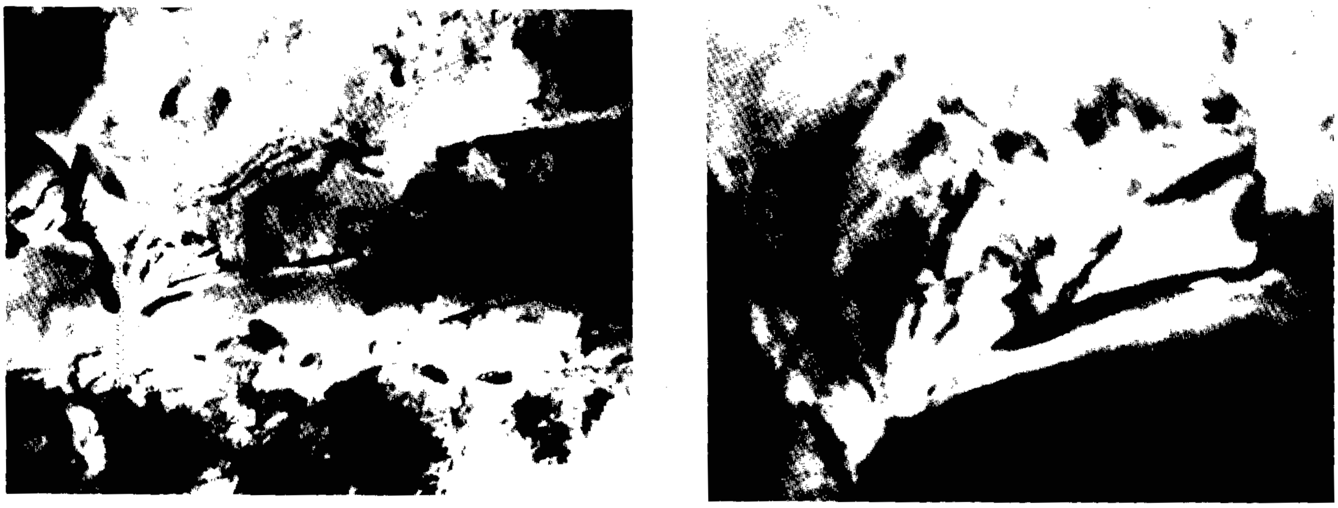
(a) (b)

Fig. G4-23—TEM microstructural morphologies in Gleeble simulated CGHAZ sample of UT5 after a PWHT at 1250°F for 15 min; (a) 20,000×; (b) 100,000×

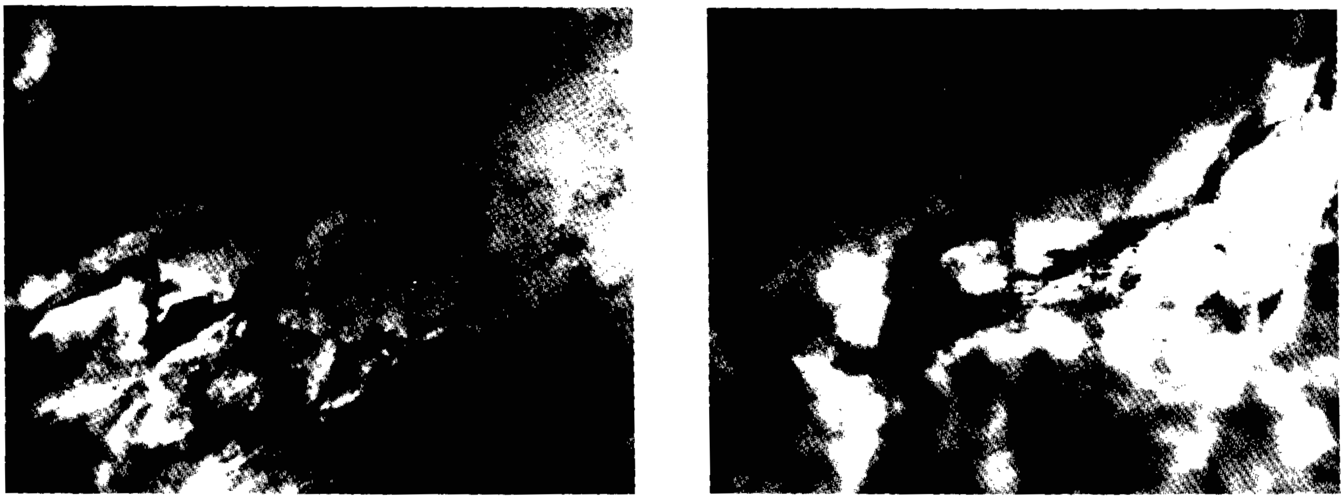
(a) (b)

Fig. G4-24—TEM microstructural morphologies in Gleeble simulated CGHAZ sample of UT5 after a PWHT at 1250°F for 15 min; (a) 20,000×; (b) 100,000×

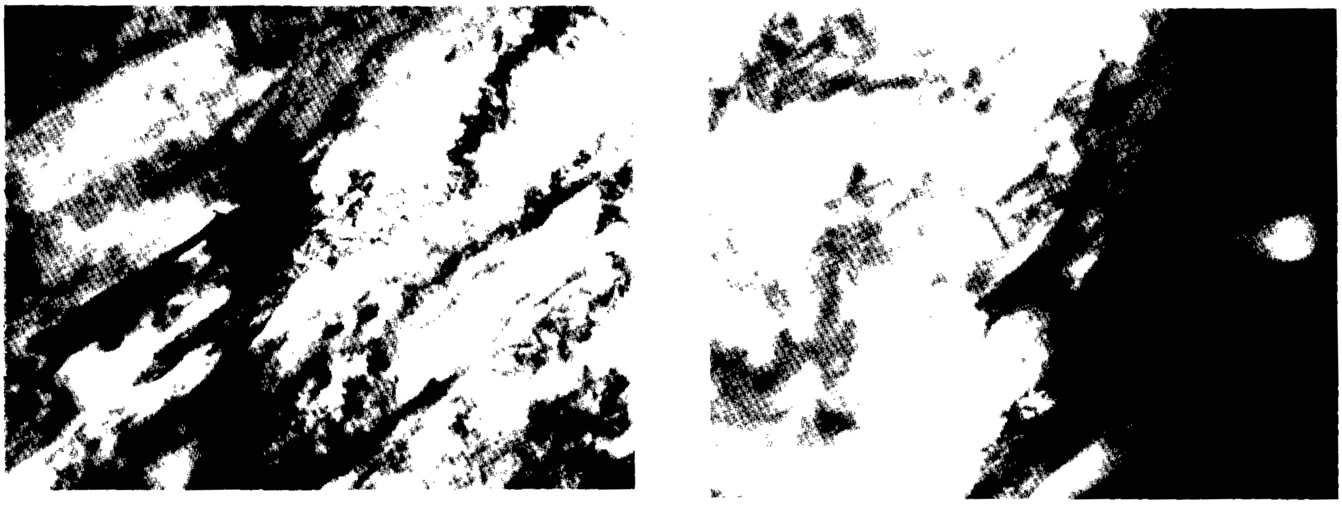
(a) (b)

Fig. G4-25—TEM microstructural morphologies in Gleeble simulated CGHAZ sample of UT5 after a PWHT at 1350°F for 8 hours; (a) 20,000×; (b) 100,000×

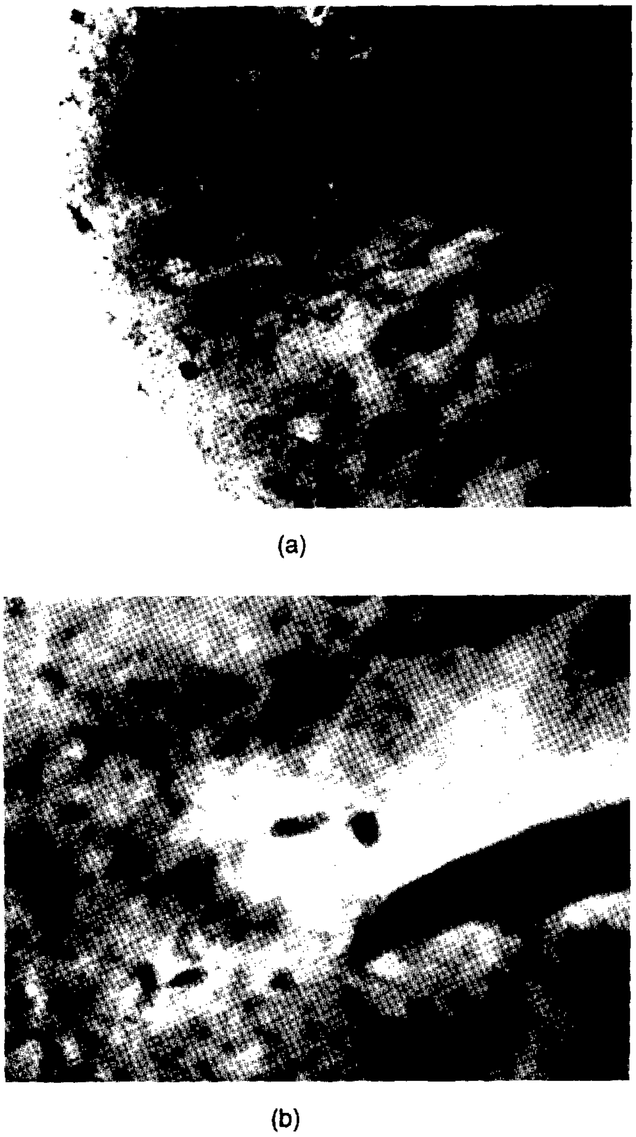

Fig. G4-26—TEM microstructural morphologies in Gleeble simulated CGHAZ sample of UT5 after a PWHT at 1350°F for 8 hours; (a) 20,000×; (b) 100,000×

According to the carbon replica examination results most are $M_{23}C_6$-type carbides. A significantly reduced interaction between carbides and dislocations is observed under this PWHT.

Discussions

Interactions between fine precipitates and dislocations play a significant role on the ratio of intragrain strength to grain boundary strength. It is generally considered that reheat cracking takes place when the grain matrix strength is greater than the grain boundary strength. Therefore, the extent of interaction between precipitates and dislocations affects the reheat cracking tendency.

The TEM microstructural investigation results indicate that those materials that rapidly nucleate carbides in the CGHAZ during PWHT have a higher reheat cracking tendency. Thus, the cracking sensitivity for UT3 and UT5 is greatest in UT2. Mo_2C-type carbides play an important role in the grain matrix strengthening, a delay in more formation in the CGHAZ can reduce the reheat cracking tendency. Many researchers point out that Mo_2C, V_4C_3 and Fe_3C play great roles in the intragranular strengthening of the CGHAZ during PWHT. However, the type and shape of the precipitates may not be as important as the size of the particles thus the precipitation strengthening effect. If fine particles of Mo_2C, Fe_3C, V_4C_3 or $M_{23}C_6$ form intragranularly during the on-cooling portion of the welding thermal cycle or during initial PWHT, a significant effect on the ratio of grain matrix strength to grain boundary strength occurs and the reheat cracking tendency is increased.

A factor that should be considered is that solid solution strengthening in the CGHAZ contributes to the intragranular strength and is higher in the as-simulated condition and initial stage of PWHT. With an increase in severity, carbide formation take places the grain matrix solid solution strengthening effect decreases and a reduction of the strain level occurs more readily. The ductility of CGHAZ will also increase with PWHT extent.

Appendix H—Creep Rupture Behavior of the Coarse Grained HAZ

Appendix H-1—Notch Bar and Smooth Bar Creep/Stress Rupture Testing

Approach and Method

The basis for the smooth and notched bar stress rupture study was the concept that long term cracking in-service was a manifestation of notch sensitivity (shortened life at stress concentrations). Comparisons were to be made of the relative lives of smooth and notch specimens at a selected temperature and stress that would be discriminatory.

Utilizing MPCs specially designed Gleeble specimens (Appendix H-2) valid elongations and creep rates could be obtained from the smooth bars to help understand behavior. Then the effects of composition, heat input and PWHT might be systematically studied. Earlier work by MPC (Ref. H1) on one of the steels studied showed that the simulated heat affected zones displayed the classic behavior of short notch bar life at low stresses and low creep temperatures. The results shown in Figure H1-1 were for tests at 950 and 1000°F for material tempered at 1175°F for 12 hours.

For this study a number of test conditions were considered. It is generally recognized that notch sensitivity decreases with increasing temperature and increasing stress. However, tests at design stresses and temperatures would be unduly long. The compromise condition selected for most tests was 1025°F and 20 ksi. The resulting range of test durations, about 400–5000 hours, was practical yet the conditions were not far removed from those that might be encountered in petroleum industry service and lead to failure in a time frame of 5–10 years. For example, on a Larson-Miller Parameter basis (using C = 20), 5000 hours at 1025°F equals about 10 years at 950°F. Slightly higher and lower stresses (25 and 16 ksi) and higher temperatures were examined to determine if there was sensitivity to stress or temperature. It was concluded that increasing stress or temperature provided less discrimination among the heats while decreasing stress unacceptably prolonged tests for some materials without changing the ranking.

Heat inputs studied were 45, 80 and 120 Kj/in. while PWHTs evaluated ranged from 1150–1375°F. The materials used were UT2, UT3, UT4, UT5 and UT8. These ranged from excellent (UT2) to poor (UT3 and UT4) in weldability and included marginal materials as well (UT5 and UT8).

The notched specimens used had 0.3-in. minor diameter and proportions that conformed to ASTM E292 0.0085-in. notch radius and 0.43-in. major diameter) to provide a K_t of 3.9. Some specimens had two notches, one about one-half in. above the other so that partially cracked material might be studied without interference from oxidation of the fracture surface. The smooth bar specimens had a gage length of about 1-in. They were prepared by resistance heating to provide a relatively uniform microstructure over that length as described in Section H-2.

The complete test results are presented by heat in Tables H1-1 to H1-5 and representative creep curves can be found in Section H-3. Figs. H1-2 and H1-3 compare all the results to a Reference curve for smooth base metal specimens of 1¼Cr-½Mo steel. While the smooth bar HAZ data are in reasonable agreement with base metal (Fig. H1-2) it can be seen

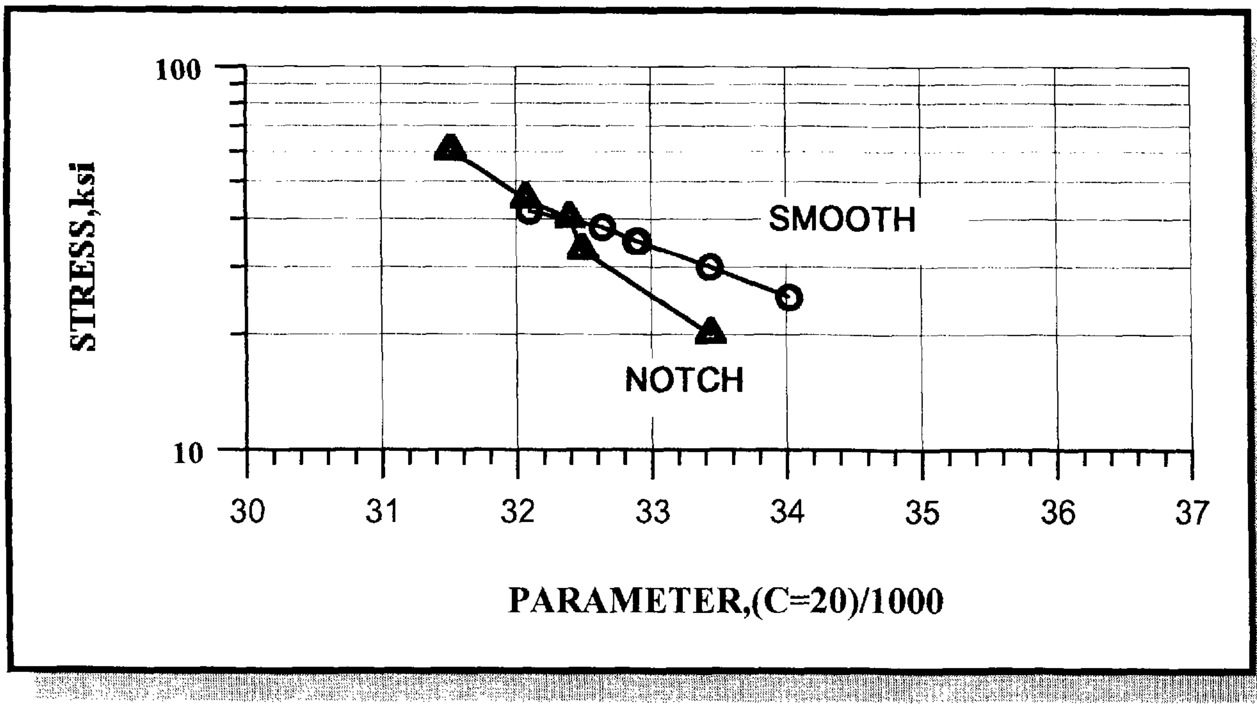

Fig. H1-1—Comparison of smooth and notch bar life for UT5, PWHT 1175°F, 12 hr

Table H1-1—Smooth and Notched Stress-Rupture and Creep Rate Test Results for UT2

Heat Input (kj/in)	*Temper. Temp. (F)*	*Temper. Time (hrs)*	*Test Temp. (F)*	*Stress (ksi)*	*Notched Life (hrs)*	*Smooth Life (hrs)*	*Ratio Notch/Smooth*	*MPC Creep Rate/hr*	*Last Strain* (%)*
80	1150	1	1125	20	154.2	158.0	0.98	1.0E-04	4.7
80	1150	1	1100	20	257.1	396.2	0.65	4.8E-05	6.2
80	1150	1	1075	20	510.2			1.5E-05	0.8
80	1150	1	1050	20	1111.9	1830.8	0.61	8.0E-06	5.0
80	1150	1	1025	20	2376.8	3998.7	0.59	3.0E-06	4.4
80	1150	1	1025	20	2376.8	3998.7	0.59	3.0E-06	4.4
80	1150	1	1025	25	439.4	1642.7	0.27	6.0E-06	2.8
80	1250	1	1075	20	951.6	883.1	1.08	2.4E-05	7.3
80	1250	1	1025	20	3488.7	4591.3	0.76	4.0E-06	6.3
80	1250	1	1025	25	1237.5	1363.8	0.91	2.0E-05	6.7
120	1300	3	1025	20	3202.7	4952.5	0.65	3.7E-06	6.8
120	1325	3	1025	20	3431.2	4588.1	0.75	5.0E-06	6.1
120	1350	3	1025	20	2794.2	3166.5	0.88	4.4E-06	5.3

*The last strain is the final elongation in the creep rupture test.

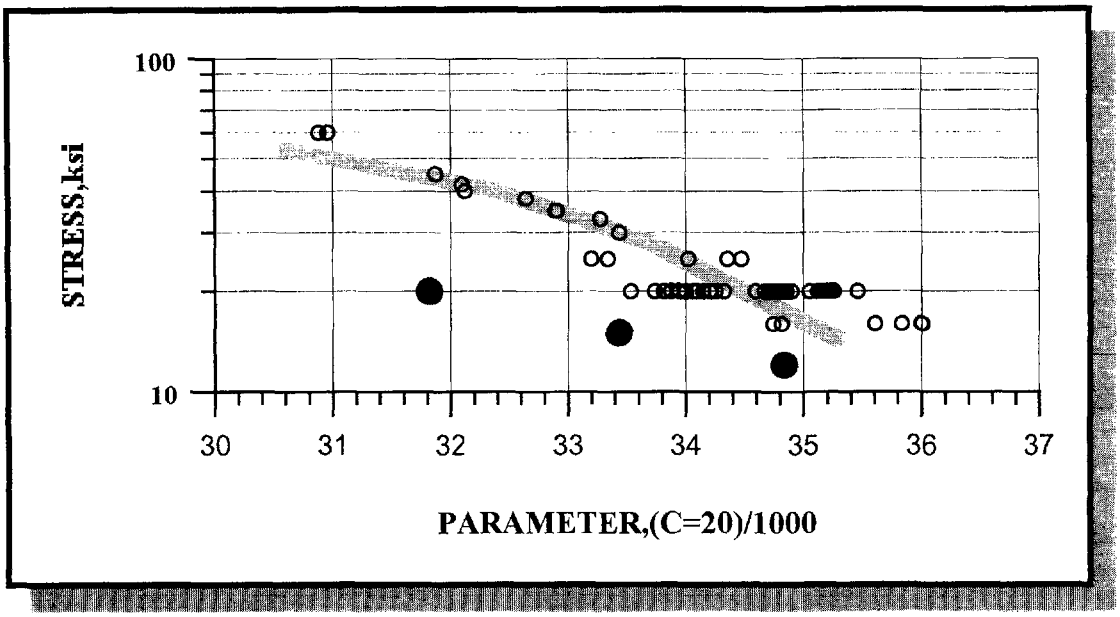

Fig. H1-2—HAZ smooth bar stress rupture parameter plot. Filled points are for service exposed base metal

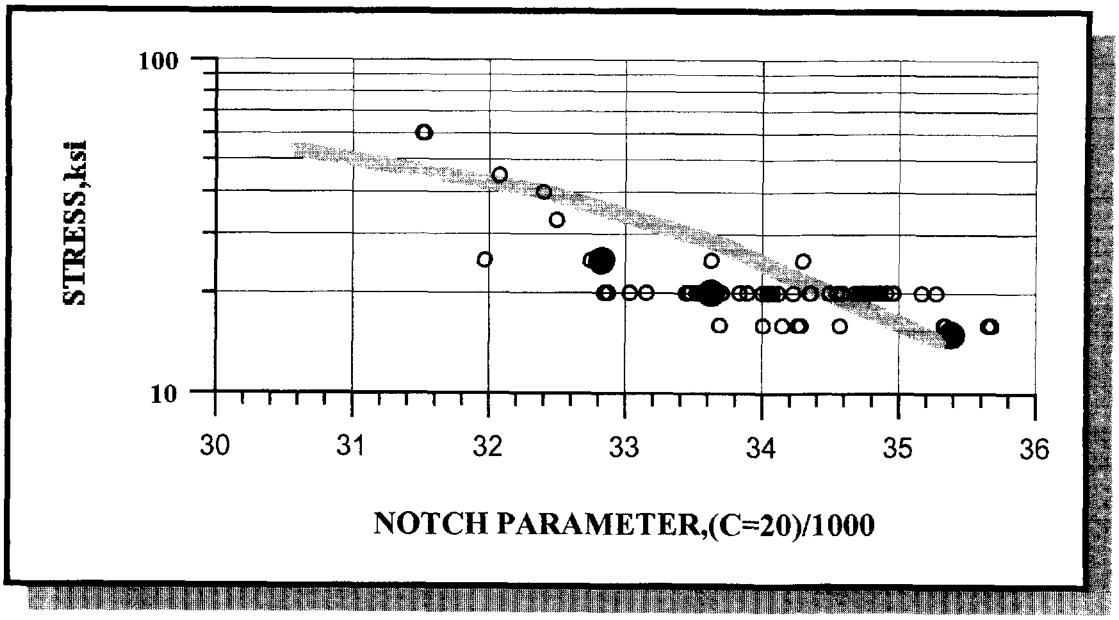

Fig. H1-3—HAZ notch bar stress rupture parameter plot. Filled points are for service-exposed base metal

Table H1-2—Smooth and Notched Stress-Rupture and Creep Rate Test Results for UT3

Heat Input (kj/in)	*Temper. Temp. (F)*	*Temper. Time (hrs)*	*Test Temp. (F)*	*Stress (ksi)*	*Notched Life (hrs)*	*Smooth Life (hrs)*	*Ratio Notch/Smooth*	*MPC Creep Rate/hr*	*Last Strain* (%)*
45	1325	3	1025	20	454.8				
45	1350	3	1025	20	784.4	593.8	1.32	1.6E-05	1.2
45	1375	3	1025	20	493.4	526.1	0.94	1.0E-05	2.0
80	1150	1	1025	16	481.4				
80	1150	1	1025	20	211.0	382.0	0.55	2.5E-06	0.3
80	1150	1	1025	25	33.7	228.5	0.15	4.1E-06	0.2
80	1250	1	1025	16	982.1				
80	1250	5	1025	20	130.8	786.8	0.17	3.0E-06	0.5
80	1250	1	1025	20	136.7	588.5	0.23	2.1E-06	0.4
80	1250	1	1025	25	112.0	284.2	0.39	1.0E-05	0.5
120	1325	3	1025	20	884.6	1291.7	0.68	1.7E-06	0.4
120	1325	3	1025	16	1887.0				

*The last strain is the final elongation in the creep rupture test.

Table H1-3—Smooth and Notched Stress-Rupture and Creep Rate Test Results for UT4

Heat Input (kj/in)	*Temper. Temp. (F)*	*Temper. Time (hrs)*	*Test Temp. (F)*	*Stress (ksi)*	*Notched Life (hrs)*	*Smooth Life (hrs)*	*Ratio Notch/Smooth*	*MPC Creep Rate/hr*	*Last Strain* (%)*
45	1250	5	1025	16	788.2	2771.8	0.28	6.0E-06	4.3
45	1250	5	1025	20	394.1	647.7	0.61	1.5E-05	2.5
45	1275	5	1025	16	1208.8	2487.4	0.49	7.0E-06	3.3
45	1275	5	1025	20	372.3	893.7	0.42	1.6E-05	4.2
45	1300	5	1025	16	1170.1	2489.6	0.47	5.0E-06	4.1
45	1300	5	1025	20	345.8	721.6	0.48	1.8E-05	3.7
45	1325	3	1025	20	454.1	785.4	0.58	2.0E-05	3.7
45	1350	3	1025	20	468.4	871.0	0.54	2.2E-05	5.5
120	1250	5	1025	20	175.2	907.6	0.19	1.0E-05	1.7
120	1275	5	1025	20	495.0	1161.4	0.43	9.0E-06	2.6
120	1300	5	1025	20	604.9	990.1	0.61	1.5E-05	2.9
120	1325	3	1025	20	347.9	1095.0	0.32	1.5E-05	3.2
120	1350	3	1025	20	423.9	1078.2	0.39	1.4E-05	3.8

*The last strain is the final elongation in the creep rupture test.

Table H1-4—Smooth and Notched Stress-Rupture and Creep Rate Test Results for UT5

Heat Input (kj/in)	*Temper. Temp. (F)*	*Temper. Time (hrs)*	*Test Temp. (F)*	*Stress (ksi)*	*Notched Life (hrs)*	*Smooth Life (hrs)*	*Ratio Notch/Smooth*	*MPC Creep Rate/hr*	*Last Strain** (%)*
45	1250	5	1075	16	1048.9	1564.0	0.67	1.5E-05	7.2
45	1250	5	1025	20	1931.6	2964.4	0.65	4.8E-06	5.4
45	1275	5	1075	20	437.8	418.1	1.05	6.3E-05	8.9
45	1275	5	1025	20	1352.0	2457.0	0.55	7.5E-06	7.7
45	1300	5	1075	16	1674.8	2193.8	0.76	1.2E-05	10.4
45	1300	5	1025	20	2768.9	2490.2	1.11	7.5E-06	6.9
45	1325	3	1025	20	1828.4	2563.2	0.71	8.0E-06	7.8
45	1350	3	1025	20	2262.9	2232.3	1.01	1.1E-05	10.4
80	1175	12	1000	20	803.9				
80	1175	12	1000	25		2009.5	0.30*		
80	1175	12	1000	30		795.7	0.50*		3.0
80	1175	12	1000	35		345.2	0.80*		5.5
80	1175	12	1000	40	156.0				
80	1175	12	1000	60	39.2				
80	1175	12	950	33	1115.3				
80	1175	12	950	35		2135.2	0.47*		3.4
80	1175	12	950	38		1417.6	0.63*		6.6
80	1175	12	950	42		581.0	1.12*		12.1
80	1175	12	950	45	558.8				
80	1175	12	950	60	223.3				
120	1250	5	1075	16	1027.9	2812.6	0.37	2.7E-06	1.7
120	1250	5	1025	20	1960.0	5357.0	0.37	7.0E-07	1.1
120	1275	5	1075	20	459.3	1258.5	0.36	3.5E-06	1.0
120	1275	5	1025	20	1685.6	4898.2	0.34	7.0E-07	1.4
120	1300	5	1075	16	1744.9	2862.6	0.61	3.3E-06	2.8
120	1300	5	1025	20	2871.2	4999.0	0.57	2.5E-06	T
120	1325	3	1025	20	2402.8	4657.4	0.52	1.5E-06	2.2
120	1350	3	1025	20	2482.7	4462.2	0.56	3.3E-06	4.0

*Estimated from notch parameter behavior.
**The last strain is the final elongation in the creep rupture test.

Table H1-5—Smooth and Notched Stress-Rupture and Creep Rate Test Results for UT8

Heat Input (kj/in)	*Temper. Temp. (F)*	*Temper. Time (hrs)*	*Test Temp. (F)*	*Stress (ksi)*	*Notched Life (hrs)*	*Smooth Life (hrs)*	*Ratio Notch/Smooth*	*MPC Creep Rate/hr*	*Last Strain** (%)*
0*	1005	200000*	1025	12		2888.3		4.0E-05	41.5
0*	1005	200000*	1025	15	6703.0	327.5	20.47	4.1E-04	45.0
0*	1005	200000*	1025	20	437.6	26.7	16.39	5.0E-03	41.3
0*	1005	200000*	1025	25	127.3				
120	1250	5	1050	20	366.4	1178.7	0.31	7.5E-06	1.5
120	1250	5	1025	20	829.8	2705.1	0.31	2.9E-06	1.8
120	1275	5	1050	20	393.0	1121.9	0.35	1.1E-05	2.7
120	1275	5	1025	20	661.8	2972.3	0.22	4.0E-06	2.1
120	1300	5	1050	20	557.5	1148.7	0.49	1.0E-05	2.6
120	1300	5	1025	20	859.7	2555.8	0.34	4.5E-06	2.5
120	1325	3	1025	20	1116.7	2668.0	0.42	3.9E-06	3.5
120	1350	3	1025	20	1368.0	2522.9	0.54	3.4E-06	2.5

*Base metal, estimated service exposure.
**The last strain is the final elongation in the creep rupture test.

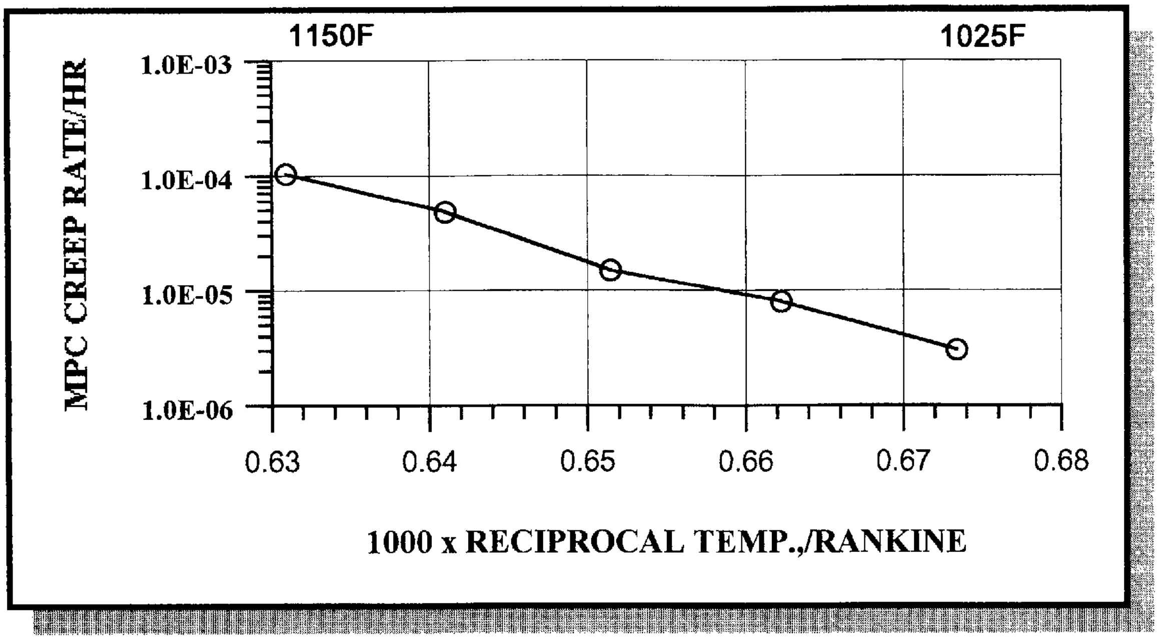

Fig. H1-4—Effect of temperature on creep rate for UT2 HAZ at 20 ksi

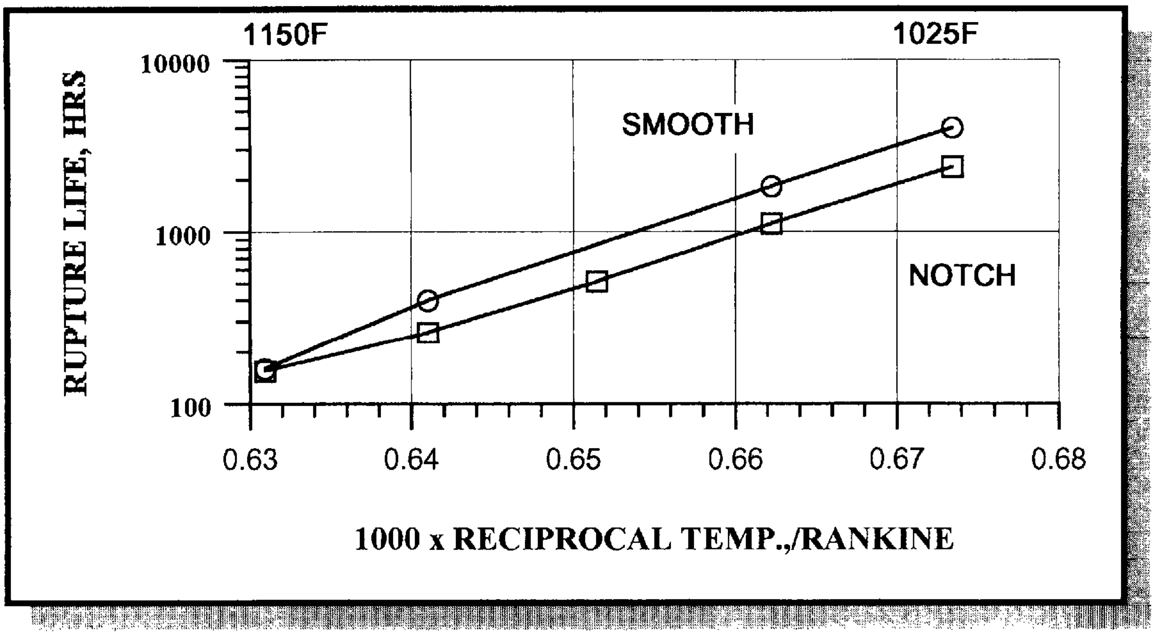

Fig. H1-5—Effect of temperature on smooth and notch bar lives for UT2 HAZ at 20 ksi that the notch bar results scatter excessively on the low side. The filled points shown are for one of the heats tested (UT8) when removed from electric utility service in a highly softened condition (not a heat affected zone). It can be seen by comparing Figs. H1-2 and H1-3 and from Table H1-5 that for this material severely service-aged base metal displayed short smooth bar life, but was significantly notch strengthened.

Before proceeding to a description of the results, it should be noted that increasing temperature increased creep rate in a roughly linear manner (with the reciprocal) of temperature as predicted by the Larson-Miller parameter (Fig. H1-4). Notch bar and smooth bar lives tended to diverge with decreasing temperature and hence the life ratios decreased with decreasing temperature (Figs. H1-5 and H1-6).

The creep rates reported are not the minimum creep rates that are comprised of a mixture of primary and tertiary behavior. A method used to establish the time equal zero creep rate of material (not yet damaged by creep) developed by MPC was utilized instead (Ref. H2). Also, since elongations were low, the last creep extension measurement prior to fracture is reported as the elongation. Fitting broken specimens together for the measurement of elongation is too imprecise.

Early tests showed that materials UT2 and UT3 displayed significantly differing weldability. Smooth and notched-bar tests showed the same trend after small amounts of tempering. Creep rates were not very different after tempering at 1150 and 1250°F for material given 80 Kj/in. heat input (Fig. H1-7a). However, notch bar lives differed greatly (Fig. H1-7b).

Smooth bar lives and elongation at failure were radically different with the UT2 displaying nearly satisfactory lives and relatively high elongations despite the small amount of tempering (Figs. H1-8 and H1-9). The UT3 specimen showed only a fraction of a percent strain (last reading before failure).

High Heat Input Simulation. Four heats (UT2, 4, 5 and 8) were studied utilizing materials exposed to 120 KJ/in. simulation. The creep rates observed varied over an order of magnitude (Fig. H1-10) with UT4 displaying the highest rate and practically no effect of tempering temperature. UT8 was similarly insensitive to tempering temperature. UT5 showed the lowest rate, which increased with tempering temperature. Note that creep rate was not at all a function of carbon content alone, as UT4 and UT5 have virtually the same carbon content while UT2 has the lowest carbon content. UT2 and UT5 recorded the same creep rates after tempering at 1300 or 1350°F.

Elongation measured before fracture tended to increase with increasing tempering temperature (Fig. H1-11) as did the notch-to-smooth bar life ratio (Fig. H1-12). While the ratio increased notably, all of these materials remained notch sensitive.

At low tempering temperatures the higher carbon materials displayed very low elongation. Smooth bar life was virtually unaffected by tempering temperature (Fig. H1-13) with the high and low carbon materials (UT5 and 2) showing the same performance. The generally long life of UT2 was possible because of its high ductility.

Notch bar lives varied considerably (Fig. H1-14). While UT8 tended to improve with increasing

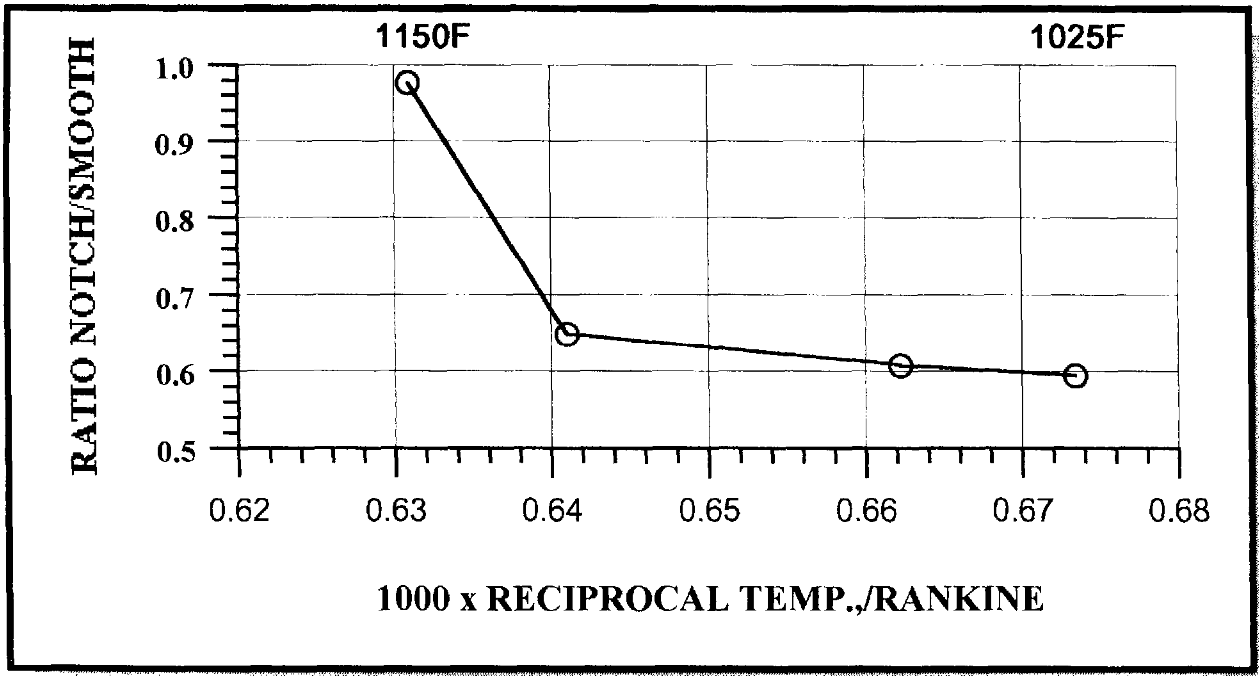

Fig. H1-6—Effect of temperature on notch/smooth bar life ratio for UT2 HAZ at 20 ksi

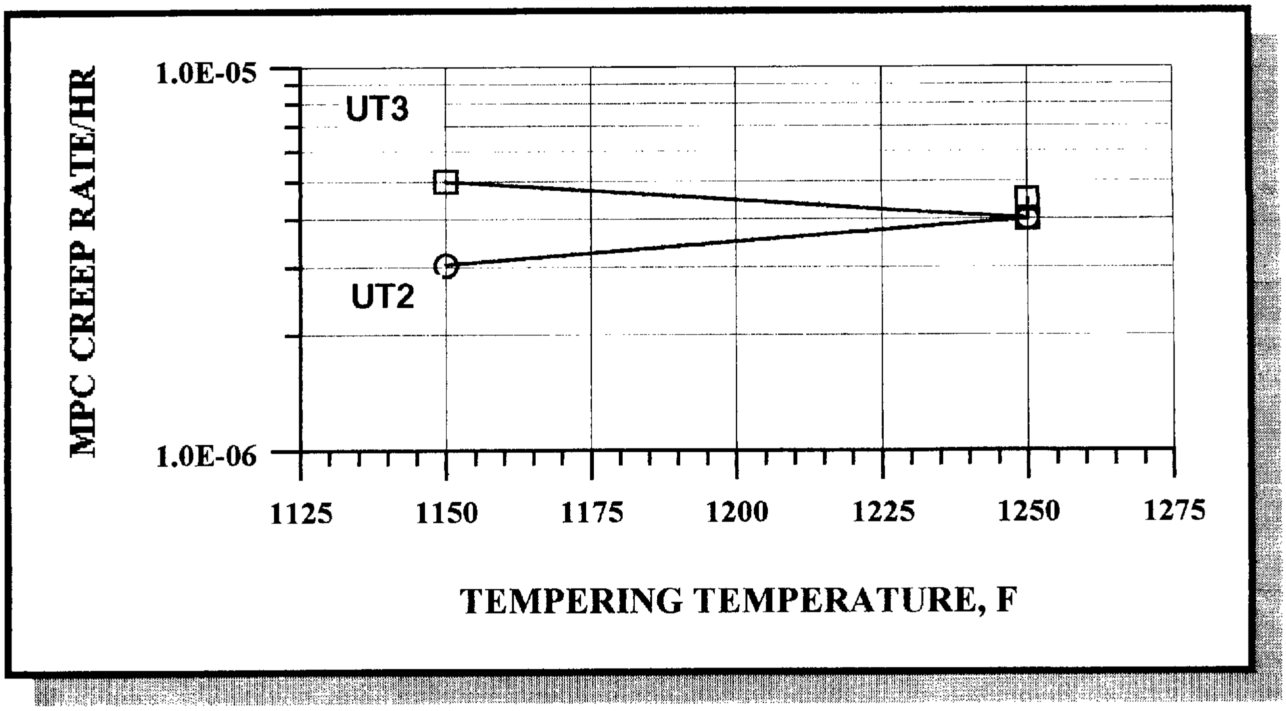

Fig. H1-7a—80 Kj/in. HAZ creep rate vs. tempering temperature

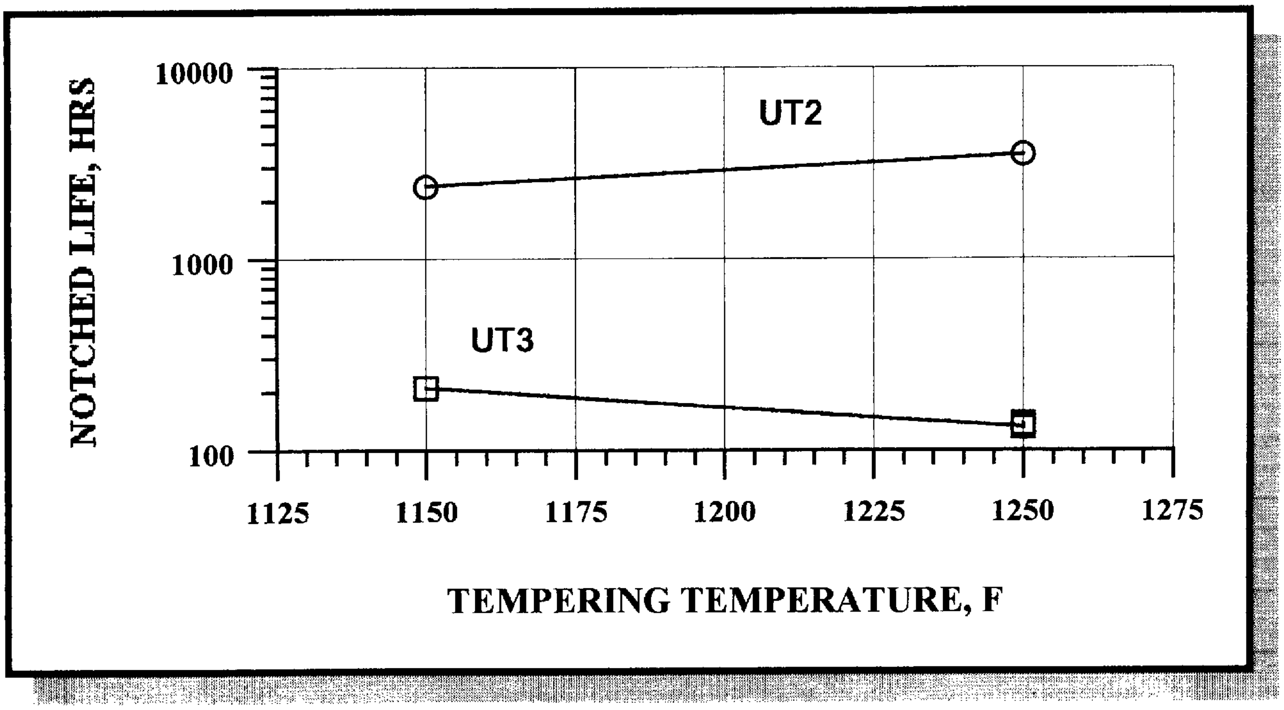

Fig. H1-7b—80 Kj/in. HAZ notch bar lives

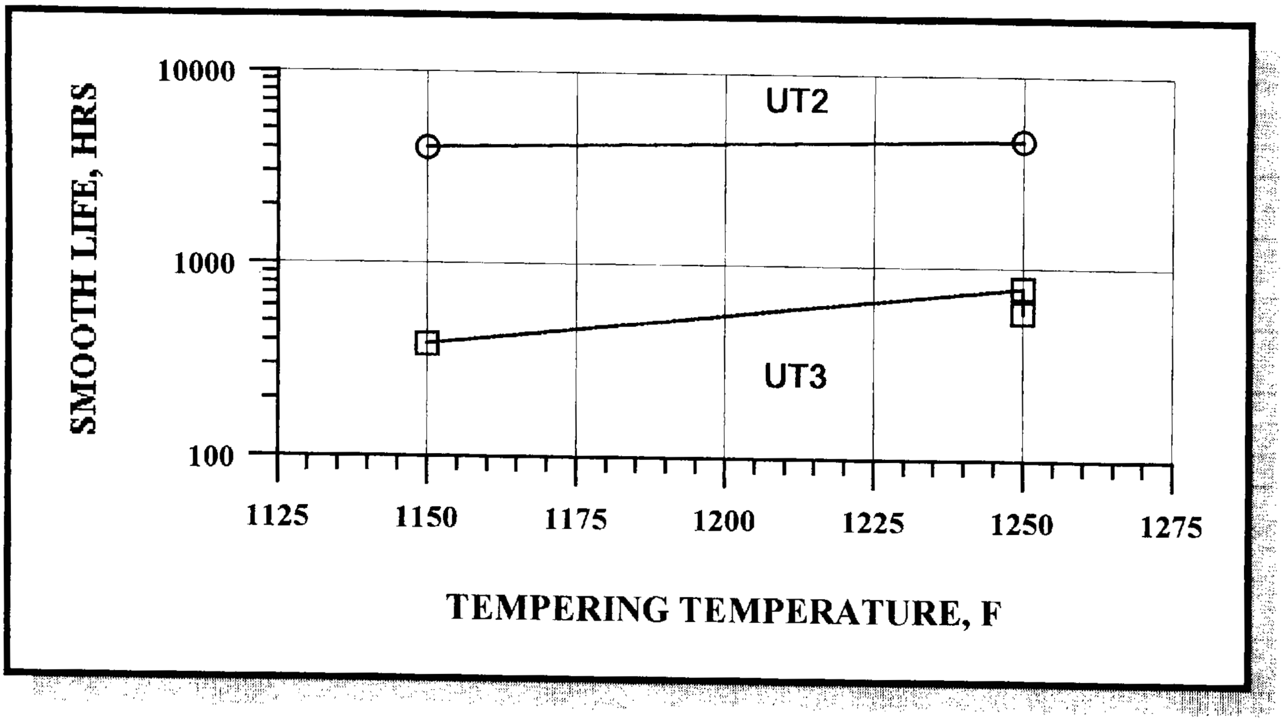

Fig. H1-8—80 Kj/in. HAZ smooth bar lives

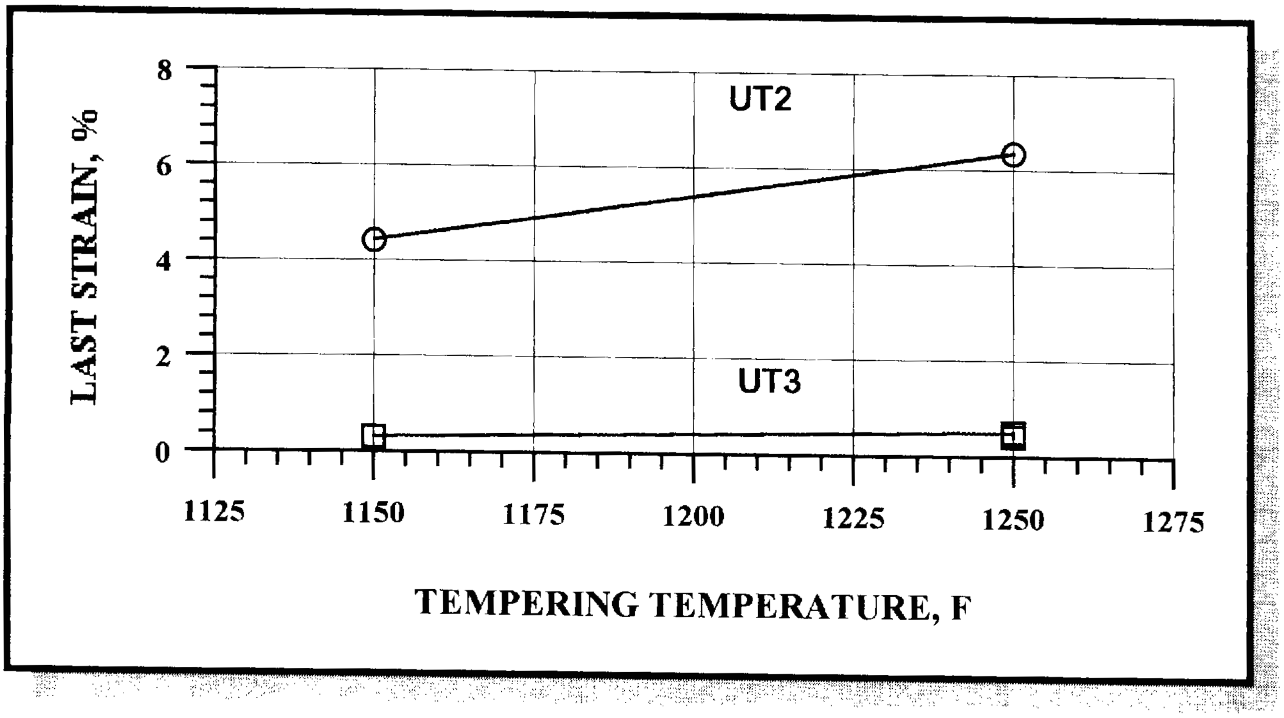

Fig. H1-9—80 Kj/in. HAZ last strain measurement before failure

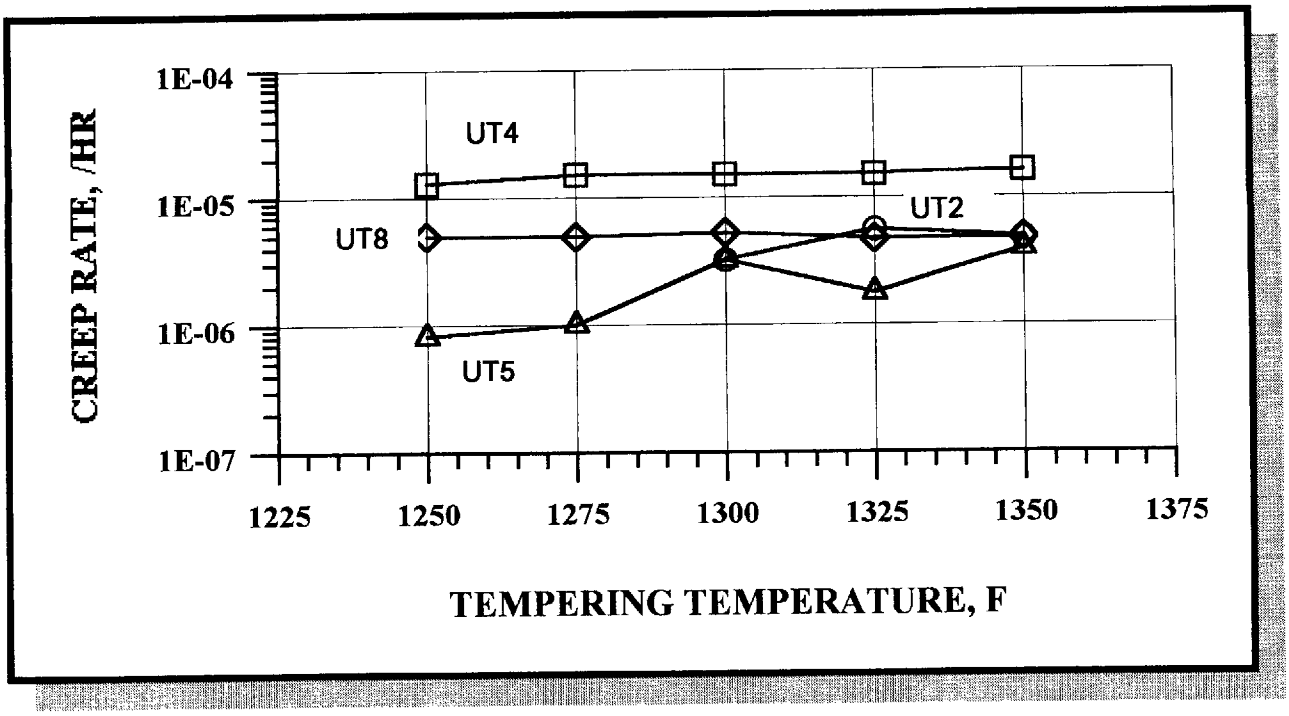

Fig. H1-10—Creep rates vs. tempering temperature for high heat input HAZ

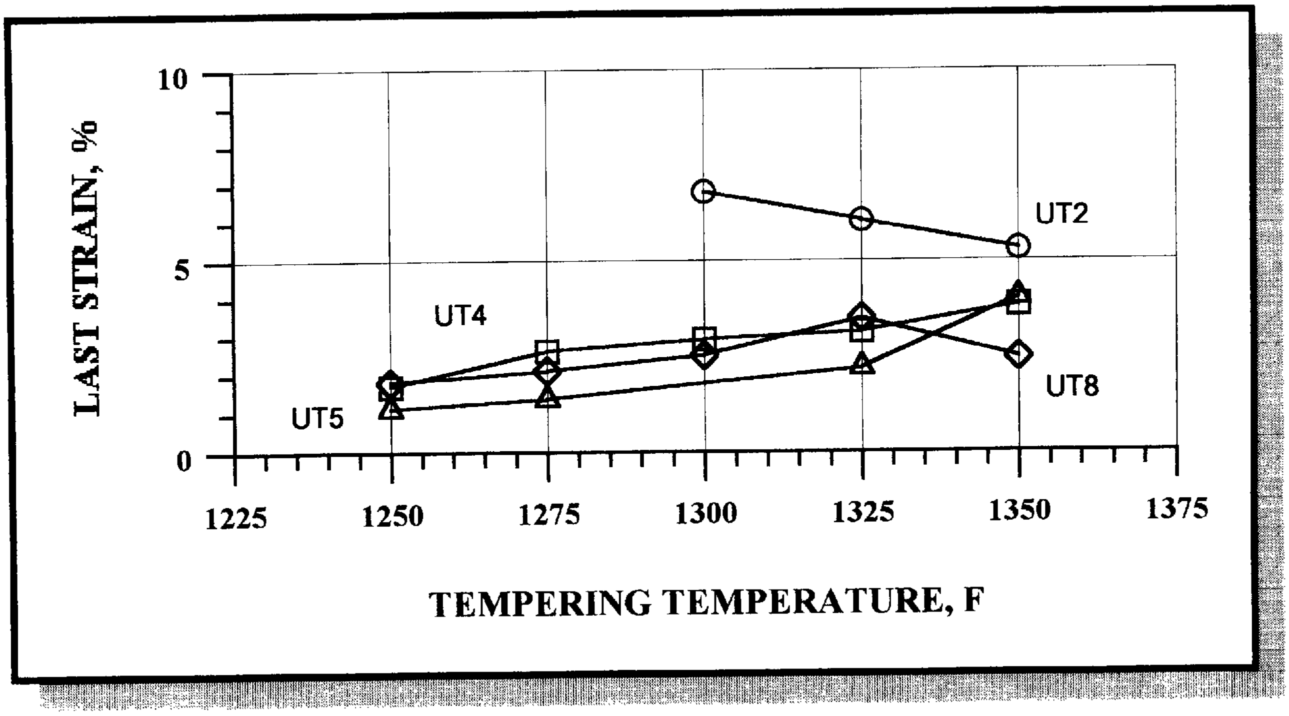

Fig. H1-11—Last strain measured before failure vs. tempering temperature for high heat input HAZ

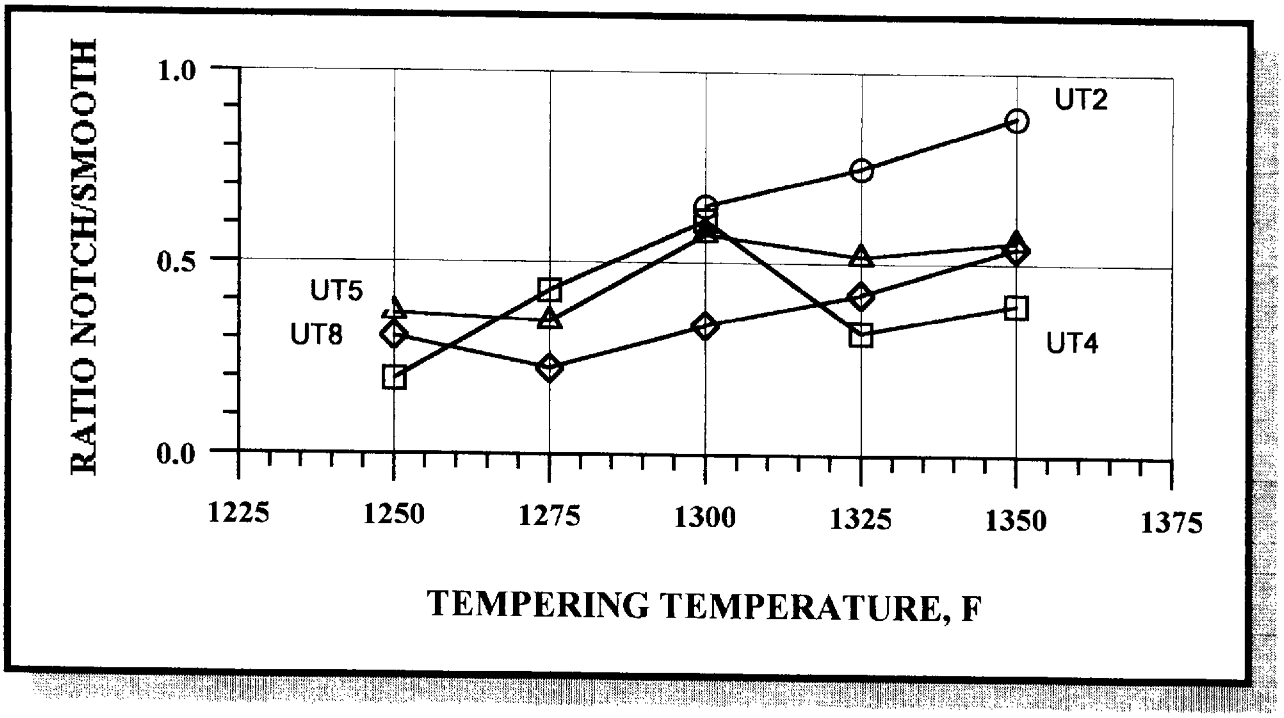

Fig. H1-12—Notch/smooth bar life ratios for high heat input HAZ

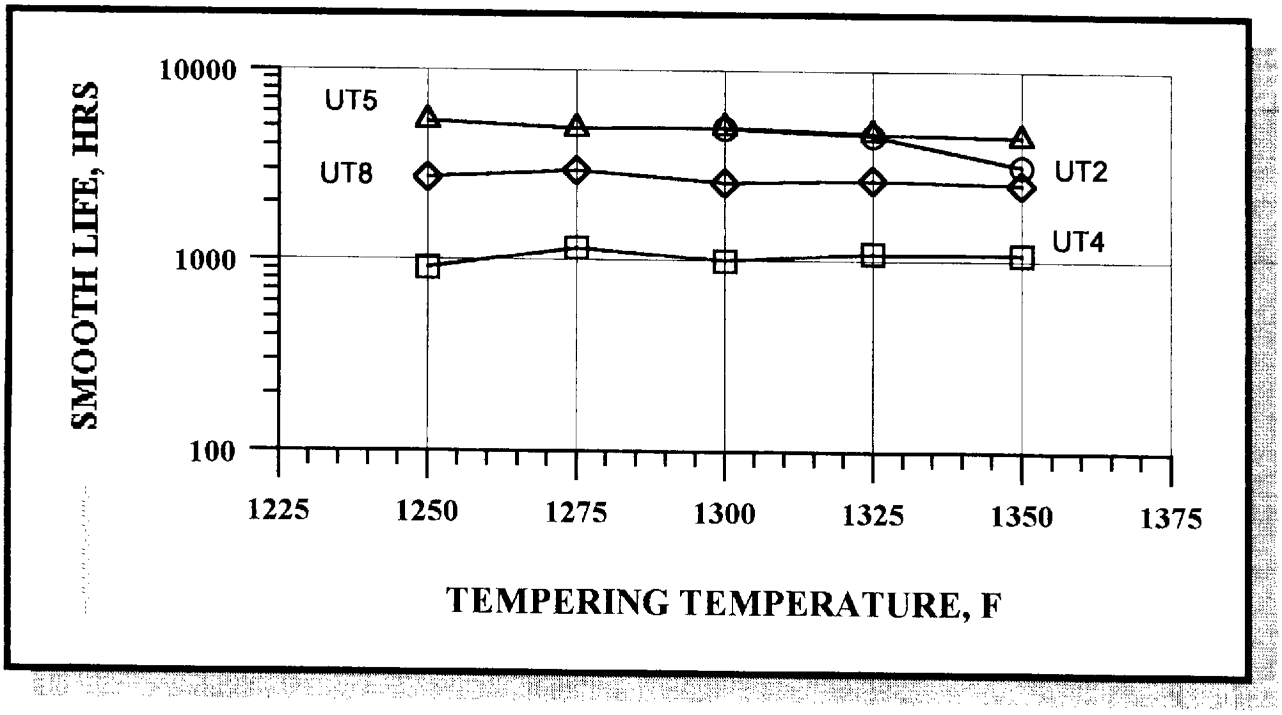

Fig. H1-13—Smooth bar rupture life for high heat input HAZ

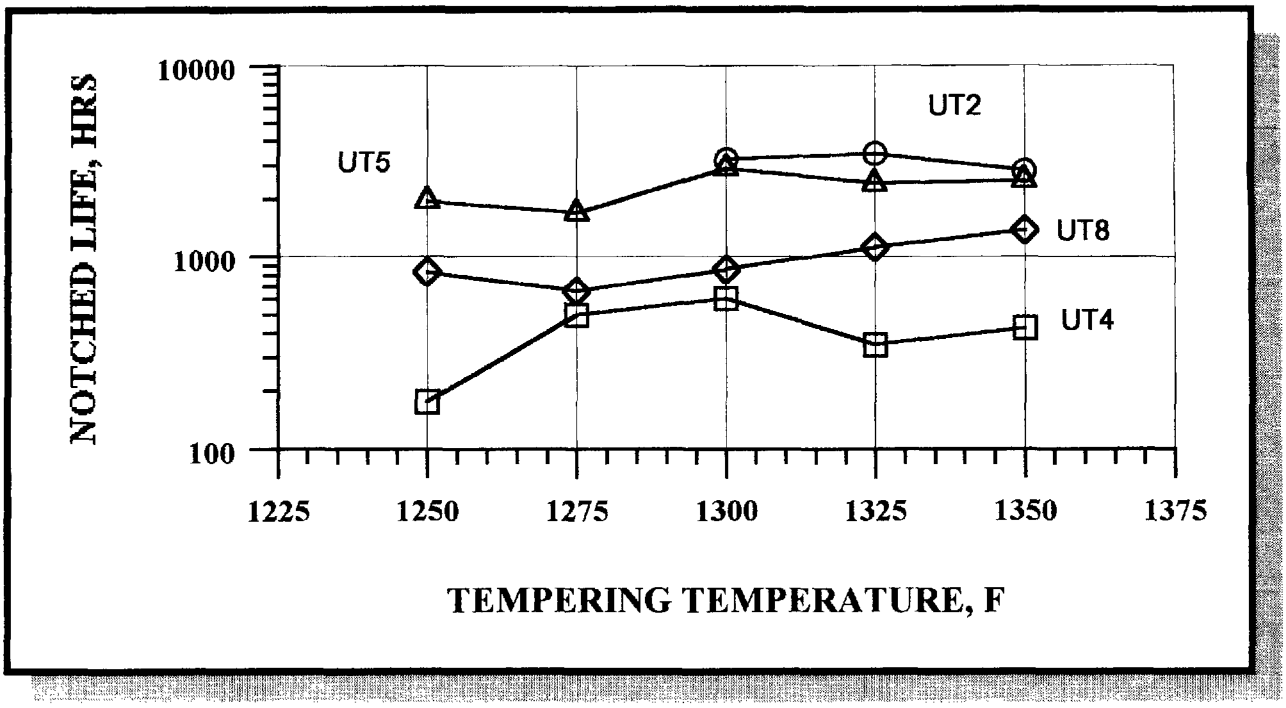

Fig. H1-14—Notch bar rupture life for high heat input HAZ

temper-ing temperature, it is not apparent that UT4 improved above 1275°F. Certainly, tempering below 1275°F did not provide good performance for UT4.

Low Heat Input Results. In this series of tests, UT3, 4 and 5 were compared. All had relatively high carbon content. As with the high heat input welds, UT4 displayed more rapid creep rates than UT5, although the difference was not so great (Fig. H1-15). The last measured strain before failure was lowest at 1250°F and highest at 1350°F (Fig. H1-16). UT3 was poor, irrespective of tempering temperature. Smooth and notch bar lives varied considerably with UT3 displaying very short life despite low creep rates, apparently because of its low ductility (Figs. H1-17

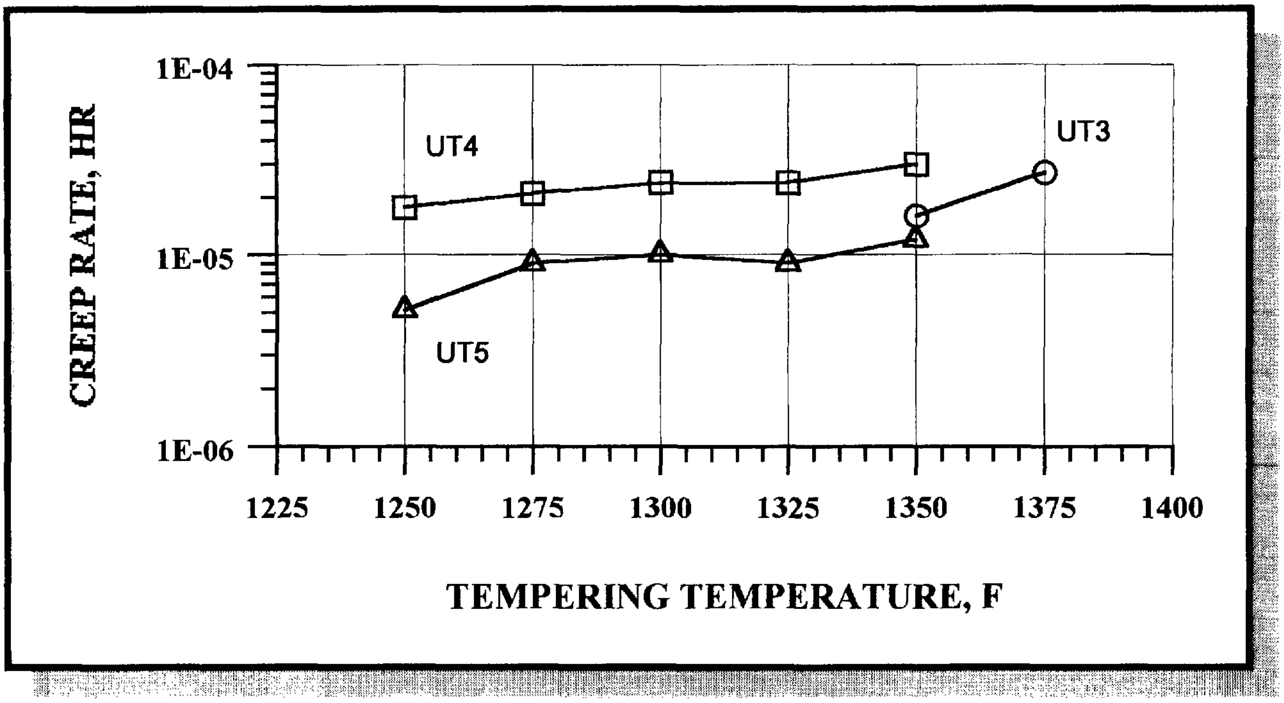

Fig. H1-15—Creep rates vs. tempering temperature for low heat input HAZ

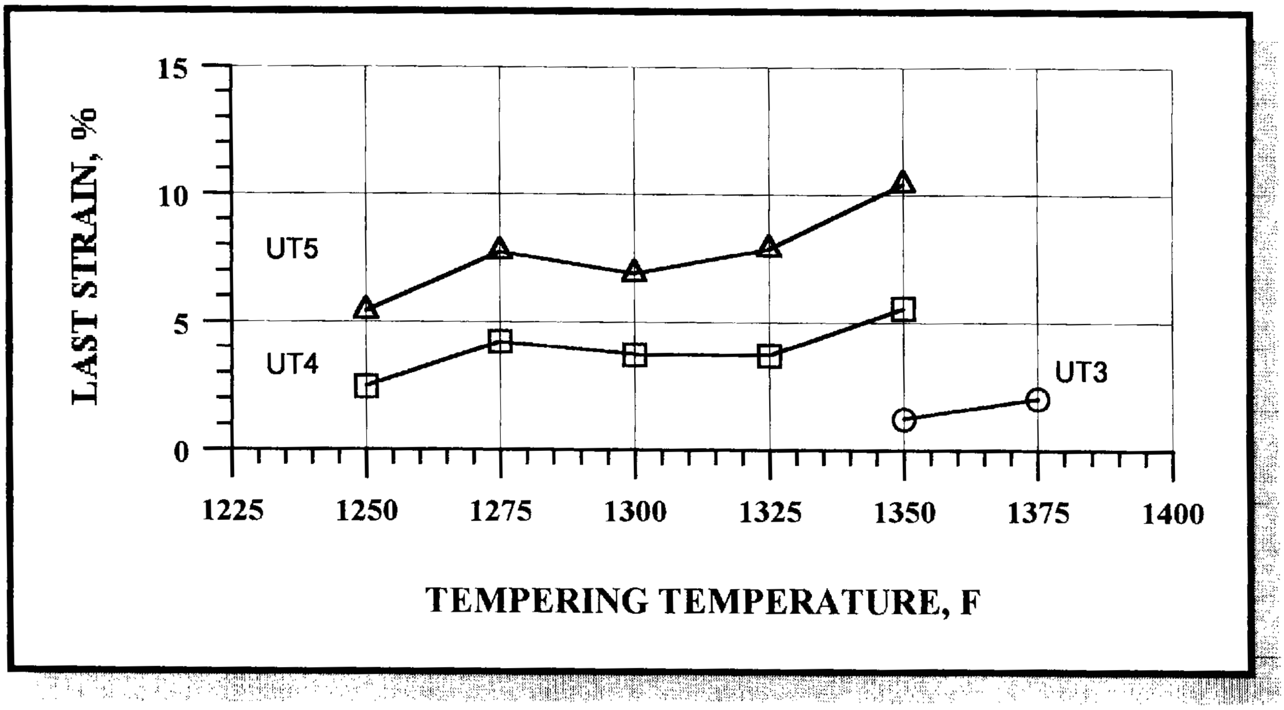

Fig. H1-16—Last strain measured vs. tempering temperature for low heat input HAZ

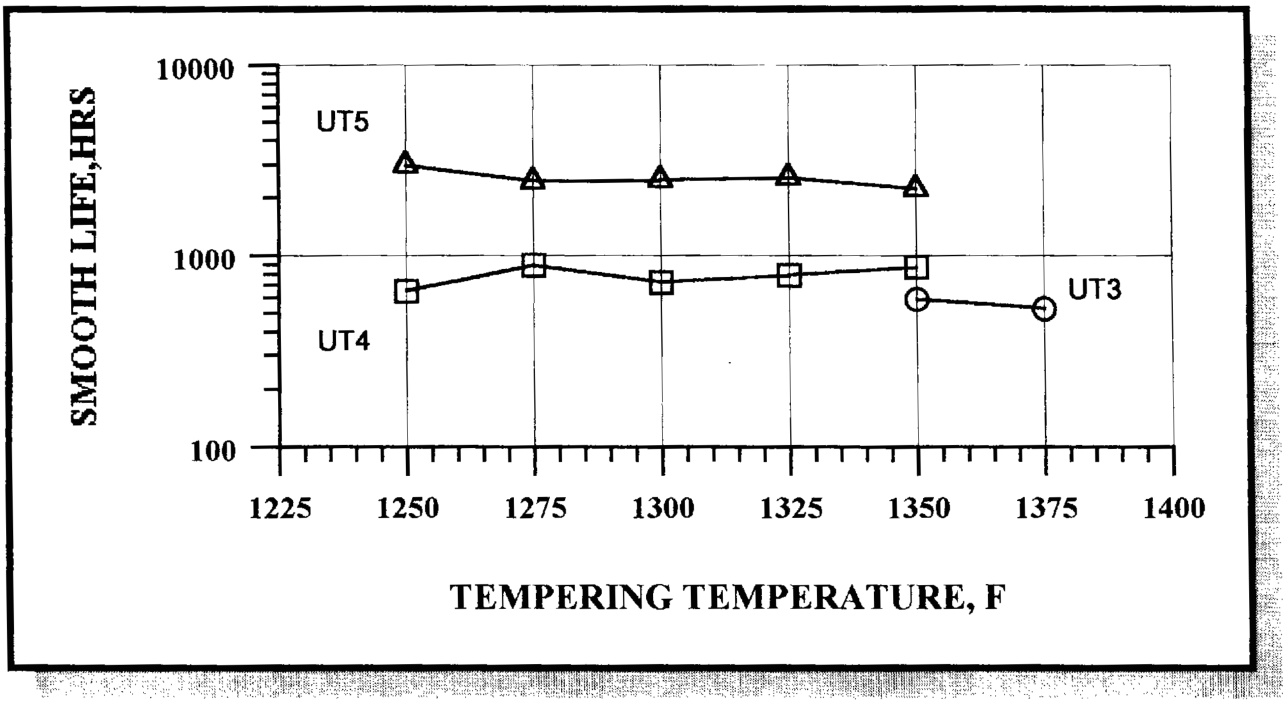

Fig. H1-17—Smooth bar rupture life for low heat input HAZ

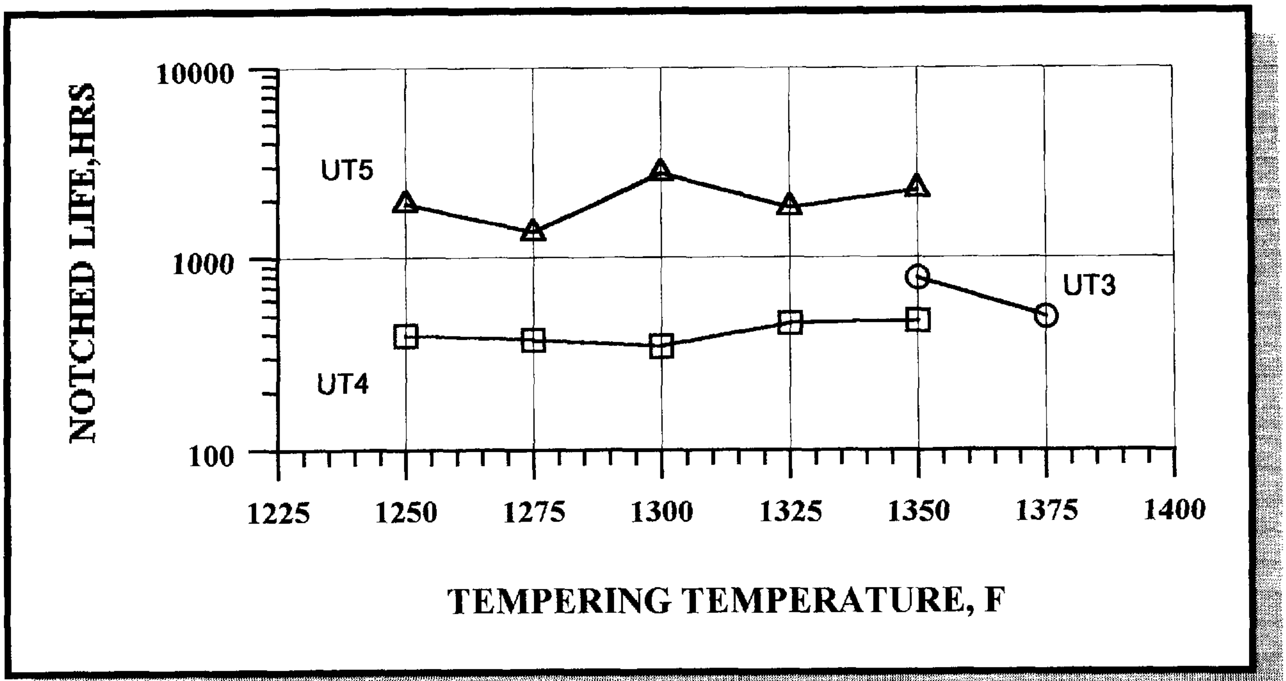

Fig. H1-18—Notch bar rupture life for low heat input HAZ

and H1-18). The life ratios of UT5 were relatively high and even exceeded unity at some temperatures-(Fig. H1-19). The ratios of lives for UT3 were high because smooth bars failed quickly because ductility was so low. Tempering cannot be viewed as having imparted favorable properties to UT3.

Comparison of High and Low Heat Input. Materials UT4 and UT5 were studied in the high and low heat input conditions. Creep rates of low heat input materials were consistently higher, although the difference was much greater for UT5 (Figs. H1-20 and H1-21). Smooth bar lives displayed less variations (Figs. H1-22 and H1-23) while notch bar lives were substantially independent of heat input (Figs. H1-24 and H1-25).

Hardness and Metallographic Studies. Data were taken regarding the hardnesses of specimens before and after testing. Sample data may be found in Table H1-6. Hardness seemed to correlate only with total tempering and test thermal exposure and not elongation, life ratio or total life.

Microhardness measurements at the uncracked notch failed to show any significant softening pattern in the vicinity of the notch. The hardness transverse locations and representative data may be seen in Figs. H1-26 to H1-30. Typically, cracks were found to have initiated subsurface and propagated intergranularly radially outward toward the surface and then inward before fracture (Figs. H1-31 to H1-33).

Conclusions

The smooth/notch bar study corroborated the conclusions of the reheat cracking study and provided insight into some cause and effect relations. At the test stresses and temperatures the materials displayed very low ductility despite tempering. The effect of tempering on creep rate and life was very small. Notch sensitivity appeared to decline as ductility increased and hardness decreased. The superior ductility of low heat input materials was attributed to differences in transformation products (Appendix C). It is apparent that for a given material, a low heat input weld provides higher ductility and creep rates. The effect on smooth bar life is small, but notch bar life improves.

The extraordinarily high creep rate for UT4 in the high heat input condition and the small differences as compared to low heat input material suggests unusual transformation behavior leading to similar transformation products irrespective of heat input. This material was noted to have an abnormally high manganese content which could favor martensite in the products as noted in Appendix C.

Ductility may also be influenced by impurities. Heats with excessive Sn, Cu (correlated variables), etc. tended to display low ductility after PWHT. The combination of high creep rates and low ductility would lead to very short life.

Tempering tended to have beneficial effects on notch ratios and ductility. The behavior of materials tempered below 1275°F was notably inferior. It is expected that markedly superior results (ratios) would be obtained if the hardness of the HAZ could be reduced by tempering to values closer to that of the base metal. This appeared to occur most readily with

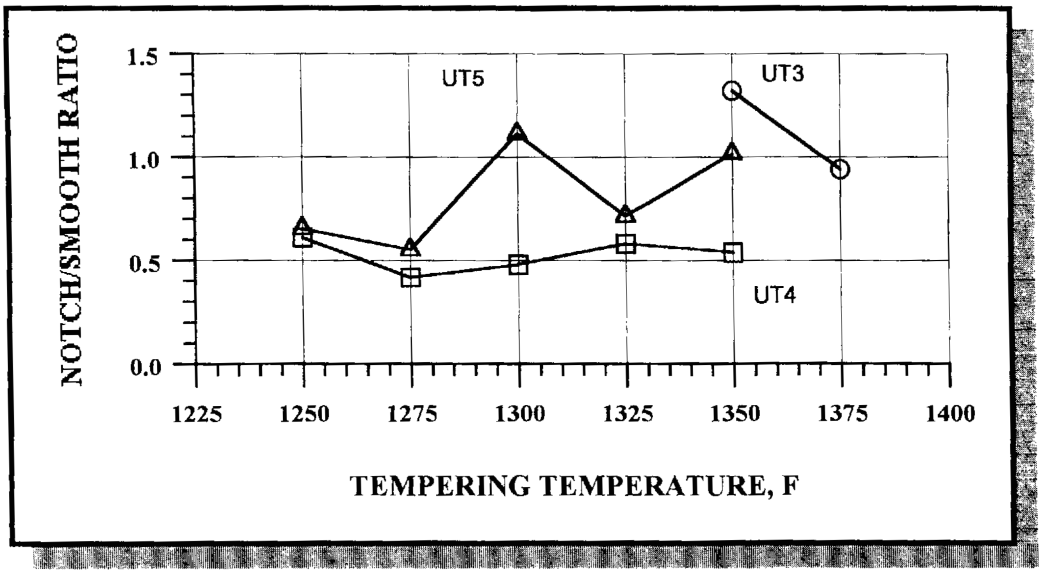

Fig. H1-19—Ratio of notch to smooth bar lives vs. tempering temperature for low heat input welds

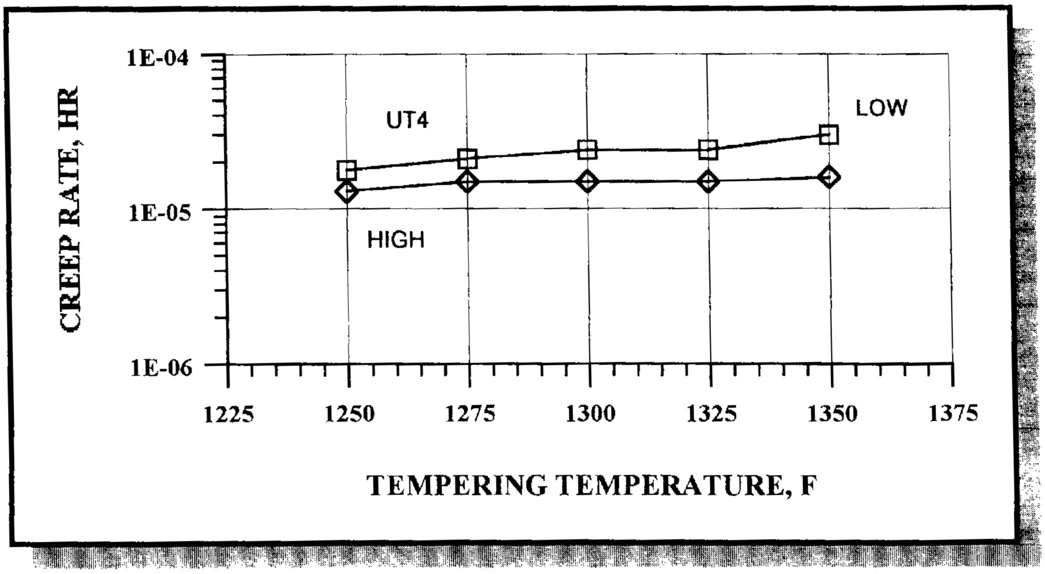

Fig. H1-20—Comparison of creep rates for UT4 at low and high heat inputs

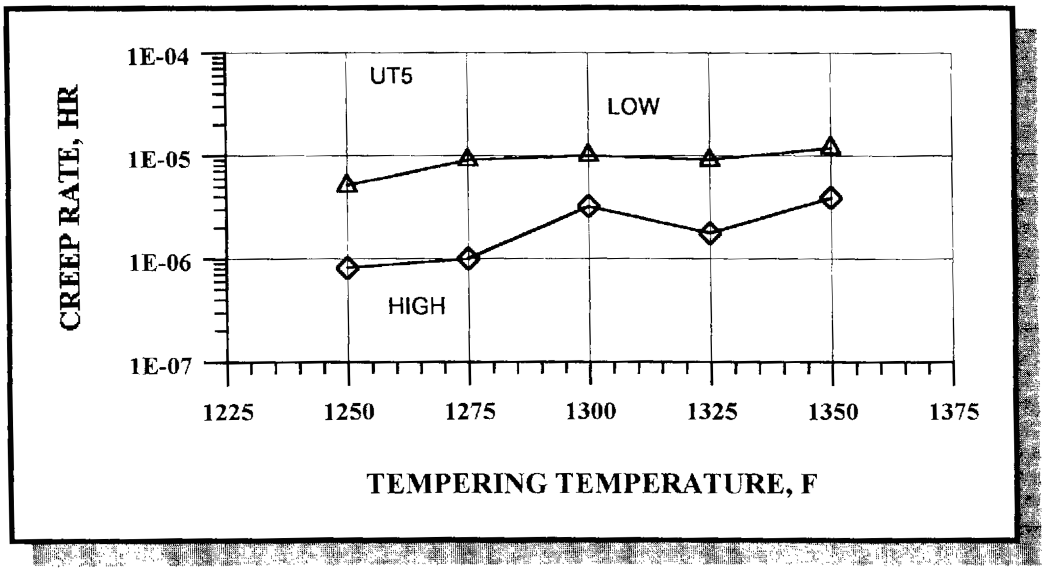

Fig. H1-21—Comparison of creep rates for UT5 at low and high heat inputs

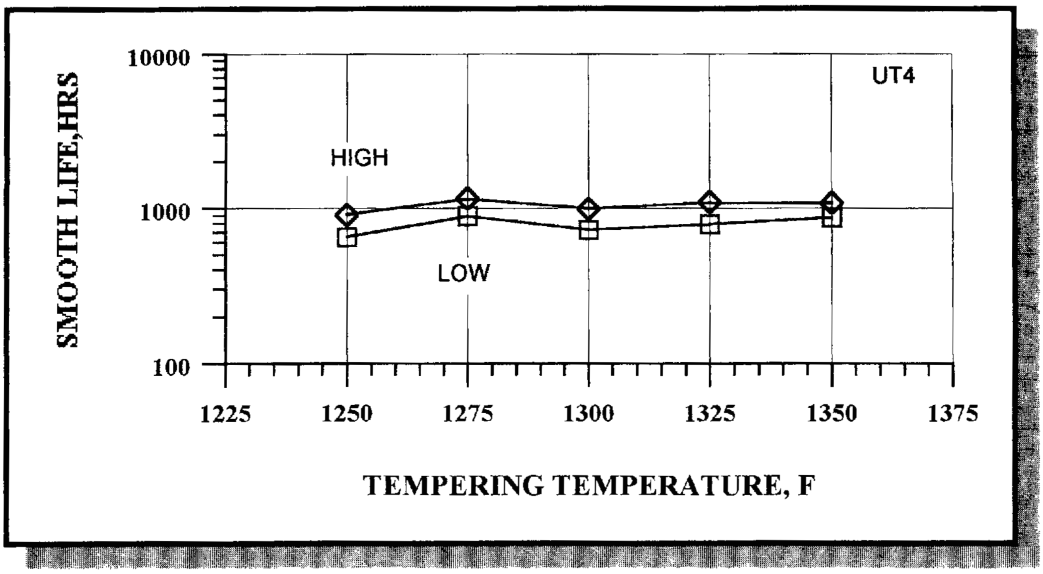

Fig. H1-22—Comparison of smooth bar lives for UT4 at low and high heat inputs

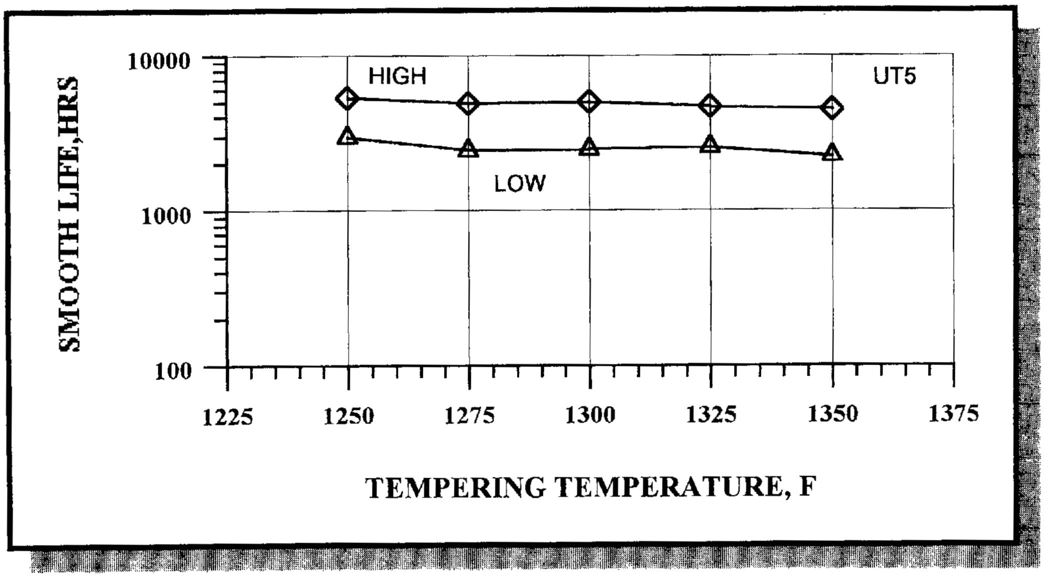

Fig. H1-23—Comparison of smooth bar lives of UT5 at low and high heat inputs

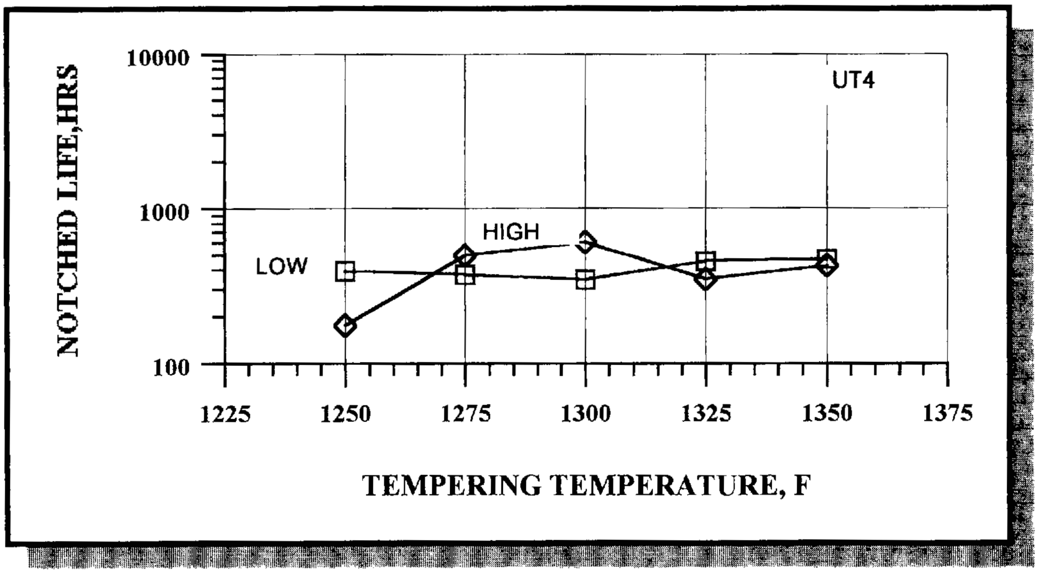

Fig. H1-24—Comparison of notch bar lives of UT4 at low and high heat inputs

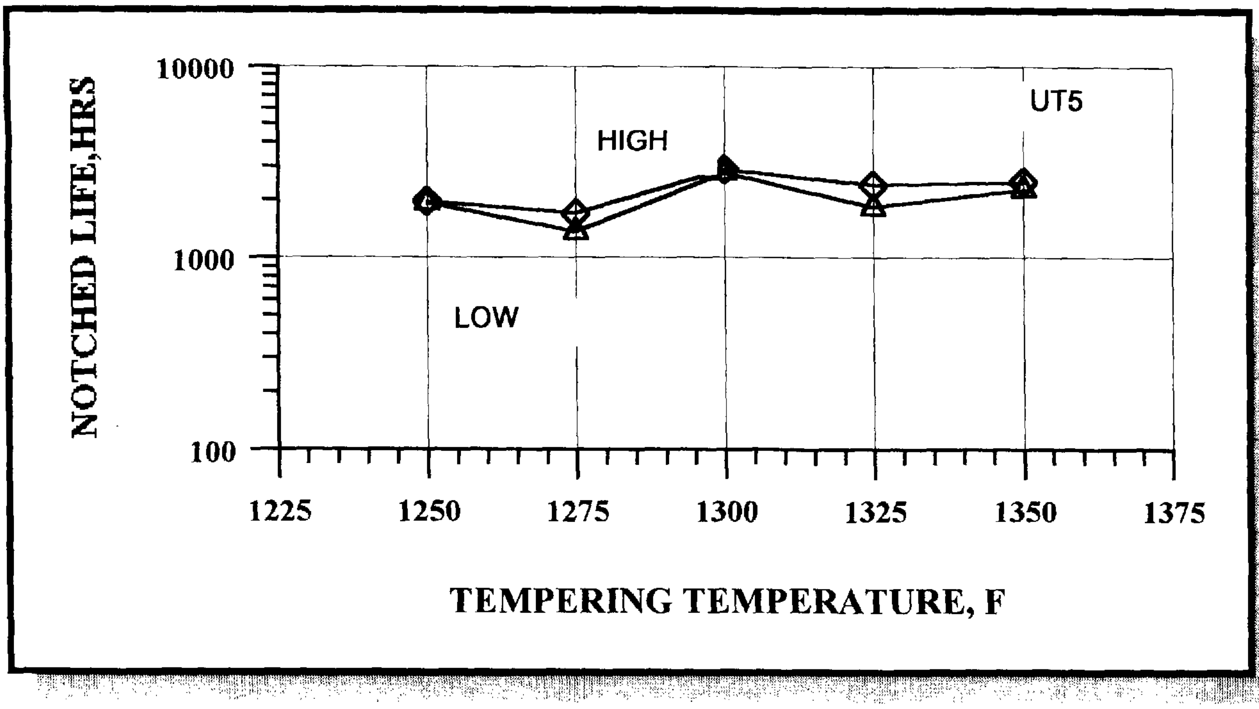

Fig. H1-25—Comparison of notch bar lives of UT5 at low and high heat inputs

Table H1-6—Hardness of Notched Stress Rupture Samples Test Condition: 1025°F-20Ksi

					Hardness, HV			
Materials	*MPC Code*	*Heat Input KJ/in.*	*PWHT °F/hrs*	*Rupture Time (hrs)*	*UTK*	*A*	*B*	*C*
UT2	1250/1H	80	1250/1	3488.7	188	—	—	192
UT2	1325/3	80	1325/3	3431.2	186	246	180	172
UT2	1350/3	80	1350/3	2794.2	183	244	176	169
UT3	J	80	1250/1	130.8	222	—	—	216
UT3	L-P	45	1325/3	454.8	218	—	—	207
UT3	L-Q	45	1350/3	784.4	176	—	—	205
UT3	H-J	120	1250/5	—*	—*	—*	—*	—*
UT3	H-P	120	1325/3	884.6	183	—	—	195
UT3	H-Q	120	1350/3	—*	—*	—*	—*	—*
UT4	L-J	45	1250/5	394.1	218	—	—	237
UT4	L-P	45	1325/3	454.1	200	269	202	—
UT4	L-Q	45	1350/3	468.4	184	270	185	—
UT4	H-J	120	1250/5	175.2	237	—	—	237
UT4	H-P	120	1325/3	347.9	193	263	210	200
UT4	H-Q	120	1350/3	423.9	185	262	190	180
UT5	L-J	45	1250/5	1931.6	199	—	—	210
UT5	L-P	45	1325/3	1828.4	202	252	192	187
UT5	L-Q	45	1350/3	2262.9	176	246	176	152
UT5	H-J	120	1250/5	1960	198	—	—	210
UT5	H-P	120	1325/3	2402.8	197	252	192	187
UT5	H-Q	120	1350/3	2482.7	182	246	176	170
UT8	H-J	120	1250/5	366.4	194	—	—	200
UT8	H-P	120	1325/3	1116.7	178	240	190	190
UT8	H-Q	120	1350/3	1368	183	247	—	180

Abbreviations: UTK, After creep rupture test (UTK); A, As-simulated (MPC); B, After tempering at MTC (MPC); C, After creep rupture test (MPC).

*Under test.

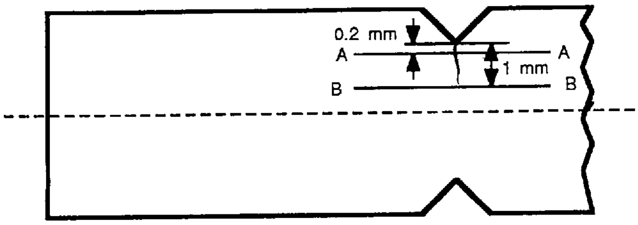

HARDNESS MEASUREMENT ALONG A-A
AND B-B IN CREEP RUPTURE SAMPLE

Fig. H1-26—Locations for microhardness traverses in double notch rupture bars

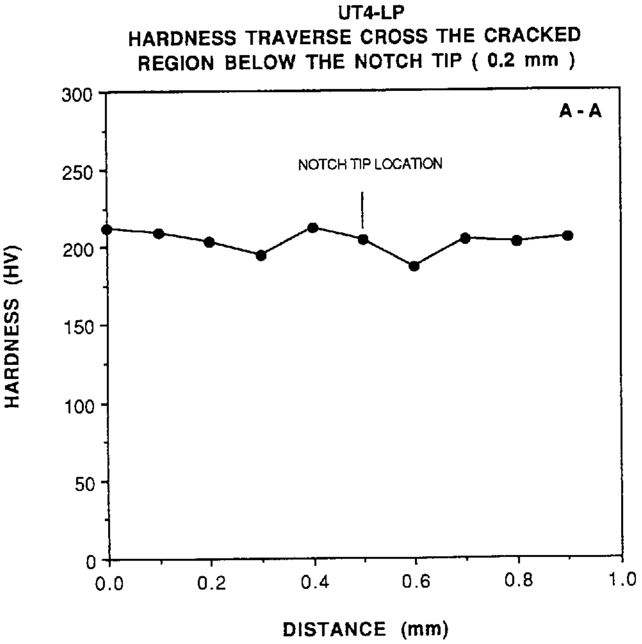

Fig. H1-27—Hardness traverse of notch specimens of UT4, low heat input tempered at 1325°F, Section AA

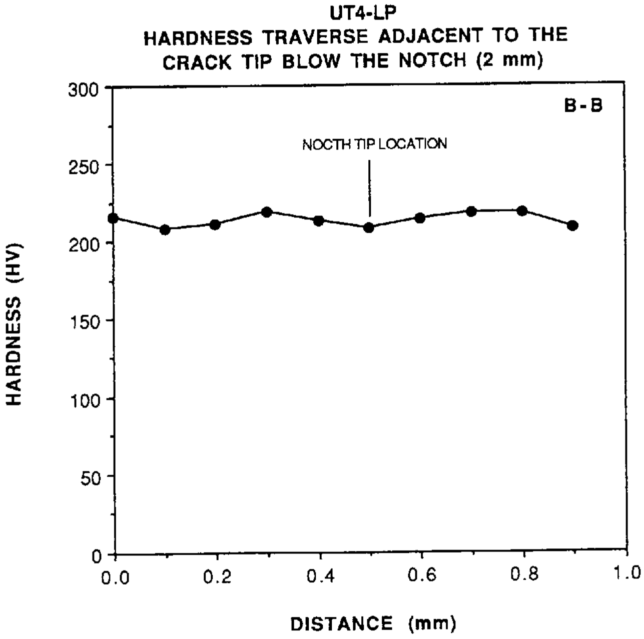

Fig. H1-28—Hardness traverse of notch specimens of UT4, low heat input tempered at 1325°F, Section BB

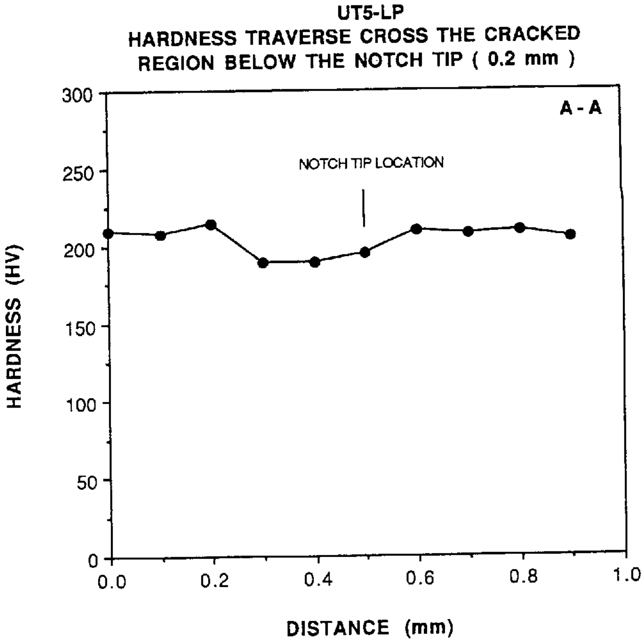

Fig. H1-29—Hardness traverse of notch specimens of UT8, low heat input tempered at 1325°F, Section AA

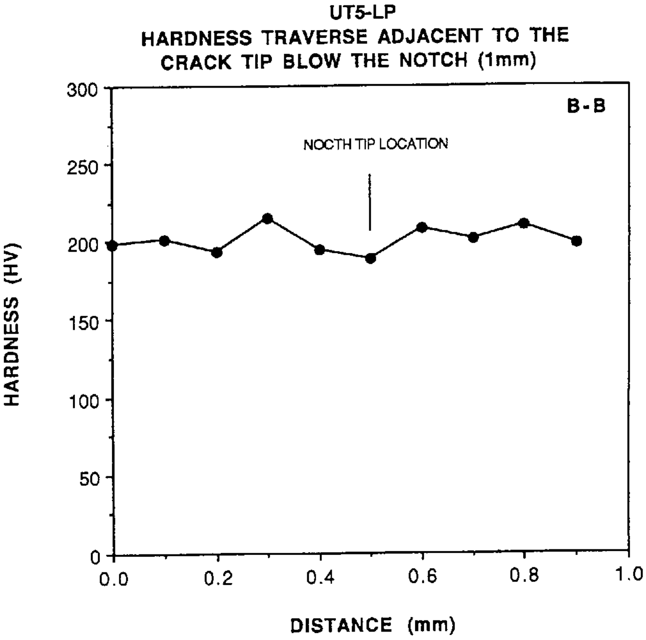

Fig. H1-30—Hardness traverse of notch specimens of UT5, low heat input tempered at 1325°F

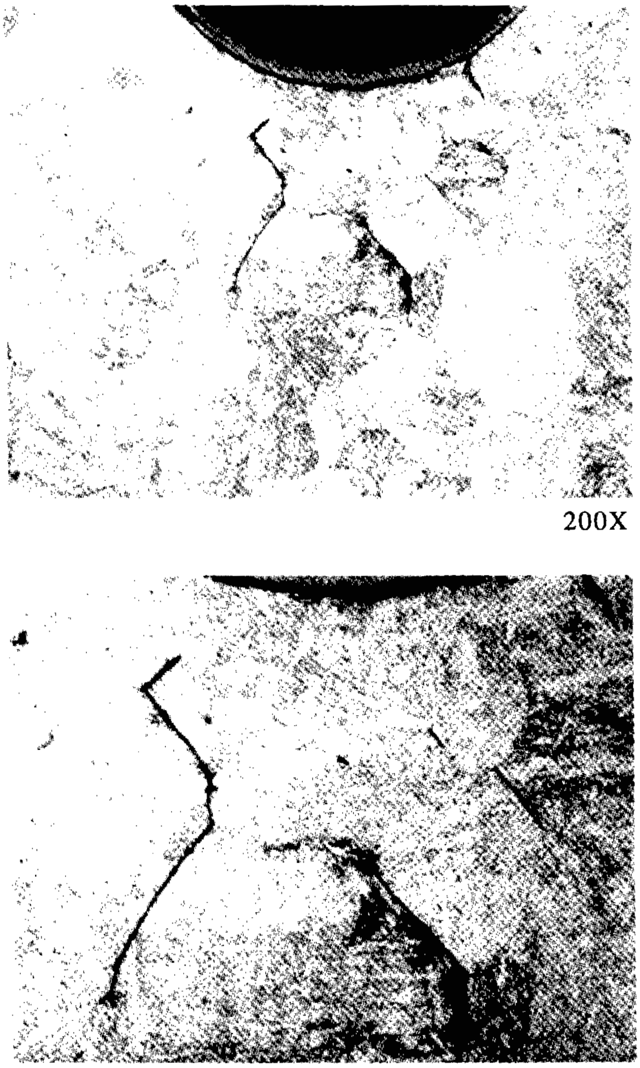

200X

400X

Fig. H1-31—Crack initiated beneath the second notch tip of creep ruptured sample, UT4, heat input 45 Kj/in., PWHT 1325°F, 3 hrs, tested at 1025°F, 20 ksi for 454.1 hrs

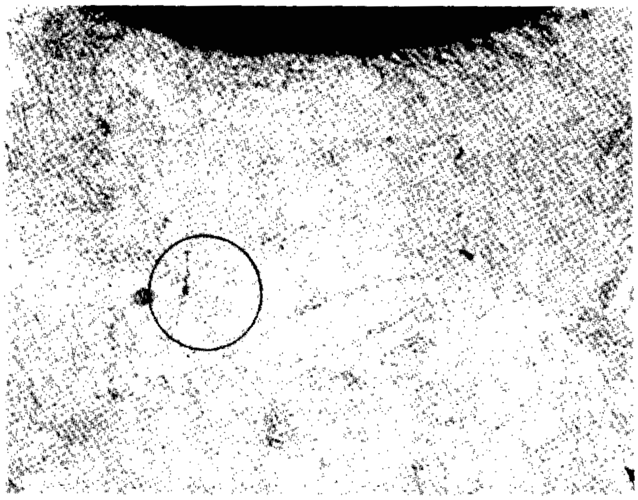

400X

Fig. H1-32—Microcrack initiated beneath the second notch tip of creep ruptured sample, UT5, heat input 45 Kj/in., PWHT 1325°F, 3 hrs, tested at 1025°F, 20 ksi for 1828.4 hrs

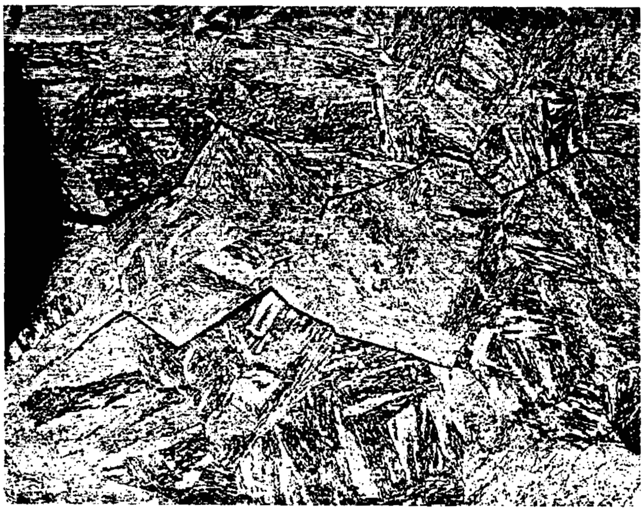

Fig. H1-33—Intergranularly propagated crack in UT4 specimen

the low carbon material UT2 and when low heat input was used.

References to Appendix H1

1. Hashimoto, K., Tokuno, K., Takeda, T., Tsuchida, Y. and Prager, M. Creep Embrittlement of V-Modified 2.25Cr-1Mo Steels, *Serviceability of Petroleum, Process and Power Equipment* (ASME PVP Vol. 239/MPC Vol. 33), 1992.
2. Prager, M. Development of the MPC OMEGA Method for Life Assessment in the Creep Range, PVP Vo. 288, ASME Pressure Vessel & Piping Conference, June 1994.

Appendix H2—Preparation of Extended Length HAZ Simulation Specimens by the Gleeble Technique

A technique for the preparation of extended length Gleeble HAZ simulation specimens suitable for creep rupture testing was developed so that reasonable sized and uniform microstructural HAZ zones could be accurately evaluated. A 125 mm long 11 mm gage diameter specimen was designed with 19 mm diameter ends. The extended specimen with large diameter ends gripped at the ends permits an extended (40 mm long) hot zone of uniform temperature. Because of increased jaw spacing, heat extraction during the cooling part of the thermal cycle is limited and thus externally applied cooling is utilized to obtain the desired cooling rate characteristic of the welding thermal cycle in the HAZ region of interest. For this external cooling, a 50 mm long cooling fixture was designed capable of impinging helium on the specimen surface along the specimen length. The helium flow was initiated beyond the peak temperature (1315°C–2400°F for CGHAZ simulation) and the flow rate of the helium was regulated to obtain a uniform and desired cooling rate along the gage length.

Subsequent metallographic and hardness evaluations on longitudinal sections of simulated specimens revealed uniform microstructure and hardness along a 35 mm length of the sample. This permits the machining of a 30 mm gage length with uniform microstructure for creep testing. The gage diameter is machined to 9 mm to provide a proper transition into the larger diameter specimen shoulders and to eliminate any microstructural gradients.

There is no other technique to study the mechanical behavior of a single region of the HAZ in a reasonable sized creep sample. Creep testing of these specimens generates data that is characteristic of the elevated temperature behavior of the CGHAZ of the material. Thus by using this unique method, very valuable data on the elevated temperature behavior of the CGHAZ of API materials was obtained which aided in the understanding of the differences in in-service cracking behavior between heats.

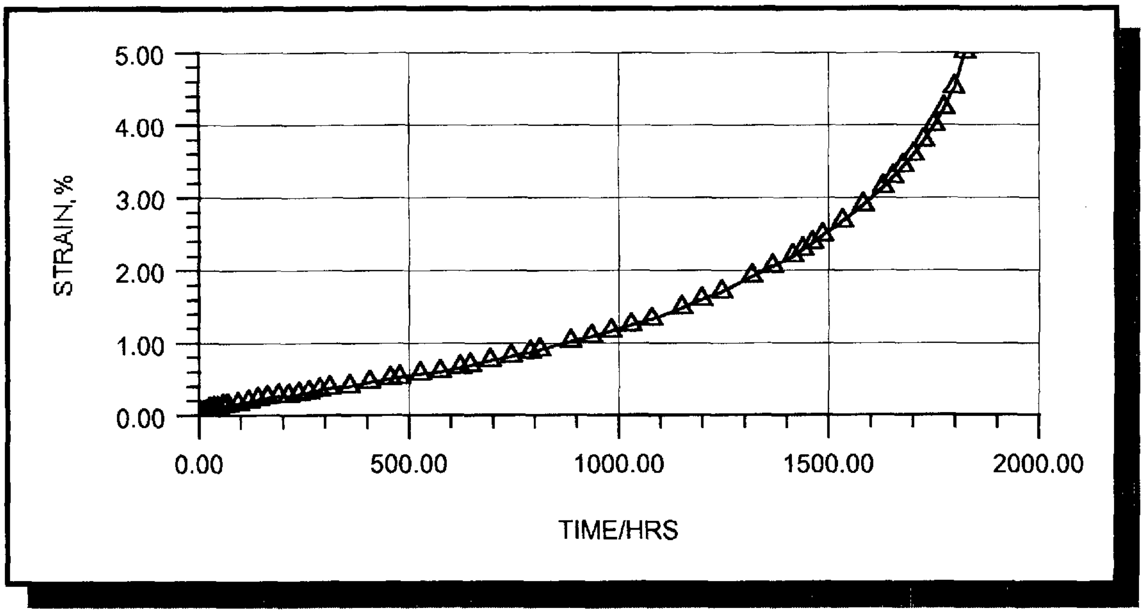

Fig. H3-1—UT2 1¼ CR ½ MO, HAZ, 1050F/20ksi specimen AB/BD-3

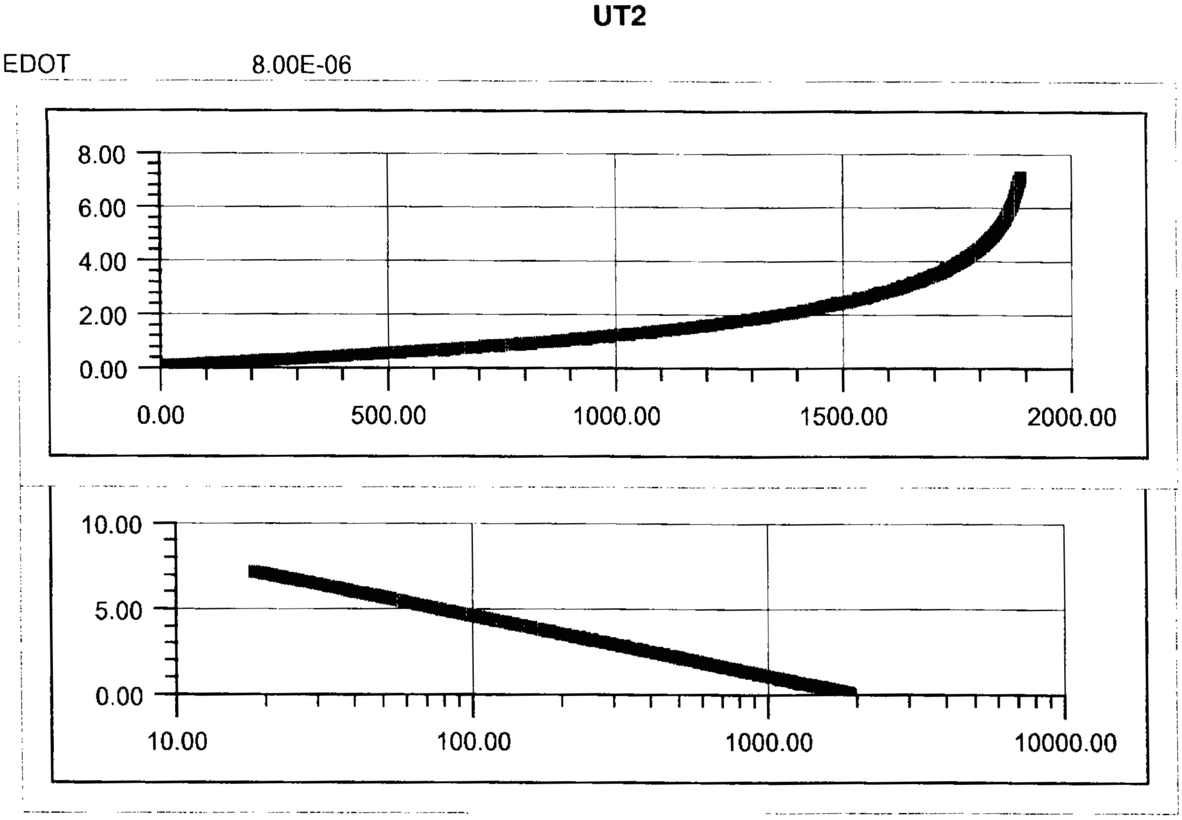

Fig. H3-2—Curve fitting per Ref. H2 to obtain MPC creep rate

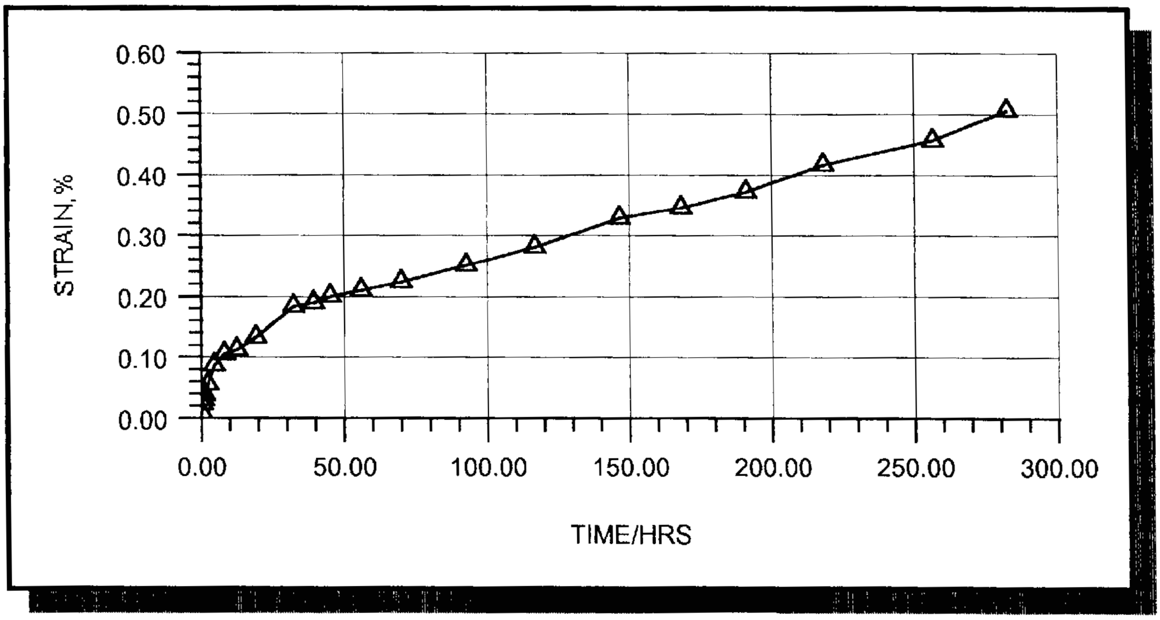

Fig. H3-3—UT3 1¼ CR ½ MO, Gleebled, 1025F/25KSI specimen LD-13

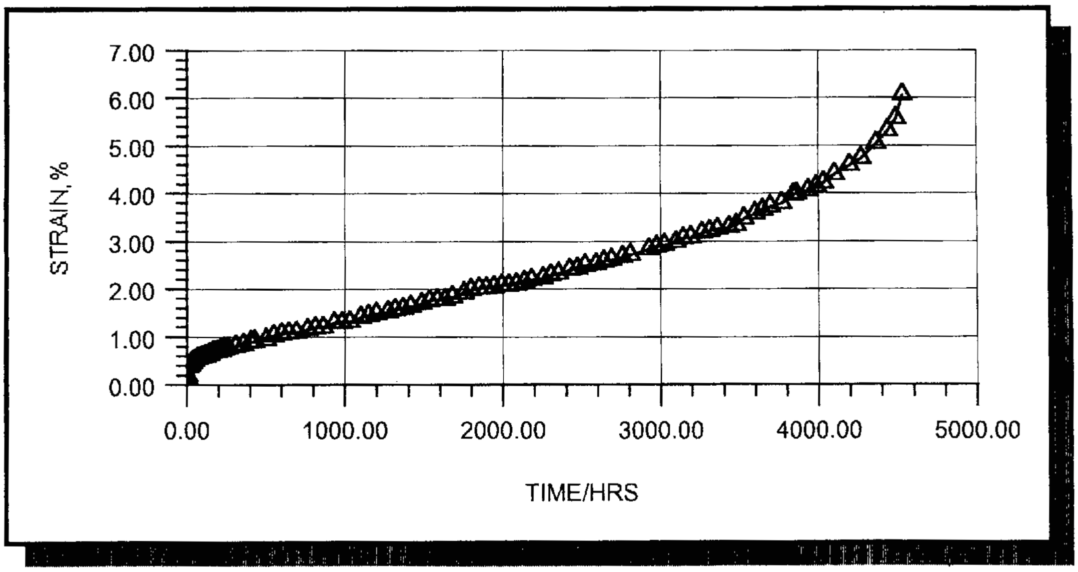

Fig. H3-4—UT2 1¼ CR ½ MO, HAZ, 1025F/20ksi specimen AB2H-P1

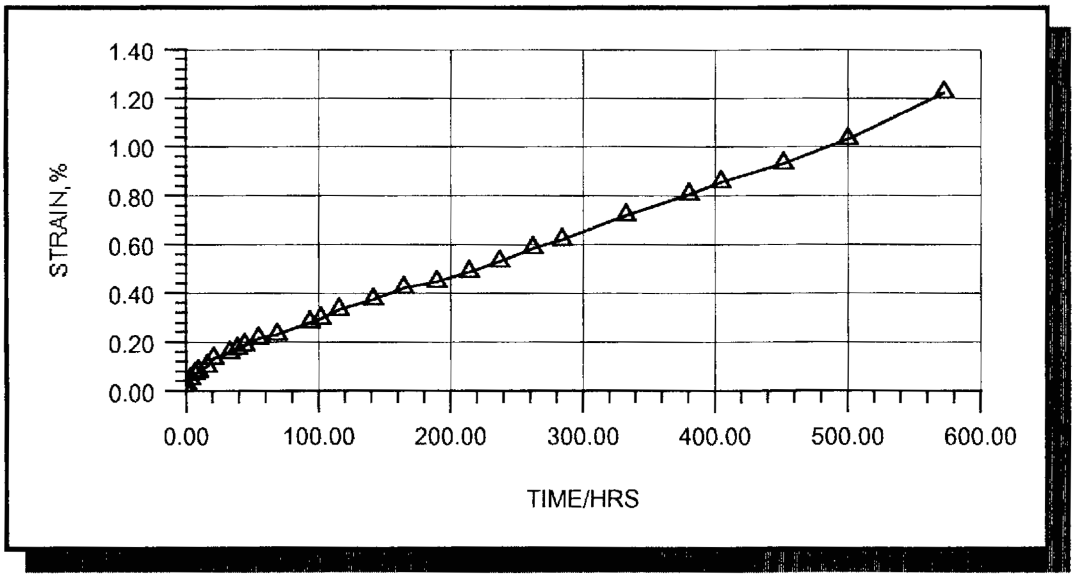

Fig. H3-5—UT3 1¼ CR ½ MO, HAZ, 1025F/20K specimen AB3L-Q2

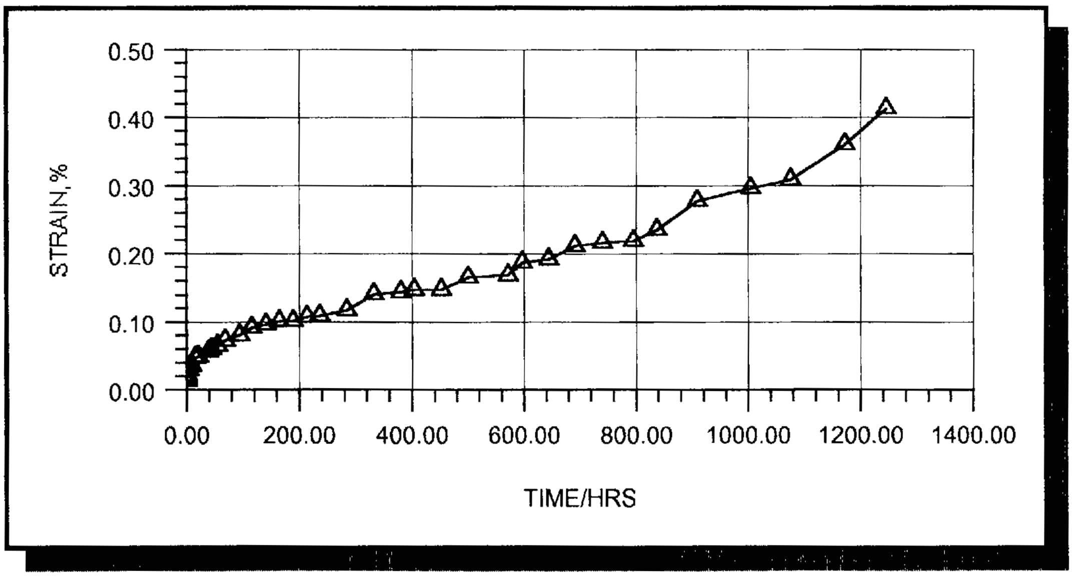

Fig. H3-6—UT3 1¼ CR ½ MO, HAZ, 1025F/20ksi specimen AB3H-P3

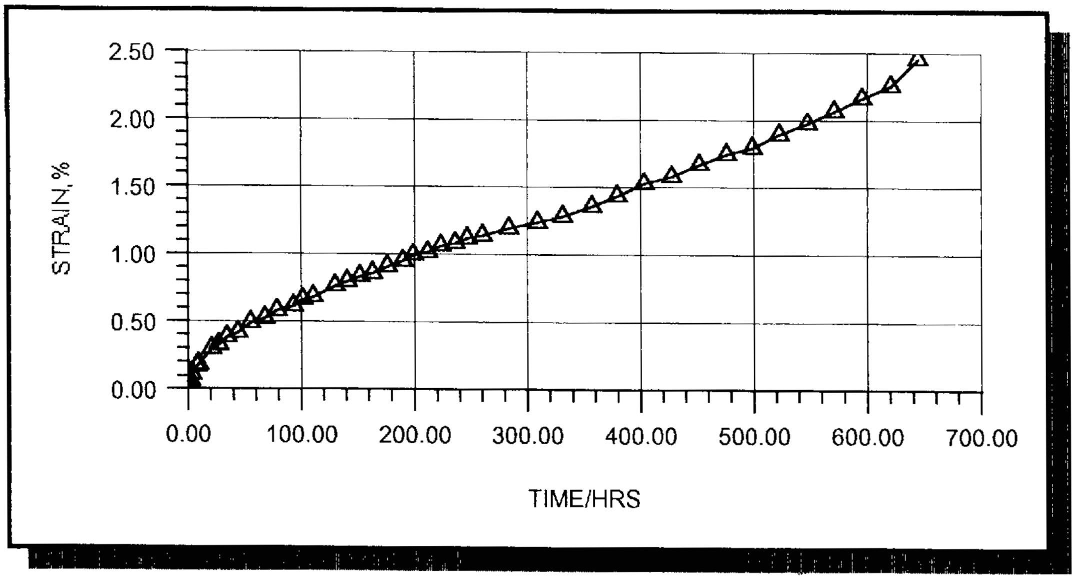

Fig. H3-7—UT4 1¼ CR ½ MO, HAZ, 1025F/20ksi specimen AB4L-J3

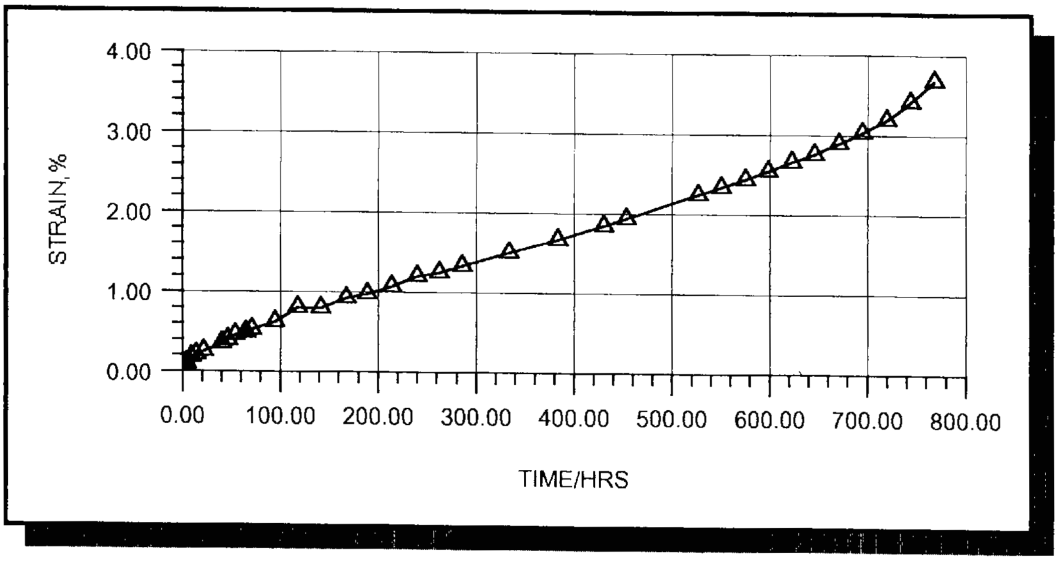

Fig. H3-8—UT4 1¼ CR ½ MO, HAZ, 1025F/20ksi specimen AB4L-P1

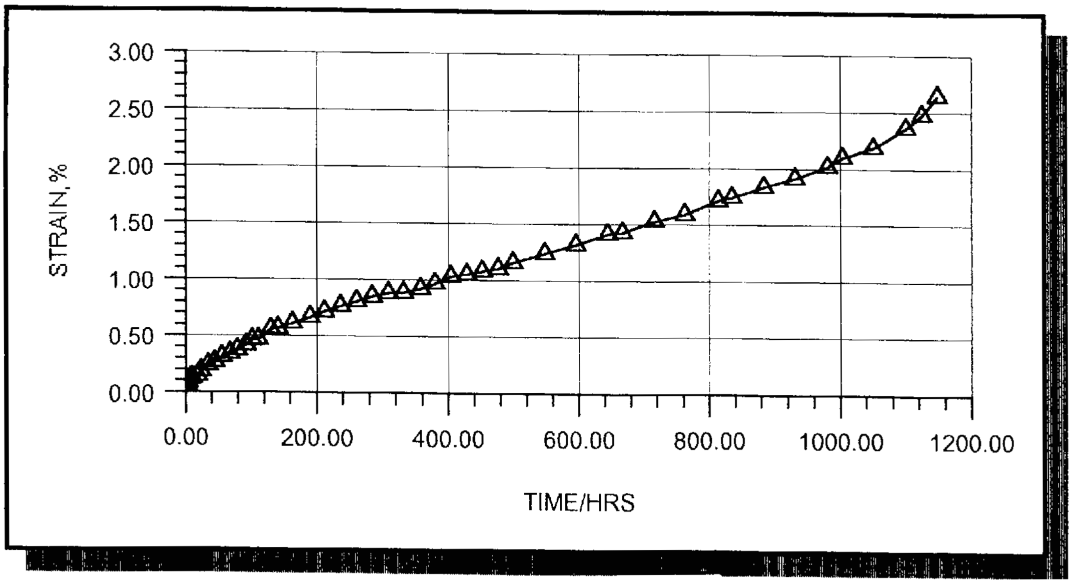

Fig. H3-9—UT4 1¼ CR ½ MO, HAZ, 1025F/20ksi specimen AB4H-K1

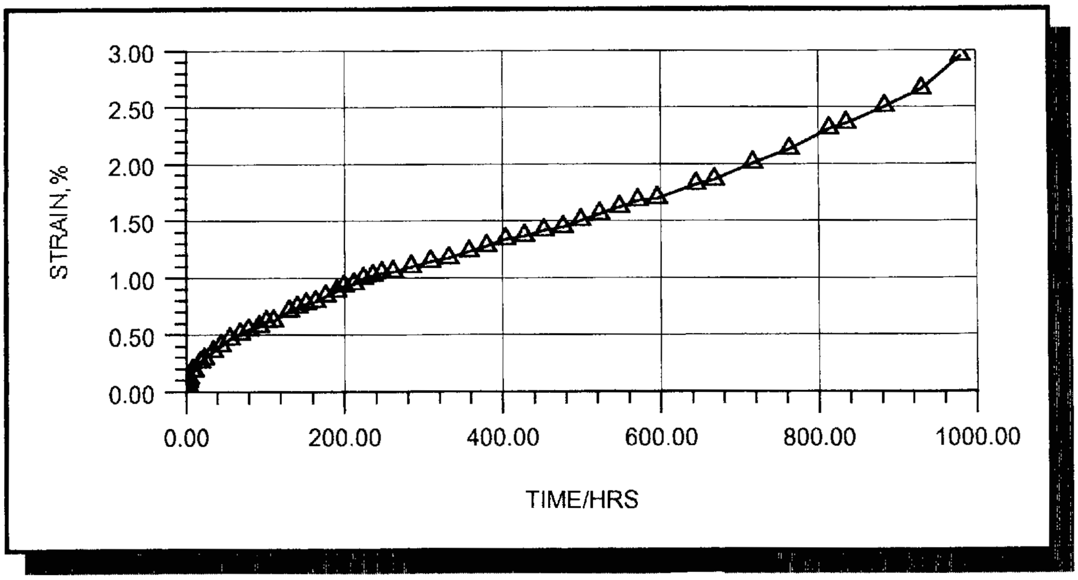

Fig. H3-10—UT4 1¼ CR ½ MO, HAZ, 1025F/20ksi specimen AB4H-M1

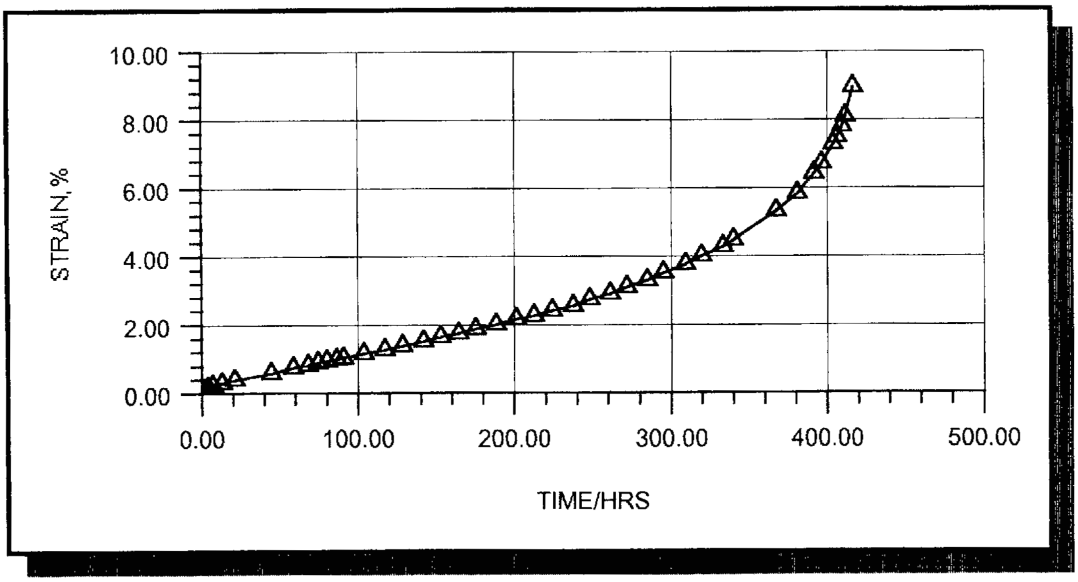

Fig. H3-11—UT5 1¼ CR ½ MO, HAZ, 1075F/20ksi specimen AB5L-K4

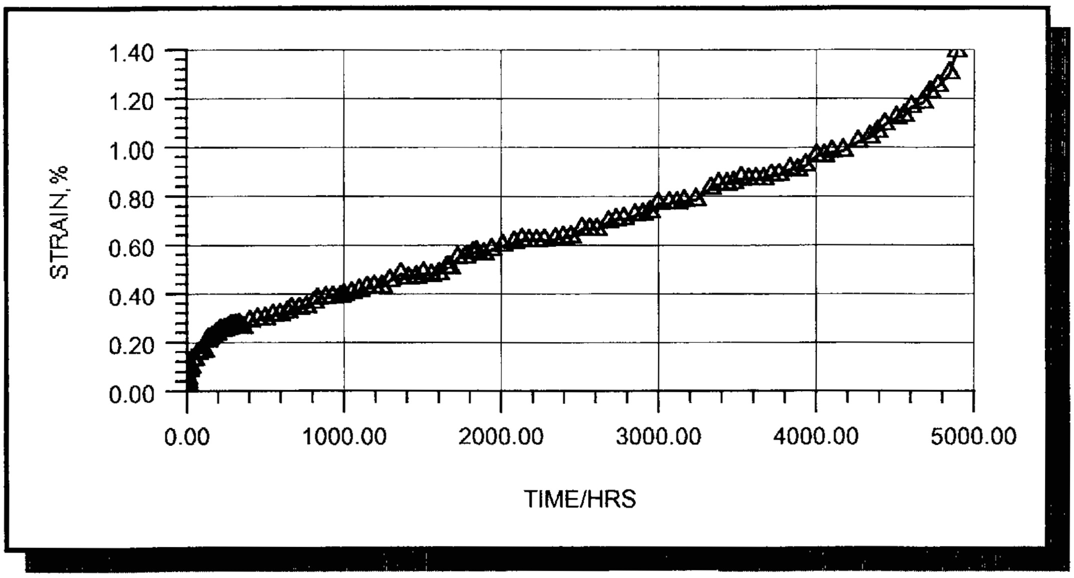

Fig. H3-12—UT5 1¼ CR ½ MO, HAZ, 1025F/20ksi specimen AB5H-K1

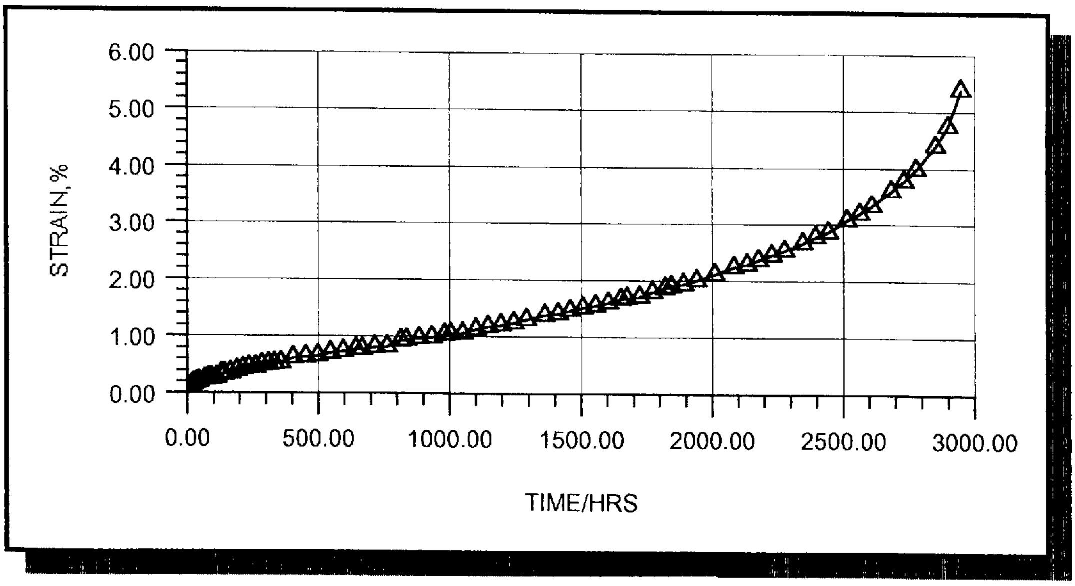

Fig. H3-13—UT5 1¼ CR ½ MO, HAZ, 1025F/20ksi specimen AB5L-J3

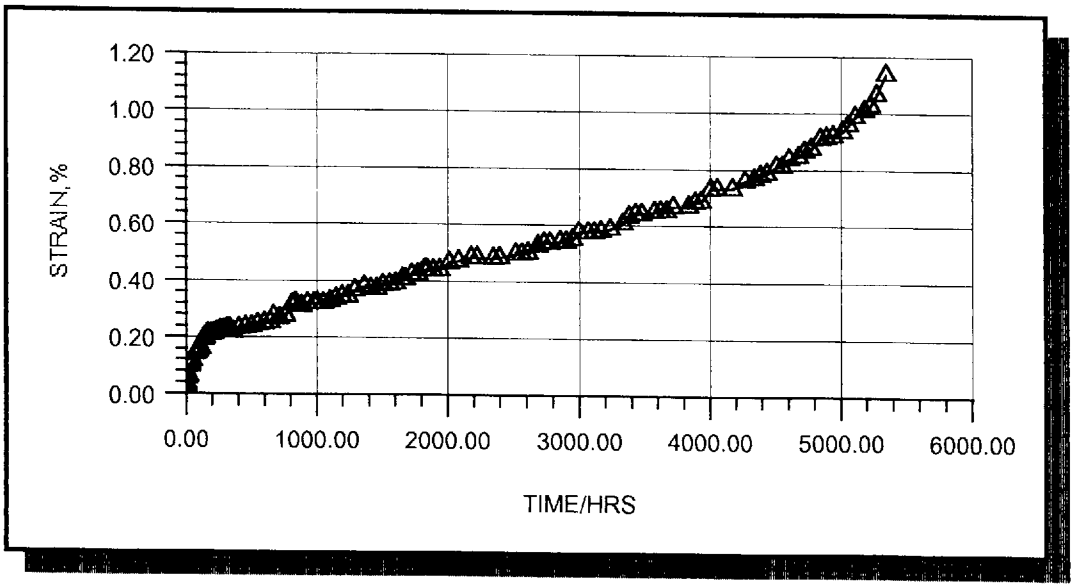

Fig. H3-14—UT5 1¼ CR ½ MO, HAZ, 1025F/20ksi specimen AB5H-J1

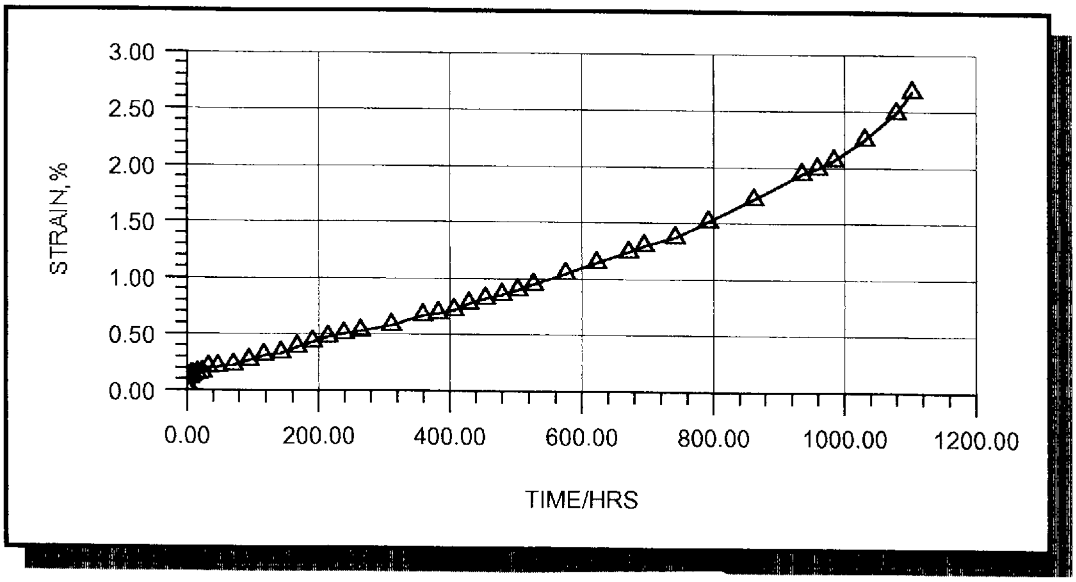

Fig. H3-15—UT8 1¼ CR ½ MO, HAZ, 1050F/20ksi specimen AB8H-K2

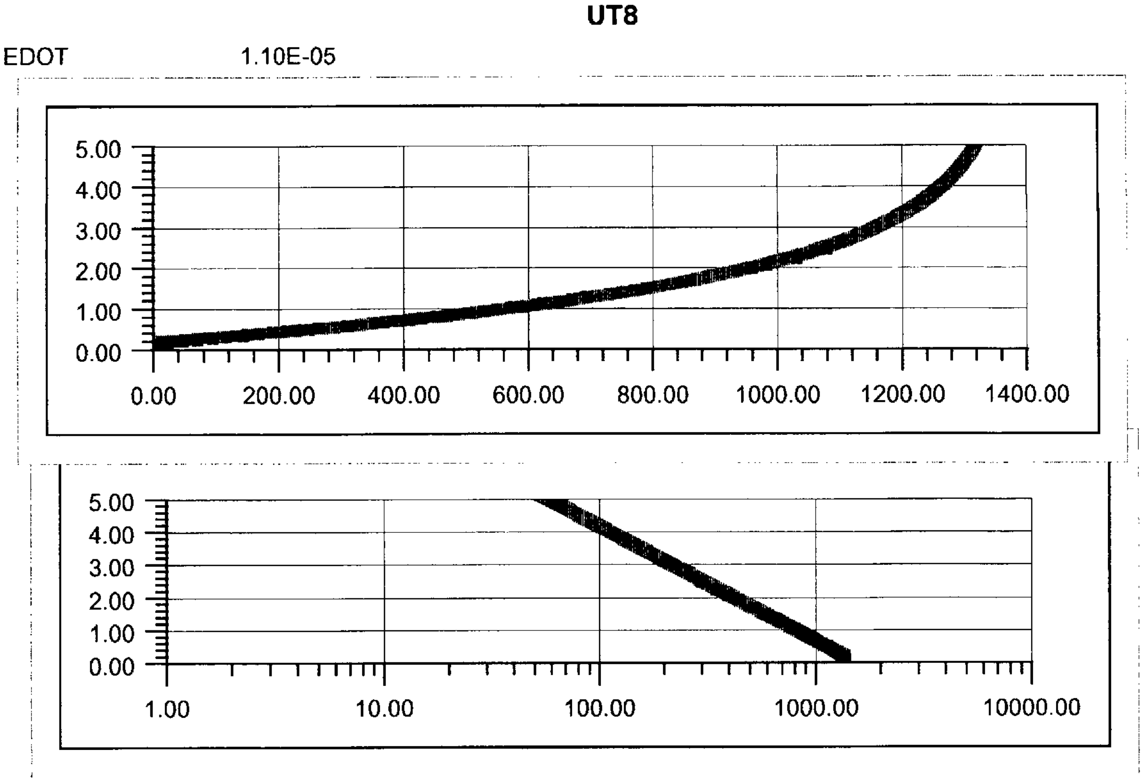

Fig. H3-16—Curve fitting per Ref. H2 to obtain MPC creep rate

Appendix I—Repair Welding Procedures

Behavior of Low Carbon Weld Metal and Repaired Weldments

It has long been reported that the use of low carbon weld metal in fabrication and especially repair of Cr-Mo components enhances the success of complicated joints. However, the creep service suitability of the lower carbon weld deposits has been questioned.

Recent studies by PVRC, the Edison Welding Institute and Ontario Hydro have shown that temper-bead or controlled deposition procedures that aim at refinement of the CGHAZ can mitigate reheat cracking and low toughness problems in the CGHAZ. When coupled with low carbon weld metal these studies, which emphasize the use of a refined HAZ, may provide for equivalent properties in the HAZ and weld metal thus enhancing the possibility for extended life and improved repair weld deposition.

A study that is currently in progress at the University of Tennessee under PVRC guidance addresses the efficacy of the utilization of low carbon Cr-Mo weld metal for repairs in Cr-Mo vessels and piping. Testing for the determination of elevated temperature behavior of the low carbon 1¼Cr-½Mo weld metal in the as-welded, postweld heat treated and N&T condition is underway. The results obtained thus far reveal that the properties fall in the virgin base metal (ASTM DS50) data band. In addition, full thickness repairs in two elevated temperature service exposed piping welds were conducted and the properties of the repairs in the as-welded, postweld heat treated (1350°F, 1 hour) condition are equivalent to the service exposed, unrepaired welds.[1]

The repair was conducted using low carbon SMA weld metal deposition and controlled deposition techniques, the procedure for which is presented following this discussion. This procedure was developed as a part of a PVRC project and is aimed at complete (approaching 100%) refinement of the CGHAZ in the base metal.

Another concern regarding low carbon weld metal toughness was also addressed in this study and it was found that low carbon weld metal has adequate toughness in the as-welded condition (exceeding 40 ft-lbs at −40°F). Upon PWHT at 1350°F for 8 hours the toughness was found to improve significantly. The toughness data and curves are also included in this appendix. Thus, it can be concluded that use of a low carbon consumable may improve the possibility of a successful repair and maintain suitable elevated temperature creep and toughness.

Reference to Appendix I

1. Lundin, C. D., Khan, K. K., Zhou, G. and Liu, P. "Efficacy of Low Carbon 1¼Cr-½Mo Weld Metal for Repair Welding of Elevated Temperature Service Exposed Cr-Mo Components," Pressure Vessel & Piping Conference and Exchanging International Technology, ASME/JSME, July 23–27, 1995, Hawaii, USA.

Temper-Bead Welding Procedure for Repair Welding

Position of Welding. Flat

Preheat & Interpass Temperature. 250°F minimum, 400°F maximum

Electrode Type. Generally E8018 B2L (AWS A5.5) for 1¼Cr-½Mo

Welding Technique:

- Bead Overlap: For the first three layers, weld with the electrode tip directed at the toe of the previous pass in order to achieve a 50% bead overlap (see sketch (a) below).
- Electrode Angle: The electrode should be positioned at an angle of 80–90° to surface of the repair cavity (see sketch (b) below).

Welding Parameters:

- *First Layer* (use stringer beads)
  Electrode Size: 3⁄32″ diameter E8018 B2L
  Current: 80–85 amps
  Travel Speed: 10–11 inches per minute
  Heat Input: Approximately 9 KJ/in
- *Second & Third Layers* (use stringer beads)
  Electrode Size: ⅛″ diameter E8018 B2L
  Current: 130–140 amps
  Travel Speed: 10 inches per minute
  Heat Input: Approximately 17 KJ/in
- *Remaining Layer* (use stringer beads)
  Electrode Size: ⅛″ & 5⁄32″ diameter E8018 B2L as required

Cavity Welding. For the first three layers, weld from the center of the cavity out and lap the last pass on each side over the top edge of the plate.

Final Temper Layer of Weld Metal and Removal:

1. Overfill the cavity one layer above the surface using the numbered sequence shown below.
2. Grind the entire weld surface flat/smooth.
3. Add one additional layer of weld metal as shown to temper underlying weld metal (without overlapping the base metal—1⁄16″ from the edge of the weld and using the numbered sequence shown). Remove this additional layer of weld metal by grinding flat/smooth.

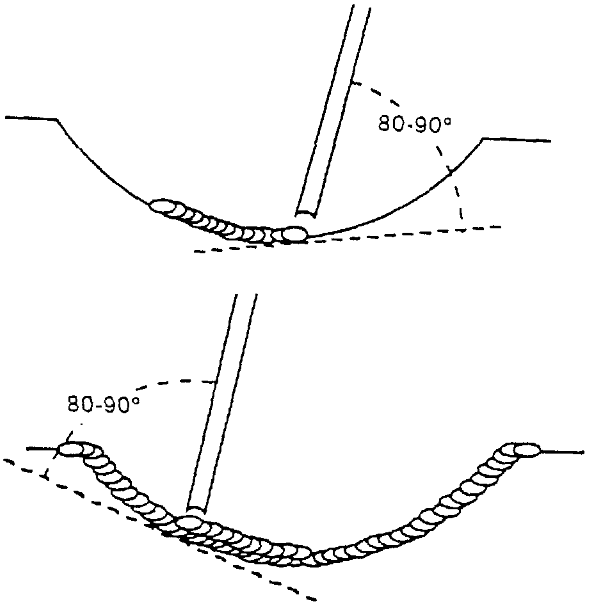

Fig. I-1

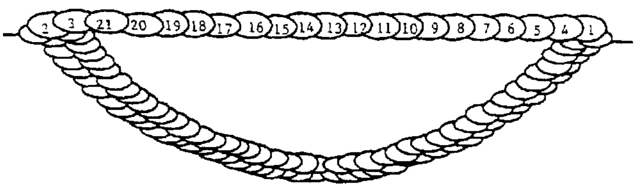

Fig. I-2

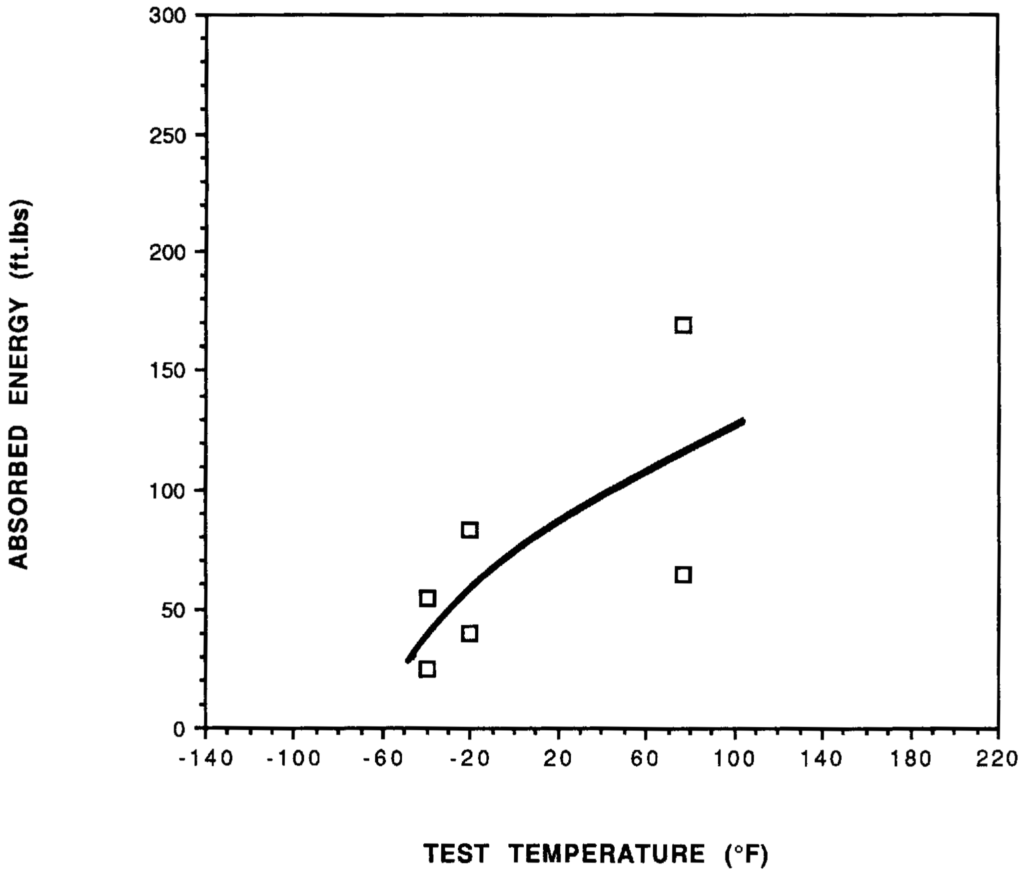

Fig. I-3—CVN-absorbed energy low C SMA repair weld metal (E8018 B2L) in as-welded condition

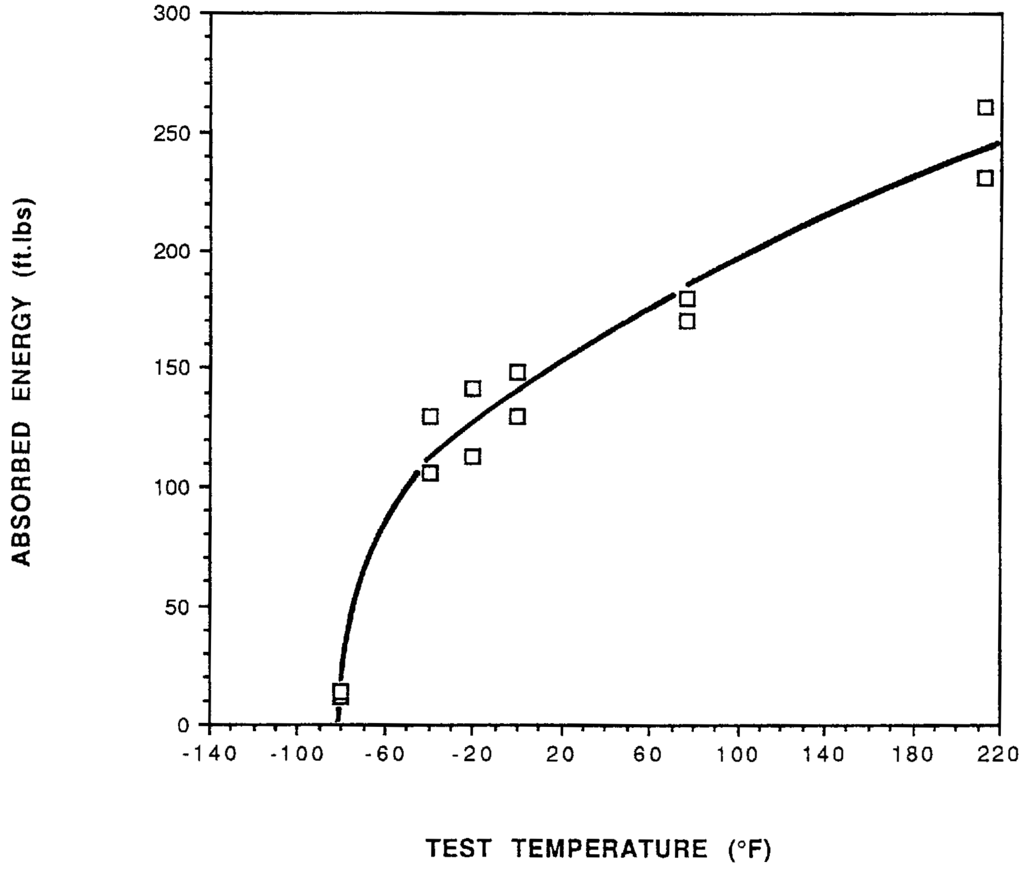

Fig. I-4—CVN-absorbed energy low C SMA repair weld metal (E8018 B2L) PWHT 1350°F, 8 hrs

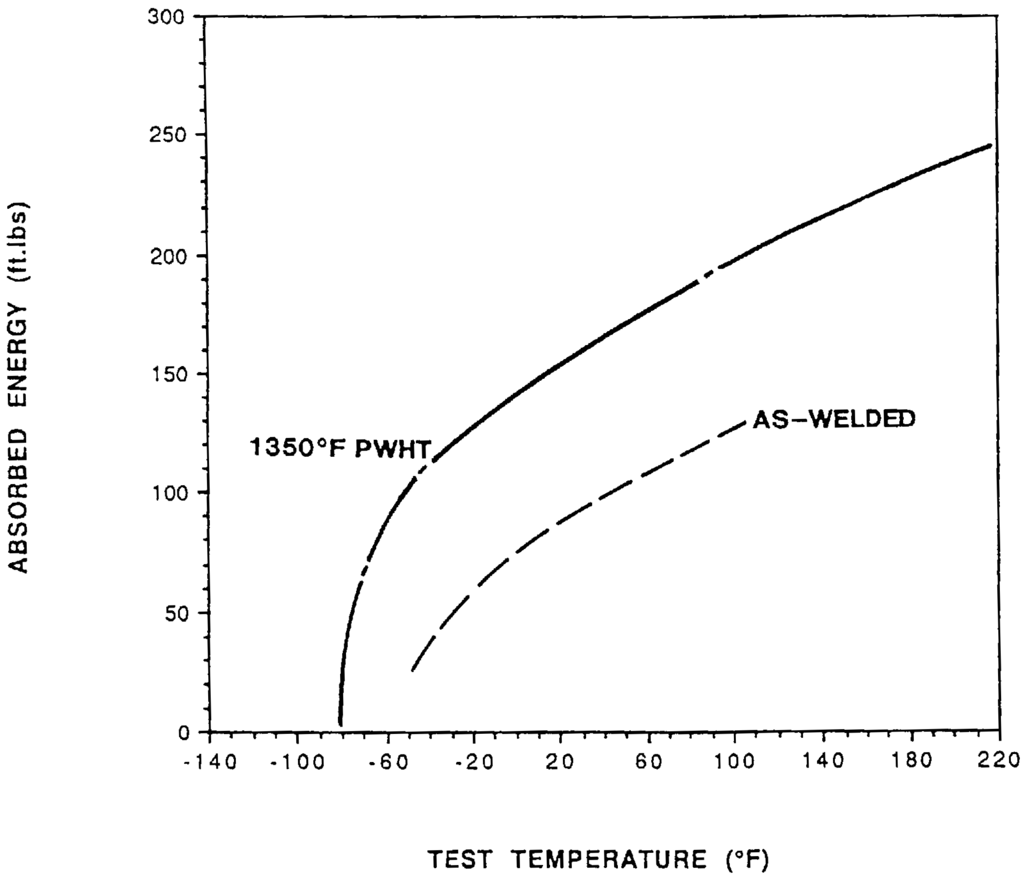

Fig. I-5—CVN-absorbed energy low C SMA repair weld metal (8018 B2L) PWHT 1350°F, 8 hrs/as-welded

Results of Charpy V-Notch Toughness Study

Low C SMA Repair Weld Metal, 1350°F, 8 hrs PWHT

Test Temperature (°F)	*Energy Absorbed (ft-lbs)*
212	260
212	231
RT	170
RT	180
0	149
0	130
−20	113
−20	142
−40	130
−40	106
−80	14
−80	12

Low C SMA Repair Weld Metal, As-Welded

Test Temperature (°F)	*Energy Absorbed (ft-lbs)*
RT	64
RT	169
−20	83
−20	40
−40	25
−40	54

Appendix J—Program Tasks

Task I—Fabrication and Welding

Problems may be caused by preheat and postheat procedures and the consumables used during welding. The resulting hydrogen cold cracks may appear or propagate under service conditions. The effectiveness of welding guidelines offered by this program will be demonstrated by large scale tests based on a bent beam concept with a stress concentration at the edge of a transverse weld. The same specimen can be used to identify the time-temperature window for PWHT cracking. This work will be done on crack sensitive heats as identified in preliminary small scale tests (Task II).

Small scale, simulated HAZ tests of Gleeble specimens will establish crack prone microstructures. Notch sensitivity under accelerated service-like conditions can be studied to determine the influence of PWHT and other thermal treatments. The full range of PWHTs covering possibilities under Class I and Class II requirements will be examined regarding sensitivity to in-service cracking.

Task 2—Materials Variables

Materials variables can be systematically screened with a validated small scale test. The compositional variables include J Factor, X, P, S, Cu, Ca, Ti, C, B, N, grain size, Cr and Si. Before proceeding too far, small scale SRC rankings will be validated by large scale tests. Then the remainder of the variables will be studied. Materials will be obtained from retired vessels with the cooperation of steelmakers and prepared by possibly abusive thermal treatments. The primary tool involved will be a spiral notch test of a simulated HAZ. The comparative behavior of Class I and Class II heat treatments can be studied here jointly under Tasks 1 and 2. Comparing the tendency for SRC cracking of Class I and Class II weldments will require full scale testing.

Task 3—Controlled Deposition Repair Procedures

Crack susceptible materials will be used. The techniques will be demonstrated by preparing actual weldments and utilizing the full scale test to determine improvements in resistance to stress relief cracking tendencies. Simulated HAZ specimens both exposed and not exposed to PWHT will be stress-rupture tested to validate suitability for service.

Task 4—Filler Metals

The objective here is to reduce susceptibility of repairs to stress-relief or in-service cracking when they are made with undermatching (low carbon) filler metals. The concern, on the other hand, is their ultimate suitability for service. The study of the former will be exactly analogous the study of controlled deposition techniques. Again, crack susceptible materials will be used. Cracking susceptibility of the base metal may be enhanced by prewelding heat treatment or selecting materials of unsatisfactory composition. The full scale weldment tests will be exposed to the most severe postwelding heat treatment cycle. This activity will improve understanding of the interplay of carbon level with preheat/postheat requirements with respect to hydrogen cracking. Service performance will be studied by stress-rupture testing weldments given the maximum PWHT at Code allowable stresses.

Task 5—Hydrogen Effects

This work will be patterned on crack propagation studies now in progress on 2¼Cr-1Mo steel. Compact tension specimens under hydrogen pressure and operating temperature are monitored using d.c. potential drop techniques. Hydrogen pressure and temperature can be varied to see the effect on creep crack growth or even on crack growth at lower temperatures, including ambient. Actual weld heat affected zones will be studied as will materials of varying stress-rupture notch sensitivity and PWHT. If needed, creep rates under hydrogen may be obtained in the MPC test stands at temperatures to 950°F.

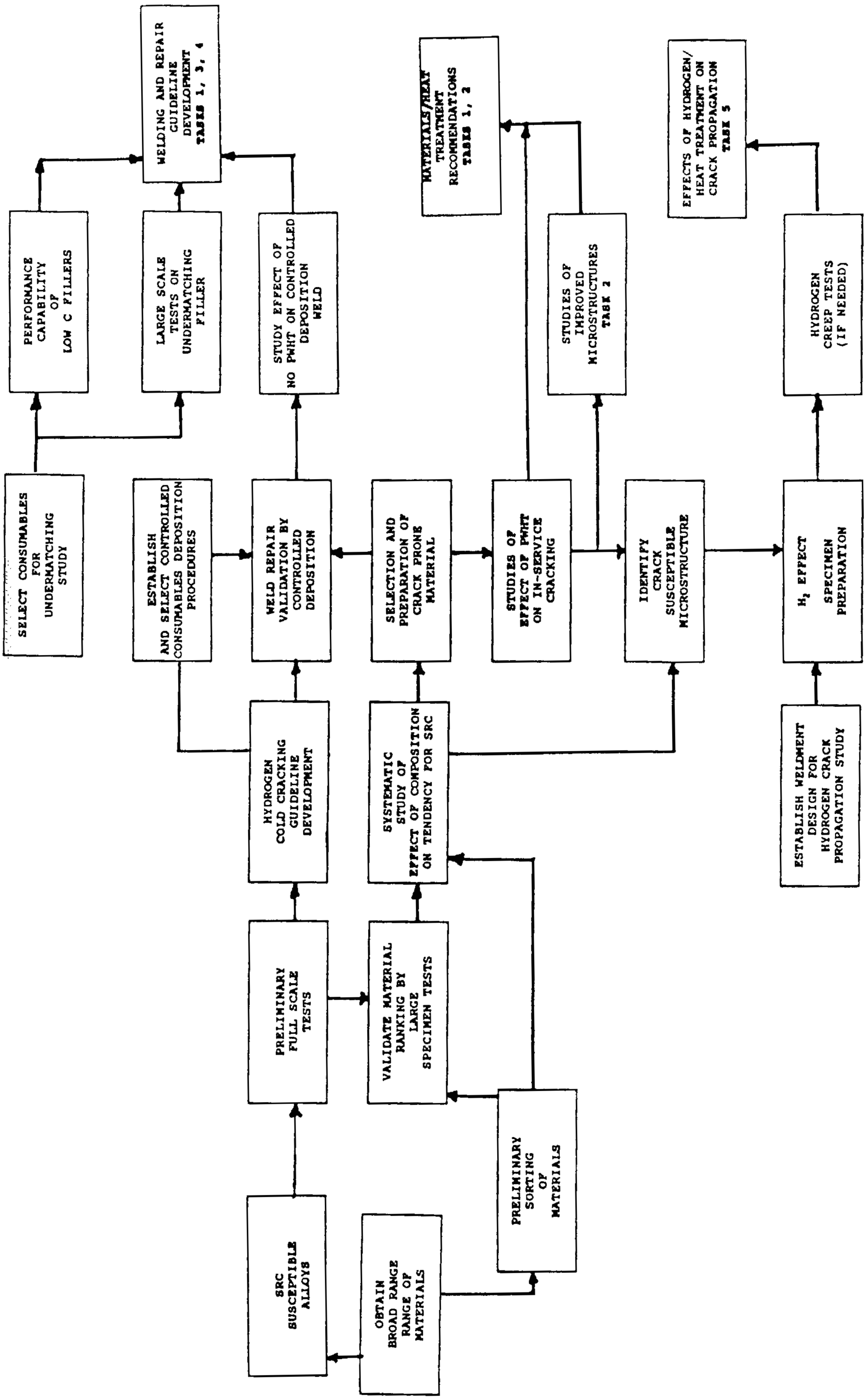

Fig. J-1—Research plan

American Petroleum Institute
1220 L Street, Northwest
Washington, D.C. 20005

Order No. C93801